frontiers | Research Topics

Antiviral innate immune sensing, regulation, and viral immune evasion

Edited by
Chenhe Su, Rongtuan Lin, Junji Xing and Hongjuan You

Published in
Frontiers in Immunology

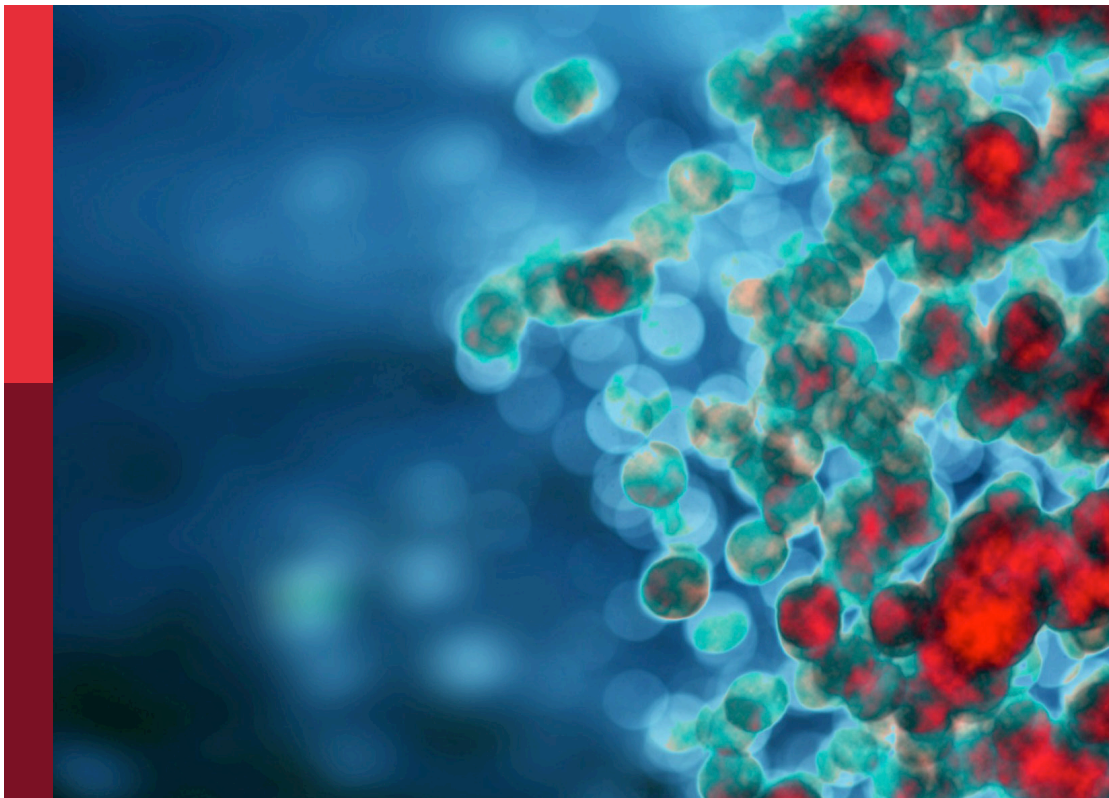

ISSN 1664-8714
ISBN 978-2-8325-5296-4
DOI 10.3389/978-2-8325-5296-4

About Frontiers

Frontiers is more than just an open access publisher of scholarly articles: it is a pioneering approach to the world of academia, radically improving the way scholarly research is managed. The grand vision of Frontiers is a world where all people have an equal opportunity to seek, share and generate knowledge. Frontiers provides immediate and permanent online open access to all its publications, but this alone is not enough to realize our grand goals.

Frontiers journal series

The Frontiers journal series is a multi-tier and interdisciplinary set of open-access, online journals, promising a paradigm shift from the current review, selection and dissemination processes in academic publishing. All Frontiers journals are driven by researchers for researchers; therefore, they constitute a service to the scholarly community. At the same time, the *Frontiers journal series* operates on a revolutionary invention, the tiered publishing system, initially addressing specific communities of scholars, and gradually climbing up to broader public understanding, thus serving the interests of the lay society, too.

Dedication to quality

Each Frontiers article is a landmark of the highest quality, thanks to genuinely collaborative interactions between authors and review editors, who include some of the world's best academicians. Research must be certified by peers before entering a stream of knowledge that may eventually reach the public - and shape society; therefore, Frontiers only applies the most rigorous and unbiased reviews. Frontiers revolutionizes research publishing by freely delivering the most outstanding research, evaluated with no bias from both the academic and social point of view. By applying the most advanced information technologies, Frontiers is catapulting scholarly publishing into a new generation.

What are Frontiers Research Topics?

Frontiers Research Topics are very popular trademarks of the *Frontiers journals series*: they are collections of at least ten articles, all centered on a particular subject. With their unique mix of varied contributions from Original Research to Review Articles, Frontiers Research Topics unify the most influential researchers, the latest key findings and historical advances in a hot research area.

Find out more on how to host your own Frontiers Research Topic or contribute to one as an author by contacting the Frontiers editorial office: frontiersin.org/about/contact

Antiviral innate immune sensing, regulation, and viral immune evasion

This ebook is split into several files; this is part two of the ebook, please see the overview text of the Research Topic page to access the first part of the ebook.

Topic editors
Chenhe Su — Henan Normal University, China
Rongtuan Lin — McGill University, Canada
Junji Xing — Houston Methodist Research Institute, United States
Hongjuan You — Xuzhou Medical University, China

Citation
Su, C., Lin, R., Xing, J., You, H., eds. (2024). *Antiviral innate immune sensing, regulation, and viral immune evasion*. Lausanne: Frontiers Media SA.
doi: 10.3389/978-2-8325-5296-4

Table of contents

frontiers | Frontiers in Immunology

TYPE Review
PUBLISHED 15 August 2022
DOI 10.3389/fimmu.2022.963923

OPEN ACCESS

EDITED BY
Chenhe Su,
Wistar Institute, United States

REVIEWED BY
Zhonghan Li,
Sichuan University, China
Xiaochuan Liu,
University of California, Riverside, United States

*CORRESPONDENCE
Zhiwen Xu
abtcxzw@126.com

†These authors have contributed equally to this work and share first authorship

SPECIALTY SECTION
This article was submitted to Viral Immunology, a section of the journal Frontiers in Immunology

RECEIVED 08 June 2022
ACCEPTED 13 July 2022
PUBLISHED 15 August 2022

CITATION
Jian Z, Ma R, Zhu L, Deng H, Li F, Zhao J, Deng L, Lai S, Sun X, Tang H and Xu Z (2022) Evasion of interferon-mediated immune response by arteriviruses. *Front. Immunol.* 13:963923. doi: 10.3389/fimmu.2022.963923

Evasion of interferon-mediated immune response by arteriviruses

Zhijie Jian[1†], Rui Ma[1†], Ling Zhu[1,2], Huidan Deng[1], Fengqin Li[1,3], Jun Zhao[1,2], Lishuang Deng[1], Siyuan Lai[1], Xiangang Sun[1], Huaqiao Tang[1] and Zhiwen Xu[1,2*]

[1]College of Veterinary Medicine, Sichuan Agricultural University, Cheng Du, China, [2]Key Laboratory of Animal Disease and Human Health of Sichuan Province, Sichuan Agricultural University, Cheng Du, China, [3]College of Animal Science, Xichang University, Xichang, China

IFN is the most potent antiviral cytokine required for the innate and adaptive immune responses, and its expression can help the host defend against viral infection. Arteriviruses have evolved strategies to antagonize the host cell's innate immune responses, interfering with IFN expression by interfering with RIG, blocking PRR, obstructing IRF-3/7, NF-κB, and degrading STAT1 signaling pathways, thereby assisting viral immune evasion. Arteriviruses infect immune cells and may result in persistence in infected hosts. In this article, we reviewed the strategies used by Arteriviruses to antagonize IFN production and thwart IFN-activated antiviral signaling, mainly including structural and nonstructural proteins of Arteriviruses encoding IFN antagonists directly or indirectly to disrupt innate immunity. This review will certainly provide a better insight into the pathogenesis of the arthritis virus and provide a theoretical basis for developing more efficient vaccines.

KEYWORDS

arteriviruses, interferon (IFN), viral proteins, innate immunity, immune evasion

Introduction

The mammalian immune system can effectively detect and fight against viral infections by inducing the production of type I interferon, which forms the first line of defense. The type I interferon response consists of two parts. The first part is triggered by viral stimulation when cells produce type I interferon and secrete IFN. In the second part of the response, both the IFN-producing cell and adjacent cells sense IFN, leading to the production of IFN-stimulated genes (ISG) (1).

Arteriviruses include porcine reproductive and respiratory syndrome virus (PRRSV), equine arteritis virus (EAV), lactate dehydrogenase-elevating virus (LDV), simian hemorrhagic fever virus (SHFV), and swing possum virus (SPV). They can persist in infected animals, PRRSV can persist for six months in pigs, EAV can persist for life in

horses, LDV can usually persist in mice without pathological consequences for the host, and SHFV can show different symptoms in macaques and baboons, with macaques showing fatal hemorrhagic fever but baboons showing only persistent asymptomatic infection (2–5). EAV and PRRSV are considered important pathogens in veterinary studies among these arteriviruses. They can cause significant economic losses in the equine and swine industries, share similar molecular characteristics, and cause reproductive disorders in livestock (6). Therefore, effective Arterivirus control and prevention methods are urgently needed. This review summarizes research advances for the different pathways of anti-IFN responses to Arteriviruses (Figure 1). We want to provide creative insights to guide the development of innovative strategies to achieve Arteriviruses prevention and control.

Overview of interferon response

IFN is a soluble factor discovered in 1957 in viral infections and is named for its ability to interfere in viral replication (7). Interferons are classified into types I, II, and III IFNs (IFN-I, II, and III). In mammals, IFN-I is composed of 19 IFN proteins: 14 IFN-α subtypes (IFN-α1 to α14), IFN-ω, IFN-ε, IFN-τ, IFN-κ, and IFN-β and IFN-I signaling is mediated through the IFN-I receptor (IFNAR), which is a common cell surface receptor. IFN-II family is mainly produced by T lymphocytes and natural killer cells (NK cells), which are mediated by IFNGR (a receptor composed of IFNGR1 and IFNGR2). IFN-III comprises 4 subtypes, IFN-λ1, IFN-λ2, IFN-λ3, and IFN-λ4, and it is mediated by IFNLR (a receptor composed of IFNLR1 and IL10R2) (8–12). IFN-III is associated with IFN-I and IL-10, which have antiviral activity (10). IFN-λ is an epithelial cytokine that limits viral replication in epithelial cells and forms an additional protective layer at mucosal sites (13).

The activation of IFN-I response is divided into three phases: ①pattern recognition receptors (PRRs) on the cell membrane or cytoplasm PRRs recognize pathogen-associated molecular patterns (PAMPs); ②IFN triggers JAK-STAT *via* paracrine or autocrine signaling; ③expression of a large number of antiviral ISG genes, which puts the host into an antiviral state (14).

Most PRRs in the innate immune system of vertebrates can be classified into the following five types: Toll-like receptors (TLRs), retinoic acid-inducible gene I (RIG-I)-like receptors (RLRs), nucleotide oligomerization domain (NOD)-like receptors (NLRs), C-type lectin receptors (CLRs), and absent in melanoma-2 (AIM2)-like receptors (ALRs) (15). We will discuss two classes of viral sensing PRRs in this review. These include TLRs and RLRs, which are important for inducing the type I IFN response. TLRs primarily recognize viral RNA or DNA in the endosomes, and RLRs primarily recognize viral RNA in the cytoplasm. They play a key role in the induction of host IFN expression (16–18). Still, another is a set of structurally unrelated viral DNA sensors (Cyclic GMP-AMP synthase) and IFI16 located in the cytoplasm and/or nucleus, and it also plays a critical role in inducing the expression of host IFN (19). Interferon is normally secreted and binds to cell surface receptors in response to viral infection and activates a JAK/STAT-dependent signaling cascade that produces ISG and puts the cell in a state of resistance (20).

The prolonged infection caused by arteriviruses has a greater association with immune evasion, mainly through the suppression of interferon by various pathways to promote viral proliferation and long-term infection. Clarifying the antagonism between arteriviruses and interferon is important to understand the pathogenesis and find relevant targets as a basis for vaccine

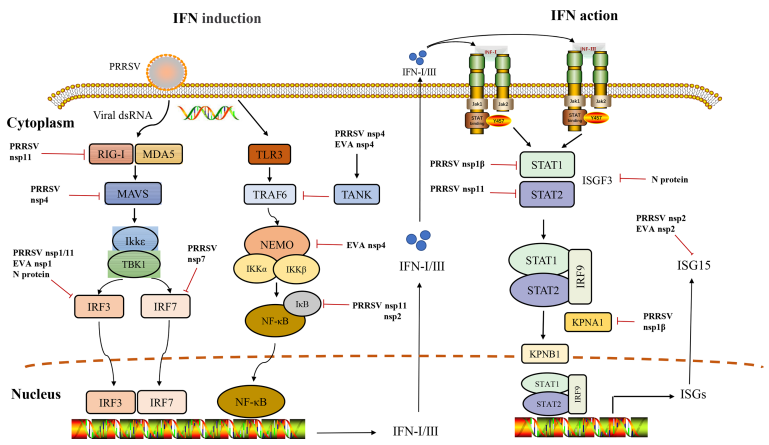

FIGURE 1
Interference of IFN induction and its downstream signaling pathway by Arteriviruses.

development. Therefore, this review will summarize the underlying immune evasion mechanisms by arteriviruses.

Arteriviruses induce mainly low levels of IFN expression

Arteriviruses use different mechanisms to suppress interferon responses to evade the host's innate immune response. Early studies have shown that PRRSV infection in pigs leads to a weak induction of the natural immune response. Detection of interferon in alveolar lavage fluid reveals that interferon is maintained at very low levels, suggesting that PRRSV can interfere with IFN-I transcription directly at the level of IFN-β gene transcription in the early stages of infection (21–23). Before the challenge, IFN-pretreatment of pigs *in vivo* reduced PRRSV-induced symptoms. However, it appears that IFN therapy could not rescue PRRSV-infected swine from death, but it extended survival time (24). *In vitro* study, the inhibition of IFNs expression by PRRSV was similarly observed in MARC-145 cells infected with PRRSV and PAMs cells (23, 25).

Similarly, IFN-β production in Equine endothelial cells (EECS) was significantly inhibited after EAV infection, in contrast to SeV infection, which stimulated high levels of IFN-I expression, and EAV infection also significantly inhibited SeV-induced IFN-I production (26). All of the above studies suggest that Arteriviruses induce IFN inhibition, and the main mechanisms responsible for this phenomenon are reviewed next.

Arteriviruses proteins inhibit the IFN response

Different arteritis virus structural and nonstructural proteins exercise different functions in IFN inhibition (Table 1).

ORF2, 2a, 3, 4, 5, 6, and 7 of PRRSV encode GP2, E, GP3, GP4, GP5, M protein, and N protein, respectively (41). Mechanistic studies of PRRSV antagonism to type I interferon have focused on IFN-α/β, two factors that play a major role in the fight against PRRSV infection. At least two structural proteins (M and N proteins) and four nonstructural proteins of PRRSV, nsp1, nsp2, nsp11, and nsp4, have been identified as exhibiting inhibitory effects on IFN-β promoter activation, with nsp1 showing the strongest inhibitory effect and self-cleavage of nsp1 during infection to produce NSP1α and NSP1β. NSP1β can inhibit IRF3 phosphorylation and NF-κB-dependent nuclear translocation (30, 31). Nsp4 is a 3C-like serine protease that antagonizes type I interferon production by cleaving mitochondria antiviral signaling protein (MAVS) and NF-κB essential regulators (NEMO) (32, 33, 42). PRRSV nsp7 inhibits IRF7 expression, downregulates IFN and downstream ISG expression, and promotes viral replication (38). Nsp11 can suppress the activation of IFN-β by cleaving the mRNA of MAVS (also known as IPS-1, Cardif, and VISA) *via* the endoribonuclease domain (43). PRRSV N protein is distributed in both cytoplasm and nucleus, suggesting that altered localization of N protein may affect its IFNs inhibitory activity (28). Some studies have demonstrated that N protein prevents IFN-β induction like that of nsp2 (44). IFN-γ plays an important role in the immune response against PRRSV. The duration of viremia and the degree of morbidity did not correlate well, but ELISA experiments showed that N, M protein, and nsp2 were indeed associated with PRRSV-specific induction of IFN-γ secretion by lymphocytes (27).

Among the EAV nsp, four nonstructural proteins, nsp1, nsp2, nsp4, and nsp11, have been identified as potential interferon antagonists. It was shown that the homolog of PRRSV nsp1α/β, EAV nsp1, has the strongest ability to inhibit type I IFN synthesis (26). EAV nsp2-encoded papain-like proteinase (PLP2) inhibits Ub- and ISG15-dependent innate immune responses (36). Similarly, EAV nsp4 can inhibit virus-induced IFN-β production by targeting NEMO for protein cleavage, and cleavage occurs at four sites, including E166,

TABLE 1 Arteriviruses proteins inhibit IFN downstream signaling pathway.

Arteriviruses proteins	The molecular mechanisms	References
M	PRRSV-specific IFN-γ secretion is correlated with N and M proteins, but the exact mechanism is unclear.	(27)
N	N proteins can inhibit interferon-induced elevated STAT2 levels and ISGF3 nuclear translocation, and their altered localization may also affect the inhibitory activity of IFNs.	(28, 29)
nsp1	Inhibition of IRF3 and IκBα phosphorylation, blocking nuclear translocation of STAT1 and each signaling step upstream of NF-κB activation, cleavage of MAVS and NEMO to antagonize interferon production	(30–35)
nsp2	nsp2 is a potential ISG15 production and binding antagonist and can inhibit Ub and ISG15-dependent innate immune responses.	(36, 37)
nsp4	Targeted cleavage of NEMO and NF-κB activator (TANK) to block NF-κB signaling, cleavage of MAVS and blocking RLR signaling, and inhibition of IFN-β promoter activation.	(33, 34)
nsp7	Inhibits IRF7 expression, thereby downregulating IFN and downstream ISG expression, and promotes viral replication	(38)
nsp11	nsp11 can induce STAT2 degradation directly through the ubiquitin-proteasome degradation pathway and inhibit the NF-κB signaling pathway by de-ubiquitination-dependent activity	(39, 40)

E171, Q205, and E349, consistent with PRRSV cleavage sites (34).

Arteriviruses interference with host interferon induction

Blocking the recognition of TLR-mediated pathways

The RLRs group consisted of RIG-I, melanoma differentiation-associated gene 5 (MDA5), and Laboratory of Genetics and Physiology 2 (LGP2). RIG-I recognizes the triphosphate and diphosphate at the stem end of dsRNA, which is the hallmark of viral RNA of most RNA viruses (45). MDA5 perceives long dsRNA, which is believed to represent the intermediate replication product of many RNA viruses (46). LGP2, a protein structurally related to both RIG-I and MDA5, appears to be a cofactor for viral RNA sensing by a mechanism that is not completely understood and likely involves making viral RNA more accessible to RIG-I or MDA5 (47). RIG-I and MDA5 are important sensors for IFN-I production in the porcine innate immune system (48). RIG-1 and MDA-5 detect specific viral RNA PAMPs, while LGP2 negatively regulates RIG-I signaling and promotes RNA binding to MDA5 (49). RIG-I-like receptor-mediated type I IFN production plays an important role in the host's defense against viral invasion (50). dsRNA is a specific secondary structure of viral RNA detected by RIG-I/MDA5 and induces IFN-α/β production through cascade activation of the RLR pathway (51). Viral dsRNA can trigger RIG-I, and the CARD domain of RIG-I interacts with the CARD domain of MAVS, and activation of MAVS recruits multiple downstream signaling components to the mitochondria, leading to activation of κ-B kinase inhibitor ϵ (Iκκϵ) and TANK-binding kinase 1 (TBK1), which in turn causes IRF3 phosphorylation. Phosphorylated IRF3 forms a dimer and translocates to the nucleus, activating transcription of the IFN-I gene (52, 53).

PRRSV infection inhibits IFN-β production mainly by interfering with MAVS activation in the RIG-I signaling pathway (54). The porcine reproductive and respiratory syndrome virus (PRRSV) 3C-like protease (3CLSP), by contrast, cleaves MAVS in a proteasome- and caspase-independent manner at Glu268 (E268/G269). Both cleavage products fail to activate the type I IFN response (55). Further studies showed that the highly pathogenic porcine reproductive and respiratory syndrome virus (HP-PRRSV) protein nsp4 cleaves MAVS and blocks RLR signaling, and causes specific downregulation of the MAVS, but nsp4 in the typical PRRSV strain CH-1a has no effect on MAVS, so this may be a strategy evolved by the virulent strain (32). Nsp11 reduces RIG-I mRNA dependent on its endoribonuclease activity. Nsp11 inhibits IRF3 and NF-κB activity when stimulated with dsRNA analogs and TNF-α, respectively, suggesting that this inhibition also depends on RLR (56).

Recent studies have shown that MDA5 senses the EAV genome to induce IFN expression (57).

Evasion of the IRF3/7 signaling pathway

Interferon regulatory factors (IRFs) are a family of transcription factors with 9 members identified so far. IRF4, 5, and 6 have no substantial role in IFN regulation and are also not described. IRF-1 and IRF-2 mRNA were expressed in multiple cell types, whereas IRF-8 expression was restricted to myeloid and lymphoid cell lines, and its mRNA was significantly upregulated in response to viral infection or IFN stimulation (58, 59). IRF-9 was originally identified as the DNA-binding subunit of ISGF3 and was proven essential for the antiviral response to IFN-α/β and IFN-γ (60, 61). IRF-3 and IRF-7 are closely related in their primary structure, and recent studies have identified an important and distinct role for these two factors in IFN-α/β gene induction in arteritis virus infection.

It has been suggested that IFN-λ expression is more flexible than IFN-α/β expression, which may allow IFN-III to be expressed in response to a wider range of stimuli than IFN-I, and would potentially make IFN-III expression less sensitive to microbial evasion strategies targeting the IRF pathway (62, 63). IRF3 is a target factor for various viruses and can impair natural immune signaling. Most viruses inhibit IRF3 phosphorylation and thus also IRF3 dimerization and translocation. In the absence of IRF-3 activation and IFN-β production, alternative pathways allow IFN-λ to be induced without IRF-3 activation. IRF-3 is a virus targeting factor and can impair innate immune signaling. Most viruses inhibit IRF3 phosphorylation, dimerization, and nuclear translocation. TBK1 and IKKϵ can induce IRF3 and IRF7 phosphorylation and be affected by K63-linked polyubiquitination (64, 65). The ubiquitin chain may serve as a platform for the assembly of the TBK1 signaling complex, so for TBK1, polyubiquitination of the K63 linkage appears to be important for TLR and RLR-induced IFN production (65, 66). Activated TBK1/IKKϵ phosphorylates IRF3 and/or IRF7 at specific serine residues in the cell membrane, which are subsequently transferred to the nucleus to recruit the coactivator CBP/p300 and form a complex to bind the IRF-3 response element of the IFN-β promoter (PRD I and III) (67–69). Interestingly, IRF7 was induced during IFN signaling at low levels in most cells, suggesting that IRF7 can strongly enhance IFN production (70).

Viral proteins target TBK1 to block IFNβ production by preventing TBK1 activation from MAVS or inhibiting IRF3 activation from TBK1. Once activated, MAVS signaling recruits multiple kinases, ubiquitin ligases, and adapters, leading to phosphorylation and activation of potential transcription factors involved in IFN promoter activation.

These transcription factors, IRF factors, especially IRF3 and IRF7, are essential for IFN induction (71, 72). In addition, IRFs are also required for IFN induction during TLR activation. Therefore, it is unsurprising that virally encoded IFN antagonists can inhibit IRFs.

PRRSV nsp1 is the most potent interferon repressor protein among the nonstructural proteins. Studies have shown that the inhibition of type I IFN is due to PRRSV nsp1α/β blocking dsRNA-induced activation of IRF-3. In the presence of nsp1α/β, phosphorylation of IRF-3 and its nuclear translocation occurred normally, but the association of IRF3 with cAMP response element-binding protein(CBP) in the nucleus was inhibited, thereby blocking IRF-3 activation (73, 74). Nsp4 was reported to inhibit IRF-3-mediated activation of the IFN-β promoter, an inhibition derived from the hydrolytic activity of the nsp4 3C-like serine protease (75, 76). Recently, it has been shown that N proteins can inhibit poly(I:C)-mediated IRF-3 phosphorylation and nuclear translocation, thereby suppressing the expression of IFN-β (44). Therefore, IRF3 can be a direct viral target to block IFN production and a key target for vaccine development. IRF7 is another important regulator in the interferon signaling pathway. IRF7 can inhibit the early replication of PRRSV. While PRRSV nsp7 significantly down-regulates IRF7 expression, nsp4 and nsp5 do not down-regulate IRF7 expression. Instead, nsp11 upregulates IRF7 expression, which may result from complex virus-protein interactions (38).

Similarly, EVA nsp1α and NSP1β mediated the inactivation of MAVS, leading to inhibition of IRF-3 activity, which is similar to the role of PRRSV nsp1 (77). It was also found that EAV nsp1 blocked every signaling step upstream of IRF-3, suggesting that EAV nsp1 acts downstream of all these tested steps in this signaling pathway and, interestingly, does not have much effect on the nuclear accumulation of IRF-3, presumably having an effect on the IFN-β promoter in the nucleus (26).

Blocking TLR-mediated recognition pathway and activation of transcription factor NF-κB

Pathogen-associated molecular patterns in viral RNAs are recognized by various pattern recognition receptors, such as TLR3. TLR-3, -7, -8, and -9 are all capable of inducing type I IFN gene expression, and they exercise the function of detecting different forms of nucleic acids. They scan the extracellular and endosomal space to detect RNA and DNA, detect the viral genome from extracellularly lysis viral particles and initiate signaling cascades that lead to the secretion of IFN and other proinflammatory molecules, such as TLR3 recognition of dsRNA, initiating a TRIF-dependent signaling cascade (52, 78).

Suppressors of cytokine signaling (SOCS) are intracellular family proteins involved in the negative regulation of the immune response (79). Lung epithelial cells can induce IFN-β production and are the first to interact with pathogens, and plasmacytoid dendritic cells (PDCs) can rapidly establish a connection with TLR7 and induce IFN-I expression (80, 81). Recent studies have also shown that SOCS1 and SOCS3 strongly inhibit TLR7-mediated IFN-I production (82, 83) and that PRRSV N proteins can significantly activate SOCS1 promoter activity and induce SOCS1 expression at the protein level in Marc-145 cells, ultimately leading to IFN inhibition (84). Interestingly, TLR3-mediated IFN production after infection with Herpes simplex virus 1 (HSV-1) is cell type-dependent, with TLR3 limiting HSV-1 replication in mouse fibroblasts and CNS-resident cells (neurons, astrocytes), whereas no such protective mechanism is produced in mouse macrophages (85).

TLR3 interacts with TRIF by interacting with upstream adaptors. TRIF undergoes conformational changes and recruits the downstream TNF receptor-associated factor (TRAF)6 (86). The kinase receptor-interacting protein-1 (RIP-1) is part of the signaling pathways downstream of TLR3 and RIG-I. It can interact with TRIF to induce NF-κB activation (87). In its inactive state, the transcription factor NFκB is complexed with its inhibitor IκB (88). Upon stimulation, IκB is phosphorylated by the IκB kinase (IKK) complex, which is composed of two catalytic subunits, such as IKKα and IKKβ, and a regulatory subunit, such as NF-κB essential modulator (NEMO) (89). NF-κB regulates more than 100 genes that play key roles in inflammation, the innate immune response, and the initiation of adaptive immunity (90).

PRRSV nsp1 and nsp2 inhibit the NF-κB signaling pathway to antagonize IFN-β production (91, 92). Nsp1α inhibits the phosphorylation of IκBα, resulting in the nuclear localization of p65 being blocked, thereby aborting NF-κB function, which is associated with its C-terminal 14 amino acids (92). The nsp2 ovarian tumor protease (OUT) structural domain has deubiquitination activity, and IκB degradation is a necessary step for NF-κB activation, which can act on the IκB polyubiquitination process to prevent its degradation and ultimately inhibit NF-κB-mediated production of IFNs (91). PRRSV nsp4 cleaves TRAF family member-associated NFκB activator (TANK), which inhibits TRAF6-mediated NFκB activation (93). PRRSV nsp4 can also block NF-κB signaling targeting NEMO at a single locus E349 (33). Interestingly, the cleaved fragment of NEMO (1-349) still activates IFN and NF-κB promoter production, suggesting that nsp4 may fail to completely prevent NEMO-mediated IFN-β activation *via* cleavage at NEMO E349 (34). PRRSV nsp11 has also been reported to inhibit the NF-κB signaling pathway in response to deubiquitination activity (39).

EAV nsp1 inhibits IFN-β activation mainly through the NF-κB-dependent signaling pathway, which blocks each signaling step upstream of NF-κB activation, but nsp1 has little effect on NF-κB nuclear accumulation. It is speculated that EAV nsp1 may affect the IFN-β promoter in the nucleus (26). It has also

been shown that EAV Nsp4 can cleave TANK to inhibit NF-κB expression (93).

Interference with type I IFN-activated JAK/STAT signaling pathway and antiviral ISGs

Interferons are normally produced and secreted upon viral infection, and secreted IFN binds to the IFN receptor and activates Janus kinase 1 (JAK1) and tyrosine kinase 2 (TYK2) which phosphorylate signal transducers and activators of transcription proteins (STAT1 and STAT2) (94). Phosphorylated STAT1 and STAT2 form heterodimers that bind to IRF9 to form IFN-stimulated gene factor 3 (ISGF3). ISGF3 translocates to the nucleus and binds to the IFN-stimulated response element (ISRE), triggering the expression of hundreds of ISGs with antiviral functions and putting the cell in an antiviral state (20). Antiviral ISG plays a crucial role in eliminating viral infections (95). Many ISGs are signaling molecules or regulatory proteins in innate and adaptive immunity, and their induction of ISGs can further amplify and develop immune responses (including IFN responses) (96, 97).

PRRSV inhibits the IFN-activated JAK/STAT signal transduction and ISG expression in both MARC-145 and PAM cells (29, 98). Further research found that PRRSV nsp1β could block the nuclear translocation of STAT1 and significantly inhibit the expression of ISGs (35). IFN induces IFN-stimulated gene expression by activating phosphorylation of STAT1 and STAT2, which can form a heterotrimer with IRF9 (ISGF3) and translocate to the nucleus. Severe acute respiratory syndrome (SARS) and PRRSV both interfere with the host innate immune responses. Still, mechanisms that block nuclear translocation of ISGF3 are different, and SARS ORF6 can block nuclear translocation of STAT1 by sequestering KPNA2 alone (99). However, no interaction between nsp1β and any KPNAs was found in PRRSV-infected cells. PRRSV VR2385 can inhibit IFN-α signaling in MARC-145 and PAMs by interfering with ISGF3 nuclear translocation, but PRRSV modified live virus (MLV) infection of PAMs can directly activate IFN signaling, suggesting that there may be different effects of IFN induction between the two PRRSV strains, which may provide reference implications for PRRSV vaccine design (35). PRRSV nsp11 can induce STAT2 degradation directly *via* the ubiquitin-proteasome degradation pathway, in which amino acid residue K59 in nsp11 plays a key role but does not depend on endoribonuclease activity (40). Similarly, N proteins can inhibit interferon-induced elevation of STAT2 levels and ISGF3 nuclear translocation (29). PAM cells are affected by IFN-γ and microbial products such as lipopolysaccharide (LPS) and viral infection, and LPS-activated PAMs inhibit PRRSV replication, and genes in the JAK/STAT signaling pathway were found to be significantly upregulated, suggesting that it might play a key role in cellular activation (100).

Among the antiviral ISGs, the best-studied ones are ISG15, 2 ',5'-oligoadenylate synthetases (OASs), ribonuclease L (RNaseL), the dsRNA-activated protein kinase (PKR), p56 [ISG56, interferon-induced protein with tetratricopeptide repeats 1 (IFIT1)], and Mx1 (Myxovirus (influenza virus) resistance 1), and IFNs induce upregulation of transcriptional expression of several hundred interferon-stimulated genes (101, 102). ISG15 is a ubiquitin-like antiviral protein [59, 60]. ISG15 conjugation (ISGylation) to substrate proteins follows a process similar to ubiquitin conjugation (103, 104). Many viruses target STAT1 and STAT2 to inhibit the induction of ISG. ISG can inhibit nucleic acid nuclear input and RNA and protein synthesis or enhance viral degradation (102). ISG15 and ISGylation act in different cellular pathways, particularly in regulating antiviral innate immune responses. PRRSV nsp2 was previously identified as a potential antagonist of ISG15 production and ISGylation, overexpression of ISG15 inhibited PRRSV replication in cell culture, and the antiviral activity of interferon was reduced by inhibition of ISG15 binding (37). Interestingly, the pseudoknot region of the 3' untranslated region (UTR) of the PRRSV genome can be recognized by RIG-I and TLR3 and strongly induces the expression of ISGs in PAMs, and importantly, similar structures predicted for other arterivirus members, including EAV, LDV, and SHFV, also show strong IFN-inducing activity (105).

The interferon-induced PKR plays an important role in antiviral response. PKR mediates translational control by phosphorylating the protein translation initiation factor eIF2α, inhibiting protein synthesis and viral replication (106). The addition inhibitor of PKR (2-AP) restored PRRSV replication in IFN-γ-treated cells (107). Research shows that PRRSV inhibited PKR activation during its early stage infection of PAMs (108).

Conclusion

Arteriviruses have evolved much to evade the host's innate immune system to better survive in the host over the long term. The sustained low level of interferon expression is a fundamental reason for their ability to persist. Current studies have identified at least six viral proteins identified as IFN antagonists of PRRSV, further understanding of the immune regulation of viruses and strategies to evade the host immune system is necessary. The development of antiviral drugs can be facilitated by understanding the relationship between Arteriviruses and IFN antagonism to identify key immune evasion proteins. Also, understanding current antiviral strategies can enhance known antiviral pathways and further facilitate the development of safe and effective vaccine strains.

Author Contributions

LZ, MR, and ZX conceived the scope of the review article writing, HD and FL assisted with language revisions. JZ, LD, SL, XS, and HT assisted with reviewing relevant literature. ZJ wrote the review with the help of other authors. All authors contributed to the article and approved the submitted version.

Funding

This article was supported by the Sichuan Province's "14th Five-Year Plan" Sichuan Pig Major Science and Technology Project (No. 2021ZDZX0010) and the Key R&D Program in Rural Areas of Sichuan Provincial Department of Science and Technology (No. 2020YFN0147).

Conflict of Interest

The authors declare that the research was conducted in the absence of any commercial or financial relationships that could be construed as a potential conflict of interest.

Publisher's note

References

1. Nagarajan U. Induction and function of IFNβ during viral and bacterial infection. *Crit Rev Immunol* (2011) 31(6):459–74. doi: 10.1615/CritRevImmunol.v31.i6.20

2. Anderson GW, Rowland RR, Palmer GA, Even C, Plagemann PG. Lactate dehydrogenase-elevating virus replication persists in liver, spleen, lymph node, and testis tissues and results in accumulation of viral RNA in germinal centers, concomitant with polyclonal activation of b cells. *J Virol* (1995) 69(8):5177–85. doi: 10.1128/jvi.69.8.5177-5185.1995

3. Vatter HA, Brinton MA. Differential responses of disease-resistant and disease-susceptible primate macrophages and myeloid dendritic cells to simian hemorrhagic fever virus infection. *J Virol* (2014) 88(4):2095–106. doi: 10.1128/JVI.02633-13

4. Plagemann PG, Rowland RR, Even C, Faaberg KS. Lactate dehydrogenase-elevating virus: an ideal persistent virus? *Springer Semin Immunopathol* (1995) 17 (2-3):167–86. doi: 10.1007/BF00196164

5. Gulyaeva A, Dunowska M, Hoogendoorn E, Giles J, Samborskiy D, Gorbalenya AE. Domain organization and evolution of the highly divergent 5' coding region of genomes of arteriviruses, including the novel possum nidovirus. *J Virol* (2017) 91(6):JVI.02096-16. doi: 10.1128/JVI.02096-16

6. Socha W, Rola J, Żmudziński JF. Variability of nonstructural proteins of equine arteritis virus during persistent infection of the stallion. *Pol J Vet Sci* (2015) 18(2):255–9. doi: 10.1515/pjvs-2015-0033

7. Isaacs A, Lindenmann J, Valentine RC. Virus interference. II. some properties of interferon. *Proc R Soc Lond Ser B Biol Sci* (1957) 147(927):268–73. doi: 10.1098/rspb.1957.0049

8. Sadler AJ, Williams BR. Interferon-inducible antiviral effectors. *Nat Rev Immunol* (2008) 8(7):559–68. doi: 10.1038/nri2314

9. Donnelly RP, Kotenko SV. Interferon-lambda: a new addition to an old family. *J Interferon Cytokine Res* (2010) 30(8):555–64. doi: 10.1089/jir.2010.0078

10. Kotenko SV, Gallagher G, Baurin VV, Lewis-Antes A, Shen M, Shah NK, et al. IFN-lambdas mediate antiviral protection through a distinct class II cytokine receptor complex. *Nat Immunol* (2003) 4(1):69–77. doi: 10.1038/ni875

11. Swiecki M, Colonna M. Type I interferons: diversity of sources, production pathways and effects on immune responses. *Curr Opin Virol* (2011) 1(6):463–75. doi: 10.1016/j.coviro.2011.10.026

12. Pestka S, Krause CD, Walter MR. Interferons, interferon-like cytokines, and their receptors. *Immunol Rev* (2004) 202:8–32. doi: 10.1111/j.0105-2896.2004.00204.x

13. Zanoni I, Granucci F, Broggi A. Interferon (IFN)-λ takes the helm: Immunomodulatory roles of IFN-III. *Front Immunol* (2017) 8:1661. doi: 10.3389/fimmu.2017.01661

14. Takeuchi O, Akira S. Innate immunity to virus infection. *Immunol Rev* (2009) 227(1):75–86. doi: 10.1111/j.1600-065X.2008.00737.x

15. Li D, Wu M. Pattern recognition receptors in health and diseases. *Signal Transduct Target Ther* (2021) 6(1):291. doi: 10.1038/s41392-021-00687-0

16. Rathinam VAK, Fitzgerald KA. Cytosolic surveillance and antiviral immunity. *Curr Opin Virol* (2011) 1(6):455–62. doi: 10.1016/j.coviro.2011.11.004

17. Yoneyama M, Onomoto K, Jogi M, Akaboshi T, Fujita T. Viral RNA detection by RIG-i-like receptors. *Curr Opin Immunol* (2015) 32:48–53. doi: 10.1016/j.coi.2014.12.012

18. Kawai T, Akira S. Toll-like receptor and RIG-i-like receptor signaling. *Ann N Y Acad Sci* (2008) 1143:1–20. doi: 10.1196/annals.1443.020

19. Sparrer KM, Gack MU. Intracellular detection of viral nucleic acids. *Curr Opin Microbiol* (2015) 26:1–9. doi: 10.1016/j.mib.2015.03.001

20. Pervolaraki K, Stanifer ML, Münchau S, Renn LA, Albrecht D, Kurzhals S, et al. Type I and type III interferons display different dependency on mitogen-activated protein kinases to mount an antiviral state in the human gut. *Front Immunol* (2017) 8:459. doi: 10.3389/fimmu.2017.00459

21. Albina E, Carrat C, Charley B. Interferon-alpha response to swine arterivirus (PoAV), the porcine reproductive and respiratory syndrome virus. *J Interferon Cytokine Res* (1998) 18(7):485–90. doi: 10.1089/jir.1998.18.485

22. Van Reeth K, Labarque G, Nauwynck H, Pensaert M. Differential production of proinflammatory cytokines in the pig lung during different respiratory virus infections: correlations with pathogenicity. *Res Vet Sci* (1999) 67(1):47–52. doi: 10.1053/rvsc.1998.0277

23. Miller LC, Laegreid WW, Bono JL, Chitko-McKown CG, Fox JM. Interferon type I response in porcine reproductive and respiratory syndrome virus-infected MARC-145 cells. *Arch Virol* (2004) 149(12):2453–63. doi: 10.1007/s00705-004-0377-9

24. Dong S, Yin Y, Shen S, Guo Y, Gao M, Zhang W, et al. Inhibitory effects of recombinant porcine interferon-α on high- and low-virulence porcine reproductive and respiratory syndrome viruses. *Res Vet Sci* (2012) 93(2):1060–5. doi: 10.1016/j.rvsc.2011.12.006

25. Buddaert W, Van Reeth K, Pensaert M. *In vivo* and *in vitro* interferon (IFN) studies with the porcine reproductive and respiratory syndrome virus (PRRSV). *Adv Exp Med Biol* (1998) 440:461–7. doi: 10.1007/978-1-4615-5331-1_59

26. Go YY, Li Y, Chen Z, Han M, Yoo D, Fang Y, et al. Equine arteritis virus does not induce interferon production in equine endothelial cells: identification of nonstructural protein 1 as a main interferon antagonist. *BioMed Res Int* (2014) 2014:420658. doi: 10.1155/2014/420658

27. Molina RM, Cha SH, Chittick W, Lawson S, Murtaugh MP, Nelson EA, et al. Immune response against porcine reproductive and respiratory syndrome virus during acute and chronic infection. *Vet Immunol Immunopathol* (2008) 126(3-4):283–92. doi: 10.1016/j.vetimm.2008.08.002

28. Rowland RR, Kervin R, Kuckleburg C, Sperlich A, Benfield DA. The localization of porcine reproductive and respiratory syndrome virus nucleocapsid protein to the nucleolus of infected cells and identification of a

potential nucleolar localization signal sequence. *Virus Res* (1999) 64(1):1–12. doi: 10.1016/S0168-1702(99)00048-9

29. Wang R, Nan Y, Yu Y, Zhang YJ. Porcine reproductive and respiratory syndrome virus Nsp1β inhibits interferon-activated JAK/STAT signal transduction by inducing karyopherin-α1 degradation. *J Virol* (2013) 87(9):5219–28. doi: 10.1128/JVI.02643-12

30. Beura LK, Sarkar SN, Kwon B, Subramaniam S, Jones C, Pattnaik AK, et al. Porcine reproductive and respiratory syndrome virus nonstructural protein 1beta modulates host innate immune response by antagonizing IRF3 activation. *J Virol* (2010) 84(3):1574–84. doi: 10.1128/JVI.01326-09

31. Ke H, Yoo D. The viral innate immune antagonism and an alternative vaccine design for PRRS virus. *Vet Microbiol* (2017) 209:75–89. doi: 10.1016/j.vetmic.2017.03.014

32. Huang C, Du Y, Yu Z, Zhang Q, Liu Y, Tang J, et al. Highly pathogenic porcine reproductive and respiratory syndrome virus Nsp4 cleaves VISA to impair antiviral responses mediated by RIG-i-like receptors. *Sci Rep* (2016) 6:28497. doi: 10.1038/srep28497

33. Huang C, Zhang Q, Guo XK, Yu ZB, Xu AT, Tang J, et al. Porcine reproductive and respiratory syndrome virus nonstructural protein 4 antagonizes beta interferon expression by targeting the NF-κB essential modulator. *J Virol* (2014) 88(18):10934–45. doi: 10.1128/JVI.01396-14

34. Chen J, Wang D, Sun Z, Gao L, Zhu X, Guo J, et al. Arterivirus nsp4 antagonizes interferon beta production by proteolytically cleaving NEMO at multiple sites. *J Virol* (2019) 93(12):1568-72. doi: 10.1128/JVI.00385-19

35. Patel D, Nan Y, Shen M, Ritthipichai K, Zhu X, Zhang YJ. Porcine reproductive and respiratory syndrome virus inhibits type I interferon signaling by blocking STAT1/STAT2 nuclear translocation. *J Virol* (2010) 84(21):11045–55. doi: 10.1128/JVI.00655-10

36. van Kasteren PB, Bailey-Elkin BA, James TW, Ninaber DK, Beugeling C, Khajehpour M, et al. Deubiquitinase function of arterivirus papain-like protease 2 suppresses the innate immune response in infected host cells. *Proc Natl Acad Sci U S A* (2013) 110(9):E838–47. doi: 10.1073/pnas.1218464110

37. Sun Z, Li Y, Ransburgh R, Snijder EJ, Fang Y. Nonstructural protein 2 of porcine reproductive and respiratory syndrome virus inhibits the antiviral function of interferon-stimulated gene 15. *J Virol* (2012) 86(7):3839–50. doi: 10.1128/JVI.06466-11

38. Liu K, Ma G, Liu X, Lu Y, Xi S, Ou A, et al. Porcine reproductive and respiratory syndrome virus counteracts type I interferon-induced early antiviral state by interfering IRF7 activity. *Vet Microbiol* (2019) 229:28–38. doi: 10.1016/j.vetmic.2018.12.015

39. Wang D, Fan J, Fang L, Luo R, Ouyang H, Ouyang C, et al. The nonstructural protein 11 of porcine reproductive and respiratory syndrome virus inhibits NF-κB signaling by means of its deubiquitinating activity. *Mol Immunol* (2015) 68(2 Pt A):e00385-19. doi: 10.1016/j.molimm.2015.08.011

40. Yang L, He J, Wang R, Zhang X, Lin S, Ma Z, et al. Nonstructural protein 11 of porcine reproductive and respiratory syndrome virus induces STAT2 degradation to inhibit interferon signaling. *J Virol* (2019) 93(22):997-1001. doi: 10.1128/JVI.01352-19

41. Meng XJ, Paul PS, Halbur PG, Lum MA. Characterization of a high-virulence US isolate of porcine reproductive and respiratory syndrome virus in a continuous cell line, ATCC CRL11171. *J Vet Diagn Invest* (1996) 8(3):374–81. doi: 10.1177/104063879600800317

42. Tian X, Lu G, Gao F, Peng H, Feng Y, Ma G, et al. Structure and cleavage specificity of the chymotrypsin-like serine protease (3CLSP/nsp4) of porcine reproductive and respiratory syndrome virus (PRRSV). *J Mol Biol* (2009) 392(4):977–93. doi: 10.1016/j.jmb.2009.07.062

43. Shi X, Wang L, Li X, Zhang G, Guo J, Zhao D, et al. Endoribonuclease activities of porcine reproductive and respiratory syndrome virus nsp11 was essential for nsp11 to inhibit IFN-β induction. *Mol Immunol* (2011) 48(12-13):1568–72. doi: 10.1016/j.molimm.2011.03.004

44. Sagong M, Lee C. Porcine reproductive and respiratory syndrome virus nucleocapsid protein modulates interferon-β production by inhibiting IRF3 activation in immortalized porcine alveolar macrophages. *Arch Virol* (2011) 156(12):2187–95. doi: 10.1007/s00705-011-1116-7

45. Pichlmair A, Schulz O, Tan CP, Näslund TI, Liljeström P, Weber F, et al. RIG-i-mediated antiviral responses to single-stranded RNA bearing 5'-phosphates. *Science* (2006) 314(5801):997–1001. doi: 10.1126/science.1132998

46. Kato H, Takeuchi O, Sato S, Yoneyama M, Yamamoto M, Matsui K, et al. Differential roles of MDA5 and RIG-I helicases in the recognition of RNA viruses. *Nature* (2006) 441(7089):101–5. doi: 10.1038/nature04734

47. Venkataraman T, Valdes M, Elsby R, Kakuta S, Caceres G, Saijo S, et al. Loss of DExD/H box RNA helicase LGP2 manifests disparate antiviral responses. *J Immunol* (2007) 178(10):6444–55. doi: 10.4049/jimmunol.178.10.6444

48. Dong XY, Liu WJ, Zhao MQ, Wang JY, Pei JJ, Luo YW, et al. Classical swine fever virus triggers RIG-I and MDA5-dependent signaling pathway to IRF-3 and NF-κB activation to promote secretion of interferon and inflammatory cytokines in porcine alveolar macrophages. *Virol J* (2013) 10:286. doi: 10.1186/1743-422X-10-286

49. Chan YK, Gack MU. Viral evasion of intracellular DNA and RNA sensing. *Nat Rev Microbiol* (2016) 14(6):360–73. doi: 10.1038/nrmicro.2016.45

50. Yoneyama M, Fujita T. RIG-I family RNA helicases: cytoplasmic sensor for antiviral innate immunity. *Cytokine Growth Factor Rev* (2007) 18(5-6):545–51. doi: 10.1016/j.cytogfr.2007.06.023

51. Jin HS, Suh HW, Kim SJ, Jo EK. Mitochondrial control of innate immunity and inflammation. *Immune Netw* (2017) 17(2):77–88. doi: 10.4110/in.2017.17.2.77

52. Fitzgerald KA, Rowe DC, Barnes BJ, Caffrey DR, Visintin A, Latz E, et al. LPS-TLR4 signaling to IRF-3/7 and NF-kappaB involves the toll adapters TRAM and TRIF. *J Exp Med* (2003) 198(7):1043–55. doi: 10.1084/jem.20031023

53. Liu S, Cai X, Wu J, Cong Q, Chen X, Li T, et al. Phosphorylation of innate immune adaptor proteins MAVS, STING, and TRIF induces IRF3 activation. *Science* (2015) 347(6227):aaa2630. doi: 10.1126/science.aaa2630

54. Luo R, Xiao S, Jiang Y, Jin H, Wang D, Liu M, et al. Porcine reproductive and respiratory syndrome virus (PRRSV) suppresses interferon-beta production by interfering with the RIG-I signaling pathway. *Mol Immunol* (2008) 45(10):2839–46. doi: 10.1016/j.molimm.2008.01.028

55. Dong J, Xu S, Wang J, Luo R, Wang D, Xiao S, et al. Porcine reproductive and respiratory syndrome virus 3C protease cleaves the mitochondrial antiviral signalling complex to antagonize IFN-β expression. *J Gen Virol* (2015) 96(10):3049–58. doi: 10.1099/jgv.0.000257

56. Sun Y, Ke H, Han M, Chen N, Fang W, Yoo D. Nonstructural protein 11 of porcine reproductive and respiratory syndrome virus suppresses both MAVS and RIG-I expression as one of the mechanisms to antagonize type I interferon production. *PloS One* (2016) 11(12):e0168314. doi: 10.1371/journal.pone.0168314

57. van Kasteren PB, Beugeling C, Ninaber DK, Frias-Staheli N, van Boheemen S, García-Sastre A, et al. Arterivirus and nairovirus ovarian tumor domain-containing deubiquitinases target activated RIG-I to control innate immune signaling. *J Virol* (2012) 86(2):773–85. doi: 10.1128/JVI.06277-11

58. Miyamoto M, Fujita T, Kimura Y, Maruyama M, Harada H, Sudo Y, et al. Regulated expression of a gene encoding a nuclear factor, IRF-1, that specifically binds to IFN-beta gene regulatory elements. *Cell* (1988) 54(6):903–13. doi: 10.1016/S0092-8674(88)91307-4

59. Nelson N, Kanno Y, Hong C, Contursi C, Fujita T, Fowlkes BJ, et al. Expression of IFN regulatory factor family proteins in lymphocytes. induction of stat-1 and IFN consensus sequence binding protein expression by T cell activation. *J Immunol* (1996) 156(10):3711–20. doi: 10.1016/j.bcp.2013.01.007

60. Bluyssen AR, Durbin JE, Levy DE. ISGF3 gamma p48, a specificity switch for interferon activated transcription factors. *Cytokine Growth Factor Rev* (1996) 7(1):11–7. doi: 10.1016/1359-6101(96)00005-6

61. Taniguchi T, Tanaka N, Ogasawara K, Taki S, Sato M, Takaoka A. Transcription factor IRF-1 and its family members in the regulation of host defense. *Cold Spring Harb Symp Quant Biol* (1999) 64:465–72. doi: 10.1101/sqb.1999.64.465

62. Iversen MB, Paludan SR. Mechanisms of type III interferon expression. *J Interferon Cytokine Res* (2010) 30(8):573–8. doi: 10.1089/jir.2010.0063

63. Levy DE, Marié IJ, Durbin JE. Induction and function of type I and III interferon in response to viral infection. *Curr Opin Virol* (2011) 1(6):476–86. doi: 10.1016/j.coviro.2011.11.001

64. Verhelst K, Verstrepen L, Carpentier I, Beyaert R. IκB kinase ϵ (IKKϵ): a therapeutic target in inflammation and cancer. *Biochem Pharmacol* (2013) 85(7):873–80. doi: 10.1016/j.bcp.2013.01.007

65. Weil R, Laplantine E, Génin P. Regulation of TBK1 activity by optineurin contributes to cell cycle-dependent expression of the interferon pathway. *Cytokine Growth Factor Rev* (2016) 29:23–33. doi: 10.1016/j.cytogfr.2016.03.001

66. Zhao W. Negative regulation of TBK1-mediated antiviral immunity. *FEBS Lett* (2013) 587(6):542–8. doi: 10.1016/j.febslet.2013.01.052

67. Randall RE, Goodbourn S. Interferons and viruses: an interplay between induction, signalling, antiviral responses and virus countermeasures. *J Gen Virol* (2008) 89(Pt1):1–47. doi: 10.1099/vir.0.83391-0

68. Yoneyama M, Suhara W, Fukuhara Y, Fukuda M, Nishida E, Fujita T. Direct triggering of the type I interferon system by virus infection: activation of a transcription factor complex containing IRF-3 and CBP/p300. *EMBO J* (1998) 17(4):1087–95. doi: 10.1093/emboj/17.4.1087

69. Yang H, Ma G, Lin CH, Orr M, Wathelet MG. Mechanism for transcriptional synergy between interferon regulatory factor (IRF)-3 and IRF-7 in activation of the interferon-beta gene promoter. *Eur J Biochem* (2004) 271(18):3693–703. doi: 10.1111/j.1432-1033.2004.04310.x

70. Ikushima H, Negishi H, Taniguchi T. The IRF family transcription factors at the interface of innate and adaptive immune responses. *Cold Spring Harb Symp Quant Biol* (2013) 78:105–16. doi: 10.1101/sqb.2013.78.020321

71. Honda K, Yanai H, Negishi H, Asagiri M, Sato M, Mizutani T, et al. IRF-7 is the master regulator of type-I interferon-dependent immune responses. *Nature* (2005) 434(7034):772–7. doi: 10.1038/nature03464

72. Sato M, Tanaka N, Hata N, Oda E, Taniguchi T. Involvement of the IRF family transcription factor IRF-3 in virus-induced activation of the IFN-beta gene. *FEBS Lett* (1998) 425(1):112–6. doi: 10.1016/S0014-5793(98)00210-5

73. Kim O, Sun Y, Lai FW, Song C, Yoo D. Modulation of type I interferon induction by porcine reproductive and respiratory syndrome virus and degradation of CREB-binding protein by nonstructural protein 1 in MARC-145 and HeLa cells. *Virology* (2010) 402(2):315–26. doi: 10.1016/j.virol.2010.03.039

74. Han M, Du Y, Song C, Yoo D. Degradation of CREB-binding protein and modulation of type I interferon induction by the zinc finger motif of the porcine reproductive and respiratory syndrome virus nsp1α subunit. *Virus Res* (2013) 172 (1-2):54–65. doi: 10.1016/j.virusres.2012.12.012

75. Zhang J, Hu MM, Shu HB, Li S. Death-associated protein kinase 1 is an IRF3/7-interacting protein that is involved in the cellular antiviral immune response. *Cell Mol Immunol* (2014) 11(3):245–52. doi: 10.1038/cmi.2013.65

76. Chen Z, Li M, He Q, Du J, Zhou L, Ge X, et al. The amino acid at residue 155 in nonstructural protein 4 of porcine reproductive and respiratory syndrome virus contributes to its inhibitory effect for interferon-β transcription in vitro. *Virus Res* (2014) 189:226–34. doi: 10.1016/j.virusres.2014.05.027

77. Chen Z, Lawson S, Sun Z, Zhou X, Guan X, Christopher-Hennings J, et al. Identification of two auto-cleavage products of nonstructural protein 1 (nsp1) in porcine reproductive and respiratory syndrome virus infected cells: nsp1 function as interferon antagonist. *Virology* (2010) 398(1):87–97. doi: 10.1016/j.virol.2009.11.033

78. O'Neill LA, Golenbock D, Bowie AG. The history of toll-like receptors - redefining innate immunity. *Nat Rev Immunol* (2013) 13(6):453–60. doi: 10.1038/nri3446

79. Linossi EM, Calleja DJ, Nicholson SE. Understanding SOCS protein specificity. *Growth Factors (Chur Switzerland)* (2018) 36(3-4):104–17. doi: 10.1080/08977194.2018.1518324

80. Crotta S, Davidson S, Mahlakoiv T, Desmet CJ, Buckwalter MR, Albert ML, et al. Type I and type III interferons drive redundant amplification loops to induce a transcriptional signature in influenza-infected airway epithelia. *PloS Pathog* (2013) 9(11):e00099-20. doi: 10.1371/journal.ppat.1003773

81. Kawai T, Akira S. The role of pattern-recognition receptors in innate immunity: update on toll-like receptors. *Nat Immunol* (2010) 11(5):373–84. doi: 10.1038/ni.1863

82. Yu CF, Peng WM, Schlee M, Barchet W, Eis-Hübinger AM, Kolanus W, et al. SOCS1 and SOCS3 target IRF7 degradation to suppress TLR7-mediated type I IFN production of human plasmacytoid dendritic cells. *J Immunol* (2018) 200 (12):4024–35. doi: 10.4049/jimmunol.1700510

83. Olière S, Hernandez E, Lézin A, Arguello M, Douville R, Nguyen TL, et al. HTLV-1 evades type I interferon antiviral signaling by inducing the suppressor of cytokine signaling 1 (SOCS1). *PloS Pathog* (2010) 6(11):e1001177. doi: 10.1016/s0969-2126(99)80002-1

84. Luo X, Chen XX, Qiao S, Li R, Xie S, Zhou X, et al. Porcine reproductive and respiratory syndrome virus enhances self-replication *via* AP-1-Dependent induction of SOCS1. *J Immunol* (2020) 204(2):394–407. doi: 10.4049/jimmunol.1900731

85. Zhu H, Zheng C. The race between host antiviral innate immunity and the immune evasion strategies of herpes simplex virus 1. *Microbiol Mol Biol Rev* (2020) 84(4):7832-46. doi: 10.1128/MMBR.00099-20

86. Hyun J, Kanagavelu S, Fukata M. A unique host defense pathway: TRIF mediates both antiviral and antibacterial immune responses. *Microbes Infect* (2013) 15(1):1–10. doi: 10.1016/j.micinf.2012.10.011

87. Meylan E, Burns K, Hofmann K, Blancheteau V, Martinon F, Kelliher M, et al. RIP1 is an essential mediator of toll-like receptor 3-induced NF-kappa b activation. *Nat Immunol* (2004) 5(5):503–7. doi: 10.1038/ni1061

88. Cramer P, Müller CW. A firm hand on NF-kappaB: structures of the IkappaBalpha-NFkappaB complex. *Structure (London Engl 1993)* (1999) 7(1):R1–6. doi: 10.1074/jbc.M115.660761

89. Yamamoto Y, Gaynor RB. IkappaB kinases: key regulators of the NF-kappaB pathway. *Trends Biochem Sci* (2004) 29(2):72–9. doi: 10.1016/j.tibs.2003.12.003

90. Santoro MG, Rossi A, Amici C. NF-kappaB and virus infection: who controls whom. *EMBO J* (2003) 22(11):651-62. doi: 10.1093/emboj/cdg267

91. Sun Z, Chen Z, Lawson SR, Fang Y. The cysteine protease domain of porcine reproductive and respiratory syndrome virus nonstructural protein 2 possesses deubiquitinating and interferon antagonism functions. *J Virol* (2010) 84(15):7832–46. doi: 10.1128/JVI.00217-10

92. Song C, Krell P, Yoo D. Nonstructural protein 1α subunit-based inhibition of NF-κB activation and suppression of interferon-β production by porcine reproductive and respiratory syndrome virus. *Virology* (2010) 407(2):268–80. doi: 10.1016/j.virol.2010.08.025

93. Huang L, Liu Q, Zhang L, Zhang Q, Hu L, Li C, et al. Encephalomyocarditis virus 3C protease relieves TRAF family member-associated NF-κB activator (TANK) inhibitory effect on TRAF6-mediated NF-κB signaling through cleavage of TANK. *J Biol Chem* (2015) 290(46):27618–32. doi: 10.1074/jbc.M115.660761

94. Levy DE. STATs: transcriptional control and biological impact. *Nat Rev Mol Cell Biol* (2002) 164:493-503. doi: 10.1038/nrm909

95. Schoggins JW, Rice CM. Interferon-stimulated genes and their antiviral effector functions. *Curr Opin Virol* (2011) 1(6):519–25. doi: 10.1016/j.coviro.2011.10.008

96. Yang E, Li MMH. All about the RNA: Interferon-stimulated genes that interfere with viral RNA processes. *Front Immunol* (2020) 11:605024. doi: 10.3389/fimmu.2020.605024

97. Schneider WM, Chevillotte MD, Rice CM. Interferon-stimulated genes: a complex web of host defenses. *Annu Rev Immunol* (2014) 32:513–45. doi: 10.1146/annurev-immunol-032713-120231

98. Wang R, Nan Y, Yu Y, Yang Z, Zhang YJ. Variable interference with interferon signal transduction by different strains of porcine reproductive and respiratory syndrome virus. *Vet Microbiol* (2013) 166(3-4):e01352-19. doi: 10.1016/j.vetmic.2013.07.022

99. Frieman M, Yount B, Heise M, Kopecky-Bromberg SA, Palese P, Baric RS. Severe acute respiratory syndrome coronavirus ORF6 antagonizes STAT1 function by sequestering nuclear import factors on the rough endoplasmic reticulum/Golgi membrane. *J Virol* (2007) 81(18):9812–24. doi: 10.1128/JVI.01012-07

100. Liu Q, Zhang YL, Hu W, Hu SP, Zhang Z, Cai XH, et al. Transcriptome of porcine alveolar macrophages activated by interferon-gamma and lipopolysaccharide. *Biochem Biophys Res Commun* (2018) 503(4):2666–72. doi: 10.1016/j.bbrc.2018.08.021

101. Samuel CE. Antiviral actions of interferons. *Clin Microbiol Rev* (2001) 14 (4):778–809, table of contents. doi: 10.1128/CMR.14.4.778-809.2001

102. Fensterl V, Sen GC. Interferons and viral infections. *BioFactors (Oxford England)* (2009) 35(1):14–20. doi: 10.1002/biof.6

103. Recht M, Borden EC, Knight EJr. A human 15-kDa IFN-induced protein induces the secretion of IFN-gamma. *J Immunol* (1991) 147(8):2617–23. doi: 10.1073/pnas.0607038104

104. Lenschow DJ, Lai C, Frias-Staheli N, Giannakopoulos NV, Lutz A, Wolff T, et al. IFN-stimulated gene 15 functions as a critical antiviral molecule against influenza, herpes, and sindbis viruses. *Proc Natl Acad Sci U S A* (2007) 104 (4):1371–6. doi: 10.1073/pnas.0607038104

105. Xie S, Chen XX, Qiao S, Li R, Sun Y, Xia S, et al. Identification of the RNA pseudoknot within the 3' end of the porcine reproductive and respiratory syndrome virus genome as a pathogen-associated molecular pattern to activate antiviral signaling *via* RIG-I and toll-like receptor 3. *J Virol* (2018) 92(12):e00097-18. doi: 10.1128/JVI.00097-18

106. Clemens MJ, Elia A. The double-stranded RNA-dependent protein kinase PKR: structure and function. *J Interferon Cytokine Res* (1997) 17(9):503–24. doi: 10.1089/jir.1997.17.503

107. Rowland RR, Robinson B, Stefanick J, Kim TS, Guanghua L, Lawson SR, et al. Inhibition of porcine reproductive and respiratory syndrome virus by interferon-gamma and recovery of virus replication with 2-aminopurine. *Arch Virol* (2001) 146(3):539–55. doi: 10.1007/s007050170161

108. Xiao Y, Ma Z, Wang R, Yang L, Nan Y, Zhang YJ. Downregulation of protein kinase PKR activation by porcine reproductive and respiratory syndrome virus at its early stage infection. *Vet Microbiol* (2016) 187:1–7. doi: 10.1016/j.vetmic.2016.03.004

frontiers | Frontiers in Immunology

TYPE Original Research
PUBLISHED 17 August 2022
DOI 10.3389/fimmu.2022.918692

OPEN ACCESS

EDITED BY
Pei-Hui Wang,
Shandong University, China

REVIEWED BY
Rawan Muhammad Shady,
Cairo University, Egypt
Amam Zonaed Siddiki,
Chattogram Veterinary and Animal Sciences University, Bangladesh

*CORRESPONDENCE
Tofazzal Islam
tofazzalislam@bsmrau.edu.bd
Chunfu Zheng
zheng.alan@hotmail.com
Md. Salim Khan
k2salim@yahoo.com

SPECIALTY SECTION
This article was submitted to Viral Immunology, a section of the journal Frontiers in Immunology

RECEIVED 12 April 2022
ACCEPTED 27 June 2022
PUBLISHED 17 August 2022

CITATION
Hoque MN, Sarkar MMH, Khan MA, Hossain MA, Hasan MI, Rahman MH, Habib MA, Akter S, Banu TA, Goswami B, Jahan I, Nafisa T, Molla MMA, Soliman ME, Araf Y, Khan MS, Zheng C and Islam T (2022) Differential gene expression profiling reveals potential biomarkers and pharmacological compounds against SARS-CoV-2: Insights from machine learning and bioinformatics approaches. *Front. Immunol.* 13:918692. doi: 10.3389/fimmu.2022.918692

Differential gene expression profiling reveals potential biomarkers and pharmacological compounds against SARS-CoV-2: Insights from machine learning and bioinformatics approaches

M. Nazmul Hoque[1], Md. Murshed Hasan Sarkar[2], Md. Arif Khan[3,4], Md. Arju Hossain[4], Md. Imran Hasan[5], Md. Habibur Rahman[5], Md. Ahashan Habib[2], Shahina Akter[2], Tanjina Akhtar Banu[2], Barna Goswami[2], Iffat Jahan[2], Tasnim Nafisa[6], Md. Maruf Ahmed Molla[6], Mahmoud E. Soliman[7], Yusha Araf[8,9], M. Salim Khan[2]*, Chunfu Zheng[9,10]* and Tofazzal Islam[11]*

[1]Department of Gynecology, Obstetrics and Reproductive Health, Bangabandhu Sheikh Mujibur Rahman Agricultural University, Gazipur, Bangladesh, [2]Bangladesh Council of Scientific & Industrial Research (BCSIR), Dhaka, Bangladesh, [3]Department of Biotechnology and Genetic Engineering, University of Development Alternative, Dhaka, Bangladesh, [4]Department of Biotechnology and Genetic Engineering, Mawlana Bhashani Science and Technology University, Tangail, Bangladesh, [5]Department of Computer Science and Engineering, Islamic University, Kushtia, Bangladesh, [6]National Institute of Laboratory Medicine and Referral Center, Dhaka, Bangladesh, [7]Molecular Bio-computation and Drug Design Laboratory, School of Health Sciences, University of KwaZulu-Natal, Durban, South Africa, [8]Department of Genetic Engineering and Biotechnology, School of Life Sciences, Shahjalal University of Science and Technology, Sylhet, Bangladesh, [9]Department of Immunology, School of Basic Medical Sciences, Fujian Medical University, Fuzhou, China, [10]Department of Microbiology, Immunology and Infectious Diseases, University of Calgary, Calgary, AB, Canada, [11]Institute of Biotechnology and Genetic Engineering (IBGE), Bangabandhu Sheikh Mujibur Rahman Agricultural University (BSMRAU), Gazipur, Bangladesh

The COVID-19 pandemic, caused by Severe Acute Respiratory Syndrome Coronavirus 2 (SARS-CoV-2), has created an urgent global situation. Therefore, it is necessary to identify the differentially expressed genes (DEGs) in COVID-19 patients to understand disease pathogenesis and the genetic factor(s) responsible for inter-individual variability and disease comorbidities. The pandemic continues to spread worldwide, despite intense efforts to develop multiple vaccines and therapeutic options against COVID-19. However, the precise role of SARS-CoV-2 in the pathophysiology of the nasopharyngeal tract (NT) is still unfathomable. This study utilized machine learning approaches to analyze 22 RNA-seq data from COVID-19 patients (n = 8), recovered individuals (n = 7), and healthy individuals (n = 7) to find disease-related differentially expressed genes (DEGs). We compared

10.3389/fimmu.2022.918692

dysregulated DEGs to detect critical pathways and gene ontology (GO) connected to COVID-19 comorbidities. We found 1960 and 153 DEG signatures in COVID-19 patients and recovered individuals compared to healthy controls. In COVID-19 patients, the DEG–miRNA, and DEG–transcription factors (TFs) interactions network analysis revealed that E2F1, MAX, EGR1, YY1, and SRF were the highly expressed TFs, whereas hsa-miR-19b, hsa-miR-495, hsa-miR-340, hsa-miR-101, and hsa-miR-19a were the overexpressed miRNAs. Three chemical agents (Valproic Acid, Alfatoxin B1, and Cyclosporine) were abundant in COVID-19 patients and recovered individuals. Mental retardation, mental deficit, intellectual disability, muscle hypotonia, micrognathism, and cleft palate were the significant diseases associated with COVID-19 by sharing DEGs. Finally, the detected DEGs mediated by TFs and miRNA expression indicated that SARS-CoV-2 infection might contribute to various comorbidities. Our results provide the common DEGs between COVID-19 patients and recovered humans, which suggests some crucial insights into the complex interplay between COVID-19 progression and the recovery stage, and offer some suggestions on therapeutic target identification in COVID-19 caused by the SARS-CoV-2.

KEYWORDS

SARS-CoV-2, functional enrichment, gene regulatory networks, therapeutic targets, RNA-seq, genomics

Introduction

In late December 2019, a novel respiratory disease, now popularly termed "COVID-19", caused by severe acute respiratory syndrome coronavirus 2 (SARS-CoV-2), emerged in Wuhan, China (1–3). Immediately after its first outbreak in China, this fearsome virus has emerged as one of the deadliest human pathogens (4, 5). As of June 22, 2022, COVID-19 disease affected 217 countries and territories, and more than 545 million cases have been confirmed around the globe, with more than 6.3 million deaths (6). Due to its worldwide spread and severity, the World Health Organization (WHO) has declared the disease a public health emergency of international concern (7–9). In the early stage of the outbreak, the spectrum of clinical manifestations of COVID-19 ranges from the common cold to respiratory failure depending on the demography and environment (2, 7, 10). However, recent data show that the clinical episodes of COVID-19 may range from asymptomatic infection to critical illness, with a dysregulated inflammatory response to infection a hallmark of severe cases (11) and life-threatening multiorgan failure (10, 12–14). In most cases (~80%), patients exhibit mild symptoms, while the remaining ~20% may develop severe lung injury and death from respiratory failure (15–17). Some of the clinically infected patients may suffer from acute respiratory distress syndrome (ARDS) and multiple organ failures, requiring intensive care unit (ICU) facilities for life support and medication (16). Risk factors for severe SARS-CoV-2 include age, smoking status, ethnicity, and male sex (13, 18). Notably, the persistence and prognosis of COVID-19 are greatly influenced by the patients' underlying health conditions and age (12, 19). With no effective antiviral treatment and slow vaccine rollout, COVID-19 continues to threaten public health worldwide seriously (20).

Despite increasing global threats of COVID-19, the host immune response against SARS-CoV-2 infection remains poorly understood, and the perturbations result in a severe outcome (15, 21). The nasal epithelium is a portal for initial infection and transmission of the SARS-CoV-2 (7). SARS-CoV-2 employs ACE2 (Angiotensin-converting enzyme 2) as a receptor for cellular entry (22, 23), and the binding affinity of the S protein and ACE2 was found to be a major determinant of SARS-CoV-2 replication rate and disease severity (21, 24). After the entrance into the susceptible host, SARS-CoV-2 infects cells of the respiratory epithelium and mucous membranes, such as those of the nose or eyes (22, 25). The host immune response to SARS-CoV-2 infection involves activation of both cellular and humoral arms. The innate immune system recognizes the SARS-CoV-2 RNAs through three major classes of cytoplasmic pattern recognition receptors: Toll-like receptors (TLRs), RIG-I-like receptors (RLRs), and NOD-like receptors (NLRs) (21, 26). This response involves the release of interferons (IFNs) and inflammatory cytokines, including the IL-1 family, IL-6, and

TNF, that activates a local and systemic response to infection (7, 21). This inflammatory response cascade involves the recruitment, activation, and differentiation of innate and adaptive immune cells, including neutrophils, inflammatory myeloid cells, CD8 T cells, and natural killer (NK) cells (15). The infection resolution largely depends on the cytotoxic activity of CD8 T cells and NK cells, which enable the clearance of virus-infected cells (7, 21). It is believed that dysregulated host immune response leads to the persistence of virus-infected cells and may facilitate a hyper-inflammatory state termed Macrophage (MΦ) activation syndrome (MAS) or "cytokine storm", and ultimately damage the infected lung (15, 21, 27). However, the underlying molecular mechanisms of the aberrant inflammatory responses in serology and histopathology under SARS-CoV-2 infection are still not clear.

The ongoing pandemic of SARS-CoV-2 and lack of comprehensive knowledge regarding the progression of COVID-19 has constrained our ability to develop effective treatments for infected patients. One way to understand the host response to SARS-CoV2 is to examine gene expression in relevant tissues. Until now, a scant amount of gene expression profiles are available from patients with COVID-19 and have yielded some insights into the pathogenic processes triggered by infection with SARS-CoV-2 (15, 21, 28). Transcriptomic analyses of cells upon viral infections are extremely useful for identifying the host immune response dynamics and gene regulatory networks (15, 29). However, because of the limited number of samples and preliminary analysis, a full picture of the physical state of SARS-CoV-2 affected tissues has not emerged. To address this, we have employed RNA-seq techniques to investigate the upper airway (nasopharyngeal tract) gene expression profile in 22 specimens of COVID-19 patients (n = 8), COVID-19 recovered (n = 7) and healthy (n = 7) individuals using several orthogonal bioinformatic tools to provide a complete view of the nature of the COVID-19 inflammatory response and the potential points of therapeutic intervention. Through DEG analyses in these datasets, we identified several genes coding for translational activities (e. g. RPL4, RPS4X, RPL19, RPS12, RPL19, EIF3E), ATP-synthesis (MT-CYB, MT-ATP6), transcription factors (e. g. E2F1, MAX, EGR1, YY1, SRF), hub-proteins (e. g. KIAA0355, DCUN1D3, FEM1C, ARHGEF12, THBS1), and mi-RNA (e. g. hsa-miR-19b, hsa-miR-495, hsa-miR-340, hsa-miR-101, and hsa-miR-19a) evidencing a sustained inflammation and cytokine storm in the COVID-19 patients.

Materials and methods

Ethical statement and consent of participants

his study was conducted following Bangladesh's Director-General of Health Services (DGHS) guidelines. The protocol for a sample collection from COVID-19 recovered, and healthy humans, sample processing, transport, and RNA extraction was approved by the National Institute of Laboratory Medicine and Referral Center of Bangladesh. The study participants provided written informed consent consistent with the experiment.

Study subject and sample collection

COVID-19 diagnosis, laboratory testing, and treatment in this cohort have been previously described (30). Patients with confirmed COVID-19 were classified as having mild/moderate (MM) or severe/critical (SC) disease based on symptomatology (22). We recruited seven recovered COVID-19 patients (post-hospital discharge) from this cohort and seven healthy subjects with no history of SARS-CoV-2 infection (negative control. Twenty-two (N = 22) nasopharyngeal samples (including COVID-19 = 8, recovered = 7, and healthy = 7) were collected from Dhaka city of Bangladesh. Collected samples were preserved at -20°C until further use for RNA extraction and RT-qPCR assay. The RT-qPCR was performed for *ORF1ab* and *N* genes of SARS-CoV-2 using a novel Coronavirus (2019-nCoV) Nucleic Acid Diagnostic Kit (PCR-Fluorescence Probing, Sansure Biotech Inc.) according to the manufacturer's instructions. Viral RNA was extracted using a Pure Link viral RNA/DNA mini kit (Thermo Fisher Scientific, USA). Thermal cycling was performed at 50°C for 30 min for reverse transcription, followed by 95°C for 1 min, and then 45 cycles of 95°C for 15 s, 60°C for 30 s on an Analytik-Jena qTOWER instrument (Analytik Jena, Germany).

RNA sequencing

We utilized the total RNA-seq approach for this study. According to the manufacturer's instructions, the cDNA of all 22 samples was used to prepare paired-end libraries with the Nextera DNA Flex library preparation kit (Illumina, Inc., San Diego, CA). Paired-end (2 x 150 bp reads) sequencing of the prepared library pool of the samples was performed using a NextSeq high throughput kit with an Illumina NextSeq 550 sequencer at the Genomic Research Laboratory, Bangladesh Council of Scientific and Industrial Research (BCSIR), Dhaka, Bangladesh.

Overview of the proposed bioinformatics pipelines

Network-based approaches are common to identify and analyze the pathogenesis of SARS-CoV-2. Datasets required in this work were constructed and collected at the initial phase and

detailed in the following subsections. Gene expression analysis was performed to identify the DEGs from each dataset (Figure 1). Next, the common DEGs between two groups of COVID-19 datasets were identified. These common DEGs were further used to discover their protein-protein interactions (PPIs) and to perform gene set enrichment analysis (GSEA) to identify enriched cell signaling pathways and functional gene ontology (GO) terms. Next, the same common DEGs were used to discover three types of GRNs: DEGs–micro RNAs (miRNA) network, DEGs–transcription factors (TFs) network, and TF-miRNA network. Finally, protein-chemical compound and protein-drug interactions were also investigated for the common DEGs (Figure 1).

Dataset preparation and analysis of differentially expressed genes

To assess the DEGs of COVID-19 and their genetic association with host cells, we collected and analyzed the RNA-seq datasets from our lab experiment. In this study, we prepared two datasets as COVID-19 positive patients versus

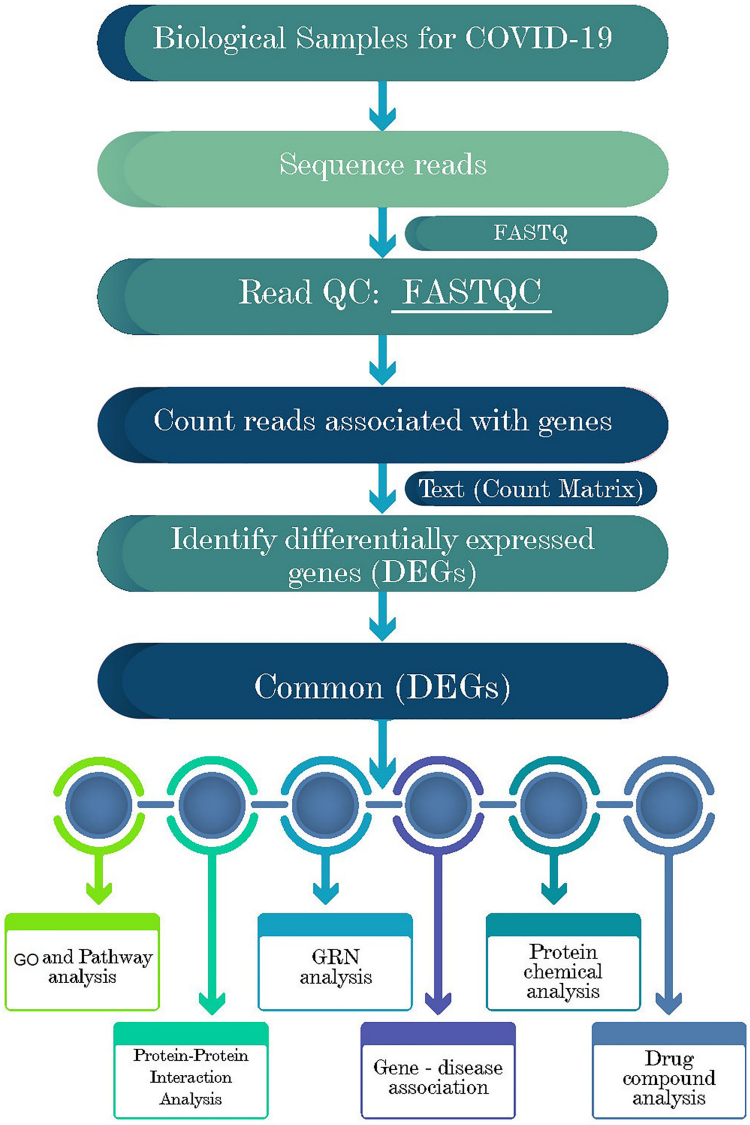

FIGURE 1
Schematic representations of the paths for differentially expressed genes (DEGs) analysis in RNA-seq data of the COVID-19 patients, recovered humans, and healthy controls nasopharyngeal tract.

COVID-19 recovered humans with the same healthy control group for analytical purposes. We performed several statistical operations on the datasets to determine the DEGs. Moreover, the Benjamini–Hochberg false discovery rate method was used to balance the discovery of statistically significant genes and the limitation of false positives. The BioJupies generator (31) online server (https://maayanlab.cloud/biojupies/) was used for RNA-seq raw data analysis. In this study, genes with adjusted *P*-value < 0.05 and absolute value of $\log_2$ fold-change ≥ 1 were considered DEGs. Next, we compared two COVID-19 datasets to determine the shared DEGs using the Venny v2.1 web tool (32). In this article, we use the term combined DEGs' to refer to the collection of these two sets of DEGs, which have been used in the downstream bioinformatics analyses.

Functional enrichment analysis

We utilized Enrichr (33) with Fisher's exact test to conduct the functional enrichment analysis with the combined DEGs. After performing an overrepresentation analysis, a collection of enriched cell signaling pathways and functional GO keywords were discovered, revealing the biological importance of the previously detected DEGs. In Enrichr analysis, we combined the signaling pathways from two libraries, including KEGG (Kyoto Encyclopedia of Genes and Genomes) and Reactome (https://reactome.org/), to create a single route. Only the important paths for which the *P*-value was less than 0.05 were evaluated and considered after deleting duplicate pathways. For functional GO annotations, we looked at the GO biological process, GO molecular function, and GO cellular component datasets in Enrichr and selected the most important GO terms based on set criteria and with an adjusted *P*-value < 0.05.

Protein-protein interaction network analysis

Protein-protein interaction (PPI) of the shared DEGs was analyzed using the STRING database (34). We applied different local- and global-based methods using the cytoHubba plugin in Cytoscape v3.8.2 (35) to determine potential hubs within the PPI network. While the local method ranked hubs based on the relationship between the node and its direct neighbor, the global method ranked hubs based on the interaction between the node and the whole network. In total, five different methods were considered, including three local rank methods, i.e., degree, maximum neighborhood component (MNC), maximal clique centrality (MCC), and two global rank methods, i.e., edge percolated component (EPC) and betweenness. Next, we compared the results and identified the common nodes as the most potential hubs. Finally, the protein networks were analyzed through Cytoscape v3.8.2.

Differential gene regulatory network analysis

The findings of DEG–miRNA, TF–DEG, and TF-miRNA interaction networks are part of the GRN analysis. Using the Network Analyst platform (36), the commonly dysregulated genes were utilized to identify GRN networks. Discovering DEG–miRNA interaction networks was accomplished through the miRTarBase database (37). To identify the TF–DEG interaction network, the JASPAR database (38) was used. Employing TF-miRNA coregulatory network database, the TF-miRNA interaction was analyzed. The networks were filtered with a betweenness value of 100 and degree centrality of 0 to 10 to remove unnecessary information.

Protein–chemical compound analysis

Analyses of protein–chemical compounds can be used to identify the chemical molecules responsible for the interaction of proteins in comorbidities. For example, this study found protein–chemical interactions using the enriched gene (common DEGs) that COVID-19 patients developed several digestive problems. Furthermore, using the Comparative Toxicogenomics Database (39), we have identified the protein–chemical interactions through Network Analyst (36).

Protein–drug interaction network

One of the key goals of this study is to identify potential therapeutic compounds that could effectively mitigate SARS-CoV-2 pervasiveness. Using the shared DEGs, we constructed the protein-drug interaction (PDI) network through the Network Analyst v3.0 web server (36) in conjunction with the DrugBank v5.0 database (https://go.drugbank.com/docs/drugbank_v5.0.xsd). To aid the analysis, we downloaded the network data and configured the data with Cytoscape v3.8.2 (35).

Gene-disease association prediction

DisGeNET (https://www.uniprot.org/database/DB-0218) is a standardized gene-disease association database that incorporates correlations from various sources involving various biological features of disorders (40). It emphasizes the increasing understanding of human genetic illnesses. We examined the gene-disease connection using a network analyzer (36) to find diseases and chronic problems associated with common DEGs.

Results

Differentially expression and distribution of DEGs

To elucidate whether differentially expressed genes (DEGs) contribute to the SAR-CoV-2 inflammatory response and the potential points of therapeutic intervention, we analyzed 22 RNA-seq data of nasopharyngeal epithelial tissue of COVID-19 patients, recovered humans, and healthy controls. To perform RNA-seq analysis, we retrieved datasets from the National Center for Biotechnology Information (NCBI) that belonged to previously published BioProject under accession number PRJNA720904 (https://www.ncbi.nlm.nih.gov/bioproject). We identified 1960 and 153 gene signatures in COVID-19 patients and recovered human NT epithelial tissues, which were differentially expressed compared with healthy controls. We particularly focused on the dysregulation (up or down-regulation) of the identified DEGs during SARS-CoV-2 pathophysiology and its overlap with the recovered or healthy states of the humans. The volcano plots in Figure 2 show the DEGs for COVID-19 with the red dots. The number of shared DEGs between COVID-19 and recovered datasets is presented in the Venn diagrams (Figures 2C, D). Thirty-seven shared DEGs were identified between COVID-19 patients and recovered subjects. Of the detected DEGs, 1,510 (77.04%) genes were upregulated (Up) during SARS-CoV-2 pathogenesis, of which 1,489 (98.61%) genes had a sole association with COVID-19 patients. Likewise, 90 (58.82%) genes were upregulated in recovered humans, and of them, 69 (76.67%) genes had a sole association with the recovery phage of SARS-CoV-2 infection (Figure 2C). By comparing the upregulated genes between COVID-19 patients and recovered individuals, we found that 21 genes (i.e., RPL4, MT-ND2, SCD5, MT-CYB, EZR) were shared between the conditions (Figure 2C). On the other hand, 450 (22.96%) and 63 (41.18%) DEGs were downregulated (Down) in COVID-19 patients and recovered subjects, respectively, and of them, only 12 genes (i.e., MAFF,

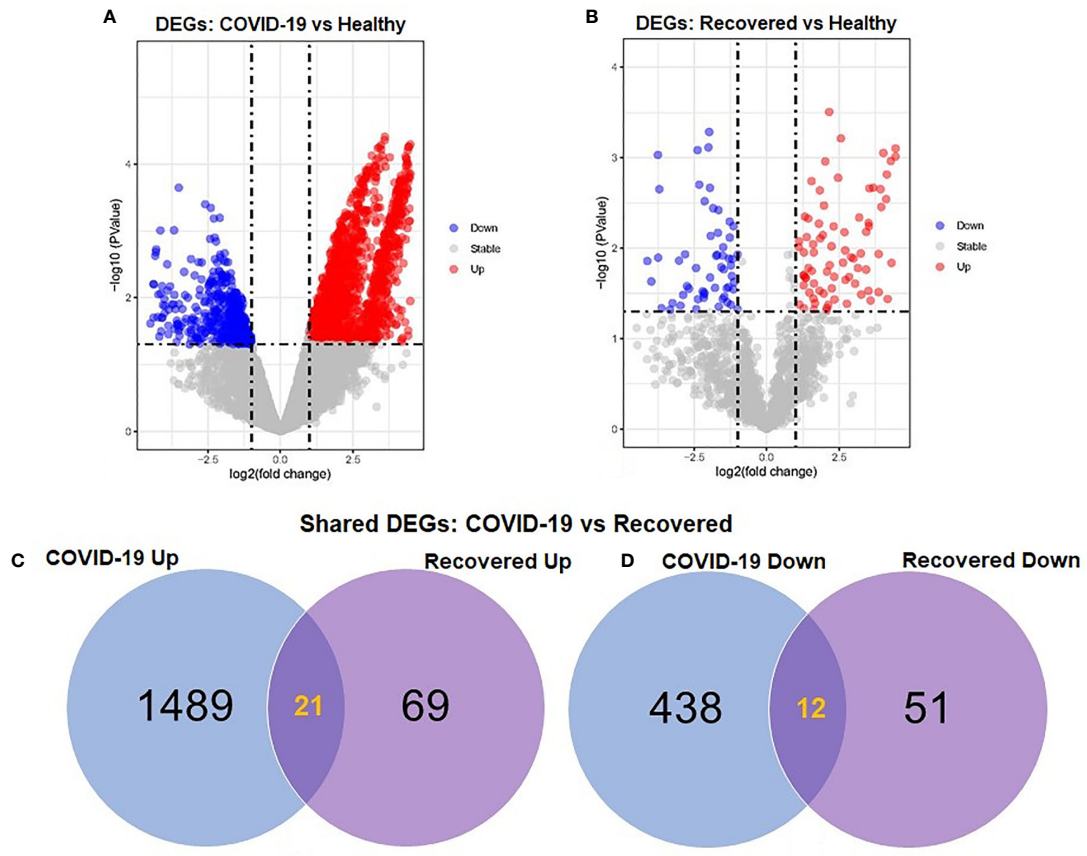

FIGURE 2
Volcano plots showing dysregulated genes in **(A)** COVID-19 patients vs. healthy control and **(B)** recovered humans vs. healthy controls. The red and blue dots indicate the expressions of the upregulated (Up) and down-regulated (Down) DEGs, respectively. Venn diagrams depict the unique and shared DEGs **(C)** upregulated and **(D)** down-regulated under the given conditions.

ARHGEF12, DCUN1D3, DR1, MT-CO1.) were found to be shared between COVID-19 and recovered cases (Figure 2D). The DEGs shared between COVID-19 positive and recovered people and their relationships from the perspective of adjusted *P*-value, and log2 fold-change is presented in the heatmaps, respectively (Figures 3A, B). Finally, 33 common dysregulated (Up or Down) genes were presented in a bubble plot to show relationships with 10 log fold-change values (Figure 3C).

Functional enrichment analysis identifies significant cell signaling pathways and gene ontology

We used the Enrichr tool to conduct a functional enrichment analysis on the DEGs to identify the signaling pathways and functional GO keywords significantly enriched with DEGs in the nasopharyngeal epithelial cells from COVID-19 patients. The 33 shared DEGs were used to identify key pathways and GOs that may be linked to COVID-19 comorbidities. We combined the KEGG and Reactome pathway databases with Enrichr tools to create a single pathway database. We looked at the pathways whose significance was determined by the *P*-value and plotted the top 20 pathways for each condition (Figure 4). Consideration was given to the paths having a higher logarithmic *P*-value. The most significant pathways were the ribosome signaling pathway, coronavirus signaling pathway, and c-type-lectin receptor signaling pathway for KEGG analysis (Figure 4B) and forming a pool of free 40S subunits 3-UTR-mediated translational regulation, and eukaryotic translational initiation signaling pathways for the Reactome database (Figure 4B).

We used the Enrichr tool to identify significantly enriched cellular signaling pathways and functional GO terms (molecular function, biological process, and cellular component) with DEGs in the nasopharyngeal epithelial cells from COVID-19 patients. The 33 shared DEGs were used to identify key pathways and GOs that may be linked to COVID-19 comorbidities. We looked at the pathways whose significance was determined by the *P*-value (having a higher logarithmic *P*-value) and plotted the top 20 pathways for each condition (Figure 4).

We further conducted GO functional enrichment analysis using the same common DEGs. We employed the GO biological process, the GO molecular function, and the GO cellular component databases obtained from Enrichr libraries. The significantly enriched GO terms were identified if the enrichment yielded the adjusted *P*-value's high logarithmic value. The top 20 cellular signaling pathways in the COVID-19 patient's nasopharyngeal epithelial cells were selected in this study (Figure 5) in relevance to the recovered phase. The most significant GO pathways were the ceramide 1-phosphate transfer activity, and ceramide 1-phosphate binding pathways for the molecular functions (Figure 5A), database nuclear-transcribed mRNA catabolic process and regulation of epithelial cell differentiation pathways for biological process (Figure 5B), and membrane raft, and cytosolic sizeable ribosomal subunit pathways for cellular component (Figure 5C).

Protein-protein interaction network construction and interaction analysis

A Protein-protein interaction (PPI) network was built from the common DEGs interactions, consisting of 24 nodes and 72 edges. The PPI network clustering highlighted RPL4, RPL18A, EIF3E, EIF3D, RPS4X, RPL19, EIF3K, RPS12, MT-ND2, MT-CO1, MT-ATP6, and MT-CYB with high interaction activity (Figure 6). The proteins with several connecting edges can be identified as hub proteins. Figure 7 shows the top 10 hub nodes within the PPI network. As anticipated by five different methods (i.e., maximum neighborhood component; MNC, betweenness, degree, edge percolated component; EPC and maximal clique centrality; MCC), we recognized eight hub-nodes as potential hub-proteins (i.e., RPL4, RPS4X, RPL19, RPS12, RPL19, EIF3E, MT-CYB, and MT-ATP6) (Figures 7A–E). Interestingly, these eight hub proteins were common in all methods. Only RPS4X was found from 4 methods except for betweenness (Figure 7B). Conversely, the betweenness method predicted only three proteins (i.e., SCD5, EZR, and RIMS1) from the shared DEGs as hubs that were not found by other methods (Figure 7B).

GRN analysis identifies DEGs–miRNA and transcription factor–gene interactions

The common DEGs between COVID-19 patients and recovered humans were used in this study. The DEG–miRNA interactions network is depicted in Figure 8A. The dysregulated genes are shown by the circles in the picture, while the squares represent the miRNAs. The association among different nodes of DEGs and miRNA (circles or squares) is represented by different lines linking them. Significant nodes are those in a network that connect several edges because they are more crucial. Out of 21 miRNAs detected, hsa-let-7e-5p, hsa-mir-7977, hsa-mir-155-5p, hsa-mir-186-5p, and hsa-mir-1827 were the most expressed miRNAs and had a stronger association with DEGs (Figure 8A). Likewise, among the DEGs, DMD, AHDC1, BAG4, EMP2, TIMM50, RPL7L1, and THBS1 were more significant since these DEGs have a higher degree (number of connecting edges) than the others and miRNAs (Figure 8A). We further studied the interactions between TF and DEGs and identified 14 TFs, of which FOXC1, FOXL1, NFIC, YY1, and PPARG were significantly enriched and showed more interactions with DEGs (Figure 8B).

Apart from these, the present study included TFs and miRNAs highly relevant to SARS-CoV-2 interactions. This

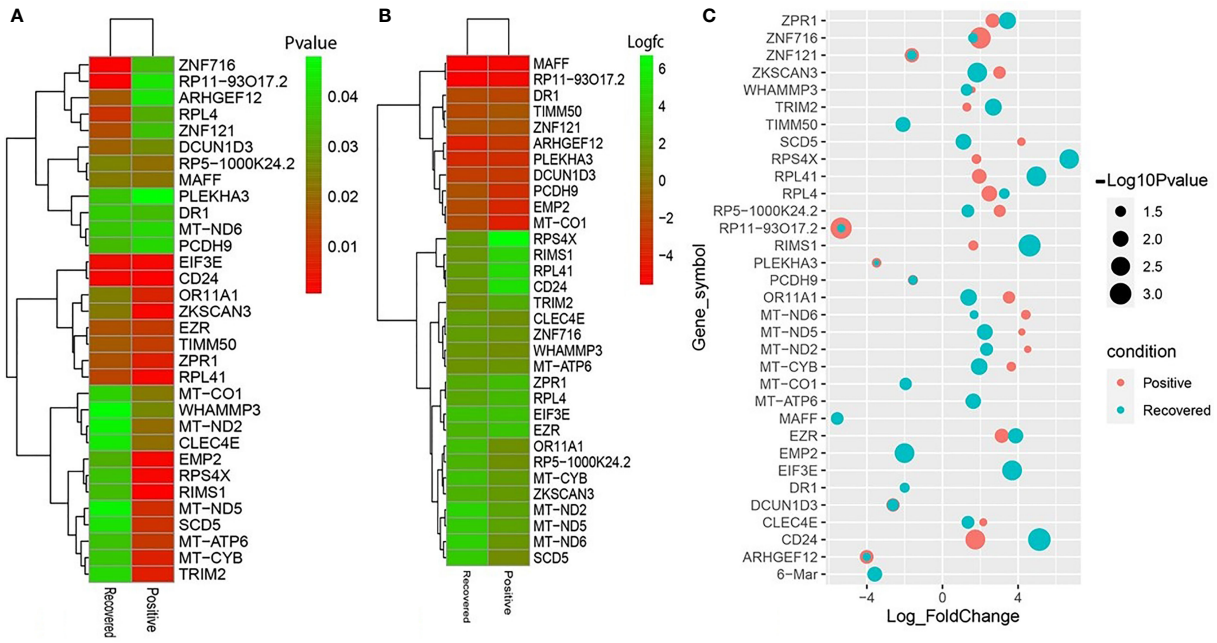

FIGURE 3
Heatmaps depicting the relationships among common DEGs in COVID-19 patients and recovered subjects based on **(A)** adjusted *p*-value and **(B)** logFC values. **(C)** Bubble plots showing the combined Log_{10} fold-changes and *p*-values for the shared common genes between COVID-19 patients and recovered humans. The red color indicates the genes of COVID-19 patients, and the green color presents the genes of the recovered people, while the mixed color indicates the overlapping genes.

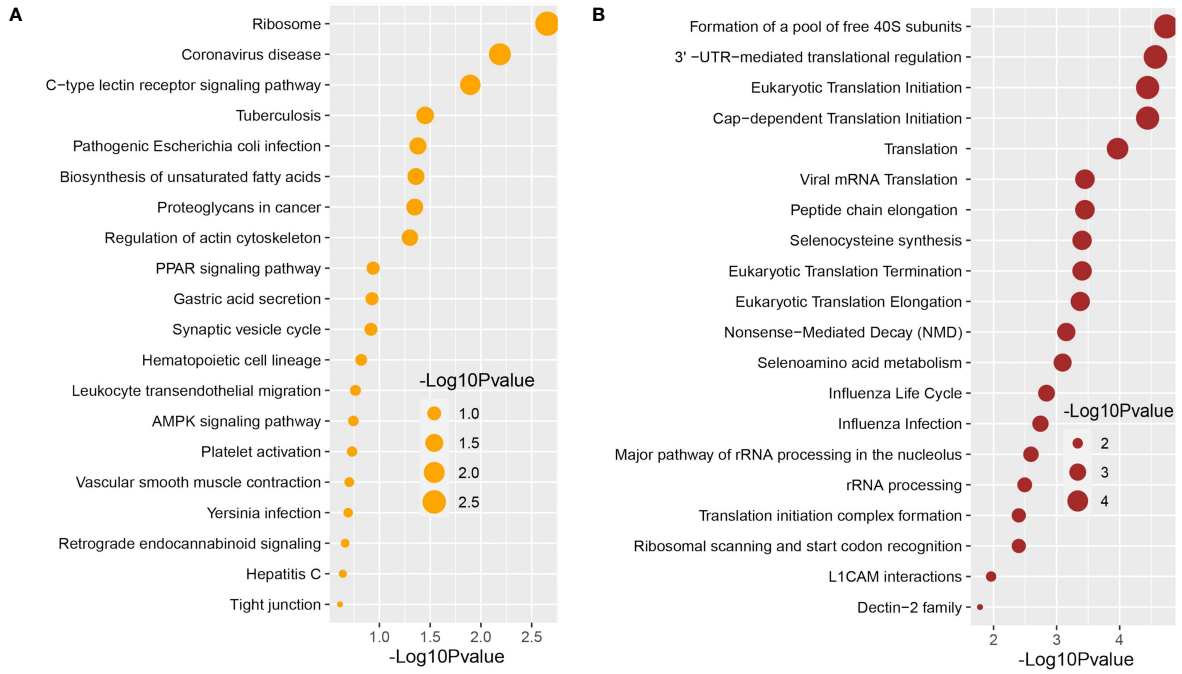

FIGURE 4
Signaling pathway analysis of nasopharyngeal epithelial cells on COVID-19 patients. We find that the top 20 terms depend on the *P*-value. **(A)** KEGG pathway and **(B)** Reactome pathway.

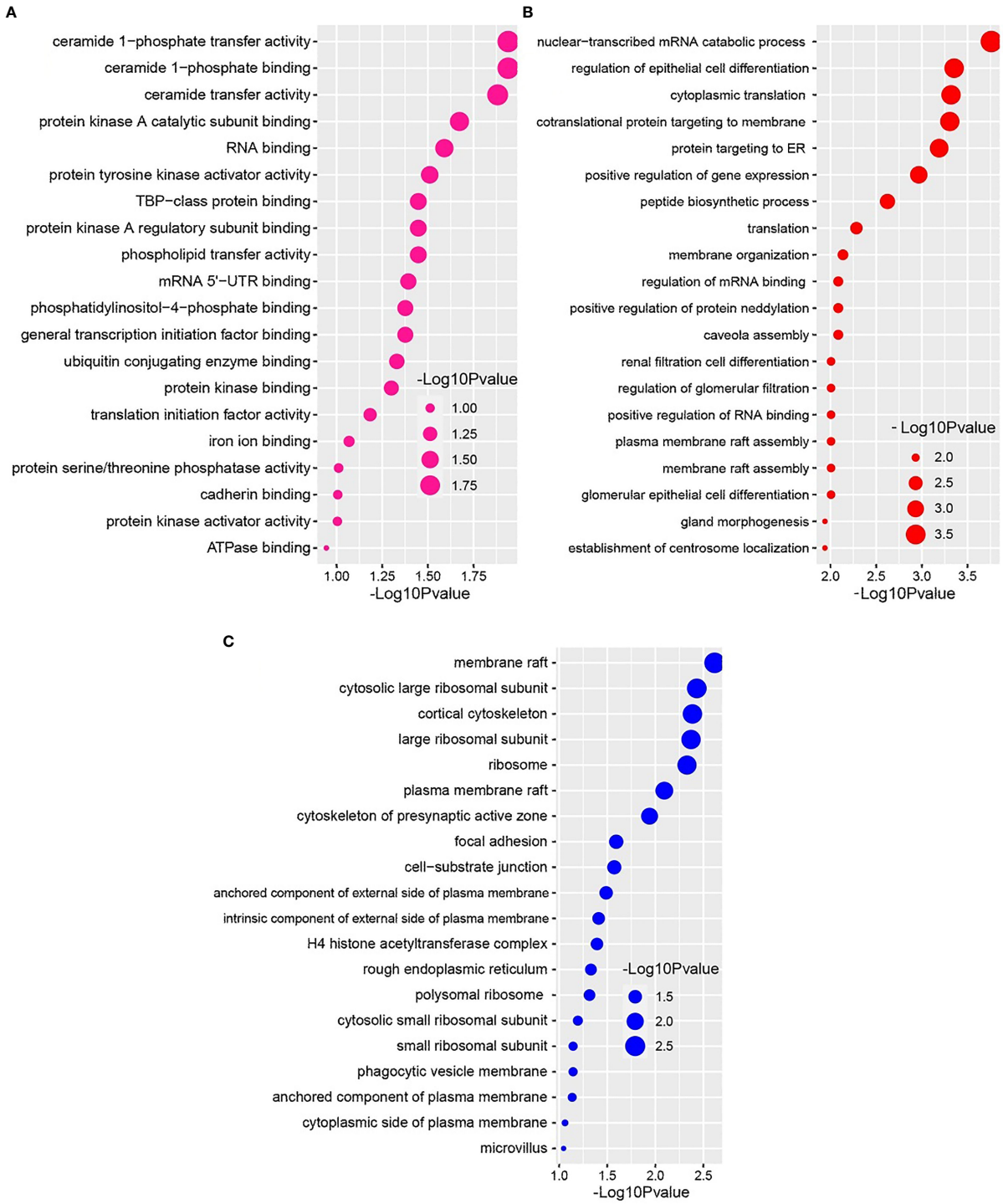

FIGURE 5
Based on the adjusted *P*-value, the top 20 cell signaling pathways in the nasopharyngeal epithelial cells in COVID-19 patients. The pathways have been formed by combining the DEGs that are common in the **(A)** gene ontology (GO) molecular function, **(B)** GO biological process, and **(C)** GO cellular component.

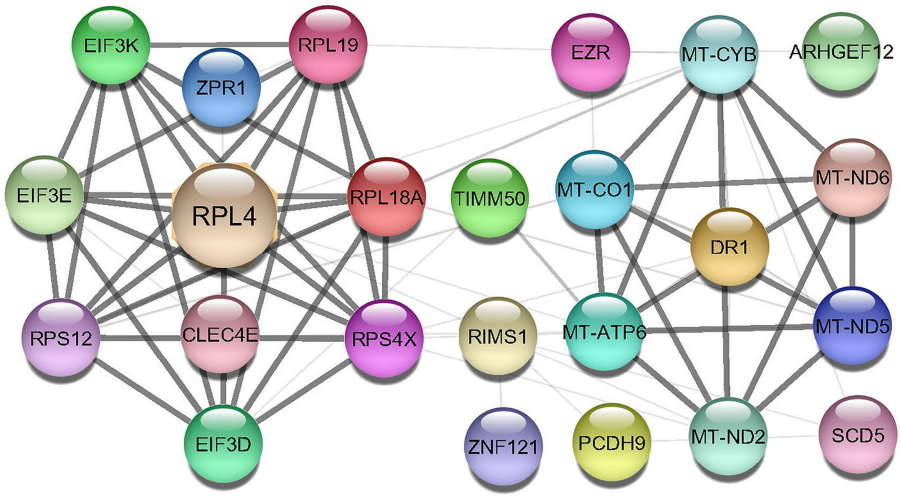

FIGURE 6
Protein-protein interaction (PPIs) network of common DEGs in COVID-19 patients. The nodes represent the proteins, and the edges represent the interactions across the proteins. Proteins having more edges are highly expressed, and thickness between the edges indicates the strength of interactions.

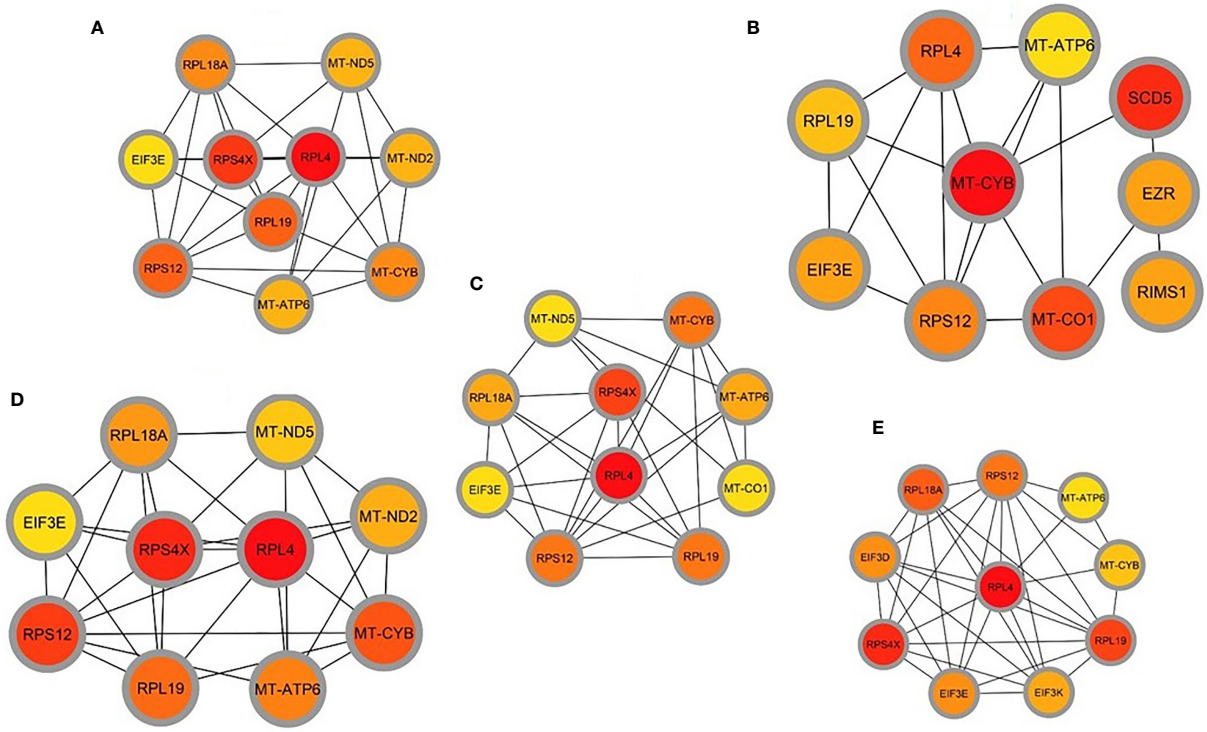

FIGURE 7
Determination of hub genes from the protein-protein interaction (PPI) network by using the Cytohubba plugin in Cytoscape. We applied five algorithms of the Cytohubba plugin to obtain the hub genes. Here **(A)** maximum neighborhood component (MNC), **(B)** betweenness, **(C)** degree, **(D)** edge percolated component (EPC), and **(E)** maximal clique centrality (MCC). Red to yellow color gradients indicate the higher ranking of hub genes.

analysis identified 19 hub proteins, 10 TFs, and 5 miRNAs (Figure 9A). In COVID-19 interaction, the TF–miRNA network showed that E2F1, MAX, EGR1, YY1, and SRF were the highly expressed TFs, and hsa-miR-19b, hsa-miR-495, hsa-miR-340, hsa-miR-101, and hsa-miR-19a were among significant miRNAs (Figure 9B).

Protein-drug and protein-chemical interactions reveal possible drugs for COVID-19 patients

Protein-drug interaction (PDI) networks provide a wealth of information about possible pathogenesis mechanisms and drug interactions that may not be evident using conventional approaches. To disrupt the SARS-CoV-2 pervasiveness, we sought to find pharmaceutical compounds that interact with viral proteins (Methods). We detected nine pharmacological compounds (for example, famoxadone, ubiquinone-2, 2-nonyl-4-hydroxyquinoline, 5-n-undecyl-6-hydroxy-4,7-dioxobenzothiazole) acting against one protein, the human mitochondrial cytochrome b (MT-CYB) (Figure 9B).

Protein–chemical interaction (PCI) is an important study to understand the functionality of proteins underpinning the molecular mechanisms within the cell, which may also help in drug discovery. For example, it has been discovered that SARS-CoV-2 infection causes PCI networks in the COVID-19 patients and recovered humans. Figure 10A depicts a network of PCI among significant proteins. The significant proteins identified from this network include FEM1C, NCALD, THBS1, PCDH9, DMD, and PDGFA. Similarly, we identified three chemical agents, Valproic Acid, Alfatoxin B1, and Cyclosporine, enriched in this interaction analysis (Figure 10A).

Gene-disease network finds different diseases associated with COVID-19

This study hypothesizes that many conditions can be associated or connected with COVID-19 by sharing some common genes. Disorder-specific therapeutic interface strategies attempt to discover the link between genes and diseases. In this study, we found 14 other diseases associated with COVID-19 by sharing four DEGs (i.e., DMD, C2CD3, WNT3, and AHDC1) most prevalent in COVID-19. Of the detected diseases, mental retardation, mental deficiency, intellectual disability, muscle hypotonia, micrognathism, and cleft palate were the significant diseases interconnected with COVID-19 (Figure 10B).

Discussion

The SARS-CoV-2 infection causes a wide spectrum of diseases ranging from minimal, often asymptomatic, respiratory illness to severe pneumonia with multisystem failure and death. The ongoing rapid transmission and global spread of COVID-19 have raised intriguing questions whether the evolution and adaptation of SARS-CoV-2 is driven by

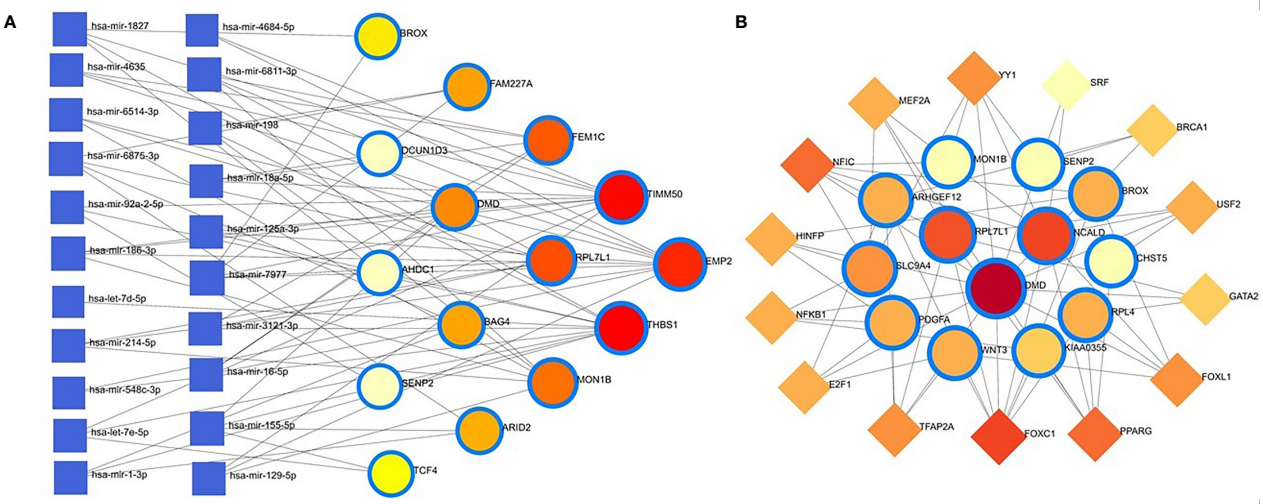

FIGURE 8
Genes' regulatory networks. **(A)** Gene regulatory networks (gene-miRNA) of the nasopharyngeal epithelial cell in COVID- 19 patients with the shared dysregulated genes. The square shapes and circular shapes represent the miRNA and genes, respectively. **(B)** Gene regulatory networks (transcription factors; TF) of the nasopharyngeal epithelial cell in COVID- 19 patients with the shared dysregulated genes. The square shapes and circular shapes represent the TF and genes, respectively.

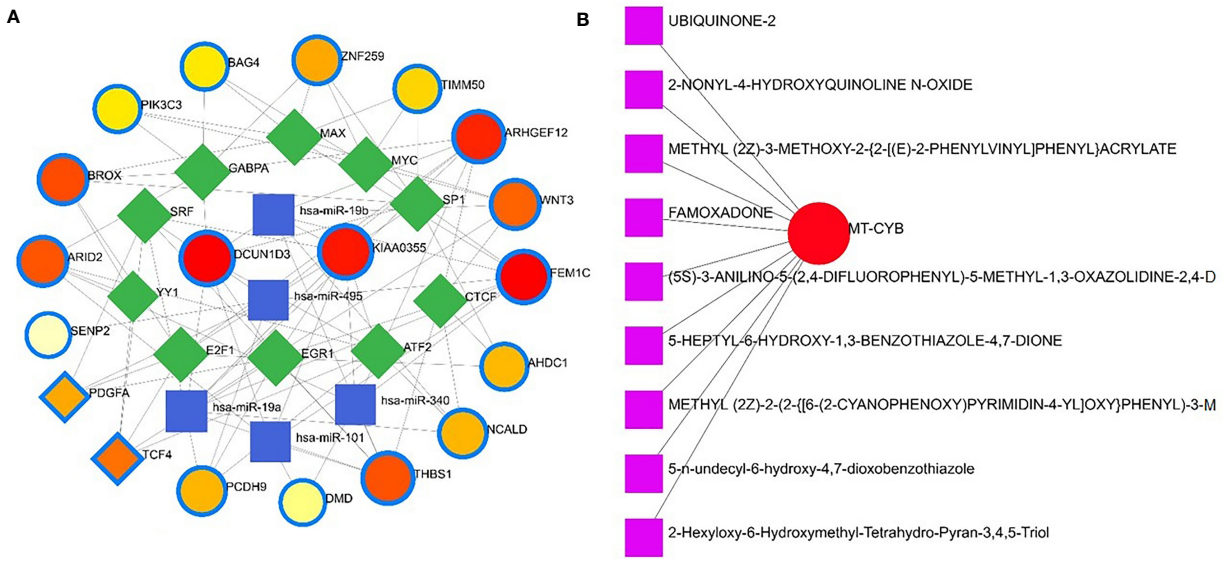

FIGURE 9
Gene regulatory and protein-drug interactions. **(A)** Gene regulatory networks (TF-miRNA) of the nasopharyngeal epithelial cell in COVID- 19 patients with the shared dysregulated genes. The blue color and square shapes indicate the miRNA, while the green color is square-shapes, representing TF. **(B)** Protein-drug interaction network. Nine pharmacological compounds are indicated by squares (pink color), while one circle shape (red) represents the hub node.

changes at the gene levels (41). Therefore, this work investigates the influences of SARS-CoV-2 infection on differential gene expressions (DEGs) in the nasopharyngeal epithelial cells of the COVID-19 patients and recovered individual. We identified 1960 and 153 DEGs in COVID-19 patients and recovered humans with different expressions than healthy controls. Among these DEGs, 77.0% were upregulated during SARS-CoV-2 pathogenesis, and more than 98.0% of the upregulated gene signature had a sole association with COVID-19 patients. Therefore, relatively higher genes were upregulated in COVID-19 patients compared to recovered and healthy humans. Earlier studies reported that certain differences in gene expression

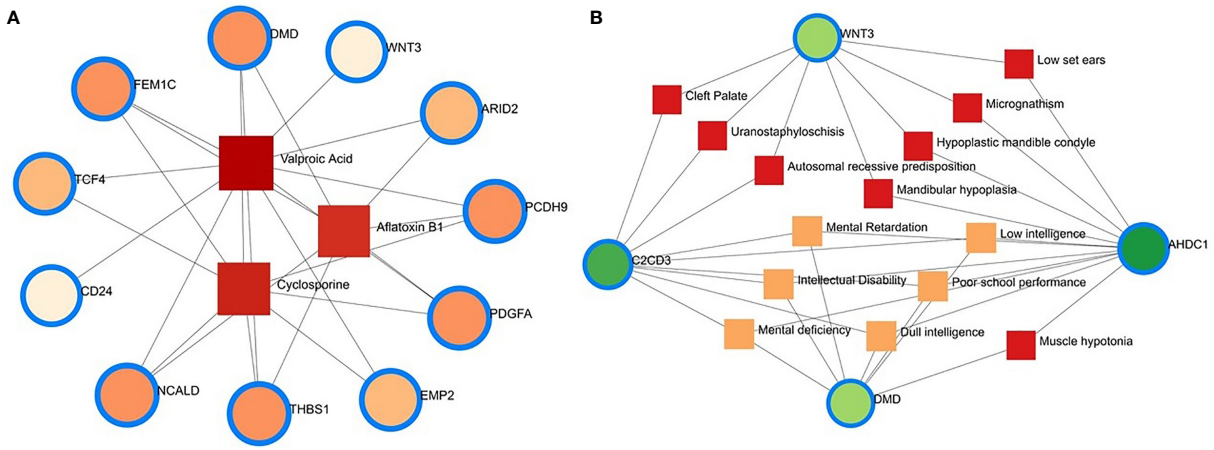

FIGURE 10
Protein-chemical and gene-disease association. **(A)** Protein-chemical interaction network. Three phytochemical compounds were found against 11 genes. Circles showed the shared DEGs, while square shapes indicated interacting phytochemical compounds. **(B)** Gene-disease association network. Circles indicate the common differential genes, and the 14 square shapes represent the common diseases interconnected to the COVID-19 patients.

between patient groups might be driven by changes in tissues' cellular composition, including through the recruitment of immune cell types to the site of infection (14). By analyzing the RNA-seq dataset of lung epithelial cells infected with SARS-CoV-2, Jha et al. (42) identified 338 DEGs, including 92 increased and 246 decreased genes across the datasets. In this study, top abundant DEGs such as genes encoding for ribosomal protein (RPL4), controlling the production of the mitochondrial reactive oxygen species (MT-ND2) (43), modulating cell proliferation and differentiation (SCD5) (44), mitochondrial deficiencies and associated disorders (MT-CYB) (45), epithelial marker ezrin (EZR) associated with cell surface structure adhesion, migration and organization of the SARS-CoV-2 (46) were found to be co-expressed in the nasopharyngeal epithelial cells of COVID-19 patients and recovered humans (Figure 2C). Conversely, SARS-CoV-2 infection suppressed the expression of genes associated with transcription factors (MAFF) (47), erythropoiesis (ARHGEF12) (48), membrane neddylation (DCUN1D3) (49), a global regulator of transcription (DR1) (50), and cytochrome-c oxidase activity (MT-CO1) (51) in both COVID-19 patients and recovered humans (Figure 2D).

We next investigated whether host gene expression during SARS-CoV-2 pathophysiology is associated with functional enrichment, for example, cell signaling pathways and gene ontology. Our results showed that DEGs related to ribosome signaling pathway, coronavirus signaling pathway, c-type-lectin receptor signaling pathway, forming a pool of free 40S subunits, 3-UTR-mediated translational regulation, and eukaryotic translational initiation signaling pathways were significantly enriched in the nasopharyngeal epithelial cells on COVID-19 patients. These findings corroborated with the previously published studies conducted to understand host transcriptional response to influenza A virus and SARS-CoV-2 in primary human bronchial epithelial cells (28, 42). Gene ontology analysis identified several pathways: ceramide 1-phosphate transfer activity, ceramide 1-phosphate binding pathways, nuclear-transcribed mRNA catabolic process, regulation of epithelial cell differentiation pathways for biological process, membrane raft and cytosolic sizeable ribosomal subunit pathways for cellular component significantly enriched in COVID-19 patients. Ceramide 1 phosphate (C1P) can augment immunity and control COVID-19 infection by enhancing autophagy, adaptive immunity (Th1 programming), and MHC-I-dependent cytotoxic T lymphocytes (CTL) response (52). The epithelium lining the airways plays a key role in the defense against infections. Several lines of evidence showed that SARS-CoV-2 infection induces epithelial barrier function, as documented by decreased trans-epithelial resistance, increased permeability, and altered tight junction protein distribution (53, 54). However, this functional impairment remained transient, with signs of epithelial regeneration during the recovery phage of SARS-CoV-2 infection. Basal cell mobilization and replication can also be observed to exert a moderate effect on epithelial barrier integrity (53). With these dysregulated genes, we have conducted the PPI network analyses. PPIs network analysis is the most prominent section of the study as hub gene detection, analysis of modules and drug identification thoroughly depends on the PPIs network. According to the PPIs network (Figures 6, 7), ribosomal proteins (RPL4, RPS4X, RPL19, RPS12, RPL19), translation initiation factor 3 subunit E (EIF3E), mitochondrial deficiencies and associated disorders (MT-CYB) (45), and cytochrome-c oxidase activity (MT-CO1) (51), and mitochondrial oxidative phosphorylation (MT-ATP6) proteins were declared as hub genes because of their high interaction rate or degree value. SARS-CoV-2 infection regulates the mitochondrial transcription of the proteins (MT-CO1 and MT-ATP6) involved in ATP synthesis, respiratory activity, oxidative stress, pro-inflammatory state, and cytokine production (55). The increased expression of ribosomal proteins can be attributed to the virus hijacking the host's translational machinery for its survival by the mechanisms such as ribosome shunting and phosphorylation of ribosomal proteins (42). The PPI and gene enrichment analyses of these hyper-interactive proteins showed significant biological functions connected to COVID-19 related to the cell signaling pathway and the host response to SARS-CoV-2 infections (56). As discussed earlier, these proteins are involved in several other disorders (28, 55, 56).

We further studied relationships of the common DEGs between COVID-19 patients and recovered humans concerning protein-protein, gene-miRNA, TF-gene, protein-drug, and protein-chemical interactions. Our results showed that hsa-miR-19b, hsa-miR-495, hsa-miR-340, hsa-miR-101 and hsa-miR-19a were the mostly expressed miRNAs (Figure 8A), and E2F1, MAX, EGR1, YY1 and SRF were the highly expressed transcription factors (TFs) (Figure 8B). While host responses to infection are critical in differential outcomes of SARS-CoV-2 infection, the role of miRNAs in COVID-19 pathogenesis is poorly understood. We observed that most of these miRNAs were strongly upregulated in COVID-19 patients, which could be used as the circulating biomarkers for the diagnosis or prognosis of COVID-19 (57). Circulating miRNAs are extracellular serum/plasma miRNAs that could be involved in cell-cell communication and might contribute to disease progression. Besides their diagnostic value, miRNAs are well known for their therapeutic potential, especially in viral diseases. A recent report has compared the miRNA signature in the peripheral blood of COVID-19 patients versus healthy donors and several miRNAs have been identified to be deregulated, and interfered with the shaping of the immune responses (58). Therefore, the upregulated levels of miRNAs could be involved in the inflammatory storm seen in COVID-19 patients by inhibiting the immunosuppressive and anti-inflammatory role ensured by the transcription signaling pathway. Recent studies reported that transcription of mRNAs in epithelial cells is

induced by TNF-α and triggers a negative feedback loop involving E-selectin to control inflammatory signaling (42, 59). Although we identified the 14 TF-genes showing more interactions with DEGs, we have to assess further whether these genes have the potential causal effects on the COVID-19 development. Our network-based approach identified TF hubs that likely regulate many cellular functions (e.g., cytokine storm) overexpressed in COVID-19 patients. Previous research identified 95 TFs in cytokines upregulated in the COVID-19 patients, and of them, 19 TFs are targets of FDA-approved drugs (60). Targeting TFs associated with the cytokine-releasing syndrome provides candidate drugs and targets to treat COVID-19 (60). However, additional research is needed to determine whether these combinations elicit the same immunomodulatory response in the context of SARS-CoV-2 infection.

Nine pharmacological compounds were found to be effective against SARS-CoV-2, and of them, fungicide (famoxadone), blood pressure controlling coenzyme (ubiquinone-2), secondary metabolite producing quinoline (2-nonyl-4-hydroxyquinoline), and xenobiotic compound (5-n-undecyl-6-hydroxy-4,7-dioxobenzothiazole) showed their activity against the human mitochondrial cytochrome b (MT-CYB). These compounds have significant antimicrobial, antidiabetic, anti-inflammatory, antiviral, and antioxidant activities (61) against SARS-CoV-2 infections. Furthermore, protein-chemical interaction (PCI) showed that FEM1C, NCALD, THBS1, PCDH9, DMD, and PDGFA proteins interacted with three chemical agents such as Valproic acid (VPA), Alfatoxin B1, and cyclosporine. Numerous promising antiviral therapies against SARS-CoV-2 are being investigated to prevent interindividual transmission and severe complications of the COVID-19. The VPA can reduce the SARS-CoV-2 receptor ACE-2 expression level and can be used as a potential drug candidate for the prevention strategy against COVID-19 (62). Aflatoxin B1 (AFB1), which alters immune responses to mammals, is one of the most common mycotoxins in feeds and food and a potential aggravating risk factor in COVID-19 patients (63). The effect of cyclosporine on coronaviruses, including the new SARS-CoV2, has been extensively studied (64). Several earlier studies showed that cyclosporine has the potential to prevent uncontrolled inflammatory response, SARS-CoV-2 replication, and acute lung injury (64, 65). Therefore, effective drugs are urgently needed to target this life-threatening complication, particularly for patients developing acute respiratory distress syndrome. In addition, we identified 14 other diseases associated with COVID-19 by sharing four DEGs (i.e., DMD, C2CD3, WNT3 and AHDC1) which were most prevalent in COVID-19. People with SARS-CoV-2 infections often have coexisting conditions like mental retardation, mental deficiency, intellectual disability, muscle hypotonia, micrognathism, and cleft palate. There is a dearth of information regarding the impact of COVID-19 in patients with tuberculosis, HIV, chronic hepatitis, and other concurrent infections (66). COVID-19 patients developed serious symptoms, including difficulty breathing, chest pain, loss of muscle control, severe inflammation, and organ damage. The adverse health and economic impact of the COVID-19 pandemic influenced mental health, causing distress, anxiety, and depression (67). These complications are not necessarily short-lived and can cause long-term effects of multiorgan injury following SARS-CoV-2 infections. COVID-19 presents a greater risk to people with intellectual and developmental disabilities, especially younger ones, and recent evidence suggests that mental health problems significantly increased worldwide during this pandemic (68, 69). Since muscle possesses the ACE2 receptor to which SARS-Cov-2 binds, it follows that the involvement of the muscle could be due not only to the secondary effects of the infection (e.g., reduced oxygen supply from persistent lung disease, perfusion defects from cardiovascular defects and vascular damage), but also to the direct action of virus (SARS-CoV-2 myositis) (70).

Conclusions

Gene expression analysis may potentially reveal disease-pathogenesis pathways and point to novel targets for potential therapeutic approaches. This study examines the RNA-seq data of COVID-19 patients, recovered persons, and healthy individuals to find DEGs and biomarkers between the SARS-CoV-2 pathogenesis and recovery stage from a molecular and cellular standpoint. We found that COVID-19 patients had a much larger number of DEGs than recovered humans and healthy controls and that some of these were co-expressed in both COVID-19 patients and recovered humans. We used gene expression analysis with the biomarker to identify cellular signaling pathways and GO terms. In the COVID-19 patients, we found several genes coding for translational activities, transcription factors, hub-proteins, and miRNA expressions, all of which indicated a persistent inflammation and cytokine storm. The signaling pathways, GO terms, and chemical compounds discovered in this study could help researchers figure out how genes are linked together to find possible therapeutic approaches. However, the DEGs' direct molecular biological functions and significant pathways discovered in this study should be investigated further to understand better the mechanisms underlying the host response to SARS-CoV-2 and identify potential therapeutic targets and drug candidates for COVID-19.

Data availability statement

The data presented in the study are deposited in the National Center for Biotechnology Information (NCBI) repository under BioProject accession number PRJNA720904.

Ethics statement

The protocol for sample collection from COVID-19, recovered and healthy humans, sample processing, transport, and RNA extraction was approved by the National Institute of Laboratory Medicine and Referral Center of Bangladesh. Written informed consent was obtain from the participants.

Author contributions

MNH conceived and designed the experiments, analysed data, and wrote the manuscript. MAK, MAH, MIH and MHR contributed to data analysis and interpreting results. MMHS, MAH, SA, TAB, BG, IJ, TN, and MMAM collected samples and performed sequencing. MES edited the manuscript. YA reviewed and edited the manuscript. MSK coordinated the study and performed sequencing. CZ critically evaluated the results and edited the manuscript. TI conceived and designed the experiments, coordinated the study, and critically edited the manuscript. All authors contributed to the article and approved the submitted version.

Acknowledgments

The authors would like to thank the individuals who helped in sample collection.

Conflict of interest

The authors declare that the research was conducted in the absence of any commercial or financial relationships that could be construed as a potential conflict of interest.

The reviewer AZS declared a past collaboration with the author MNH to the handling editor at the time of review.

Publisher's note

References

1. Huang C, Wang Y, Li X, Ren L, Zhao J, Hu Y, et al. Clinical features of patients infected with 2019 novel coronavirus in wuhan, China. *Lancet* (2020) 395 (10223):497–506. doi: 10.1016/S0140-6736(20)30183-5

2. Hoque MN, Chaudhury A, Akanda MAM, Hossain MA, Islam MT. Genomic diversity and evolution, diagnosis, prevention, and therapeutics of the pandemic COVID-19 disease. *PeerJ* (2020) 8:e9689. doi: 10.7717/peerj.9689

3. Zhang T, Wu Q, Zhang Z. Probable pangolin origin of SARS-CoV-2 associated with the COVID-19 outbreak. *Curr Biol* (2020) 30(7):1346–51.e2. doi: 10.1016/j.cub.2020.03.022

4. Rahman MS, Hoque MN, Islam MR, Akter S, Alam ARU, Siddique MA, et al. Epitope-based chimeric peptide vaccine design against s, m and e proteins of SARS-CoV-2, the etiologic agent of COVID-19 pandemic: an in silico approach. *PeerJ* (2020) 8:e9572. doi: 10.7717/peerj.9572

5. Islam MR, Hoque MN, Rahman MS, Alam A, Akther M, Puspo JA, et al. Genome-wide analysis of SARS-CoV-2 virus strains circulating worldwide implicates heterogeneity. *Sci Rep* (2020) 10(1):1–9. doi: 10.1038/s41598-020-70812-6

6. Hopkins JJohns Hopkins coronavirus resource center. *COVID-19 case tracker* (2020). Available at: https://ccp.jhu.edu/kap-covid/?gclid=Cj0KCQjwgMqSBhDCARIsAIIVN1XZXbLT6Dr8AJW6UL1jMd-lbvg7wBz3EK_Sklpj6hcq6U1POShYGNkaAvEyEALw_wcB (Accessed April 10, 2022).

7. Hoque MN, Akter S, Mishu ID, Islam MR, Rahman MS, Akhter M, et al. Microbial co-infections in COVID-19: Associated microbiota and underlying mechanisms of pathogenesis. *Microb Pathog* (2021), 104941. doi: 10.1016/j.micpath.2021.104941

8. Sohrabi C, Alsafi Z, O'neill N, Khan M, Kerwan A, Al-Jabir A, et al. World health organization declares global emergency: A review of the 2019 novel coronavirus (COVID-19). *Int J Surg* (2020) 76:71–6. doi: 10.1016/j.ijsu.2020.02.034

9. Hoque MN, Faisal GM, Chowdhury FR, Haque A, Islam T. The urgency of wider adoption of one health approach for the prevention of a future pandemic. *Int J One Health* (2022) 8(1):20–33. doi: 10.14202/IJOH.2022.20-33

10. Bajgain KT, Badal S, Bajgain BB, Santana MJ. Prevalence of comorbidities among individuals with COVID-19: A rapid review of current literature. *Am J Infect Control* (2021) 49(2):238–46. doi: 10.1016/j.ajic.2020.06.213

11. Rafiqul Islam S, Foysal M, Hoque MN, Mehedi H, Rob M, Salauddin A, et al. Dysbiosis of oral and gut microbiomes in SARS-CoV-2 infected patients in Bangladesh: elucidating the role of opportunistic gut microbes. *Front Med* (2022) 163:821777. doi: 10.3389/fmed.2022.821777

12. Zhou F, Yu T, Du R, Fan G, Liu Y, Liu Z, et al. Clinical course and risk factors for mortality of adult inpatients with COVID-19 in wuhan, China: a retrospective cohort study. *Lancet* (2020) 395(10229):1054–62. doi: 10.1016/S0140-6736(20)30566-3

13. Bui LT, Winters NI, Chung M-I, Joseph C, Gutierrez AJ, Habermann AC, et al. Chronic lung diseases are associated with gene expression programs favoring SARS-CoV-2 entry and severity. *Nat Commun* (2021) 12:4314. doi: 10.1038/s41467-021-24467-0

14. Mick E, Kamm J, Pisco AO, Ratnasiri K, Babik JM, Castañeda G, et al. Upper airway gene expression reveals suppressed immune responses to SARS-CoV-2 compared with other respiratory viruses. *Nat Commun* (2020) 11(1):1–7. doi: 10.1038/s41467-020-19587-y

15. Daamen AR, Bachali P, Owen KA, Kingsmore KM, Hubbard EL, Labonte AC, et al. Comprehensive transcriptomic analysis of COVID-19 blood, lung, and airway. *Sci Rep* (2021) 11(1):1–19. doi: 10.1038/s41598-021-86002-x

16. Liu T, Jia P, Fang B, Zhao Z. Differential expression of viral transcripts from single-cell RNA sequencing of moderate and severe COVID-19 patients and its implications for case severity. *Front Microbiol* (2020) 11:603509. doi: 10.3389/fmicb.2020.603509

17. Hoque MN, Rahman MS, Ahmed R, Hossain MS, Islam MS, Islam T, et al. Diversity and genomic determinants of the microbiomes associated with COVID-19 and non-COVID respiratory diseases. *Gene Rep* (2021) 23:101200. doi: 10.1016/j.genrep.2021.101200

18. Zheng Z, Peng F, Xu B, Zhao J, Liu H, Peng J, et al. Risk factors of critical & mortal COVID-19 cases: A systematic literature review and meta-analysis. *J Infect* (2020) 81(2):e16–25. doi: 10.1016/j.jinf.2020.04.021

19. Nain Z, Barman SK, Sheam MM, Syed SB, Samad A, Quinn JM, et al. Transcriptomic studies revealed pathophysiological impact of COVID-19 to predominant health conditions. *Brief Bioinform* (2021) 22(6):bbab197. doi: 10.1093/bib/bbab197

20. Dong E, Du H, Gardner L. An interactive web-based dashboard to track COVID-19 in real time. *Lancet Infect Dis* (2020) 20(5):533–4. doi: 10.1016/S1473-3099(20)30120-1

21. Xiong Y, Liu Y, Cao L, Wang D, Guo M, Jiang A, et al. Transcriptomic characteristics of bronchoalveolar lavage fluid and peripheral blood mononuclear cells in COVID-19 patients. *Emerg Microbes Infect* (2020) 9(1):761–70. doi: 10.1080/22221751.2020.1747363

22. Li S, Duan X, Li Y, Li M, Gao Y, Li T, et al. Differentially expressed immune response genes in COVID-19 patients based on disease severity. *Aging (Albany NY)* (2021) 13(7):9265. doi: 10.18632/aging.202877

23. Rahman MS, Islam MR, Hoque MN, Alam ASMRU, Akther M, Puspo JA, et al. Comprehensive annotations of the mutational spectra of SARS-CoV-2 spike protein: a fast and accurate pipeline. *Transbound Emerg Dis* (2021) 68(3):1625–38. doi: 10.1111/tbed.13834

24. Sungnak W, Huang N, Bécavin C, Berg M, Queen R, Litvinukova M, et al. SARS-CoV-2 entry factors are highly expressed in nasal epithelial cells together with innate immune genes. *Nat Med* (2020) 26(5):681–7. doi: 10.1038/s41591-020-0868-6

25. Subbarao K, Mahanty S. Respiratory virus infections: understanding COVID-19. *Immunity* (2020) 52(6):905–9. doi: 10.1016/j.immuni.2020.05.004

26. Nelemans T, Kikkert M. Viral innate immune evasion and the pathogenesis of emerging RNA virus infections. *Viruses* (2019) 11(10):961. doi: 10.3390/v11100961

27. Abassi Z, Knaney Y, Karram T, Heyman SN. The lung macrophage in SARS-CoV-2 infection: a friend or a foe? *Front Immunol* (2020) 11:1312. doi: 10.3389/fimmu.2020.01312

28. Blanco-Melo D, Nilsson-Payant BE, Liu W-C, Uhl S, Hoagland D, Møller R, et al. Imbalanced host response to SARS-CoV-2 drives development of COVID-19. *Cell* (2020) 181(5):1036–45.e9. doi: 10.1016/j.cell.2020.04.026

29. Monaco G, Lee B, Xu W, Mustafah S, Hwang YY, Carre C, et al. RNA-Seq signatures normalized by mRNA abundance allow absolute deconvolution of human immune cell types. *Cell Rep* (2019) 26(6):1627–40.e7. doi: 10.1016/j.celrep.2019.01.041

30. Hoque MN, Sarkar M, Hasan M, Rahman MS, Akter S, Banu TA, et al. SARS-CoV-2 infection reduces human nasopharyngeal commensal microbiome with inclusion of pathobionts. *Sci Rep* (2021) 11(1):1–17, 24042. doi: 10.1038/s41598-021-03245-4

31. Torre D, Lachmann A, Ma'ayan A. BioJupies: automated generation of interactive notebooks for RNA-seq data analysis in the cloud. *Cell Syst* (2018) 7(5):556–61.e3. doi: 10.1016/j.cels.2018.10.007

32. Venny OJ. *An interactive tool for comparing lists with venn's diagrams. 2007–2015* (2016). Available at: http://bioinfogp.cnb.csic.es/tools/venny/index.html (Accessed 28 December 2021).

33. Chen EY, Tan CM, Kou Y, Duan Q, Wang Z, Meirelles GV, et al. Enrichr: interactive and collaborative HTML5 gene list enrichment analysis tool. *BMC Bioinform* (2013) 14(1):1–14. doi: 10.1186/1471-2105-14-128

34. Snel B, Lehmann G, Bork P, Huynen MA. STRING: a web-server to retrieve and display the repeatedly occurring neighborhood of a gene. *Nucleic Acids Res* (2000) 28(18):3442–4. doi: 10.1093/nar/28.18.3442

35. Lopes CT, Franz M, Kazi F, Donaldson SL, Morris Q, Bader GD. Cytoscape web: an interactive web-based network browser. *Bioinformatics* (2010) 26(18):2347–8. doi: 10.1093/bioinformatics/btq430

36. Zhou G, Soufan O, Ewald J, Hancock RE, Basu N, Xia J. NetworkAnalyst 3.0: a visual analytics platform for comprehensive gene expression profiling and meta-analysis. *Nucleic Acids Res* (2019) 47(W1):W234–W41. doi: 10.1093/nar/gkz240

37. Huang H-Y, Lin Y-C-D, Li J, Huang K-Y, Shrestha S, Hong H-C, et al. miRTarBase 2020: updates to the experimentally validated microRNA–target interaction database. *Nucleic Acids Res* (2020) 48(D1):D148–D54. doi: 10.1093/nar/gkz896

38. Sandelin A, Alkema W, Engström P, Wasserman WW, Lenhard B. JASPAR: an open-access database for eukaryotic transcription factor binding profiles. *Nucleic Acids Res* (2004) 32(suppl_1):D91–D4. doi: 10.1093/nar/gkh012

39. Davis AP, Grondin CJ, Johnson RJ, Sciaky D, McMorran R, Wiegers J, et al. The comparative toxicogenomics database: update 2019. *Nucleic Acids Res* (2019) 47(D1):D948–54. doi: 10.1093/nar/gky868

40. Piñero J, Queralt-Rosinach N, Bravo A, Deu-Pons J, Bauer-Mehren A, Baron M, et al. DisGeNET: a discovery platform for the dynamical exploration of human diseases and their genes. *Database* (2015) bav028. doi: 10.1093/database/bav028

41. Rahman MS, Hoque MN, Islam MR, Islam I, Mishu ID, Rahaman MM, et al. Mutational insights into the envelope protein of SARS-CoV-2. *Gene Rep* (2021) 22:100997. doi: 10.1016/j.genrep.2020.100997

42. Jha PK, Vijay A, Halu A, Uchida S, Aikawa M. Gene expression profiling reveals the shared and distinct transcriptional signatures in human lung epithelial cells infected with SARS-CoV-2, MERS-CoV, or SARS-CoV: potential implications in cardiovascular complications of COVID-19. *Front Cardiovasc Med* (2021) 7:623012. doi: 10.3389/fcvm.2020.623012

43. Zhang W, Hou L, Wang T, Lu W, Tao Y, Chen W, et al. The expression characteristics of mt-ND2 gene in chicken. *Mitochondrial DNA Part A* (2016) 27(5):3787–92. doi: 10.3109/19401736.2015.1079904

44. Igal RA, Sinner DI. Stearoyl-CoA desaturase 5 (SCD5), a Δ-9 fatty acyl desaturase in search of a function. *Biochim Biophys Acta - Mol Cell Biol Lipids* (2021) 1866(1):158840. doi: 10.1016/j.bbalip.2020.158840

45. Scozzi D, Cano M, Ma L, Zhou D, Zhu JH, O'Halloran JA, et al. Circulating mitochondrial DNA is an early indicator of severe illness and mortality from COVID-19. *JCI Insight* (2021) 6(4):e143299. doi: 10.1172/jci.insight.143299

46. Giobbe GG, Bonfante F, Jones BC, Gagliano O, Luni C, Zambaiti E, et al. SARS-CoV-2 infection and replication in human gastric organoids. *Nat Commun* (2021) 12(1):1–14. doi: 10.1038/s41467-021-26762-2

47. Kannan MB, Solovieva V, Blank V. The small MAF transcription factors MAFF, MAFG and MAFK: current knowledge and perspectives. *Biochim Biophys Acta Mol Cell Res* (2012) 1823(10):1841–6. doi: 10.1016/j.bbamcr.2012.06.012

48. Xie Y, Gao L, Xu C, Chu L, Gao L, Wu R, et al. ARHGEF12 regulates erythropoiesis and is involved in erythroid regeneration after chemotherapy in acute lymphoblastic leukemia patients. *Haematologica* (2020) 105(4):925. doi: 10.3324/haematol.2018.210286

49. Meyer-Schaller N, Chou Y-C, Sumara I, Martin DD, Kurz T, Katheder N, et al. The human Dcn1-like protein DCNL3 promotes Cul3 neddylation at membranes. *Proc Natl Acad Sci (U.S.A.)* (2009) 106(30):12365–70. doi: 10.1073/pnas.0812528106

50. Kim S, Na JG, Hampsey M, Reinberg D. The Dr1/DRAP1 heterodimer is a global repressor of transcription *in vivo*. *Proc Natl Acad Sci (U.S.A.)* (1997) 94(3):820–5. doi: 10.1073/pnas.94.3.820

51. Shoubridge EA. Cytochrome c oxidase deficiency. *Am J Med Genet* (2001) 106(1):46–52. doi: 10.1002/ajmg.1378

52. Prakash H, Upadhyay D, Bandapalli OR, Jain A, Kleuser B. Host sphingolipids: Perspective immune adjuvant for controlling SARS-CoV-2 infection for managing COVID-19 disease. *Prostaglandins Other Lipid Mediat* (2021) 152:106504. doi: 10.1016/j.prostaglandins.2020.106504

53. Robinot R, Hubert M, de Melo GD, Lazarini F, Bruel T, Smith N, et al. SARS-CoV-2 infection induces the dedifferentiation of multiciliated cells and impairs mucociliary clearance. *Nat Commun* (2021) 12(1):1–16. doi: 10.1038/s41467-021-24521-x

54. Zhu N, Zhang D, Wang W, Li X, Yang B, Song J, et al. A novel coronavirus from patients with pneumonia in China, 2019. *N Engl J Med* (2020) 382:727–33. doi: 10.1056/NEJMoa2001017

55. de Las Heras N, Martín Giménez VM, Ferder L, Manucha W, Lahera V. Implications of oxidative stress and potential role of mitochondrial dysfunction in COVID-19: Therapeutic effects of vitamin d. *Antioxidants* (2020) 9(9):897. doi: 10.3390/antiox9090897

56. Taz TA, Ahmed K, Paul BK, Kawsar M, Aktar N, Mahmud SH, et al. Network-based identification genetic effect of SARS-CoV-2 infections to idiopathic pulmonary fibrosis (IPF) patients. *Briefings Bioinform* (2021) 22(2):1254–66. doi: 10.1093/bib/bbaa235

57. Fayyad-Kazan M, ElDirani R, Hamade E, El Majzoub R, Akl H, Bitar N, et al. Circulating miR-29c, miR-30c, miR-193a-5p and miR-885-5p: Novel potential biomarkers for HTLV-1 infection diagnosis. *Inf Genet Evol* (2019) 74:103938. doi: 10.1016/j.meegid.2019.103938

58. Li C, Hu X, Li L, Li JH. Differential microRNA expression in the peripheral blood from human patients with COVID-19. *J Clin Lab Anal* (2020) 34(10):e23590. doi: 10.1002/jcla.23590

59. Li D, Peng H, Qu L, Sommar P, Wang A, Chu T, et al. miR-19a/b and miR-20a promote wound healing by regulating the inflammatory response of keratinocytes. *J Invest Dermatol* (2021) 141(3):659–71. doi: 10.1016/j.jid.2020.06.037

60. Santoso CS, Li Z, Rottenberg JT, Liu X, Shen VX, Bass JIF. Therapeutic targeting of transcription factors to control the cytokine release syndrome in COVID-19. *Front Pharmacol* (2021) 12:67348512. doi: 10.3389/fphar.2021.67348512

61. Sharma PC, Sinhmar A, Sharma A, Rajak H, Pathak DP. Medicinal significance of benzothiazole scaffold: an insight view. *J Enzyme Inhib Med Chem* (2013) 28(2):240–66. doi: 10.3109/14756366.2012.720572

62. Unal G, Turan B, Balcioglu YH. Immunopharmacological management of COVID-19: Potential therapeutic role of valproic acid. *Med Hypotheses* (2020) 143:109891. doi: 10.1016/j.mehy.2020.109891

63. Vamadevaiah RM, Santhekadur PK. Herbal immunity booster-associated liver injury during COVID-19 pandemic and aflatoxins. *J Clin Exp Hepatol* (2021) 12(1):252–3. doi: 10.1016/j.jceh.2021.08.021

64. Poulsen NN, von Brunn A, Hornum M, Blomberg Jensen M. Cyclosporine and COVID-19: Risk or favorable? *Am J Transplant* (2020) 20(11):2975–82. doi: 10.1111/ajt.16250

65. Cour M, Ovize M, Argaud L. Cyclosporine a: a valid candidate to treat COVID-19 patients with acute respiratory failure? *Crit Care* (2020) 24(1):1–3. doi: 10.1186/s13054-020-03014-1

66. Patterson BK, Guevara-Coto J, Yogendra R, Francisco EB, Long E, Pise A, et al. Immune-based prediction of COVID-19 severity and chronicity decoded using machine learning. *Front Immunol* (2021) 12:2520. doi: 10.3389/fimmu.2021.700782

67. Ejaz H, Alsrhani A, Zafar A, Javed H, Junaid K, Abdalla AE, et al. COVID-19 and comorbidities: Deleterious impact on infected patients. *Infect Public Health* (2020) 13:1833–9. doi: 10.1016/j.jiph.2020.07.014

68. Das R, Hasan MR, Daria S, Islam MR. Impact of COVID-19 pandemic on mental health among general Bangladeshi population: a cross-sectional study. *BMJ Open* (2021) 11(4):e045727. doi: 10.1136/bmjopen-2020-045727

69. Turk MA, Landes SD, Formica MK, Goss KD. Intellectual and developmental disability and COVID-19 case-fatality trends: TriNetX analysis. *Disabil Health J* (2020) 13(3):100942. doi: 10.1016/j.dhjo.2020.100942

70. Devaux CA, Rolain J-M, Raoult D. ACE2 receptor polymorphism: Susceptibility to SARS-CoV-2, hypertension, multiorgan failure, and COVID-19 disease outcome. *J Microbiol Immunol Infect* (2020) 53(3):425–35. doi: 10.1016/j.jmii.2020.04.015

frontiers | Frontiers in Immunology

TYPE Original Research
PUBLISHED 19 August 2022
DOI 10.3389/fimmu.2022.965454

OPEN ACCESS

EDITED BY
Chenhe Su,
Wistar Institute, United States

REVIEWED BY
Xiaochuan Liu,
University of California, Riverside, United States
Hongbo Zhou,
Huazhong Agricultural University, China

*CORRESPONDENCE
Ming Liao
mliao@scau.edu.cn

†These authors have contributed equally to this work

SPECIALTY SECTION
This article was submitted to Viral Immunology, a section of the journal Frontiers in Immunology

RECEIVED 09 June 2022
ACCEPTED 03 August 2022
PUBLISHED 19 August 2022

CITATION
Ye Y, Fan H, Li Q, Zhang Z, Miao P, Zhu J, Liu J, Zhang J and Liao M (2022) Differential proteome response to H5N1 highly pathogenic avian influenza (HPAI) viruses infection in duck. *Front. Immunol.* 13:965454. doi: 10.3389/fimmu.2022.965454

Differential proteome response to H5N1 highly pathogenic avian influenza (HPAI) viruses infection in duck

Yu Ye[1,2†], Huiying Fan[1,3,4†], Qi Li[1,5], Zhen Zhang[1,6], Peisi Miao[1,7], Jun Zhu[1,8], Jie Liu[1,5,6], Jie Zhang[1,3,4] and Ming Liao[1,3,4,5,6*]

[1]College of Veterinary Medicine, South China Agricultural University, Guangzhou, China, [2]College of Animal Technology and Science, Jiangxi Agricultural University, Nanchang, China, [3]National and Regional Joint Engineering Laboratory for Medicament of Zoonosis Prevention and Control, Guangzhou, China, [4]Key Laboratory of Animal Vaccine Development, Ministry of Agriculture, Guangzhou, China, [5]Key Laboratory of Zoonoses Control and Prevention of Guangdong, Guangzhou, China, [6]Key Laboratory of Control and Prevention of Guangdong Higher Education Institutes, Guangzhou, China, [7]Jiangsu Coinnovation Center for Prevention and Control of Important Animal Infectious Diseases and Zoonoses, Yangzhou, China, [8]South China Collaborative Innovation Center for Poultry Disease Control and Product Safety, Guangzhou, China

Ducks and wild aquatic birds are the natural reservoirs of avian influenza viruses. However, the host proteome response that causes disease *in vivo* by the H5N1 HPAI virus is still unclear. This study presented a comprehensive analysis of the proteome response in Muscovy duck lung tissue during 3 days of infection with either a highly virulent DK383 or an avirulent DK212. An unbiased strategy- isobaric tags for relative and absolute quantitation (iTRAQ) in conjunction with high-performance liquid chromatography with tandem mass spectrometry (HPLC-MS/MS) was utilized to investigate the infection mechanism. Pathways derived from analysis of 292 significantly altered proteins may contribute to the high pathogenic nature and disease progression of H5N1 viruses. Global proteome profiles indicated improved correlation with the virus titers and gene expression patterns between the two strains of the H5N1 virus. DK383 replicated more efficiently and induced a stronger response specific to severe disease. While proteins involved in the immune response of neutrophils were increased markedly by DK383, DK212 evoked a distinct response characterized by an increase in proteins involved in the maturation of dendritic cells, adhesion of phagocytes, and immune response of macrophages. The differentially activated Akt/mTOR/p70S6K pathway might involve in the host response to H5N1 viruses. Therefore, systematically integrated with datasets from primary genomic and virus titer results, proteomic analyses may help reveal the potential pathogenesis.

KEYWORDS

H5N1 Highly Pathogenic Avian Influenza (HPAI) viruses, isobaric tags for relative and absolute quantitation (iTRAQ), host proteome response, mammalian target of rapamycin (mTOR) signaling, infection

Introduction

The H5N1 HPAI viruses continuously circulate among poultry in parts of Asia and northeast Africa. Since October 2021, the H5N1 strain has swept across Africa, Asia, Europe, and North America, with around 3000 outbreaks reported (1). Occasionally, H5N1 viruses infect humans, causing disease with a mortality rate of nearly 60%. H5N1-infected wild birds (including ducks) do not usually display many signs of infection, which suggests that the duck has become the "Trojan horse" in spreading H5N1 (2). RIG-I, an influenza virus sensor absent in chickens, plays a role in the innate immunity of ducks against influenza. On the other hand, this provides a plausible explanation for ducks' reduced susceptibility to influenza viruses compared with chickens (3). Many recent studies have focused on the pathogenicity of H5N1 HPAI viruses in animal models.

In 2002, there was a resurgence of the H5N1 strains that are highly pathogenic to ducks and cause death and severe neurological signs. This phenomenon may indicate that the biology of H5N1 influenza viruses in waterfowl is changing (4). Molecular mutation in some residues of the genome segment of H5N1 HPAI viruses has been demonstrated to be associated with lethality in ducks. For example, the amino acid changes of the polymerase genes PA (T515A) and PB1 (Y436H) are virulence factors (5). The substitution of two amino acids, S224P and N383D, in PA also contributes to the highly virulent phenotype (6). In addition, the HA and PA gene alteration induces high virus replication and an intense innate immune response in the brain (7). Although several virulence factors have been identified, host factors are also responsible for the pathogenesis of infections. Elevated inflammatory cytokine and chemokine production break the homeostasis of the respiratory and immune system during influenza virus infection, whereas macrophages that migrate to influenza-infected lungs play a pathogenic role in pulmonary inflammation (8). However, the studies on the host response of ducks to H5N1 influenza viruses have been far from optimal.

Previous work analyzing the host response of ducks to H5N1 influenza virus infection has primarily utilized *in vitro* systems (9). Moreover, *in vivo* studies of molecular differences in host response are confined only to RNA expression profiling analogous to *in vitro* studies (7, 10, 11). Unfortunately, little work has been done in proteome profiling to investigate the host-virus interaction within the duck model.

Our study presents a comprehensive analysis of the host proteome response to influenza virus infection based on an unbiased strategy-iTRAQ in conjunction with HPLC-MS/MS. Muscovy ducks were infected with either a highly virulent (A/Duck/Guangdong/383/2008, DK383) or an avirulent (A/Duck/Guangdong/212/2004, DK212) H5N1 HPAI virus. Lung tissue was then collected to evaluate viral titers 1, 2, and 3 days post-infection (dpi). While DK383 caused death between 3 and 4 dpi, DK212 in ducks appears asymptomatic. Based on the information presented above, the lung tissue at 3 dpi was chosen to perform proteomic analysis. 2,459 proteins were quantified, including 292 significantly altered proteins during productive infection. Functional analysis integrated with previous observation in our laboratory (10) provides a complete view of the host proteome response and in-depth characterization of viral pathogenesis.

Materials and methods

Virus, cells, and animals

The H5N1 HPAI viruses DK383 and DK212 were isolated in the Guangdong province of China (12). Viral titers of influenza stock were measured by plaque assay to prepare for duck embryonic fibroblasts (DEF) infection (13).

Fibroblasts were extracted from 12-day-old Muscovy duck embryos. Cells were plated into cell culture flasks and maintained overnight in DMEM with 10% fetal bovine serum, 100 U/ml of penicillin, and 100 μg/ml of streptomycin at 39°C, 5% CO_2.

MDCK (Madin-Darby canine kidney) cells were grown in DMEM supplemented with 10% fetal bovine serum at 37°C and 5% CO_2.

One-day-old healthy Muscovy ducks were purchased from a commercial hatchery in Guangzhou. Congenitally avian influenza-negative ducks were chosen by agar gel precipitation tests and hemagglutinin inhibition (HI) assays to be experimental animals. All experiments were carried out in Animal Biosafety Level 3 (ABSL-3) facilities.

Infection of ducks and cells

At 4 weeks old, 42 ducks were randomly assigned into 3 groups (DK383, DK212, and mock control). In each group, ducks were inoculated by the intranasal route with 10^6 EID_{50} in 0.2 ml of either DK383 or DK212 and 0.2 ml phosphate buffered saline (PBS) as mock controls. After the challenge, ducklings were observed for 14 days for clinical signs of infection. Three ducks from each group were sacrificed at 1, 2, and 3 dpi. Their lung tissues were collected and inoculated into SPF eggs, and virus titers were determined as previously described (10). All animal experiments were conducted following the guidance of CDC's Institutional Animal Care and Use Committee and in an Association for Assessment and Accreditation of Laboratory Animal Care International-accredited facility. The protocol of animal experiments in this study had been approved by the ABSL-3 Committee of South China Agricultural University.

DEF cells were infected with avian influenza viruses at a multiplicity of infection (MOI) of 0.01. Cells inoculated with serum-free DMEM were used as mock-infected controls. After incubation for 1 h, the cells were washed once with PBS, cultured with maintenance media at 39°C at 5% CO_2, and harvested at 12 hpi.

Protein preparation and iTRAQ labeling

Lung tissue was collected and washed with cold PBS. Proteins were extracted by a RIPA reagent containing a complete protease inhibitor. After vibrating several times, the lysate was sonicated for 8 cycles of 1 s on and 1 s off on ice with a JY96-II (Ningbo Scientz Biotechnology), then centrifuged at 12,000 g at 4°C for 10 min. Protein concentration was measured through BCA Protein Assay Kit (Thermo Scientific). Two biological replicates and two experimental replicates were prepared and analyzed by iTRAQ-based HPLC-MS/MS. The samples were prepared in our laboratory using a modified protein digestion method (14). The proteins were reduced to 50 mM tris-(2-carboxyethyl) phosphine (TCEP) at 60°C for 1 h and alkylation in 200 mM Methyl methanethiosulphonate (MMTS) at room temperature for 10 min. The treated samples were diluted with 0.5 M triethylammonium bicarbonate (TEAB) to reduce the urea concentration to less than 2 M, followed by trypsin digestion at 37°C overnight with an enzyme/substrate mass ratio of 1/50. The peptides digested by trypsin were labeled by iTRAQ 8-plex reagents according to the manufacturer's protocols (AB Sciex). Each sample was labeled separately with the iTRAQ tags: For experiment 1 (Group1), the two samples from the DK383 group were labeled with channels 114 and 115, and the two samples from the DK212 group were labeled with channels 116 and 117. Each tissue lysate was further prepared individually. A similar procedure was carried out in experiment 2 (Group2), except that the single sample was exchanged with the channels with the biological duplicate taken from groups DK383 and DK212 to eliminate the influence of tags.

High-pH reversed-phase chromatography

iTRAQ labeled samples were redissolved with mobile phase A (20 mM $HCOONH_4$, 2 M NaOH, pH 10) before HPLC on a Gemini-NX 3u C18 110A; 150×2.00 mm Phenomenex columns. The flow rate for reversed-phase column separation was 200 µl/min with mobile phase A and mobile phase B (20 mM $HCOONH_4$, 80% CAN, 2 M NaOH, pH 10). A solvent gradient system was conducted: 0-15 min, 5-15% B; 15-60 min, 15-50% B; 60-80 min, 50-90% B; 80–100 min, 5% B. The UV detector was calibrated at 214/280 nm, and fractions were collected every 1 min. In total, 24 fractions were pooled for each sample and dried using a vacuum centrifuge.

RPLC-MS analysis

A linear gradient was operated for peptide separation, which was formed from 5% ACN, 0.1% FA (mobile phase A) and 95% ACN, 0.1% FA (mobile phase B), from 5% to 40% of mobile phase B in 70 min at a flow rate of 300 nL/min. The eluted peptides were performed on a TripleTOF 5600 system (AB Sciex) in Information Dependent Mode. MS spectra were acquired across the mass range of 350–1,500 mass-to-charge ratio (m/z) in high-resolution mode (≥ 30,000) with 250 ms accumulation time per spectrum. A maximum of 20 precursors per cycle were chosen for fragmentation from each MS spectrum with 100 ms minimum accumulation time for each precursor and dynamic exclusion for 20 s. Tandem mass spectra were recorded in high sensitivity mode (resolution ≥ 15,000) with rolling collision energy on and iTRAQ reagent collision energy adjustment on, as reported previously (15). The m/z range for MS/MS scans was set from 100 to 1,500.

Data analysis

The raw data were converted to Protein Pilot™ 4.5 (AB Sciex) equipped with the Paragon™ Algorithm (Revision Number: 4.5.0.0, 1654) for deep proteome analysis and protein quantitation. TripleTOF 5600 system performs automatic recalibration such that typical mass errors for MS and MS/MS data were below 10 ppm. The Anas platyrhynchos database (May 7, 2014, 16,588 sequences) was downloaded from NCBI, combined with common contaminants, and used for database searching. The parameters for database searching were as follows: iTRAQ 4-plex (peptide labeled) was set as sample type; MMTS was set as the cysteine alkylation; trypsin was set as the digestion enzyme; biological modifications and amino acid substitutions were set as ID focus; search effort was set as "thorough". In Paragon™ Algorithm, iTRAQ 4-plex (peptide labeled) listed in Protein Pilot™ 4.5 were searched simultaneously with the tolerances specified as ± 0.05 Da for MS fragments and ± 0.1 Da for MS/MS fragments. A database search for the reversed database was also performed to evaluate false discovery rates (FDR) at the peptide and protein levels. Only peptide and protein identifications with FDR < 1% were retained. In addition, a strict cutoff for protein identification was controlled with an unused ProtScore ≥ 1.3, which corresponds to a confidence limit of 95%, to minimize false positive results. For iTRAQ quantitation, only peptides marked as "Auto" in Protein Pilot™ 4.5 contributed to the protein ratio calculation. Bias correction was set as "Auto" and background correction as "Yes" for protein quantitation results.

The coefficient of variance (CV) was calculated in biological and experimental replicates to assess the iTRAQ reliability. Proteins with an iTRAQ ratio higher than 20 or less than 0.05 were not quantified. Only proteins with at least two unique peptides and reasonable ratios across all channels were considered quantified. Protein quantitation values of Group1 and Group2 were obtained by calculating the mean of iTRAQ protein ratios of biological replicates of each group. The final protein quantitation information based on normalization to the mean of Group1 and Group2 (experimental replicates of this study) was used for further data analysis. The mass spectrometry proteomics data were deposited to the ProteomeXchange Consortium (http://proteomecentral.proteomexchange.org) with an identifier (PXD002719). Then the altered proteins were introduced into DAVID 2021 (https://david.ncifcrf.gov/home.jsp) to perform go ontology (GO) annotation and enrichment analysis. For further analysis, the duck gene identifiers of all significantly regulated proteins were converted to human protein gi numbers using BLAST of NCBI. Protein gi numbers and regulation values were imported into the Ingenuity Pathway Analysis software (IPA, www.ingenuity.com) for pathway analysis and network construction.

Western blot

Treated cells were scraped and re-suspended in a cold RIPA buffer. Protein quantification was measured using the Pierce® BCA protein assay kit (Thermo Scientific). Western blot analysis was performed as described (16) by sodium dodecyl sulfate-polyacrylamide gel electrophoresis (SDS-PAGE), using primary antibodies: anti-GAPDH (Bioworld Technology), anti-Akt (Sigma-Aldrich), anti-phosphorylated Akt (Bioworld Technology), anti-mTOR (Cell Signaling Technology), anti-phosphorylated mTOR (Cell Signaling Technology), anti-p70S6K (Santa Cruz), anti-phosphorylated p70S6K (Cell Signaling Technology), anti-phosphorylated rpS6 (Cell Signaling Technology), anti-phosphorylated 4EBP1 (Cell Signaling Technology), anti-HSP90a (Bioworld Technology), anti-desmin (Santa Cruz), anti-β-actin (Bioworld Technology), and anti-caplain-1 (Novus). Membranes were washed in TBST and incubated with DyLight488-conjugated goat anti-rabbit IgG or rabbit anti-mouse IgG (1:10000, Rockland) for 1 h. Membranes were then washed in TBST and visualized using the Odyssey Infrared Imaging system (Licor Biosciences).

RNA and cDNA preparation

DNase-treated total RNA was isolated from lung tissue at 3 dpi using Direct-zol™ RNA MinPrep according to the instructions provided by the manufacturer (Zymo Research). Reverse transcription (RT) was conducted using the PrimeScript™ RT Reagent Kit (Takara).

Quantitative real-time PCR (qRT-PCR)

qRT-PCR was performed using the QuantiNova™ SYBR® Green PCR kit (Qiagen). Primers were designed by the software Primer3 Web (http://bioinfo.ut.ee/primer3/) based on published target sequences and previously mentioned (7, 10). Primer pairs (Table 1) were selected based on specificity determined by dissociation curves. The levels of PCR products were monitored using a 7500 Fast Real-Time PCR system (Applied Biosystems). PCR conditions were as follows: 95°C for 2 min, followed by 40 cycles of 95°C for 5 s, and 60°C for 32 s. Dissociation curves of the products were generated by incrementally increasing the samples' temperature from 55°C to 100°C as the final step. For assay validation, purified products were cloned into pMD18-T (Takara) and sequenced to verify the specificity of target amplification.

Statistics analysis

Expression fold change of target genes in the infected group versus those in the control group was determined by the $2^{-\Delta\Delta Ct}$ method using the duck housekeeping gene glyceraldehyde-3-phosphate-dehydrogenase (GAPDH) as the endogenous reference gene to normalize the level of target gene expression (10). Standard deviations were calculated using the fold change values of three replicates for each gene. Comparisons on virus titer in lung tissues and qRT-PCR data were conducted for statistical analyses by GraphPad Prism 5 software (GraphPad Software, Inc.).

Results

In this study, the ducks were infected separately by two H5N1 HPAI strains, DK383 or DK212, and initially used iTRAQ 8-plex reagent to investigate the host proteome response to the H5N1 HPAI virus. To compare disease progression, samples from 1, 2, and 3 dpi were selected to evaluate virus load. DK383 replicated to a much greater extent within the lungs than DK212 and reached the peak, particularly at 3 dpi. This result was

TABLE 1 Primers used for qRT-PCR in this study.

Primer name	Sequence (5'-3')	Genbank accession number
IL-6F	TTCGACGAGGAGAAATGCTT	JQ728554.1
IL-6R	CCTTATCGTCGTTGCCAGAT	
TNF-αF	ATGAACCCTCCTCCGTACAC	EU375296.1
TNF-αR	TCTGAACTGGGCGGTCATAA	
IL-10F	GGGGAGAGGAAACTGAGAGATG	JN786941.1
IL-10R	TCACTGGAGGGTAAAATGCAGA	

consistent with our previous results (Figure 1). DK383 could cause a more productive infection and replicate more efficiently than DK212 (10, 12). Ducks in the DK383 group displayed more severe symptoms than those in the DK212 groups within 3 dpi. Signs included hemorrhages of the beak, torticollis, anorexia, depression, neurological symptoms on day 3 p.i., and death on 4 dpi. However, no ducks exposed to DK212 died or showed clinical signs of infection. Altogether, lung tissues of DK383 and DK212 at 3 dpi were designated for later proteomics analysis.

Reproducibility assessment of protein identification among replicates and determination of the cutoff value

Two independent iTRAQ experiments were conducted as experimental replicates on day 3 p.i. in different virulence of H5N1 influenza virus infection. Two animals of each group were analyzed in separate iTRAQ channels as biological replicates. Peptides and proteins were retained according to the values of FDR and unused ProtScore. We then assessed biological and experimental replicates by calculating the coefficient of variance (CV) (17) when the recommended cutoff point of biological replicate is at ± 50% variation, the coverages of Group1 and Group2 in protein quantification were 86% and 92%, respectively (Supplementary Figure 1). While the cutoff point at ± 50% variation for experimental replicate between Group1 and Group2, an 86% coverage interval in protein quantification was recorded (Supplementary Figure 2), which indicated greater proteome coverage and precise quantification (18).

Overall, peptides from biological and experimental replicates were pooled and characterized using a cutoff CV of 0.5. iTRAQ ratios of protein expression higher than 20 or lower than 0.05 were not considered in the further analysis. Altogether, 16,680 peptides were acquired in the two independent experiments, of which 74.6% of Group1 and 64.8% of Group2 were detected. Correspondingly, 3,000 proteins were identified, in which 90.5% of Group1 and 82.3% of Group2 were detected. From this total, 2,459 proteins were quantified across both experimental replicates, in which 89.6% of the Group1 and 94.4% of Group2 were detected (Supplementary Figure 3), for a final 85.1% reproducibility, implying that there were high correlation rates between both biological replicates and experimental replicates. The quantified proteins in two replicates fit a Gaussian distribution based on the ratios (Figure 2). The ratio distribution was narrow, with a mean of 1.034 and a standard deviation (SD) of 0.1986. According to traditional statistics, 0.6107 and 1.389 were considered significant differences ($P \leq 0.05$), which were located at the lower and upper bound, respectively. To reduce the omission of some valuable information, we slightly expanded the range of analysis. Eventually, proteins with expression ratios ≥ 1.3 or ≤ 0.7 were recognized as significantly up- and down-regulated, respectively. As a result, 297 proteins were differentially expressed, including 222 up-regulated and 70 down-regulated proteins.

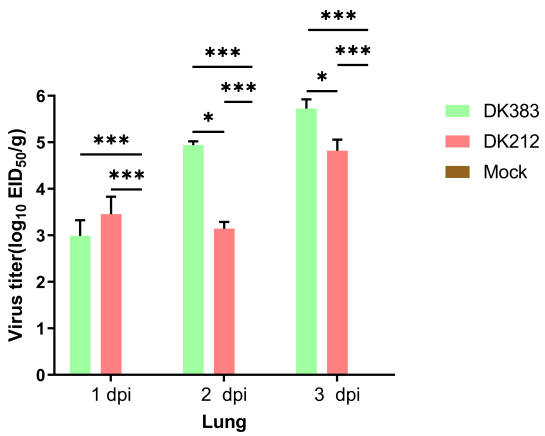

FIGURE 1
Virus titers in the lung of Muscovy ducks infected with DK383 and DK212 at 1, 2, and 3 dpi. Virus titers were calculated as means of standard deviation in log10 EID_{50}/g of tissue. * and *** indicated significant differences with $P \leq 0.05$ and $P \leq 0.001$.

Bioinformatics analysis of overexpressed proteins

To identify the host protein function manipulated by two H5N1 HPAI strains in this study, GO term enrichment analysis of the differentially expressed genes was carried out. In biological process terms, the up-regulated proteins may involve in phagocytosis, actin polymerization or depolymerization, translation, and peptide biosynthetic process, while the down-regulated proteins only may participate in purine-containing compound metabolic process, purine-containing compound metabolic process, and small molecule metabolic process. In molecular function terms, the L-ascorbic acid binding, monosaccharide binding, and structural constituent of ribosome were enriched in the up-regulated proteins, whereas sugar-phosphatase activity, carbohydrate phosphatase activity, and unfolded protein binding were enrichment in the down-regulated proteins ($P \leq 0.05$, Figure 3 and Supplementary Table 1). Since the duck genome database has inadequate annotation by contrast with the human genome, many proteins are uncharacterized or unknown. Each identifier of the altered proteins in Supplementary Table 1 was converted to its corresponding human protein gi number. Protein gi numbers and expression ratios were imported into the IPA tool, and a global molecular network and pathway were then developed from information previously reported based on the underlying biological evidence, such as protein interactions, regulation of expression, etc. We discovered that the previously characterized proteins were assigned to 26 diseases or functions annotation.

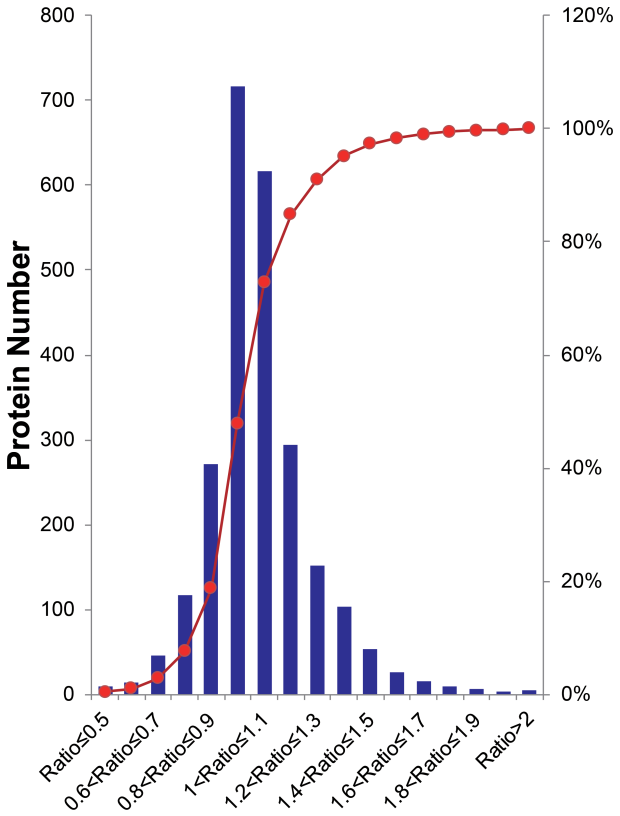

FIGURE 2
Histogram distribution of expression ratios of quantified proteins. The Red line indicates the cumulative percentage of proteins.

This bio function classification was identified at statistically significant levels ($P \leq 0.05$) displayed in Figure 4A, with additional data shown in Supplementary Table 2. The multiple protein clusters were predicated on being activated or up-regulated in the DK212 group compared with the DK383 group, including cell movement, maturation of dendritic cells, immune response of macrophages, chemotaxis of endothelial cells, and adhesion of phagocytes. By contrast, proteins in these clusters were predicated on being up-regulated in the DK383, including the immune response of neutrophils, the number of filaments, and the size of cells. The most relevant canonical pathways following the influenza virus infection included eIF2 signaling, Fcγ receptor-mediated phagocytosis in macrophages and monocytes, CD28 signaling in T helper cells, production of nitric oxide, and reactive oxygen species in macrophages, mitochondrial dysfunction, and mTOR signaling. ($P \leq 0.05$, Figure 4B and Supplementary Table 2). It is suggested that the H5N1 virus may involve manipulation and interference with immune regulatory mechanisms.

The proteins significantly regulated were subject to regulatory network analysis, which may further the investigation of possible links between influenza virus infection and diseases such as acute lung injury. Network analysis suggested these proteins were mapped to 10 specific functional networks (Figure 5 and Supplementary Table 2). The three networks of interest correspond to (1) RNA posttranscriptional modification, cancer, and cell cycle; (2) infectious disease, energy production, and lipid metabolism; (3) hereditary disorder, neurological disease, and free radical scavenging.

Validation of identified candidates by western blot

To confirm the protein quantification, immunoblotting analyses were carried out on a series of protein candidates extracted from lung tissues of DK383 and DK212 ducks. Although there are insufficient antibodies to be appropriately used for the quantified proteins, the results in Figure 6 demonstrated the ratios of the four representative proteins (HSP90a, desmin, β-actin, and caplain-1) were consistent with those data obtained from iTRAQ-identified candidates.

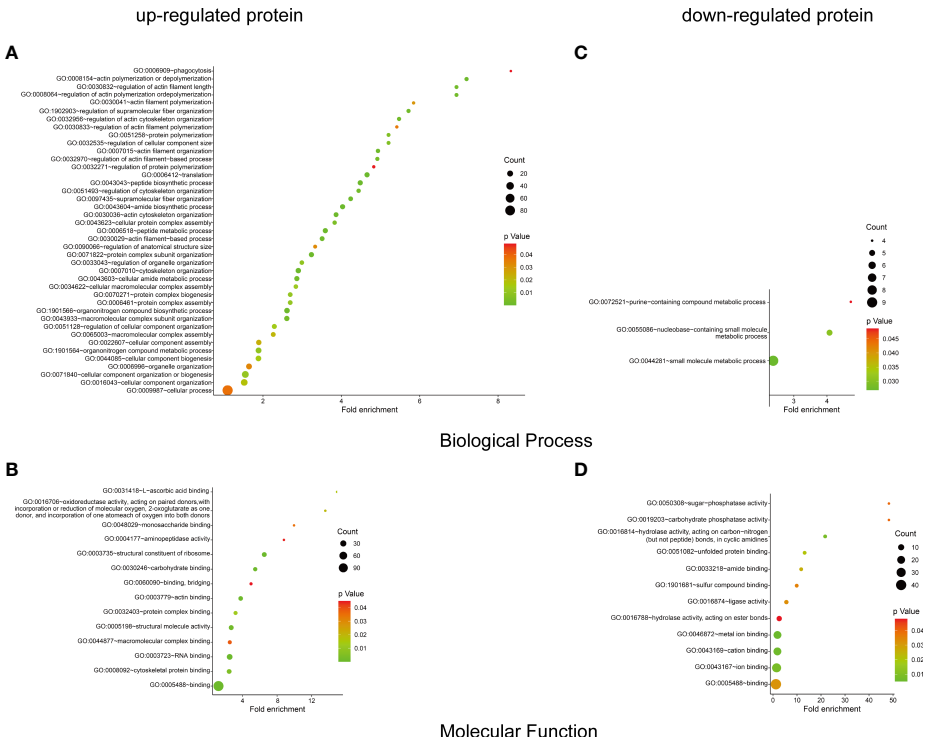

FIGURE 3
GO enrichment analysis of the differential proteins. The biological process and molecular function terms enrichment results of up-proteins **(A, B)** and down-regulated proteins **(C, D)** were conducted by DAVID. More information is available in Supplementary Table 1. The figure was created with ImageGP (http://www.ehbio.com/ImageGP/).

Akt/mTOR/p70S6K pathway is involved in the duck proteome response to influenza virus infection

As mentioned above, mTOR signaling was highlighted in the canonical pathway analysis. Several proteins in this pathway formed a group whose abundance differed between DK212 and DK383 infected ducks. For example, eIF3M, RPS8, RPS5, and RPS4X are downstream elements of mTOR signaling (Supplementary Table 2). The proteins were up-regulated in the DK212 group, indicating that mTOR signaling may be promoted more obviously than in the DK383 group. As reported previously, moderate mTOR phosphorylation induces a protective effect in influenza virus-infected cells (13). Because the sample pooling strategy could reduce the biological variation, increasing the power to detect changes (19). For each condition, pooled samples consisting of three biological replicates were collected. To measure whether members of mTOR signaling were activated in H5N1 virus-infected lung tissues, lysates from these pooled samples were evaluated by western blot. As illustrated in Figure 7, robust phosphorylation in Akt (Ser473) and mTOR (Ser2448) were observed after the duck lung tissues were treated with DK383 and DK212 at 3 dpi compared with the control, which demonstrated the activation of the Akt/mTOR pathway. p70S6K is considered an important component of mTOR signaling, and our results demonstrated that phosphorylation in p70S6K (Thr389) was not detected.

However, rpS6, downstream of p70S6K, showed enhanced phosphorylation. DK212 infection dramatically induced phosphorylation of rpS6 compared with DK383. This phenomenon indicated facilitating the initiation of mRNA translation and further confirmed the activation of the mTOR pathway. These findings were further validated by comparing them to these proteins of mTOR signaling in influenza-infected DEF. As expected, we observed that DK212 and DK383 both markedly increased the levels of p-Akt (Ser473), p-p70S6K (Thr389), and p-rpS6 (Ser235/236). When the cells were treated with DK212, these phosphorylated proteins significantly increased too much higher than those observed in cells treated with DK383 (Figure 7). Meanwhile, there was no significant difference between each group in phosphorylated 4EBP1, the other substrate of mTOR. Therefore, amplified phosphorylation of proteins in the Akt/mTOR/p70S6K pathway revealed a host response that negatively regulated this signaling cascade after infection by a virulent H5N1 virus.

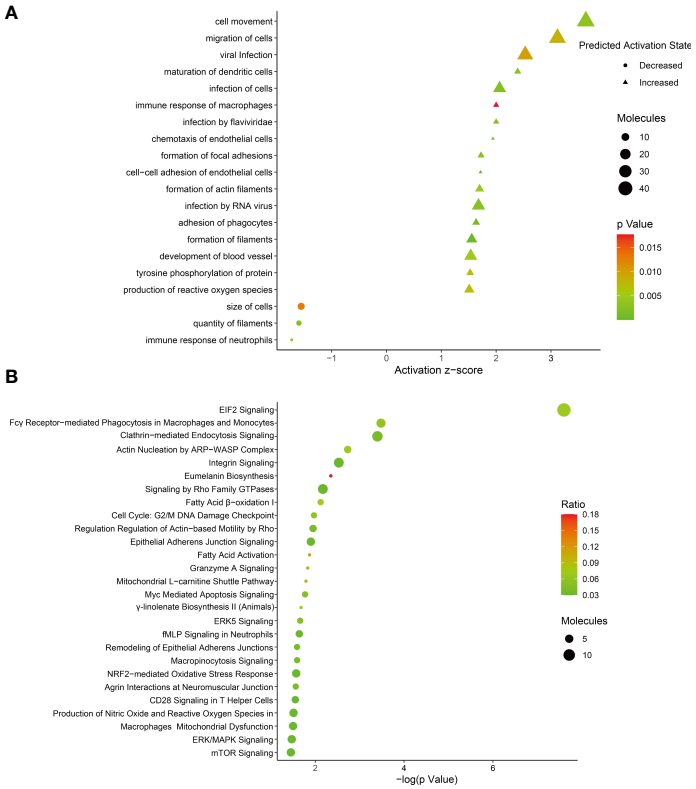

FIGURE 4
(A) bio-function analysis results of proteins with differential expression. The circle indicates increased effects on the function predicated by IPA, and the triangle indicates that the biological process or disease is trending towards a decrease; **(B)** enrichment of canonical pathways within each category was determined using IPA software. More information is available in Supplementary Table 2. The figure was created with ImageGP.

Akt/mTOR/p70S6K pathway controls cytokine bias

As we all know, mTOR complexes regulate metabolic processes of cells, including protein synthesis (20). Innate or adaptive immune signals could trigger the Akt-mTOR-p70S6K signaling cascade in innate immune cells. mTOR activation can inhibit the proinflammatory molecules, such as IL-6 and tumor necrosis factor-alpha (TNF-α), and also boost the production of anti-inflammatory cytokines such as interleukin-10 (IL-10) (21). Due to a limited number of appropriate reagents to measure these cytokines of ducks in the serum, mRNA levels of the core proteins were used to evaluate by qRT-PCR. A significant increase in mRNA levels of IL-6 was observed at 3 dpi, and the IL-6 expression in DK383 infected group was higher than that of the DK212 infected group, which was previously described (10). A similar pattern was found in TNF-α mRNA levels after infection by the virulent H5N1 virus DK383. However, the level of IL-10 mRNA was remarkably lower in DK212 infected lung tissue (Figure 8). As reported in the earlier study (22), the differences in cytokine production did not correlate with gene expression. Hence, the cytokine biasing reported in response to virulent H5N1 virus may involve posttranscriptional gene expression regulation.

Discussion

Prior work has focused on the host response to influenza virus infection in RNA expression profiles within the duck model. However, several proteomic analyses have been implemented in the influenza virus-host interactomes. This study provided a comprehensive analysis describing the host proteomes of ducks during infection with the H5N1 virus. An unbiased strategy-iTRAQ, combined with HPLC-MS/MS, enhanced the proteome coverage and protein specificity. The duck genome database annotation development also facilitated the broadened identification of peptides and proteins (11). H5N1 viruses have employed various strategies

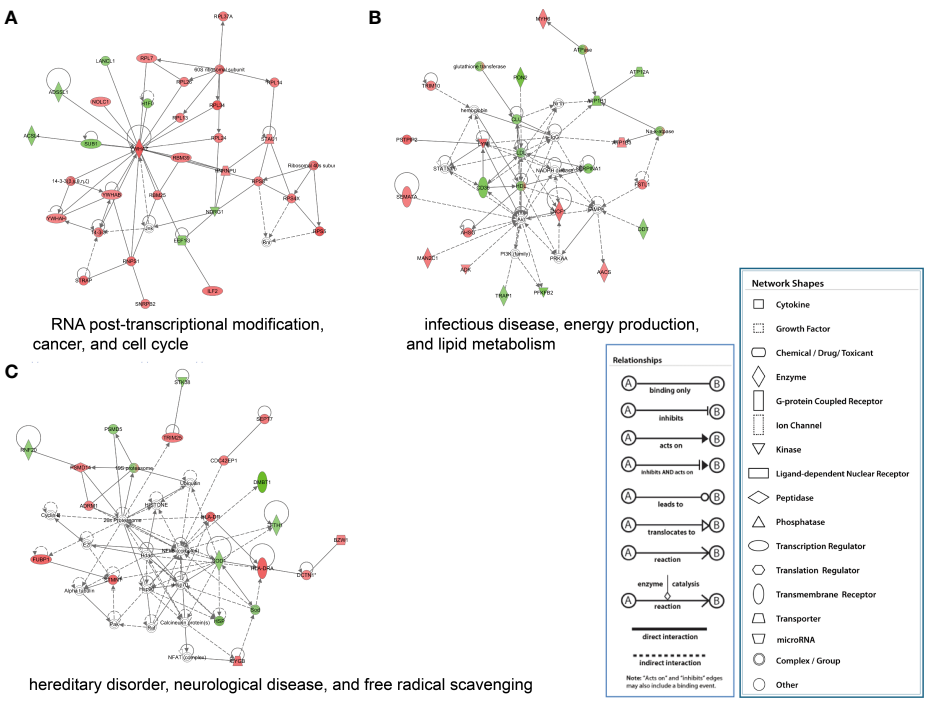

FIGURE 5
IPA of proteins that were significantly altered to construct specific functional networks. Red, up-regulated proteins; green, down-regulated proteins; white, proteins known to be in the Ingenuity Pathways Knowledge Base but were not identified in this study. The color depth indicates the magnitude of the change in protein expression level. The shapes indicate the molecular class (i.e., protein family). Lines connecting the molecules imply molecular relationships. Dashed lines indicate indirect interactions, and solid lines indicate direct interactions. The arrow styles mean specific molecular relationships and the directionality of the interaction. **(A)** RNA posttranscriptional modification, cancer, and cell cycle; **(B)** infectious disease, energy production, and lipid metabolism; **(C)** hereditary disorder, neurological disease, and free radical scavenging.

to regulate innate and adaptive immune responses to establish productive infections in an individual. While proteins involved in the immune response of neutrophils and the size of cells were elevated significantly in the lung by the virulent virus DK383, the avirulent virus DK212 induced a distinct response characterized by an increase in proteins that participated in cell movement, maturation of dendritic cells, adhesion of phagocytes, and immune response of macrophages.

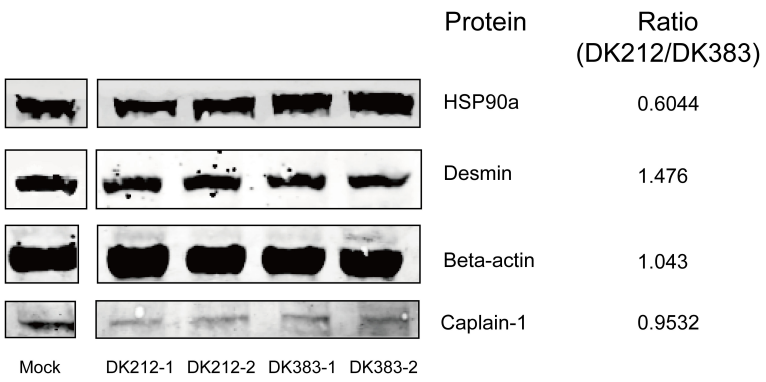

FIGURE 6
Western blot analyses of the representative proteins. Ratios of each protein between DK212 and DK383 were determined by iTRAQ. Compared with the DK383 group, decreased expression was observed for HSP90a, increased expression was found for desmin, and the expression of β-actin and caplain-1 were not altered in the DK212 group.

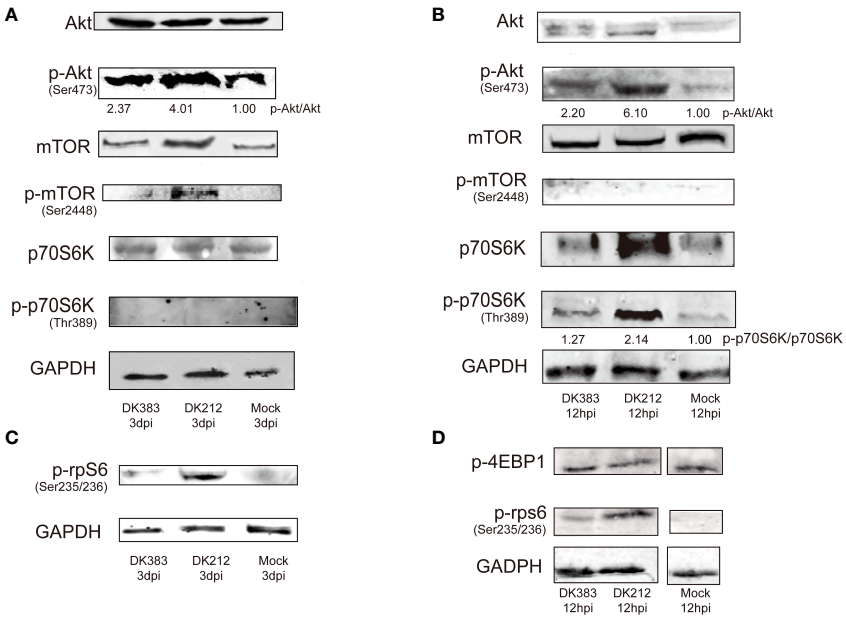

FIGURE 7
Immunoblot analysis of mTOR pathway activation in duck lung tissues at 3 dpi DEF lysates at 12 hpi infected with DK383 or DK212. Total and phosphorylation levels of Akt, mTOR, and p70S6K are shown in lung tissues **(A)** and DEF **(B)**; **(C)** shows phosphorylation of rpS6 in lung tissues; **(D)** shows phosphorylation of 4EBP1 and rpS6 in infected DEF. Densitometry of signal intensity of the phosphorylation protein normalized to the corresponding total protein was labeled under each band. The mock-infected group was used as the negative control.

There is increasing evidence for a critical role in the "maturation of dendritic cells" at the onset of antiviral immunity. Contrasting with a seasonal virus, the pandemic H1N109 influenza virus failed to induce substantial dendritic cell maturation (23). DK212 infection substantially repressed CD36, THBS1, and SERPINA1 expression, which might prevent the maturation of immature dendritic cells. ITGB2, LYN, and STAT1 were up-regulated by comparison with DK383, suggesting that the virulent virus might impede this biological process. Compared with low pathogenic H1N1 (PR8) in infected human monocyte-derived macrophages, the H5N1 HPAI virus revealed an insufficient innate immune response. This strategy contributes to virus spreading and progression to the systemic stage of disease (24). The bio-function "adhesion of phagocytes",

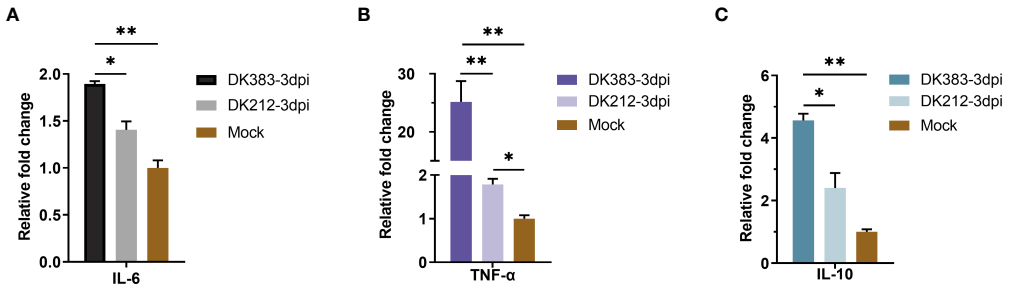

FIGURE 8
qPCR expression analysis of proinflammatory cytokine IL-6 **(A)** and TNF-α **(B)** and anti-inflammatory cytokine IL-10 **(C)** in the lungs of infected duck with the two HPAIVs at 3 dpi. Gene expression was normalized to the GAPDH gene expression level and is presented as the fold change relative to the level for the control group. Error bars indicate standard deviations. (*) $P \leq 0.05$ and (**) $P \leq 0.01$ compared with the result for DK212, respectively.

"cell movement", and "immune response of macrophages" were significantly regulated in DK212, which indicated the avirulent virus might have a positive effect on the immune response to eliminating pathogen. Moreover, the neutrophils ameliorate lung injury and facilitate the development of severe disease during influenza infection (25). Thus, the categories "immune response of neutrophils" and "size of cells" were dramatically elevated, which may aggravate the tissue injury.

To mine our data, we applied IPA software to determine which signaling pathways were enriched in each group. We discovered that multiple members in the pathways of eIF2 signaling, Fcγ receptor-mediated phagocytosis in macrophages and monocytes, and CD28 signaling in T helper cells were up-regulated in DK212. In eukaryotic cells, induction of the eIF2 signaling pathway occurs following infection with pathogens. Bacterial virulence factor YopJ reduced eIF2 signaling to repress proinflammatory cytokine expression and be susceptible to bacterial invasion. Viral infection also activates eIF2-mediated translation control. This effect causes a decrease in general protein synthesis and reduces viral replication while enhancing the translation of specific stress-related mRNA transcripts, such as ATF3 and CHOP. The highly conserved eIF2 signaling pathway is vital for antiviral responses (26). Meanwhile, Fc receptor-mediated phagocytosis plays a pivotal role in the clearance of influenza virus infections (27). The costimulatory pathway CD28 signaling is essential for activating helper T cells and protective immunity to influenza infection (28). Taken together, it appears that down-regulation of these pathways may promote the evasion of the host immune responses for productive infection in DK383.

The mTOR signaling pathway was up-regulated in DK212 compared with DK383. Akt/mTOR/p70S6K pathway plays a vital role in regulating immune function and protein translation in response to environmental stress, such as infection. Our data indicated that infection of lung tissue and DEF with either a highly virulent or avirulent H5N1 virus favored ubiquitinylation of Akt, mTOR, p70S6K, and rpS6. The avirulent virus-induced mTOR pathway more noticeably than the virulent virus indicates that this pathway was differentially regulated in response to influenza infection. In the previous research, alterations in phosphorylation of the PI3K/Akt/mTOR signaling pathway suggests that influenza viruses highjack the host response responsible for aiding viral replication and pathogenesis (29). Suppression of mTOR function inhibited translation and boosted proinflammatory cytokine secretion (22). Influenza A virus NS1, a known multifunction protein, has been reported to activate Akt phosphorylation (30). This phenomenon indicates NS1 may serve as an inducer of mTOR. However, NS1 has a negligible influence on the accumulation of mTOR in the H1N1-infected cells (31). In the duck model, it is unknown whether the regulator of NS1 in cells infected with the H5N1 virus is analogous to the effect of H1N1. Therefore, further work should be directed to understand the precise regulatory mechanism better.

To gain a more detailed understanding of changes in host response proteome during H5N1 virus infection, we focused on an early infection event about interferon (IFN) response by searching the known interferon-stimulated genes to determine which might be associated with influenza virus infection. Influenza virus NS1 protein can impair antiviral IFN response by antagonizing RIG-I's ubiquitination (32). Our results demonstrated that many tripartite motif-containing proteins (TRIM) were up-regulated in the DK212, which could mediate ubiquitination and enhance innate immune signaling, including TRIM10, 25, and 47. Most importantly, TRIM25 can augment the production of biologically functional, antiviral cytokines and reduce virus replication (33). Meanwhile, the expression of the final effector STAT1 in the IFN response pathway was markedly increased at 3 dpi. It may be reasonable to assume that the DK212 group could have induced more robust antiviral immunity than the DK383 group.

In contrast to Lys172 residue of human RIG-I critical for efficient TRIM25-mediated ubiquitination, duck RIG-I activated by TRIM25 is independent of anchored ubiquitin (34, 35). However, little is known about whether TRIM25 was regulated differentially by NS1 proteins of various virulent strains. This finding is promising and should be explored in the next stage. Not all genomic and proteomic data were in good agreement (36). Discrepancies that are always difficult to explain might provide objective answers concerning influenza virus pathogenesis. Future advances in biological system analyses integrating these approaches will potentially refine our understanding of the influenza virus infection.

In conclusion, in the present work, an iTRAQ-based quantitative proteomics strategy was developed to dissect Muscovy duck lung tissue infected by H5N1 HPAI viruses to quantify changes in host protein expression. Bioinformatics analysis of these proteomics data suggested multiple signaling pathways may be involved in the host response to H5N1 HPAI viruses, which provide insights into the mechanisms of infection. To validate our results, Akt/mTOR/p70S6K pathway was confirmed to be activated during the infection of H5N1 HPAI viruses. In summary, our data highlights the interaction between the H5N1 HPAI virus and the host and may help to elucidate the potential mechanism of pathogenicity and inflammation.

Data availability statement

The data presented in the study are deposited in the ProteomeXchange Consortium repository (http://proteomecentral.proteomexchange.org), accession number PXD002719.

Ethics statement

The animal study was reviewed and approved by ABSL-3 Committee of South China Agricultural University.

Author contributions

HF and ML conceived the study. YY, QL, ZZ, PM, JuZ, JL, and JiZ performed the experiments. YY and HF analyzed the data. YY wrote the draft. HF and ML revised the manuscript. All authors contributed to the article and approved the submitted version.

Funding

This work was supported by the Natural Science Foundation of Guangdong Province, China (2014A030313462), Science & technology nova Program of Pearl River of Guangzhou (2012J2200086), Programs for Science and Technology Development on H7N9 Avian Influenza of Guangdong Province (20140224), the China Agricultural Research System (CARS-42-G09), Joint Research Projects on H7N9 Influenza ((2014) no.1046), and the Modern Agriculture Talents Support Program ((2012) no.160).

Acknowledgments

We thank Hejia Ye for the technical assistance in the animal experiment.

Conflict of interest

The authors declare that the research was conducted without any commercial or financial relationships construed as a potential conflict of interest.

Publisher's note

Supplementary material

The Supplementary Material for this article can be found online at: https://www.frontiersin.org/articles/10.3389/fimmu.2022.965454/full#supplementary-material

References

1. Wille M, Barr IG. Resurgence of avian influenza virus. *Science* (2022) 376 (6592):459–60. doi: 10.1126/science.abo1232

2. Kim JK, Negovetich NJ, Forrest HL, Webster RG. Ducks: The "Trojan horses" of H5N1 influenza. *Influenza Other Resp* (2009) 3(4):121–8. doi: 10.1111/j.1750-2659.2009.00084.x

3. Barber MR, Aldridge JRJr., Webster RG, Magor KE. Association of RIG-I with innate immunity of ducks to influenza. *Proc Natl Acad Sci U S A* (2010) 107 (13):5913–8. doi: 10.1073/pnas.1001755107

4. Hulse-Post DJ, Sturm-Ramirez KM, Humberd J, Seiler P, Govorkova EA, Krauss S, et al. Role of domestic ducks in the propagation and biological evolution of highly pathogenic H5N1 influenza viruses in Asia. *Proc Natl Acad Sci U S A* (2005) 102(30):10682–7. doi: 10.1073/pnas.0504662102

5. Hulse-Post DJ, Franks J, Boyd K, Salomon R, Hoffmann E, Yen HL, et al. Molecular changes in the polymerase genes (PA and PB1) associated with high pathogenicity of H5N1 influenza virus in mallard ducks. *J Virol* (2007) 81 (16):8515–24. doi: 10.1128/jvi.00435-07

6. Song J, Feng H, Xu J, Zhao D, Shi J, Li Y, et al. The PA protein directly contributes to the virulence of H5N1 avian influenza viruses in domestic ducks. *J Virol* (2011) 85(5):2180–8. doi: 10.1128/jvi.01975-10

7. Hu J, Hu Z, Mo Y, Wu Q, Cui Z, Duan Z, et al. The PA and HA gene-mediated high viral load and intense innate immune response in the brain contribute to the high pathogenicity of H5N1 avian influenza virus in mallard ducks. *J Virol* (2013) 87(20):11063–75. doi: 10.1128/jvi.00760-13

8. Fukuyama S, Kawaoka Y. The pathogenesis of influenza virus infections: The contributions of virus and host factors. *Curr Opin Immunol* (2011) 23(4):481–6. doi: 10.1016/j.coi.2011.07.016

9. Cui Z, Hu J, He L, Li Q, Gu M, Wang X, et al. Differential immune response of mallard duck peripheral blood mononuclear cells to two highly pathogenic avian influenza H5N1 viruses with distinct pathogenicity in mallard ducks. *Arch Virol* (2014) 159(2):339–43. doi: 10.1007/s00705-013-1820-6

10. Wei L, Jiao P, Song Y, Cao L, Yuan R, Gong L, et al. Host immune responses of ducks infected with H5N1 highly pathogenic avian influenza viruses of different pathogenicities. *Vet Microbiol* (2013) 166(3-4):386–93. doi: 10.1016/j.vetmic.2013.06.019

11. Huang Y, Li Y, Burt DW, Chen H, Zhang Y, Qian W, et al. The duck genome and transcriptome provide insight into an avian influenza virus reservoir species. *Nat Genet* (2013) 45(7):776–83. doi: 10.1038/ng.2657

12. Sun H, Jiao P, Jia B, Xu C, Wei L, Shan F, et al. Pathogenicity in quails and mice of H5N1 highly pathogenic avian influenza viruses isolated from ducks. *Vet Microbiol* (2011) 152(3-4):258–65. doi: 10.1016/j.vetmic.2011.05.009

13. Datan E, Shirazian A, Benjamin S, Matassov D, Tinari A, Malorni W, et al. mTOR/p70S6K signaling distinguishes routine, maintenance-level autophagy from autophagic cell death during influenza a infection. *Virology* (2014) 452-453:175–90. doi: 10.1016/j.virol.2014.01.008

14. Sun LL, Bertke MM, Champion MM, Zhu GJ, Huber PW, Dovichi NJ. Quantitative proteomics of xenopus laevis embryos: Expression kinetics of nearly 4000 proteins during early development. *Sci Rep* (2014) 4:4365. doi: 10.1038/srep04365

15. Li XZ, Zhang SN, Wang KX, Liu SM, Lu F. iTRAQ-based quantitative proteomics study on the neuroprotective effects of extract of acanthopanax senticosus harm on SH-SY5Y cells overexpressing A53T mutant alpha-synuclein. *Neurochem Int* (2014) 72:37–47. doi: 10.1016/j.neuint.2014.04.012

16. Fan H, Ye Y, Luo Y, Tong T, Yan G, Liao M. Quantitative proteomics using stable isotope labeling with amino acids in cell culture reveals protein and pathway regulation in porcine circovirus type 2 infected PK-15 cells. *J Proteome Res* (2012) 11(2):995–1008. doi: 10.1021/pr200755d

17. Gan CS, Chong PK, Pham TK, Wright PC. Technical, experimental, and biological variations in isobaric tags for relative and absolute quantitation (iTRAQ). *J Proteome Res* (2007) 6(2):821–7. doi: 10.1021/pr060474i

18. Chong PK, Gan CS, Pham TK, Wright PC. Isobaric tags for relative and absolute quantitation (iTRAQ) reproducibility: Implication of multiple injections. *J Proteome Res* (2006) 5(5):1232–40. doi: 10.1021/pr060018u

19. Bauer KM, Lambert PA, Hummon AB. Comparative label-free LC-MS/MS analysis of colorectal adenocarcinoma and metastatic cells treated with 5-fluorouracil. *Proteomics* (2012) 12(12):1928–37. doi: 10.1002/pmic.201200041

20. Battaglioni S, Benjamin D, Wälchli M, Maier T, Hall MN. mTOR substrate phosphorylation in growth control. *Cell* (2022) 185(11):1814–36. doi: 10.1016/j.cell.2022.04.013

21. Martin S, Saha B, Riley JL. The battle over mTOR: An emerging theatre in host-pathogen immunity. *PLoS Pathog* (2012) 8(9):e1002894. doi: 10.1371/journal.ppat.1002894

22. Ivanov SS, Roy CR. Pathogen signatures activate a ubiquitination pathway that modulates the function of the metabolic checkpoint kinase mTOR. *Nat Immunol* (2013) 14(12):1219–28. doi: 10.1038/ni.2740

23. Chin R, Earnest-Silviera L, Gordon CL, Olsen K, Barr I, Brown LE, et al. Impaired dendritic cell maturation in response to pandemic H1N109 influenza virus. *J Clin Virol* (2013) 56(3):226–31. doi: 10.1016/j.jcv.2012.11.009

24. Friesenhagen J, Boergeling Y, Hrincius E, Ludwig S, Roth J, Viemann D. Highly pathogenic avian influenza viruses inhibit effective immune responses of human blood-derived macrophages. *J Leukoc Biol* (2012) 92(1):11–20. doi: 10.1189/jlb.0911479

25. Tate MD, Deng Y-M, Jones JE, Anderson GP, Brooks AG, Reading PC. Neutrophils ameliorate lung injury and the development of severe disease during influenza infection. *J Immunol* (2009) 183(11):7441–50. doi: 10.4049/jimmunol.0902497

26. Shrestha N, Bahnan W, Wiley DJ, Barber G, Fields KA, Schesser K. Eukaryotic initiation factor 2 (eIF2) signaling regulates proinflammatory cytokine expression and bacterial invasion. *J Biol Chem* (2012) 287(34):28738–44. doi: 10.1074/jbc.M112.375915

27. Huber VC, Lynch JM, Bucher DJ, Le J, Metzger DW. Fc receptor-mediated phagocytosis makes a significant contribution to clearance of influenza virus infections. *J Immunol* (2001) 166(12):7381–8. doi: 10.4049/jimmunol.166.12.7381

28. Linterman MA, Denton AE, Divekar DP, Zvetkova I, Kane L, Ferreira C, et al. CD28 expression is required after T cell priming for helper T cell responses and protective immunity to infection. *Elife* (2014) 3:e03180. doi: 10.7554/eLife.03180

29. Ranadheera C, Coombs KM, Kobasa D. Comprehending a killer: The Akt/mTOR signaling pathways are temporally highjacked by the highly pathogenic 1918 influenza virus. *EBioMedicine* (2018) 32:142–63. doi: 10.1016/j.ebiom.2018.05.027

30. Hale BG, Jackson D, Chen Y-H, Lamb RA, Randall RE. Influenza a virus NS1 protein binds p85beta and activates phosphatidylinositol-3-kinase signaling. *Proc Natl Acad Sci United States America* (2006) 103(38):14194–9. doi: 10.1073/pnas.0606109103

31. Zhirnov OP, Klenk HD. Influenza a virus proteins NS1 and hemagglutinin along with M2 are involved in stimulation of autophagy in infected cells. *J Virol* (2013) 87(24):13107–14. doi: 10.1128/jvi.02148-13

32. Gack MU, Albrecht RA, Urano T, Inn K-S, Huang IC, Carnero E, et al. Influenza a virus NS1 targets the ubiquitin ligase TRIM25 to evade recognition by the host viral RNA sensor RIG-I. *Cell Host Microbe* (2009) 5(5):439–49. doi: 10.1016/j.chom.2009.04.006

33. Versteeg GA, Rajsbaum R, Sanchez-Aparicio MT, Maestre AM, Valdiviezo J, Shi M, et al. The E3-ligase TRIM family of proteins regulates signaling pathways triggered by innate immune pattern-recognition receptors. *Immunity* (2013) 38(2):384–98. doi: 10.1016/j.immuni.2012.11.013

34. Miranzo-Navarro D, Magor KE. Activation of duck RIG-I by TRIM25 is independent of anchored ubiquitin. *PLoS One* (2014) 9(1):e86968. doi: 10.1371/journal.pone.0086968

35. Gack MU, Shin YC, Joo C-H, Urano T, Liang C, Sun L, et al. TRIM25 RING-finger E3 ubiquitin ligase is essential for RIG-i-mediated antiviral activity. *Nature* (2007) 446(7138):916–20. doi: 10.1038/nature05732

36. Brown JN, Palermo RE, Baskin CR, Gritsenko M, Sabourin PJ, Long JP, et al. Macaque proteome response to highly pathogenic avian influenza and 1918 reassortant influenza virus infections. *J Virol* (2010) 84(22):12058–68. doi: 10.1128/JVI.01129-10

frontiers | Frontiers in Immunology

TYPE Original Research
PUBLISHED 23 August 2022
DOI 10.3389/fimmu.2022.972499

OPEN ACCESS

EDITED BY
Rongtuan Lin,
McGill University, Canada

REVIEWED BY
Fu Chen,
Qingdao Agricultural University, China
Yunhuan Liu,
Nanjing Agricultural University, China

*CORRESPONDENCE
Zhanyong Wei
zhanyong_wei@126.com

†These authors have contributed equally to this work and share the first authorship

SPECIALTY SECTION
This article was submitted to Viral Immunology, a section of the journal Frontiers in Immunology

RECEIVED 18 June 2022
ACCEPTED 28 July 2022
PUBLISHED 23 August 2022

CITATION
Ren Z, Yu Y, Zhang X, Wang Q, Deng J, Chen C, Shi R, Wei Z and Hu H (2022) Exploration of PDCoV-induced apoptosis through mitochondrial dynamics imbalance and the antagonistic effect of SeNPs. *Front. Immunol.* 13:972499. doi: 10.3389/fimmu.2022.972499

Exploration of PDCoV-induced apoptosis through mitochondrial dynamics imbalance and the antagonistic effect of SeNPs

Zhihua Ren[1,2†], Yueru Yu[2†], Xiaojie Zhang[2†], Qiuxiang Wang[2], Junliang Deng[2], Chaoxi Chen[3], Riyi Shi[4], Zhanyong Wei[1*] and Hui Hu[1]

[1]College of Veterinary Medicine, Henan Agricultural University, Zhengzhou, China, [2]Key Laboratory of Animal Disease and Human Health of Sichuan Province, College of Veterinary Medicine, Sichuan Agricultural University, Chengdu, China, [3]College of Animal and Veterinary Sciences, Southwest Minzu University, Chengdu, China, [4]Department of Basic Medical Sciences, College of Veterinary Medicine, Weldon School of Biomedical Engineering, Purdue University, West Lafayette, IN, United States

Porcine Deltacoronavirus (PDCoV), an enveloped positive-strand RNA virus that causes respiratory and gastrointestinal diseases, is widely spread worldwide, but there is no effective drug or vaccine against it. This study investigated the optimal Selenium Nano-Particles (SeNPs) addition concentration (2 - 10 μg/mL) and the mechanism of PDCoV effect on ST (Swine Testis) cell apoptosis, the antagonistic effect of SeNPs on PDCoV. The results indicated that 4 μg/mL SeNPs significantly decreased PDCoV replication on ST cells. SeNPs relieved PDCoV-induced mitochondrial division and antagonized PDCoV-induced apoptosis *via* decreasing Cyt C release and Caspase 9 and Caspase 3 activation. The above results provided an idea and experimental basis associated with anti-PDCoV drug development and clinical use.

KEYWORDS

Porcine Deltacoronavirus, selenium nano-particles, apoptosis, mitochondrial dynamics, swine testicular cells

Abbreviations: Caspase, Cysteinyl aspartate specific proteinase; Cyt C, Cytochrome C; Drp1, Dynamin-like protein1; Fis1, Mitochondrial fission protein1; LLC-PK, LLC porcine kidney cell line; Mfn1/2, Mitofusin1/2; OPA1, Optic Atrophy1; PDCoV, Porcine deltacoronavirus; qPCR, Quantitative Real-time PCR; SeNPs, Selenium Nano-Particles; ST, Swine testis; WB, Western Blotting.

Introduction

Porcine Deltacoronavirus (PDCoV), an enveloped RNA virus, is a swine gastrointestinal pathogenic virus. Infection with the virus causes diarrhea, dehydration, and vomiting in sows and piglets (1–3). PDCoV was first detected in Hong Kong, China, in 2012 (4) and has spread to many regions and countries worldwide (5–10), causing colossal impact and economic losses to the global swine industry. In recent years, many studies have reported the isolation of PDCoV from other species, such as cattle and poultry (11–13). In addition to infecting animals, researchers identified PDCoV, which come from two distinct viral lineages in plasma samples of three Haitian children with acute undifferentiated febrile illness (14). These indicate that PDCoV has the capability of cross-species transmissions, which deserve high priority. Furthermore, studies have reported that added trypsin could increase virus titer, accompanied by visible CPE compared to no or lower trypsin concentrations (15, 16).

Apoptosis is programmed cell death that reduces the size of apoptotic cells, chromatin consolidation in the nucleus, and degradation and fragmentation of DNA under physiological or pathological conditions (17, 18). PDCoV infection induces tissue or cell apoptosis. Duan et al. detected a great number of apoptotic signals in the jejunum and ileum of pigs infected with the PDCoV strain CHN-HN-1601 by oral administration with 1 × 106 $TCID_{50}$ (19). The experiment of Jung et al. showed that piglets inoculated orally with 8.8 - 11.0 log_{10} genomic equivalents (GE) of US PDCoV strain OH-FD22 do not induce apoptosis in gut cells but induce LLC-PK and ST cells apoptosis *in vitro* (1). Therefore, the effect of this virus on apoptosis deserves further study.

Cytochrome C (Cyt C) is a crucial apoptotic signaling molecule, and its release from mitochondria is a key event in apoptosis (20). Cyt C released into the cytoplasm binds to Apoptosis protease activating factor-1 (Apaf-1) to form an apoptotic complex, which activates Caspase 9 and Caspase 3 to activate the apoptotic cascade pathway and ultimately induce apoptosis (21, 22). Mitochondria are important organelles in cells. Many studies have shown that the abnormal function of mitochondria is closely related to the occurrence of apoptosis. According to previous studies, approximately 15% of Cyt C is bound to the outer and inner membrane of the mitochondrial membrane gap in a normal physiological environment. Still, this binding is not tight and is easily separated by external stimuli. The remaining 85% of Cyt C is located in the mitochondrial cristae (23, 24), and Cyt C release is associated with mitochondrial dynamics homeostasis and its associated proteins. Mitochondrial dynamics is an important event that affects the morphology and number of mitochondrial networks; this process is regulated by mitochondrial fission proteins (Drp1, Fis1) and mitochondrial fusion proteins (Mfn1, Mfn2, and OPA1); when the dynamic balance of mitochondria is disrupted, it can lead to changes in mitochondrial morphology and number or structural damage, which affects many biological processes, including apoptosis (22).

Selenium is a trace element that is essential in the body and inhibits the replication of many viruses, making it an excellent candidate for treating viral infections. According to research, selenium-deficient mice are more susceptible to Coxsackie virus B (CVB) and influenza virus (IV), as well as having more severe organ and tissue damage (25, 26). Furthermore, the cure rates of the new coronavirus (SARS-CoV-2) is strongly related to selenium intake and status in different Chinese areas (27). Serum selenium levels are linked to the prognosis of Corona Virus Disease 2019 (COVID-19), and higher serum selenium levels are related to a higher cure rate (28). In a previous study by our group, it was discovered that Se-Met inhibited PDCoV replication *in vitro*, and selenium could alleviate the viral infection-induced oxidative stress, and increased the levels of various cytokines in host cells, boosting the level of cellular immunity to inhibit virus replication (29). To sum up, selenium may be a promising drug for treating COVID-19 and other virus infections, allowing for the development of new and highly effective antiviral drugs. Furthermore, Selenium Nano-Particles (SeNPs) are characterized by high activity, low toxicity, and easy absorption by the human body, and exhibit good antiviral activity against dengue virus (DENV) in Hela and HepG2 cells (30). SeNPs has powerful antioxidant and cytotoxicity-reducing properties (31). On the one hand, SeNPs can promote apoptosis of cancer cells *in vitro* through the mitochondrial pathway (32), and on the other hand, they have antioxidant, anti-oxidative stress, and anti-apoptotic effects on focal tissues (33). In addition, SeNPs can reduce mitochondrial dysfunction in disease states, thereby reducing apoptosis (34).

We cultured swine testis (ST) cells *in vitro*, performed and compared the optimal trypsin addition concentration in PDCoV infection, and investigated the potential relationship between mitochondrial homeostasis-related proteins and apoptosis and apoptotic proteins under PDCoV infection, as well as the effect of SeNPs addition on virus replication and apoptosis, providing a theoretical foundation for drug research and development and clinical medication against PDCoV.

Materials and methods

Cells and virus

Porcine testicular cells were cultured with 90% DMEM high sugar medium, 9% fetal bovine serum, 1% Penicillin-Streptomycin-Mycoplasma Removal Agent Solution, incubated at 37°C. The PDCoV HNZK-04 strain (GenBank accession no: MH708124.1) isolated and preserved according to the method of Jin (35) et al. was used in this experiment. ST cells were infected with PDCoV (MOI=0.07).

Drugs

SeNPs were purchased from Yantai Jialong Nano Industry Co., Ltd., lot 202107027, 100g, red liquid. Trypsin (powder) was purchased from Sigma Aldrich.

Characterisation and identification of SeNPs

SeNPs were characterized using transmission electron microscopy (TEM) and Energy Dispersive X-ray (EDX). TEM was used to observe the morphological structure of the SeNPs, including shape and size, and EDX was used to identify some of the elements. The experimental characterization was carried out at the Fuda testing group in Shanghai.

CCK-8 assay for cytotoxicity of trypsin and SeNPs

The CCK-8 method was used to assess the cytotoxicity of trypsin and SeNPs *in vitro*. A control group (cells and culture medium) and a test group (cell culture medium, trypsin, or SeNPs) were set up. In 96-well plates, cells were seeded and incubated overnight. After two D-Hanks washes, trypsin was added at 2, 3, 4, 5, 6, 7, 8, 9, and 10 μg/mL (n=6). After washing the cells twice with D-Hanks solution, CCK-8 solution was added, and absorbance at 450 nm was measured using an enzyme marker. After pre-experimentation, SeNPs were added to the culture medium at final concentrations of 0, 1, 2, 4, 6, 8, 10, 12, 14 μg/mL. The preceding experimental steps were followed.

The detection of viral replication and mitochondrial dynamics related-protein mRNA expression by RT-qPCR

Total cellular RNA was extracted using the traditional Trizol method. cDNA was synthesized and amplified using the TransScript All-in-One First-Strand cDNA Synthesis SuperMix for the qPCR kit, and cDNA was quantified in the CFX Connect real-time PCR detection system (BIO-RAD). Relative gene expression levels were calculated using Equation $2^{-(\Delta\Delta Ct)}$ (using β-actin as the reference gene). Primers were designed according to the NCBI database, and Primer Premier 5 software and the primer sequences shown in Table 1 were pre-experimentally screened.

The experiment "The effect of trypsin on PDCoV-infected ST cells" was divided into two groups: virus (respectively added 1, 2, 3 and 4 μg/mL trypsin) and control and PDCoV replication were measured 48 h after viral infection (n=6).

TABLE 1 Primer sequence.

Gene name	Sequence (5'-3')
Mpro	F: CTTATTCTGCTTTGGCTGCTC
	R: GGATATGAAGGTTAGTACGGC
β-actin	F: GGCACCACACCTTCTACAACGAG
	R: TCATCTTCTCACGGTTGGCTTTGG
Drp1	F: AATTGAGGCCGAGACAGACC
	R: GGAACTCGATGTCAGGAGGC
Fis1	F: ACAGAGCCACAGAACAACC
	R: AGTCCAATGAGTCCAGCC
Mfn1	F: AAGGAACGGATGGAGATAAAGC
	R: TGCGACCAAAACGAAGACATC
Mfn2	F: GGGCATTCTCGTTGTTGG
	R: AGCTTCTCGCTGGCGTACT
OPA1	F: CGAAAGAACCTTGAATCCC
	R: AATAGAAGCCTCTCCGACA

The experiment "The mRNA expression of mitochondrial dynamics-related proteins in ST cells after PDCoV infection" was divided into two groups: virus and control, and RT-qPCR assays were performed at 6, 24, and 48 h after PDCoV infection (n=6).

The experiment "The inhibitory effect of SeNPs on PDCoV replication" was divided into four groups: virus, virus plus 2μg/mL SeNPs, virus plus 4μg/mL SeNPs and virus plus 8μg/mL SeNPs. RT-qPCR was used to assess intracellular viral replication 6, 24, and 48 h after PDCoV infection (n=6).

Infectivity of PDCoV on ST cells at different trypsin concentrations by indirect immunofluorescence assay

The cells were seeded with cell slides, and after culturing for a certain time, the slides were stained, and the fluorescence was observed using an Olympus inverted biological microscope.

The test was grouped into control and viral groups and tested at 48 h post-infection.

Western blotting detects the expression of ST cell apoptosis-related proteins and mitochondrial dynamics-related proteins after PDCoV infection

Total Protein: Cellular proteins were extracted according to the extraction kit, and concentrations were determined using the BCA Protein Concentration Assay Kit. Mitochondrial proteins: the cell pellet was collected after the cells were digested, triturated 30 - 40 times on ice with a homogenizer added to HEPES solution, and after multiple centrifugal cleavages, the

supernatant was collected to determine the protein concentration using a BCA protein concentration assay kit.

The experiment "Effect of SeNPs on the expression of mitochondrial dynamics-related proteins in ST cells after PDCoV infection" was grouped into virus ,control, SeNPs, and virus plus SeNPs groups, and WB assays were performed at 6, 24, and 48 h (n=3).

The experiment "Effect of SeNPs on the expression of apoptosis-related proteins in PDCoV-infected cells" was divided into four groups: control, virus, SeNPs, and virus plus SeNPs groups, with WB assay at 6, 24, and 48 h (n=3).

Flow Cytometry- Annexin-FITC/PI double-staining assay for apoptosis detection

Cells were stained according to the Annexin V-FITC Apoptosis Detection Kit (Wuhan servicebio Technology Co., Ltd.), followed by 100 - 200 μL cell suspension for apoptosis detection using flow cytometry FITC and PE passages, with blank and isotype control tubes first, followed by tubes to be tested. Flowjo V10 software was used to analyze the results.

The test "Inhibition of PDCoV-induced ST cell apoptosis by SeNPs" was divided into control, virus, SeNPs, and virus plus SeNPs groups and assayed by flow cytometry at 6, 24, and 48 h (n=3).

Statistical analysis

The test results are expressed as mean ± standard deviation. The experimental data were sorted and unified in Excel, and SPSS 21.0 software was used for significant difference analysis, and the least significant difference (LSD) method was used to compare the data, respectively. $P < 0.05$ indicates statistical significance.

Results

Optimal trypsin concentration selected under PDCoV infection

The addition of trypsin at ≤ 4 μg/mL had a non-significant promotion effect on ST cell viability compared to the control group ($P > 0.05$), while the addition of trypsin at ≥ 5 μg/mL inhibited the growth of ST cells, with a significant difference between 7 - 10 μg/mL of trypsin ($P < 0.01$) (Figure 1). Based on the results of the CCK-8 test, settings of 1, 2, 3, and 4 μg/mL of trypsin were used for subsequent tests.

Following that, we looked at the expression of PDCoV M protein mRNA at various trypsin concentrations. As shown in Figure 2, in the concentration range of 1 - 4 μg/mL, viral replication increased significantly ($P < 0.01$) with the increase of trypsin concentration compared to the group without trypsin, in which the viral replication was highest after the addition of 4 μg/mL trypsin, about 70.4 times higher than that of the group without trypsin.

To further confirm the optimal trypsin concentration for PDCoV infection of ST cells, we used the indirect immunofluorescence method to observe the infection of ST cells by PDCoV after adding different concentrations of trypsin. As shown in Figure 3, the cells with different concentrations of trypsin added could all observe obvious green fluorescence, whereas no fluorescence was observed in the group of cells without added trypsin; and the density of fluorescence increased with the increase of trypsin concentration in the range of 1 - 4 μg/mL, indicating that the higher the concentration of trypsin, the higher the expression of N protein, i.e., the more ST cells were infected with PDCoV. The density of cells infected with PDCoV was greatest at a trypsin concentration of 4 μg/mL, and therefore the addition of 4 μg/mL of trypsin was chosen for all subsequent experiments.

Characterisation of SeNPs

The nanoparticles were subsequently analyzed by EDX (Figures 4, 5). The characteristic absorption peaks of SeNPs were present in the spectra at 1.37, 11.22, and 12.49 keV, respectively. in addition, signals of elements such as C and O were also present. the SeNPs The concentration of SeNPs was 2.8 mg/mL.

Assay SeNPs on cell viability

The cytotoxicity of SeNPs to ST cells in the range of 0 - 14 μg/mL (as determined by pre-experiment) was assessed using the CCK-8 method. As a result, SeNPs were not significantly cytotoxic in the range of 0 - 8 μg/mL, and the cell survival rate was greater than 100% (Figure 6). The data showed that the maximum concentration of SeNPs was 8 μg/mL. Based on this, 2, 4, and 8 μg/mL were selected for subsequent SeNPs antiviral assays.

SeNPs inhibit the replication of PDCoV in ST cells

PDCoV-infected ST cells were treated with 2, 4, and 8 μg/mL of SeNPs, and the expression of viral M protein mRNA was measured after 6, 24, and 48 h. As a result, all three concentrations of SeNPs inhibited viral replication significantly ($P < 0.01$) after 6 h of treatment, with the replication of 4 μg/mL SeNPs reaching approximately 0.318 times that of the non-SeNPs group (Figure 7). As the treatment time increased, the inhibitory effect of SeNPs became more significant, with the

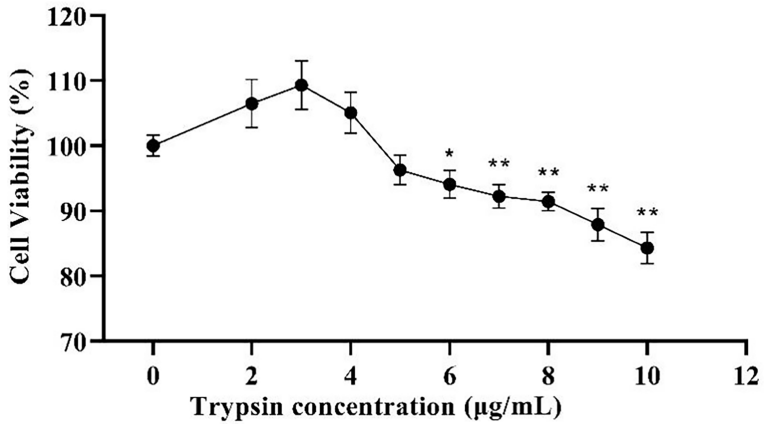

FIGURE 1
Effects of different trypsin concentrations on the viability of ST cells. * indicates that the difference is significant ($P < 0.05$) compared with the group added with 0 μg/mL trypsin, ** indicates that the difference is extremely significant ($P<0.01$), and no indication indicates that the difference is not significant ($P > 0.05$), n=6.

three concentrations at 24 h being 0.042, 0.030, and 0.021 times compared to the replication of the PDCoV groups, and at 48 h reaching 0.026, 0.003, and 0.004 times compared to the replication of the PDCoV groups, respectively. The above results demonstrate that SeNPs have a good anti-PDCoV effect and that this effect is enhanced with increasing duration of infection. Therefore, 4 μg/mL SeNPs were selected for subsequent experimental studies in this trial.

SeNPs repress PDCoV-induced apoptosis in ST cells

It has been reported that PDCoV infection induces apoptosis in LLC-PK and ST cells. Our experiments demonstrated the inhibitory effect of SeNPs on PDCoV replication. To investigate whether SeNPs inhibit PDCoV-induced apoptosis, we measured the apoptosis rate by Annexin-FITC/PI double-staining assay

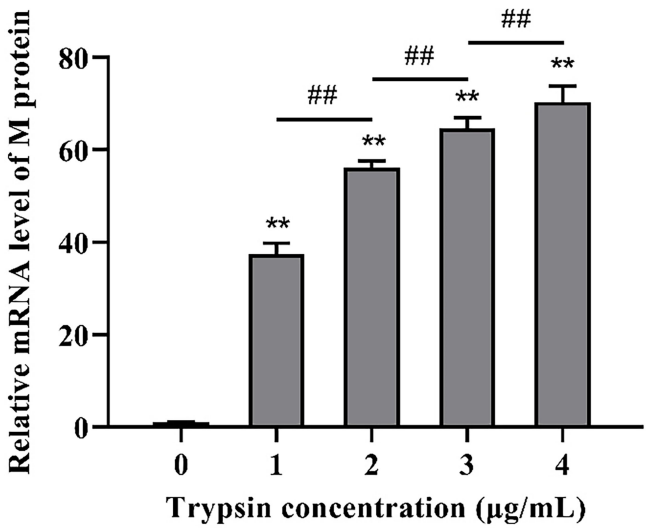

FIGURE 2
Effects of different trypsin concentrations on PDCoV replication. **indicates that the difference is extremely significant compared with the 0 μg/mL trypsin group ($P < 0.01$); ## indicates extremely significant difference ($P < 0.01$); No notation indicates that the difference is not significant ($P > 0.05$), n=6.

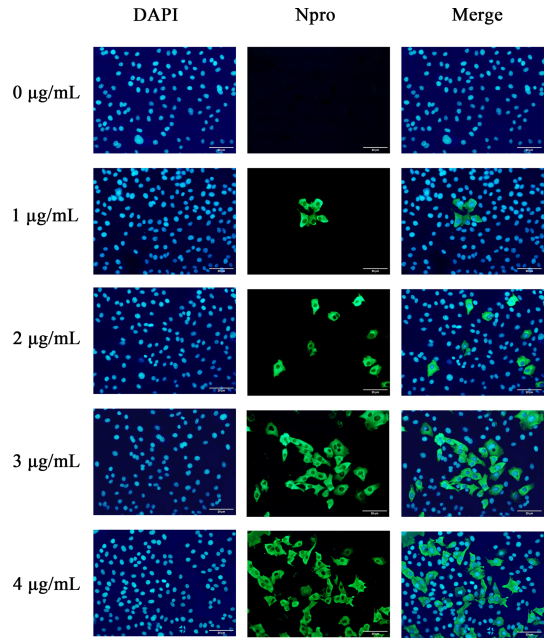

FIGURE 3
Changes in ST cells infected with PDCoV under different trypsin concentrations (400×). DAPI-stained nuclei are blue after UV light excitation and green after blue light excitation after primary and secondary antibodies binding to viral proteins.

after 6, 24, and 48 h treatment of infected cells with SeNPs. According to the findings in Figure 8, after 6h of PDCoV infection, the apoptosis rate increased slightly compared to the control group. There was no significant difference between the apoptosis rate in the SeNPs-treated group and the PDCoV group ($P > 0.05$), indicating that PDCoV infection had a lower effect on apoptosis in the early stage. The addition of SeNPs treatment did not inhibit the early infection-induced apoptosis few cells. With the increase in infection time, the late apoptosis rate, and total apoptosis rate were all significant increases in the PDCoV group compared with the control group after 24 h ($P < 0.01$). After SeNPs treatment of infected cells, the difference in early apoptosis rate was not significant ($P > 0.05$), late apoptosis and total apoptosis rates were significantly decreased ($P < 0.01$), and there was no significant change in the SeNPs group compared to the control group ($P > 0.05$). At 48h, compared to the controlgroup, the early apoptosis rate, late apoptosis rate and total apoptosis rateof the viral group were significantly increased ($P < 0.01$ or $P < 0.05$), and the late apoptosis rate and total apoptosis rate were significantly decreased after SeNPs treatment ($P < 0.01$). The above results indicated that PDCoV could induce apoptosis of ST cells *in vitro*, and the addition of SeNPs could significantly inhibit the apoptosis induced by virus. And the longer the infection time, the more the number of apoptotic cells, the more obvious the effect of its inhibition.

SeNPs inhibit PDCoV-induced Cyt C release

Cyt C is an important apoptotic factor normally found in mitochondria and is released from mitochondria to the cytoplasm when apoptosis is stimulated, which is a critical event in apoptosis. The cytoplasmic Cyt C content was determined, and the results are shown in Figure 9. At the three time points, the control group had very few protein amounts of Cyt C in the cytoplasm, and the cytoplasm contained almost no Cyt C at 6 and 24 h, indicating that mitochondria release little or almost no Cyt C into the cells

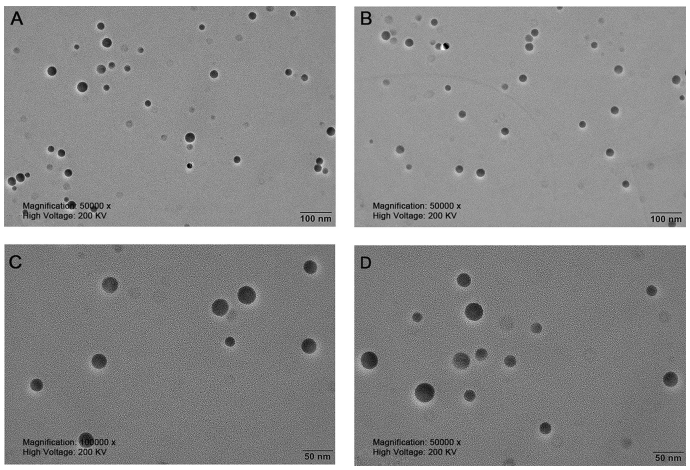

FIGURE 4
Transmission electron microscopy of SeNPs. **(A, B)** are magnified 50,000 times. **(C, D)** are magnified 100,000 times.

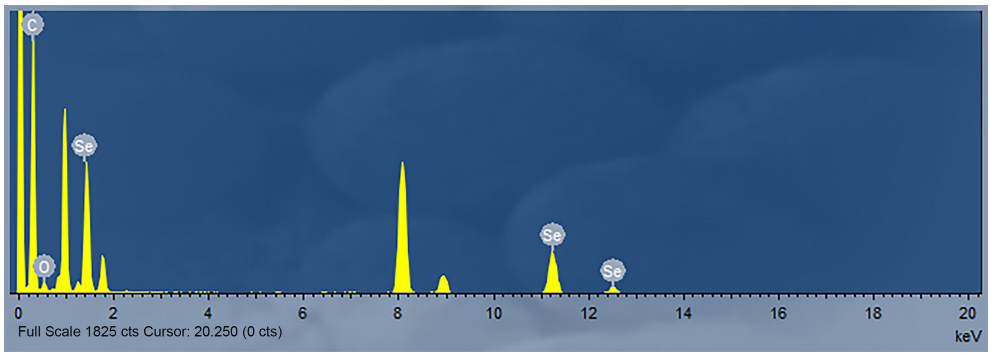

FIGURE 5
Energy Spectrum Analysis of SeNPs.

under normal conditions. In contrast, the cytoplasmic Cyt C contents were significantly higher in the PDCoV-infected groups at 6, 24, and 48 h than those in the control groups ($P < 0.01$) and increased with increasing infection duration, indicating that PDCoV infection could conduce the release of Cyt C from mitochondria, and the longer the duration of infection, the greater the amount of release. Cyt C content in the cytoplasm of the SeNPs-treated group (PDCoV+SeNPs) was significantly lower compared with the PDCoV group, and the differences were all highly significant ($P < 0.01$), while the SeNPs-treated group was significant ($P < 0.05$) at 6 h compared with the Control group. The SeNPs group was higher than the Control group at 6 h, 24 h and 48 h, but the differences were not significant ($P > 0.05$). The above results suggest that SeNPs treatment reduced Cyt C release, while the addition of SeNPs alone had no significant effect on Cyt C release.

SeNPs inhibit PDCoV-induced Caspase 3 and 9 activation

After Cyt C is released into the cells, it activates downstream Caspase 9 and Caspase 3, further triggering the apoptotic cascade. To explore whether the two apoptotic proteins are activated after PDCoV infection and the effect of SeNPs treatment, we examined the activated Caspase 9 and Caspase 3 in the cells by the WB method, and the results are presented in Figure 10. The amount of activated Caspase 9 and Caspase 3 protein increased significantly after PDCoV infection compared

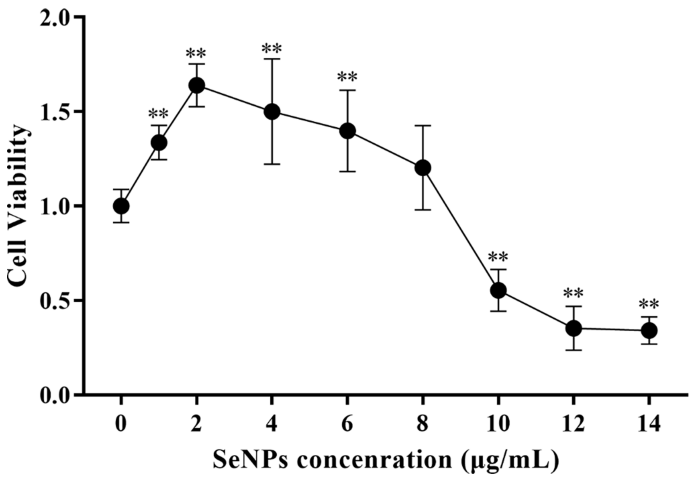

FIGURE 6
Effects of different SeNPs concentrations on the viability of ST cells In the figure ** indicates that the difference is extremely significant compared with the group added with 0 μg/mL SeNPs ($P < 0.01$), and no indication indicates that the difference is not significant ($P > 0.05$), n=6.

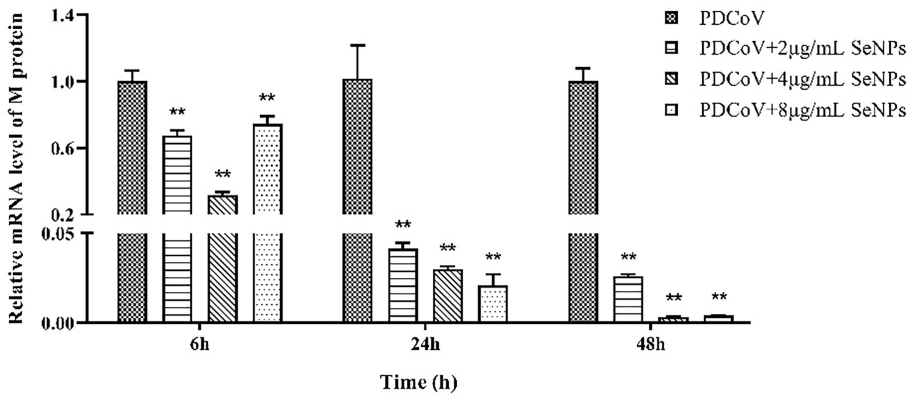

FIGURE 7
Effects of different concentrations of SeNPs on PDCoV replication in ST cells. ** indicates an extremely significant difference between different concentrations of SeNPs treatment group and PDCoV group (P <; 0.01), and no indication indicates no significant difference ($P > 0.05$), n=6.

to the control group, and the difference was significant ($P < 0.01$). And the longer the infection, the higher the expression of the two proteins. At 24 h and 48 h, after SeNPs were added, Caspase 9 protein content was lower than that of the PDCoV group, and the difference was significant ($P < 0.01$), and there was no significant change in protein content in the SeNPs group compared to the control group. Meanwhile, Caspase 3 levels were significantly lower in the SeNPs-treated group than in the PDCoV-infected group at 24 and 48 h ($P < 0.01$).

SeNPs alleviate PDCoV-induced increased mitochondrial division

To see if SeNPs' inhibition of PDCoV-induced Cyt C release was associated with mitochondrial dynamics, we examined the changes in dynamics-related proteins in mitochondria after PDCoV infection and SeNPs treatment. The outcomes are depicted in Figure 11. Drp1 protein expression was significantly increased ($P < 0.05$ or $P < 0.01$) after 24h and 48 h PDCoV infection, but there was no effect on Fis1 protein expression. In contrast, the expression of mitochondrial fusion proteins Mfn1, Mfn2, and OPA1 significantly reduced after 24h and 48 h PDCoV infection ($P < 0.05$ or $P < 0.01$). According to the data presented above, PDCoV infection increases mitochondrial fission protein levels while decreasing fusion protein levels. And, within a certain range, the longer the infection time, the greater the amount of change. After adding SeNPs to infected cells, Drp1 protein levels reduced, while Mfn1, Mfn2, and OPA1 protein levels improved compared to the virus-infected group. In summary, PDCoV disrupted the dynamic balance of mitochondria in ST cells, resulting in increased mitochondrial division and decreased fusion, and SeNPs treatment can mitigate the excessive mitochondrial division to some extent.

Discussion

PDCoV primarily affects the digestive tract of piglets *in vivo*, but studies have revealed that LLC-PK and ST cells are most susceptible to PDCoV *in vitro* (16) and that PDCoV can be isolated and passed continuously in these two cells, making them the most commonly used for PDCoV proliferation *in vitro*. Trypsin has been demonstrated to increase viral infectivity in cells (36). In a similar vein, after 24 h of incubation on ST cells without trypsin, no cells were infected with PDCoV by immunofluorescence, and when 4 μg/mL of trypsin was added, virus replication increased 70.4 times that of the non-addition group, which could be because trypsin promotes PDCoV attachment to cells (37) cleaving and activating the PDCoV S protein, allowing the virus to enter cells (38). Trypsin has also been proposed to promote viral replication by provoking the fusion of infected cells' intercellular membranes (39).

In this experiment, we used an apoptosis assay to show that PDCoV caused a significant increase in the apoptosis rate of ST cells after 24 and 48 h of infection and that the longer the infection duration, the higher the apoptosis rate, indicating that PDCoV-induced apoptosis of ST cells in the middle and late stages of infection, and the induction of apoptosis became more obvious with the increase of infection duration, consistent with results by Jung et al. (1). Several studies showed that it promoted viral infection and replication by regulating apoptosis. The cytomegalovirus (CMV) viral protein vMIA blocks apoptosis by binding to the pro-apoptotic protein Bax, which is recruited to and bound to mitochondria. Rotavirus (RV) promotes the

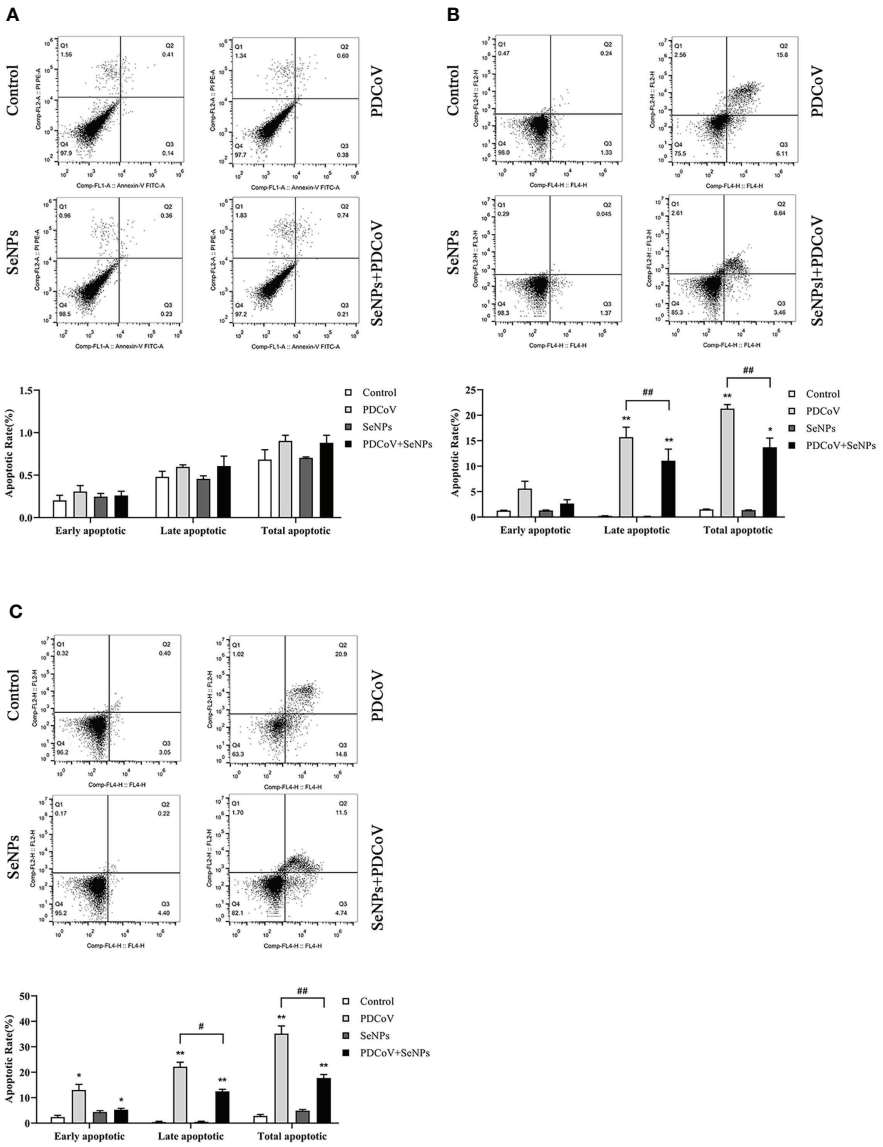

FIGURE 8
Effect of SeNPs on apoptosis induced by PDCoV. **(A–C)** are the flow quadrant diagram and apoptosis rate change diagram of each treatment group at 6, 24, and 48 h, respectively. * indicates that the difference is significant compared with the control group ($P < 0.05$), ** indicates that the difference is extremely significant compared with the control group ($P < 0.01$); # indicates that there is a significant difference between the PDCoV group and the PDCoV+SeNPs group ($P < 0.05$), ## indicates that there is a significant difference between the PDCoV group and the PDCoV+SeNPs group ($P < 0.01$), and there is no significant difference ($P > 0.05$) in the unlabeled expression, n=3.

spread of virus progeny by activating the mitochondrial route of apoptosis in the late stages of infection, allowing viral particles to spread to surrounding cells (40, 41).

In most cell death models, the release of Cyt C from mitochondria results in the formation of an apoptosome with Apaf-1, which sequentially activates Caspase 9 and Caspase 3, triggering the apoptotic cascade response (23, 24). This experiment found that the amount of Cyt C protein in the cytoplasm significantly increased with time after PDCoV infection. Subsequent detection showed that the expression of Cyt C downstream proteins Caspase 9 and Caspase 3 increased after virus infection, and the content was positively correlated with the infection time, indicating that PDCoV induces the mitochondrial release of Cyt C and then activates the Caspase apoptosis cascade. Mitochondrial dynamics are tightly linked to apoptosis. Many studies have argued that increased mitochondrial division leads to apoptosis, and many viruses take advantage of this to disrupt the dynamics balance to induce apoptosis (42). Therefore, we investigated whether PDCoV disrupts mitochondrial morphology by interfering with

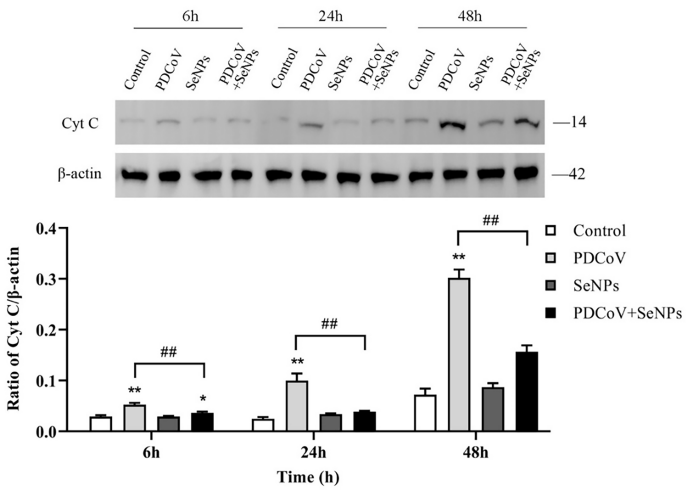

FIGURE 9
Effects of SeNPs on Cyt C content in the cytoplasm of ST cells infected with PDCoV. Top is immunoblot bands of Cyt C in each treatment group at 6, 24, and 48 h. At the bottom is a histogram after analyzing and calculating the ratio of grayscale values of Cyt C. * indicates that the difference is significant compared with the control group ($P < 0.05$), ** indicates that the difference is extremely significant compared with the control group ($P < 0.01$); ## indicates that there is a significant difference between the PDCoV group and the PDCoV + SeNPs group ($P < 0.01$), and there is no significant difference ($P > 0.05$) in the unlabeled expression, n=3.

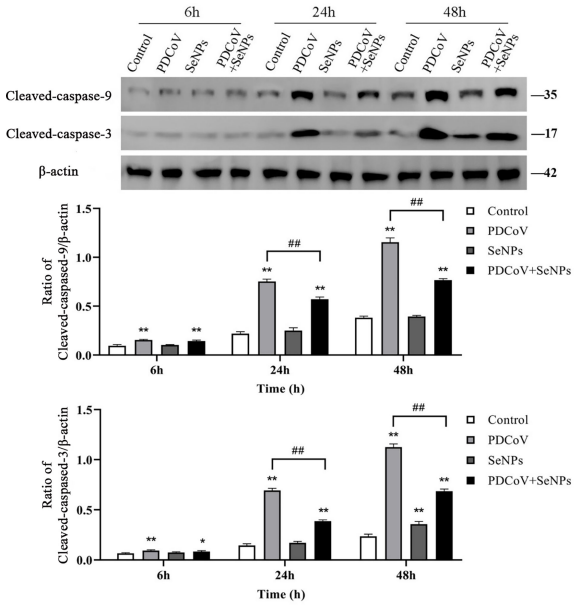

FIGURE 10
Effect of SeNPs on apoptosis-related proteins of ST cells infected with PDCoV. Top is immunoblot bands of Cleaved-caspase-3 and Cleaved-caspase-9 in each treatment group at 6, 24, and 48 h. At the bottom is a histogram after analyzing and calculating the ratio of grayscale values of the Cleaved-caspase-3 and Cleaved-caspase-9. * indicates that the difference is significant compared with the control group ($P < 0.05$), ** indicates that the difference is extremely significant compared with the control group ($P < 0.01$); ## indicates that there is a significant difference between the PDCoV group and the PDCoV + SeNPs group ($P < 0.01$), and there is no significant difference ($P > 0.05$) in the unlabeled expression, n=3.

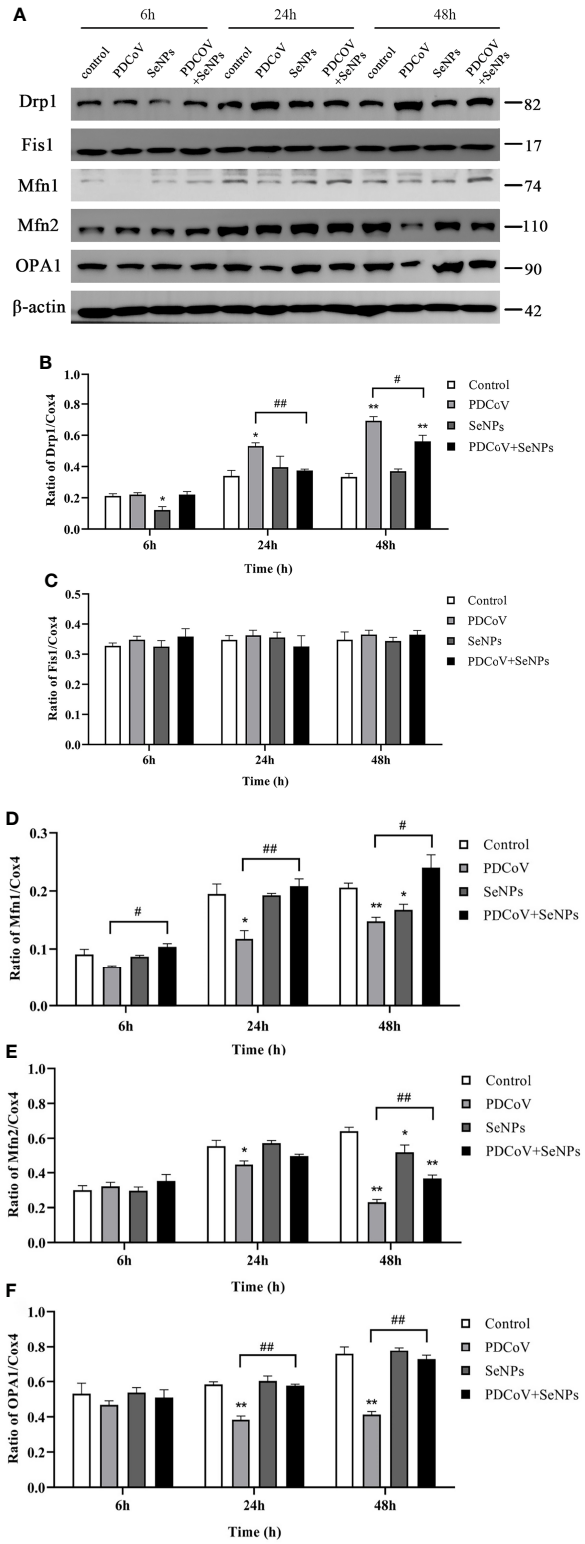

FIGURE 11 (Continued)

FIGURE 11 (Continued)
Effect of SeNPs on mitochondria dynamics-related proteins of ST cells infected with PDCoV. **(A)** Immunoblot bands of mitochondrial dynamic-related proteins Drp1, OPA1, Fis1, Mfn1, and Mfn2 in each treatment group at 6, 24, and 48 h; **(B–F)** are the histograms after analyzing and counting the gray value ratios of the target protein and the reference protein of Drp1, OPA1, Fis1, Mfn1, and Mfn2 respectively. * indicates that the difference is significant compared with the control group ($P < 0.05$), ** indicates that the difference is extremely significant compared with the control group ($P < 0.01$); # indicates that there is a significant difference between the PDCoV group and the PDCoV+SeNPs group ($P < 0.05$), ## indicates that there is a significant difference between the PDCoV group and the PDCoV+SeNPs group ($P < 0.01$), and there is no significant difference ($P > 0.05$) in the unlabeled expression, n=3.

mitochondrial dynamics, further leading to the release of Cyt C. After PDCoV infection, we identified a substantial increase in the mitochondrial fission protein Drp1 and a decrease in the expression of the fusion proteins Mfn1, Mfn2, and OPA1, indicating that the virus causes excessive mitochondrial division. Similar to the results of this assay, Mukherjee et al. discovered that RV infection of cells resulted in increased mitochondrial division, the release of Cyt C, and consequent activation of the apoptotic pathway by promoting the expression of the fission protein Drp1 and degradation of the fusion protein Mfn1 (41). It has also been demonstrated that Drp1-mediated mitochondrial division induces the release of Cyt C. When Drp1 expression is inhibited, it reduces fragmented mitochondria and inhibits Cyt C release and nuclear DNA fragmentation (43). OPA1 is a mitochondrial cristae remodeling protein stabilizing cristae morphology and limiting intracristae protein release. The significant decrease in OPA1 expression observed in this experiment could also be a crucial factor in the release of Cyt C from mitochondrial cristae. The relationship between mitochondrial division and apoptosis is still being debated. Although mitochondrial division is commonly thought to be an early event in apoptosis, some studies have found that inhibiting mitochondrial division only had a minor effect on Cyt C release and had no effect on the release of other apoptotic factors in mitochondria, implying that mitochondrial division may not be the primary cause of Cyt C release (44). It has also been argued that mitochondrial division is only essential when large amounts of Cyt C are required to activate the Caspase pathway (45). Hence more studies are needed to clarify the relationship between the two in the future.

In our another experiment, ST cells were treated by four kinds of interactions between SeNPs and virus *in vitro*. Samples were collected to detect the amount of virus replication in cells to explore the antiviral effect of SeNPs. The experiment contains anti-adsorption effect of SeNPs (equal volumes of virus and SeNPs were added directly to the cells, incubated for 1 h at 4°C refrigerator, washed, added to trypsin culture medium, and incubated in the cell incubator), preventive effect of SeNPs (virus was added to the cells pretreated with SeNPs for 1 h, incubated for 1 h in the cell incubator, washed, added to culture medium, and incubated in the cell incubator), therapeutic of SeNPs (virus pretreated cells, incubated in the cell incubator for 1 h, washed, added to the culture medium containing trypsin and SeNPs and placed in the cell incubator), and direct inactivation of SeNPs (virus and SeNPs mixture preincubated at 4°C for 1 h, incubated in the cell incubator for 1 h, washed, added to the culture medium and placed in the cell incubator). It was found (data not shown in this paper) that direct inactivation of the virus by SeNPs was nor significant. And the optimal effect related to SeNPs is therapeutic effect compared to anti-PDCoV adhesion effect, protective effect, direct inactivation effect. Therefore, we suggest that SeNPs inhibits apoptosis caused by viruses by alleviating excessive mitochondrial division, but deeper mechanism needs further trials to verify.

There are no effective drugs for PDCoV treatment or prevention. Although many studies have shown that certain drugs can inhibit PDCoV replication (46–49), these drugs are not used in production. As a result, finding an anti-PDCoV drug that can be applied in production is a problem that must be solved. In this study, we discovered that the viral M-gene replication reached 0.318, 0.030, and 0.003 times respectively compared to the control groups at 6, 24, and 48 h after adding 4 μg/mL of SeNPs, indicating that SeNPs had a strong anti-PDCoV ability. The inhibition of virus replication by selenium *in vitro* has been reported in various reports. Diphenyl diselenide (PhSe) inhibited the replication of herpes simplex virus 2 (HSV-2) in Vero cells (50). Na_2SeO_3 inhibited the replication of the hepatitis B virus (HBV), and the inhibitory effect increased with increasing Na_2SeO_3 concentration or treatment time (51). In Madin-Darby Canine Kidney (MDCK) cells, modified SeNPs inhibit the H1N1 influenza virus and Caspase 3-mediated apoptosis caused by virus infection (52, 53). Our previous research found that selenomethionine (Se-Met) inhibited PDCoV replication on LLC-PK cells (29). However, most of the above studies are on inorganic and organic selenium, and there are few studies on the antiviral effects of SeNPs. We compared the results of this trial to the previous ones and discovered that SeNPs had better anti-PDCoV effects than Se-Met, which could be due to SeNPs' easier absorption, implying that SeNPs have greater antiviral potential than organic and inorganic selenium and could be a viable drug for the treatment of PDCoV and other virus infections.

Current studies associated selenium are primarily focused on its antiviral and antioxidant properties, with few reports linking selenium to apoptosis. Some studies have shown that selenium can inhibit apoptosis caused by certain toxic agents. Wang et al. discovered that L-selenomethionine reduced excessive apoptosis induced by Ammonia (NH3) and abnormal changes in

mitochondrial dynamics-related proteins (54). Selenium-rich yeast (SeY) attenuated potassium dichromate ($K_2Cr_2O_7$) induced apoptosis in poultry kidney tissue *via* modulating the mitogen-activated protein kinase pathway (55). Wang et al. manifested that sodium selenite (SS) and (Se-Met) could reduce tertbutyl hydroperoxide (TBHP) induced oxidative stress, inhibited mitochondrial fission and apoptosis of nucleus pulposus cells (NPCs) (56). *In vitro* studies have shown that selenium supplementation can inhibit viral infection by increasing glutathione peroxidase 1 (Gpx1) activity and reducing reactive oxygen species (ROS) content, JNK phosphorylation levels (57–59).

According to our findings, adding SeNPs to infected cells significantly reduced the apoptosis rate and inhibited the release of Cyt C and the activation of Caspase 9 and Caspase 3, implying that SeNPs inhibit PDCoV-induced apoptosis. Subsequent experiments revealed that SeNPs could, to some extent, reduce the increase in Drp1 protein level caused by PDCoV and elevate the decrease in Mfn1, Mfn2, and OPA1 protein levels caused by PDCoV. In summary, it may be inferred that SeNPs exerted antiviral effects by alleviating excessive mitochondrial division and inhibiting Cyt C release in the middle and late stages of PDCoV infection, thereby antagonizing virus-induced apoptosis and thus inhibiting the propagation and spread of virus particles, but more studies are needed to confirm this point.

Data availability statement

The original contributions presented in the study are included in the article/supplementary materials. Further inquiries can be directed to the corresponding author.

Ethics statement

Ethical review and approval was not required for the study on human participants in accordance with the local legislation and institutional requirements. Written informed consent from the patients/participants OR patients/participants legal guardian/next of kin was not required to participate in this study in accordance with the national legislation and the institutional requirements.

Author contributions

ZR, ZW, and HH contributed to the conception and design of the study. ZR, YY, XZ, QW performed the experiments. CC, JD, ZW, RS performed statistical analysis. YY and RS wrote the first draft of the manuscript. The rest reviewed and revised the manuscript. All authors reviewed the manuscript, read and approved the submitted version.

Funding

This study was supported by the National Key Research and Development Program of China (2021YFD1801103-4), and the National Natural Science Foundation of China (32130106).

Conflict of interest

The authors declare that the research was conducted in the absence of any commercial or financial relationships that could be construed as a potential conflict of interest.

Publisher's note

References

1. Jung K, Hu H, Saif LJ. Porcine deltacoronavirus induces apoptosis in swine testicular and llc porcine kidney cell lines *in vitro* but not in infected intestinal enterocytes *in vivo*. *Vet Microbiol* (2016) 182:57–63. doi: 10.1016/j.vetmic.2015.10.022

2. Chen Q, Gauger P, Stafne M, Thomas J, Arruda P, Burrough E, et al. Pathogenicity and pathogenesis of a united states porcine deltacoronavirus cell culture isolate in 5-Day-Old neonatal piglets. *Virology* (2015) 482:51–9. doi: 10.1016/j.virol.2015.03.024

3. Dong N, Fang L, Yang H, Liu H, Du T, Fang P, et al. Isolation, genomic characterization, and pathogenicity of a Chinese porcine deltacoronavirus strain chn-Hn-2014. *Vet Microbiol* (2016) 196:98–106. doi: 10.1016/j.vetmic.2016.10.022

4. Woo PC, Lau SK, Lam CS, Lau CC, Tsang AK, Lau JH, et al. Discovery of seven novel mammalian and avian coronaviruses in the genus deltacoronavirus supports bat coronaviruses as the gene source of alphacoronavirus and betacoronavirus and avian coronaviruses as the gene source of gammacoronavirus and deltacoronavirus. *J Virol* (2012) 86(7):3995–4008. doi: 10.1128/JVI.06540-11

5. Le VP, Song S, An BH, Park GN, Pham NT, Le DQ, et al. A novel strain of porcine deltacoronavirus in Vietnam. *Arch Virol* (2018) 163(1):203–7. doi: 10.1007/s00705-017-3594-8

6. Tang P, Cui E, Song Y, Yan R, Wang J. Porcine deltacoronavirus and its prevalence in China: A review of epidemiology, evolution, and vaccine

development. *Arch Virol* (2021) 166(11):2975–88. doi: 10.1007/s00705-021-05226-4

7. Jang G, Lee KK, Kim SH, Lee C. Prevalence, complete genome sequencing and phylogenetic analysis of porcine deltacoronavirus in South Korea, 2014-2016. *Transbound Emerg Dis* (2017) 64(5):1364–70. doi: 10.1111/tbed.12690

8. Lorsirigool A, Saeng-Chuto K, Temeeyasen G, Madapong A, Tripipat T, Wegner M, et al. The first detection and full-length genome sequence of porcine deltacoronavirus isolated in lao pdr. *Arch Virol* (2016) 161(10):2909–11. doi: 10.1007/s00705-016-2983-8

9. Saeng-Chuto K, Lorsirigool A, Temeeyasen G, Vui DT, Stott CJ, Madapong A, et al. Different lineage of porcine deltacoronavirus in Thailand, Vietnam and Lao pdr in 2015. *Transbound Emerg Dis* (2017) 64(1):3–10. doi: 10.1111/tbed.12585

10. Li G, Chen Q, Harmon KM, Yoon KJ, Schwartz KJ, Hoogland MJ, et al. Full-length genome sequence of porcine deltacoronavirus strain USA/Ia/2014/8734. *Genome Announc* (2014) 2(2):e00278–14. doi: 10.1128/genomeA.00278-14

11. Jung K, Hu H, Saif LJ. Calves are susceptible to infection with the newly emerged porcine deltacoronavirus, but not with the swine enteric alphacoronavirus, porcine epidemic diarrhea virus. *Arch Virol* (2017) 162 (8):2357–62. doi: 10.1007/s00705-017-3351-z

12. Boley PA, Alhamo MA, Lossie G, Yadav KK, Vasquez-Lee M, Saif LJ, et al. Porcine deltacoronavirus infection and transmission in poultry, United States(1). *Emerg Infect Dis* (2020) 26(2):255–65. doi: 10.3201/eid2602.190346

13. Liang Q, Zhang H, Li B, Ding Q, Wang Y, Gao W, et al. Susceptibility of chickens to porcine deltacoronavirus infection. *Viruses* (2019) 11(6):573. doi: 10.3390/v11060573

14. Lednicky JA, Tagliamonte MS, White SK, Elbadry MA, Alam MM, Stephenson CJ, et al. Independent infections of porcine deltacoronavirus among Haitian children. *Nature* (2021) 600(7887):133–7. doi: 10.1038/s41586-021-04111-z

15. Jung K, Miyazaki A, Hu H, Saif LJ. Susceptibility of porcine ipec-J2 intestinal epithelial cells to infection with porcine deltacoronavirus (Pdcov) and serum cytokine responses of gnotobiotic pigs to acute infection with ipec-J2 cell culture-passaged pdcov. *Vet Microbiol* (2018) 221:49–58. doi: 10.1016/j.vetmic.2018.05.019

16. Hu H, Jung K, Vlasova AN, Chepngeno J, Lu Z, Wang Q, et al. Isolation and characterization of porcine deltacoronavirus from pigs with diarrhea in the United States. *J Clin Microbiol* (2015) 53(5):1537–48. doi: 10.1128/JCM.00031-15

17. Saraste A, Pulkki K. Morphologic and biochemical hallmarks of apoptosis. *Cardiovasc Res* (2000) 45(3):528–37. doi: 10.1016/s0008-6363(99)00384-3

18. Taylor RC, Cullen SP, Martin SJ. Apoptosis: Controlled demolition at the cellular level. *Nat Rev Mol Cell Biol* (2008) 9(3):231–41. doi: 10.1038/nrm2312

19. Duan C, Wang J, Liu Y, Zhang J, Si J, Hao Z, et al. Antiviral effects of ergosterol peroxide in a pig model of porcine deltacoronavirus (Pdcov) infection involves modulation of apoptosis and tight junction in the small intestine. *Vet Res* (2021) 52(1):86. doi: 10.1186/s13567-021-00955-5

20. Yamamoto T, Yamada A, Yoshimura Y, Terada H, Shinohara Y. [the mechanisms of the release of cytochrome c from mitochondria revealed by proteomics analysis]. *Yakugaku Zasshi* (2012) 132(10):1099–104. doi: 10.1248/yakushi.12-00220-2

21. Xiong S, Mu T, Wang G, Jiang X. Mitochondria-mediated apoptosis in mammals. *Protein Cell* (2014) 5(10):737–49. doi: 10.1007/s13238-014-0089-1

22. Ren Z, Zhang X, Ding T, Zhong Z, Hu H, Xu Z, et al. Mitochondrial dynamics imbalance: A strategy for promoting viral infection. *Front Microbiol* (2020) 11:1992. doi: 10.3389/fmicb.2020.01992

23. Liu X, Kim CN, Yang J, Jemmerson R, Wang X. Induction of apoptotic program in cell-free extracts: Requirement for datp and cytochrome c. *Cell* (1996) 86(1):147–57. doi: 10.1016/s0092-8674(00)80085-9

24. Scorrano L, Ashiya M, Buttle K, Weiler S, Oakes SA, Mannella CA, et al. A distinct pathway remodels mitochondrial cristae and mobilizes cytochrome c during apoptosis. *Dev Cell* (2002) 2(1):55–67. doi: 10.1016/s1534-5807(01)00116-2

25. Beck MA, Nelson HK, Shi Q, Van Dael P, Schiffrin EJ, Blum S, et al. Selenium deficiency increases the pathology of an influenza virus infection. *FASEB J* (2001) 15(8):1481–3. doi: 10.1096/fj.00-0721fje

26. Beck MA, Kolbeck PC, Shi Q, Rohr LH, Morris VC, Levander OA. Increased virulence of a human enterovirus (Coxsackievirus B3) in selenium-deficient mice. *J Infect Dis* (1994) 170(2):351–7. doi: 10.1093/infdis/170.2.351

27. Zhang J, Taylor EW, Bennett K, Saad R, Rayman MP. Association between regional selenium status and reported outcome of covid-19 cases in China. *Am J Clin Nutr* (2020) 111(6):1297–9. doi: 10.1093/ajcn/nqaa095

28. Moghaddam A, Heller RA, Sun Q, Seelig J, Cherkezov A, Seibert L, et al. Selenium deficiency is associated with mortality risk from Covid-19. *Nutrients* (2020) 12(7):2098. doi: 10.3390/nu12072098

29. Ren Z, Jia G, He H, Ding T, Yu Y, Zuo Z, et al. Antiviral effect of selenomethionine on porcine deltacoronavirus in pig kidney epithelial cells. *Front Microbiol* (2022) 13:846747. doi: 10.3389/fmicb.2022.846747

30. Ramya S, Shanmugasundaram T, Balagurunathan R. Biomedical potential of actinobacterially synthesized selenium nanoparticles with special reference to anti-biofilm, anti-oxidant, wound healing, cytotoxic and anti-viral activities. *J Trace Elem Med Biol* (2015) 32:30–9. doi: 10.1016/j.jtemb.2015.05.005

31. Varlamova EG, Gudkov SV, Plotnikov EY, Turovsky EA. Size-dependent cytoprotective effects of selenium nanoparticles during oxygen-glucose deprivation in brain cortical cells. *Int J Mol Sci* (2022) 23(13):7464. doi: 10.3390/ijms23137464

32. Jiao J, Yu J, Ji H, Liu A. Synthesis of macromolecular astragalus polysaccharide-nano selenium complex and the inhibitory effects on Hepg2 cells. *Int J Biol Macromol* (2022) 211:481–9. doi: 10.1016/j.ijbiomac.2022.05.095

33. El-Azab MF, Al-Karmalawy AA, Antar SA, Hanna PA, Tawfik KM, Hazem RM. A novel role of nano selenium and sildenafil on streptozotocin-induced diabetic nephropathy in rats by modulation of inflammatory, oxidative, and apoptotic pathways. *Life Sci* (2022) 303:120691. doi: 10.1016/j.lfs.2022.120691

34. Rao S, Lin Y, Lin R, Liu J, Wang H, Hu W, et al. Traditional Chinese medicine active ingredients-based selenium nanoparticles regulate antioxidant selenoproteins for spinal cord injury treatment. *J Nanobiotechnol* (2022) 20 (1):278. doi: 10.1186/s12951-022-01490-x

35. Jin XH, Zhang YF, Yuan YX, Han L, Zhang GP, Hu H. Isolation, characterization and transcriptome analysis of porcine deltacoronavirus strain hnzk-02 from Henan Province, China. *Mol Immunol* (2021) 134:86–99. doi: 10.1016/j.molimm.2021.03.006

36. Tan Y, Sun L, Wang G, Shi Y, Dong W, Fu Y, et al. The trypsin-enhanced infection of porcine epidemic diarrhea virus is determined by the S2 subunit of the spike glycoprotein. *J Virol* (2021) 95(11):e02453–20. doi: 10.1128/JVI.02453-20

37. Yuan Y, Zu S, Zhang Y, Zhao F, Jin X, Hu H. Porcine deltacoronavirus utilizes sialic acid as an attachment receptor and trypsin can influence the binding activity. *Viruses* (2021) 13(12):2442. doi: 10.3390/v13122442

38. Zhang J, Chen J, Shi D, Shi H, Zhang X, Liu J, et al. Porcine deltacoronavirus enters cells *via* two pathways: A protease-mediated one at the cell surface and another facilitated by cathepsins in the endosome. *J Biol Chem* (2019) 294 (25):9830–43. doi: 10.1074/jbc.RA119.007779

39. Yang YL, Meng F, Qin P, Herrler G, Huang YW, Tang YD. Trypsin promotes porcine deltacoronavirus mediating cell-to-Cell fusion in a cell type-dependent manner. *Emerg Microbes Infect* (2020) 9(1):457–68. doi: 10.1080/22221751.2020.1730245

40. Bhowmick R, Halder UC, Chattopadhyay S, Chanda S, Nandi S, Bagchi P, et al. Rotaviral enterotoxin nonstructural protein 4 targets mitochondria for activation of apoptosis during infection. *J Biol Chem* (2012) 287(42):35004–20. doi: 10.1074/jbc.M112.369595

41. Mukherjee A, Patra U, Bhowmick R, Chawla-Sarkar M. Rotaviral nonstructural protein 4 triggers dynamin-related protein 1-dependent mitochondrial fragmentation during infection. *Cell Microbiol* (2018) 20(6): e12831. doi: 10.1111/cmi.12831

42. Vilmen G, Glon D, Siracusano G, Lussignol M, Shao Z, Hernandez E, et al. Bhrf1, a Bcl2 viral homolog, disturbs mitochondrial dynamics and stimulates mitophagy to dampen type I ifn induction. *Autophagy* (2021) 17(6):1296–315. doi: 10.1080/15548627.2020.1758416

43. Szabadkai G, Simoni AM, Chami M, Wieckowski MR, Youle RJ, Rizzuto R. Drp-1-Dependent division of the mitochondrial network blocks intraorganellar Ca2+ waves and protects against Ca2+-mediated apoptosis. *Mol Cell* (2004) 16 (1):59–68. doi: 10.1016/j.molcel.2004.09.026

44. Estaquier J, Arnoult D. Inhibiting Drp1-mediated mitochondrial fission selectively prevents the release of cytochrome c during apoptosis. *Cell Death Differ* (2007) 14(6):1086–94. doi: 10.1038/sj.cdd.4402107

45. Martinou JC, Youle RJ. Which came first, the cytochrome c release or the mitochondrial fission? *Cell Death Differ* (2006) 13(8):1291–5. doi: 10.1038/sj.cdd.4401985

46. Zhai X, Wang N, Jiao H, Zhang J, Li C, Ren W, et al. Melatonin and other indoles show antiviral activities against swine coronaviruses *in vitro* at pharmacological concentrations. *J Pineal Res* (2021) 71(2):e12754. doi: 10.1111/jpi.12754

47. Kong F, Niu X, Liu M, Wang Q. Bile acids lca and cdca inhibited porcine deltacoronavirus replication *in vitro*. *Vet Microbiol* (2021) 257:109097. doi: 10.1016/j.vetmic.2021.109097

48. Brown AJ, Won JJ, Graham RL, Dinnon KH3rd, Sims AC, Feng JY, et al. Broad spectrum antiviral remdesivir inhibits human endemic and zoonotic deltacoronaviruses with a highly divergent rna dependent rna polymerase. *Antiviral Res* (2019) 169:104541. doi: 10.1016/j.antiviral.2019.104541

49. Duan C, Ge X, Wang J, Wei Z, Feng WH, Wang J. Ergosterol peroxide exhibits antiviral and immunomodulatory abilities against porcine deltacoronavirus (Pdcov) *via* suppression of nf-kappab and P38/Mapk signaling pintimp.2020.107317athways *in vitro*. *Int Immunopharmacol* (2021) 93:107317. doi: 10.1016/j.intimp.2020.107317

50. Sartori G, Jardim NS, Marcondes Sari MH, Dobrachinski F, Pesarico AP, Rodrigues LC Jr., et al. Antiviral action of diphenyl diselenide on herpes simplex virus 2 infection in female Balb/C mice. *J Cell Biochem* (2016) 117(7):1638–48. doi: 10.1002/jcb.25457

51. Cheng Z, Zhi X, Sun G, Guo W, Huang Y, Sun W, et al. Sodium selenite suppresses hepatitis b virus transcription and replication in human hepatoma cell lines. *J Med Virol* (2016) 88(4):653–63. doi: 10.1002/jmv.24366

52. Wang C, Chen H, Chen D, Zhao M, Lin Z, Guo M, et al. The inhibition of H1n1 influenza virus-induced apoptosis by surface decoration of selenium nanoparticles with beta-thujaplicin through reactive oxygen species-mediated akt and P53 signaling pathways. *ACS Omega* (2020) 5(47):30633–42. doi: 10.1021/acsomega.0c04624

53. Lin Z, Li Y, Gong G, Xia Y, Wang C, Chen Y, et al. Restriction of H1n1 influenza virus infection by selenium nanoparticles loaded with ribavirin *via* resisting caspase-3 apoptotic pathway. *Int J Nanomedicine* (2018) 13:5787–97. doi: 10.2147/IJN.S177658

54. Wang J, Li Y, Wang J, Wang Y, Liu H, Bao J. Selenium alleviates ammonia-induced splenic cell apoptosis and inflammation by regulating the interleukin Family/Death receptor axis and Nrf2 signaling pathway. *Biol Trace Elem Res* (2022). doi: 10.1007/s12011-022-03279-3

55. Zhao Y, Zhang H, Hao D, Wang J, Zhu R, Liu W, et al. Selenium regulates the mitogen-activated protein kinase pathway to protect broilers from hexavalent chromium-induced kidney dysfunction and apoptosis. *Ecotoxicol Environ Saf* (2022) 239:113629. doi: 10.1016/j.ecoenv.2022.113629

56. Wang P, Zhang S, Liu W, Chen S, Lv X, Hu B, et al. Selenium attenuates tbhp-induced apoptosis of nucleus pulposus cells by suppressing mitochondrial fission through activating nuclear factor erythroid 2-related factor 2. *Oxid Med Cell Longev* (2022) 2022:7531788. doi: 10.1155/2022/7531788

57. Chen X, Ren F, Hesketh J, Shi X, Li J, Gan F, et al. Selenium blocks porcine circovirus type 2 replication promotion induced by oxidative stress by improving Gpx1 expression. *Free Radic Biol Med* (2012) 53(3):395–405. doi: 10.1016/j.freeradbiomed.2012.04.035

58. Shao C, Yu Z, Luo T, Zhou B, Song Q, Li Z, et al. Chitosan-coated selenium nanoparticles attenuate prrsv replication and Ros/Jnk-mediated apoptosis *in vitro*. *Int J Nanomedicine* (2022) 17:3043–54. doi: 10.2147/IJN.S370585

59. Liu X, Chen D, Su J, Zheng R, Ning Z, Zhao M, et al. Selenium nanoparticles inhibited H1n1 influenza virus-induced apoptosis by ros-mediated signaling pathways. *RSC Adv* (2022) 12(7):3862–70. doi: 10.1039/d1ra08658h

frontiers | Frontiers in Immunology

TYPE Original Research
PUBLISHED 25 August 2022
DOI 10.3389/fimmu.2022.958801

OPEN ACCESS

EDITED BY
Chenhe Su,
Wistar Institute, United States

REVIEWED BY
Xun Zhang,
University of Strathclyde, United Kingdom
Lihong Liu,
Columbia University, United States

*CORRESPONDENCE
Dongming Zhou
zhoudongming@tmu.edu.cn
Hongbo Zhang
hongboflood@163.com

SPECIALTY SECTION
This article was submitted to Viral Immunology, a section of the journal Frontiers in Immunology

RECEIVED 01 June 2022
ACCEPTED 04 July 2022
PUBLISHED 25 August 2022

CITATION
Zhang H, Alford T, Liu S, Zhou D and Wang J (2022) Influenza virus causes lung immunopathology through down-regulating PPARγ activity in macrophages.
Front. Immunol. 13:958801.
doi: 10.3389/fimmu.2022.958801

Influenza virus causes lung immunopathology through down-regulating PPARγ activity in macrophages

Hongbo Zhang[1]*, Taylor Alford[2], Shuangquan Liu[1,3], Dongming Zhou[4]* and Jieru Wang[1,2]

[1]Department of Pediatrics, University of Pittsburgh School of Medicine, Pittsburgh, PA, United States, [2]Department of Medicine, National Jewish Health, Denver, CO, United States, [3]Department of Clinical Laboratory, The First Affiliated Hospital of University of Southern China, Hengyang, Hunan, China, [4]Department of Pathogen Biology, School of Basic Medical Sciences, Tianjin Medical University, Tianjin, China

Fatal influenza (flu) virus infection often activates excessive inflammatory signals, leading to multi-organ failure and death, also referred to as cytokine storm. PPARγ (Peroxisome proliferator-activated receptor gamma) agonists are well-known candidates for cytokine storm modulation. The present study identified that influenza infection reduced PPARγ expression and decreased PPARγ transcription activity in human alveolar macrophages (AMs) from different donors. Treatment with PPARγ agonist Troglitazone ameliorated virus-induced proinflammatory cytokine secretion but did not interfere with the IFN-induced antiviral pathway in human AMs. In contrast, PPARγ antagonist and knockdown of PPARγ in human AMs further enhanced virus-stimulated proinflammatory response. In a mouse model of influenza infection, flu virus dose-dependently reduced PPARγ transcriptional activity and decreased expression of PPARγ. Moreover, PPARγ agonist troglitazone significantly reduced high doses of influenza infection-induced lung pathology. In addition, flu infection reduced PPARγ expression in all mouse macrophages, including AMs, interstitial macrophages, and bone-marrow-derived macrophages but not in alveolar epithelial cells. Our results indicate that the influenza virus specifically targets the PPARγ pathway in macrophages to cause acute injury to the lung.

KEYWORDS

lung macrophage, PPARγ, influenza, PPARγ agonist, acute lung injury

Introduction

Influenza A virus (IAV) is a common pathogen causing respiratory illness. Pathology is determined by pathogens and the host (1). The easy-mutation nature of the influenza virus made it a challenging to develop a universal vaccine to protect the susceptible population (2, 3). Therefore, identifying the host-derived mechanism for influenza-associated diseases is critical for developing an effective prevention or treatment strategy for combating influenza infection.

Peroxisome proliferator-activated receptor gamma (PPARγ) is a member of the nuclear hormone receptor superfamily of ligand-activated transcription factors that regulate the expression of genes involved in reproduction, metabolism, development, and immune responses (4, 5). PPARγ is a well-known anti-inflammatory transcription factor (6, 7). It has been reported that respiratory virus, such as a respiratory syncytial virus (RSV), alter PPARγ expression (6, 7). In addition, PPARγ ligands are proposed as anti-SARS-CoV-2 drugs based on their anti-inflammatory, antioxidant and immunomodulatory properties (8, 9). Several PPARγ agonists have been documented to attenuate inflammation and alleviate influenza infection in mouse studies. Cloutier et al. found that 15-Deoxy-Delta-12,14-prostaglandin J2 (15d-PGJ2), a ligand of PPARγ, protects mice against lethal influenza infection (10). Several reports suggest that IAV infection downregulates PPAR-γ expression in mouse macrophages (11, 12). However, it is not known whether the influenza A virus directly hijacks PPARγ signaling in human primary alveolar macrophages.

PPARγ is predominantly expressed in alveolar macrophages (AMs) (13). Alveolar macrophages are the lung's immune effector and play a central role in maintaining lung homeostasis by repairing tissue damage and phagocytosis of invading pathogens (14). During infection, AMs release a lot of proinflammatory cytokines to recruit immune cells to the infection site (13). However, the excessive proinflammatory response, the so-called cytokine storm, contributes significantly to the tissue damage (15). Our previous study with genome profiling of human AMs in response to influenza infection suggests that influenza may reduce PPARγ gene expression (16). Therefore, we hypothesize that the influenza A virus surpresses the PPARγ pathway, therefore contributes to the dysregulation of the host immune response.

The present study first examined whether influenza infection impaired PPARγ signaling *in vitro* in human primary lung cells, including the alveolar epithelial and macrophage cells. We then addressed whether activation of PPARγ by a commercial agonist would reduce the proinflammatory response in human AMs *in vitro* and protect infected mice from severe lung injury and inflammation *in vivo*. We demonstrated that influenza infection impaired PPARγ signaling, which led to an excessive proinflammatory response in human AMs but not in epithelial cells and lung inflammation and pathology *in vivo*. Our results revealed a novel mechanism of influenza-induced acute lung injury.

Materials and methods

Influenza infection of human AMs

Influenza H1N1 virus A/PR8/Puerto Rico/34 (PR8) and 2009 H1N1 pandemic virus A/California/04 (CA04) were prepared as described previously (17–19). According to the standard procedure, the contemporary H3N2 virus vz18B2 was created by reverse genetics directly from a human swab specimen collected in New York State a human swab collected in New York state and kindly provided by Dr. Wentworth (20). Human AMs were isolated from unidentified donor lungs, which were not suitable for transplantation, and donated for medical studies as described previously (18, 19). Cultured AMs were inoculated with the influenza virus at a multiplicity of infection (moi) of 1 for 1 h. Cells were harvested at 24 h post-inoculation (hpi). The Committee for the Protection of Human Subjects at National Jewish Health and University of Pittsburgh Committee for Oversight of Research and Clinical Training involving Decedents (CORID) have approved this study.

Mouse influenza infection

Eight to ten-week-old C57BL/6 mice were purchased from The Jackson Laboratory (Bar Harbor, Maine). Mice were maintained under specific pathogen-free conditions within the animal facility at the Children's Hospital of Pittsburgh of University of Pittsburgh Medical Center. Animal studies were conducted with approval from the University of Pittsburgh Institutional Animal Care and Use Committee. For influenza infection, mice were intranasally challenged with 1000 pfu of PR8 virus diluted in 50 µl of sterile PBS or 50 µl of PBS control. Following infection, mice were monitored daily for weight loss and signs of clinical illness and 3 or 5 mice were sacrificed 3 days after the virus challenge.

Mouse bronchoalveolar lavage and lung tissue processing

At the indicated time, mice were euthanized by intraperitoneal injection of a leathal dose of sodium pentobarbital. The whole-lungs lavage was performed with 1 ml sterile saline solution, and bronchoalveolar lavage fluid (BALF) was collected and centrifuged at 4°C, 3000 rpm for 10 min. An aliquot of 100ul cell-free BALF was snap-frozen by the dry ice-ethanol bath to evaluate viral burden by standard Plaque Assay as previously described (18, 19). The remaining BALF was stored at -80°C for

detection of albumin, lactate dehydrogenase (LDH), and cytokine by ELISA. BAL cell cytospin slides were stained with a HEMA-3 stain kit (Fisher Scientific, Waltham, MA) for inflammatory cell differential counts. For histology staining, the right superior lobe was fixed in 10% neutral buffered formalin. The right lobe was saved at -80°C for protein extraction. The remaining lung lobes were collected and homogenized in 1 ml of sterile ice-cold PBS at 4°C using a gentle MACS Dissociator (Miltenyi Biotech, San Diego, CA). The post-caval lobe was saved at -80°C for RNA extraction.

Treatment with PPARγ agonist and antagonist

For a PPARγ agonist and antagonist experiment in human AMs, troglitazone (5 μM) (Sigma, St Louis, MO) was given 1 h before or right after infection. PPARγ antagonist T0070907 or GW9662 (Sigma, St Louis, MO) were given 1h before infection. After infection, cells were cultured with agonists or antagonists for another 24 h.

For treatment with mice, 10 mg/kg troglitazone was injected intraperitoneally prior to flu infection and daily after infection for 5 days. Mice were observed daily for daily activity and weight loss. On Day 5 post flu inoculation, mice were sacrificed. 2 mg/kg T0070907 or GW9662 was injected intraperitoneally 1 day prior to flu infection and daily after infection for 2 days. Mice were observed daily for daily activity, weight loss, and the mice were sacrificed on Day 3 post flu infection.

PPARγ transcription activity assay

The nuclear protein from control and virus-infected human AMs and mouse lungs was extracted using Pierce nuclear/cytoplasmic protein extraction kit (ThermoFisher Scientific, Waltham, MA). Following the manufacturer's instruction, an equal amount of nuclear protein from control and infected samples was used to evaluate the PPARγ activity using the TransAM PPARγ kit (Active Motif Inc., Rixensart, Belgium). The kit includes a 96-well plate coated with with an immobilized oligonucleotide containing the PPARγ response element (5'-AACTAGGTCAAAGGTCA-3') for measuring PPARγ activity. The active form of PPARγ contained in nuclear extract specifically binds to the oligonucleotide. The primary antibodies used in the TransAM PPARγ kit recognize an accessible epitope on PPARγ protein upon DNA binding. A horseradish peroxidase-conjugated secondary antibody is used for the spectrophotometric quantification.

Real-time RT-PCR

Total RNA was extracted from human and mouse cells using the RNeasy kit (QIAGEN S.A., Courtaboeuf, France). RNA purity and integrity were examined by Nanodrop spectrophotometric analysis. Following the manufacturer's instructions, 1 μg of total RNA was reverse-transcribed into cDNA using the qScript™ cDNA Synthesis kit (Quanta Bioscience, Gaithersburg, MD). cDNA was then used in standard real-time PCR to measure gene expression using the Applied Biosystems 7900HT. Reaction conditions were 95°C for 15 s and 60°C for 1min, repeated for 40 cycles, with a 10 min hot start at 95°C. Relative mRNA level was quantified using the $2^{\Delta Ct}$ method and standardized by GAPDH. All TaqMan real-time PCR probes were purchased from Life Technologies (Carlsbad, CA). They are human PPARγ (Hs00234592_m1), human IL-1B (Hs00174097_m1), human GAPDH (Hs02758991_g1), mouse PPARγ (Mm00440940_m1), mouse Mx1 (Mm00487796_m1), and mouse GAPDH (Mm99999915_g1).

Statistical analysis

All data analyses were performed with Prism 9.3.0 (GraphPad, La Jolla, CA). Mann–Whitney U test was used to compare gene expression and viral replication between two groups. The two-tailed Student *t*-test was used for the comparisons between the two groups. A one-way ANOVA test was used for the comparison of the three groups.

Results

Influenza infection impairs the PPARγ pathway in human primary AMs

To confirm whether influenza A infection impairs PPARγ anti-inflammatory pathway in human primary AMs, cultured cells were infected with H1N1 virus PR8, and gene expression and transcription activity of PPARγ was measured at 4 and 24 h post-infection (hpi). Our results suggested that PR8 infection decreased mRNA of PPARγ in human AMs from 10 tested donors at 4 hpi and a further reduction at 24 hpi (Figure 1A). Since PPARγ is a transcription factor, we extracted cellular nuclear protein from infected cells at 24 hpi and further determined the transcription activity of PPARγ using the TransAM kit (Active motif) in cells isolated from 4 donors. The data in Figure 1B show a dose-dependent decrease in PPARγ activity and virus.

In addition, we infected human AMs with the 2009 pandemic (H1N1pdm09) virus CA04. As we previously reported, this virus caused a much lower infection than PR8 (19), but it still significantly reduced PPARγ expression (Figure 1C) at both 4 and 24 hpi. Our previous study found that PR8 infection reduced the expression of important scavenger receptors, including CD36, the direct target gene of PPARγ in human AMs (16). Altogether, these data indicate that H1N1 infection impairs the PPARγ signaling pathway in human AMs.

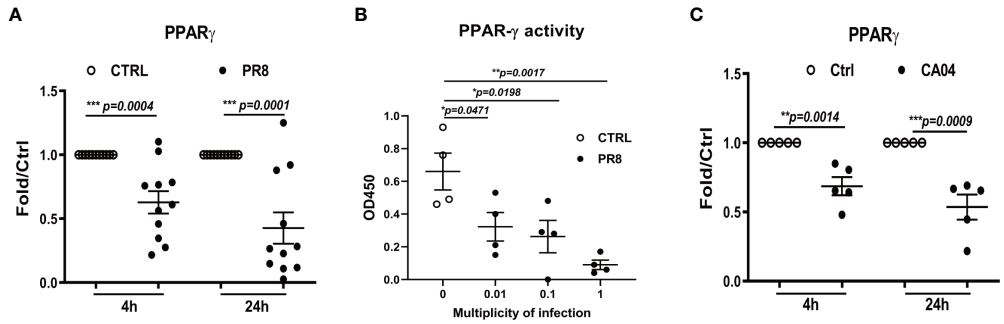

FIGURE 1
Influenza infection reduces PPARG gene expression and transcription activity in human alveolar macrophages(AMs). Cultured human AMs were infected with PR8 virus **(A, B)** or CA04 virus **(C)** at MOI=1, at 4 or 24 hpi, the cell pellet was harvested for RNA extraction, and the mRNA level of PPARγ was determined by RT-qPCR **(A, C)**. Human AM was infected with PR8 at MOI=0.01, 0.1, or 1, harvested the cell pellet for the nuclear protein extraction at 24 hpi, and the PPARγ transcriptional activity of PPARγ was determined **(B)**. Unpaired t test was applied for the statistical analysis of **(A, C)** and Ordinary one-way ANOVA was applied for B. *p < 0.05, **p < 0.01, and ***p < 0.001.

PPARγ is critical for controlling influenza virus-induced proinflammatory response in human AMs.

We and others reported that the influenza A virus stimulated a predominant proinflammatory response in human AMs (16, 18, 19). To determine if this strong inflammatory response is due to dampened PPARγ signaling, we did several experiments to knockdown PPARγ using PPARγ-specific siRNA or alter PPARγ activity using a commercially available PPARγ agonist or antagonists prior to virus infection and measured proinflammatory cytokine secretion. PPARγ-specific siRNA treatment reduced around 90% of PPARγ expression (Figure 2A) and resulted in significantly upregulated secretion of TNF-α, IL-6, IL-8, and RANTES, but not IP-10 (Figures 2B–F). On the other hand, activated PPARγ by an agonist, Trog, significantly reduced virus-stimulated TNF- α, IL-8, and RANTES but not IP-10 (Figures 2G-J). Similar results were observed in contemporary H3N2 viral infection treated with PPARγ agonist (Supplementary Figure 1). On the contrary, PPARγ antagonist further enhanced virus-stimulated TNF-α (Figure 2K). As expected, the decreased secretion of IL-8 and RANTES caused by PPARγ agonist treatment was restored by subsequent antagonist treatment (Figures 2L, M). These results indicate that PPARγ is critical for keeping the proinflammatory response on check.

PPARγ agonist does not alter influenza-induced IFN production as well as IFN downstream signaling

Production of IFN is a major antiviral defense of human AMs in response to influenza infection. To determine whether the administration of PPARγ agonist alters IFN response, we examined gene expression of interferons. Treatment of human AMs with PPARγ agonists did not alter PR8-induced mRNA production of IFN-α, IFN-β, and IFN-λ1 (Figures 3A–C). PPARγ agonist also did not alter CA04-induced expression of IFN genes and antiviral genes Mx1 and ISG56 (Figures 3D, E). These results suggest that activation of PPARγ does not interfere with the host antiviral pathway.

Influenza infection reduces mRNA and transcription activity of PPARγ in mice

To investigate whether the influenza virus impairs PPARγ signaling *in vivo*, we investigated PPARγ in a mouse model of flu infection. We infected C57B/6 mice with different doses of PR8 by intranasal inoculation. Data in Figure 4A shows that PR8 infection decreased PPARγ activity dose-dependently. Figures 4B, C shows that viral infection significantly decreased PPARγ mRNA. To verify that influenza virus infection decreases the PPARγ activity in mouse macrophages, we isolated other macrophages, including alveolar macrophage, lung intestinal macrophage, bone marrow macrophage, and type II alveolar epithelial cell (ATII) from the mouse and then infected these cells with PR8. 24 hpi after PR8 infection, determined the mRNA level of PPARγ. Our results suggested that PR8 only decreased PPARγ activity in mouse macrophages but not in ATII, similar to our observation in primary human cells (Figures 4D–G).

Activation of PPARγ ameliorated influenza-induced lung injury and improved survival

To further determine whether the acute lung injury is due to an impaired PPARγ pathway. We treated mice with PPARγ

10.3389/fimmu.2022.958801

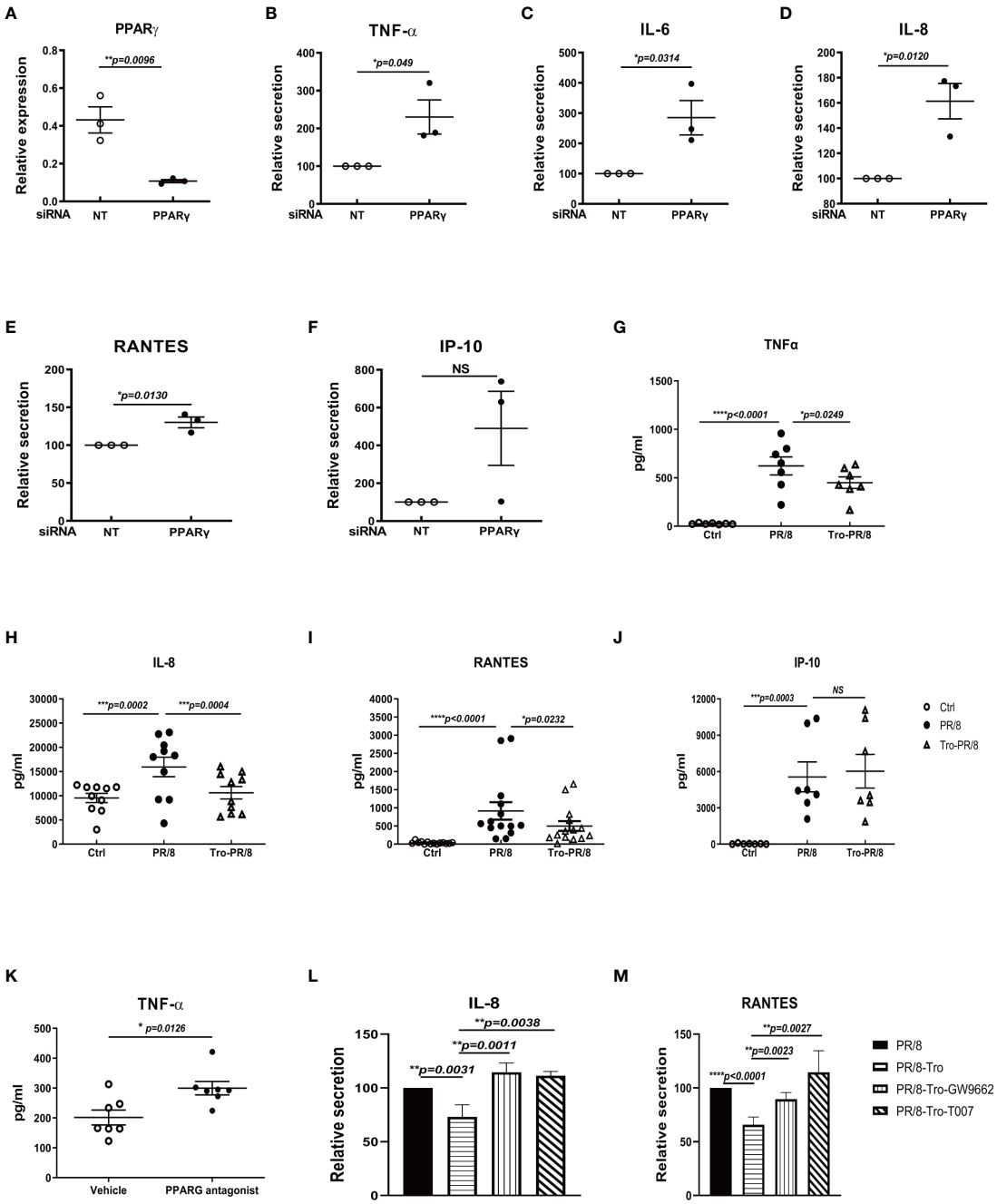

FIGURE 2
PPARγ is critical for controlling influenza virus-induced proinflammatory response in human AMs. Human AMs isolated from three donors were transfected with PPARγ specific siRNA or nontarget control siRNA(NT) 48 h before infections with PR8(MOI=1). At 24 h after infection, RNA(A-F) was extracted for examining PPARγ gene expression, and cell-free culture supernatants were collected to detect cytokines using DuoSet ELISA kits from R&D Systems. **(A)** PPARγ mRNA level. **(B)** TNFα. **(C)** IL-6. **(D)** IL-8. **(E)** RANTES. **(F)** IP-10. **(G–J)** For the experiment with PPARγ agonist, troglitazone (5 μM) (Sigma, St Louis, MO) in human AMs, was given right after infection. PPARγ antagonist T0070907 or GW9662 (Sigma) were given 1h before infection. At 24 h after infection, cell-free culture supernatants were collected to detect cytokines using DuoSet ELISA kits from R&D Systems. **(G)** TNFα. **(H)** IL-8. **(I)** RANTES. **(J)** IP-10. Isolated human AMs were treated with PPARγ agonist, troglitazone (5 μM) in human AMs right after PR/8 infection. PPARγ antagonist T0070907 or GW9662 (Sigma) were given 1h before infection. After infection, cells were treated with agonists or antagonists for another 24 h. At 24 h after infection, cell-free culture supernatants were collected to detect cytokines using DuoSet ELISA kits from R&D Systems. **(K)** TNFα. **(L)** IL-8. **(M)** RANTES. Unpaired t test was applied for comparison of two groups, while one-way ANOVA was used for comparison of more than two groups. ns means no significance. *p < 0.05, **p < 0.01, and ***p < 0.001.

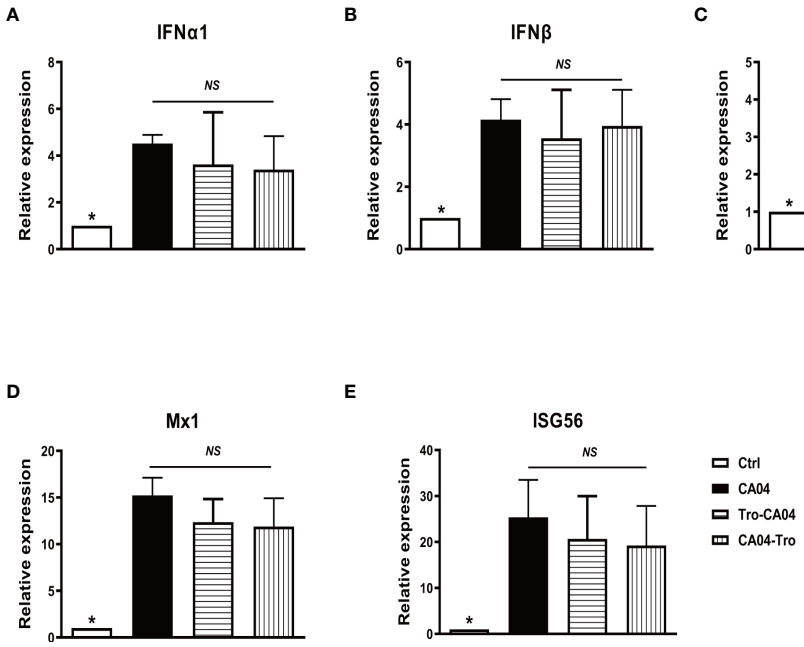

FIGURE 3
PPARγ agonist does not alter influenza-induced IFN production and IFN downstream signaling. Cultured human AMs were infected with CA04 at MOI=1, and PPARγ agonist troglitazone (5 μM) (Sigma, St Louis, MO) was given 1 h before or after infection. After infection, cells were cultured with an agonist for another 24 h. At 4 or 24 hpi, the cell pellet was harvested for RNA extraction, and the expression level of indicated genes was determined by RT-qPCR. **(A)** IFNα. **(B)** IFNβ. **(C)** IFNλ. **(D)** Mx1. **(E)** ISG56. Mann-Whitney test was apllied for the statistical analysis between CA04 and non- infected control conditions. Ordinary one-way ANOVA was applied for the statistical analysis among CA04, Tro-CA04 & CA04-Tro conditions. ns means no significance. *p < 0.05.

agonist troglitazone prior to influenza infection and evaluated viral burden, weight loss, inflammatory cell differentiation in bronchoalveolar lavage fluid (BALF), and acute lung injury. Compared to the vehicle control-treated group, troglitazone-treated mice displayed elevated PPARγ activity (Figure 5A), reduced viral burden (Figure 5B), and attenuated weight loss (Figure 5C). There was a significantly decreased total protein and LDH, total cell number, percentage of neutrophils, and an increased percentage of monocytes in the infected BAL (Figures 5D-H). These data indicate that virus-induced lung injury is dependent on the downregulation of the PPARγ pathway.

PPARγ antagonist enhanced the inflammatory response and exacerbated damage in the lung of influenza-infected mice

Since PPARγ agonist ameliorated the lung injury during flu infection in mice, we investigated whether the PPARγ antagonist could worsen the lung injury or not. In the antagonist treatment group, albumin and LDH, the two important indicators of lung injury, were significantly elevated in antagonist-treated mice lungs (Figures 6A, B). In addition, the total inflammatory cell number and the portion of monocytes were also significantly elevated under the treatment of the antagonist (Figures 6C, D).

Discussion

The influenza virus is a common public health problem and can cause serious complications, including events leading to hospitalization and death (21). The mortality due to influenza has been associated with excessive inflammatory response and cytokemia (22). Recently, several studies have highlighted the importance of therapies targeting host inflammatory responses. Alveolar macrophages are target cells in the lung infected by influenza virus and release many proinflammatory modulators during influenza infection to restrain viral infection (17, 23). PPARγ is expressed in monocytes and macrophages (24). In addition to its well-known regulatory effects on lipid and glucose metabolism, PPARγ is an important anti-inflammatory transcription factor that antagonizes NF-κB mediated cytokine production (25).

In this study, we have demonstrated that IAV infection decreased gene expression and transcript activity of PPARγ in human primary AMs, and there is a dose-dependent relationship between the PR8 infection and decreased PPARγ activity, as shown

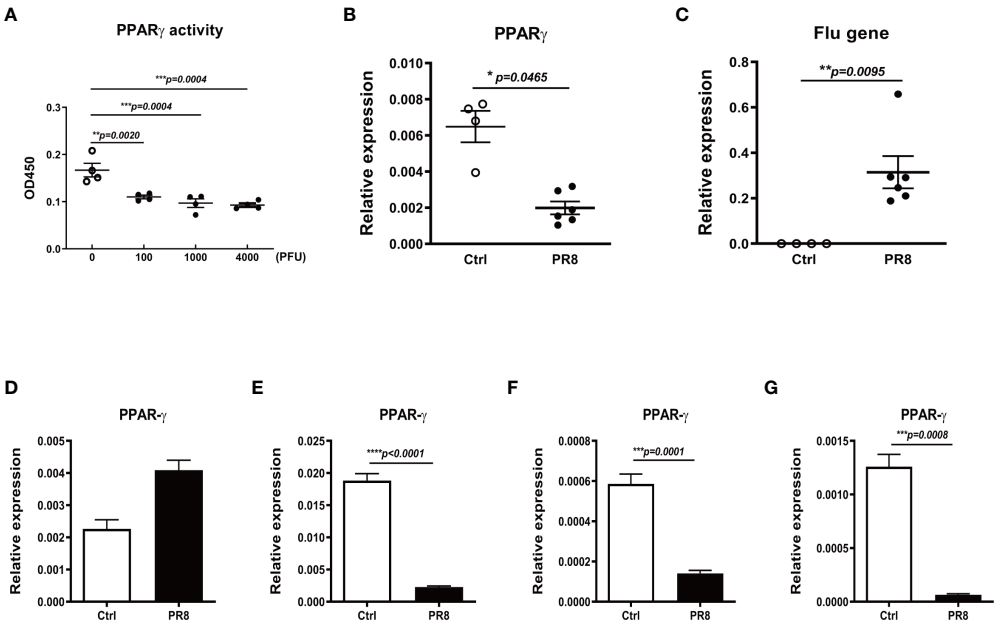

FIGURE 4
Influenza infection reduces PPARγ expression and activity in mouse lungs and macrophages. C57B/6 mice were infected with different doses of PR8 or saline by intranasal inoculation, and the lung tissue was collected on day 3 after infection. The PPARγ activity **(A)** and mRNA **(B)** in the mouse lung tissue were determined. The viral RNA in mice lungs was also determined by RT-PCR **(C)**. The isolated mouse lung alveolar epithelial type II cells (ATII **(D)**), alveolar macrophages (AM **(E)**), lung interstitial macrophages (IM **(F)**), and bone marrow-derived macrophages (BMDM **(G)**) were infected with PR8 at MOI=1, harvested the cell pellet at 24 h after infection for RNA extraction. The PPARγ mRNA was determined by RT-PCR. Unpaired t test was applied for the statistical analysis. *p < 0.05, **p < 0.01, ***p < 0.001 and ****p < 0.0001.

in Figure 1. Furtherly, knock-down of PPARγ by siPPARγ enhanced the secretion of multiple cytokines in primary human AMs (Figures 2B-E). On the other hand, activation of PPARγ in human AMs treated by PPARγ agonist reduced secretion of multiple cytokines. (Figure 2G-J). Also, PPARγ agonist treated mouse AMs showed less secretion of TNFα during IAV infection (Figure 2K). At the same time, the antagonist diminished the inflammatory inhibition effect of the PPARγ agonist during IAV infection (Figures 2L, M). Taken together, these results suggested that PPARγ plays an important role in the IAV infection-induced inflammatory response in human AMs. Although a reduction of multiple inflammatory factors was observed in PPARγ-activated AM, the expression of IFN was not significantly reduced (Figure 3). We got the similar resuts in H3N2 infected human primary AMs (Supplementary Figure 1).

In addition to investigate the role of PPARγ during IAV infection in human primary AMs, we infected mice with IAV and harvested the lungs to investigate the PPARγ activity and mRNA level. We found that the IAV infection decreased the PPARγ activity and mRNA level (Figures 4A–C) in mouse lung. In order to verify the IAV infection inhibited the expressing level of PPARγ in what kind cells, ATII cells and different macrophages, including alveolar macrophages, interstitial macrophages, and bone-marrow-derived macrophages were isolated from the naive mice and cultured for IAV infection. Our results suggested that IAV infection only inhibited the PPARγ expressing in macropahges but not in the ATII cells (Figures 4D–G).

Since the IAV infection significantly reduced the PPARγ activity in mouse lung, we hypothesized that activated the PPARγ activity *in vivo* moderate inflammatory response and immunopathological damage caused by IAV. As expected, PPARγ activation protected against IAV-induced lung injury and mortality in mice (Figure 5). Conversely, PPARγ antagonist treated mice displayed worsened mortality and delayed viral clearance (Figure 6).

Cytokine storm, the consequence of misregulation of inflammatory cytokines and hyperactivation of the innate immune response, has been recognized as a key mediator of influenza-induced lung disease and may be the key to COVID-19 infection (15, 26). Stimulation of PPARγ by natural or synthetic agonists may modulate the cytokine storm typical of viral infection by preventing cytokine overproduction and the inflammatory cascade (6) (27). Several natural PPARγ ligands have been proposed to treat COVID-19 (8). Due to its ability to reduce inflammatory parameters, the PPARγ agonist pioglitazone has also been proposed as an effective treatment for COVID-19 patients with diabetes, hypertension, and cardiovascular comorbidities (28).

There are several recent studies reported that treatment with PPARγ agonists significantly reduced flu-associated pathogenesis. Our results are consistent with the results from

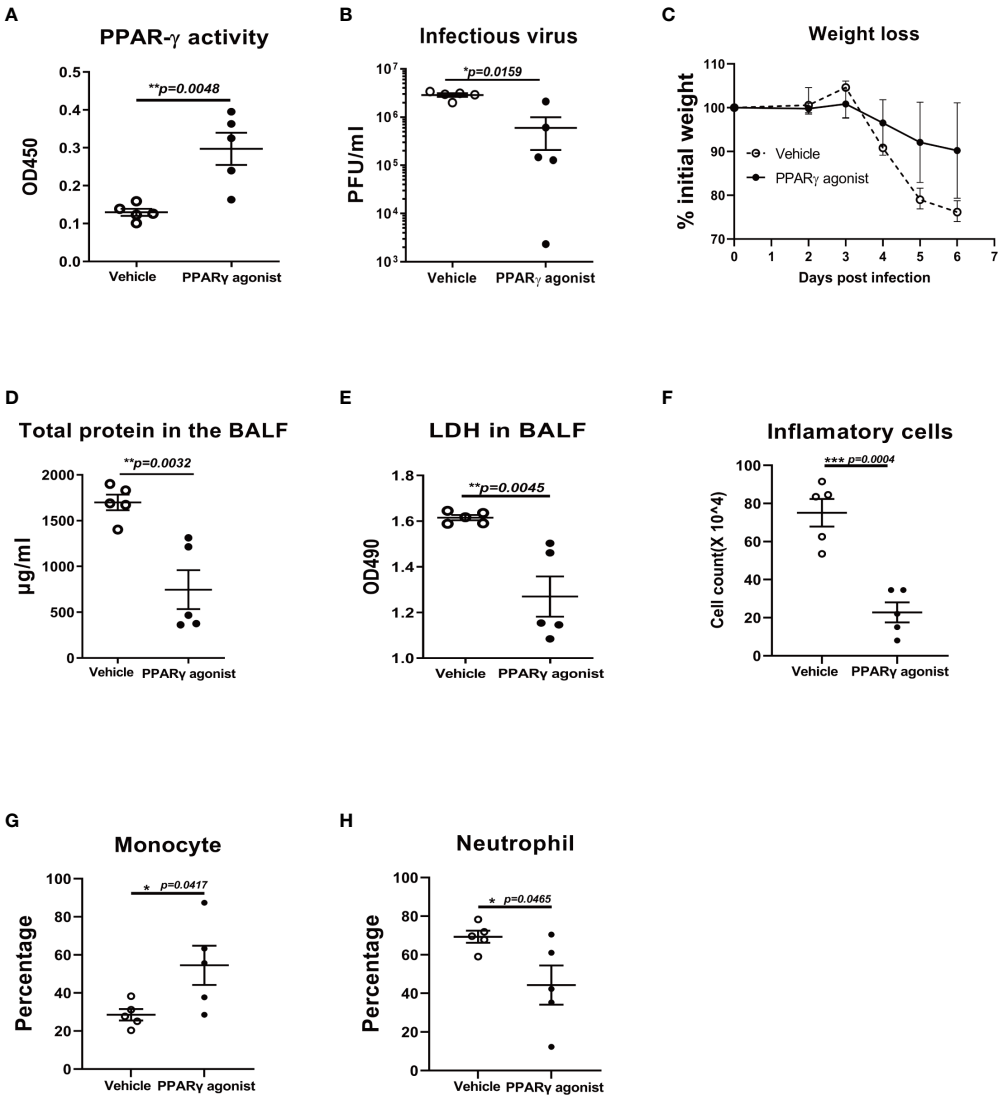

FIGURE 5
PPARγ agonist reduces viral replication and virus-induced weight loss in influenza virus-infected mice. C57B/6 mice were treated with PPARγ agonist troglitazone prior to influenza infection and evaluated viral burden, weight loss, and inflammatory cell differentiation in bronchoalveolar lavage fluid (BALF) and acute lung injury. Compared to the vehicle control-treated group, troglitazone-treated mice displayed elevated PPARγ activity **(A)**, reduced viral burden **(B)** and attenuated weight loss **(C)**. There was a significantly decreased total protein **(D)** and LDH **(E)**, reduced total cell number **(F)**, reduced percentage of neutrophils **(G)**, and an increased percentage of monocytes in the infected BALF **(H)**. Unpaired t test was applied for statistical analysis. *p < 0.05, **p < 0.01, and ***p < 0.001.

Jie Sun's group that PPARγ deficiency enhaces mouse susceptibility to influenza-induced mortality (12).

Gopal et al. did not reveal that PPARγ plays a key anti-inflammatory role in what kind of cells (29). To our knowledge, there is no published paper using human primary macrophages to investigate the role of PPARγ during IAV infection. In the present study, we tested and verified the decreased PPARγ activity in human primary lung macrophages and different mouse macrophages including AM, IM, and BMDM during influenza virus infection. Our results revealed that PPARγ mainly exerts anti-inflammatory effects in human macrophages during IAV infection which had not been reported in any published paper. Some other published papers also investigated the anti-inflammatory effects of PPARγ, but these studies focused on different pathogens and the role of PPARγ in different kind cells like neutrophil but not in the macrophages (30–32). Our study used *in vitro* human primary cell culture and an *in vivo* mouse model of IAV infections, whereas the other focused solely on a mouse model.

Our results have shown that flu infection directly targets macrophages to reduce PPARγ activity and expression, causing

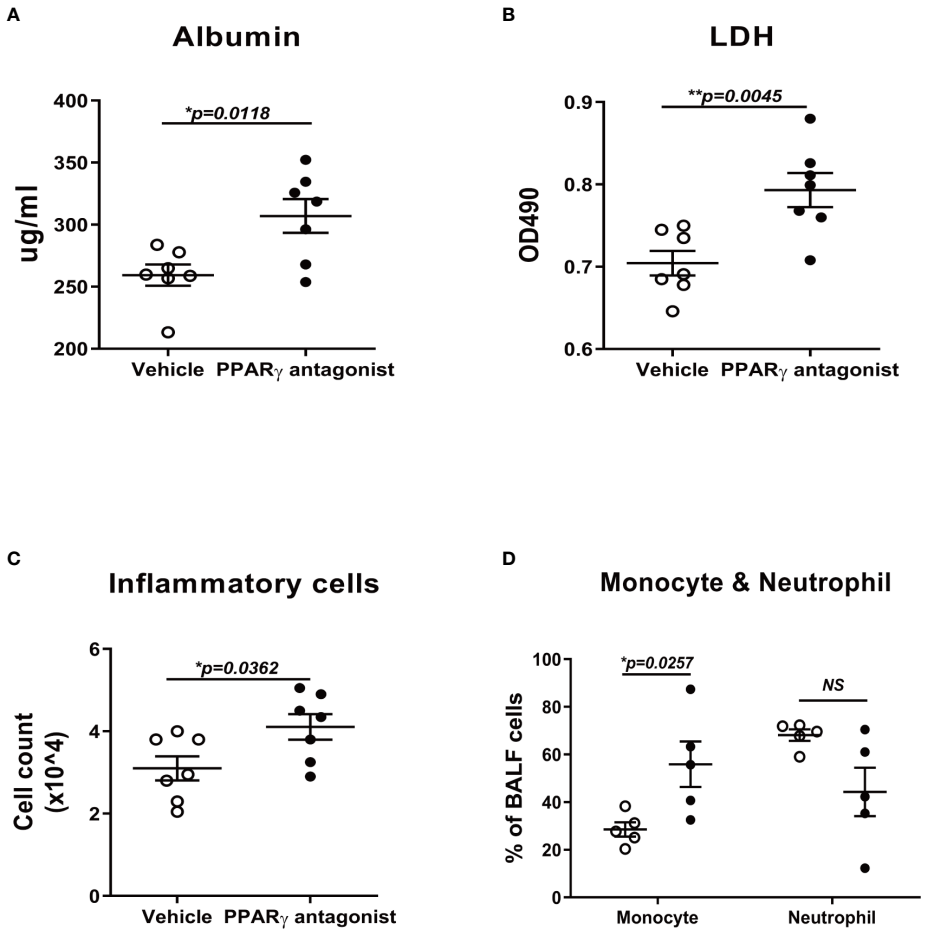

FIGURE 6
PPARγ antagonist promotes influenza-induced lung injury and inflammation. C57B/6 mice were treated with PPARγ antagonist, T0070907, prior to influenza infection and evaluated inflammatory cell differentiation in bronchoalveolar lavage fluid (BALF) and acute lung injury. Compared to the vehicle control-treated group, T0070907 treated mice displayed elevated albumin **(A)**, LDH **(B)**, TNFα **(C)**, and total cell number **(D)**. Unpaired t test was applied for the statistical analysis. ns means no significance. *p < 0.05, **p < 0.01.

lung injury and inflammation. In addition, a study with the respiratory syncytial virus (RSV) has shown a down-regulation of PPARγ expression by a nonstructural protein of RSV virus, and PPARγ agonists have beneficial effects in the suppression of the inflammatory response during RSV infection and therefore might have clinical efficacy in the course of severe RSV-infection (33). To this point, our study provides the mechanistic rationale for anti-inflammatory therapy through PPARγ for influenza and maybe other respiratory infections, including RSV and SARS-Cov2. Further studies to evaluate the effect of the various PPARγ agonists against viral infection will be worthwhile.

The current study provides a novel mechanism by which the influenza virus destroys the anti-inflammatory balance in the lung and causes acute lung injury. In conclusion, we performed *in vitro* and *in vivo* studies to determine the role of PPARγ in influenza infection. This study demonstrates that IAV reduces the transcriptional activity of PPARγ, which is critical for influenza-induced acute lung injury and mortality. Our findings suggest that PPARγ agonists have the potential to be used to limit influenza-related mortality and morbidity.

Data availability statement

The original contributions presented in the study are included in the article/Supplementary Material. Further inquiries can be directed to the corresponding authors.

Ethics statement

The animal study was reviewed and approved by The University of Pittsburgh Institutional Animal Care and Use Committee. Human AMs were isolated from de-identified donors.

Author contributions

HZ performed in vitro and in vivo experiments, collected data, and wrote the manuscript. TA performed PPARg agonist and antagonist experiments in human AMs. SL participated in vivo experiments. DZ edited the manuscript. JW designed experiments, summarized the data, and edited the manuscript. All authors contributed to the article and approved the submission.

Funding

This work was supported by National Institutes of Health grants R03AI101953 (to J.W.), R01HL113655 (to J.W.), and startup funding from the University of Pittsburgh (to J.W.).

Conflict of interest

The authors declare that the research was conducted in the absence of any commercial or financial relationships that could be construed as a potential conflict of interest.

Publisher's note

Supplementary material

The Supplementary Material for this article can be found online at: https://www.frontiersin.org/articles/10.3389/fimmu.2022.958801/full#supplementary-material

SUPPLEMENTARY FIGURE 1
PPARγ agonist inhibits H3N2 induced secretion of IL-8 and TNFα but not IP-10. Isolated human AMs were treated with PPARγ agonist, troglitazone (5 μM) in human Ams after H3N2 virus infection. After infection, cells were cultured with troglitazone for another 24 h. At 24 h after infection, cell-free culture supernatants were collected to detect cytokines using DuoSet ELISA kits from R&D Systems. **(A)** IL-8. **(B)** TNFα. **(C)** IP-10. Unpaired t test was applied for the statistical analysis.γ

References

1. Taubenberger JK, Morens DM. The pathology of influenza virus infections. *Annu Rev Pathol* (2008) 3:499–522. doi: 10.1146/annurev.pathmechdis.3.121806.154316

2. Angeletti D, Yewdell JW. Is it possible to develop a "Universal" influenza virus vaccine? outflanking antibody immunodominance on the road to universal influenza vaccination. *Cold Spring Harb Perspect Biol* (2018) 10(7):1–9. doi: 10.1101/cshperspect.a028852

3. Nachbagauer R, Palese P. Is a universal influenza virus vaccine possible? *Annu Rev Med* (2020) 71:315–27. doi: 10.1146/annurev-med-120617-041310

4. Feige JN, Gelman L, Michalik L, Desvergne B, Wahli W. From molecular action to physiological outputs: peroxisome proliferator-activated receptors are nuclear receptors at the crossroads of key cellular functions. *Prog Lipid Res* (2006) 45(2):120–59. doi: 10.1016/j.plipres.2005.12.002

5. Janani C, Ranjitha Kumari BD. PPAR gamma gene–a review. *Diabetes Metab Syndr* (2015) 9(1):46–50. doi: 10.1016/j.dsx.2014.09.015

6. Arnold R, Konig W. Peroxisome proliferator-activated receptor-gamma agonists inhibit the replication of respiratory syncytial virus (RSV) in human lung epithelial cells. *Virology* (2006) 350(2):335–46. doi: 10.1016/j.virol.2006.03.008

7. Bassaganya-Riera J, Song R, Roberts PC, Hontecillas R. PPAR-gamma activation as an anti-inflammatory therapy for respiratory virus infections. *Viral Immunol* (2010) 23(4):343–52. doi: 10.1089/vim.2010.0016

8. Fantacuzzi M, Amoroso R, Ammazzalorso A. PPAR ligands induce antiviral effects targeting perturbed lipid metabolism during SARS-CoV-2, HCV, and HCMV infection. *Biol (Basel)* (2022) 11(1):114–29. doi: 10.3390/biology11010114

9. Ciavarella C, Motta I, Valente S, Pasquinelli G. Pharmacological (or synthetic) and nutritional agonists of PPAR-gamma as candidates for cytokine storm modulation in COVID-19 disease. *Molecules* (2020) 25(9):2076–90. doi: 10.3390/molecules25092076

10. Cloutier A, Marois I, Cloutier D, Verreault C, Cantin AM, Richter MV. The prostanoid 15-deoxy-Delta12,14-prostaglandin-j2 reduces lung inflammation and protects mice against lethal influenza infection. *J Infect Dis* (2012) 205(4):621–30. doi: 10.1093/infdis/jir804

11. Huang S, Jiang L, Cheon IS, Sun J. Targeting peroxisome proliferator-activated receptor-gamma decreases host mortality after influenza infection in obese mice. *Viral Immunol* (2019) 32(4):161–9. doi: 10.1089/vim.2019.0016

12. Huang S, Zhu B, Cheon IS, Goplen NP, Jiang L, Zhang R, et al. Limper AH et al: PPAR-gamma in macrophages limits pulmonary inflammation and promotes host recovery following respiratory viral infection. *J Virol* (2019) 93(9):1–15. doi: 10.1128/JVI.00030-19

13. Smith MR, Standiford TJ, Reddy RC. PPARs in alveolar macrophage biology. *PPAR Res* (2007) 2007:23812. doi: 10.1155/2007/23812

14. Bain CC, MacDonald AS. The impact of the lung environment on macrophage development, activation and function: diversity in the face of adversity. *Mucosal Immunol* (2022) 15(2):223–34. doi: 10.1038/s41385-021-00480-w

15. Lukan N. "Cytokine storm", not only in COVID-19 patients. mini-review. *Immunol Lett* (2020) 228:38–44.

16. Wang J, Nikrad MP, Travanty EA, Zhou B, Phang T, Gao B, et al. Hartshorn K et al: Innate immune response of human alveolar macrophages during influenza a infection. *PLoS One* (2012) 7(3):e29879. doi: 10.1371/journal.pone.0029879

17. Wang J, Nikrad MP, Phang T, Gao B, Alford T, Ito Y, et al. Hartshorn K et al: Innate immune response to influenza a virus in differentiated human alveolar type II cells. *Am J Respir Cell Mol Biol* (2011) 45(3):582–91. doi: 10.1165/rcmb.2010-0108OC

18. Wang J, Oberley-Deegan R, Wang S, Nikrad M, Funk CJ, Hartshorn KL, et al. Differentiated human alveolar type II cells secrete antiviral IL-29 (IFN-lambda 1) in response to influenza a infection. *J Immunol* (2009) 182(3):1296–304. doi: 10.4049/jimmunol.182.3.1296

19. Travanty E, Zhou B, Zhang H, Di YP, Alcorn JF, Wentworth DE, et al. Differential susceptibility of human lung primary cells to H1N1 influenza viruses. *J Virol* (2015)89(23):11935–44. doi: 10.1128/JVI.01792-15

20. Zhou B, Li Y, Belser JA, Pearce MB, Schmolke M, Subba AX, et al. Garcia-Sastre a et al: NS-based live attenuated H1N1 pandemic vaccines protect mice and ferrets. *Vaccine* (2010) 28(50):8015–25. doi: 10.1016/j.vaccine.2010.08.106

21. Rothberg MB, Haessler SD, Brown RB. Complications of viral influenza. *Am J Med* (2008) 121(4):258–64. doi: 10.1016/j.amjmed.2007.10.040

22. Price I, Mochan-Keef ED, Swigon D, Ermentrout GB, Lukens S, Toapanta FR, et al. The inflammatory response to influenza a virus (H1N1): An experimental and mathematical study. *J Theor Biol* (2015) 374:83–93. doi: 10.1016/j.jtbi.2015.03.017

23. Travanty E, Zhou B, Zhang H, Di YP, Alcorn JF, Wentworth DE, et al. Differential susceptibilities of human lung primary cells to H1N1 influenza viruses. *J Virol* (2015) 89(23):11935–44. doi: 10.1128/JVI.01792-15

24. Poznyak AV, Nikiforov NG, Starodubova AV, Popkova TV, Orekhov AN. Macrophages and foam cells: Brief overview of their role, linkage, and targeting potential in atherosclerosis. *Biomedicines* (2021) 9(9) :1221–32. doi: 10.3390/biomedicines9091221

25. Scirpo R, Fiorotto R, Villani A, Amenduni M, Spirli C, Strazzabosco M. Stimulation of nuclear receptor peroxisome proliferator-activated receptor-gamma limits NF-kappaB-dependent inflammation in mouse cystic fibrosis biliary epithelium. *Hepatology* (2015) 62(5):1551–62. doi: 10.1002/hep.28000

26. Miyazawa M. Immunopathogenesis of SARS-CoV-2-induced pneumonia: lessons from influenza virus infection. *Inflammation Regener* (2020) 40:39. doi: 10.1186/s41232-020-00148-1

27. Wang L, Waltenberger B, Pferschy-Wenzig EM, Blunder M, Liu X, Malainer C, et al. Natural product agonists of peroxisome proliferator-activated receptor gamma (PPARgamma): a review. *Biochem Pharmacol* (2014) 92(1):73–89.

28. Dhurandhar NV, Akheruzzaman M, Hegde V. Potentially modifiable factors to reduce severity of COVID-19 in type 2 diabetes. *Nutr Diabetes* (2020) 10(1):30–2. doi: 10.1038/s41387-020-00133-0

29. Gopal R, Mendy A, Marinelli MA, Richwalls LJ, Seger PJ, Patel S, et al. Peroxisome proliferator-activated receptor gamma (PPAR) suppresses inflammation and bacterial clearance during influenza-bacterial super-infection. *Viruses* (2019) 11(6):505–22. doi: 10.3390/v11060505

30. Birrell MA, Patel HJ, McCluskie K, Wong S, Leonard T, Yacoub MH, et al. PPAR-gamma agonists as therapy for diseases involving airway neutrophilia. *Eur Respir J* (2004) 24(1):18–23. doi: 10.1183/09031936.04.00098303

31. Milam JE, Keshamouni VG, Phan SH, Hu B, Gangireddy SR, Hogaboam CM, et al. PPAR-gamma agonists inhibit profibrotic phenotypes in human lung fibroblasts and bleomycin-induced pulmonary fibrosis. *Am J Physiol Lung Cell Mol Physiol* (2008) 294(5):L891–901. doi: 10.1152/ajplung.00333.2007

32. Sharma R, Kaundal RK, Sharma SS. Amelioration of pulmonary dysfunction and neutrophilic inflammation by PPAR gamma agonist in LPS-exposed guinea pigs. *Pulm Pharmacol Ther* (2009) 22(3):183–9. doi: 10.1016/j.pupt.2008.11.011

33. Arnold R, Neumann M, Konig W. Peroxisome proliferator-activated receptor-gamma agonists inhibit respiratory syncytial virus-induced expression of intercellular adhesion molecule-1 in human lung epithelial cells. *Immunology* (2007) 121(1):71–81. doi: 10.1111/j.1365-2567.2006.02539.x

frontiers | Frontiers in Immunology

TYPE Review
PUBLISHED 02 September 2022
DOI 10.3389/fimmu.2022.989298

OPEN ACCESS

EDITED BY
Rongtuan Lin,
McGill University, Canada

REVIEWED BY
Chunsheng Hou,
Institute of Bast Fiber Crops, (CAAS), China
Xuefeng Qi,
Northwest A&F University, China
Xiaochuan Liu,
University of California, Riverside, United States

*CORRESPONDENCE
Anchun Cheng
chenganchun@vip.163.com

†These authors have contributed equally to this work and share first authorship

SPECIALTY SECTION
This article was submitted to Viral Immunology, a section of the journal Frontiers in Immunology

RECEIVED 08 July 2022
ACCEPTED 12 August 2022
PUBLISHED 02 September 2022

CITATION
Wang J, Sun D, Wang M, Cheng A, Zhu Y, Mao S, Ou X, Zhao X, Huang J, Gao Q, Zhang S, Yang Q, Wu Y, Zhu D, Jia R, Chen S and Liu M (2022) Multiple functions of heterogeneous nuclear ribonucleoproteins in the positive single-stranded RNA virus life cycle. *Front. Immunol.* 13:989298. doi: 10.3389/fimmu.2022.989298

Multiple functions of heterogeneous nuclear ribonucleoproteins in the positive single-stranded RNA virus life cycle

Jingming Wang[1,2,3†], Di Sun[1,2,3†], Mingshu Wang[1,2,3], Anchun Cheng[1,2,3*], Yukun Zhu[1,2,3], Sai Mao[1,2,3], Xuming Ou[1,2,3], Xinxin Zhao[1,2,3], Juan Huang[1,2,3], Qun Gao[1,2,3], Shaqiu Zhang[1,2,3], Qiao Yang[1,2,3], Ying Wu[1,2,3], Dekang Zhu[2,3], Renyong Jia[1,2,3], Shun Chen[1,2,3] and Mafeng Liu[1,2,3]

[1]Institute of Preventive Veterinary Medicine, Sichuan Agricultural University, Chengdu City, China, [2]Key Laboratory of Animal Disease and Human Health of Sichuan Province, Sichuan Agricultural University, Chengdu City, China, [3]Avian Disease Research Center, College of Veterinary Medicine, Sichuan Agricultural University, Chengdu City, China

The heterogeneous nuclear ribonucleoproteins (hnRNPs) are a diverse family of RNA binding proteins that are implicated in RNA metabolism, such as alternative splicing, mRNA stabilization and translational regulation. According to their different cellular localization, hnRNPs display multiple functions. Most hnRNPs were predominantly located in the nucleus, but some of them could redistribute to the cytoplasm during virus infection. HnRNPs consist of different domains and motifs that enable these proteins to recognize predetermined nucleotide sequences. In the virus-host interactions, hnRNPs specifically bind to viral RNA or proteins. And some of the viral protein-hnRNP interactions require the viral RNA or other host factors as the intermediate. Through various mechanisms, hnRNPs could regulate viral translation, viral genome replication, the switch of translation to replication and virion release. This review highlights the common features and the distinguish roles of hnRNPs in the life cycle of positive single-stranded RNA viruses.

KEYWORDS

host-pathogen interaction, positive single-stranded RNA virus, heterogeneous nuclear ribonucleoprotein, viral life cycle, immune response

Introduction

Positive single-stranded RNA viruses include a broad group of well-known pathogens in the *Picornaviridae*, *Flaviviridae*, *Coronaviridae* and other viral families (1). These viruses generally endanger human health and cause economic burdens as well as societal costs. For example, severe acute respiratory syndrome-coronavirus-2 (SARS-CoV-2, belonging to the *Coronaviridae* family) has spread worldwide for the past two years, threatening lives by causing severe symptoms in patients and resulting in millions of deaths (2). Hepatitis C virus (HCV, belonging to the *Flaviviridae* family) was estimated to infect 71 million people worldwide, and the number of infected people has increased by nearly 2 million a year, causing cirrhosis, hepatocellular carcinoma, liver failure and even death (3, 4). And enterovirus (belonging to the *Picornaviridae* family) threats human health by its extensive outbreak and causing deaths (5). Positive single-stranded RNA viruses mostly contain a limited-sized genome that encodes several or at most dozens of proteins (6). Viruses require assistance from host factors to replicate successfully in cells and also develop diverse mechanisms to exploit host factors to aid the different life cycle stages for maintaining viral efficient propagation (6–8). Positive single-stranded RNA viruses can translocate host factors to the cytoplasm and support their life cycle (9–11). And some proteins in host cells are closely related to viral proteins or RNAs to inhibit virus propagation (12). A recent study revealed that 104 host proteins could interact with SARS-CoV-2 RNA and participate in viral translational initiation, transcription and immune response. Additionally, 23 of these proteins could be targeted with existing drugs (13). To defend themselves from virus infection, host cells also develop some strategies to drive proteins or other host factors to confine viral proteins or RNA to restrain the virus replication (14). Therefore, studying host proteins that interact with viral genomics or viral proteins is beneficial for understanding RNA virus pathogenesis and providing information on developing antiviral therapies and vaccines (15).

HnRNPs constitute a group of RNA-binding proteins that recognize specific RNA sequences and are reported to be frequently involved in RNA metabolism processes such as pre-mRNA splicing, transcription and translation regulation (16). The hnRNP family mainly comprises 20 proteins, and they are named in alphabetical order from hnRNP A1 to hnRNP U (and RALY, which is also known as HNRPCL2 or P542), with molecular weights ranging from 34 kDa to 120 kDa (16). HnRNPs can bind to heterogenous nuclear RNAs (hnRNAs) or pre-mRNAs, which are primary transcripts generated by polymerase II (17). This binding activity is linked with pre-mRNA splicing, causing impaired binding capacity of hnRNP A, B, C and I and leading to splicing inhibition (18). Heterogeneous ribonucleoproteins (hnRNPs) are proteins identified to associate with the virus components during positive-strand RNA virus infection (19–21).

The structure of hnRNPs usually includes RNA-binding/RNA recognition motifs and other domains/motifs related to cytoplasmic redistribution or the binding of nucleotide sequences (22, 23). Although hnRNPs share some similar structural features, they can be very different from each other (see Figure 1). Many members of hnRNPs possess RNA recognition motifs/RNA binding domains (RRMs/RBDs), while hnRNP E and hnRNP K possess specific RNA binding domains called K-homology domains (KH domains) (16). These structures identify and bind to specific RNA sequences, so different hnRNPs have distinctive sequence affinities. For example, the RRM1 of hnRNP A2/B1 recognizes adenine-guanine–guanine (AGG) motifs, and its RRM2 recognizes uridine-adenine-guanine (UAG) motifs (24). Most hnRNPs are confined within the nucleus, while a few others can shuttle between the cytoplasm and nucleus (18, 25). Several structures are responsible for their localization rearrangement. Some hnRNPs contain a nuclear localization sequence (NLS), which is in charge of nuclear import (26). The other sequence that mediates the hnRNPs nuclear import/export is the M9 sequence (27). However, more information on the mechanisms by which hnRNPs are exported from the nucleus to the cytoplasm remains to be defined. It is also worth mentioning that the abundance of hnRNPs is distinctive in different organisms (for example, hnRNP C was identified to be highly expressed in the neurons and testicles of mice but not detectable in the lung or pancreas) (28). In addition to binding RNA, hnRNPs are also associated with DNA biogenesis as they are involved in DNA replication, damage repair and telomere functioning (29). For instance, it has been shown that hnRNP K can modulate neurotransmitter gene biosynthesis and participate in activation-induced cytidine deaminase-mediated antibody diversification (30, 31).

HnRNPs are involved in many steps of viral infection process, including replication, translation, the switch of translation to replication, as well as virion release (19, 32, 33). For example, the SARS-CoV-2 N protein can partition into liquid condensates with hnRNP A2 and hnRNP P to promote viral replication (19). The negative-stranded RNA of poliovirus (PV) could interact with hnRNP C to enable positive-stranded RNA synthesis (32). During enterovirus 71 (EV71) infection, hnRNP A1 can bind to viral internal ribosome entry site (IRES), which leads to enhanced IRES-mediated translation, and hnRNP K interacts with stem-loops I, II, and IV to participate in viral replication (34, 35). Some viruses could take advantage of hnRNPs by rearranging these proteins from the nucleus to the cytoplasm (36, 37). With positive-stranded RNA viruses replicate in the cytoplasm, distributed hnRNPs are able to interact with viral proteins or RNA to either assist or hinder virus multiplication (1, 36, 37). Therefore, discussing the

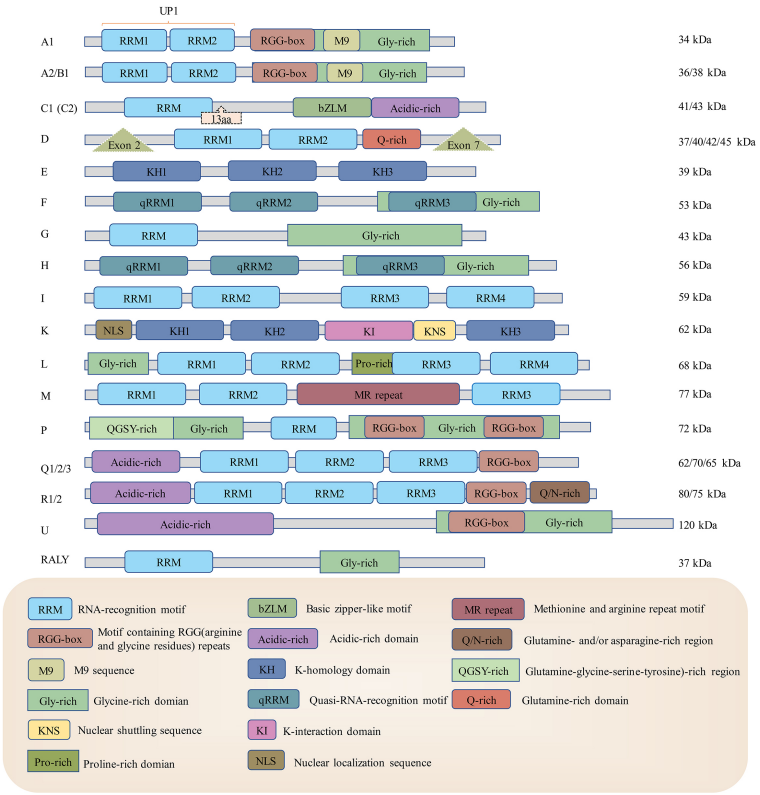

FIGURE 1
The structures of heterogeneous ribonucleoproteins from hnRNP A1 to RALY. HnRNPs have different structures using some shared and distinctive elements. RRM: RNA recognition motif, KH: K-homology domain, RGG-box: motifs containing arginine and glycine repeats, M9: M9 sequence, Gly-rich: glycine-rich domain, bZLM: basic leucine zipper-like motif, Acidic-rich: acidic-rich domain, Q-rich: Glutamine-rich domain, Exon: The splicing site of enzyme to create various mRNAs, therefore translated into different proteins, NLS: nuclear localization sequence, KI: K-interaction domain, Pro-rich: Proline-rich domain, KNS: nuclear shuttling domain, MR-repeat: methionine and arginine repeat motif, QGSY-rich: (glutamine-glycine-serine-tyrosine)-rich region, Q/N-rich: glutamine- and/or asparagine-rich region. RRMs and KH domains are usually responsible for virus RNA recognition and binding, and M9 and NLS are mainly responsible for hnRNP nuclear retention.

interactions between viruses and hnRNPs improves our understanding of the molecular mechanisms of viral attacks on host cells and the strategies through which our bodies resist these invasions (38).

Roles of heterogeneous nuclear ribonucleoproteins in the positive-strand virus life cycle

HnRNP A/B

The four paralogues of hnRNP A/B proteins are hnRNP A1, A2/B1, A3 and A0, and all of them were reported to have several isoforms except for A0. The structures of hnRNP A/B proteins are highly conserved among each other and they normally locate at the nucleus (39). Another study suggested that although hnRNP A/B colocalized with spliceosomal complexes within the nucleus, hnRNP A1 was abundant at the membrane of the nucleus while A2/B1 and A3 accumulated in perinucleolar areas (40). HnRNP A/B are responsible for RNA splicing, trafficking and mRNA translation regulation (both Cap-dependent and IRES-dependent). Besides, hnRNP A1 and A2/B1 also possess DNA-binding ability (39).

Among these subgroup proteins, hnRNP A1 is one of the most abundant and ubiquitously expressed proteins (27). HnRNP A1 contains an unwinding protein 1 (UP1) domain comprising two RNA-recognition motifs (RRM1 and RRM2) in the N-terminus followed by specific motifs, an RGG box, a prion-like domain and a nuclear-shuttling sequence called the M9 sequence in the C-terminus (26, 41). UP1 and the RGG-box affect the ability of hnRNP A1 to unfold DNA G-quadruplexes, and the prion-like domain is closely related to stress granule assembly (41, 42). HnRNP A1 shuttles rapidly between the cytosol and the nucleus, and its M9 is vital for its import back into the nucleus. A study revealed that TMG-induced O-linked N-acetylglucosaminylation reinforces hnRNP A1 nuclear

localization and that sorbitol-induced phosphorylation of hnRNP A1 results in its cytoplasmic accumulation (43). Notably, although hnRNP A1 is expressed in most tissues, it was identified to be most abundant in neurons of the central nervous system (28). HnRNP A2/B1 is crucial to oligodendrocyte and neural mRNA trafficking (44).

Some coronaviruses were reported to be associated with hnRNP A1 (45–51). An early study suggested that the nucleocapsid protein (N protein) of SARS coronavirus had a high affinity with hnRNP A1, and the protein-protein interaction requires 161-220 aa of SARS coronavirus N protein and 203-320 aa of hnRNP A1 (45). It was also suggested that hnRNP A1 might participate in the switch from viral translation to replication because N6-methyl adenosine (m6A) marked SARS-CoV-2 RNA recruit hnRNP A1 and enhance viral genome transcription while suppressing translation. And this interaction could be inhibited by 3-Deazaneplanocin A (DZNep) (46). And During SARS-CoV-2 infection, the cellular location of hnRNP A2/B1 is rearranged by NSP1, leading to restrained immune response and enhancing infection by SARS-CoV-2 and β-coronavirus, but the mechanism by which this occurs remains to be explained (36). And a recent study pointed out that hnRNP A2/B1 could associate with SARS-CoV-2 RNA to promote viral replication, which could be targetable for antiviral drugs (52).

HnRNP A1 interacts with the porcine epidemic diarrhoea virus (PEDV) N protein to promote viral replication, and inhibition of hnRNP A1 could result in reduced virus copy numbers of different strains of PEDV in CCL81 cells (47) (see Figure 2A). Despite the lack of evidence, hnRNP A1 was hypothesized to facilitate PEDV replication through binding to the 5' end sequence and intergenic IG sequence, which is required for coronavirus optical transcription of nested subgenomic mRNA (47). Interestingly, the hnRNP A1 level was downregulated during PEDV YN144 strain infectin, a finding different from that in cells infected with the YN13 strain, where the hnRNP A1 levels were not remarkably changed. This phenomenon was presumed to be related to the weaker virulence of YN144 (48). Mouse hepatitis virus (MHV) infection could result in cytoplasm retention of hnRNP A1 and binding of hnRNP A1 to transcription regulation areas of MHV negative-stranded RNA (49). Interestingly, C-terminal deletion of hnRNP A1 inhibited MHV replication, while full-length hnRNP A1 reinforced MHV replication (50). hnRNP A1 was also detected to interact with MHV N proteins in the cytoplasm, but the effect of this interaction during MHV infection remained unexplored (51). As mentioned above, the N protein of SARS-CoV-2, PEDV and MHV could interact with hnRNP A1, and the interaction favours the virus replication (47).

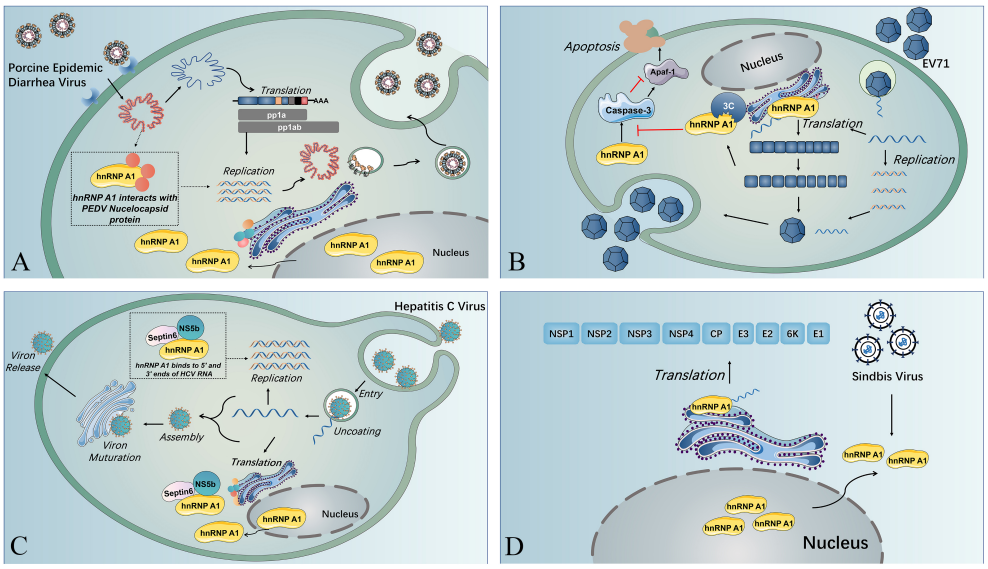

FIGURE 2
The multiple functions of hnRNP A1 in viral life cycles. **(A)** Nuclear translocation of SV induces cytoplasmic retention of hnRNP A1, and hnRNP A1 binds to the 5′ UTR of SV RNA, resulting in enhanced viral translation. **(B)** HnRNP A1 interacts with the nucleocapsid of PEDV and facilitates PEDV replication near the nucleus. **(C)** HnRNP A1 binding to the 5′ UTR and 3′ UTR of HCV RNA and forming a complex with septin 6 and NSb5 induces the cyclization of HCV RNA and reinforces HCV RNA replication. **(D)** HnRNP A1 could bind to Apaf-1 mRNA to promote Apaf-1 translation and then upregulate the expression of caspase-3, resulting in cell apoptosis and virion release. EV71 3C protease could splice hnRNP A1 and abolish its capacity to bind to Apaf-1 mRNA and downregulate caspase-3 expression, guaranteeing sufficient virus replication before virion release.

HnRNP A1 also affect the replication of viruses from other virus families (20, 53). HnRNP A1 usually affects the viral translation by associating with the IRES within viral RNA (20, 53, 54). The IRES trans-acting factor (ITAF) activity of hnRNP A1 could be regulated through posttranslational modifications (PTMs). HnRNP A1 PTMs are recognized by different viruses to modulate their IRES-dependent translation (55). HnRNP A1 acts as an ITAF with EV71 IRES to regulate IRES-dependent translation, and hnRNP A2 shows a similar function during EV71 infection. Furthermore, EV71 infection stimulates the phosphorylation of p38 mitogen-activated protein kinase (MARK), which induces the cytoplasmic relocalization of hnRNP A1 and induces IRES-mediated viral protein translation (56). A study indicated that EV71 translation could be restrained by inhibition of hnRNP A1 shuttling from the nucleus to the cytoplasm through the use of an inhibitor (SB203580) that can inhibit p38 MAPK (57). The association of hnRNP A1 and A2 on EV71 IRES was demonstrated to be inhibited by a dietary flavonoid called apigenin, and virus infection was downregulated when cells were given apigenin (53), which could be that apigenin target the glycine-rich domain of hnRNP A2, disrupting its multimerization and splicing activity (58). HnRNP A1 can trigger IRES-mediated translation of human rhinovirus (HRV) RNA and inhibit IRES activity of apoptotic peptidase activating factor 1 (apaf-1) mRNA. The binding of hnRNP A1 to the apaf-1 IRES hinders apaf-1 from hampering cell apoptosis and guaranteeing that the virus propagates sufficiently before releasing virions (59). The EV71 3C protease cleaves hnRNP A1, promoting apaf-1 translation and apoptosis and enables virus spreading (54) (see Figure 2B). Besides, hnRNP A1 could bind to the 5'-untranslated region (UTR) and 3'-UTR of the HCV genome, forming a complex with NS5b and septin 6 to promote viral replication (20) (see Figure 2C). In addition to IRES-mediated translation of RNA viruses, hnRNP A1 could also affect non-IRES-initiated translation, such as that of Sindbis virus (SINV). And during SINV infection, hnRNP A1 also undergoes retention in the cytoplasm, binding to the 5' UTR of SINV RNA and promoting SINV translation, but the exact mechanism remains to be explored (60) (see Figure 2D).

HnRNP A2 has been confirmed to interact with Japanese encephalitis virus (JEV) NS5 by binding to the 5' UTR of the negative-stranded RNA to enhance viral replication (61). Additionally, hnRNP A2 also binds to the 3' UTR of DENV (62). And hnRNP A2 has been discovered to show RNA-binding activity similar to that of hnRNP A1 to MHV, modulating MHV RNA synthesis (63). During persistent Junín virus (JUNV) infection, not only was the location of hnRNP A/B rearranged to the cytoplasm, but the expression level of hnRNP A/B was also lowered than that under normal conditions (64). And when hnRNP A1 and hnRNP A2 were silenced, the replication of JUNV was significantly reduced, and JUNV infection caused the cytoplasmic distribution of hnRNP A1 but not hnRNP A2 (61, 65).

HnRNP C

HnRNP C is a critical RNA-binding protein with functions in RNA expression, stability, mRNA splicing, nonspecific sequence exportation and 3'-end processing (66, 67). HnRNP C is predominantly located in the nucleus, and its expression level was upregulated in multiple tumours, including lung cancer, hepatocellular carcinoma, glioblastoma, melanoma and breast cancer (68–71). HnRNP C1/C2 consists of a RRM, a basic leucine zipper-like motif (bZLM), a NLS and an acid-rich C-terminal domain. There are 13 amino acid residues between RRM and bZLM in hnRNP C2, distinguishing it from hnRNP C1 (67). HnRNP C proteins can form $C1_3C2$ tetramers in native hnRNP complexes (32, 66, 72).

Although HnRNP C1/C2 is normally located in the nucleus, its trafficking from the nucleus to the cytoplasm is observed during PV and RV infection (68). This relocalization may be attributed to either of the two mechanisms: the degradation of the nuclear pore complex (NPC) or the interaction with viral proteins and cellular proteins (66). The NPC forms a channel that allows macromolecules to shuttle between the cytoplasm and nucleus (69). Degradation of the NPC components Nup153 and p62 during RV or PV infection may be related to the inhibition of nuclear import pathways, resulting in cytoplasmic accumulation of hnRNP C1/C2 (70, 71).

HnRNP C can interact with PV RNA and proteins to stimulate viral RNA synthesis, as hnRNP C serves as an important component of RNP during PV infection-induced complex formation that promotes the initiation of positive-strand RNA synthesis (72). HnRNP C binds to both termini of virus negative-stranded RNA, forming a multimer that facilitates PV RNA synthesis. And C-terminal truncated hnRNP C1/C2 inhibits PV replication, suggesting that hnRNP C1/C2 associates with PV RNA through its C-terminus (72). During picornavirus infection, negative-stranded RNA is the template for viral replication, and the circulation of viral RNA is crucial for efficient replication, so the hnRNP C stabilizing interaction between the 5'-UTR and 3'-UTR of negative-stranded RNA contributes to viral replication (32).

Other members of the *Picornaviridae* family may show the same regulatory action due to the highly conserved sequence within the IRES (73). During Coxsackie B virus (CVB3) infection, hnRNP C1/C2 could bind to the 5' UTR of virus RNA and replace polypyrimidine tract-binding protein (PTBP, or hnRNP I) and bind to stem-loop V in the CVB3 IRES, inhibiting the translation of CVB3. And it could mediate the translation-replication switch without the help of CVB3 3CD (73, 74). Interestingly, hnRNP C1/C2 exhibits a higher affinity

for negative-stranded viral RNA than positive-strand viral RNA, although positive-strand viral RNA outnumbered negative-stranded viral RNA (74). During CVB3 infection, the positive-stranded/negative-stranded viral RNA ratio altered under the control of hnRNP C1/C2 (74).

In addition to interacting with picornavirus RNA, hnRNP C1/C2 has been discovered to bind to precursors of PV 3CD, P2 and P3 precursors, which likely recruit 3CD to the replication complex/replication organelle (RC/RO) (68). The RC/RO is a unique structure that forms in positive RNA virus-infected cells and contains several viral proteins and host factors required for efficient replication of viral RNA (75). And how the association of hnRNP C1/C2 and RC/RO contribute to the viral replication require further investigation.

Multiplication of a member of *Flaviviridae* family is also reported to be regulated by hnRNP C1/C2 (76). Knockdown of hnRNP C1/C2 using specific siRNA, and the hnRNP C1/C2 knockdown cells were less infected by DENV compared to normal cells. And the viral RNA level and relative expression level of viral proteins declined while hnRNP C1/C2 is knocked down (but not through directly resisting viral translation). Notably, the supernatant virus titers were also lowered in hnRNP C1/C2 knockdown cells (77). HnRNP C1/C2 can also interact with the DENV NS1 protein, but whether it affects DENV infection remains unknown, and further exploration is required (76).

HnRNP D

Due to alternative exon splicing, four protein isoforms of hnRNP D (also known as AU-rich element RNA-binding protein 1, AUF1) have been identified and named based on their molecular weight: $p37^{AUF1}$, $p40^{AUF1}$, $p42^{AUF1}$ and $p45^{AUF1}$. All these isoforms contain two RRMs and a glutamine-rich (Q-rich) motif (16). Isoforms $p37^{AUF1}$ and $p40^{AUF1}$ have a nuclear import signal, while $p42^{AUF1}$ and $p45^{AUF1}$ have a nuclear export sequence within exon 7, while the two smaller isoforms lack the sequence (78). All four isoforms of hnRNP D were reported to be mainly located in the nucleus, but they could shuttle between the cytoplasm and nucleus in a transcription-dependent manner. It was also suggested that the interaction between the smaller two isoforms and two larger isoforms might contribute to the shuttle function of hnRNP D. HnRNP D is an extensively studied AU-rich-binding protein predominantly responsible for rapid mRNA degradation. In addition, hnRNP D regulates the stabilization of ARE-mRNAs and the transcription of certain genes (79).

Among the hnRNP D isoforms, $p45^{AUF1}$ significantly promotes the replication of several members of the *Flaviviridae* family, including Zika virus (ZIKV), West Nile virus (WNV), DENV and HCV (80). It was reported that $p45^{AUF1}$ could reinforce WNV RNA synthesis by inducing a structural shift of WNV RNA and enhancing the WNV RNA 5'- 3' interaction by binding the AU-rich region of the WNV RNA 3' UTR and destabilizing the 3' stem structure of the 3' CL of WNV RNA (81). The same research group reported that although hnRNP D is generally considered an AU-rich binding protein, the AU-rich sequence of WNV RNA was not required for $p45^{AUF1}$-mediated WNV replication reinforcement *in vitro* but was necessary *in cellulo* (81). In addition to acting as an RNA chaperone for WNV RNA, $p45^{AUF1}$ was also suggested to have an annealing function over WNV RNA, and the RNA chaperone activity is regulated by arginine methylation at the C-terminus of $p45^{AUF1}$. The methylation of $p45^{AUF1}$ mediated by methyltransferase PRMT1 remarkably increases $p45^{AUF1}$ affinity to WNV RNA, thereby strengthening the binding ability of $p45^{AUF1}$ to viral RNA and supporting efficient WNV RNA synthesis (82).

Similar to the function of hnRNP D during WNV infection, a later study demonstrated that $p45^{AUF1}$ also destabilizes DENV and ZIKV RNA 3' stem-loops as well as 5' stem-loops to facilitate negative-stranded RNA synthesis by aiding in shifting viral translation to replication. As expected, depletion of $p45^{AUF1}$ reduced DENV and ZIKV replication in human cells (80). The interaction of hnRNP D and HCV IRES facilitates viral translation ($p45^{AUF1}$ had the strongest effect), and siRNA-mediated knockdown of hnRNP D remarkably downregulated viral replication (83). Encouragingly, HCV RNA can move from heavy polysomes to light polysomes when hnRNP D is reduced (83).

Unlike the roles of hnRNP D in the *Flavivirus* family, hnRNP D is predominantly a restriction factor of viral replication for enteroviruses (37, 84). All four isoforms were reported to bind to stem-loop IV of both PV and HRV, and the copy numbers of the viruses were increased in the absence of hnRNP D, suggesting that hnRNP D somehow limited the virus infection (85). HnRNP D could restrict PV and CVB3 replication by inhibiting viral RNA synthesis and IRES-driven translation, and the inhibition of hnRNP D on viral RNA synthesis is not due to interacting with the 3' NCR of viral RNA or inducing viral RNA decay (86). Interestingly, EV71 translation is affected by hnRNP D but not EMCV RNA synthesis (86). Although cytoplasmic retention of hnRNP D was discovered in PV-, CVB3-, HRV-, EV71- and EMCV-infected cells, EMCV uses a different approach from other enteroviruses (37). And unlike other enterovirus 2A protein acting as a protease, the 2A protein of EMCV does not exhibit protease activity. However, it was indicated that Nup62 and Nup153 were targeted by both enterovirus 2A protein (through cleavage) and EMCV L protein (through phosphorylation), and thus, the nucleocytoplasmic transport feature of them was altered (70, 87). HnRNP D colocalizes with the 2A protein near the predicted replication complex in the cytoplasm in PV- and HRV16-infected cells (85).

In addition to changing the properties of the nuclear pore complex, the 3C/3CD of several enteroviruses blocks the restriction activity of hnRNP D by impairing their multiplication (86). HnRNP D was confirmed to be cleaved by 3C/3CD of PV, HRV and CVB3 (86). This cleavage results in disruption of hnRNP D binding to stem-loop IV of the viral RNA strand and thus resists restriction of hnRNP D on virus propagation, possibly caused by cleavage at the N-terminus to impair the dimerization of hnRNP D (85). Furthermore, because the CVB3 genome contains AU-rich sequences within the 3' UTR, the cleavage of hnRNP D by CVB3 3CD can disrupt the binding of hnRNP D to the 3' UTR of CVB3; thus, the stability of viral RNA is reinforced (84) (see Figure 3). Unlike the situation during enterovirus infection, there were not observable cleavage of hnRNP D was detected during EMCV infection (37). According to the studies mentioned above, the distinct behaviour of hnRNP D during EMCV infection might attribute to the alternative function of EMCV 2A protein (85–87).

Notably, hnRNP D was also reported to be recruited to stress granules (SGs) during high-dose infection with CVB3 and EV71 (88). Stress granules are complexes without membrane structures that form under stress pressure, such as viral infection, and can stall overall translation, including viral translation (89), so figuring out relationships of hnRNP D and viral RNA/proteins within SGs might reveal a mechanism that affect viral translation.

HnRNP E

HnRNPs E1 and E2 are also known as poly(C)-binding protein-1 (PCBP-1) and PCBP-2. The remaining two members (hnRNP E3 and E4) are divergent from hnRNP E1 and E2 (16, 90). Unlike hnRNP E1 and E2, which are located in the nucleus, hnRNP E3 and E4 are identified to be predominantly in the cytoplasm, and are generally not considered as hnRNPs. And they all contain 3 KH domains (16). Each KH domain contains three α-helices and three β-folds and can target specific RNA and DNA. The sequences in KH domains are highly conserved, but sequences outside the KH domains vary. Both hnRNP E1 and E2 are highly expressed in the nucleus, exhibiting 89% similarity in sequence homology. However, the cytoplasmic roles of hnRNP E1 and E2 have attracted considerable attention because of their roles in alternative splicing, mRNA stability and translation. As an RNA chaperone, hnRNP E1 can unfold the secondary structure of the IRES, facilitating the binding of hnRNP I and recruitment of ribosomes to initiate translation (17, 90).

HnRNP E were predominantly reported to be associated with stem-loops of viral RNA, within cloverleaf or IRES (91–97). During PV infection, hnRNP E2 was confirmed to bind to stem-loop V of PV IRES and required for PV translation (91, 92). Both hnRNP E1 and hnRNP E2 bind to stem-loop IV and cloverleaf, and they form heterodimers to interact with PV RNA to reinforce viral translation (93). Another study pointed out that although hnRNP E1 and E2 both have the capacity to bind to PV cloverleaf and stem-loop IV, these two isoforms have different affinities: hnRNP E2 was identified to have a much stronger capacity to bind to PV stem-loop IV than hnRNP E1, while the binding ability of PV cloverleaf was similar (97). Furthermore, hnRNP E binds to stem-loop B of PV RNA cloverleaf to remarkably strengthen PV 3CD binding to stem-loop D of PV RNA cloverleaf, and they form a hnRNP E-RNA-3CD ternary complex (93) (see Figure 4). Together, hnRNP E and PV 3CD

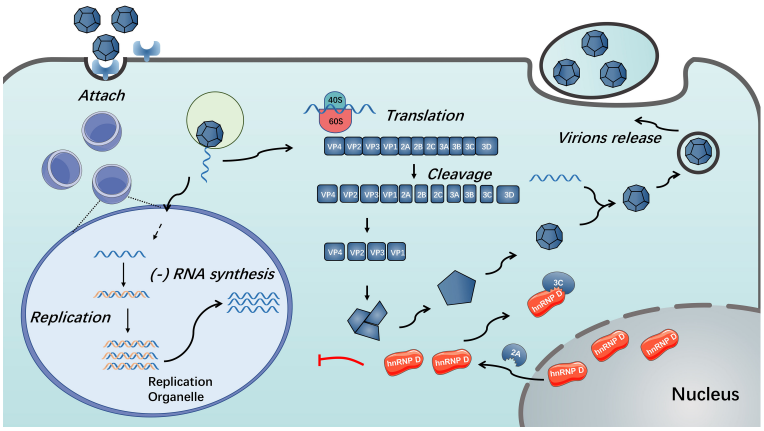

FIGURE 3
Functions of hnRNP D in enterovirus replication. During enterovirus infection, hnRNP D translocates from nucleus to cytoplasm in a 2A protein-dependent manner. The presence of hnRNP D could restrict enterovirus RNA replication. Enterovirus 3C/3CD could cleave hnRNP D and disable it from inhibiting virus RNA replication (85, 86).

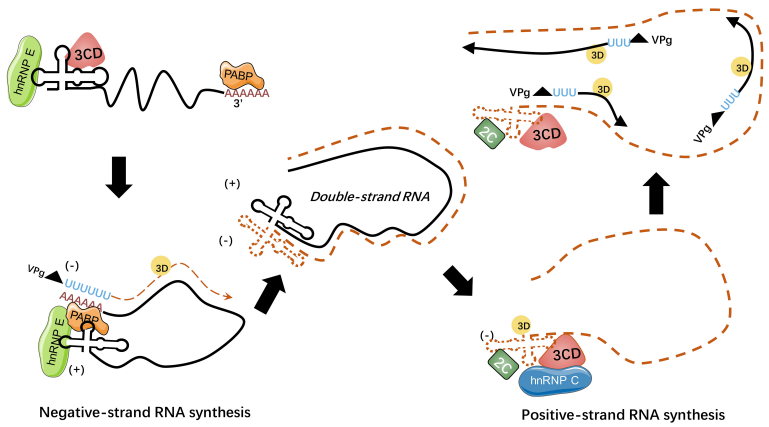

FIGURE 4
HnRNPs regulate picornaviral RNA synthesis. During picornavirus infection, viral genome circularizes through the interaction of hnRNP E-cloverleaf-3CD complex with PABP to initiate the synthesis of minus-strand RNA. The hnRNP E could bind to cloverleaf of positive-strand RNA with 3CD precursor while hnRNP C could bind to the minus-strand RNA with viral 2C ATPase to stabilize the cloverleaf structure. The processes of RNA replication rely on the interaction between hnRNPs and viral template RNA (98).

can modulate the switch from viral translation to replication (94). It was assumed that cleavage of hnRNP E by PV 3C/3CD mediates the viral translation-replication shift because the cleavage between the KH2 and KH3 domains results in the truncated hnRNP E that lacks the KH3 domain, with intact function in replication but impaired function in translation (95). Interestingly, a study indicated that PV 3CD binds to cloverleaf stem-loop D of PV RNA to rearrange hnRNP E from binding PV cloverleaf to stem-loop IV to some degree, while the importance of this activity remained unspecified (96).

During EV71 infection, hnRNP E1 binds to stem-loops I and IV within the 5'-UTR after being recruited to the viral membrane-associated complex to facilitate replication (99). APOBEC3G (A3G), a broad-spectrum antiviral factor, competitively binds to the EV71 5'-UTR to restrain the interaction between the 5'-UTR and hnRNP E1 and inhibiting viral replication and protein synthesis (100). Whether A3G could inhibit 5' UTR-hnRNP E1 interaction of other viruses awaits future studying.

This KH domain-dependent hnRNP E-viral RNA interaction could protect PV RNA from 5' exonuclease and maintain viral RNA stability of coxsackieviruses, echoviruses, and rhinoviruses (101). Stabilized viral RNA is essential not only for viral polysome formation but also for efficient viral translation and replication (101, 102). The interaction of the hnRNP E2 KH3 domain and PV cloverleaf could stimulate PV translation, along with the interaction between PV 2A and poly (A) tail (103). CVB3, another enterovirus member, was also reported to interact with hnRNP E (104). HnRNP E2 was identified to interact with cloverleaf and IRES IV of CVB3 RNA, with its KH1 domain binding to subdomain C of IRES IV and the KH3 domain binding to subdomain B of IRES IV (105). Similar to the findings in PV-infected cells, hnRNP E binding to the cloverleaf of CVB3 RNA to facilitate the synthesis of viral subgenomic negative-stranded RNA (106).

Calicivirus IRES was slightly distinct from type I IRES of PV, it constituted an important GNRA tetraloop in subdomain d10c. This tetraloop was identified to bind to the KH1 and KH2 domain of hnRNP E2, along with another subdomain d10b within IRES binding to the KH3 domain of hnRNP E2. And the KH2 domain of hnRNP E2 is required for efficient calicivirus replication initiation (107). HnRNP E1 and E2 also interact with HCV 5' UTR RNA, but their roles during HCV infection require more research to specify (108). A later study demonstrated that hnRNP E2 could bind to HCV IRES to promote viral translation. hnRNP E2 partially localize to the detergent-resistant membrane fraction and associate with HCV nonstructural protein NS5 to facilitate viral replication by circularizing the HCV genome within the HCV replication complex (109). Porcine reproductive and respiratory syndrome virus (PRRSV) was also associated with hnRNP E1 and E2 (110). HnRNPs E1 and E2 were discovered to interact with the PRRSV RNA 5' UTR and nonstructural protein 1β (nsp1β) to be involved in PRRSV genome replication and transcription and colocalize with the viral replication and transcription complex in the cytoplasm (110). Another study confirmed that the nsp1β-hnRNP E2 interaction requires the C-terminal extension (CTE) domain and C-terminal papain-like cysteine protease domain (PCPβ) domain of PRRSV nsp1β and the KH2 domain of hnRNP E2, and its putative mechanism for modulating viral translation and

replication is through controlling the translation-replication switch (111). Both hnRNP E1 and hnRNP E2 can interact with the P protein of vesicular stomatitis virus (VSV) and antagonize viral infection by reducing viral gene expression (112).

HnRNP I

HnRNP I, also known as PTBP, regulates splicing by binding to polypyrimidine stretches at a branch point upstream of exons. Similar to the structure of hnRNP L, hnRNP I composed of four RRMs. Both hnRNP L and hnRNP I participate in RNA-related biological processes, including mRNA stabilization, pre-mRNA and translation. Both PTBP1 and PTBP2 can interact with CU repeats to repress nonconserved cryptic exons (113).

During positive single-stranded RNA virus infection, hnRNP I can regulate viral IRES-dependent translation and viral replication (114–117). As for picornaviruses, the IRES-mediated translation of EMCV and FMDV can be enhanced by hnRNP I (114, 115). More specifically, it has been shown that hnRNP I can bind to the FMDV IRES, forming an initiation complex with 48S and 80S (115). HnRNP I has also been shown to bind to the 3' terminus of HCV RNA and support viral replication (116, 117). However, the role of hnRNP I during HCV infection is controversial; some articles suggest that hnRNP I promotes HCV translation and replication, while several articles have opposite opinions (118–122). A small-molecule compound, 6-methoxyethylamino-numonafide (MEAN), can inhibit HCV replication by hampering the expression level and redistribution of hnRNP I (123). Interestingly, during PV (sabin strain)-infection, an isoform of hnRNP I that is specifically expressed in neurons was identified to have a different function. Although neuron-specific hnRNP I shares 70% of the amino acids, it failed to rescue viral translation in hnRNP I-knockdown cells (124).

HnRNP K

HnRNP K is a versatile RNA-/DNA-binding protein that is involved in multiple fundamental processes of gene expression and signalling, including chromatin remodelling, RNA splicing, mRNA stability, transcription and translation (125). Furthermore, hnRNP K is critical for cellular DNA damage repair and tumorigenesis (126). Similar to hnRNP E, hnRNP K contains three KH domains (KH1, KH2 and KH3), a K-interaction (KI) domain, a NLS, a nuclear shuttling domain (KNS), a proline-rich domain and an interactive region with a C-terminal kinase (cKBR) (125).

During HCV infection, hnRNP K was identified to interact with the HCV core protein and 5' UTR of HCV RNA (127, 128). It was confirmed that amino acids 1-155 of the HCV core protein and amino acids 250-392 of hnRNP K (consist of 3 proline-rich domains) were responsible for the binding (127). Although how the modulation occurs remained unclarified, binding of hnRNP K to stem-loop I within the 5' UTR of HCV RNA could aid HCV replication. Notably, hnRNP K was partially rearranged from the nucleus to the cytoplasm to colocalize with NS5A, a viral protein that is related to HCV replication complex formation (128). Interestingly, miR-122, as a highly expressed microRNA in livers, was also confirmed to bind to hnRNP K. And the interaction between miR-122 and hnRNP K would increase the stability of miR-122 and may possess the capacity to modulate HCV replication (129). Another study pointed out that hnRNP K binds to positive-stranded RNA of HCV and is recruited to lipid droplets to suppress HCV particle production, possibly by restraining the genome from packaging into virions without impairing viral replication, but viral RNA-hnRNP K interaction or downregulation of viral particles producing was not found during DENV infection (130). However, a study indicated that hnRNP K could affect viral multiplication and release by associating with vimentin and DENV NS1 because disruption of vimentin reduced nuclear expression of hnRNP K and downregulated virus titers of cell-associated DENV and culture supernatant (33). A similar phenomenon was observed during JEV infection, and JEV NS1 also interacted with vimentin and hnRNP K to support viral propagation (131).

HnRNP K was suggested to bind to the IRES of both EV71 and FMDV RNA, although the binding sites of hnRNP K on the IRES were slightly different (34, 132). Stem-loop I, II and IV of FMDV RNA were determined to interact with hnRNP K, and this interaction may result in enhanced viral RNA synthesis (34). During FMDV infection, hnRNP K binds to domains II, III and IV of FMDV IRES and thus inhibits FMDV translation by replacing PTB, which functions as an ITAF to promote FMDV translation (132). Notably, FMDV 3CD protease could cleave hnRNP K at Glu-364, producing two cleavage products, hnRNP K (aa 1-364), remining a minor restriction on FMDV IRES-mediated translation, and hnRNP K (aa 364-465), which was confirmed to promote FMDV propagation (132). HnRNP K could also be cleaved by PV and CVB3 3C protease, although hnRNP K could benefit the virus infection (133).

For JUNV, hnRNP K was confirmed to be recruited from the nucleus to the cytoplasm during infection to favour virus propagation (65). SINV nsP1, nsP2 and nsP3 were found to be coimmunoprecipitated with hnRNP K, and nsP2 could colocalize with hnRNP K in infected cells (134). HnRNP K could also interact with Chikungunya virus (CHIKV) nsP2 and capsid, and knockdown of hnRNP K induces lower virus copies, suggesting that it may play an essential role in CHIKV multiplication (135). HnRNP K is also required for VSV infection by several mechanisms (136). First, hnRNP K suppresses the apoptosis of VSV-infected cells, promoting cell survival for efficient viral propagation (136). Notably, hnRNP K

restricts the expression of T-cell-restricted intracellular antigen isoforms 1a and 1b (TIA1a and TIA1a), both of which can suppress VSV replication. Additionally, hnRNP K maintains the level of cellular proteins that are required for VSV infection, such as the alanine deaminase-like (ADAL) proteins GBF1 and ARF1 (136).

HnRNP L

Similar to other members of hnRNPs, hnRNP L is involved in mRNA stabilization, mRNA transportation, pre-mRNA splicing and IRES-mediated translation. HnRNP L was first identified as a member of the hnRNP family. In particular, it has been reported that hnRNP L-directed RNA switches regulate the stress-dependent translation of vascular endothelial growth factor A (VEGFA) and promote cell apoptosis (137). Furthermore, hnRNP L mediates cryptic exon repression by acting as a splicing factor and utilizing CA-rich elements (138). HnRNP L can also interact with other hnRNP family members, including hnRNP K, hnRNP I and hnRNP E2 (139, 140). HnRNP L has four consensus RRM domains, and although it is primarily distributed in the nucleus, it can be localized to the cytoplasm under hypoxic conditions (137).

HCV could recruit cellular eukaryotic initiation factors (eIFs) and ITAFs to the IRES elements, initiating and modulating translation through a complicated network of RNA–protein and protein–protein interactions and the contact between the 5'- and 3'-ends of the viral genome (21). HnRNP L specifically binds to the HCV IRES, promoting viral translation. And HCV IRES-mediated translation enhanced by hnRNP L could be blocked by an RNA aptamer specific for hnRNP L (21). In addition, HCV infection mediates the coprecipitation of hnRNP L with NS5A and increases the amount of hnRNP L associated with viral replication complexes (141). Depleting hnRNP L impairs viral replication and attenuates viral yield but does not affect HCV IRES-driven translation (141). FMDV IRES can specifically bind hnRNP L, negatively regulating viral replication in a manner that differs from IRES-dependent translation. Because hnRNP L could interact with FMDV $3D^{Pol}$ in the presence of FMDV RNA, it was speculated that hnRNP L inhibits viral RNA synthesis in the replication complex (142). And for the limited amounts of studies on how hnRNP L affect positive singe-stranded RNA viruses life cycle (21, 141, 142), more investigations are needed to explain its function during virus infection.

HnRNP M

As a component of the spliceosome complex, hnRNP M (or CEAR) is abundant in the nucleus and comprises four different isoforms generated by alternative splicing. The four isoforms constitute three RRMs with shifting locations (29, 143). HnRNP M is a critical splicing regulatory protein for some receptors with divergent physiological functions, such as fibroblast growth factor receptor 2 (FGFR2) and dopamine D2 receptor (D2R) (144, 145). Recent studies have revealed well-documented roles for hnRNP M in cancer metastasis, muscle differentiation and innate immune gene expression (146–148).

HnRNP M silencing can increase the replication of SINV, CHIKV and Semliki Forest virus (SFV), indicating hnRNP M could impede virus infection. And it is worth mentioning that hnRNP M, hnRNP C and hnRNP E1 colocalize with viral replicases in the cytoplasm (149). In contrast, knockdown of hnRNP M and hnRNP F significantly decreased DENV production, indicating the proteins are required for efficient viral production (150).

A subsequent study reported that loss of hnRNP M results in hyperinduction of a cohort of inflammatory and antimicrobial genes in VSV-infected macrophages, enhancing macrophage antiviral defences and controlling virus infection. This finding reveals that hnRNP M could restrain macrophage antiviral functions and positively regulate virus replication (151). During picornavirus infection, hnRNP M is cleaved by 3C/3CD of CVB3 and PV at position Q389/G390 between RRM2 and RRM3. Although the four isoforms of hnRNP M differ in length, all isoforms have this cleavage site (152). In addition, hnRNP M and/or its cleavage products were identified to facilitate protein synthesis and replication of PV, but they were not required for PV IRES-mediated translation or viral RNA stability maintenance (152).

HnRNP M also associate with innate immune pathways to regulate virus infection (148, 153). When retinoic acid-inducible gene-I (RIG-I)-like receptors (RLRs) recognize the viral genome, and the innate immune response is triggered against invading pathogens (153). During virus infection, hnRNP M can interact with RIG-I and MDA5 in a viral infection-dependent manner and negatively regulate the induction of antiviral genes triggered by Sendai virus (SeV) or EMCV (153). Moreover, hnRNP M could bind to viral RNA and weaken its binding affinity to RIG-I and MDA5, suggesting that hnRNP M could inhibit the innate antiviral response by antagonizing the sensing of viral RNA by RLRs (148).

Other hnRNPs

Unlike other hnRNP proteins, hnRNP F and H appear to bind poly(G)-rich tracts, whose RRMs are not conserved and described as quasi-RRMs (qRRMs). In addition to regulating the maturation and posttranscriptional processing of pre-mRNA, hnRNP H/F protein was recently found to localize to stress granules in response to cellular stress. Although recognizing similar sequences, hnRNP F was upregulated, while hnRNP H and H2 were significantly down-regulated during Nipah virus

infection (154). With 2D-gel electrophoresis and MALDI-TOF analysis, hnRNP H was identified to regulate DENV multiplication by affecting TNF-α production (155). HnRNP H was also reported to interact with the NS1 protein of DENV, aiding viral propagation, although the exact mechanism still remained unclear (156). The hnRNP U (also known as scaffold attachment factor-A, SAF-A), a key RNA-binding protein in processing newly transcribed RNA and chromatin organisation in interphase, was identified to interfere induction of some antiviral immune genes during VSV infection, and it may result from VSV-induced cleavage of hnRNP U which depleted C-terminal RGG domain, the RNA binding domain (157).

Other than interacting with positive single-stranded RNA viruses, hnRNPs could also affect life cycle of retrovirus (158). For example, hnRNP A1, AB, H and F were identified as HIV splicing factors that regulate HIV-1 splicing (158, 159). The splicing of HIV RNA increases the coding potential of the viral genome and controls viral gene expression. HnRNP A1, Q, K, R and U can bind to Rev protein specifically, which is a significant regulator in the HIV replication cycle. The knockdown of hnRNP A1, Q, K and R has a negative impact on HIV replication, while knockdown of hnRNP U can increase viral production (160). It is worth noting that the N-terminal 86 amino acids of hnRNP U could downregulate HIV mRNA transcription in the cytoplasm (139). HnRNP associated with lethal yellow (RALY), which shares a high sequence similarity with hnRNP C, regulates the expression of the HIV coreceptor CCR5 by binding to its 3'UTR (161). Thus, hnRNP proteins modulate HIV-1 gene expression by a series of multiple mechanisms. Using a proteomic strategy to define polysome specialization during RNA virus infection, hnRNP R has been identified as a novel ITAF recruited by PV for translation (162). HnRNP P (also known as FUS/TLS) directly inhibits the transcription and translation of CVB3 by inducing the formation of SGs, the production of IFN-I and inflammatory cytokines (163). Because of their key roles in the regulation of gene expression, it is not surprising that hnRNP proteins are involved in viral infection. These hnRNP proteins directly or indirectly influence viral translation and replication.

Conclusion

Despite their diversity in structure (from hnRNP A1 to U), hnRNPs are involved in multiple cellular processes, including pre-mRNA processing, mRNA transport, regulation of translation, and controlling miRNAs (164, 165). To date, it has become clear that hnRNPs are crucial players in the cancer and neurodegenerative disease, and they are also established as playing either antiviral or pro-viral roles (44, 166).

Given their diverse and important functionalities, it is not at all surprising that many hnRNPs have been linked either directly or indirectly to viral replication and pathogenesis. Normally, hnRNP I involves in pre-mRNA splicing, IRES-dependent translation initiation, RNA polyadenylation, transportation and stability, and cell differentiation (164). During infection, hnRNP I could act as an ITAF for HRV and FMDV IRES, which stimulates and controls viral translation (114, 115). Similar to hnRNP I, many hnRNPs could be manipulated by single-stranded RNA viruses *via* interacting with viral RNA or proteins to aid their life cycle proceeding (46, 74, 81, 91, 114). And a few hnRNPs display distinctive effects when host cells are infected with different positive-stranded RNA viruses. Here, we summarize the functions of hnRNPs that participate in different stages of positive single-stranded RNA viruses (see Figure 5).

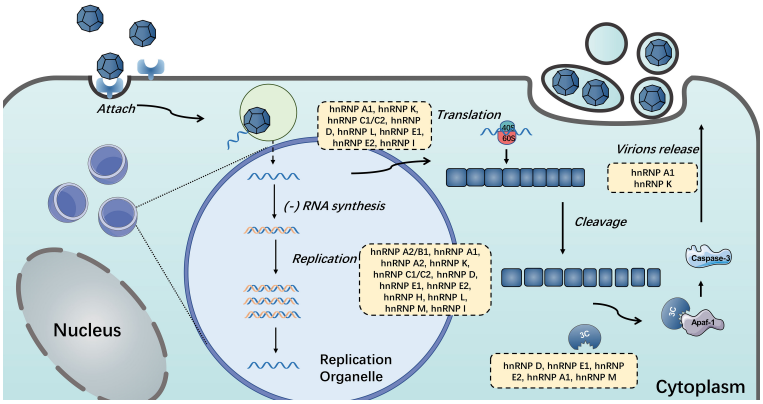

FIGURE 5
HnRNPs in the positive single-stranded RNA virus life cycle. HnRNPs play important roles in the life cycle of single-stranded RNA viruses, including viral translation, replication, the switch of translation to replication and the release of mature virions. The hnRNPs in yellow boxes were discovered to participate in these processes.

Notably, most hnRNPs shuttle continuously between the nucleus and the cytoplasm, which means the localization of hnRNPs is also vital for virus infection (65, 85, 110, 111). Positive-stranded RNA viruses replicate in the cytoplasm, which is associated with virus-induced membrane structures (99). Many nuclear resident hnRNPs underwent cytoplasmic relocalization during viral infection, including hnRNP A1, hnRNP C, hnRNP D, hnRNP E, hnRNP K and hnRNP M (49, 70, 85, 110, 128, 149). In term of hnRNP A1, the best-known member of hnRNP family, can interact with multiple viral proteins or RNA and regulate their life cycles, including SARS, HCV, DENV, MHV, PEDV, EV71, JUNV and SINV (35, 46, 47, 50, 54, 64). Like hnRNP A1, the common effects of hnRNPs on positive single-stranded RNA viruses reported were promotion of viral replication or translation (55, 81, 98).

The positive single-stranded RNA viruses take advantage of hnRNP family for their sufficient proliferation. In the case of *Picornaviridae*, PV infection requires hnRNP C, hnRNP D, hnRNP E, hnRNP R, hnRNP K, hnRNP M and hnRNP I (72, 85, 95, 103, 124, 152, 162). Meanwhile, PV applies strategy to cleave hnRNP E, hnRNP K, hnRNP M and hnRNP I by viral 3C protease and abolish their binding capacity (96, 133, 152). And

TABLE 1 A brief summary of the functions of hnRNPs in the positive single-stranded RNA virus life cycle.

HnRNP	Virus		Functions during positive single-stranded virus life cycle	Viral RNA/protein that harm interplay with	References
A/B	*Flaviviridae* *Picornaviridae* *Coronaviridae* *Arenaviridae* *Togaviridae*	HCV, DENV EV71, HRV SARS-CoV-2, PEDV, MHV JUNV SINV	Enhance virus RNA replication, enhance viral translation, modulate virions release	SARS-CoV-2 N protein, PEDV N protein, EV71 3C protein, IRES of EV71 RNA, 5' UTR and 3' UTR of HCV RNA, SARS-CoV-2 RNA	(45–52, 55–60)
C1/C2	*Flaviviridae* *Picornaviridae*	HCV, DENV PV, CVB3	Enhance virus RNA replication, enhance/inhibit viral translation, mediate switch of viral translation to replication	DENV NS1 protein, negative-strand RNA of PV, IRES of CVB3 RNA	(32, 72–74, 76, 77)
D	*Flaviviridae* *Picornaviridae*	HCV, WNV, ZIKV, DENV PV, CVB3. HRV, EMCV	Enhance viral translation, enhance virus RNA replication Inhibit virus RNA replication	IRES of HCV RNA, 3' end and 5' end of DENV RNA, WNV and ZIKV RNA, PV and HRV 3C protein, PV and CVB3 2A protein	(80–86)
E	*Flaviviridae* *Picornaviridae* *Rhabdoviridae* *Togaviridae*	DENV EV71, PV VSV SFV	Enhance viral translation Inhibit viral gene expressing	5' CL of PV RNA, 5' UTR of EV71 RNA, PV 3C/3CD protein, DENV core protein, VSV P protein	(91–97, 99–106)
I	*Flaviviridae* *Picornaviridae* *Hepeviridae*	HCV ECMV, FMDV, PV HEV	Enhance viral translation, enhance virus replication	IRES of EMCV RNA, 5' UTR (IRES) of PV RNA, 3' terminal of HCV RNA, PV 3C protein	(114–124)
K	*Flaviviridae* *Picornaviridae* *Arenaviridae* *Rhabdoviridae* *Togaviridae*	DENV, HCV EV71, FMDV JUNV VSV CHIKV, SINV	Enhance viral translation, enhance virus replication, virion assembly and release Inhibit viral protein synthesis	IRES of HCV and EV71 RNA, HCV core protein, DENV core protein, HCV NS3 and core protein	(33, 34, 127–134)
L	*Flaviviridae* *Picornaviridae*	HCV FMDV, EMCV, CVB3	Enhance viral translation, inhibit viral RNA replication Inhibit viral translation	RCs of FMDV and HCV, FMDV 3CD protein, CVB3 2A protein and 3C protein	(21, 137–142)
M	*Flaviviridae* *Picornaviridae* *Togaviridae* *Rhabdoviridae*	DENV PV, CVB3, EMCV SINV, SFV, CHIKV VSV	Enhance viral translation, enhance viral RNA replication, evade immune response inhibit virus replication	PV and CVB3 3C/3CD protein	(148–153)

many other positive single-stranded RNA viruses and hnRNPs share this similar pattern (54, 133). Furthermore, some hnRNPs have been reported to interact with other host proteins to modulate viral propagation (20). HnRNP A1 could interact with HCV NSb5 and septin 6 to enhance viral RNA circulation and eventually reinforce viral replication (20).

This review focuses on the interactions between hnRNPs and positive single-stranded RNA viruses. Here, we compared and discussed the function of hnRNPs in regulating the activity of viral translation (see Table 1) *via* protein-RNA interaction during different viral infection. And it seems that hnRNPs particularly bind to IRES of virus RNA to achieve this (21, 53, 107). Although the importance of hnRNPS during single-stranded RNA virus infection are explored in some extent (45, 74, 83), the exact mechanisms by which these interactions affect viral life cycle are not fully understood. Investigations into the precise function of these hnRNPs in viral infection are likely to provide great mechanistic insights and potential therapeutic targets for these infectious diseases.

Author contributions

JW and DS conceived, designed and wrote this manuscript. MW and AC revised the manuscript. YZ, SM, XO, XZ, JH, QG, SZ, QY, YW, DZ, RJ, SC and ML provided ideas contributing to the structure of this manuscript. All authors listed contributed to the completion of the manuscript and reviewed and approved the final manuscript.

Funding

This work was supported by the Applied Basic Research Programs of Science and Technology Department of Sichuan Province (2022NSFSC0080), the China Postdoctoral Science Foundation (2020M683651XB), the earmarked fund for China Agriculture Research System (CARS-42-17), China Agriculture Research System of MOF and MARA and the Sichuan Veterinary Medicine and Drug Innovation Group of China Agricultural Research System (SCCXTD-2020-18).

Conflict of interest

The authors declare that the research was conducted in the absence of any commercial or financial relationships that could be construed as a potential conflict of interest.

Publisher's note

References

1. Modrow S, Falke D, Truyen U, Schatzl H. Molecular virology. *Springer* (2013). doi: 10.1007/978-3-642-20718-1

2. Wang MY, Gao XF, Wang DP, Cao JM. SARS-CoV-2: Structure, biology, and structure-based therapeutics development. *Front Cell Infect Microbiol* (2020) 10:587269. doi: 10.3389/fcimb.2020.587269

3. Martinello M, Hajarizadeh B, Grebely J, Dore GJ, Matthews GV. Management of acute HCV infection in the era of direct-acting antiviral therapy. *Nat Rev Gastroenterol Hepatol* (2018) 15(7):412–24. doi: 10.1038/s41575-018-0026-5

4. Sulkowski MS, Moon JS, Sherman KE, Morelli G, Darling JM, Muir AJ, et al. A pragmatic, randomized controlled trial of oral antivirals for the treatment of chronic hepatitis c: The PRIORITIZE study. *Hepatology* (2021) 74(6):2952–64. doi: 10.1002/hep.32053

5. Kobayashi K, Koike S. Adaptation and virulence of enterovirus-A71. *Viruses* (2021) 13(8):1661. doi: 10.3390/v13081661

6. Ahlquist P, Noueiry AO, Lee WM, Kushner DB, Dye BT. Host factors in positive-strand RNA virus genome replication. *J Virol* (2003) 77(15):8181–6. doi: 10.1128/JVI.77.15.8181-8186.2003

7. Wang A. Dissecting the molecular network of virus-plant interactions: the complex roles of host factors. *Annu Rev Phytopathol* (2015) 53:45–66. doi: 10.1146/annurev-phyto-080614-120001

8. Zhang K, Miorin L, Makio T, Dehghan I, Gao S, Xie Y, et al. Nsp1 protein of SARS-CoV-2 disrupts the mRNA export machinery to inhibit host gene expression. *Sci Adv* (2021) 7(6):eabe7386. doi: 10.1126/sciadv.abe7386

9. Lizcano-Perret B, Michiels T. Nucleocytoplasmic trafficking perturbation induced by picornaviruses. *Viruses* (2021) 13(7):1210. doi: 10.3390/v13071210

10. Yarbrough ML, Mata MA, Sakthivel R, Fontoura BM, Schmidt N, Lareau CA, et al. Viral subversion of nucleocytoplasmic trafficking. *Traffic* (2014) 15 (2):127–40. doi: 10.1111/tra.12137

11. Le Sage V, Mouland AJ. Viral subversion of the nuclear pore complex. *Viruses* (2013) 5(8):2019–42. doi: 10.3390/v5082019

12. Lloyd RE. Nuclear proteins hijacked by mammalian cytoplasmic plus strand RNA viruses. *Virology* (2015) 479-480:457–74. doi: 10.1016/j.virol.2015.03.001

13. Schmidt N, et al. The SARS-CoV-2 RNA-protein interactome in infected human cells. *Nat Microbiol* (2021) 6(3):339–53. doi: 10.1038/s41564-020-00846-z

14. Haddad C, Davila-Calderon J, Tolbert BS. Integrated approaches to reveal mechanisms by which RNA viruses reprogram the cellular environment. *Methods* (2020) 183:50–6. doi: 10.1016/j.ymeth.2020.06.013

15. Chen N, Zhang B, Deng L, Liang B, Ping J. Virus-host interaction networks as new antiviral drug targets for IAV and SARS-CoV-2. *Emerg Microbes Infect* (2022) 11(1):1371–89. doi: 10.1080/22221751.2022.2071175

16. Geuens T, Bouhy D, Timmerman V. The hnRNP family: insights into their role in health and disease. *Hum Genet* (2016) 135(8):851–67. doi: 10.1007/s00439-016-1683-5

17. Gorlach M, Burd CG, Portman DS, Dreyfuss G. The hnRNP proteins. *Mol Biol Rep* (1993) 18(2):73–8. doi: 10.1007/BF00986759

18. Dreyfuss G, Matunis MJ, Piñol-Roma S, Burd CG. hnRNP proteins and the biogenesis of mRNA. *Annu Rev Biochem* (1993) 62:289–321. doi: 10.1146/annurev.bi.62.070193.001445

19. Perdikari TM, Murthy AC, Ryan VH, Watters S, Naik MT, Fawzi NL. SARS-CoV-2 nucleocapsid protein phase-separates with RNA and with human hnRNPs. *EMBO J* (2020) 39(24):e106478. doi: 10.15252/embj.2020106478

20. Kim CS, Seol SK, Song OK, Park JH, Jang SK. An RNA-binding protein, hnRNP A1, and a scaffold protein, septin 6, facilitate hepatitis c virus replication. *J Virol* (2007) 81(8):3852–65. doi: 10.1128/JVI.01311-06

21. Hwang B, Lim JH, Hahm B, Jang SK, Lee SW. hnRNP l is required for the translation mediated by HCV IRES. *Biochem Biophys Res Commun* (2009) 378 (3):584–8. doi: 10.1016/j.bbrc.2008.11.091

22. Rossi A, Moro A, Tebaldi T, Cornella N, Gasperini L, Lunelli L, et al. Identification and dynamic changes of RNAs isolated from RALY-containing ribonucleoprotein complexes. *Nucleic Acids Res* (2017) 45(11):6775–92. doi: 10.1093/nar/gkx235

23. Bampton A, Gittings LM, Fratta P, Lashley T, Gatt A. The role of hnRNPs in frontotemporal dementia and amyotrophic lateral sclerosis. *Acta Neuropathol* (2020) 140(5):599–623. doi: 10.1007/s00401-020-02203-0

24. Wu B, Su S, Patil DP, Liu H, Gan J, Jaffrey SR, Ma J, et al. Molecular basis for the specific and multivariant recognitions of RNA substrates by human hnRNP A2/B1. *Nat Commun* (2018) 9(1):420. doi: 10.1038/s41467-017-02770-z

25. Mizutani A, Fukuda M, Ibata K, Shiraishi Y, Mikoshiba K. SYNCRIP, a cytoplasmic counterpart of heterogeneous nuclear ribonucleoprotein r, interacts with ubiquitous synaptotagmin isoforms. *J Biol Chem* (2000) 275(13):9823–31. doi: 10.1074/jbc.275.13.9823

26. Siomi H, Dreyfuss G. A nuclear localization domain in the hnRNP A1 protein. *J Cell Biol* (1995) 129(3):551–60. doi: 10.1083/jcb.129.3.551

27. Jean-Philippe J, Paz S, Caputi M. hnRNP A1: the Swiss army knife of gene expression. *Int J Mol Sci* (2013) 14(9):18999–9024. doi: 10.3390/ijms140918999

28. Kamma H, Portman DS, Dreyfuss G. Cell type-specific expression of hnRNP proteins. *Exp Cell Res* (1995) 221(1):187–96. doi: 10.1006/excr.1995.1366

29. Han SP, Tang YH, Smith R. Functional diversity of the hnRNPs: past, present and perspectives. *Biochem J* (2010) 430(3):379–92. doi: 10.1042/BJ20100396

30. Banerjee K, Wang M, Cai E, Fujiwara N, Baker H, Cave JW. Regulation of tyrosine hydroxylase transcription by hnRNP K and DNA secondary structure. *Nat Commun* (2014) 5:5769. doi: 10.1038/ncomms6769

31. Yin Z, Kobayashi M, Hu W, Higashi K, Begum NA, Kurokawa K, et al. RNA-Binding motifs of hnRNP K are critical for induction of antibody diversification by activation-induced cytidine deaminase. *Proc Natl Acad Sci USA* (2020) 117(21):11624–35. doi: 10.1073/pnas.1921115117

32. Ertel KJ, Brunner JE, Semler BL. Mechanistic consequences of hnRNP c binding to both RNA termini of poliovirus negative-strand RNA intermediates. *J Virol* (2010) 84(9):4229–42. doi: 10.1128/JVI.02198-09

33. Kanlaya R, Pattanakitsakul SN, Sinchaikul S, Chen ST, Thongboonkerd V. Vimentin interacts with heterogeneous nuclear ribonucleoproteins and dengue nonstructural protein 1 and is important for viral replication and release. *Mol Biosyst* (2010) 6(5):795–806. doi: 10.1039/b923864f

34. Lin JY, Li ML, Huang PN, Chien KY, Horng JT, Shih SR. Heterogeneous nuclear ribonuclear protein K interacts with the enterovirus 71 5' untranslated region and participates in virus replication. *J Gen Virol* (2008) 89(Pt 10):2540–9. doi: 10.1099/vir.0.2008/003673-0

35. Levengood JD, Tolbert M, Li ML, Tolbert BS. High-affinity interaction of hnRNP A1 with conserved RNA structural elements is required for translation and replication of enterovirus 71. *RNA Biol* (2013) 10(7):1136–45. doi: 10.4161/rna.25107

36. Zhou F, Wan Q, Chen S, Chen Y, Wang PH, Yao X, et al. Attenuating innate immunity and facilitating beta-coronavirus infection by NSP1 of SARS-CoV-2 through specific redistributing hnRNP A2/B1 cellular localization. *Signal Transduct Target Ther* (2021) 6(1):371. doi: 10.1038/s41392-021-00786-y

37. Cathcart AL, Semler BL. Differential restriction patterns of mRNA decay factor AUF1 during picornavirus infections. *J Gen Virol* (2014) 95(Pt 7):1488–92. doi: 10.1099/vir.0.064501-0

38. Nakamura T, Isoda N, Sakoda Y, Harashima H. Strategies for fighting pandemic virus infections: Integration of virology and drug delivery. *J Control Release* (2022) 343:361–78. doi: 10.1016/j.jconrel.2022.01.046

39. Thibault PA, Ganesan A, Kalyaanamoorthy S, Clarke JWE, Salapa HE, Levin MC, et al. hnRNP A/B proteins: An encyclopedic assessment of their roles in homeostasis and disease. *Biol (Basel)* (2021) 10(8):712. doi: 10.3390/biology10080712

40. Friend LR, Han SP, Rothnagel JA, Smith R. Differential subnuclear localisation of hnRNPs A/B is dependent on transcription and cell cycle stage. *Biochim Biophys Acta* (2008) 1783(10):1972–80. doi: 10.1016/j.bbamcr.2008.05.021

41. Ghosh M, Singh M. RGG-box in hnRNPA1 specifically recognizes the telomere G-quadruplex DNA and enhances the G-quadruplex unfolding ability of UP1 domain. *Nucleic Acids Res* (2018) 46(19):10246–61. doi: 10.1093/nar/gky854

42. Kim HJ, Kim NC, Wang YD, Scarborough EA, Moore J, Diaz Z, et al. Mutations in prion-like domains in hnRNPA2B1 and hnRNPA1 cause multisystem proteinopathy and ALS. *Nature* (2013) 495(7442):467–73. doi: 10.1038/nature11922

43. Roth S, Khalaila I. The effect of O-GlcNAcylation on hnRNP A1 translocation and interaction with transportin1. *Exp Cell Res* (2017) 350(1):210–7. doi: 10.1016/j.yexcr.2016.11.023

44. Liu Y, Shi SL. The roles of hnRNP A2/B1 in RNA biology and disease. *Wiley Interdiscip Rev RNA* (2021) 12(2):e1612. doi: 10.1002/wrna.1612

45. Luo H, Chen Q, Chen J, Chen K, Shen X, Jiang H. The nucleocapsid protein of SARS coronavirus has a high binding affinity to the human cellular heterogeneous nuclear ribonucleoprotein A1. *FEBS Lett* (2005) 579(12):2623–8. doi: 10.1016/j.febslet.2005.03.080

46. Kumar R, Khandelwal N, Chander Y, Nagori H, Verma A, Barua A, et al. S-adenosylmethionine-dependent methyltransferase inhibitor DZNep blocks transcription and translation of SARS-CoV-2 genome with a low tendency to select for drug-resistant viral variants. *Antiviral Res* (2022) 197:105232. doi: 10.1016/j.antiviral.2021.105232

47. Li Z, Zeng W, Ye S, Lv J, Nie A, Zhang B, et al. Cellular hnRNP A1 interacts with nucleocapsid protein of porcine epidemic diarrhea virus and impairs viral replication. *Viruses* (2018) 10(3):127. doi: 10.3390/v10030127

48. Li Z, Chen F, Ye S, Guo X, Muhanmmad Memon A, Wu M, et al. Comparative proteome analysis of porcine jejunum tissues in response to a virulent strain of porcine epidemic diarrhea virus and its attenuated strain. *Viruses* (2016) 8(12):323. doi: 10.3390/v8120323

49. Li HP, Zhang X, Duncan R, Comai L, Lai MM. Heterogeneous nuclear ribonucleoprotein A1 binds to the transcription-regulatory region of mouse hepatitis virus RNA. *Proc Natl Acad Sci USA* (1997) 94(18):9544–9. doi: 10.1073/pnas.94.18.9544

50. Shi ST, Huang P, Li HP, Lai MM. Heterogeneous nuclear ribonucleoprotein A1 regulates RNA synthesis of a cytoplasmic virus. *EMBO J* (2000) 19(17):4701–11. doi: 10.1093/emboj/19.17.4701

51. Wang Y, Zhang X. The nucleocapsid protein of coronavirus mouse hepatitis virus interacts with the cellular heterogeneous nuclear ribonucleoprotein A1 *in vitro* and *in vivo*. *Virology* (1999) 265(1):96–109. doi: 10.1006/viro.1999.0025

52. Labeau A, Fery-Simonian L, Lefevre-Utile A, Pourcelot M, Bonnet-Madin L, Soumelis V, et al. Characterization and functional interrogation of the SARS-CoV-2 RNA interactome. *Cell Rep* (2022) 39(4):110744. doi: 10.1016/j.celrep.2022.110744

53. Zhang W, Qiao H, Lv Y, Wang J, Chen X, Hou Y, et al. Apigenin inhibits enterovirus-71 infection by disrupting viral RNA association with trans-acting factors. *PloS One* (2014) 9(10):e110429. doi: 10.1371/journal.pone.0110429

54. Li ML, Lin JY, Chen BS, Weng KF, Shih SR, Calderon JD, et al. EV71 3C protease induces apoptosis by cleavage of hnRNP A1 to promote apaf-1 translation. *PloS One* (2019) 14(9):e0221048. doi: 10.1371/journal.pone.0221048

55. Barrera A, Ramos H, Vera-Otarola J, Fernández-García L, Angulo J, Olguín V, et al. Post-translational modifications of hnRNP A1 differentially modulate retroviral IRES-mediated translation initiation. *Nucleic Acids Res* (2020) 48 (18):10479–99. doi: 10.1093/nar/gkaa765

56. Wang C, Gao L, Jin Y, Cardona CJ, Xing Z. Regulation of host responses and viral replication by the mitogen-activated protein kinases in intestinal epithelial cells infected with enterovirus 71. *Virus Res* (2015) 197:75–84. doi: 10.1016/j.virusres.2014.12.016

57. Leong SY, Ong BK, Chu JJ. The role of misshapen NCK-related kinase (MINK), a novel Ste20 family kinase, in the IRES-mediated protein translation of human enterovirus 71. *PloS Pathog* (2015) 11(3):e1004686. doi: 10.1371/journal.ppat.1004686

58. Arango D, Morohashi K, Yilmaz A, Kuramochi K, Parihar A, Brahimaj B, et al. Molecular basis for the action of a dietary flavonoid revealed by the comprehensive identification of apigenin human targets. *Proc Natl Acad Sci U.S.A.* (2013) 110(24):E2153–62. doi: 10.1073/pnas.1303726110

59. Cammas A, Pileur F, Bonnal S, Lewis SM, Lévêque N, Holcik M, et al. Cytoplasmic relocalization of heterogeneous nuclear ribonucleoprotein A1 controls translation initiation of specific mRNAs. *Mol Biol Cell* (2007) 18(12):5048–59. doi: 10.1091/mbc.e07-06-0603

60. Lin JY, Shih SR, Pan M, Li C, Lue CF, Stollar V, et al. hnRNP A1 interacts with the 5' untranslated regions of enterovirus 71 and sindbis virus RNA and is required for viral replication. *J Virol* (2009) 83(12):6106–14. doi: 10.1128/JVI.02476-08

61. Katoh H, Mori Y, Kambara H, Abe T, Fukuhara T, Morita E, et al. Heterogeneous nuclear ribonucleoprotein A2 participates in the replication of Japanese encephalitis virus through an interaction with viral proteins and RNA. *J Virol* (2011) 85(21):10976–88. doi: 10.1128/JVI.00846-11

62. Paranjape SM, Harris E. Y box-binding protein-1 binds to the dengue virus 3'-untranslated region and mediates antiviral effects. *J Biol Chem* (2007) 282 (42):30497–508. doi: 10.1074/jbc.M705755200

63. Shi ST, Yu GY, Lai MM. Multiple type A/B heterogeneous nuclear ribonucleoproteins (hnRNPs) can replace hnRNP A1 in mouse hepatitis virus RNA synthesis. *J Virol* (2003) 77(19):10584–93. doi: 10.1128/JVI.77.19.10584-10593.2003

64. Maeto CA, Knott ME, Linero FN, Ellenberg PC, Scolaro LA, Castilla V, et al. Differential effect of acute and persistent junin virus infections on the nucleo-cytoplasmic trafficking and expression of heterogeneous nuclear ribonucleoproteins type a and b. *J Gen Virol* (2011) 92(Pt 9):2181–90. doi: 10.1099/vir.0.030163-0

65. Brunetti JE, Scolaro LA, Castilla V. The heterogeneous nuclear ribonucleoprotein K (hnRNP K) is a host factor required for dengue virus and junin virus multiplication. *Virus Res* (2015) 203:84–91. doi: 10.1016/j.virusres.2015.04.001

66. Cienikova Z, Jayne S, Damberger FF, Allain FH, Maris C. Evidence for cooperative tandem binding of hnRNP c RRMs in mRNA processing. *RNA* (2015) 21(11):1931–42. doi: 10.1261/rna.052373.115

67. Whitson SR, LeStourgeon WM, Krezel AM. Solution structure of the symmetric coiled coil tetramer formed by the oligomerization domain of hnRNP c: implications for biological function. *J Mol Biol* (2005) 350(2):319–37. doi: 10.1016/j.jmb.2005.05.002

68. Brunner JE, Nguyen JH, Roehl HH, Ho TV, Swiderek KM, Semler BL, et al. Functional interaction of heterogeneous nuclear ribonucleoprotein c with poliovirus RNA synthesis initiation complexes. *J Virol* (2005) 79(6):3254–66. doi: 10.1128/JVI.79.6.3254-3266.2005

69. Beck M, Hurt E. The nuclear pore complex: understanding its function through structural insight. *Nat Rev Mol Cell Biol* (2017) 18(2):73–89. doi: 10.1038/nrm.2016.147

70. Gustin KE, Sarnow P. Effects of poliovirus infection on nucleo-cytoplasmic trafficking and nuclear pore complex composition. *EMBO J* (2001) 20(1-2):240–9. doi: 10.1093/emboj/20.1.240

71. Gustin KE, Sarnow P. Inhibition of nuclear import and alteration of nuclear pore complex composition by rhinovirus. *J Virol* (2002) 76(17):8787–96. doi: 10.1128/JVI.76.17.8787-8796.2002

72. Brunner JE, Ertel KJ, Rozovics JM, Semler BL. Delayed kinetics of poliovirus RNA synthesis in a human cell line with reduced levels of hnRNP c proteins. *Virology* (2010) 400(2):240–7. doi: 10.1016/j.virol.2010.01.031

73. Kafasla P, Morgner N, Robinson CV, Jackson RJ. Polypyrimidine tract-binding protein stimulates the poliovirus IRES by modulating eIF4G binding. *EMBO J* (2010) 29(21):3710–22. doi: 10.1038/emboj.2010.231

74. Dave P, George B, Balakrishnan S, Sharma DK, Raheja H, Dixit NM, et al. Strand-specific affinity of host factor hnRNP C1/C2 guides positive to negative-strand ratio in coxsackievirus B3 infection. *RNA Biol* (2019) 16(9):1286–99. doi: 10.1080/15476286.2019.1629208

75. Li X, Wang M, Cheng A, Wen X, Ou X, Mao S, et al. Enterovirus replication organelles and inhibitors of their formation. *Front Microbiol* (2020) 11:1817. doi: 10.3389/fmicb.2020.01817

76. Noisakran S, Sengsai S, Thongboonkerd V, Kanlaya R, Sinchaikul S, Chen ST, et al. Identification of human hnRNP C1/C2 as a dengue virus NS1-interacting protein. *Biochem Biophys Res Commun* (2008) 372(1):67–72. doi: 10.1016/j.bbrc.2008.04.165

77. Dechtawewat T, Songprakhon P, Limjindaporn T, Puttikhunt C, Kasinrerk W, Saitornuang S, et al. Role of human heterogeneous nuclear ribonucleoprotein C1/C2 in dengue virus replication. *Virol J* (2015) 12:14. doi: 10.1186/s12985-014-0219-7

78. Gratacos FM, Brewer G. The role of AUF1 in regulated mRNA decay. *Wiley Interdiscip Rev RNA* (2010) 1(3):457–73. doi: 10.1002/wrna.26

79. Moore AE, Chenette DM, Larkin LC, Schneider RJ. Physiological networks and disease functions of RNA-binding protein AUF1. *Wiley Interdiscip Rev RNA* (2014) 5(4):549–64. doi: 10.1002/wrna.1230

80. Friedrich S, Engelmann S, Schmidt T, Szczepankiewicz G, Bergs S, Liebert UG, et al. The host factor AUF1 p45 supports flavivirus propagation by triggering the RNA switch required for viral genome cyclization. *J Virol* (2018) 92(6):e01647-17. doi: 10.1128/JVI.01647-17

81. Friedrich S, Schmidt T, Geissler R, Lilie H, Chabierski S, Ulbert S, et al. AUF1 p45 promotes West Nile virus replication by an RNA chaperone activity that supports cyclization of the viral genome. *J Virol* (2014) 88(19):11586–99. doi: 10.1128/JVI.01283-14

82. Friedrich S, Schmidt T, Schierhorn A, Lilie H, Szczepankiewicz G, Bergs S, et al. Arginine methylation enhances the RNA chaperone activity of the West Nile virus host factor AUF1 p45. *RNA* (2016) 22(10):1574–91. doi: 10.1261/rna.055269.115

83. Paek KY, Kim CS, Park SM, Kim JH, Jang SK. RNA-Binding protein hnRNP d modulates internal ribosome entry site-dependent translation of hepatitis c virus RNA. *J Virol* (2008) 82(24):12082–93. doi: 10.1128/JVI.01405-08

84. Wong J, Si X, Angeles A, Zhang J, Shi J, Fung G, et al. Cytoplasmic redistribution and cleavage of AUF1 during coxsackievirus infection enhance the stability of its viral genome. *FASEB J* (2013) 27(7):2777–87. doi: 10.1096/fj.12-226498

85. Cathcart AL, Rozovics JM, Semler BL. Cellular mRNA decay protein AUF1 negatively regulates enterovirus and human rhinovirus infections. *J Virol* (2013) 87 (19):10423–34. doi: 10.1128/JVI.01049-13

86. Ullmer W, Semler BL. Direct and indirect effects on viral translation and RNA replication are required for AUF1 restriction of enterovirus infections in human cells. *mBio* (2018) 9(5):e01669-18. doi: 10.1128/mBio.01669-18

87. Porter FW, Brown B, Palmenberg AC. Nucleoporin phosphorylation triggered by the encephalomyocarditis virus leader protein is mediated by mitogen-activated protein kinases. *J Virol* (2010) 84(24):12538–48. doi: 10.1128/JVI.01484-09

88. Wu S, Lin L, Zhao W, Li X, Wang Y, Si X, et al. AUF1 is recruited to the stress granules induced by coxsackievirus B3. *Virus Res* (2014) 192:52–61. doi: 10.1016/j.virusres.2014.08.003

89. Hofmann S, Kedersha N, Anderson P, Ivanov P.. Molecular mechanisms of stress granule assembly and disassembly. *Biochim Biophys Acta Mol Cell Res* (2021) 1868(1):118876. doi: 10.1016/j.bbamcr.2020.118876

90. Chkheidze AN, Liebhaber SA. A novel set of nuclear localization signals determine distributions of the alphaCP RNA-binding proteins. *Mol Cell Biol* (2003) 23(23):8405–15. doi: 10.1128/MCB.23.23.8405-8415.2003

91. Blyn LB, Swiderek KM, Richards O, Stahl DC, Semler BL, Ehrenfeld E. Poly (rC) binding protein 2 binds to stem-loop IV of the poliovirus RNA 5' noncoding region: identification by automated liquid chromatography-tandem mass spectrometry. *Proc Natl Acad Sci U.S.A.* (1996) 93(20):11115–20. doi: 10.1073/pnas.93.20.11115

92. Blyn LB, Towner JS, Semler BL, Ehrenfeld E. Requirement of poly(rC) binding protein 2 for translation of poliovirus RNA. *J Virol* (1997) 71(8):6243–6. doi: 10.1128/jvi.71.8.6243-6246.1997

93. Gamarnik AV, Andino R. Two functional complexes formed by KH domain containing proteins with the 5' noncoding region of poliovirus RNA. *RNA* (1997) 3 (8):882–92.

94. Gamarnik AV, Andino R. Switch from translation to RNA replication in a positive-stranded RNA virus. *Genes Dev* (1998) 12(15):2293–304. doi: 10.1101/gad.12.15.2293

95. Perera R, Daijogo S, Walter BL, Nguyen JH, Semler BL. Cellular protein modification by poliovirus: the two faces of poly(rC)-binding protein. *J Virol* (2007) 81(17):8919–32. doi: 10.1128/JVI.01013-07

96. Gamarnik AV, Andino R. Interactions of viral protein 3CD and poly(rC) binding protein with the 5' untranslated region of the poliovirus genome. *J Virol* (2000) 74(5):2219–26. doi: 10.1128/JVI.74.5.2219-2226.2000

97. Walter BL, Parsley TB, Ehrenfeld E, Semler BL. Distinct poly(rC) binding protein KH domain determinants for poliovirus translation initiation and viral RNA replication. *J Virol* (2002) 76(23):12008–22. doi: 10.1128/JVI.76.23.12008-12022.2002

98. Paul AV, Wimmer E. Initiation of protein-primed picornavirus RNA synthesis. *Virus Res* (2015) 206:12–26. doi: 10.1016/j.virusres.2014.12.028

99. Luo Z, et al. PolyC-binding protein 1 interacts with 5'-untranslated region of enterovirus 71 RNA in membrane-associated complex to facilitate viral replication. *PloS One* (2014) 9(1):e87491. doi: 10.1371/journal.pone.0087491

100. Li Z, Ning S, Su X, Liu X, Wang H, Liu Y, et al. Enterovirus 71 antagonizes the inhibition of the host intrinsic antiviral factor A3G. *Nucleic Acids Res* (2018) 46 (21):11514–27. doi: 10.1093/nar/gky840

101. Murray KE, Roberts AW, Barton DJ. Poly(rC) binding proteins mediate poliovirus mRNA stability. *RNA* (2001) 7(8):1126–41. doi: 10.1017/S1355838201010044

102. Kempf BJ, Barton DJ. Poly(rC) binding proteins and the 5' cloverleaf of uncapped poliovirus mRNA function during de novo assembly of polysomes. *J Virol* (2008) 82(12):5835–46. doi: 10.1128/JVI.01513-07

103. Ogram SA, Spear A, Sharma N, Flanegan JB. The 5'CL-PCBP RNP complex, 3' poly(A) tail and 2A(pro) are required for optimal translation of poliovirus RNA. *Virology* (2010) 397(1):14–22. doi: 10.1016/j.virol.2009.11.006

104. Zell R, Ihle Y, Seitz S, Gündel U, Wutzler P, Görlach M. Poly(rC)-binding protein 2 interacts with the oligo(rC) tract of coxsackievirus B3. *Biochem Biophys Res Commun* (2008) 366(4):917–21. doi: 10.1016/j.bbrc.2007.12.038

105. Zell R, Ihle Y, Effenberger M, Seitz S, Wutzler P, Görlach M. Interaction of poly(rC)-binding protein 2 domains KH1 and KH3 with coxsackievirus RNA. *Biochem Biophys Res Commun* (2008) 377(2):500–3. doi: 10.1016/j.bbrc.2008.09.156

106. Sharma N, Ogram SA, Morasco BJ, Spear A, Chapman NM, Flanegan JB, et al. Functional role of the 5' terminal cloverleaf in coxsackievirus RNA replication. *Virology* (2009) 393(2):238–49. doi: 10.1016/j.virol.2009.07.039

107. Asnani M, Pestova TV, Hellen CU. PCBP2 enables the cadicivirus IRES to exploit the function of a conserved GRNA tetraloop to enhance ribosomal initiation complex formation. *Nucleic Acids Res* (2016) 44(20):9902–17. doi: 10.1093/nar/gkw609

108. Sp Ngberg K, Schwartz S. Poly(C)-binding protein interacts with the hepatitis c virus 5' untranslated region. *J Gen Virol* (1999) 80(Pt 6):1371–6. doi: 10.1099/0022-1317-80-6-1371

109. Wang L, Jeng KS, Lai MM. Poly(C)-binding protein 2 interacts with sequences required for viral replication in the hepatitis c virus (HCV) 5' untranslated region and directs HCV RNA replication through circularizing the viral genome. *J Virol* (2011) 85(16):7954–64. doi: 10.1128/JVI.00339-11

110. Beura LK, Dinh PX, Osorio FA, Pattnaik AK. Cellular poly(c) binding proteins 1 and 2 interact with porcine reproductive and respiratory syndrome virus nonstructural protein 1beta and support viral replication. *J Virol* (2011) 85 (24):12939–49. doi: 10.1128/JVI.05177-11

111. Wang L, He Q, Gao Y, Guo X, Ge X, Zhou L, et al. Interaction of cellular poly(C)-binding protein 2 with nonstructural protein 1beta is beneficial to Chinese highly pathogenic porcine reproductive and respiratory syndrome virus replication. *Virus Res* (2012) 169(1):222–30. doi: 10.1016/j.virusres.2012.08.002

112. Dinh PX, Beura LK, Panda D, Das A, Pattnaik AK.. Antagonistic effects of cellular poly(C) binding proteins on vesicular stomatitis virus gene expression. *J Virol* (2011) 85(18):9459–71. doi: 10.1128/JVI.05179-11

113. Ling JP, Chhabra R, Merran JD, Schaughency PM, Wheelan SJ, Corden JL, et al. PTBP1 and PTBP2 repress nonconserved cryptic exons. *Cell Rep* (2016) 17 (1):104–13. doi: 10.1016/j.celrep.2016.08.071

114. Kaminski A, Hunt SL, Patton JG, Jackson RJ. Direct evidence that polypyrimidine tract binding protein (PTB) is essential for internal initiation of translation of encephalomyocarditis virus RNA. *RNA (New York NY)* (1995) 1 (9):924–38.

115. Niepmann M, et al. Functional involvement of polypyrimidine tract-binding protein in translation initiation complexes with the internal ribosome entry site of foot-and-mouth disease virus. *J Virol* (1997) 71(11):8330–9. doi: 10.1128/jvi.71.11.8330-8339.1997

116. Chung RT, Kaplan LM. Heterogeneous nuclear ribonucleoprotein I (hnRNP-I/PTB) selectively binds the conserved 3′ terminus of hepatitis c viral RNA. *Biochem Biophys Res Commun* (1999) 254(2):351–62. doi: 10.1006/bbrc.1998.9949

117. Chang KS, Luo G. The polypyrimidine tract-binding protein (PTB) is required for efficient replication of hepatitis c virus (HCV) RNA. *Virus Res* (2006) 115(1):1–8. doi: 10.1016/j.virusres.2005.06.012

118. Tischendorf JJ, Beger C, Korf M, Manns MP, Krüger M, et al. Polypyrimidine tract-binding protein (PTB) inhibits hepatitis c virus internal ribosome entry site (HCV IRES)-mediated translation, but does not affect HCV replication. *Arch Virol* (2004) 149(10):1955–70. doi: 10.1007/s00705-004-0341-8

119. Domitrovich AM, Diebel KW, Ali N, Sarker S, Siddiqui A. Role of la autoantigen and polypyrimidine tract-binding protein in HCV replication. *Virology* (2005) 335(1):72–86. doi: 10.1016/j.virol.2005.02.009

120. Brocard M, Paulous S, Komarova AV, Deveaux V, Kean KM. Evidence that PTB does not stimulate HCV IRES-driven translation. *Virus Genes* (2007) 35(1):5–15. doi: 10.1007/s11262-006-0038-z

121. Anwar A, Ali N, Tanveer R, Siddiqui A. Demonstration of functional requirement of polypyrimidine tract-binding protein by SELEX RNA during hepatitis c virus internal ribosome entry site-mediated translation initiation. *J Biol Chem* (2000) 275(44):34231–5. doi: 10.1074/jbc.M006343200

122. Lu H, Li W, Noble WS, Payan D, Anderson DC. Riboproteomics of the hepatitis c virus internal ribosomal entry site. *J Proteome Res* (2004) 3(5):949–57. doi: 10.1021/pr0499592

123. Xue J, Liu Y, Yang Y, Wu S, Hu Y, Yang F, et al. MEAN inhibits hepatitis c virus replication by interfering with a polypyrimidine tract-binding protein. *J Cell Mol Med* (2016) 20(7):1255–65. doi: 10.1111/jcmm.12798

124. Guest S, Pilipenko E, Sharma K, Chumakov K, Roos RP. Molecular mechanisms of attenuation of the Sabin strain of poliovirus type 3. *J Virol* (2004) 78(20):11097–107. doi: 10.1128/JVI.78.20.11097-11107.2004

125. Bomsztyk K, Denisenko O, Ostrowski J. hnRNP K: one protein multiple processes. *Bioessays* (2004) 26(6):629–38. doi: 10.1002/bies.20048

126. Gallardo M, Hornbaker MJ, Zhang X, Hu P, Bueso-Ramos C, Post SM, et al. Aberrant hnRNP K expression: All roads lead to cancer. *Cell Cycle* (2016) 15 (12):1552–7. doi: 10.1080/15384101.2016.1164372

127. Hsieh TY, Matsumoto M, Chou HC, Schneider R, Hwang SB, Lee AS, et al. Hepatitis c virus core protein interacts with heterogeneous nuclear ribonucleoprotein K. *J Biol Chem* (1998) 273(28):17651–9. doi: 10.1074/jbc.273.28.17651

128. Fan B, Lu KY, Reymond Sutandy FX, Chen YW, Konan K, Zhu H, et al. A human proteome microarray identifies that the heterogeneous nuclear ribonucleoprotein K (hnRNP K) recognizes the 5' terminal sequence of the hepatitis c virus RNA. *Mol Cell Proteomics* (2014) 13(1):84–92. doi: 10.1074/mcp.M113.031682

129. Fan B, Sutandy FX, Syu GD, Middleton S, Yi G, Lu KY, et al. Heterogeneous ribonucleoprotein K (hnRNP K) binds miR-122, a mature liver-specific MicroRNA required for hepatitis c virus replication. *Mol Cell Proteomics* (2015) 14(11):2878–86. doi: 10.1074/mcp.M115.050344

130. Poenisch M, Metz P, Blankenburg H, Ruggieri A, Lee JY, Rupp D, Rebhan I, et al, et al. Identification of HNRNPK as regulator of hepatitis c virus particle production. *PloS Pathog* (2015) 11(1):e1004573. doi: 10.1371/journal.ppat.1004573

131. Wang P, Liu X, Li Q, Wang J, Ruan W. Proteomic analyses identify intracellular targets for Japanese encephalitis virus nonstructural protein 1 (NS1). *Virus Res* (2021) 302:198495. doi: 10.1016/j.virusres.2021.198495

132. Liu W, Yang D, Sun C, Wang H, Zhao B, Zhou G, et al. hnRNP K is a novel internal ribosomal entry site-transacting factor that negatively regulates foot-and-Mouth disease virus translation and replication and is antagonized by viral 3C protease. *J Virol* (2020) 94(17):e00803-20. doi: 10.1128/JVI.00803-20

133. Jagdeo JM, Dufour A, Klein T, Solis N, Kleifeld O, Kizhakkedathu J, et al. N-terminomics TAILS identifies host cell substrates of poliovirus and coxsackievirus B3 3C proteinases that modulate virus infection. *J Virol* (2018) 92 (8):e02211-17. doi: 10.1128/JVI.02211-17

134. Burnham AJ, Gong L, Hardy RW. Heterogeneous nuclear ribonuclear protein K interacts with sindbis virus nonstructural proteins and viral subgenomic mRNA. *Virology* (2007) 367(1):212–21. doi: 10.1016/j.virol.2007.05.008

135. Bourai M, Lucas-Hourani M, Gad HH, Drosten C, Jacob Y, Tafforeau L, et al. Mapping of chikungunya virus interactions with host proteins identified nsP2 as a highly connected viral component. *J Virol* (2012) 86(6):3121–34. doi: 10.1128/JVI.06390-11

136. Dinh PX, Das A, Franco R, Pattnaik AK. Heterogeneous nuclear ribonucleoprotein K supports vesicular stomatitis virus replication by regulating cell survival and cellular gene expression. *J Virol* (2013) 87(18):10059–69. doi: 10.1128/JVI.01257-13

137. Venkata Subbaiah KC, Wu J, Potdar A, Yao P. hnRNP l-mediated RNA switches function as a hypoxia-induced translational regulon. *Biochem Biophys Res Commun* (2019) 516(3):753–9. doi: 10.1016/j.bbrc.2019.06.106

138. McClory SP, Lynch KW, Ling JP. HnRNP l represses cryptic exons. *RNA* (2018) 24(6):761–8. doi: 10.1261/rna.065508.117

139. Kim JH, Hahm B, Kim YK, Choi M, Jang SK.. Protein-protein interaction among hnRNPs shuttling between nucleus and cytoplasm. *J Mol Biol* (2000) 298 (3):395–405. doi: 10.1006/jmbi.2000.3687

140. Hahm B, Cho OH, Kim JE, Kim YK, Kim JH, Oh YL. Polypyrimidine tract-binding protein interacts with HnRNP l. *FEBS Lett* (1998) 425(3):401–6. doi: 10.1016/S0014-5793(98)00269-5

141. Li Y, Masaki T, Shimakami T, Lemon SM. hnRNP l and NF90 interact with hepatitis c virus 5'-terminal untranslated RNA and promote efficient replication. *J Virol* (2014) 88(13):7199–209. doi: 10.1128/JVI.00225-14

142. Sun C, Liu M, Chang J, Yang D, Zhao B, Wang H, et al. Heterogeneous nuclear ribonucleoprotein l negatively regulates foot-and-Mouth disease virus replication through inhibition of viral RNA synthesis by interacting with the internal ribosome entry site in the 5' untranslated region. *J Virol* (2020) 94(10): e00282-20. doi: 10.1128/JVI.00282-20

143. Datar KV, Dreyfuss G, Swanson MS. The human hnRNP m proteins: identification of a methionine/arginine-rich repeat motif in ribonucleoproteins. *Nucleic Acids Res* (1993) 21(3):439–46. doi: 10.1093/nar/21.3.439

144. Hovhannisyan RH, Carstens RP. Heterogeneous ribonucleoprotein m is a splicing regulatory protein that can enhance or silence splicing of alternatively spliced exons. *J Biol Chem* (2007) 282(50):36265–74. doi: 10.1074/jbc.M704188200

145. Park E, Iaccarino C, Lee J, Kwon I, Baik SM, Kim M, et al. Regulatory roles of heterogeneous nuclear ribonucleoprotein m and Nova-1 protein in alternative splicing of dopamine D2 receptor pre-mRNA. *J Biol Chem* (2011) 286(28):25301–8. doi: 10.1074/jbc.M110.206540

146. Chen WY, Lin CL, Chuang JH, Chiu FY, Sun YY, Liang MC, et al. Heterogeneous nuclear ribonucleoprotein m associates with mTORC2 and regulates muscle differentiation. *Sci Rep* (2017) 7:41159. doi: 10.1038/srep41159

147. Passacantilli I, Frisone P, De Paola E, Fidaleo M, Paronetto MP. hnRNPM guides an alternative splicing program in response to inhibition of the PI3K/AKT/mTOR pathway in Ewing sarcoma cells. *Nucleic Acids Res* (2017) 45(21):12270–84. doi: 10.1093/nar/gkx831

148. Cao P, Luo WW, Li C, Tong Z, Zheng ZQ, Zhou L. The heterogeneous nuclear ribonucleoprotein hnRNPM inhibits RNA virus-triggered innate

immunity by antagonizing RNA sensing of RIG-i-like receptors. *PloS Pathog* (2019) 15(8):e1007983. doi: 10.1371/journal.ppat.1007983

149. Varjak M, Saul S, Arike L, Lulla A, Peil L, Merits A, et al. Magnetic fractionation and proteomic dissection of cellular organelles occupied by the late replication complexes of semliki forest virus. *J Virol* (2013) 87(18):10295–312. doi: 10.1128/JVI.01105-13

150. Viktorovskaya OV, Greco TM, Cristea IM, Thompson SR. Identification of RNA binding proteins associated with dengue virus RNA in infected cells reveals temporally distinct host factor requirements. *PloS Negl Trop Dis* (2016) 10(8): e0004921. doi: 10.1371/journal.pntd.0004921

151. West KO, Scott HM, Torres-Odio S, West AP, Patrick KL, Watson RO, et al. The splicing factor hnRNP m is a critical regulator of innate immune gene expression in macrophages. *Cell Rep* (2019) 29(6):1594–1609.e5. doi: 10.1016/j.celrep.2019.09.078

152. Jagdeo JM, Dufour A, Fung G, Luo H, Kleifeld O, Overall CM, et al. Heterogeneous nuclear ribonucleoprotein m facilitates enterovirus infection. *J Virol* (2015) 89(14):7064–78. doi: 10.1128/JVI.02977-14

153. Kato H, Takeuchi O, Sato S, Yoneyama M, Yamamoto M, Matsui K, et al. Differential roles of MDA5 and RIG-I helicases in the recognition of RNA viruses. *Nature* (2006) 441(7089):101–5. doi: 10.1038/nature04734

154. Chang LY, Ali AR, Hassan SS, AbuBakar S, et al. Human neuronal cell protein responses to Nipah virus infection*Virol J* (2007) 4:54. doi: 10.1186/1743-422X-4-54

155. Mishra KP, Shweta Diwaker D, Ganju L. Dengue virus infection induces upregulation of hn RNP-h and PDIA3 for its multiplication in the host cell. *Virus Res* (2012) 163(2):573–9. doi: 10.1016/j.virusres.2011.12.010

156. Diwaker D, Mishra KP, Ganju L, Singh SB, et al. Dengue virus non-structural 1 protein interacts with heterogeneous nuclear ribonucleoprotein h in human monocytic cells. *Asian Pac J Trop Med* (2016) 9(2):112–8. doi: 10.1016/j.apjtm.2016.01.015

157. Cao L, Luo Y, Guo X, Liu S, Li S, Li J, et al. SAFA facilitates chromatin opening of immune genes through interacting with anti-viral host RNAs. *PloS Pathog* (2022) 18(6):e1010599. doi: 10.1371/journal.ppat.1010599

158. Kutluay SB, Emery A, Penumutchu SR, Townsend D, Tenneti K, Madison MK, et al. Genome-wide analysis of heterogeneous nuclear ribonucleoprotein (hnRNP) binding to HIV-1 RNA reveals a key role for hnRNP H1 in alternative viral mRNA splicing. *J Virol* (2019) 93(21):e01048-19. doi: 10.1128/JVI.01048-19

159. Shema Mugisha C, Tenneti K, Kutluay SB. Clip for studying protein-RNA interactions that regulate virus replication. *Methods* (2020) 183:84–92. doi: 10.1016/j.ymeth.2019.11.011

160. Hadian K, Vincendeau M, Mäusbacher N, Nagel D, Hauck SM, Ueffing M, et al. Identification of a heterogeneous nuclear ribonucleoprotein-recognition region in the HIV rev protein. *J Biol Chem* (2009) 284(48):33384–91. doi: 10.1074/jbc.M109.021659

161. Kulkarni S, Lied A, Kulkarni V, Rucevic M, Martin MP, Walker-Sperling V, et al. CCR5AS lncRNA variation differentially regulates CCR5, influencing HIV disease outcome. *Nat Immunol* (2019) 20(7):824–34. doi: 10.1038/s41590-019-0406-1

162. Aviner R, Li KH, Frydman J, Andino R. Cotranslational prolyl hydroxylation is essential for flavivirus biogenesis. *Nature* (2021) 596(7873):558–64. doi: 10.1038/s41586-021-03851-2

163. Xue YC, Ng CS, Mohamud Y, Fung G, Liu H, Bahreyni A. FUS/TLS suppresses enterovirus replication and promotes antiviral innate immune responses. *J Virol* (2021) 95(12):e00304-21. doi: 10.1128/JVI.00304-21

164. Romanelli MG, Diani E, Lievens PM. New insights into functional roles of the polypyrimidine tract-binding protein. *Int J Mol Sci* (2013) 14(11):22906–32. doi: 10.3390/ijms141122906

165. Taniguchi K, Uchiyama K, Akao Y. PTBP1-targeting microRNAs regulate cancer-specific energy metabolism through the modulation of PKM1/M2 splicing. *Cancer Sci* (2021) 112(1):41–50. doi: 10.1111/cas.14694

166. Barboro P, Ferrari N, Balbi C. Emerging roles of heterogeneous nuclear ribonucleoprotein K (hnRNP K) in cancer progression. *Cancer Lett* (2014) 352 (2):152–9. doi: 10.1016/j.canlet.2014.06.019

frontiers | Frontiers in Immunology

TYPE Review
PUBLISHED 12 September 2022
DOI 10.3389/fimmu.2022.1005586

OPEN ACCESS

EDITED BY
Chenhe Su,
Wistar Institute, United States

REVIEWED BY
Wenyu Lin,
Massachusetts General Hospital and Harvard Medical School, United States
Wei Zhao,
Shandong University, China

*CORRESPONDENCE
Leiliang Zhang
armzhang@hotmail.com

†These authors share first authorship

SPECIALTY SECTION
This article was submitted to Viral Immunology, a section of the journal Frontiers in Immunology

RECEIVED 28 July 2022
ACCEPTED 23 August 2022
PUBLISHED 12 September 2022

CITATION
Liu Y, Yuan Y and Zhang L (2022) Innate immune evasion by alphaviruses.
Front. Immunol. 13:1005586.
doi: 10.3389/fimmu.2022.1005586

Innate immune evasion by alphaviruses

Yihan Liu[1,2,3†], Yupei Yuan[2,3†] and Leiliang Zhang[1,2,3*]

[1]Department of Infectious Diseases, Shandong Provincial Hospital Affiliated to Shandong First Medical University, Jinan, China, [2]Department of Pathogen Biology, School of Clinical and Basic Medical Sciences, Shandong First Medical University & Shandong Academy of Medical Sciences, Jinan, China, [3]Medical Science and Technology Innovation Center, Shandong First Medical University & Shandong Academy of Medical Sciences, Jinan, China

Alphaviruses contain many human and animal pathogens, such as CHIKV, SINV, and VEEV. Accumulating evidence indicates that innate immunity plays an important role in response to alphaviruses infection. In parallel, alphaviruses have evolved many strategies to evade host antiviral innate immunity. In the current review, we focus on the underlying mechanisms employed by alphaviruses to evade cGAS-STING, IFN, transcriptional host shutoff, translational host shutoff, and RNAi. Dissecting the detailed antiviral immune evasion mechanisms by alphaviruses will enhance our understanding of the pathogenesis of alphaviruses and may provide more effective strategies to control alphaviruses infection.

KEYWORDS

innate immune evasion, alphavirus, CHIKV, interferon, STING

Introduction

Alphaviruses are positive-stranded RNA viruses and belong to the *Togaviridae* family (1). It contains many important human and animal pathogens, such as chikungunya virus (CHIKV), Sindbis virus (SINV), and Venezuelan equine encephalitis virus (VEEV). Affected by geographical factors and climatic conditions, alphaviruses distribute on all continents except Antarctica and many islands. CHIKV can be found in tropical and subtropical regions of Africa and Southeast Asia, where winter temperatures are above 18°C. This virus is famous for causing Chikungunya fever, with the symptoms of acute febrile illness, arthralgia, and severe neurological complications (2).SINV exists in Europe, Asia, and Africa, including many Philippine Islands and the South Pacific areas. Fever, malaise, rash, and chronic musculoskeletal pain are the main symptoms of SINV (3). VEEV is mainly in circulation in the American continent and can cause severe encephalitis (4). The major transmission vectors of alphaviruses are mosquitoes, including *Aedes aegypti*, *Aedes albopictus*, and *Aedes africanus* (5).

Alphavirus particles are round with a diameter of about 70 nanometers. The viral nucleocapsid has an icosahedral symmetry with a diameter of 30-40 nanometers.

Alphavirus genome comprises a 5'-methylguanylate cap, a 3'-polyadenylic acid tail, and two open reading frames (ORFs), which encode four nonstructural proteins and six structural proteins (6). Nonstructural proteins include nsP1, nsP2, nsP3 and nsP4, and they play critical roles in the transcription and replication of the virus (7). nsP1 is required for cap synthesis and plasma membrane-anchoring. nsP2 is necessary for polyproteins processing as its C terminus obtains an N-terminal RNA helicase and cysteine protease (8). ADP ribosyl-binding and hydrolase activities in nsP3 are crucial for viral replication. nsP4 activity depends on its RNA polymerase activity. Structural proteins of alphaviruses are capsid, 6K, transferase protein (TF), E1, E2, and E3 (7). The capsid protein is used for packaging the viral nucleic acid (7). 6K participates in the infected cell surface's vial assembly and budding stages. Shared with the same coding regions with 6K, TF is generated due to a ribosomal frameshift and promotes virus replication by reducing the early IFN-I response (9). E1 and E2 mediate the entry of the virus. 6K and E3 work together to transport the precursor membrane protein to the endoplasmic reticulum (ER) (7).

The host innate immune system is the first line of defense against viral infection. For example, the Cyclic GMP-AMP Synthase (cGAS)-stimulator of interferon genes (STING) pathway could stimulate and promote the production of type I interferon to achieve antiviral effects (10). Degradation of the key regulator of eukaryotic messenger RNA transcription, RPB1, will induce transcriptional host shutoff (11). Signal transduction of the PKR-like ER kinases (PERK) pathway and the unfolded protein response (UPR) phosphorylates eukaryotic translation initiation factor 2 (eIF2), which causes translational shutoff (11). RNA-induced silencing complex (RISC) can cleave viral RNA and activate RNAi (12).

However, with the evolution of viruses and their long-term confrontation with host cells, many viruses have established effective antagonisms to host antiviral innate immune pathways and immune factors (13–21). This review has summarized different mechanisms of how alphaviruses antagonize the host's innate immunity. Alphavirus is highly infectious as it can transmit by the mosquito and pose a huge threat to public health. So understanding the antiviral innate immune pathway and the antagonistic effects induced by the viral proteins of alphaviruses could provide more strategies to control the diseases caused by alphaviruses.

Restraint of cGAS-STING pathway

When infected by a virus, activation of cytoplasmic DNA sensors such as cGAS in immune cells is adapted to intracellular damage caused by the released viral DNA. The 2'-3' cyclic-guanosine monophosphate (GMP)-adenosine monophosphate (AMP) (GAMP) is synthesized to bind to STING, which then forms dimerization and translocates to the Trans-Golgi-Network (TGN) and associate with TANK-Binding Kinase 1 (TBK1), resulting in the phosphorylation of Interferon Regulatory Factor 3 (IRF3) (22). The transcription and expression of the cGAS-STING innate immune pathway could inhibit virus replication, whereas viruses could antagonize this process.

In the first four hours of CHIKV infection, the expression of cGAS is reduced sharply, while there is no significant change in the expression of STING (23). The degradation of cGAS is mediated by capsid protein through ATG7-dependent autophagy (Figure 1). When the chemical inhibitor of autophagy 3-methyladenine (3-MA) is used, cGAS can be restored. Capsid-mediated cGAS degradation directly limits the antiviral effect of the cGAS-STING pathway (23). The interaction between nsP1 and STING is mediated by the cytoplasmic loop of STING, mainly due to the palmitoylation that occurs at 88 and 91 amino acids. The level of viral protein will be significantly reduced, and the cGAS-STING-mediated induction of type I IFN will be impaired when this interaction is lost (23). Interestingly, nsP1-STING interaction significantly inhibits IFNβ promotor activation induced by cGAS-STING (23). Other viruses degrade components of the cGAS-STING signaling to achieve evasion. For example, DENV NS2B3 protease inhibits type I IFN production in infected cells by cleaving STING (23), and papain-like protease (PLpro)-transmembrane domain (TM) in SARS disrupts IRF3 phosphorylation and dimerization (24). Interestingly, nsP2, nsP4, and capsid proteins have separate or synergistic effects on the degradation of cGAS, and their mechanisms are worthy of further study and discussion.

Inhibition of IFN pathway

Type I interferon (IFN) is a cytokine is crucial for the antiviral response and activation of the innate and adaptive immune system. Its production is often triggered by pattern recognition receptors (PRRs), including Toll-like receptors (TLRs), retinoic acid-inducible gene I (RIG-I)-like receptors (RIG-I-like receptors, RLRs), nucleotide-binding and oligomerization domain (NOD)-like receptors (NLRs), and intracellular DNA receptors (25, 26). After the cytoplasmic receptor recognizes the viral nucleic acid, melanoma differentiation-associated gene 5 (MDA5) and RIG-I will expose the caspase recruitment domain (CARD) domain to induce the aggregation and activation of the mitochondrial antiviral signal protein (MAVS). Then the signal is transmitted downwards to activate TBK1 and IKKεso that IRF3/7 is phosphorylated and transported to the nucleus to promote the transcription of type I interferons (27). The viral genome contains two ORFs. The first encodes precursor proteins, and the second encodes structural polyproteins, where the 6K protein causes a ribosomal frameshifting during translation

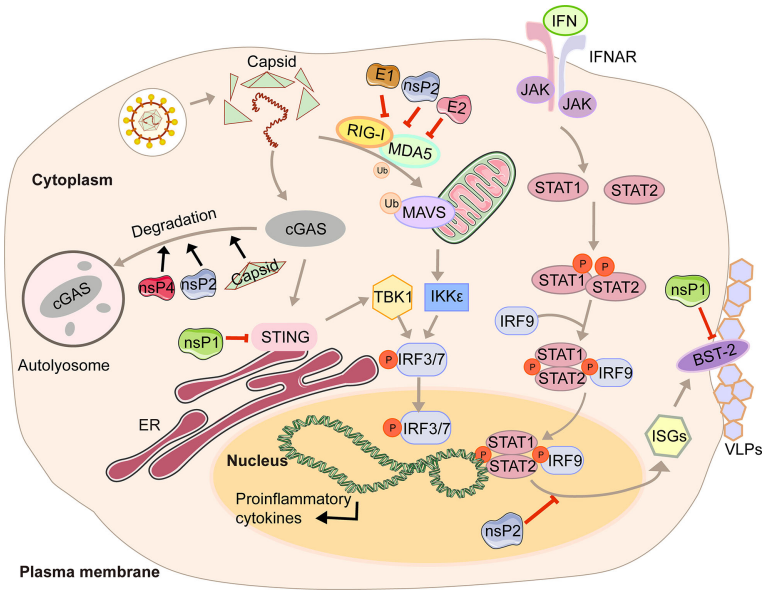

FIGURE 1
A diagram of alphavirus-mediated inhibition of the innate immune pathways leading to the production of IFN and ISG induction.

and produces the TF (9). Virus modification of host protein often occurs through post-translational modifications, such as palmitoylation and phosphorylation. Palmitoylation is a 16-carbon palmitoyl covalent bond attached to cysteine residues. This modification imparts hydrophobicity to the protein and is usually targeted at the cell membrane (28). TF has been demonstrated to be modified by palmitoylation (29, 30). 6K mutation indicates that hexanucleotide cannot be reduced to produce TF protein (31, 32). The loss of TF palmitoylation will result in the enrichment of the type I IFN production and the attenuation of toxicity caused by SINV infection (33). Palmitoylated TF is necessary for its localization and the subsequent production of virus particles, which also helps to enhance the ability to antagonize the host interferon response. Meanwhile, nsP2, E1, and E2 proteins of CHIKV can strongly antagonize the activation of the IFN-β signaling pathway (Figure 1). Co-expression of nsP2, E1, E2, and MDA5/RIG-I allows the inhibition of more than 80% of the MDA5/RIG-I-mediated IFN-β promoter activity in the presence of viral proteins (34).

In response to IFN, IFN receptors phosphorylate signal transducer and activator of transcription 1 (STAT1) (35). Then the importin-α5 transports the phosphorylation form of STAT1 (pSTAT1) to the nucleus, together with IFN response factor 9 (IRF9), and binds to the IFN-stimulated response element (ISRE) so that the transcription of the IFN-stimulated genes (ISGs) is activated (35). With the help of chromosome region maintenance 1 (CRM1), STAT1 is shuttled back into the cytoplasm when achieving the goal of releasing from its target promoter (35). This signaling pathway restricts CHIKV propagation and abolishes CHIKV-induced diseases (36). However, CHIKV infection effectively inhibits IFN-mediated phosphorylation of STAT1, thereby hindering the transmission of JAK-STAT immune signals (36). CHIKV nsP2 is responsible for regulating the IFN-induced JAK-STAT signaling (Figure 1) (37). By mutating the KR649AA site in NLS of nsP2 or redirecting nsP2 C-terminal methyltransferase-like domain into the nucleus, JAK-STAT signaling is no longer inhibited mechanically due to the reduction of pSTAT nuclear accumulation (38, 39).

Antiviral effects of IFN are fulfilled by antiviral IFN-stimulate genes (ISGs). One well-characterized ISG is bone marrow stromal antigen 2 (BST-2). Its transmembrane domain and lumenal GPI anchor allow virus particles to adhere to the surface of infected cells, thereby preventing release and bystander cells' infection (40). Although BST-2 could block the release of the virus, many of which have evolved multiple mechanisms to antagonize the inhibitory effect (40, 41), which is also the case for CHIKV. CHIKV protein co-localizes with BST-2 when expressed in VLPs, namely E1 and nsP1 (42). There are interactions between BST-2 and E1 and nsP1, but the protein that antagonizes its inhibitory effect on virus release is nsP1. In the presence of BST-2, a CHIKV virus-like particle (VLP) is adhered to the cell membrane and cannot be released from the surface. However, acting as an antagonist, upregulation of nsP1 counteracts the effect of BST-2, which enables the progeny virions to attach to the membrane (Figure 1) (42). The same effects can be observed in HIV-1 Vpu and HIV-2 Env, which can

redirect the BST-2 from the cell surface and form a perinuclear compartment (41, 43). The prerequisite is that Vpu must have both transmembrane/ion channel domain and conserved proteins (40).

In addition, the alphavirus can not only use its viral protein to inhibit the production, translation, and transcription of interferon but also use the host antiviral protein to achieve immune escape, such as zinc-finger antiviral protein (ZAP). ZAP is a host antiviral factor stimulated by IFN, inhibiting the replication of some viruses, including HBV, Sindbis virus, and Ebola (44–46). Due to the interaction between ZAP-responsible elements (ZRE) and viral RNA, some exosomes are recruited to degrade RNA substrates (44, 47). Sometimes ZAP could disturb the polysome association/translation of RNA (45). In ZAP gene knockout mice models, virus replications are greatly enhanced in lymphoid tissues, while this phenomenon could not be observed in brain tissues. Those results imply that viral infection can evade immune surveillance by suppressing the expression of ZAP antiviral protein in the brain tissues (47). However, there may be other ways for the virus to achieve antiviral effects and immune escape in the host, which requires further research.

Suppression of transcriptional host shutoff pathway

A basic feature of massive alphavirus replication in vertebrates is the cytopathic effect (CPE). Alphavirus inhibits the occurrence and efficacy of the host antiviral response by antagonizing cell transcription so that it can replicate *in vivo*, which is achieved through different mechanisms mediated by alphavirus proteins.

nsP2 from old world alphaviruses, including SINV and SFV, is the key regulator of the interaction between the virus and the host cell. Not only does nsP2 serves as a component of the replicase complex required for viral RNA replication and transcription, but also it can directly participate in the inhibition of host transcription (48, 49). As a subunit that catalyzes the polymerase reaction, RPB1 determines the initiation and extension of eukaryotic messenger RNA transcription. nsP2 could induce the ubiquitination and degradation of RPB1 (Figure 2) (50). In the experiment of mice infected with SINV containing a single nsP2 substitution (P726→G), a significant increase in the secretion of IFN can be seen due to the shutdown of host transcription (50). Normally, cells can remove the extended RNAPII complex during the transcription-coupled repair. Once the complex is blocked by large amounts of DNA damage, RPB1 can be modified by ubiquitination and then degraded by the proteasome (51). Mutating amino acids 674-688 can resist virus-induced degradation of RPB1 and make SINV a powerful inducer of type I interferon (48). It is worth noting that this phenomenon does not affect virus replication.

The amino terminal region of alphavirus nsP3 has the effect of a single ADP-ribosylhydrolase, and the N24A mutation in this region eliminates the hydrolase activity (52). A single mutation in N24A still induces the degradation of RPB1, while the double mutation of SINV nsP2-683S and nsP3-N24A no longer degrades RPB1 (48). Mayaro virus (MAYV) nsP2 associates with RPB1 and transcription initiation factor IIE subunit 2

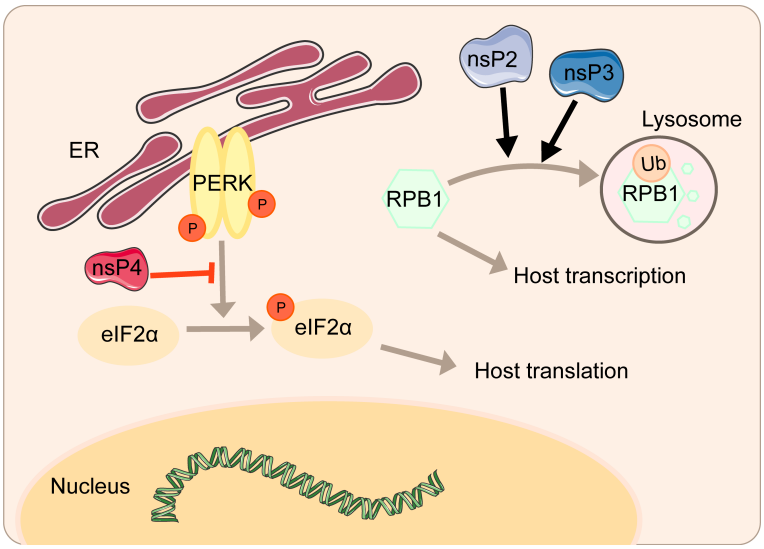

FIGURE 2
Inhibition of host transcriptional and translational shutoff by alphaviruses.

(TFIIE2) (53). Overexpression of MAYV nsP2 mediates inhibition of host cell transcription by reducing RPB1 and TFIIE2 (53).

The cytotoxicity of the new world alphaviruses represented by VEEV and EEEV differs from that of the old world alphaviruses. VEEV and EEEV-derived replicons produce fewer cytopathic changes, and at the same time, durable viral nucleic acid replication can be established (54). This host transcription shutoff in VEEV and EEEV depends on the presence of viral capsid protein (55). The capsid is distributed in the cytoplasm of infected cells and may interfere with the antiviral response. Capsid could inhibit cell messenger and ribosomal RNA transcription and downregulate RNA synthesis. Interestingly, western equine encephalitis virus (WEEV) inhibits the host transcription depending on both nsP2 and capsid, consisting of the current concept of forming WEEV from SINV- and EEEV-like ancestors (55).

Suppression of translational host shutoff pathway

After mammals are infected with alphavirus, the replication of viral RNA in the cell often leads to more serious cytopathic changes. That is, selective inhibition of host protein synthesis and viral mRNA will be in this case. The ER is responsible for the proper folding and processing of polypeptide chains into functional proteins. Factors affecting the function of the ER, such as viral infection, will lead to the accumulation of misfolded or unfolded proteins. To protect cells from over accumulation, repression of protein synthesis, so-called (UPR), maintains cellular protein homeostasis (56). These regulatory signalings contain (PERK), transcription factor 6 (ATF6), and the ER transmembrane protein kinase/endoribonuclease inositol-requiring enzyme 1 (IRE1), with the involvement of ER chaperone immunoglobulin heavy chain binding protein (BIP) (56). PERK can be activated through self-dimerization and phosphorylation, then pPERK can phosphorylate eIF2α on amino acid 51, during which GADD34 can play an inhibitory role against this process (57). Induction of C/EBP homologous protein (CHOP) is to mediate apoptosis when ER is impaired severely. The IRE pathway is activated similarly. The catalytic of IRE will trigger a sequence of gene transcription, such as components of ER-associated degradation (ERAD). ATF6 activates transcription of the chaperone, thus helping translational recovery (58, 59).

However, the virus can regulate the activity of some key factors to influence the antagonism of protein synthesis, ensuring the effective translation of virus mRNAs and the shutoff of host translation. CHIKV can regulate the signal transduction of the PERK pathway by inhibiting the phosphorylation of eIF2α during early infection (Figure 2). Upon significant expression of CHIKV nsP4, the phosphorylation of eIF2α on serine 51 regulating the signal transduction of PERK is suppressed, thereby ensuring the translation of viral proteins (58). Overexpression of CHIKV nsP2 inhibits the expression of functional UPR transcription factors ATF4 and activation of XBP1 and thus blocks the UPR, which is another strategy to shut off host translation (60).

Inhibition of RNAi pathway

Eukaryotes have evolved many antiviral immune defenses to prevent viral infection, such as RNA interference(RNAi) (12). RNAi is a conservative post-transcriptional gene silencing mechanism (12). As a member of the RNase III family of nucleases, Dicer has a helicase domain and dual RNase III motif, and it can cleave double-stranded RNAs specifically. In the process of antiviral RNAi, host cells respond rapidly to the dsRNA derived from the invading viruses, activating Dicer to cleave the dsRNA into virus-derived small interfering RNA (viRNA) with a size of 21 to 23 nucleotides, which is crucial for the antiviral response (12). One of the components of the RISC, Argonaute (AGO), plays an indispensable role in degrading the target dsRNA achieved through the RNase-H-like PiWi domain or recruiting additional proteins, thereby inhibiting viral infection (12). However, protection against RNAi attack enables the virus to encode specific virulence proteins, the so-called viral suppressors of RNAi (VSRs) (12).

The Semliki forest virus (SFV) capsid protein is demonstrated as VSR (61). SFV capsid protects viral RNA from interpretation at two stages. On the one hand, capsid binds to dsRNA to block Dicer cleavage and thus antagonizes the production of viRNA (Figure 3). The experiments of SFV capsid mutants suggest that K124/K128 and K139/K142 are essential for VSR activity (61). On the other hand, capsid associates with viRNA and thus prevents the interaction between viRNA and RISC (61). Consequently, the inactivation of the VSR function will inhibit SFV replication.

Conclusion and perspectives

In this review, we have described in detail the different mechanisms by which each viral protein of alphavirus antagonizes the host's innate immunity. The host will recognize virus invasion through the sensor proteins, including cGAS and MAVS, and activate the antiviral innate immune pathway. The downstream signals further activate the TBK1-IRF3 and IKK-NF-κB pathways, increasing type I interferon production and inhibiting viral infection. Almost all alphavirus proteins antagonize innate immunity in different mechanisms and degrees. Through the interaction with cGAS-STING, nsP1 degrades cGAS to stabilize the virus protein (Figure 1). nsP1 also down-regulates the expression of BST-2 to inhibit the adhesion

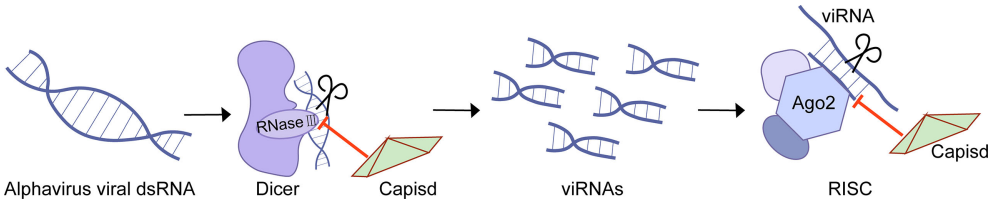

FIGURE 3
Inhibition of RNAi by alphaviruses.

of VLPs on the plasma membrane and promote the release of the virus. The mechanism of nsP2 antagonizing immune response is more complex. The type I interferon response can be counteracted by inhibiting the general transcription of host cells and reducing the phosphorylation of STAT1 in the JAK-STAT pathway (Figure 1). In addition, degradation of RPB1 occurs by nsP2-mediated ubiquitination, through which the transcription of the host proteins can be shut down (Figure 2). At the same time, nsP2 exerts a profound impact on the phosphorylation of STAT1 and STAT2 and thus inhibits the host translation (Figure 1). Both nsP3 and nsP4 could induce the host transcriptional shutdown (Figure 2). NsP4 inhibits the phosphorylation of eIF2alpha in the PERK pathway. Among the structural proteins, the capsid protein can effectively inhibit RNAi in insect and mammalian cells by separating double-stranded RNA and small interfering RNA (Figure 3). E2 and E1 inhibit the activation of the IFN-β promoter induced by the MDA5/RIG-I receptor signaling pathway. TF antagonizes the host interferon response. In addition to the structural and nonstructural proteins of alphavirus, the virus also uses the immune escape phenomenon of ZAP to antagonize the host's antiviral response.

As more and more studies are performed, a deeper and more comprehensive understanding of alphavirus antagonizing host antiviral innate immunity is revealed. However, some mechanisms are not clear enough, and there may be other ways and mechanisms to antagonize antiviral immunity that are worthy of further research and exploration. At the same time, the strategies of antagonizing antiviral immunity by alphaviruses will provide important insights into controlling viral infections.

Author contributions

LZ conceived the work. YL and YY wrote the draft. YL generated Figures. LZ revised the manuscript. All approved the final version for publication.

Funding

This work was supported by grants from the National Natural Science Foundation of China [81871663 and 82072270] and the Academic Promotion Program of Shandong First Medical University [2019LJ001].

Conflict of interest

The authors declare that the research was conducted in the absence of any commercial or financial relationships that could be construed as a potential conflict of interest.

Publisher's note

References

1. Strauss JH, Strauss EG. The alphaviruses: gene expression, replication, and evolution. *Microbiol Rev* (1994) 58:491–562. doi: 10.1128/mr.58.3.491-562.1994

2. de Lima Cavalcanti TYV, Pereira MR, de Paula SO, Franca RFO. A review on chikungunya virus epidemiology, pathogenesis and current vaccine development. *Viruses* (2022) 14(5):969. doi: 10.3390/v14050969

3. Adouchief S, Smura T, Sane J, Vapalahti O, Kurkela S. Sindbis virus as a human pathogen-epidemiology, clinical picture and pathogenesis. *Rev Med Virol* (2016) 26:221–41. doi: 10.1002/rmv.1876

4. Sharma A, Knollmann-Ritschel B. Current understanding of the molecular basis of Venezuelan equine encephalitis virus pathogenesis and vaccine development. *Viruses* (2019) 11(2):164. doi: 10.3390/v11020164

5. Fang Y, Khater EIM, Xue JB, Ghallab EHS, Li YY, Jiang TG, et al. Epidemiology of mosquito-borne viruses in Egypt: A systematic review. *Viruses* (2022) 14(7):1577. doi: 10.3390/v14071577

6. Moizéis RNC, Fernandes T, Guedes P, Pereira HWB, Lanza DCF, Azevedo JWV, et al. Chikungunya fever: A threat to global public health. *Pathog Global Health* (2018) 112:182–94. doi: 10.1080/20477724.2018.1478777

7. Ahola T, McInerney G, Merits A. Alphavirus RNA replication in vertebrate cells. *Adv Virus Res* (2021) 111:111–56. doi: 10.1016/bs.aivir.2021.07.003

8. Law YS, Utt A, Tan YB, Zheng J, Wang S, Chen MW, et al. Structural insights into RNA recognition by the chikungunya virus nsP2 helicase. *Proc Natl Acad Sci U States America* (2019) 116:9558–67. doi: 10.1073/pnas.1900656116

9. Ramsey J, Mukhopadhyay S. Disentangling the frames, the state of research on the alphavirus 6K and TF proteins. *Viruses* (2017) 9(8):228. doi: 10.3390/v9080228

10. Wu J, Chen ZJ. Innate immune sensing and signaling of cytosolic nucleic acids. *Annu Rev Immunol* (2014) 32:461–88. doi: 10.1146/annurev-immunol-032713-120156

11. Fros JJ, Pijlman GP. Alphavirus infection: Host cell shut-off and inhibition of antiviral responses. *Viruses* (2016) 8(6):166. doi: 10.3390/v8060166

12. Li WX, Ding SW. Mammalian viral suppressors of RNA interference. *Trends Biochem Sci* (2022) S0968-0004(22):00115–3. doi: 10.1016/j.tibs.2022.05.001

13. Lu Y, Zhang L. DNA-Sensing antiviral innate immunity in poxvirus infection. *Front Immunol* (2020) 11:1637. doi: 10.3389/fimmu.2020.01637

14. Antia A, Pinski AN, Ding S. Re-examining rotavirus innate immune evasion: Potential applications of the reverse genetics system. *mBio* (2022) 13(4): e0130822. doi: 10.1128/mbio.01308-22

15. Ouyang Y, Liao H, Hu Y, Luo K, Hu S, Zhu H. Innate immune evasion by human respiratory syncytial virus. *Front Microbiol* (2022) 13:865592. doi: 10.3389/fmicb.2022.865592

16. Zheng X, Nie S, Feng WH. Regulation of antiviral immune response by African swine fever virus (ASFV). *Virol Sin* (2022) 37:157–67. doi: 10.1016/j.virs.2022.03.006

17. Zhang K, Lin S, Li J, Deng S, Zhang J, Wang S. Modulation of innate antiviral immune response by porcine enteric coronavirus. *Front Microbiol* (2022) 13:845137. doi: 10.3389/fmicb.2022.845137

18. Zhu H, Zheng C. The race between host antiviral innate immunity and the immune evasion strategies of herpes simplex virus 1. *Microbiol Mol Biol Rev MMBR* (2020) 84(4):e00099–20. doi: 10.1128/MMBR.00099-20

19. Zheng C. Evasion of cytosolic DNA-stimulated innate immune responses by herpes simplex virus 1. *J Virol* (2018) 92(6):e00099–17. doi: 10.1128/JVI.00099-17

20. Lee J, Ou JJ. Hepatitis c virus and intracellular antiviral response. *Curr Opin Virol* (2022) 52:244–9. doi: 10.1016/j.coviro.2021.12.010

21. Elrefaey AME, Hollinghurst P, Reitmayer CM, Alphey L, Maringer K. Innate immune antagonism of mosquito-borne flaviviruses in humans and mosquitoes. *Viruses* (2021) 13(11):2116. doi: 10.3390/v13112116

22. Ablasser A, Chen ZJ. cGAS in action: Expanding roles in immunity and inflammation. *Sci (New York NY)* (2019) 363(6431):eaat8657. doi: 10.1126/science.aat8657

23. Webb LG, Veloz J, Pintado-Silva J, Zhu T, Rangel MV, Mutetwa T, et al. Chikungunya virus antagonizes cGAS-STING mediated type-I interferon responses by degrading cGAS. *PloS Pathog* (2020) 16:e1008999. doi: 10.1371/journal.ppat.1008999

24. Chen X, Yang X, Zheng Y, Yang Y, Xing Y, Chen Z. SARS coronavirus papain-like protease inhibits the type I interferon signaling pathway through interaction with the STING-TRAF3-TBK1 complex. *Protein Cell* (2014) 5:369–81. doi: 10.1007/s13238-014-0026-3

25. Akira S, Uematsu S, Takeuchi O. Pathogen recognition and innate immunity. *Cell* (2006) 124:783–801. doi: 10.1016/j.cell.2006.02.015

26. Natarajan K, Dimasi N, Wang J, Mariuzza RA, Margulies DH. Structure and function of natural killer cell receptors: Multiple molecular solutions to self, nonself discrimination. *Annu Rev Immunol* (2002) 20:853–85. doi: 10.1146/annurev.immunol.20.100301.064812

27. Honda K, Takaoka A, Taniguchi T. Type I interferon [corrected] gene induction by the interferon regulatory factor family of transcription factors. *Immunity* (2006) 25:349–60. doi: 10.1016/j.immuni.2006.08.009

28. Aicart-Ramos C, Valero RA, Rodriguez-Crespo I. Protein palmitoylation and subcellular trafficking. *Biochim Biophys Acta* (2011) 1808:2981–94. doi: 10.1016/j.bbamem.2011.07.009

29. Ramsey J, Renzi EC, Arnold RJ, Trinidad JC, Mukhopadhyay S. Palmitoylation of sindbis virus TF protein regulates its plasma membrane localization and subsequent incorporation into virions. *J Virol* (2017) 91(3): e2000–16. doi: 10.1128/JVI.02000-16

30. Yin H, Yin P, Zhao H, Zhang N, Jian X, Song S, et al. Intraviral interactome of chikungunya virus reveals the homo-oligomerization and palmitoylation of structural protein TF. *Biochem Biophys Res Commun* (2019) 513:919–24. doi: 10.1016/j.bbrc.2019.04.098

31. Kendra JA, de la Fuente C, Brahms A, Woodson C, Bell TM, Chen B, et al. Ablation of programmed -1 ribosomal frameshifting in Venezuelan equine encephalitis virus results in attenuated neuropathogenicity. *J Virol* (2017) 91(3): e01766–16. doi: 10.1128/JVI.01766-16

32. Chung BY, Firth AE, Atkins JF. Frameshifting in alphaviruses: A diversity of 3' stimulatory structures. *J Mol Biol* (2010) 397:448–56. doi: 10.1016/j.jmb.2010.01.044

33. Rogers KJ, Jones-Burrage S, Maury W, Mukhopadhyay S. TF protein of sindbis virus antagonizes host type I interferon responses in a palmitoylation-dependent manner. *Virology* (2020) 542:63–70. doi: 10.1016/j.virol.2020.01.001

34. Bae S, Lee JY, Myoung J. Chikungunya virus-encoded nsP2, E2 and E1 strongly antagonize the interferon-β signaling pathway. *J Microbiol Biotechnol* (2019) 29:1852–9. doi: 10.4014/jmb.1910.10014

35. Stark GR, Darnell JEJr. The JAK-STAT pathway at twenty. *Immunity* (2012) 36:503–14. doi: 10.1016/j.immuni.2012.03.013

36. Randall RE, Goodbourn S. Interferons and viruses: An interplay between induction, signalling, antiviral responses and virus countermeasures. *J Gen Virol* (2008) 89:1–47. doi: 10.1099/vir.0.83391-0

37. Simmons JD, White LJ, Morrison TE, Montgomery SA, Whitmore AC, Johnston RE, et al. Venezuelan Equine encephalitis virus disrupts STAT1 signaling by distinct mechanisms independent of host shutoff. *J Virol* (2009) 83:10571–81. doi: 10.1128/JVI.01041-09

38. Göertz GP, McNally KL, Robertson SJ, Best SM, Pijlman GP, Fros JJ. The methyltransferase-like domain of chikungunya virus nsP2 inhibits the interferon response by promoting the nuclear export of STAT1. *J Virol* (2018) 92(17):e01008–18. doi: 10.1128/JVI.01008-18.

39. Fros JJ, van der Maten E, Vlak JM, Pijlman GP. The c-terminal domain of chikungunya virus nsP2 independently governs viral RNA replication, cytopathicity, and inhibition of interferon signaling. *J Virol* (2013) 87:10394–400. doi: 10.1128/JVI.00884-13

40. Van Damme N, Goff D, Katsura C, Jorgenson RL, Mitchell R, Johnson MC, et al. The interferon-induced protein BST-2 restricts HIV-1 release and is downregulated from the cell surface by the viral vpu protein. *Cell Host Microbe* (2008) 3:245–52. doi: 10.1016/j.chom.2008.03.001

41. Hauser H, Lopez LA, Yang SJ, Oldenburg JE, Exline CM, Guatelli JC, et al. HIV-1 vpu and HIV-2 env counteract BST-2/tetherin by sequestration in a perinuclear compartment. *Retrovirology* (2010) 7:51. doi: 10.1186/1742-4690-7-51

42. Jones PH, Maric M, Madison MN, Maury W, Roller RJ, Okeoma CM. BST-2/tetherin-mediated restriction of chikungunya (CHIKV) VLP budding is counteracted by CHIKV non-structural protein 1 (nsP1). *Virology* (2013) 438:37–49. doi: 10.1016/j.virol.2013.01.010

43. Neil SJ, Zang T, Bieniasz PD. Tetherin inhibits retrovirus release and is antagonized by HIV-1 vpu. *Nature* (2008) 451:425–30. doi: 10.1038/nature06553

44. Mao R, Nie H, Cai D, Zhang J, Liu H, Yan R, et al. Inhibition of hepatitis b virus replication by the host zinc finger antiviral protein. *PloS Pathog* (2013) 9: e1003494. doi: 10.1371/journal.ppat.1003494

45. Bick MJ, Carroll JW, Gao G, Goff SP, Rice CM, MacDonald MR. Expression of the zinc-finger antiviral protein inhibits alphavirus replication. *J Virol* (2003) 77:11555–62. doi: 10.1128/JVI.77.21.11555-11562.2003

46. Müller S, Möller P, Bick MJ, Wurr S, Becker S, Günther S, et al. Inhibition of filovirus replication by the zinc finger antiviral protein. *J Virol* (2007) 81:2391–400. doi: 10.1128/JVI.01601-06

47. Wang X, Li MMH, Zhao J, Li S, MacDonald MR, Rice CM, et al. Sindbis virus can exploit a host antiviral protein to evade immune surveillance. *J Virol* (2016) 90:10247–58. doi: 10.1128/JVI.01487-16

48. Akhrymuk I, Frolov I, Frolova EI. Sindbis virus infection causes cell death by nsP2-induced transcriptional shutoff or by nsP3-dependent translational shutoff. *J Virol* (2018) 92(23):e01388–18. doi: 10.1128/JVI.01388-18

49. Garmashova N, Gorchakov R, Frolova E, Frolov I. Sindbis virus nonstructural protein nsP2 is cytotoxic and inhibits cellular transcription. *J Virol* (2006) 80:5686–96. doi: 10.1128/JVI.02739-05

50. Frolova EI, Fayzulin RZ, Cook SH, Griffin DE, Rice CM, Frolov I. Roles of nonstructural protein nsP2 and Alpha/Beta interferons in determining the outcome of sindbis virus infection. *J Virol* (2002) 76:11254–64. doi: 10.1128/JVI.76.22.11254-11264.2002

51. Nguyen VT, Giannoni F, Dubois MF, Seo SJ, Vigneron M, Kédinger C, et al. *In vivo* degradation of RNA polymerase II largest subunit triggered by alpha-amanitin. *Nucleic Acids Res* (1996) 24:2924–9. doi: 10.1093/nar/24.15.2924

52. Eckei L, Krieg S, Bütepage M, Lehmann A, Gross A, Lippok B, et al. The conserved macrodomains of the non-structural proteins of chikungunya virus and

other pathogenic positive strand RNA viruses function as mono-ADP-ribosylhydrolases. *Sci Rep* (2017) 7:41746. doi: 10.1038/srep41746

53. Ishida R, Cole J, Lopez-Orozco J, Fayad N, Felix-Lopez A, Elaish M, et al. Mayaro virus non-structural protein 2 circumvents the induction of interferon in part by depleting host transcription initiation factor IIE subunit 2. *Cells* (2021) 10 (12):3510. doi: 10.3390/cells10123510

54. Petrakova O, Volkova E, Gorchakov R, Paessler S, Kinney RM, Frolov I. Noncytopathic replication of Venezuelan equine encephalitis virus and eastern equine encephalitis virus replicons in mammalian cells. *J Virol* (2005) 79:7597–608. doi: 10.1128/JVI.79.12.7597-7608.2005

55. Garmashova N, Gorchakov R, Volkova E, Paessler S, Frolova E, Frolov I. The old world and new world alphaviruses use different virus-specific proteins for induction of transcriptional shutoff. *J Virol* (2007) 81:2472–84. doi: 10.1128/JVI.02073-06

56. Frakes AE, Dillin A. The UPR(ER): Sensor and coordinator of organismal homeostasis. *Mol Cell* (2017) 66:761–71. doi: 10.1016/j.molcel.2017.05.031

57. Novoa I, Zhang Y, Zeng H, Jungreis R, Harding HP, Ron D. Stress-induced gene expression requires programmed recovery from translational repression. *EMBO J* (2003) 22:1180–7. doi: 10.1093/emboj/cdg112

58. Rathore AP, Ng ML, Vasudevan SG. Differential unfolded protein response during chikungunya and sindbis virus infection: CHIKV nsP4 suppresses eIF2α phosphorylation. *Virol J* (2013) 10:36. doi: 10.1186/1743-422X-10-36

59. Bertolotti A, Zhang Y, Hendershot LM, Harding HP, Ron D. Dynamic interaction of BiP and ER stress transducers in the unfolded-protein response. *Nat Cell Biol* (2000) 2:326–32. doi: 10.1038/35014014

60. Fros JJ, Major LD, Scholte FEM, Gardner J, van Hemert MJ, Suhrbier A, et al. Chikungunya virus non-structural protein 2-mediated host shut-off disables the unfolded protein response. *J Gen Virol* (2015) 96:580–9. doi: 10.1099/vir.0.071845-0

61. Qian Q, Zhou H, Shu T, Mu J, Fang Y, Xu J, et al. The capsid protein of semliki forest virus antagonizes RNA interference in mammalian cells. *J Virol* (2020) 94(3):e01233–19. doi: 10.1128/JVI.01233-19

frontiers | Frontiers in Immunology

TYPE Original Research
PUBLISHED 13 September 2022
DOI 10.3389/fimmu.2022.958898

OPEN ACCESS

EDITED BY
Chenhe Su,
Wistar Institute, United States

REVIEWED BY
Xiaochuan Liu,
University of California, Riverside, United States
Huibin Yu,
Yale University, United States
Jun Yan,
Fudan University, China

*CORRESPONDENCE
Junjiang Fu
fujunjiang@swmu.edu.cn
Dabing Li
lidabing2018@163.com
Xiaoyan Liu
405071800@qq.com

†These authors have contributed equally to this work

SPECIALTY SECTION
This article was submitted to Viral Immunology, a section of the journal Frontiers in Immunology

RECEIVED 01 June 2022
ACCEPTED 26 August 2022
PUBLISHED 13 September 2022

CITATION
Cheng J, Fu J, Tan Q, Liu Z, Guo K, Zhang L, He J, Zhou B, Liu X, Li D and Fu J (2022) The regulation of ISG20 expression on SARS-CoV-2 infection in cancer patients and healthy individuals.
Front. Immunol. 13:958898.
doi: 10.3389/fimmu.2022.958898

The regulation of ISG20 expression on SARS-CoV-2 infection in cancer patients and healthy individuals

Jingliang Cheng[1†], Jiewen Fu[1†], Qi Tan[1†], Zhiying Liu[1†], Kan Guo[1], Lianmei Zhang[1,2], Jiayue He[1], Baixu Zhou[1,3], Xiaoyan Liu[1*], Dabing Li[1,4*] and Junjiang Fu[1*]

[1]Key Laboratory of Epigenetics and Oncology, The Research Center for Preclinical Medicine, Southwest Medical University, Luzhou, China, [2]Department of Pathology, The Affiliated Huaian No. 1 People's Hospital of Nanjing Medical University, Huai'an, China, [3]Department of Gynecology and Obstetrics, Guangdong Women and Children Hospital, Guangzhou, China, [4]Basic Medical School, Southwest Medical University, Luzhou, China

ISG20 inhibits viruses such as SARS-CoV-2 invasion; however, details of its expression and regulation with viral susceptibility remain to be elucidated. The present study analyzed ISG20 expression, isoform information, survival rate, methylation patterns, immune cell infiltration, and COVID-19 outcomes in healthy and cancerous individuals. Cordycepin (CD) and N6, N6-dimethyladenosine ($m^6{}_2A$) were used to treat cancer cells for ISG20 expression. We revealed that *ISG20* mRNA expression was primarily located in the bone marrow and lymphoid tissues. Interestingly, its expression was significantly increased in 11 different types of cancer, indicating that cancer patients may be less vulnerable to SARS-CoV-2 infection. Among them, higher expression of ISG20 was associated with a long OS in CESC and SKCM, suggesting that ISG20 may be a good marker for both viral prevention and cancer progress. *ISG20* promoter methylation was significantly lower in BLCA, READ, and THCA tumor tissues than in the matched normal tissues, while higher in BRCA, LUSC, KIRC, and PAAD. Hypermethylation of *ISG20* in KIRC and PAAD tumor tissues was correlated with higher expression of *ISG20*, suggesting that methylation of *ISG20* may not underlie its overexpression. Furthermore, ISG20 expression was significantly correlated with immune infiltration levels, including immune lymphocytes, chemokine, receptors, immunoinhibitors, immunostimulators, and MHC molecules in pan-cancer. STAD exhibited the highest degree of *ISG20* mutations; the median progression-free survival time in months for the unaltered group was 61.84, while it was 81.01 in the mutant group. Isoforms ISG20-001 and ISG20–009 showed the same RNase_T domain structure, demonstrating the functional roles in tumorigenesis and SARS-CoV-2 invasion inhibition in cancer patients. Moreover, CD and $m^6{}_2A$ increase ISG20 expression in various cancer cell lines, implying the antiviral/anti-SARS-CoV-2 therapeutic potential. Altogether, this study highlighted the value of combating cancer by targeting ISG20 during the COVID-19 pandemic, and small molecules extracted from traditional Chinese medicines, such as CD,

may have potential as anti-SARS-CoV-2 and anticancer agents by promoting ISG20 expression.

KEYWORDS

ISG20 expression, cancer, SARS-CoV-2, cordycepin (CD), N6, N6-dimethyladenosine (m 6 2A)

1 Introduction

Interferon stimulated exonuclease gene 20 (ISG20, OMIM: 604533) aliases HEM45, CD25, Promyelocytic leukemia nuclear body-associated protein ISG20, interferon-stimulated exonuclease gene 20 kDa, interferon-stimulated gene 20 KDa protein, estrogen-regulated transcript 45 protein, and EC 3.1.13.1. ISG20 cytogenetic locates on chromosome 15q26.1 and genomic coordinates (GRCh38) between 15:88,635,631 and 88,656,4820 was first isolated by Gongora et al. in 1997 as a cDNA encoding an interferon-induced protein, called ISG20, by screening an IFN-treated Daudi cell cDNA library (1). Pentecost (1998) identified a cDNA that encoded a 181-amino acid protein with a predicted molecular weight of 20,363 Da; the expression of *ISG20* mRNA was increased in response to estrogen in estrogen receptor-expressing cells in the presence of cycloheximide (2).

ISG20 is predicted to exhibit a broad spectrum of antiviral activity, including hepatitis A virus (HAV), hepatitis B virus (HBV), hepatitis C virus (HCV), Influenza A virus (IAV), and yellow fever virus (YFV) in an exonuclease-dependent manner, through the degradation of viral RNA as a 3'-5'-exoribonuclease (3, 4). Additional antiviral mechanisms by ISG20 include translational inhibition of viral RNA and non-self RNAs and degradation of deaminated viral DNA (3, 5–7). ISG20 has also been reported to inhibit the replication of bluetongue virus (BTV) in ovine (8) and to inhibit the proliferation of pseudorabies virus (PRV) (9, 10). Furthermore, a recent study suggested that ISG20 can degrade SARS-CoV-2 (severe acute respiratory syndrome coronavirus 2) sub-replicon RNA through exonuclease activity (11). The SARS-CoV-2 is the pathogen underlying the current COVID-19 (coronavirus disease 2019) pandemic, leading to more than 596 million positive cases and 6 million deaths worldwide (https://coronavirus.jhu.edu/).

Similarly, ISG20 acts as a SARS-CoV-2 RNase and is critical in inhibiting the SARS-CoV-2 replicon in host cells. Therefore, the expression and distribution of ISG20 may explain the differences in COVID-19 severity after the SARS-CoV-2 invasion. Cellular and humoral immunity participate in the prevention of viral invasion, and the pathological process of COVID-19 is likely correlated with the dysregulation of the immune response, particularly of T cells. Targeting ISG20 may thus be a potential therapeutic strategy for managing SARS-CoV-2 infection.

A large body of evidence has indicated the effect of COVID-19 on the clinical outcomes of cancer patients. According to cohort studies of COVID-19 on the Cancer Consortium and systematic reviews, patients with cancer and COVID-19 exhibit increased mortality rates (12–15). Thus, increased attention should be paid to patients with cancer during the COVID-19 pandemic.

Herein, we performed comprehensive and integrative profiling of ISG20 expression in healthy individuals and patients using a pan-cancer dataset using genomic, transcriptomic, and epigenomic data. The relationships between the expression of ISG20 and immune cell infiltration were investigated. These results may highlight the significance of SARS-CoV-2 infection in patients with different cancer types and the potential therapeutic value of using small molecules such as cordycepin (CD) and N6, N6-dimethyladenosine ($m^6{}_2A$) in managing SARS-CoV-2 infection.

2 Materials and methods

2.1 Online databases

ISG20 homologs in humans from GenBank (Protein: NP_001290162.2, Gene: NM_001303233.2) and others were obtained from NCBI (National Center for Biotechnology Information) (https://www.ncbi.nlm.nih.gov/homologene/31081) (16, 17). Data on gene and protein expression levels of ISG20 in the normal and cancerous tissues (https://www.proteinatlas.org/ENSG00000172183-ISG20/tissue), in different types of immune cells (RNA) (https://www.proteinatlas.org/ENSG00000172183-ISG20/immune+cell), in single cells (https://www.proteinatlas.org/ENSG00000172183-ISG20/single+cell+type), and brain tissues (https://www.proteinatlas.org/ENSG00000172183-ISG20/brain) were obtained from the Human Protein Atlas (HPA) (18, 19). *ISG20* expression in different types of cancer tissues and the corresponding normal tissues, isoform, distribution, and domain structures were

analyzed using GEPIA 2 (gene expression profiling interactive analysis 2) (http://gepia2.cancer-pku.cn/#analysis) and (http://gepia2.cancer-pku.cn/#isoform) (20, 21). DNA methylation analysis of the *ISG20* promoter was performed using DNMIVD (DNA methylation interactive visualization database) (http://119.3.41.228/dnmivd/query_gene/?cancer=pancancer&gene=ISG20) (22). Data on *ISG20* mutations were obtained from cBioPortal for cancer genomics (https://www.cbioportal.org/results/cancerTypesSummary?case_set_id=all&gene_list=ISG20&cancer_study_list=5c8a7d55e4b046111fee2296) (23). Survival analysis of *ISG20* expressions was performed using GEPIA 2, DNMIVD, and cBioPortal. Analysis of the relationships between the abundance of tumor-infiltrating lymphocytes (TILs) and expression was performed using TISIDB (an integrated repository portal for tumor-immune system interactions) (http://cis.hku.hk/TISIDB/browse.php?gene=ISG20) (24).

2.2 Immunohistochemistry analysis

Immunohistochemistry (IHC) in formalin-fixed, paraffin-embedded breast cancer tissue sections from Chinese patients was performed as described previously (17, 25–27). The ISG20 antibody (C-12, cat #: sc-514979) for IHC and western blotting was purchased from Santa Cruz Biotechnology, Inc., USA. For details, 5μm deparaffinized and rehydrated sections were incubated in 10 μM sodium citrate buffer at 95°C for 12 min for antigen retrieval, and treated with 3% hydrogen peroxide. Then blocking with 5% bovine serum albumin (BSA). Primary ISG20 antibody (1:50 dilution) was applied overnight and then incubated with appropriate biotin-conjugated secondary antibodies (SP-9000, ZSGB-Bio, CN) for 60 min at 25°C. Immunostaining signals were visualized by the Streptavidin-conjugated horseradish peroxidase (HRP) and 3,3-diaminobenzidine (DAB) (ZLI-9017, ZSGB-Bio, CN). Slides were counterstained with hematoxylin, dehydrated, and mounted.

2.3 Cell culture

Cancer cell lines A549, H1975, HepG2, 22RV1, PC3, BT549, MDA-MB-231, and HeLa were obtained from ATCC (American Type Culture Collection), and cultured in DMEM or RPM1640 supplemented with 10% serum and 1% penicillin-streptomycin (Gibco; Thermo Fisher Scientific, Inc.) in 12-well plates. CD (Cat #: A0682) was obtained from Chengdu Must Bio-Technology Co. Ltd (Chengdu, Sichuan, China), $m^6{}_2A$ (CAS #: 2620-62-4) from BOC Sciences (Shirley, NY, USA), and uridine-5'-monophosphate (UMP, CAS #: 58-97-9) from Shanghai Aladdin Biochemical Technology company (Shanghai, China). Total RNA and protein were extracted after UMP, CD, or $m^6{}_2A$ treatment with the indicated concentrations for 24 h. The cells were lysed using EBC buffer (20 mM Tris-HCl, pH 8.0, 125 mM NaCl, 2 mM EDTA, and 0.5% NP-40) supplemented with a protease and phosphatase inhibitor cocktail. The harvested protein was stored at -20°C until required.

2.4 Western blotting

SDS-PAGE was used for western blotting. After electrophoresis at 100v for 100 min, the proteins were transferred to membranes at 100v for approximately 90 min. Then the membranes were blocked with fresh 5% fat-free milk at room temperature for 2 h. Primary antibodies against ISG20, β-actin, or HSP90 were incubated in the fresh 2% fat-free milk at 4° C overnight. The following day, membranes were washed three times with TBST (Tris-buffered saline containing 0.1% Tween20) for 15 min each time, and the blots were incubated with an anti-mouse HRP secondary antibody (1:5000 dilution) in 2% fat-free milk for a further 2 h. Subsequently, the membranes were three times as above. The protocol for western blot in breast cancer tissues and its matched healthy tissues from Chinese breast cancer patients was described previously (25, 26). All experiments were repeated three times.

2.5 Semi-quantitative reverse transcription-polymerase chain reaction

The harvested total RNA was reverse transcribed into cDNA. The sequences of the primers targeting *ISG20* (NM_001303233.2) were: RT-ISG20-5: 5'-cttccaggcactgaaagagg-3' (forward primer), RT-ISG20-3: 5'-aagccgaaagcctctagtcc-3' (reverse primer). The expected product size was 309 bp. These primers would expect to detect isoforms ISG20-001 and ISG20–009, two main isoforms for ISG20 in Figure 5C. *ACTB* was used as the internal control. The sequences of the primers ACTB were: RT-ACTB-5: 5'-CTCTTCCAGCCTTCCTTCCT-3' (forward primer), RT-ACTB-3:5'-CACCTTCACCGTTCCAGTTT-3' (reverse primer). The expected product size was 510 bp. Semi-quantitative RT-PCR was performed as described previously (28). All experiments were repeated three times.

2.6 Statistical analysis

To compare the expression of ISG20 in pan-cancer and in the matched healthy tissues, |log2FC| values were used and log-rank $P<0.05$ was considered statistically significant. For comparison of the methylation of the ISG20 promoter region in cancer tissues and the corresponding healthy tissues, a student's t-test was used, and *P-value* <0.05 was considered significant.

3 Results

3.1 Expression of ISG20 in normal tissues

The transcriptional data on *ISG20* expression in human organs and tissues is presented in Figure 1A; *ISG20* mRNA was mainly located in the bone marrow and lymphoid tissues, followed by the gastrointestinal tract, respiratory system, liver and gallbladder, endocrine tissues, and kidney and urinary bladder, with no expression in the eyes. High expression of *ISG20* in the respiratory system (lung, 63.3nTPM) demonstrated its antiviral role in the lungs. The expression of *ISG20* mRNA was further validated in the consensus data set (Figure 1B). In agreement with the above results, the top nine tissues/organs for *ISG20* mRNA expressions in this consensus dataset were the lymph node, spleen, thymus, appendix, and tonsils (they are bone marrow and lymphoid tissues), stomach, duodenum, and small intestine (they are gastrointestinal tract), and lungs (Figure 1B). Then, the mRNA expression levels of *ISG20* were examined in human tissues of immune cells, single cell types, and the brain. The results of 18 immune cell types and total peripheral blood mononuclear cells (PBMCs) indicated that *ISG20* mRNA expression was very high in neutrophils, T-regs, memory B-cells, and naive B-cells (all >1,150 nPTM) (Figure 1C). The *ISG20* mRNA expression in single-cell-type specificity indicated it was predominantly expressed in the plasma cells (663.4 nTPM), Langerhans cells (500.2 nTPM), B-cells (424.2 nTPM), dendritic cells (378.8 nTPM), T-cells (318.4 nTPM), urothelial cells (538.6 nTPM), and paneth cells (476.1 nTPM) (Figure 1D). The mRNA expression levels of *ISG20* in the brain were very low but remained detectable, with the highest levels observed in the cerebral cortex (11.3 nPTM) (Figure 1E). The *ISG20* expression was unavailable (NA) in human blood cells from HPA.

Next, we conducted IHC of breast cancer tissues; representative results are shown in Figures 2A–F. ISG20 staining showed high expression in the cytoplasm and membranes in the breast tissues (Figures 2A, B) and breast cancer tissues (Figures 2, D). ISG20 was primarily located in the cytoplasm and membrane (highest in the cytoplasm), indicating its role in viral prevention. As a control, we also showed IHC images of breast tissues and breast cancer tissues without antibodies, respectively, in Figures 2E, F.

3.2 *ISG20* expression is increased in cancer tissues compared with the corresponding normal tissues

Increasing evidence has shown that cancer patients are more vulnerable to SARS-Cov-2. As an enigmatic antiviral factor, it is important to know the expression levels of ISG20 in cancer

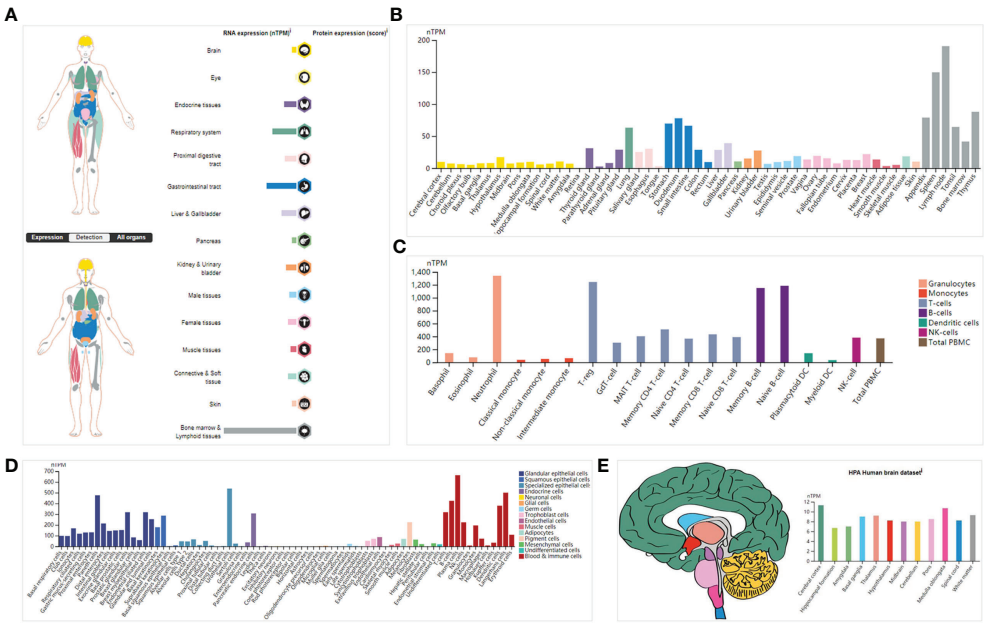

FIGURE 1
The expression of ISG20 in healthy individuals. **(A)** Overview of ISG20 expression and distribution across different types of healthy human tissues. **(B)** mRNA expression of ISG20 in healthy human tissues from the consensus data set. **(C)** mRNA expression of ISG20 in human tissues in different types of immune cells. **(D)** mRNA expression of ISG20 in human tissues in different types of single cells. **(E)** mRNA expression of ISG20 in human brain tissues.

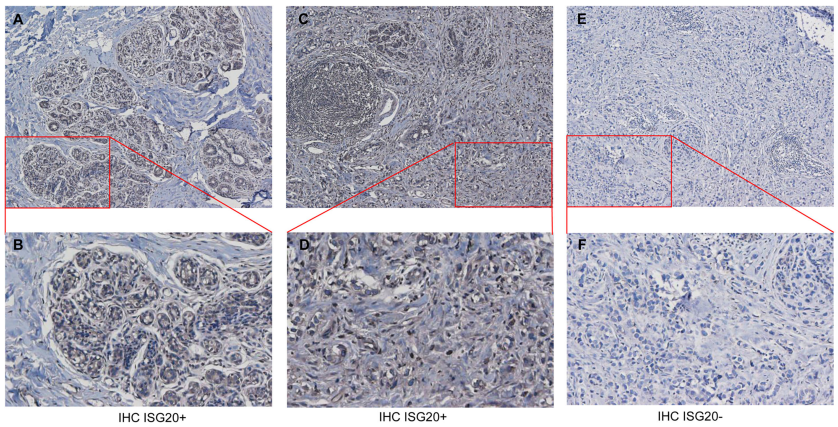

FIGURE 2
Immunohistochemistry (IHC) analysis of ISG20 expression healthy and cancer tissues from breast cancer patients. **(A, B)** IHC analysis of ISG20 in breast tissues. **(C, D)** IHC analysis of ISG20 in breast cancer tissues. **(E, F)** Control IHC of breast tissues without antibody. Panels **(B, D)** show enlarged insets from **(A, C)**, respectively.

tissues compared with corresponding healthy tissues. Surprisingly, *ISG20* mRNA expression was significantly increased in eleven types of cancer, including ACC (adrenocortical carcinoma), CESC (cervical squamous cell carcinoma and endocervical), DLBC (lymphoid neoplasm diffuse large B-cell lymphoma), GBM (glioblastoma multiforme), KIRC (Kidney renal clear cell carcinoma), LIHC (liver hepatocellular carcinoma), KIRP (kidney renal papillary cell carcinoma), PAAD (pancreatic adenocarcinoma), SKCM (skin cutaneous melanoma), TGCT (testicular germ cell tumors), and UCEC (uterine corpus endometrial carcinoma) (Figures 3A, B) compared with the matching normal tissue. Thus, high ISG20 expression in cancer may prevent viral invasion in these cancer patients.

To further validate the expression results, samples of breast cancer tissues and their matched healthy tissues were selected for collection and western blot since ISG20 levels are increased even though not significantly (Supplementary Figure 1A). It is also easy for us to collect breast tumor tissues. After western blot and the results were presented in Supplementary Figure 1B, ISG20 protein levels were increased significantly in 6 of 10 samples/patients (60%) of cancer tissues compared with the matched healthy tissues (Supplementary Figure 1B). These results validated the mRNA results from the TCGA database for BRCA (breast invasive carcinoma) patients.

3.3 The prognostic value of *ISG20* in pan-cancer

Further exploration of the prognostic value of *ISG20* revealed that higher expression was associated with a shorter OS in ACC, DLBC, LAML (acute myeloid leukemia), LGG (lower grade glioma), and UVM (uveal melanoma) (Figures 3C–G), but with a long OS in CESC, OV (ovarian serous cystadenocarcinoma), and SKCM (Figures 3H–J). It was reported that ISG20 overexpression suppressed the proliferation, migration, and invasion *in vitro* and the growth of xenograft tumors *in vivo* in ovarian cancer (29), and it may be associated with a long OS in OV patients.

High expression of *ISG20* in CESC and SKCM was associated with a longer OS, suggesting that ISG20 may be a good marker. However, high expression of ISG20 in ACC and DLBC was associated with a shorter OS, suggesting that ISG20 may be a marker of unfavorable outcomes in these types of cancer. Together, ISG20 may serve as a double-edged sword in viral prevention and cancer progression in certain types of cancer.

3.4 Methylation of the *ISG20* promoter region in cancer and the matched normal tissues

DNA methylation can regulate gene expression. We'd like to know whether ISG20 expression changes are due to methylation modification. By analyzing the DNMIVD database, we found that *ISG20* promoter methylation was significantly lower in BLCA, READ, and THCA tumor tissues compared to the matching normal tissue (Figures 4A–C), while higher in BRCA, LUSC, KIRC, and PAAD (Figures 4D–G). Hypermethylation of *ISG20* in KIRC and PAAD tumor tissues was correlated with the higher expression, suggesting that methylation of *ISG20* may not be the cause of overexpression. Thus, other mechanisms may be involved in regulating *ISG20* expression.

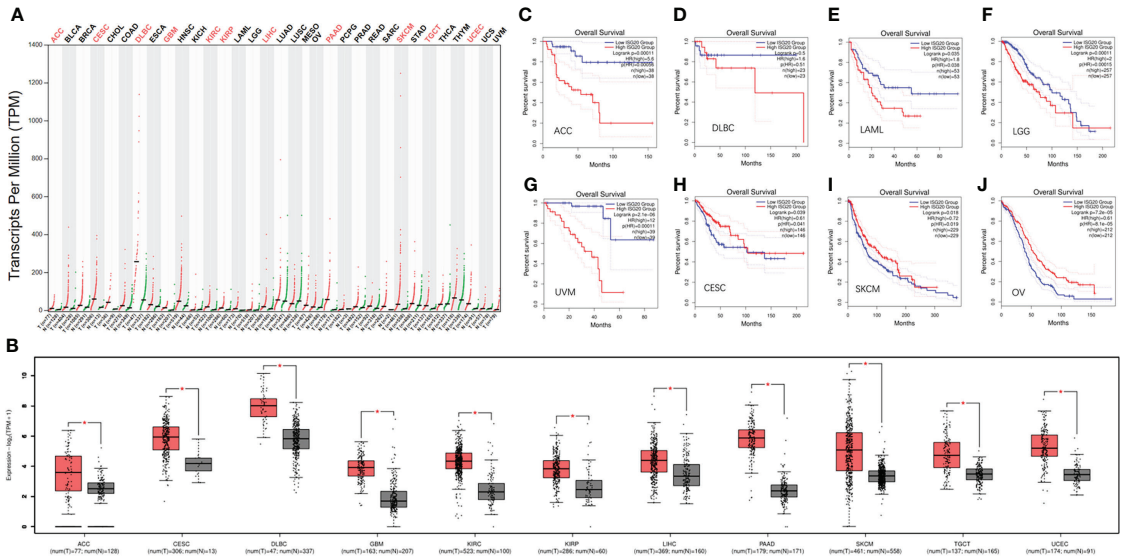

FIGURE 3
The expression of ISG20 in pan-cancer and the respectively matched healthy tissues. **(A)** The expression of ISG20 in different types of cancer and the corresponding normal tissues. **(B)** The expression of ISG20 was significantly higher in the cancer tissues compared with the corresponding normal tissues. **(C–J)**. Survival and ISG20 expression in ACC, DLBC, LAML, LGG, UVM, CESC, SKCM, and OV patients. |log2FC| values were used, and log-rank *P*<0.05 was considered statistically significant. *indicates the significant difference.

3.5 Expression distribution, utilization, and structure of *ISG20* in pan-cancer, and conservation across different species

Different *ACE2* isoforms have differential roles in host susceptibility to SARS-CoV-2 entry (30, 31). We analyzed *ISG20* isoform prevalence and structures in pan-cancer and found 11 isoforms that exhibited differential expression levels (Figure 5A). Except for very low or no expression of isoforms ENST00000558992.1 (ISG20−010), ENST00000558942.5 (ISG20−003), and ENST00000558236.1 (ISG20−011), the remaining eight *ISG20* isoforms were detectable in all cancers.

The utilization of isoform ENST00000560741.5 (ISG20−009) was the highest across all 31 cancer types, followed by ENST00000559876.1 (ISG20−006); others showed very low or no utilization (Figure 5B). The genomic structures of *ISG20* isoforms in pan-cancer are shown in Figure 5C. The isoforms ENST00000306072.9 (ISG20-001) and ENST00000560741.5 (ISG20−009) showed the same structure consisting of 181 amino acids with an RNase_T domain as reported previously; isoforms ENST00000559876.1 (ISG20-006) with 155 amino acids and ENST00000379224.9 (ISG20-008) with 87 amino acids, both possessed a truncated RNase_T domain (Figure 5C), demonstrating the functional role of ISG20-001 and ISG20−009 in tumorigenesis and SARS-CoV-2 invasion inhibition in cancer patients.

In addition, the ISG20 protein showed a highly conserved sequence across different species, including humans, chimpanzee, Rhesus monkey, cows, dog, mice, and rats (Figure 5D), suggesting that ISG20 may possess a similar potential function in inhibiting viral infection in other species (8). Indeed, ISG20 was also reported to inhibit the bluetongue virus (BTV) replication in sheep (8).

3.6 Mutation profiles of *ISG20* in pan-cancer

Gene mutations can cause cancer, recurrence, and/or therapeutic resistance. By analyzing the *ISG20* mutation profile in 32 types of cancer based on data obtained from TCGA, we found that STAD (stomach adenocarcinoma) had the highest mutational frequency, with 3.64% of 440 cases possessing a mutation, followed by SARC (3.53% of 255 cases), whereas BLGG (brain lower grade glioma) had the lowest frequency of mutations (0.19% of 514 cases) (Figure 6A). No *ISG20* mutations were found in the other 11 types of cancer shown in Figure 6A. The detailed landscape of mutations shows the presence of missense mutations, truncations, and SV/fusions in the ISG20 gene, with missense mutations being the most common (Figure 6B).

To further explore the resulting prognostic value, we analyzed the survival correlation between *ISG20* mutant groups and unaltered groups in cancer. However, no significant difference was observed (*P*=0.0679), and the median number of months of progression-free survival for the unaltered

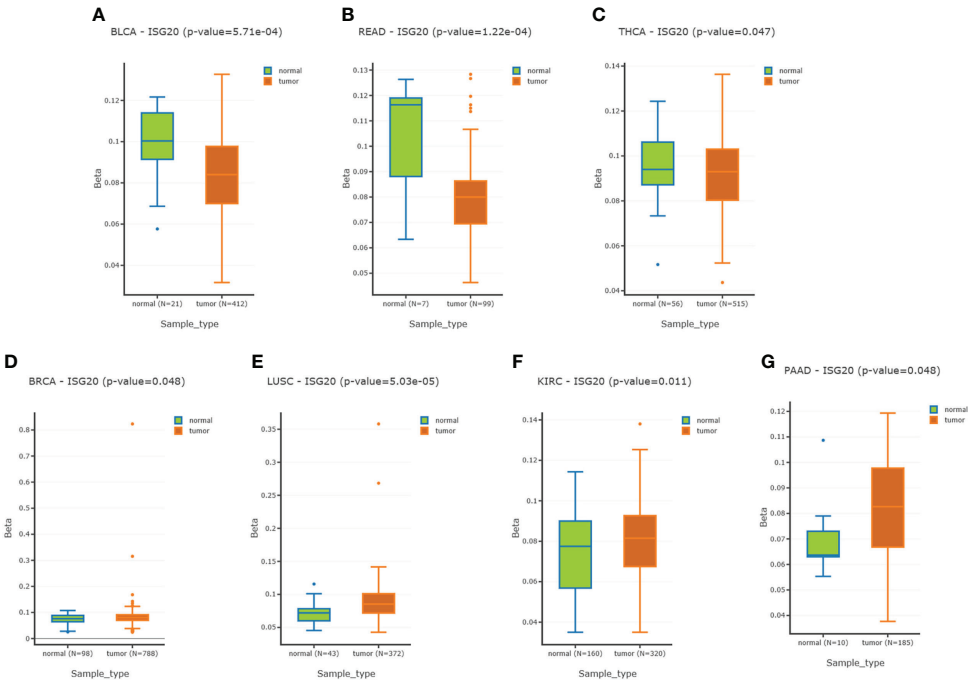

FIGURE 4
Methylation of the ISG20 promoter region in cancer tissues and the corresponding healthy tissues. **(A–C)**. Methylation of the ISG20 promoter region in cancer tissues was significantly lower than in the corresponding healthy tissues for BLCA, READ, and THCA, respectively. **(D–G)**. Methylation of the ISG20 promoter region in cancer tissues was significantly higher than in the corresponding healthy tissues for BRCA, LUSC, KIRC, and PAAD, respectively. The student's t-test was used and *P-value* <0.05 was considered significant.

group was 61.84 months (56.05-66.11, 95% CI), while in the mutant groups, it increased to 81.01 months (48.89-NA, 95% CI) (Figure 6C).

3.7 Association analysis of *ISG20* expression with the tumor-immune system in pan-cancer

Due to the indispensability of antiviral processes and anti-tumor responses of the immune system, the correlation between *ISG20* expression and immune infiltration levels in pan-cancer was analyzed in the TISDB database. We also found significant correlations between *ISG20* expression and immune lymphocytes, chemokines, receptors, immunoinhibitors, immunostimulators, and major histocompatibility complex (MHC) molecules in almost cancer types assessed (Figures 7A–F).

3.8 CD increases ISG20 expression in various cancer cell lines

Some small molecules or natural active components can affect gene expression. We wanted to determine whether small molecules or natural components targeted ISG20 expression. To do this, we first used the DrugBank database and revealed that UMP (DB03685) might target ISG20 (Table 1; Supplementary Figures 2A, B). Then, several cancer-cell lines were cultured and treated with 0, 10, 20, or 40 μM UMP for 24 h, and cells were collected for RNA extraction and RT-PCR. However, the results showed that UMP did not affect *ISG20* mRNA expression in A549 lung cancer cells, HeLa cervical cancer cells, 22RV1 and PC3 prostate cancer cells, and MDA-MB-231 and BT549 breast cancer cells (Supplementary Figures 2C–H).

Then, CD, a nucleoside derivative, was applied to determine the effect on ISG20 expression in the cancer cell lines. The results showed that CD increased ISG20 expression at both the protein and mRNA level in a dose-dependent manner in the H1975 lung cancer-cell line (Figures 8A, B) and 22RV1 prostate cancer-cell line (Figures 8C, D).

3.9 $m^6{}_2A$ increases ISG20 expression in HepG2 cancer cells

The effects of $m^6{}_2A$, another nucleoside derivative, on ISG20 expression in cancer cell lines were also determined. Our results showed that $m^6{}_2A$ increased ISG20 expression at both the

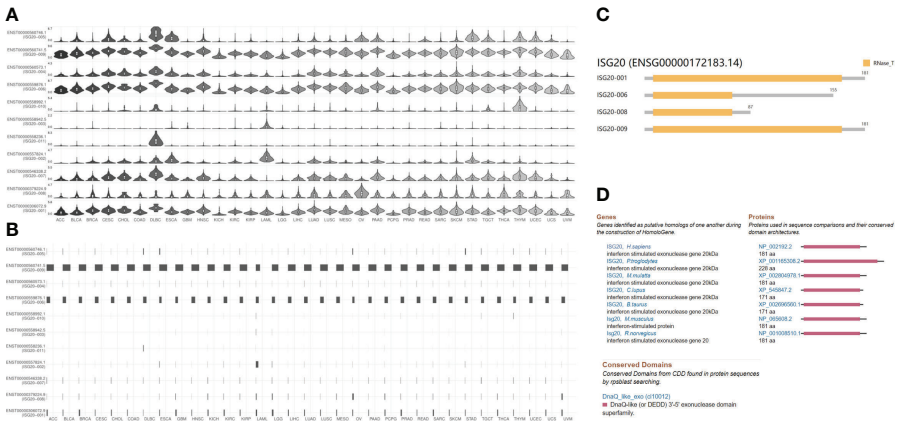

FIGURE 5
ISG20 isoform expression distribution, utilization, structure in pan-cancer, and conservation of ISG20 across different species. **(A)** The expression profiles of the ISG20 isoforms (violin plot). **(B)** Utilization profiles of the ISG20 isoforms (bar plot). **(C)** Structure of the ISG20 isoforms in pan-cancer. Information on 7 isoforms is missing; specifically, ENST00000546338.2, ENST00000557824.1, ENST00000558236.1, ENST00000558942.5, ENST00000558992.1, ENST00000560573.1, and ENST00000560746.1. **(D)** Conservation of ISG20 across different species.

protein and mRNA level in a dose-dependent manner in the HepG2 liver cancer cell line (Figures 8E, F).

Altogether, both nucleoside derivatives, CD and $m^6{}_2A$, are predicted to exhibit antiviral/anti-SARS-CoV-2 therapeutic potential by increasing ISG20 expression.

4 Discussion

In this study, we found that the *ISG20* mRNA was primarily located in the bone marrow and lymphoid tissues; interestingly, the *ISG20* mRNA expression levels were significantly increased in 11 different types of cancer, including ACC, CESC, DLBC, GBM, KIRC, KIRP, LIHC, PAAD, SKCM, TGCT, and UCEC; and no decreases were observed in any type of cancer. Among these, higher expression of ISG20 was associated with a longer OS in CESC and SKCM, suggesting that ISG20 may be a good marker in both viral prevention and cancer progression in patients with these types of cancer. Unlike other receptors, such as ACE2, TMPRSS4, and CTSL, increased ISG20 expression may prevent viral invasion in these types of cancer. DNA methylation is known to affect gene expression, and we found that ISG20 promoter methylation was significantly lower in BLCA, READ, and THCA tumor tissues compared with those in the matched normal tissues, while higher in BRCA, LUSC, KIRC, and PAAD. Hypermethylation of *ISG20* in KIRC and PAAD tumor tissues was correlated with the higher expression, suggesting that methylation of *ISG20* may not underlie the increase in its expression; thus, other mechanisms may be involved in regulating *ISG20* overexpression. Interestingly, both CD and $m^6{}_2A$ increase ISG20 expression in various cancer cell lines, even though it is unknown whether CD and $m^6{}_2A$ regulate ISG20 expression by modification of DNA methylation patterns. Due to the indispensability of antiviral processes and anti-tumor responses in the immune system, the correlation between ISG20 expression and immune infiltration levels of pan-cancer was analyzed, and we revealed significant correlations between *ISG20* expression and immune lymphocytes, chemokine, receptors, immunoinhibitors, immunostimulators, and MHC molecules in all cancer types, highlighting a potential antiviral/anti-SARS-CoV-2 role.

Certain small molecules or natural active components can affect gene expression. We first performed DrugBank database searches and revealed ISG20 as a UMP target. UMP was demonstrated to possess an anti-fibrillatory effect by activating energy metabolism (32). Unfortunately, our experiments failed to find UMP-regulated ISG20 expression in cancer cells. We, therefore, further tested whether CD and $m^6{}_2A$ could affect ISG20 expression and found that both promoted ISG20 expression at the protein and mRNA levels. CD is a natural active component of traditional Chinese medicine (TCM) fungus *cordyceps militaris*, which has anticancer properties (33–35). $m^6{}_2A$ is a modified ribonucleoside in the tRNA of *mycobacterium bovis*, according to Bacille Calmette-Guérin (36). CD and $m^6{}_2A$ are nucleoside derivatives that have been reported to inhibit the expression of CTSL, another SARS-CoV-2 receptor, in cancer cell lines (26). In addition, CD inhibited the expression of furin, another SARS-CoV-2 receptor, in several cancer cell lines (17). As CTSL inhibitors, both CD and $m^6{}_2A$ can promote ISG20

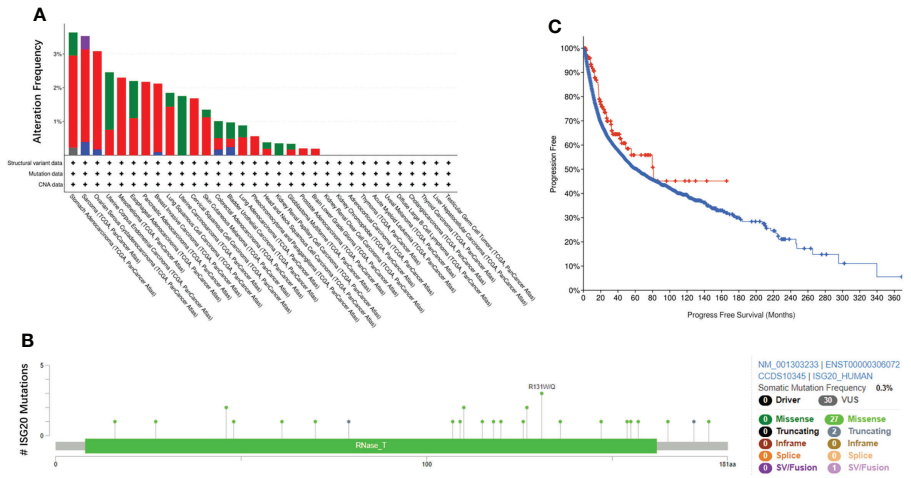

FIGURE 6
ISG20 mutations in pan-cancer. **(A)** Overview of ISG20 mutations in pan-cancer. Different colors represent different types of mutations. **(B)** ISG20 mutation hot spots in pan-cancer. **(C)** Correlation of progression-free survival between the ISG20 mutated group (red) and unaltered group (blue) of pan-cancer.

upregulation. Considering ISG20 inhibits viral replication and/or degradation, CD and $m^6{}_2A$ may play roles in preventing SARS-CoV-2 invasion and the severity of cancer.

Altogether, our study revealed the expression and distribution patterns of *ISG20* in virus/SARS-CoV-2 invasion inhibition on different tissues and organs, differential expression and methylation patterns, and the prognostic significance across several types of cancer. *ISG20* can play an important role in SARS-CoV-2 inhibition in certain types of cancer. Although future studies are needed for validation, our current study

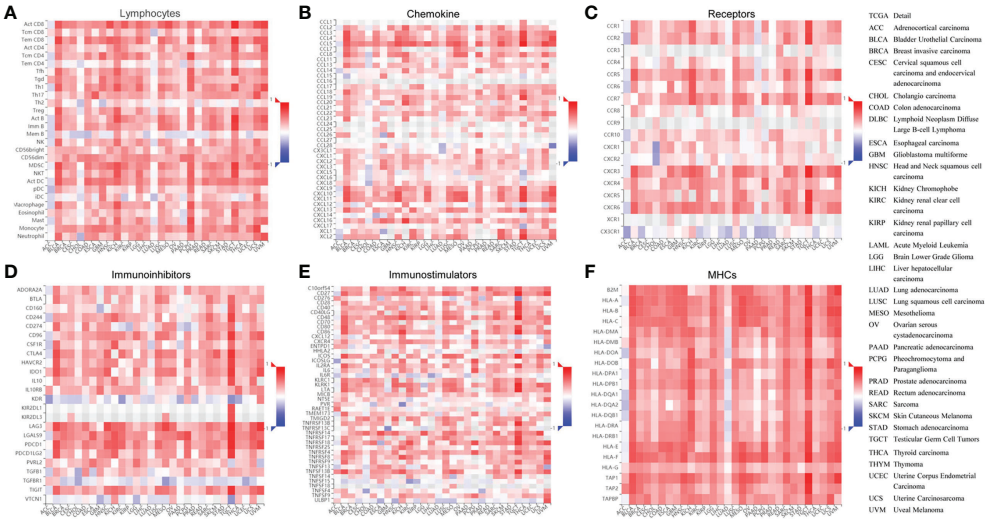

FIGURE 7
Correlation between ISG20 expressions and the tumor-immune system in pan-cancer. The correlation between ISG20 expression and **(A)** lymphocytes, **(B)** chemokines, **(C)** receptors, **(D)** immunoinhibitors, **(E)** immunostimulators, and **(F)** MHCs pan-cancer. The Y axes indicate human immune molecules, and the X axes show the human cancer type. MHC, major histocompatibility complex. The rho value was used to show the Spearman correlations with the range of -1(in blue) to 1 (in red), from the most reverse correlations to the most positive correlations of the gene expressions in the heatmaps. The right panel shows the full terms for all cancers included.

TABLE 1 Drugs predicted to target ISG20.

Drug ID	Name	Drug type	Predicted targets	Target no.
DB03685	Uridine monophosphate	Small Molecule	B4GALT1, GLT6D1, ISG20, LSM6, UCKL1	5

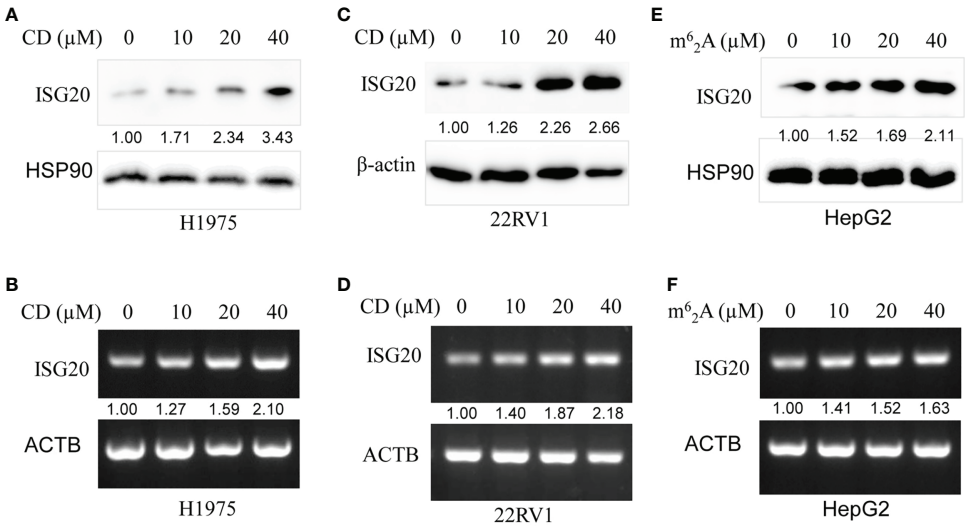

FIGURE 8
Cordycepin (CD) and N6, N6-dimethyladenosine ($m^6{}_2A$) increase ISG20 expression in various cancer cell lines. **(A, B)** CD increases ISG20 expression in the H1975 lung cancer cell line. **(C, D)** CD increases ISG20 expression in the 22RV1 prostate cancer cell line. **(E, F)** m^6a_2A increase ISG20 expression in the HepG2 live cancer cell line.

provides useful information to understand the current COVID-19 pandemic better. Moreover, small molecules from TCM or natural products may be used in the development of anti-SARS-CoV-2 drugs as well anticancer agents by upregulating ISG20 expression. Our study highlighted the value of targeting ISG20 as an alternative therapeutic strategy in combating cancer, SARS-CoV2, and other viral-caused diseases such as HAV, HBV, HCV, IAV, YFV, and BTV.

Data availability statement

The original contributions presented in the study are included in the article/Supplementary Material. Further inquiries can be directed to the corresponding authors.

Ethics statement

This study was reviewed and approved by The study was approved by the Ethical Committee of Southwest Medical University and The Affiliated Huaian No. 1 People's Hospital of Nanjing Medical University. The patients/participants provided their written informed consent to participate in this study.

Author contributions

JC, QT, JWF, ZL, XL, KG, LZ, JH, BZ, DL performed experimental studies, data acquisition, data analysis, and literature search. JJF collected and analyzed the data. JJF wrote and edited the manuscript. JJF, JC, DL revised the manuscript. All authors contributed to the article and approved the submitted version.

Funding

This work was supported by the Foundation of Science and Technology Department of Sichuan Province (grant no. 2022NSFSC0737), the Foundation of Southwest Medical University (grant nos. 2021ZKMS004, 2021ZKQN109), in part by the Research Foundation of Luzhou City (grant no. 2021-

SYF-37), and the National Natural Science Foundation of China (grant nos. 81672887 and 82073263).

Acknowledgments

The authors thank all the people from the Research Center for Preclinical Medicine, Southwest Medical University.

Conflict of interest

The authors declare that the research was conducted in the absence of any commercial or financial relationships that could be construed as a potential conflict of interest.

Publisher's note

Supplementary material

The Supplementary Material for this article can be found online at: https://www.frontiersin.org/articles/10.3389/fimmu.2022.958898/full#supplementary-material

References

1. Gongora C, David G, Pintard L, Tissot C, Hua TD, Dejean A, et al. Molecular cloning of a new interferon-induced PML nuclear body-associated protein. *J Biol Chem* (1997) 272:19457–63. doi: 10.1074/jbc.272.31.19457

2. Pentecost BT. Expression and estrogen regulation of the HEM45 MRNA in human tumor lines and in the rat uterus. *J Steroid Biochem Mol Biol* (1998) 64:25–33. doi: 10.1016/S0960-0760(97)00140-4

3. Deymier S, Louvat C, Fiorini F, Cimarelli A. ISG20: An enigmatic antiviral RNase targeting multiple viruses. *FEBS Open Bio* (2022) 12:1096–111. doi: 10.1002/2211-5463.13382

4. Qu H, Li J, Yang L, Sun L, Liu W, He H. Influenza a virus-induced expression of ISG20 inhibits viral replication by interacting with nucleoprotein. *Virus Genes* (2016) 52:759–67. doi: 10.1007/s11262-016-1366-2

5. Wu N, Nguyen XN, Wang L, Appourchaux R, Zhang C, Panthu B, et al. The interferon stimulated gene 20 protein (ISG20) is an innate defense antiviral factor that discriminates self versus non-self translation. *PLoS Pathog* (2019) 15:e1008093. doi: 10.1371/journal.ppat.1008093

6. Stadler D, Kachele M, Jones AN, Hess J, Urban C, Schneider J, et al. Interferon-induced degradation of the persistent hepatitis b virus cccDNA form depends on ISG20. *EMBO Rep* (2021) 22:e49568. doi: 10.15252/embr.201949568

7. Weiss CM, Trobaugh DW, Sun C, Lucas TM, Diamond MS, Ryman KD, et al. The interferon-induced exonuclease ISG20 exerts antiviral activity through upregulation of type I interferon response proteins. *mSphere* (2018) 3:e00209–18. doi: 10.1128/mSphere.00209-18

8. Kang D, Gao S, Tian Z, Zhang G, Guan G, Liu G, et al. ISG20 inhibits bluetongue virus replication. *Virol Sin* (2022) 37(4):521–30. doi: 10.1016/j.virs.2022.04.010

9. Chen X, Sun D, Dong S, Zhai H, Kong N, Zheng H, et al. Host interferon-stimulated gene 20 inhibits pseudorabies virus proliferation. *Virol Sin* (2021) 36:1027–35. doi: 10.1007/s12250-021-00380-0

10. Ye G, Liu H, Zhou Q, Liu X, Huang L, Weng C. A tug of war: Pseudorabies virus and host antiviral innate immunity. *Viruses* (2022) 14:547. doi: 10.3390/v14030547

11. Furutani Y, Toguchi M, Higuchi S, Yanaka K, Gailhouste L, Qin XY, et al. Establishment of a rapid detection system for ISG20-dependent SARS-CoV-2 subreplicon RNA degradation induced by interferon-alpha. *Int J Mol Sci* (2021) 22:11641. doi: 10.3390/ijms222111641

12. Elkrief A, Hennessy C, Kuderer NM, Rubinstein SM, Wulff-Burchfield E, Rosovsky RP, et al. Geriatric risk factors for serious COVID-19 outcomes among older adults with cancer: A cohort study from the COVID-19 and cancer consortium. *Lancet Healthy Longev* (2022) 3:e143–52. doi: 10.1016/S2666-7568(22)00009-5

13. Desai A, Gupta R, Advani S, Ouellette L, Kuderer NM, Lyman GH, et al. Mortality in hospitalized patients with cancer and coronavirus disease 2019: A systematic review and meta-analysis of cohort studies. *Cancer* (2021) 127:1459–68. doi: 10.1002/cncr.33386

14. Grivas P, Khaki AR, Wise-Draper TM, French B, Hennessy C, Hsu CY, et al. Association of clinical factors and recent anticancer therapy with COVID-19 severity among patients with cancer: a report from the COVID-19 and cancer consortium. *Ann Oncol* (2021) 32:787–800. doi: 10.1016/j.annonc.2021.02.024

15. Fu C, Stoeckle JH, Masri L, Pandey A, Cao M, Littman D, et al. COVID-19 outcomes in hospitalized patients with active cancer: Experiences from a major new York city health care system. *Cancer* (2021) 127:3466–75. doi: 10.1002/cncr.33657

16. Fu J, Liao L, Balaji KS, Wei C, Kim J, Peng J. Epigenetic modification and a role for the E3 ligase RNF40 in cancer development and metastasis. *Oncogene* (2021) 40:465–74. doi: 10.1038/s41388-020-01556-w

17. Li D, Liu X, Zhang L, He J, Chen X, Liu S, et al. COVID-19 disease and malignant cancers: The impact for the furin gene expression in susceptibility to SARS-CoV-2. *Int J Biol Sci* (2021) 17:3954–67. doi: 10.7150/ijbs.63072

18. Uhlen M, Fagerberg L, Hallstrom BM, Lindskog C, Oksvold P, Mardinoglu A, et al. Proteomics. Tissue-based map of the human proteome. *Science* (2015) 347:1260419. doi: 10.1126/science.1260419

19. Uhlen M, Zhang C, Lee S, Sjostedt E, Fagerberg L, Bidkhori G, et al. A pathology atlas of the human cancer transcriptome. *Science* (2017) 357(6352):eaan2507. doi: 10.1126/science.aan2507

20. Tang Z, Li C, Kang B, Gao G, Li C, Zhang Z. GEPIA: a web server for cancer and normal gene expression profiling and interactive analyses. *Nucleic Acids Res* (2017) 45:W98–W102. doi: 10.1093/nar/gkx247

21. Tang Z, Kang B, Li C, Chen T, Zhang Z. GEPIA2: an enhanced web server for large-scale expression profiling and interactive analysis. *Nucleic Acids Res* (2019) 47:W556–W60. doi: 10.1093/nar/gkz430

22. Ding W, Chen J, Feng G, Chen G, Wu J, Guo Y, et al. DNMIVD: DNA methylation interactive visualization database. *Nucleic Acids Res* (2020) 48:D856–D62. doi: 10.1093/nar/gkz830

23. Cerami E, Gao J, Dogrusoz U, Gross BE, Sumer SO, Aksoy BA, et al. The cBio cancer genomics portal: An open platform for exploring multidimensional cancer genomics data. *Cancer Discovery* (2012) 2:401–4. doi: 10.1158/2159-8290.CD-12-0095

24. Ru B, Wong CN, Tong Y, Zhong JY, Zhong SSW, Wu WC, et al. TISIDB: An integrated repository portal for tumor-immune system interactions. *Bioinformatics* (2019) 35:4200–2. doi: 10.1093/bioinformatics/btz210

25. Zhang L, Yang M, Gan L, He T, Xiao X, Stewart MD, et al. DLX4 upregulates TWIST and enhances tumor migration, invasion and metastasis. *Int J Biol Sci* (2012) 8:1178–87. doi: 10.7150/ijbs.4458

26. Zhang L, Wei C, Li D, He J, Liu S, Deng H, et al. COVID-19 receptor and malignant cancers: Association of CTSL expression with susceptibility to SARS-CoV-2. *Int J Biol Sci* (2022) 18:2362–71. doi: 10.7150/ijbs.70172

27. Wang K, Deng H, Song B, He J, Liu S, Fu J, et al. The correlation between immune invasion and SARS-COV-2 entry protein ADAM17 in cancer patients by bioinformatic analysis. *Front Immunol* (2022) 13:923516. doi: 10.3389/fimmu.2022.923516

28. Fu J, Zhou B, Zhang L, Balaji KS, Wei C, Liu X, et al. Expressions and significances of the angiotensin-converting enzyme 2 gene, the receptor of SARS-CoV-2 for COVID-19. *Mol Biol Rep* (2020) 47:4383–92. doi: 10.1007/s11033-020-05478-4

29. Yu J, Liu TT, Liang LL, Liu J, Cai HQ, Zeng J, et al. Identification and validation of a novel glycolysis-related gene signature for predicting the prognosis in ovarian cancer. *Cancer Cell Int* (2021) 21:353. doi: 10.1186/s12935-021-02045-0

30. Blume C, Jackson CL, Spalluto CM, Legebeke J, Nazlamova L, Conforti F, et al. A novel ACE2 isoform is expressed in human respiratory epithelia and is upregulated in response to interferons and RNA respiratory virus infection. *Nat Genet* (2021) 53:205–14. doi: 10.1038/s41588-020-00759-x

31. Onabajo OO, Banday AR, Stanifer ML, Yan W, Obajemu A, Santer DM, et al. Interferons and viruses induce a novel truncated ACE2 isoform and not the full-length SARS-CoV-2 receptor. *Nat Genet* (2020) 52:1283–93. doi: 10.1038/s41588-020-00731-9

32. Bul'on VV, Krylova IB, Selina EN, Rodionova OM, Evdokimova NR, Sapronov NS, et al. Antiarrhythmic effect of uridine and uridine-5'-monophosphate in acute myocardial ischemia. *Bull Exp Biol Med* (2014) 157:728–31. doi: 10.1007/s10517-014-2653-3

33. Radhi M, Ashraf S, Lawrence S, Tranholm AA, Wellham PAD, Hafeez A, et al. A systematic review of the biological effects of cordycepin. *Molecules* (2021) 26 (19):5886. doi: 10.3390/molecules26195886

34. Tima S, Tapingkae T, To-Anun C, Noireung P, Intaparn P, Chaiyana W, et al. Antileukaemic cell proliferation and cytotoxic activity of edible golden cordyceps (Cordyceps militaris) extracts. *Evid Based Complement Alternat Med* (2022) 2022:5347718. doi: 10.1155/2022/5347718

35. Wei C, Khan MA, Du J, Cheng J, Tania M, Leung EL, et al. Cordycepin inhibits triple-negative breast cancer cell migration and invasion by regulating EMT-TFs SLUG, TWIST1, SNAIL1, and ZEB1. *Front Oncol* (2022) 12:898583. doi: 10.3389/fonc.2022.898583

36. Chan CT, Chionh YH, Ho CH, Lim KS, Babu IR, Ang E, et al. Identification of N6,N6-dimethyladenosine in transfer RNA from mycobacterium bovis bacille calmette-guerin. *Molecules* (2011) 16:5168–81. doi: 10.3390/molecules16065168

frontiers | Frontiers in Immunology

TYPE Original Research
PUBLISHED 13 September 2022
DOI 10.3389/fimmu.2022.1007089

OPEN ACCESS

EDITED BY
Chenhe Su,
Wistar Institute, United States

REVIEWED BY
Zhiqiang Qin,
University of Arkansas for Medical Sciences, United States
Leyi Wang,
University of Illinois at Urbana-Champaign, United States

*CORRESPONDENCE
Jian Zhu
Jian.Zhu@osumc.edu

SPECIALTY SECTION
This article was submitted to Viral Immunology, a section of the journal Frontiers in Immunology

RECEIVED 29 July 2022
ACCEPTED 11 August 2022
PUBLISHED 13 September 2022

CITATION
Li T-W, Kenney AD, Park J-G, Fiches GN, Liu H, Zhou D, Biswas A, Zhao W, Que J, Santoso N, Martinez-Sobrido L, Yount JS and Zhu J (2022) SARS-CoV-2 Nsp14 protein associates with IMPDH2 and activates NF-κB signaling. *Front. Immunol.* 13:1007089. doi: 10.3389/fimmu.2022.1007089

SARS-CoV-2 Nsp14 protein associates with IMPDH2 and activates NF-κB signaling

Tai-Wei Li[1], Adam D. Kenney[2], Jun-Gyu Park[3], Guillaume N. Fiches[1], Helu Liu[4], Dawei Zhou[1], Ayan Biswas[5], Weiqiang Zhao[1], Jianwen Que[4], Netty Santoso[1], Luis Martinez-Sobrido[3], Jacob S. Yount[2] and Jian Zhu[1,2]*

[1]Department of Pathology, The Ohio State University Wexner Medical Center, Columbus, OH, United States, [2]Department of Microbial Infection and Immunity, The Ohio State University Wexner Medical Center, Columbus, OH, United States, [3]Texas Biomedical Research Institute, San Antonio, TX, United States, [4]Department of Medicine, Columbia University Medical Center, New York, NY, United States, [5]Department of Genetics, The University of Alabama at Birmingham, Birmingham, AL, United States

Severe acute respiratory syndrome coronavirus 2 (SARS-CoV-2) infection leads to NF-κB activation and induction of pro-inflammatory cytokines, though the underlying mechanism for this activation is not fully understood. Our results reveal that the SARS-CoV-2 Nsp14 protein contributes to the viral activation of NF-κB signaling. Nsp14 caused the nuclear translocation of NF-κB p65. Nsp14 induced the upregulation of IL-6 and IL-8, which also occurred in SARS-CoV-2 infected cells. IL-8 upregulation was further confirmed in lung tissue samples from COVID-19 patients. A previous proteomic screen identified the putative interaction of Nsp14 with host Inosine-5'-monophosphate dehydrogenase 2 (IMPDH2), which is known to regulate NF-κB signaling. We confirmed the Nsp14-IMPDH2 protein interaction and identified that IMPDH2 knockdown or chemical inhibition using ribavirin (RIB) and mycophenolic acid (MPA) abolishes Nsp14- mediated NF-κB activation and cytokine induction. Furthermore, IMPDH2 inhibitors (RIB, MPA) or NF-κB inhibitors (bortezomib, BAY 11-7082) restricted SARS-CoV-2 infection, indicating that IMPDH2-mediated activation of NF-κB signaling is beneficial to viral replication. Overall, our results identify a novel role of SARS-CoV-2 Nsp14 in inducing NF-κB activation through IMPDH2 to promote viral infection.

KEYWORDS

SARS-CoV-2, NF-κB, Nsp14, IL-8, IMPDH2, ribavirin, mycophenolic acid

Introduction

SARS-CoV-2 is a beta-coronavirus that causes the current, severe COVID-19 pandemic globally. The viral genome of SARS-CoV-2 is a ~30 kb polycistronic, positive-strand RNA that encodes multiple structural and nonstructural proteins (1, 2). SARS-CoV-2 nonstructural proteins (Nsp 1-16) play diversified roles in supporting viral RNA/protein synthesis and virion assembly, including manipulating host gene expression and host antiviral responses (3, 4). It has been recently reported that SARS-CoV-2 infection suppresses type I interferon (IFN) signaling (5, 6), while it induces the activation of NF-κB signaling that plays a central role in the production of pro-inflammatory cytokines, including interleukin (IL)- 6 and IL-8 (5, 7, 8). In certain cases, massive inflammatory responses occur due to hyper-activation of the immune system, resulting in a widespread and uncontrolled cytokine storm, leading to acute respiratory distress syndrome (ARDS), life-threatening lung damage, and increased mortality of COVID-19 patients. However, the underlying mechanism of how SARS-CoV-2 infection contributes to NF-κB-mediated inflammatory responses that are expected to determine the outcome of SARS-CoV-2 viral replication and pathogenesis is still largely uncharacterized.

Here we focused on characterizing the regulatory functions of SARS-CoV-2 Nsp14 that are required for efficient viral replication. Nsp14 is a conserved, multifunctional viral factor participating in synthesizing and modifying coronaviral sub-genomic (sg) RNAs (9). Nsp14 possesses a 3' to 5' exonuclease activity that excises mismatched base pairs during viral RNA replication (10–12), providing a proofreading function that increases the fidelity of viral RNA synthesis (13, 14). Nsp14 also possesses RNA methyltransferase activity required for guanine-N7 methylation (15). Nsp14-mediated guanine-N7 methylation cooperates with 2'-O RNA methylation mainly catalyzed by Nsp10/16, leading to 5'-capping of newly synthesized sgRNAs (16, 17), which not only prevents degradation by host RNA 5' exonucleases and recognition by host foreign RNA sensors, such as RIG-I (18) but also increases translation efficiently of host ribosomes to synthesize viral proteins (19, 20). Nsp14 has also been reported to reduce the accumulation of viral double-stranded (ds) RNAs and thus dampen the pathogen-associated molecular pattern (PAMP) mediated antiviral response (21). In addition, Nsp14 is known to facilitate recombination between different viral RNAs to generate new strains (22). Compared to these well-studied viral functions of Nsp14, its regulation of host cellular events is much less investigated. An earlier large-scale proteomic analysis reporting candidate interacting partners for all of the SARS-CoV-2 open reading frames (ORFs) indicated that the host inosine-5'-monophosphate dehydrogenase 2 (IMPDH2) protein is one binding partner of SARS-CoV-2 Nsp14 protein (23). Interestingly, IMPDH2 has been identified to play a role in regulating NF-κB signaling (24). Our new results showed that SARS-CoV-2 Nsp14 activates NF-κB signaling and induces IL-8 upregulation, which indeed requires the interaction of Nsp14 with IMPDH2.

Results

SARS-CoV-2 Nsp14 causes activation of NF-κB

We initially investigated the effect of SARS-CoV-2 Nsp14 along with Nsp10 and Nsp16 on certain immune signaling pathways. The pcDNA-V5-FLAG-Nsp14/10/16 vectors were individually transfected in HEK293T, and the expression of the individual proteins was confirmed (Figure S1A). We then utilized these expression vectors for interferon-sensitive response element (ISRE) and NF-κB luciferase reporter assays (Figures S1B, C). Nsp14 mildly increased ISRE activity at the basal level but caused its decrease in IFN-α-treated HEK293T cells, while Nsp10 and Nsp16 mildly decreased ISRE activity at both conditions, which is consistent with earlier findings (3, 4). On the contrary, only Nsp14 significantly increased NF-κB activity in both untreated and TNF-α-treated HEK293T cells. TNF-α did not affect the expression of transfected Nsp14 in HEK293T cells (Figure 1A) but induced a drastic increase of NF-κB activity that was further enhanced by Nsp14 (Figure 1B). Thus, we further investigated the Nsp14-induced activation of NF-κB signaling. The impact of Nsp14 on nuclear localization of NF-κB p65 was determined in HEK293T cells transfected with Nsp14. Indeed, Nsp14 expression led to the significant increase of nuclear but not total p65 protein (Figures 1C, D and Figure S2). These results confirmed that SARS-CoV-2 Nsp14 activates NF-κB signaling.

SARS-CoV-2 Nsp14 induces upregulation of IL-8

NF-κB plays a critical role in regulating pro-inflammatory gene expression. Since we showed that Nsp14 causes NF-κB activation, we further determined whether Nsp14 induces the expression of IL-6 and IL-8. IL-6 and IL-8 are defined gene targets of NF-κB (25–27). In HEK293T cells transfected with pcDNA-V5-FLAG-Nsp14, IL-6 and IL-8 were consistently and significantly upregulated with or without TNF-α (Figure 2A). Results were similar in Nsp14-transfected A549 cells (Figure 2B). IL-8 protein was detected in TNF-α treated A549 cells, which further increased due to Nsp14 expression along with the increase of p65 phosphorylation at ser536 (Figure 2C). The p65 phosphorylation at ser536 increases p65 nuclear accumulation and NF-κB's transactivation during

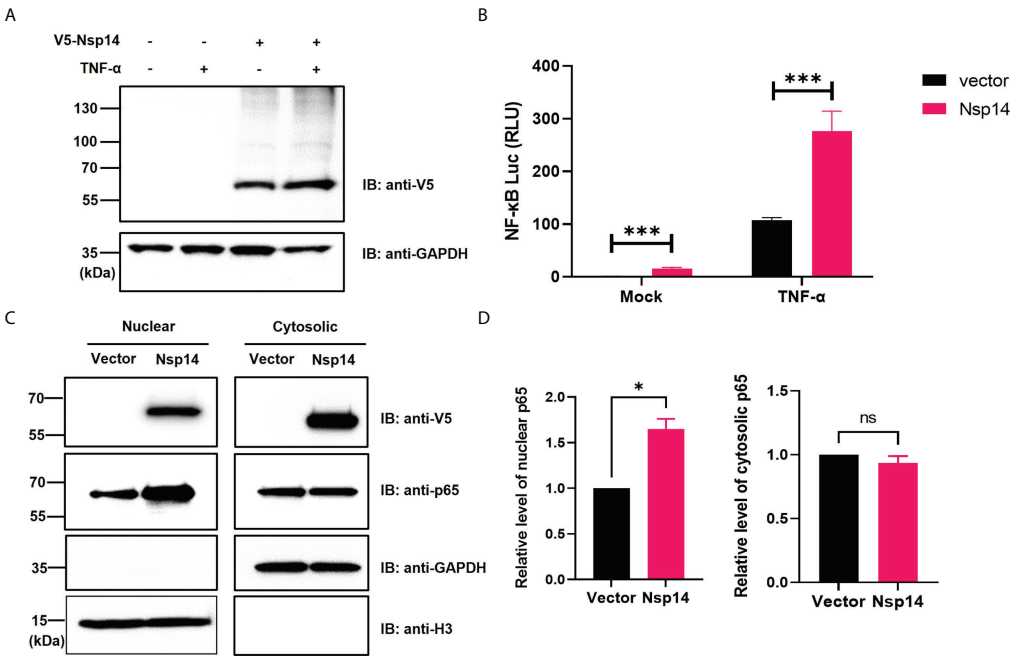

FIGURE 1
SARS-CoV-2 Nsp14 increases NF-κB activity. **(A–C)** HEK293T cells were transiently transfected with V5-FLAG-Nsp14 or empty vector for 24h and then treated with or without TNF-α for 24h. V5-FLAG-Nsp14 was analyzed by protein immunoblotting **(A)**. HEK293T cells transfected with V5-FLAG-Nsp14 or empty vector along with NF-κB-driven firefly luciferase and TK-driven renilla luciferase reporter vectors were un-treated or treated with TNF-α **(B)**. Luciferase activity (firefly/renilla) in these cells was measured and normalized to the untreated group with the empty vector. HEK293T cells transfected with V5-FLAG-Nsp14 or empty vector were subjected to the nuclear/cytosolic fractionation. V5-FLAG-Nsp14 and NF-κB p65 in the nucleus or cytosol were analyzed by protein immunoblotting **(C)**. Histone H3 was used as the nuclear marker. The intensity of the p65 protein band was quantified and normalized to the empty vector **(D)**. Results were calculated from 3 independent experiments and presented as mean +/- standard error of the mean (SEM). (ns: not significant ; * p<0.05; *** p<0.001; by unpaired Student's t-test).

inflammation or stress response (28–30). Our results suggested that Nsp14 is capable of increasing NF-κB p65 transactivation to induce IL-8 expression.

We next confirmed whether infection of cells with SARS-CoV-2 also induces upregulation of IL-6 and IL-8. HEK293T-ACE2 cells were infected with the SARS-CoV-2 viral strain USA-WA1/2020 (31). The expression of viral genes, Nsp14 and nucleocapsid (N), was readily detected (Figure 3A). The SARS-CoV-2 infection also led to the upregulation of IL-6 and IL-8 (Figure 3B). We employed immunofluorescence staining assays to determine whether IL-8 upregulation occurs in lung tissue samples dissected from deceased COVID-19 patients. The results showed that IL-8 expression is consistently higher in COVID-19 patients (Figure 3C) compared to un-infected cases (Figure 3D). Indeed, earlier studies of deceased samples of COVID-19 patients identified that IL-8 induction occurs in SARS-CoV-2 infection (5, 32). Our results suggested that Nsp14 contributes to IL-8 induction through NF-κB activation. We primarily focused on IL-8 as the target gene of NF-κB for further investigation since it is known that IL-8 has a role in favoring viral infection by inhibiting the antiviral action of IFNα (33).

IMPDH2 binds to Nsp14 and contributes to Nsp14-mediated induction of IL-8

We first confirmed the putative protein interaction of Nsp14 with IMPDH2 (23) by protein co-immunoprecipitation (co-IP) assays in HEK293T cells co-transfected with the pLEX-V5-IMPDH2 and pEZY-FLAG-Nsp14 vectors (Figure 4A). We also used the protein co-IP assays to confirm the protein interaction of FLAG-V5-Nsp14 with endogenous IMPDH2 (Figure 4B). As the next step, we determined whether endogenous IMPDH2 is required for IL-8 induction by Nsp14. IMPDH2-targeting or non-targeting (NT) siRNAs were transfected in HEK293T cells, and an efficient knockdown of endogenous IMPDH2 was confirmed (Figure 4C). Remarkably, IMPDH2 knockdown abolished the IL-8 induction by Nsp14 in HEK293T cells without or with TNF-α (Figure 4D). However, overexpression of IMPDH2 had no significant effect on NF-κB activation by Nsp14 in HEK293T cells with or without TNF-α (Figure S3). In order to further pinpoint which domain(s) of Nsp14 binding to IMPDH2, we cloned the truncated Nsp14 protein to encode the exonuclease domain (Exo, aa1-287, MW ~30 kDa) or RNA methyltransferase domain (MT, aa288-527,

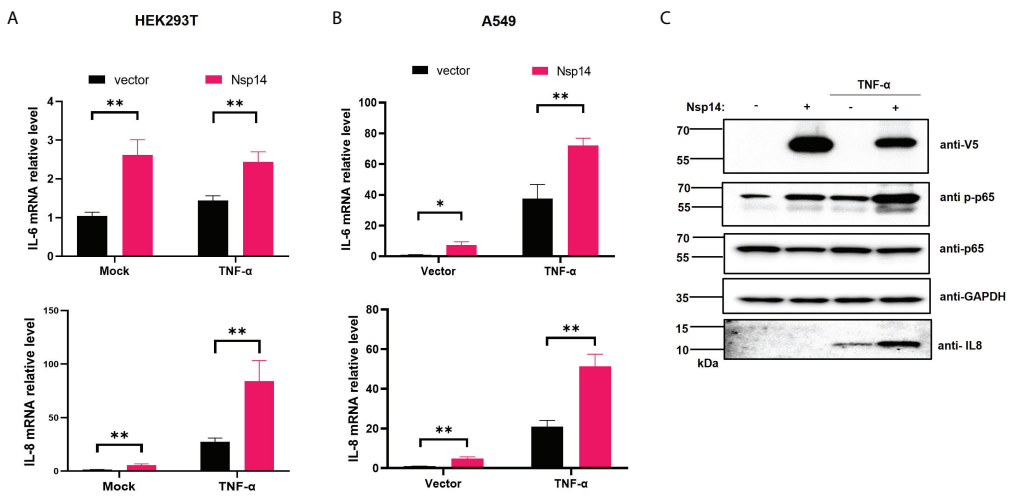

FIGURE 2
SARS-CoV-2 Nsp14 increases IL-6/8 expression. **(A)** HEK293T cells were transfected with V5-FLAG-Nsp14 or empty vector were un-treated or treated with TNF-α for 24h. The mRNA level of IL-6 and IL-8 in these cells was measured and normalized to the untreated, empty vector-transfected group. **(B)** A549 cells were treated similarly as in **(A)** and analyzed for IL-6 and IL-8 mRNA expression. **(C)** Protein level of Nsp14, phosphate, and total NF-κB p65, as well as IL-8, in A549 cells transfected with or without FLAG-V5-Nsp14 +/- TNF-α was measured by immunoblotting. Results were calculated from at least 3 independent experiments and presented as mean +/- standard error of the mean (SEM). (* p<0.05; ** p<0.01; by unpaired Student's t-test).

MW ~27 kDa) (9, 13, 34) with N-terminal FLAG and V5 tags (Figure 5A). We transfected full-length (FL), Exo, or MT Nsp14 cDNA in HEK293T cells, and NSP14 proteins were readily expressed (Figure 5B). In the above HEK293T cells, we determined the interaction of FL or truncated Nsp14 protein with endogenous IMPDH2 protein through co-IP assays. Results showed that only the FL Nsp14 protein binds to endogenous IMPDH2 (Figure 5B). Consistently, only the FL Nsp14 protein increased NF-κB-driven luciferase activities (Figure 5C). Thus, both functional domains of NSP14 involve in its interaction with IMPDH2 and the induction of NF-κB activation corporately.

IMPDH2 inhibition blocks Nsp14-mediated NF-κB activation and IL-8 induction

Since IMPDH2 is required for IL-8 induction by Nsp14, we expected that its inhibition would reduce Nsp14-mediated NF-κB activation and IL-8 induction. We tested two reported IMPDH2 inhibitors, ribavirin (RIB) and mycophenolic acid (MPA) (23, 35). RIB is a synthetic nucleoside that occupies the IMPDH2 catalytic site to inhibit IMP conversion to xanthosine 5'-phosphate (XMP) during the guanine nucleotide (GTP) biosynthesis (35–37). MPA shares similar features with the IMPDH2 cofactor, nicotinamide adenine dinucleotide (NAD^+). MPA stacks and traps the XMP intermediate at the catalytic site to inhibit IMPDH2 enzyme activity (35, 38). We confirmed that NF-κB activation by Nsp14 significantly decreases in HEK293T cells treated with RIB (Figure 6A) or MPA (Figure 6B) at multiple doses in the absence or presence of TNF-α using the NF-κB luciferase reporter assays. Treatment of HEK293T cells with RIB (Figure S4A) or MPA (Figure S4B) at the similar doses caused no obvious cytotoxicity through cell viability assays. Likewise, treatment of HEK293T cells with RIB (Figures 6C, D) or MPA (Figures 6E-F) also caused the reduction of both IL-6 and IL-8 mRNA induction by Nsp14. Furthermore, we treated Nsp14-transfected A549 cells with RIB or MPA, which decreased the TNF-a induced p65 phosphorylation and IL-8 protein expression (Figure S4C). These results supported the model that IMPDH2 is required for Nsp14's function to activate NF-κB and induce IL-8. However, these IMPDH2 inhibitors had no effect on disrupting the Nsp14-IMPDH2 protein interaction measured by co-IP assays (Figure S4D).

IMPDH2 or NF-κB inhibition restricts viral infection of SARS-CoV-2 in cell culture

We next tested whether IMPDH2 inhibitors (RIB, MPA) impact SARS-CoV-2 infection *in vitro*, considering that virus-mediated NF-κB activation modulates viral infection (39–42). Indeed, we showed that the infection rate of SARS-CoV-2 decreases in both A549-ACE2 and HEK293T-ACE2 cells treated with RIB or MPA through quantification of cells expressing N protein by immunofluorescence staining assays

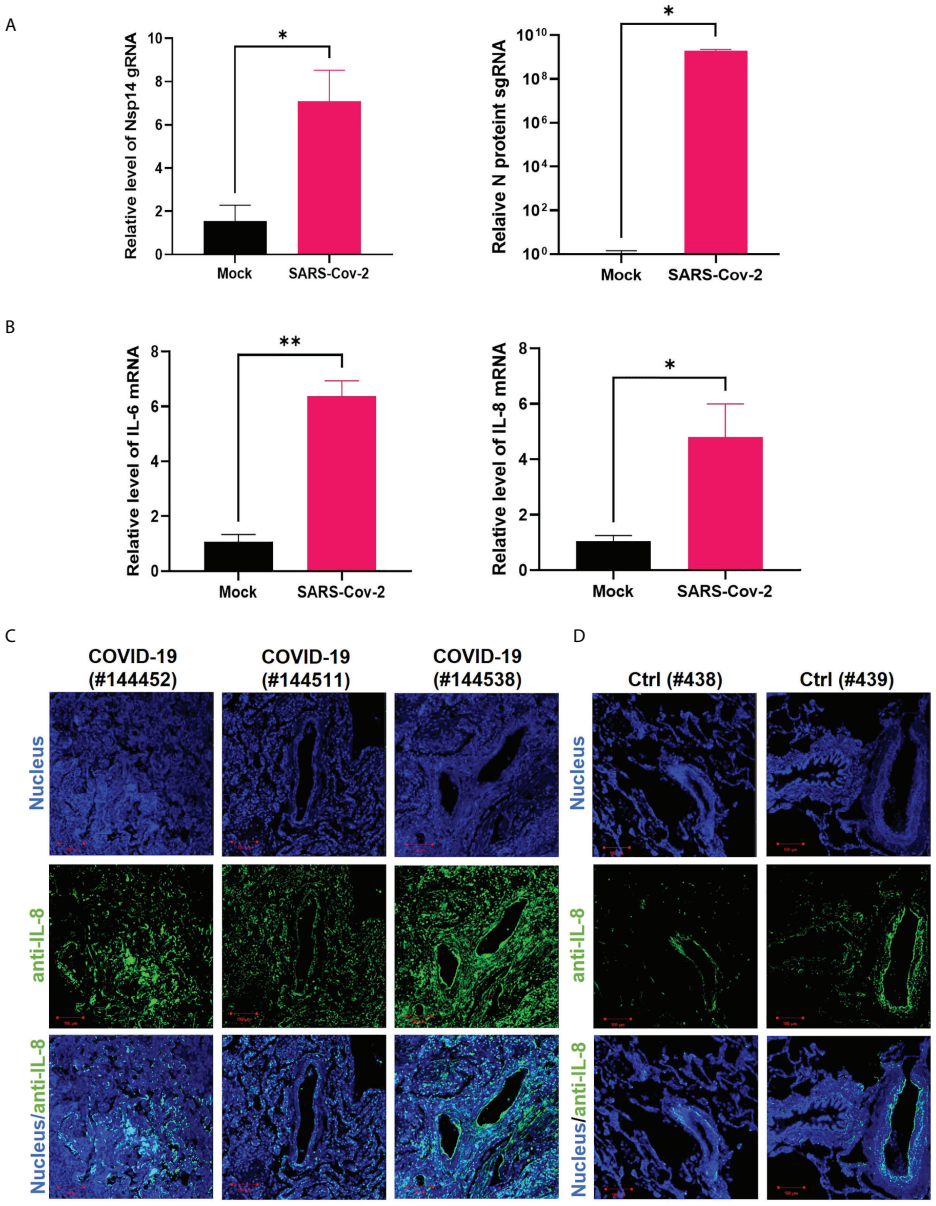

FIGURE 3
IL-8 is induced by Nsp14 and in SARS-CoV-2 infected lung tissues. **(A, B)** HEK293T-ACE2 cells were infected with wild-type SARS-Cov-2 viruses. Cells were harvested at 24 h. Total RNAs were extracted, and the expression of viral genes (Nsp14, N-protein, **A**) or cytokines (IL-6, IL-8, **B**) was analyzed by RT-qPCR and normalized to mock infection. Results were calculated from 3 technical repeats and presented as mean +/- standard error of the mean (SEM). (* $p<0.05$; ** $p<0.01$; by unpaired Student's t-test). **(C, D)** Dissected lung tissues from COVID19 patients (**C**, donors #144452, #144511, #144538) or non-infected donors (**D**, donors #438, #439) were analyzed for IL-8 expression by immunofluorescence (green). Nuclei were stained with Hoechst (blue). Scale bar: 100 μm.

(Figures 7A, B, S5A, B) or sgRNA level by RT-qPCR (Figures 7C, S5C). Consistently, we also identified that treatment of RIB or MPA leads to a significant reduction of IL-6 and IL-8 expression (Figure 7D). The results of IMPDH2 inhibitors also aligned with those of NF-κB inhibitors. Treatment of HEK293T-ACE2 cells with the NF-κB inhibitors, including BAY 11-7082 (43) and bortezomib (44), significantly reduced the sgRNA level of SARS-CoV-2 N protein measured by RT-qPCR (Figure 7E). In order to confirm the antiviral activity of NF-κB inhibitors, we further performed the plaque reduction microneutralization (PRMNT) and cell-viability assays with the serial dilution of these drugs in Vero E6 and A549-hACE2 cells (Figures 7F, G). Bortezomib potently blocked SARS-CoV-2 infection in both cells without obvious cytotoxicity, comparable to remdesivir. However, the

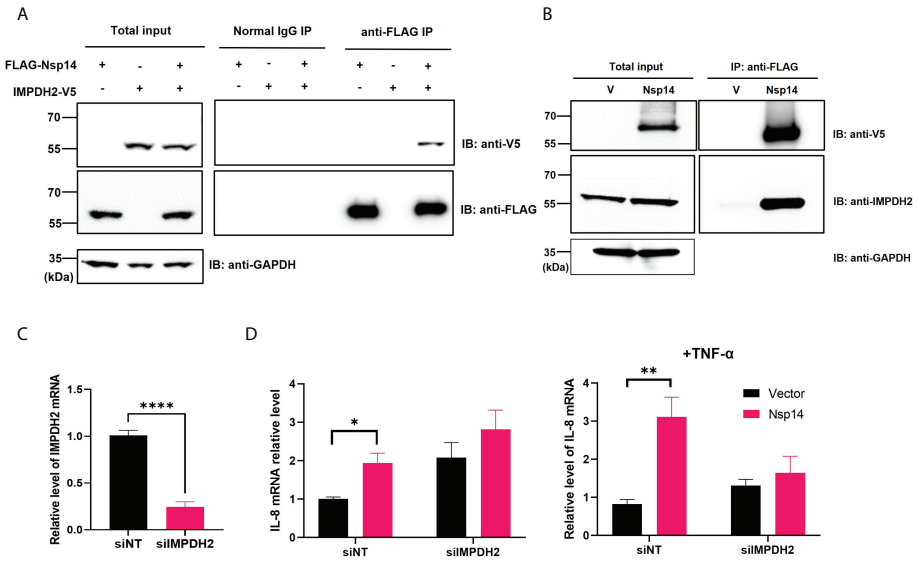

FIGURE 4
IMPDH2 associates with Nsp14 and is required for IL-8 upregulation by Nsp14. **(A)** HEK293T cells were transiently transfected with the vector expressing FLAG-Nsp14 or V5-IMPDH2, alone or together. Cell lysates were prepared and subjected to protein co-immunoprecipitation (co-IP) assays using anti-FLAG or control IgG antibody. Precipitated protein samples were analyzed by protein immunoblotting using anti-V5 and anti-FLAG antibodies. **(B)** HEK293T cells were transiently transfected with the empty vector (V) or FLAG-V5-Nsp14 vector. Cell lysates were prepared and subjected to protein co-IP assays using an anti-FLAG antibody. Precipitated protein samples were analyzed by protein immunoblotting using anti-V5 and anti-IMPDH2 antibodies. **(C)** HEK293T cells were transiently transfected with IMPDH2 or non-targeting (NT) siRNAs. The mRNA level of IMPDH2 was measured and normalized to siNT. **(D)** HEK293T cells transfected with IMPDH2 or NT siRNAs were further transfected with V5-FLAG-Nsp14 or empty vector. These cells were untreated or treated with TNF-α. Total RNAs were extracted. IL-8 mRNA was analyzed and normalized to the siNT and empty vector-transfected group. Results were calculated from 3 independent experiments and presented as mean +/- standard error of the mean (SEM). (*p<0.05; ** p<0.01; **** p<0.0001; by unpaired Student's t-test).

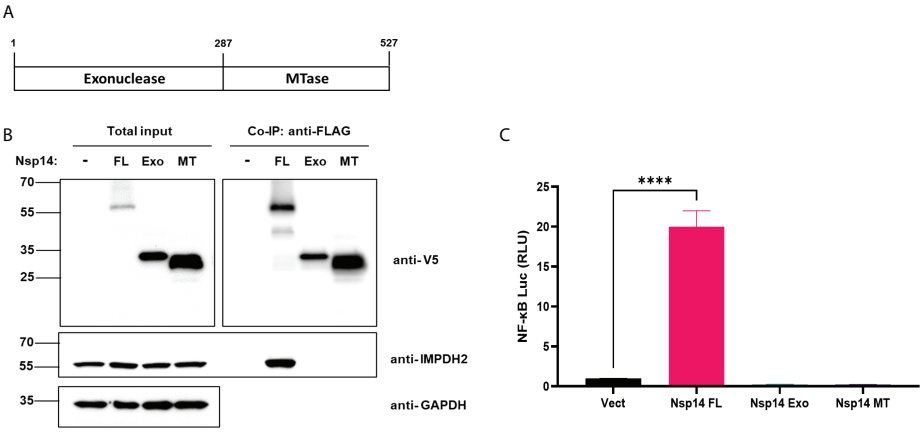

FIGURE 5
Full-length Nsp14 protein but not truncated domains interact with IMPDH2 and induce NF-κB activation. **(A)** We cloned the truncated Nsp14 protein to encode the exonuclease domain (Exo, aa1-287, MW ~30 kDa) or RNA methyltransferase domain (MT, aa288-527, MW ~27 kDa) with N-terminal FLAG and V5 tags. **(B)** pcDNA vector expressing full-length (FL), Exo, or MT Nsp14 was transfected in HEK293T cells. At 48h post of transfection, cells were harvested. Lysates were prepared and subjected to protein co-IP assays using an anti-FLAG antibody. Precipitated protein samples were analyzed by immunoblotting. **(C)** HEK293T cells were transfected with pcDNA vector expressing full-length (FL), Exo, or MT Nsp14, or empty vector, along with NF-κB-driven firefly luciferase and TK-driven renilla luciferase reporter vectors. At 48h post of transfection, luciferase activity (firefly/renilla) was measured and normalized to the empty vector. Results were calculated from 3 technical repeats and presented as mean +/- standard error of the mean (SEM). (**** p<0.001; by one-way ANOVA and Tukey's multiple comparison test).

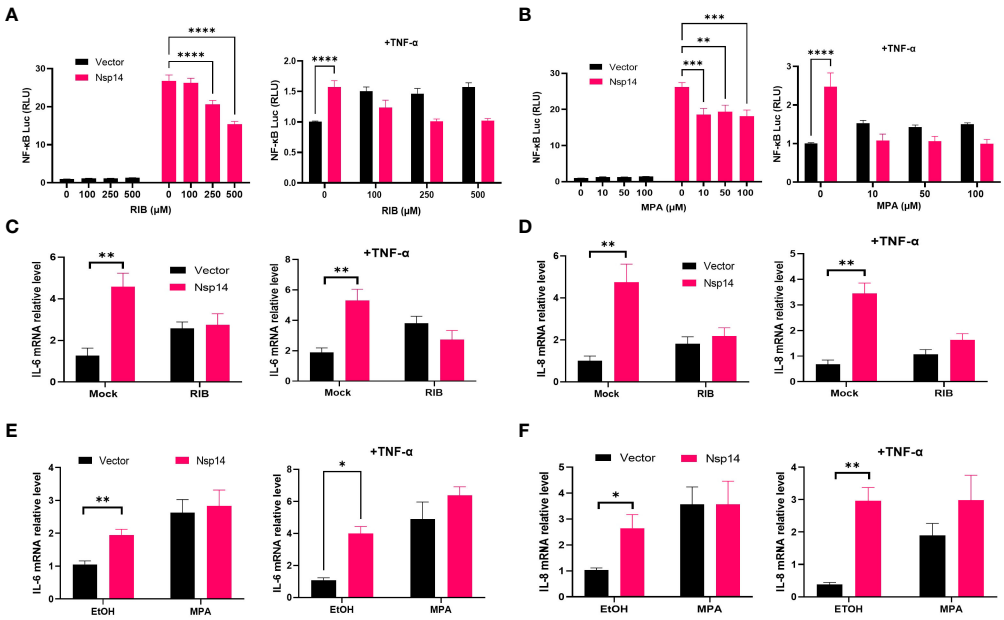

FIGURE 6
IMPDH2 inhibition reduces Nsp14-mediated NF-κB activation and IL8 induction. **(A)** HEK293T cells transfected with V5-FLAG-Nsp14 or empty vector along with NF-κB-driven firefly luciferase and TK-driven renilla luciferase reporter vectors were treated with ribavirin (RIB) at 24h post of transfection for 24h without or with TNFα stimulation. Luciferase activity (firefly/renilla) in these cells was measured and normalized to that of un-treated, empty vector-transfected cells. **(B)** Mycophenolic acid (MPA) was tested similarly as in **(A)**. Results were calculated from at least 2 independent experiments and presented as mean +/- standard error of the mean (SEM). (** p< 0.01; *** p< 0.001; **** p< 0.0001 by two-way ANOVA and Tukey's multiple comparison test). **(C, D)** HEK293T cells transfected with V5-FLAG-Nsp14 or empty vector were treated with 500 μM RIB at the basal or TNF-α-stimulated condition. Total RNAs were extracted. IL-6 **(C)** and IL-8 **(D)** mRNA was analyzed and normalized to the mock treatment of the empty vector-transfected group. **(E, F)** 100 μM MPA was tested similarly as in **(C, D)**, and results were normalized to the solvent control (0.1% ethanol, EtOH) of the empty vector-transfected group. Results were calculated from 3 independent experiments and presented as mean +/- standard error of the mean (SEM). (* p<0.05; ** p<0.01; by unpaired Student's t-test).

anti-SARS-CoV-2 activity of BAY 11-7082 correlated with the increased cytotoxicity in both cells (Figure S5D). These NF-κB inhibitors also had no effect on disrupting the Nsp14-IMPDH2 protein interaction (Figure S4E).

Discussion

Besides the well-known viral functions of SARS-CoV-2 Nsp14 to control modification and replication of viral RNA genomes, earlier studies illustrated that Nsp14 suppresses Type 1 IFN signaling and nuclear translocation of IRF3 to facilitate viral invasion of the host's antiviral immune response (3, 4). Our results showed that Nsp14, which is expressed at the early stage of primary infection (7), also affects other cell signaling pathways, such as NF-κB signaling (Figure 1), likely to support viral replication. Activation of NF-κB may further trigger the production of downstream pro-inflammatory cytokines to initiate the cytokine storm and contribute to ARDS. In this study, we identified that Nsp14 increases nuclear translocation of p65 and induces the expression of NF-κB's downstream cytokines, such as IL-6 and IL-8, which have also been detected in lung tissues of COVID-19 patients (5, 32) and animal models of SARS-CoV-2 infection (7). These cytokines are reported to play a critical role in regulating the recruitment and infiltration of immune cells (macrophages, neutrophils) during viral infection (43, 44). Infiltrating immune cells may further escalate inflammatory responses leading to lung damage. Indeed, we showed that IL-8 expression is much higher in lung tissue samples of COVID-19 patients than in uninfected controls (Figures 3C, D). We identified that only the FL Nsp14 protein binds to endogenous IMPDH2 protein (Figure 5B) and induces NF-κB activation (Figure 5C). These results align with other findings reporting that Nsp14 needs both its exonuclease and methyltransferase domains to shut down the host's protein translation (45). However, due to current technical limitations one remaining question is whether Nsp14 protein expressed from SARS-CoV-2 viral genome truly contributes to NF-κB activation and IL-6/8 induction, which needs future confirmation. A recent study showed that Nsp14 interacts with SIRT1/SIRT5 to decrease NRF2/HMOX1 signaling while increase oxidant stress and inflammatory responses (46). Nsp14 H268A mutant and other exoribonuclease-deficient mutants still inhibit NRF2/ARE-

driven transcription, suggesting that Nsp14 may affect cellular signaling *via* protein-protein interaction independent of its exoribonuclease activity. However, it is intriguing to test whether Nsp14 exoribonuclease-deficient mutants (such as H268A) have an impact on Nsp14's function to induce NF-κB signaling, since our results indeed showed that exoribonuclease domain of Nsp14 is required for NF-κB activation (Figure 5C).

Another key finding is that IMPDH2 is a host mediator of Nsp14 involved in NF-κB activation, verified by both genetic knockdown (Figure 4) and chemical inhibition (Figure 6). We confirmed the protein interaction of Nsp14 with IMPDH2, which was initially reported in earlier proteomic studies (23, 32). Previous results also suggested that IMPDH2 benefits the budding of Junín mammarenavirus (JUNV), propagation of lymphocytic choriomeningitis virus (LCMV) (47), and replication of human norovirus (HuNV) (48). IMPDH2 inhibitors have been used for treating hepatitis C virus (HCV) (35, 49). Our results suggested that IMPDH2 likely supports the SARS-CoV-2 infection and Nsp14-mediated NF-κB activation as well. IMPDH2 is a protein target of certain immunosuppressive drugs used for organ transplantation and allograft rejection (38, 50, 51), and it has been reported to regulate NF-κB signaling (24, 52). In an earlier study, RIB (the IMPDH2 inhibitor) decreased the IL-6/IL-8 secretion in the animal models of rotavirus infection (53). Another study also showed that MPA (the IMPDH2 inhibitor) decreased the NF-κB activation and induction of IL-8 (54) and IL-6 (55, 56). Nsp14 may hijack IMPDH2 for NF-κB activation (24), contributing to abnormal inflammatory responses. IL-6 from infected cells may stimulate macrophages, pathological fibroblasts, Th2 and Th17 cells, and initiate inflammatory or immunopathological responses that dysregulate extracellular matrix, impair tissue repairing, and facilitate tissue injury (57–61). IL-8 may attract neutrophils, stimulate granulocytes' response to tissue damage, and generate ARDS-related micro thrombosis (62, 63). IL-8 induction could initiate a positive feedback *via* autocrine of attracted neutrophils (63), which may also support viral replication of SARS-CoV-2 (64) and inhibit SARS-CoV-2 specific T-cell responses (65). In terms of possible molecular mechanisms, since IMPDH2 participates in regulating the host nucleotide metabolism (66, 67), it may further modulate cellular stress response and downstream NF-κB activation (67–69). This metabolism disruption caused by Nsp14 might increase the phosphorylation of IKKβ and IκBα to further promote nuclear translocation and phosphorylation of p65 (24). Future studies will be needed to understand further how Nsp14 and IMPDH2 cooperate to activate NF-κB. In addition, we also noticed that Nsp14 partially localizes in the nuclei of cells (Figures 1C, D), similar to findings from other groups (70, 71). Thus, Nsp14 may encode other cellular functions. Nsp14 may associate with and modify the host cellular RNAs *via* its exonuclease and methyltransferase activities. Nsp14 may also affect the transcriptional activity of nuclear p65 and the expression of its gene targets. Our study has translational significance since we showed that both IMPDH2 inhibitors, RIB and MPA, effectively reduce viral replication of SARS-CoV-2 and expression of NF-κB's downstream cytokines (IL-8 and IL-6) induced by SARS-CoV-2 (Figures 7A–D). The antiviral effect of IMPDH2 inhibitors is likely through inhibition of NF-κB, supported by our results showing that NF-κB inhibitors, particularly bortezomib, indeed restrict viral infection of SARS-CoV-2 in cell culture as well (Figures 7E–G). It has been reported that IL-8 increases the replication of human immunodeficiency virus-1 (HIV-1), HCV, and cytomegalovirus (CMV) (72–75). SARS-CoV-2 Nsp14 induces the NF-κB signaling and downstream cytokines, which may support the host cell proliferation and survival, or prevent cell apoptosis, thus benefiting viral replication (42, 76). As the supportive evidence, a recent study showed that knockdown of NF-κB p50 or IL-8 indeed impairs SARS-CoV-2 viral RNA expression and its replication in A549-ACE2 cells (64). RIB and MPA are both FDA-approved drugs for treating HCV infection and transplant organ rejection, respectively. Our findings are supported by recent results showcasing the therapeutic potential of RIB and MPA for treating COVID-19 and SARS-CoV-2 infection. The combination of RIB with IFN β-1b and Lopinavir–Ritonavir therapy is currently in clinical trials for treating SARS-CoV-2 infection (77), which has been shown to significantly alleviate the COVID-19 symptoms and suppress IL-6 levels in serum. In another preclinical study, MPA was reported to inhibit SARS-CoV-2 replication (78) and viral entry (79). In addition, bortezomib is an FDA-approved antineoplastic agent and would be promising to treat SARS-CoV-2, which will be further investigated. Overall, our study delineated a potentially new mode of action (MOA) for these IMPDH2 inhibitors, which may disrupt the Nsp14-IMPDH2 axis that plays a crucial role in regulating activation of NF-κB signaling and induction of its downstream cytokines (Figure 8).

Material and methods

Cell culture

HEK293T cells (Cat. # CRL-3216, ATCC) were cultured in Dulbecco's modified Eagle's medium (DMEM, Cat # D5796, Sigma). A549 cells (Cat. # CCL-185, ATCC) were cultured in F12K medium (Cat. # 21127030, Gibco™). Vero E6 cells (Cat. # CRL-1586, ATCC) were cultured in DMEM. HEK293T cells stably expressing ACE2-GFP were previously described (31). A549-ACE2 cells were obtained through BEI Resources, NIH NIAID (Cat # NR53821). Cell culture medium contained 10% fetal bovine serum (FBS, Cat. # 10437028, Thermo Fisher), penicillin (100 U/ml)/streptomycin (100 μg/ml) (Cat. # MT30002CI, Corning).

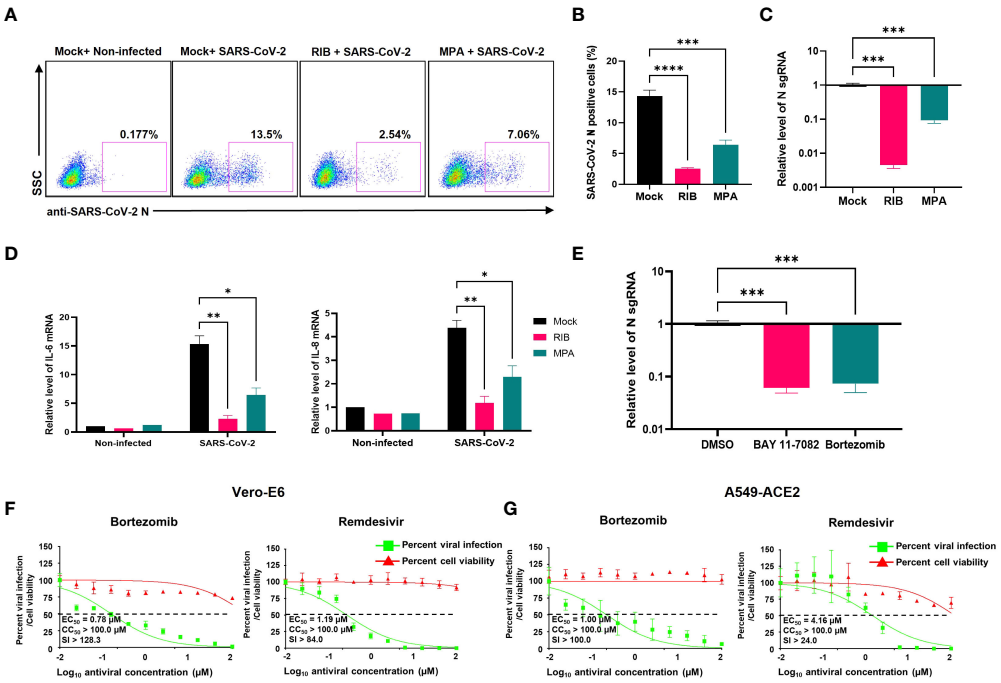

FIGURE 7
IMPDH2 and NF-κB inhibitors restrict the SARS-CoV-2 infection in cell culture. **(A-D)** A549-ACE2 cells were treated with RIB (500 μM), MPA (100 μM), or mock, and simultaneously infected with SARS-Cov-2 viruses for 24 h. The SARS-CoV-2 infection was detected by intracellular staining of SARS-CoV-2 N protein **(A)**. The percentage of SARS-CoV-2 N protein-positive cells was calculated **(B)**. Cells were harvested for RNA extraction, and N protein sgRNA was analyzed and normalized to the mock treatment **(C)**. The mRNA of IL-6 and IL-8 was analyzed and normalized to the non-infected cell with the mock treatment **(D)**. **(E)** HEK293T-ACE2 cells were infected with SARS-CoV-2 in the presence of BAY 11-7082 (10 μM), bortezomib (10 μM), or DMSO solvent control for 24 h. The sgRNA level of N protein was analyzed and normalized to DMSO. Results were calculated from 3 technical repeats and presented as mean +/- standard error of the mean (SEM). (* p<0.05; ** p<0.01; *** p<0.001; **** p<0.001; by one-way **(B, C, E)** or two-way ANOVA **(D)** and Tukey's multiple comparison test). **(F-G)** Vero E6 **(F)** or A549-ACE2 **(G)** cells were briefly infected with SARS-CoV-2, followed by treatment of indicated compounds (bortezomib, remdesivir). At 24 hpi, the above cells were subjected to PRMNT assay at four biological replicates. Results were calculated as mean +/- standard deviation (SD). The dotted line indicates the 50% inhibition. The selectivity index (SI) is presented as CC_{50}/EC_{50}.

Compounds and antibodies

Recombinant human TNF-α (Cat. # 554618) was purchased from BD. Biosciences. Ribavirin (RIB, Cat. # R0077) was purchased from Tokyo Chemical Industry (TCI). Mycophenolic acid (MPA, Cat. # M3546), BAY 11-7082 (Cat. #B5556-10MG), and bortezomib (Cat. # 5043140001) were purchased from Sigma-Aldrich. Remdesivir was purchased from AOBIOUS.

Anti-V5 (Cat. # R960-25), HRP-conjugated anti-V5, and goat HRP-conjugated anti-mouse IgG (H+L) secondary antibody (Cat. # 31430) were purchased from Thermo Fisher Scientific. Anti-GAPDH antibody (Cat. # sc-32233) was purchased from Santa Cruz Biotechnology. Anti-NF-κB p65 (Cat. #8242), anti NF-κB p65 ser536 phosphorylation (Cat. #3033), anti-FLAG (Cat. # 2368), anti-H3 (Cat. # 9715S), and goat HRP-conjugated anti-rabbit IgG (Cat. # 7074) antibodies were purchased from Cell Signaling Technology. Anti-IL8 antibody (Cat. # 554717) was purchased from BD. Biosciences. The anti-IMPDH2 antibody (Cat. # 12948-1-AP) was purchased from Proteintech Group. The anti-SARS-CoV-1/2 NP 1C7C7 antibody was purchased from Sigma-Aldrich.

Plasmids

pLEX-IMPDH2-V5 vector was picked from the MISSION TRC3 human LentiORF library from Sigma-Aldrich. The pcDNA-FLAG-V5-Nsp10/14/16 vectors were constructed from pDONR223 SARS-CoV-2 Nsp10 (Cat. # 141264, Addgene), Nsp14 (Cat. # 141267, Addgene), and Nsp16 (Cat. # 141269, Addgene) vectors to the pcDNA3.1-3xFLAG-V5-ccdB (Cat. # 87064, Addgene) destination vector using Gateway™ LR Clonase™ II Enzyme Mix (Cat. # 11791020, Invitrogen). pEZY-FLAG-Nsp14 vector was constructed from pDONR223 SARS-CoV-2 Nsp14 vector to the pEZY-FLAG (Cat # 18700, Addgene) destined vector. pcDNA-FLAG-V5-Nsp14 Exo/MT vectors were constructed. Nsp14 Exo/MT domain was PCR

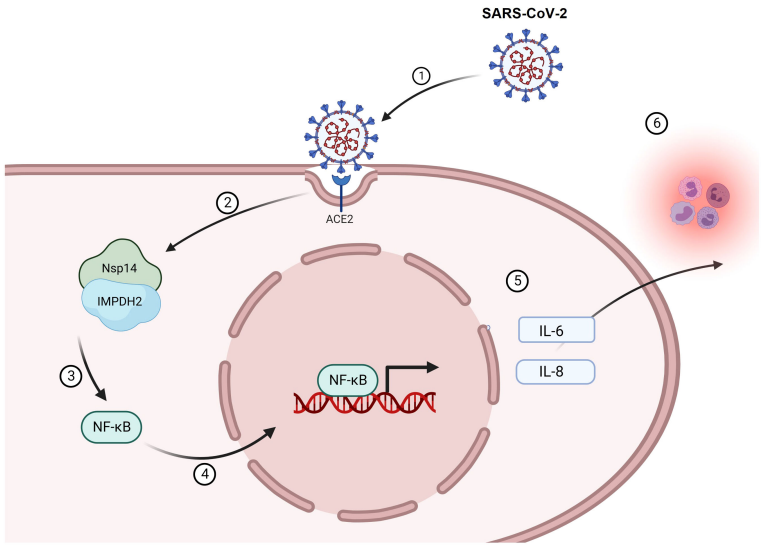

FIGURE 8
A working model of Nsp14-mediated NF-κB activation during SARS-CoV-2 infection. Infection of SARS-CoV-2 (1) leads to the expression of Nsp14 (2) that interacts with IMPDH2 (3). Such interaction promotes the nuclear translocation of NF-κb p65 (4) and its activation, which upregulates the expression of downstream cytokines, including IL-6 and IL-8 (5). Expression of IL-6 and IL-8 may further amplify the inflammatory response from immune cells contributing to viral pathology in COVID (6) and also, in return, benefit SARS-CoV-2 infection.

amplified with the Phusion Flash High-Fidelity PCR Master Mix (Cat. #F548S, Thermo Scientific) using the following primers. Exo forward: 5'-GGGGACAAGTTTGTACAAAAAAGCAGGCTGCATGGCTGAGAACGTGACCG-3'; Exo reverse: 5'-GGGGACCACTTTGTACAAGAAAGCTGGGTATTACACGAAGCACTCGTGCAC-3';MT forward: 5'-GGGGACAAGTTTGTACAAAAAAGCAGGCTGCATGAAGCGTGTGGACTGGACC-3'; MT reverse: 5'-GGGGACCACTTTGTACAAGAAAGCTGGGTATTACTGCAGCCTGGTGAAGGTG-3'.

TG-3'. The PCR products of Nsp14 domains were recombined in the pDONR223 vector *via* B/P cloning using the Gateway™ BP Clonase™ II Enzyme mix (Cat. # 11789020, Invitrogen), and subsequently in pcDNA3.1-3xFLAG-V5-ccdB vector *via* L/R cloning. The pLEX-FLAG-V5 vector was constructed by cloning the FLAG sequence to the pLEX-307 (Cat # 41392, Addgene) vector. The pNF-κB-luciferase vector ($PRDII_4$–luc in the pGL3 vector) was the gift from Dr. Jacob Yount's lab (80). The pIRES-luciferase vector (Cat. # 219092) was acquired from Agilent Technologies. The pRL-TK Renilla Luciferase vector (Cat. # AF025846) was purchased from Promega.

Transient transfection

For Nsp14 overexpression, we performed the transient transfection in HEK293T or A549 cells using TurboFect transfection reagents (Cat. # R0531, Thermo Scientific). Briefly, cells were seeded and incubated with the mixture of plasmids with Turbofect for 24 h. The medium was changed, followed by treatment of TNF-α or compounds. For IMPDH2 knockdown, 20 nM siRNA (IMPDH2 assay ID: s7417, sense: 5'-CCAAGAAAAUCACUCUUtt-3', Ambion by Life technologies; non-targeting control: Silencer™ Negative Control No. 4 siRNA, si NT, Cat. # AM4641, Invitrogen) was reversely transfected in HEK293T cells using Lipofectamine™ RNAiMAX Transfection Reagent (Cat. # 13778030, Invitrogen). Cells were kept in culture for 48h and subjected to qPCR analysis to measure gene expression.

Protein immunoblotting

Protein immunoblotting was performed following our previously published protocols (81, 82). Briefly, cells were harvested, washed by PBS, and pelleted. Cell pellets were lysed in RIPA buffer (Cat. #20-188, Millipore) containing protease inhibitor cocktail (Cat. # A32965, Thermo Scientific) on ice, followed by brief sonication to prepare cell lysate. The BCA assay kit (Cat. #23225, Thermo Scientific) was used to quantify the total protein amount in cell lysate, which was boiled in the SDS loading buffer with 5% β-mercaptoethanol (Cat. #60-24-2, Acros Organics). The denatured protein samples were separated by Novex™ WedgeWell™ 4-20% SDS-PAGE Tris-Glycine gel and

transferred to PVDF membrane (iBlot™ 2 Transfer Stacks, Invitrogen) using iBlot 2 Dry Blotting System (Cat. # IB21001, Thermo Scientific). The membranes were blocked by 5% milk in PBST and probed by the specific primary antibodies at 4°C overnight, followed by the HRP-conjugated secondary antibodies. The membranes were developed using the Clarity Max ECL substrate (Cat. # 1705062, Bio-Rad).

Luciferase reporter assays

HEK293T cells were transfected with ISRE or NF-κB luciferase vector along with pRL-TK renilla luciferase vector with or without the indicated vector expressing Nsp14. At 24 h post of transfection, the medium was changed, and cells were treated with 10 ng/ml TNF-α or un-treated for 24h. Cells were lysed using the Dual-Glo® Luciferase Assay System (Cat. #E2920, Promega). Luciferase/renilla signal intensity was detected using Biotek Cytation5 and analyzed by GEN5 software (Biotek). Cell viability assays were performed for HEK293T cells treated with inhibitors for 24h by using CellTiter-Glo® (Cat. # G7571, Promega), and the results were normalized to the solvent control.

Nuclear and cytoplasmic extraction

HEK293T cells were transfected by pcDNA-FLAG-V5-Nsp14 or control vector pLex307-FLAG-V5 for 24h and changed to fresh completed DMEM medium for further 24 h culture. Cells were collected, washed twice with 1× PBS, and subjected to the nucleus and cytoplasm extraction using NE-PER Nuclear and Cytoplasmic Extraction Reagents (Cat. #78833, Thermo Scientific) following the manufacturer's instructions and our previous studies (81). Total proteins in the whole-cell lysates from the same number of cells were extracted using 1× RIPA buffer. Extractions from nuclear, cytoplasmic proteins and the total cell lysate proteins were denatured and boiled with 4× LDS sample buffer (Cat. #NP0007, Invitrogen) and subjected to immunoblotting analysis with equal protein loading of extracts (~20 μg/lane). Anti-GAPDH and anti-histone H3 immunoblotting were used as internal controls to determine the cytoplasmic and nuclear fractions.

Protein co-immunoprecipitation

Protein co-IP assays were performed following the previously published protocol (81). Briefly, protein A/G magnetic beads (Cat. # 88802, Thermo Scientific) and anti-FLAG M2 magnetic beads (Cat. # M8823, Sigma-Aldrich) were washed with 1× RIPA buffer containing protease inhibitor cocktail. Cellular lysates were precleared with the empty magnetic beads for 1 h at 4°C on a 360° tube rocker. The cell lysate was incubated with anti-FLAG M2 magnetic beads for pull-down of FLAG-Nsp14 protein at 4°C overnight with constant rotation. Protein immunocomplexes were washed by RIPA buffer and boiled in SDS loading buffer containing 5% 2-mercaptoethanol, followed by protein immunoblotting. A normal mouse IgG antibody (Cat. # sc-2025, Santa Cruz) was used as the control in parallel.

Quantitative reverse transcription PCR

RT-qPCR assays were performed following the previously published protocol (83). Total RNAs from harvested cells were extracted using the NucleoSpin RNA extraction kit (Cat. # 740955.250, MACHEREY-NAGEL), and 0.4-1 μg RNA was reversely transcribed using the iScript™ cDNA Synthesis Kit (Cat. # 1708890, Bio-Rad). Real-time qPCR was conducted using the iTaq™ Universal SYBR® GreenSupermix (Cat. # 1727125, Bio-Rad). The PCR reaction was performed on a Bio-Rad CFX connect qPCR machine under the following conditions: 95°C for 10 m, 50 cycles of 95°C for 15 s, and 60°C for 1 m. Relative gene expression was normalized to GAPDH internal control as the $2^{-\Delta\Delta Ct}$ method: $2^{(\Delta CT \text{ of targeted gene} - \Delta CT \text{ of GAPDH})}$. The following primers were used. IL-4 forward: 5'-GTTCTACAGCCACCATGAGAA-3', reverse: 5'-CCGTTTCAGGAATCAGATCA-3'; IL-6 forward: 5'-ACTCAC CTCTTCAGAACGAATTG-3', reverse: 5'-CCATCTTTGGAA GGTTCAGGT-TG-3' (61); IL-8 forward: 5'-CTTGGC AGCCTTCCTGATTT-3'; reverse: 5'-GGGTGGAAAGGTTT-GGAGTATG-3'; Nsp14 forward: 5'-ACATGGCTTTGAGTTG ACATCT-3',reverse: 5'-AGCAGTGGAAAAGCATGTGG-3' IMP DH2 forward: 5′- CTCCCTGGGTACATCGACTT-3′, reverse: 5′-GCCTCTGTGACTGTGTCCAT-3′ (83); GAPDH forward: 5′-GCCTCTTGTCTCTTAGATTTGG-TC-3′, reverse: 5′-TAGCACTCACCATGTAGTTGAGGT-3′.

SARS-CoV-2-TRS-L (N sgRNA forward): 5′-CTCTTG TAGATCTGTTCTCTAAACGAAC-3′,

SARS-CoV-2-TRS-N (N sgRNA reverse): 5′-GGTCC ACCAAACGTAATGCG-3′ (84)

Viral infection

SARS-CoV-2 strain USA-WA1/2020 was obtained from BEI Resources, NIH, NIAHD (Cat # NR52281) and was plaque purified in Vero E6 cells to identify plaques lacking furin cleavage site mutations. A WT virus plaque was then propagated on Vero E6 cells stably expressing TMPRSS2 (kindly provided by Dr. Shan-Lu Liu, Ohio State University) for 72 h. The virus was aliquoted, flash-frozen in liquid nitrogen, and stored at -80C. The virus stock was titered on Vero E6 cells by TCID50 assay. For infection assays, the SARS-CoV-2 virus (MOI: 1.0) was added to cells along with drug treatment for 24 h

at a BSL3 laboratory of OSU Medical Center. Cells were collected by trypsinization, and either lysed with Trizol reagent (Cat # 15596026, Thermo Scientific) for RNA extraction following the manufacturer's protocol or fixed with 4% paraformaldehyde in PBS for 1 h prior to staining for flow cytometry. Staining was performed with the anti-SARS-CoV-2 nucleocapsid protein (N) antibody (Cat # 40143-MM08, Sino Biological) as described previously (31, 85). Flow cytometry was performed on a FACSCanto II machine (BD Biosciences). Data were analyzed using FlowJo software.

Human subjects

The lung specimens from deceased COVID-19 patients were obtained from Biobank at Columbia University Irving Medical Center. The control normal lung specimens were the gifts from Jahar Bhattacharya (Columbia University, NY, USA). For paraffin sections, the lungs were fixed with 4% paraformaldehyde (PFA) at 4°C overnight, dehydrated through a series of grade ethanol, and incubated with Histo-Clear (Cat.5989-27-5, National Diagnostics, USA) at room temperature for 2 hours prior to paraffin embedding. 7 µm thick sections were then prepared from the paraffin blocks and mounted on the slides for staining.

Protein immunofluorescence

Paraffin-embedded lung tissue blocks were baked on the hotplate at 75°C for 20 min and deparaffinized in xylene. The slides were rehydrated from 100%, 90%, to 70% ethanol and then to PBS. We performed the antigen unmasking using the retriever (Cat. # 62700-10, Electron Microscopy Sciences) with R-Buffer A pH 6.0 (Cat. # 62706-10, Electron Microscopy Sciences) for 2 h to complete the cycle and cool down. Slides were blocked with 20% normal goat serum (NGS) in PBST for 2 h at room temperature. Slides were incubated with an anti-IL-8 antibody (Cat. # 550419, BD Pharmingen™) in 5% NGS with PBS at 4°C overnight. Slides were washed with PBST and incubated with Alexa 488 coated goat anti-mouse antibody in 5% NGS/PBS for 2 h at room temperature. Slides were washed with PBST and stained with Hoechst (1:5000 in PBS, Invitrogen). Coverslips were mounted on slides using ProLong Glass Antifade Mountant (Cat. # P36982, Invitrogen) and dried out in the dark overnight. Confocal images were acquired using the ZEISS LSM 700 Upright laser scanning confocal microscope and ZEN imaging software (ZEISS).

Plaque reduction microneutralization

PRMNT assay was performed to evaluate the antiviral activity of drugs against SARS-CoV-2 as previously described (86). In brief, Vero-E6 and A549-ACE2 cells were seeded on 96-well plates with 4×10^4 cells/well in 96-well plates (for quadruplicates) at 24 h prior to viral infection. Cells were inoculated with SARS-CoV-2 (USA-WA1/2020 strain) viruses (100 plaque-forming units (PFU)/well) at 37°C for 1 h in the CO_2 incubator. After 1 h of viral adsorption, infection media was replaced with post-infection media containing 1% Avicel and 2-fold dilutions of the indicated compounds (starting concentration 100 µM), remdesivir (positive controls), or 0.1% DMSO (negative control), and incubated at 37°C for 24 h. At 24 h post-infection, cells were fixed with 10% neutral formalin for 24 h. Cells were permeabilized with 0.5% Triton X-100 in PBS at room temperature for 15 min and blocked with 2.5% BSA in PBS at 37°C for 1 h. Cells were stained with anti-SARS-CoV nucleocapsid (N) protein monoclonal antibody (1C7C7) in 1% BSA–PBS at 37°C for 1 h. After incubation with the primary monoclonal antibody, cells were washed with PBS and incubated with a secondary peroxidase-conjugated goat anti-mouse IgG (Dako; 1:200) in 1% BSA-PBS for 1 h at 37°C. Following the manufacturer's instructions, the labeled cells were detected by using the VECTASTAIN® ABC-HRP Kit (Vector Laboratories). Viral plaques were quantified using a CTL ImmunoSpot plate reader and counting software (Cellular Technology Limited). Infection of wild-type SARS-CoV-2 was carried out at a BSL3 laboratory of Texas Biomedical Research Institute. The percentage of viral infection was calculated as below:

$$\text{Viral infection} = \frac{(\text{Number of plaques with drug treatment} - \text{Number of plaques with "No virus"})}{(\text{Number of plaques with "No drug"; } - \text{Number of plaques with "No virus"})}$$

MTT cell viability assay

The viability of Vero and A549-ACE2 cells was determined using the MTT assay (CellTiter 96 Non-Radioactive Cell Proliferation assay, Promega) following the manufacturer's instructions and as described previously (87). Briefly, confluent monolayers (96-well plate format, 4×10^4 cells/well, quadruplicates) of Vero and A549-ACE2 cells were treated with 100 µl of DMEM containing serially diluted (2-fold dilutions, starting concentration of 100 µM) compounds, or 0.1% DMSO (negative control). Plates were incubated at 37°C in a 5% CO_2 atmosphere for 24 h. Cells and supernatants were treated with 15 µl of Dye Solution and incubated at 37°C in a 5% CO_2 atmosphere for 4 h. Then, cells were treated with 100 µl of Solubilization Solution/Stop Mix, and absorbance at 570 nm was measured using a Vmax kinetic microplate reader (BioTek). The viability of compound-treated cells was calculated as a percentage relative to values obtained with Vehicle-treated cells (0.1% DMSO). Non-linear regression curves and the

median cytotoxic concentration (CC_{50}) were calculated using GraphPad Prism software version 8.0.

Statistics

Statistical analysis was performed using the GraphPad PRISM. Data are presented as mean ± SEM of biological repeats from at least 2 independent experiments. * $p<0.05$, ** $p<0.01$, *** $p<0.001$, or **** $p<0.001$ indicated the significant difference analyzed by ANOVA or Student's t-test.

Data availability statement

The original contributions presented in the study are included in the article/Supplementary Material. Further inquiries can be directed to the corresponding author.

Author contributions

JZ and T-WL conceived and designed this study; T-WL performed most of the experiments; AK performed the SARS-CoV-2 infection and its data processing; J-GP performed the PRMNT assay and its data processing; HL prepared the tissue samples of human subjects; T-WL, NS, and JZ analyzed the results; J-GP, AK, HL, GF, DZ, AB, JQ, LM-S, and JY contributed materials and provided advice for this study. T-WL and JZ wrote the manuscript; JZ supervised the entire study. All authors contributed to the article and approved the submitted version.

Funding

This study was funded by NIH research grants R01AI150448, R01DE025447, R56AI157872, and R33AI116180 to JZ, and R03DE029716, R01CA260690 to NS.

Acknowledgments

The authors thank Dr. Mark Peeples (Nationwide Children's Hospital) and Dr. Jianrong Li (The Ohio State University) for kindly providing plaque purified SARS-CoV-2 for viral propagation. We thank Dr. Sheng-Ce Tao (Shanghai Jiao Tong University) for providing the Nsp14 cloning plasmid. We also thank Dr. Karin Musier-Forsyth and Dr. Shan-Lu Liu at The Ohio State University for their advice on our studies.

Conflict of interest

J-GP and LM-S are listed as inventors on a pending patent application describing the SARS-CoV-2 antibody 1207B4.

The remaining authors declare that the research was conducted in the absence of any commercial or financial relationships that could be construed as a potential conflict of interest.

Publisher's note

Supplementary material

The Supplementary Material for this article can be found online at: https://www.frontiersin.org/articles/10.3389/fimmu.2022.1007089/full#supplementary-material

References

1. Robson F, Khan KS, Le TK, Paris C, Demirbag S, Barfuss P, et al. Coronavirus rna proofreading: Molecular basis and therapeutic targeting. *Mol Cell* (2020) 80 (6):1136–8. doi: 10.1016/j.molcel.2020.11.048

2. Naqvi AA, Fatima K, Mohammad T, Fatima U, Singh IK, Singh A, et al. Insights into sars-Cov-2 genome, structure, evolution, pathogenesis and therapies: Structural genomics approach. *Bba-Mol Basis Dis* (2020) 1866(10):165878. doi: 10.1016/j.bbadis.2020.165878

3. Lei X, Dong X, Ma R, Wang W, Xiao X, Tian Z, et al. Activation and evasion of type I interferon responses by SARS-Cov-2. *Nat Commun* (2020) 11(1):3810. doi: 10.1038/s41467-020-17665-9

4. Yuen CK, Lam JY, Wong WM, Mak LF, Wang X, Chu H, et al. SARS-Cov-2 Nsp13, Nsp14, Nsp15 and Orf6 function as potent interferon antagonists. *Emerg Microbes Infect* (2020) 9(1):1418–28. doi: 10.1080/22221751.2020.1780953

5. Blanco-Melo D, Nilsson-Payant BE, Liu WC, Uhl S, Hoagland D, Moller R, et al. Imbalanced host response to SARS-Cov-2 drives development of covid-19. *Cell* (2020) 181(5):1036–45.e9. doi: 10.1016/j.cell.2020.04.026

6. Sa Ribero M, Jouvenet N, Dreux M, Nisole S. Interplay between SARS-Cov-2 and the type I interferon response. *PLoS Pathog* (2020) 16(7):e1008737. doi: 10.1371/journal.ppat.1008737

7. Aid M, Busman-Sahay K, Vidal SJ, Maliga Z, Bondoc S, Starke C, et al. Vascular disease and thrombosis in SARS-Cov-2-Infected rhesus macaques. *Cell* (2020) 183(5):1354–66.e13. doi: 10.1016/j.cell.2020.10.005

8. Ho JSY, Mok BW, Campisi L, Jordan T, Yildiz S, Parameswaran S, et al. Top1 inhibition therapy protects against sars-Cov-2-Induced lethal inflammation. *Cell* (2021) 184(10):2618–32e17. doi: 10.1016/j.cell.2021.03.051

9. Ma Y, Wu L, Shaw N, Gao Y, Wang J, Sun Y, et al. Structural basis and functional analysis of the sars coronavirus Nsp14-Nsp10 complex. *Proc Natl Acad Sci U S A* (2015) 112(30):9436–41. doi: 10.1073/pnas.1508686112

10. Ferron F, Subissi L, Silveira De Morais AT, Le NTT, Sevajol M, Gluais L, et al. Structural and molecular basis of mismatch correction and ribavirin excision from coronavirus rna. *Proc Natl Acad Sci USA* (2018) 115(2):E162–E71. doi: 10.1073/pnas.1718806115

11. Minskaia E, Hertzig T, Gorbalenya AE, Campanacci V, Cambillau C, Canard B, et al. Discovery of an rna virus 3' ->5' exoribonuclease that is critically involved in coronavirus rna synthesis. *Proc Natl Acad Sci USA* (2006) 103(13):5108–13. doi: 10.1073/pnas.0508200103

12. Bouvet M, Imbert I, Subissi L, Gluais L, Canard B, Decroly E. Rna 3'-end mismatch excision by the severe acute respiratory syndrome coronavirus nonstructural protein Nsp10/Nsp14 exoribonuclease complex. *Proc Natl Acad Sci USA* (2012) 109(24):9372–7. doi: 10.1073/pnas.1201130109

13. Ogando NS, Zevenhoven-Dobbe JC, van der Meer Y, Bredenbeek PJ, Posthuma CC, Snijder EJ. The enzymatic activity of the Nsp14 exoribonuclease is critical for replication of mers-cov and SARS-Cov-2. *J Virol* (2020) 94(23): e01246–20. doi: 10.1128/JVI.01246-20

14. Moeller NH, Shi K, Demir O, Banerjee S, Yin L, Belica C, et al. Structure and dynamics of sars-Cov-2 proofreading exoribonuclease exon. *Proc Natl Acad Sci USA* (2022) 119(9):e2106379119. doi: 10.1073/pnas.2106379119

15. Chen Y, Cai H, Pan J, Xiang N, Tien P, Ahola T, et al. Functional screen reveals sars coronavirus nonstructural protein Nsp14 as a novel cap N7 methyltransferase. *Proc Natl Acad Sci USA* (2009) 106(9):3484–9. doi: 10.1073/pnas.0808790106

16. Bouvet M, Debarnot C, Imbert I, Selisko B, Snijder EJ, Canard B, et al. *In vitro* reconstitution of sars-coronavirus mrna cap methylation. *PLoS Pathog* (2010) 6(4):e1000863. doi: 10.1371/journal.ppat.1000863

17. Chen Y, Su C, Ke M, Jin X, Xu L, Zhang Z, et al. Biochemical and structural insights into the mechanisms of sars coronavirus rna ribose 2'-O-Methylation by Nsp16/Nsp10 protein complex. *PLoS Pathog* (2011) 7(10):e1002294. doi: 10.1371/journal.ppat.1002294

18. Decroly E, Ferron F, Lescar J, Canard B. Conventional and unconventional mechanisms for capping viral mrna. *Nat Rev Microbiol* (2011) 10(1):51–65. doi: 10.1038/nrmicro2675

19. Jaafar ZA, Kieft JS. Viral rna structure-based strategies to manipulate translation. *Nat Rev Microbiol* (2019) 17(2):110–23. doi: 10.1038/s41579-018-0117-x

20. Jan E, Mohr I, Walsh D. A cap-to-Tail guide to mrna translation strategies in virus-infected cells. *Annu Rev Virol* (2016) 3(1):283–307. doi: 10.1146/annurev-virology-100114-055014

21. Becares M, Pascual-Iglesias A, Nogales A, Sola I, Enjuanes L, Zuniga S. Mutagenesis of coronavirus Nsp14 reveals its potential role in modulation of the innate immune response. *J Virol* (2016) 90(11):5399–414. doi: 10.1128/JVI.03259-15

22. Gribble J, Stevens LJ, Agostini ML, Anderson-Daniels J, Chappell JD, Lu X, et al. The coronavirus proofreading exoribonuclease mediates extensive viral recombination. *PLoS Pathog* (2021) 17(1):e1009226. doi: 10.1371/journal.ppat.1009226

23. Gordon DE, Jang GM, Bouhaddou M, Xu J, Obernier K, White KM, et al. A sars-Cov-2 protein interaction map reveals targets for drug repurposing. *Nature* (2020) 583(7816):459–68. doi: 10.1038/s41586-020-2286-9

24. Liao LX, Song XM, Wang LC, Lv HN, Chen JF, Liu D, et al. Highly selective inhibition of Impdh2 provides the basis of antineuroinflammation therapy. *Proc Natl Acad Sci USA* (2017) 114(29):E5986–E94. doi: 10.1073/pnas.1706778114

25. Liu T, Zhang L, Joo D, Sun SC. Nf-kappab signaling in inflammation. *Signal Transduct Target Ther* (2017) 2(1):17023. doi: 10.1038/sigtrans.2017.23

26. Grassl C, Luckow B, Schlondorff D, Dendorfer U. Transcriptional regulation of the interleukin-6 gene in mesangial cells. *J Am Soc Nephrol* (1999) 10(7):1466–77. doi: 10.1681/ASN.V1071466

27. Bezzerri V, Borgatti M, Finotti A, Tamanini A, Gambari R, Cabrini G. Mapping the transcriptional machinery of the il-8 gene in human bronchial epithelial cells. *J Immunol* (2011) 187(11):6069–81. doi: 10.4049/jimmunol.1100821

28. Perkins ND. Integrating cell-signalling pathways with nf-kappab and ikk function. *Nat Rev Mol Cell Biol* (2007) 8(1):49–62. doi: 10.1038/nrm2083

29. Perkins ND. Post-translational modifications regulating the activity and function of the nuclear factor kappa b pathway. *Oncogene* (2006) 25(51):6717–30. doi: 10.1038/sj.onc.1209937

30. Bohuslav J, Chen LF, Kwon H, Mu Y, Greene WC. P53 induces nf-kappab activation by an ikappab kinase-independent mechanism involving phosphorylation of P65 by ribosomal S6 kinase 1. *J Biol Chem* (2004) 279 (25):26115–25. doi: 10.1074/jbc.M313509200

31. Shi G, Kenney AD, Kudryashova E, Zani A, Zhang L, Lai KK, et al. Opposing activities of ifitm proteins in sars-Cov-2 infection. *EMBO J* (2021) 40 (3):e106501. doi: 10.15252/embj.2020106501

32. Leng L, Cao R, Ma J, Mou D, Zhu Y, Li W, et al. Pathological features of covid-19-Associated lung injury: A preliminary proteomics report based on clinical samples. *Signal Transduct Target Ther* (2020) 5(1):240. doi: 10.1038/s41392-020-00355-9

33. Khabar KS, Al-Zoghaibi F, Al-Ahdal MN, Murayama T, Dhalla M, Mukaida N, et al. The alpha chemokine, interleukin 8, inhibits the antiviral action of interferon alpha. *J Exp Med* (1997) 186(7):1077–85. doi: 10.1084/jem.186.7.1077

34. Romano M, Ruggiero A, Squeglia F, Maga G, Berisio R. A structural view of sars-Cov-2 rna replication machinery: Rna synthesis, proofreading and final capping. *Cells-Basel* (2020) 9(5):1267. doi: 10.3390/cells9051267

35. Hedstrom L. Imp dehydrogenase: Structure, mechanism, and inhibition. *Chem Rev* (2009) 109(7):2903–28. doi: 10.1021/cr900021w

36. Zhou S, Liu R, Baroudy BM, Malcolm BA, Reyes GR. The effect of ribavirin and impdh inhibitors on hepatitis c virus subgenomic replicon rna. *Virology* (2003) 310(2):333–42. doi: 10.1016/s0042-6822(03)00152-1

37. Leyssen P, Balzarini J, De Clercq E, Neyts J. The predominant mechanism by which ribavirin exerts its antiviral activity in vitro against flaviviruses and paramyxoviruses is mediated by inhibition of imp dehydrogenase. *J Virol* (2005) 79 (3):1943–7. doi: 10.1128/JVI.79.3.1943-1947.2005

38. Sintchak MD, Fleming MA, Futer O, Raybuck SA, Chambers SP, Caron PR, et al. Structure and mechanism of inosine monophosphate dehydrogenase in complex with the immunosuppressant mycophenolic acid. *Cell* (1996) 85 (6):921–30. doi: 10.1016/s0092-8674(00)81275-1

39. Yang CW, Lee YZ, Hsu HY, Shih C, Chao YS, Chang HY, et al. Targeting coronaviral replication and cellular Jak2 mediated dominant nf-kappab activation for comprehensive and ultimate inhibition of coronaviral activity. *Sci Rep* (2017) 7 (1):4105. doi: 10.1038/s41598-017-04203-9

40. Hemmat N, Asadzadeh Z, Ahangar NK, Alemohammad H, Najafzadeh B, Derakhshani A, et al. The roles of signaling pathways in sars-Cov-2 infection; lessons learned from sars-cov and mers-cov. *Arch Virol* (2021) 166(3):675–96. doi: 10.1007/s00705-021-04958-7

41. Yin X, Riva L, Pu Y, Martin-Sancho L, Kanamune J, Yamamoto Y, et al. Mda5 governs the innate immune response to sars-Cov-2 in lung epithelial cells. *Cell Rep* (2021) 34(2):108628. doi: 10.1016/j.celrep.2020.108628

42. Rahman MM, McFadden G. Modulation of nf-kappab signalling by microbial pathogens. *Nat Rev Microbiol* (2011) 9(4):291–306. doi: 10.1038/nrmicro2539

43. Forbester JL, Humphreys IR. Genetic influences on viral-induced cytokine responses in the lung. *Mucosal Immunol* (2021) 14(1):14–25. doi: 10.1038/s41385-020-00355-6

44. Alon R, Sportiello M, Kozlovski S, Kumar A, Reilly EC, Zarbock A, et al. Leukocyte trafficking to the lungs and beyond: Lessons from influenza for covid-19. *Nat Rev Immunol* (2021) 21(1):49–64. doi: 10.1038/s41577-020-00470-2

45. Hsu JC, Laurent-Rolle M, Pawlak JB, Wilen CB, Cresswell P. Translational shutdown and evasion of the innate immune response by sars-Cov-2 Nsp14 protein. *Proc Natl Acad Sci USA* (2021) 118(24):e2101161118. doi: 10.1073/pnas.2101161118

46. Zhang S, Wang J, Wang L, Aliyari S, Cheng G. Sars-Cov-2 virus Nsp14 impairs Nrf2/Hmox1 activation by targeting sirtuin 1. *Cell Mol Immunol* (2022) 19 (8):872–82. doi: 10.1038/s41423-022-00887-w

47. Ziegler CM, Eisenhauer P, Kelly JA, Dang LN, Beganovic V, Bruce EA, et al. A proteomics survey of junin virus interactions with human proteins reveals host factors required for arenavirus replication. *J Virol* (2018) 92(4):e01565–17. doi: 10.1128/JVI.01565-17

48. Dang W, Yin Y, Wang Y, Wang W, Su J, Sprengers D, et al. Inhibition of calcineurin or imp dehydrogenase exerts moderate to potent antiviral activity against norovirus replication. *Antimicrob Agents Chemother* (2017) 61(11):e01095–17. doi: 10.1128/AAC.01095-17

49. Hofmann WP, Herrmann E, Sarrazin C, Zeuzem S. Ribavirin mode of action in chronic hepatitis c: From clinical use back to molecular mechanisms. *Liver Int* (2008) 28(10):1332–43. doi: 10.1111/j.1478-3231.2008.01896.x

50. Quemeneur L, Gerland LM, Flacher M, Ffrench M, Revillard JP, Genestier L. Differential control of cell cycle, proliferation, and survival of primary T

lymphocytes by purine and pyrimidine nucleotides. *J Immunol* (2003) 170 (10):4986–95. doi: 10.4049/jimmunol.170.10.4986

51. Shu QN, Nair V. Inosine monophosphate dehydrogenase (Impdh) as a target in drug discovery. *Med Res Rev* (2008) 28(2):219–32. doi: 10.1002/med.20104

52. Toubiana J, Rossi AL, Grimaldi D, Belaidouni N, Chafey P, Clary G, et al. Impdhii protein inhibits toll-like receptor 2-mediated activation of nf-kappab. *J Biol Chem* (2011) 286(26):23319–33. doi: 10.1074/jbc.M110.201210

53. Jiang C, Yang H, Chen X, Qiu S, Wu C, Zhang B, et al. Macleaya cordata extracts exert antiviral effects in newborn mice with rotavirus-induced diarrhea *Via* inhibiting the Jak2/Stat3 signaling pathway. *Exp Ther Med* (2020) 20(2):1137–44. doi: 10.3892/etm.2020.8766

54. Andreucci M, Faga T, Lucisano G, Uccello F, Pisani A, Memoli B, et al. Mycophenolic acid inhibits the phosphorylation of nf-kappab and jnks and causes a decrease in il-8 release in H2o2-treated human renal proximal tubular cells. *Chem Biol Interact* (2010) 185(3):253–62. doi: 10.1016/j.cbi.2010.03.019

55. Zhang C, Tam TW, Chau MK, Garcia Cordoba CA, Yung S, Chan TM. Effect of combined mycophenolate and rapamycin treatment on kidney fibrosis in murine lupus nephritis. *Front Pharmacol* (2022) 13:866077. doi: 10.3389/fphar.2022.866077

56. von Borstel A, Abdulahad WH, Dekkema G, Rutgers A, Stegeman CA, Veldman J, et al. Mycophenolic acid and 6-mercaptopurine both inhibit b-cell proliferation in granulomatosis with polyangiitis patients, whereas only mycophenolic acid inhibits b-cell il-6 production. *PLoS One* (2020) 15(7): e0235743. doi: 10.1371/journal.pone.0235743

57. Gubernatorova EO, Gorshkova EA, Polinova AI, Drutskaya MS. Il-6: Relevance for immunopathology of sars-Cov-2. *Cytokine Growth Factor Rev* (2020) 53:13–24. doi: 10.1016/j.cytogfr.2020.05.009

58. Chomarat P, Banchereau J, Davoust J, Palucka AK. Il-6 switches the differentiation of monocytes from dendritic cells to macrophages. *Nat Immunol* (2000) 1(6):510–4. doi: 10.1038/82763

59. Diehl S, Rincon M. The two faces of il-6 on Th1/Th2 differentiation. *Mol Immunol* (2002) 39(9):531–6. doi: 10.1016/s0161-5890(02)00210-9

60. Hou W, Kang HS, Kim BS. Th17 cells enhance viral persistence and inhibit T cell cytotoxicity in a model of chronic virus infection. *J Exp Med* (2009) 206 (2):313–28. doi: 10.1084/jem.20082030

61. Melms JC, Biermann J, Huang H, Wang Y, Nair A, Tagore S, et al. A molecular single-cell lung atlas of lethal covid-19. *Nature* (2021) 595(7865):114–9. doi: 10.1038/s41586-021-03569-1

62. Barnes BJ, Adrover JM, Baxter-Stoltzfus A, Borczuk A, Cools-Lartigue J, Crawford JM, et al. Targeting potential drivers of covid-19: Neutrophil extracellular traps. *J Exp Med* (2020) 217(6):e20200652. doi: 10.1084/jem.20200652

63. Kaiser R, Leunig A, Pekayvaz K, Popp O, Joppich M, Polewka V, et al. Self-sustaining il-8 loops drive a prothrombotic neutrophil phenotype in severe covid-19. *JCI Insight* (2021) 6(18):e150862. doi: 10.1172/jci.insight.150862

64. Szachnowski U, Bhargava A, Chazal M, Foretek D, Aicher S-M, da Fonseca JP, et al. Transcriptomic landscapes of sars-Cov-2-Infected and bystander lung cells reveal a selective upregulation of nf-Kappa;b-Dependent coding and non-coding proviral transcripts. *bioRxiv* (2022). doi: 10.1101/2022.02.25.481978

65. Sacchi A, Grassi G, Bordoni V, Lorenzini P, Cimini E, Casetti R, et al. Early expansion of myeloid-derived suppressor cells inhibits sars-Cov-2 specific T-cell response and may predict fatal covid-19 outcome. *Cell Death Dis* (2020) 11 (10):921. doi: 10.1038/s41419-020-03125-1

66. Kofuji S, Hirayama A, Eberhardt AO, Kawaguchi R, Sugiura Y, Sampetrean O, et al. Imp dehydrogenase-2 drives aberrant nucleolar activity and promotes tumorigenesis in glioblastoma. *Nat Cell Biol* (2019) 21(8):1003–14. doi: 10.1038/s41556-019-0363-9

67. Kofuji S, Sasaki AT. Gtp metabolic reprogramming by Impdh2: Unlocking cancer cells' fuelling mechanism. *J Biochem* (2020) 168(4):319–28. doi: 10.1093/jb/mvaa085

68. Zhang Q, Zhou X, Wu R, Mosley A, Zeng SX, Xing Z, et al. The role of imp dehydrogenase 2 in inauhzin-induced ribosomal stress. *Elife* (2014) 3:e03077. doi: 10.7554/eLife.03077

69. Mannava S, Grachtchouk V, Wheeler LJ, Im M, Zhuang D, Slavina EG, et al. Direct role of nucleotide metabolism in c-Myc-Dependent proliferation of melanoma cells. *Cell Cycle* (2008) 7(15):2392–400. doi: 10.4161/cc.6390

70. Zhang J, Cruz-Cosme R, Zhuang MW, Liu D, Liu Y, Teng S, et al. A systemic and molecular study of subcellular localization of sars-Cov-2 proteins. *Signal Transduct Target Ther* (2020) 5(1):269. doi: 10.1038/s41392-020-00372-8

71. Meyers JM, Ramanathan M, Shanderson RL, Beck A, Donohue L, Ferguson I, et al. The proximal proteome of 17 sars-Cov-2 proteins links to disrupted antiviral signaling and host translation. *PLoS Pathog* (2021) 17(10):e1009412. doi: 10.1371/journal.ppat.1009412

72. Lane BR, Lore K, Bock PJ, Andersson J, Coffey MJ, Strieter RM, et al. Interleukin-8 stimulates human immunodeficiency virus type 1 replication and is a potential new target for antiretroviral therapy. *J Virol* (2001) 75(17):8195–202. doi: 10.1128/jvi.75.17.8195-8202.2001

73. Chen WC, Tseng CK, Chen YH, Lin CK, Hsu SH, Wang SN, et al. Hcv Ns5a up-regulates cox-2 expression *Via* il-8-Mediated activation of the Erk/Jnk mapk pathway. *PLoS One* (2015) 10(7):e0133264. doi: 10.1371/journal.pone.0133264

74. Mukaida N. Pathophysiological roles of interleukin-8/Cxcl8 in pulmonary diseases. *Am J Physiol Lung Cell Mol Physiol* (2003) 284(4):L566–77. doi: 10.1152/ajplung.00233.2002

75. Murayama T, Kuno K, Jisaki F, Obuchi M, Sakamuro D, Furukawa T, et al. Enhancement human cytomegalovirus replication in a human lung fibroblast cell line by interleukin-8. *J Virol* (1994) 68(11):7582–5. doi: 10.1128/JVI.68.11.7582-7585.1994

76. Hiscott J, Kwon H, Genin P. Hostile takeovers: Viral appropriation of the nf-kappab pathway. *J Clin Invest* (2001) 107(2):143–51. doi: 10.1172/JCI11918

77. Hung IF, Lung KC, Tso EY, Liu R, Chung TW, Chu MY, et al. Triple combination of interferon beta-1b, lopinavir-ritonavir, and ribavirin in the treatment of patients admitted to hospital with covid-19: An open-label, randomised, phase 2 trial. *Lancet* (2020) 395(10238):1695–704. doi: 10.1016/S0140-6736(20)31042-4

78. Wan W, Zhu S, Li S, Shang W, Zhang R, Li H, et al. High-throughput screening of an fda-approved drug library identifies inhibitors against arenaviruses and sars-Cov-2. *ACS Infect Dis* (2021) 7(6):1409–22. doi: 10.1021/acsinfecdis.0c00486

79. Han Y, Duan X, Yang L, Nilsson-Payant BE, Wang P, Duan F, et al. Identification of sars-Cov-2 inhibitors using lung and colonic organoids. *Nature* (2021) 589(7841):270–5. doi: 10.1038/s41586-020-2901-9

80. Prinarakis E, Chantzoura E, Thanos D, Spyrou G. S-glutathionylation of Irf3 regulates Irf3-cbp interaction and activation of the ifn beta pathway. *EMBO J* (2008) 27(6):865–75. doi: 10.1038/emboj.2008.28

81. Zhou D, Hayashi T, Jean M, Kong W, Fiches G, Biswas A, et al. Inhibition of polo-like kinase 1 (Plk1) facilitates the elimination of hiv-1 viral reservoirs in Cd4 (+) T cells ex vivo. *Sci Adv* (2020) 6(29):eaba1941. doi: 10.1126/sciadv.aba1941

82. Kong W, Biswas A, Zhou D, Fiches G, Fujinaga K, Santoso N, et al. Nucleolar protein Nop2/Nsun1 suppresses hiv-1 transcription and promotes viral latency by competing with tat for tar binding and methylation. *PloS Pathog* (2020) 16(3):e1008430. doi: 10.1371/journal.ppat.1008430

83. Huang F, Ni M, Chalishazar MD, Huffman KE, Kim J, Cai L, et al. Inosine monophosphate dehydrogenase dependence in a subset of small cell lung cancers. *Cell Metab* (2018) 28(3):369–82.e5. doi: 10.1016/j.cmet.2018.06.005

84. Yang L, Han Y, Nilsson-Payant BE, Gupta V, Wang P, Duan X, et al. A human pluripotent stem cell-based platform to study sars-Cov-2 tropism and model virus infection in human cells and organoids. *Cell Stem Cell* (2020) 27 (1):125–36.e7. doi: 10.1016/j.stem.2020.06.015

85. Larue RC, Xing E, Kenney AD, Zhang Y, Tuazon JA, Li J, et al. Rationally designed Ace2-derived peptides inhibit sars-Cov-2. *Bioconjug Chem* (2021) 32 (1):215–23. doi: 10.1021/acs.bioconjchem.0c00664

86. Park JG, Oladunni FS, Chiem K, Ye C, Pipenbrink M, Moran T, et al. Rapid in vitro assays for screening neutralizing antibodies and antivirals against sars-Cov-2. *J Virol Methods* (2021) 287:113995. doi: 10.1016/j.jviromet.2020.113995

87. Park JG, Avila-Perez G, Nogales A, Blanco-Lobo P, de la Torre JC, Martinez-Sobrido L. Identification and characterization of novel compounds with broad-spectrum antiviral activity against influenza a and b viruses. *J Virol* (2020) 94(7):e02149–19. doi: 10.1128/JVI.02149-19

frontiers | Frontiers in Immunology

TYPE Original Research
PUBLISHED 15 September 2022
DOI 10.3389/fimmu.2022.1013322

OPEN ACCESS

EDITED BY
Chenhe Su,
Wistar Institute, United States

REVIEWED BY
Yusha Araf,
Shahjalal University of Science and Technology, Bangladesh
Sharah Jabeen,
Bangladesh Agricultural University, Bangladesh

*CORRESPONDENCE
Wanming Wang
wangwm93@126.com

†These authors have contributed equally to this work

SPECIALTY SECTION
This article was submitted to Viral Immunology, a section of the journal Frontiers in Immunology

RECEIVED 06 August 2022
ACCEPTED 29 August 2022
PUBLISHED 15 September 2022

CITATION
Zheng Q, Wang D, Lin R, Lv Q and Wang W (2022) IFI44 is an immune evasion biomarker for SARS-CoV-2 and *Staphylococcus aureus* infection in patients with RA.
Front. Immunol. 13:1013322.
doi: 10.3389/fimmu.2022.1013322

IFI44 is an immune evasion biomarker for SARS-CoV-2 and *Staphylococcus aureus* infection in patients with RA

Qingcong Zheng[1†], Du Wang[2†], Rongjie Lin[1], Qi Lv[1] and Wanming Wang[1*]

[1]Department of Orthopedics, 900th Hospital of Joint Logistics Support Force, Fuzhou, China, [2]Arthritis Clinical and Research Center, Peking University People's Hospital, Beijing, China

Background: Severe acute respiratory syndrome coronavirus 2 (SARS-CoV-2) caused a global pandemic of severe coronavirus disease 2019 (COVID-19). *Staphylococcus aureus* is one of the most common pathogenic bacteria in humans, rheumatoid arthritis (RA) is among the most prevalent autoimmune conditions. RA is a significant risk factor for SARS-CoV-2 and *S. aureus* infections, although the mechanism of RA and SARS-CoV-2 infection in conjunction with *S. aureus* infection has not been elucidated. The purpose of this study is to investigate the biomarkers and disease targets between RA and SARS-CoV-2 and *S. aureus* infections using bioinformatics analysis, to search for the molecular mechanisms of SARS-CoV-2 and *S. aureus* immune escape and potential drug targets in the RA population, and to provide new directions for further analysis and targeted development of clinical treatments.

Methods: The RA dataset (GSE93272) and the *S. aureus* bacteremia (SAB) dataset (GSE33341) were used to obtain differentially expressed gene sets, respectively, and the common differentially expressed genes (DEGs) were determined through the intersection. Functional enrichment analysis utilizing GO, KEGG, and ClueGO methods. The PPI network was created utilizing the STRING database, and the top 10 hub genes were identified and further examined for functional enrichment using Metascape and GeneMANIA. The top 10 hub genes were intersected with the SARS-CoV-2 gene pool to identify five hub genes shared by RA, COVID-19, and SAB, and functional enrichment analysis was conducted using Metascape and GeneMANIA. Using the NetworkAnalyst platform, TF-hub gene and miRNA-hub gene networks were built for these five hub genes. The hub gene was verified utilizing GSE17755, GSE55235, and GSE13670, and its effectiveness was assessed utilizing ROC curves. CIBERSORT was applied to examine immune cell infiltration and the link between the hub gene and immune cells.

Results: A total of 199 DEGs were extracted from the GSE93272 and GSE33341 datasets. KEGG analysis of enrichment pathways were NLR signaling pathway, cell membrane DNA sensing pathway, oxidative phosphorylation, and viral infection. Positive/negative regulation of the immune system, regulation of

the interferon-I (IFN-I; IFN-α/β) pathway, and associated pathways of the immunological response to viruses were enriched in GO and ClueGO analyses. PPI network and Cytoscape platform identified the top 10 hub genes: RSAD2, IFIT3, GBP1, RTP4, IFI44, OAS1, IFI44L, ISG15, HERC5, and IFIT5. The pathways are mainly enriched in response to viral and bacterial infection, IFN signaling, and 1,25-dihydroxy vitamin D3. IFI44, OAS1, IFI44L, ISG15, and HERC5 are the five hub genes shared by RA, COVID-19, and SAB. The pathways are primarily enriched for response to viral and bacterial infections. The TF-hub gene network and miRNA-hub gene network identified YY1 as a key TF and hsa-mir-1-3p and hsa-mir-146a-5p as two important miRNAs related to IFI44. IFI44 was identified as a hub gene by validating GSE17755, GSE55235, and GSE13670. Immune cell infiltration analysis showed a strong positive correlation between activated dendritic cells and IFI44 expression.

Conclusions: IFI144 was discovered as a shared biomarker and disease target for RA, COVID-19, and SAB by this study. IFI44 negatively regulates the IFN signaling pathway to promote viral replication and bacterial proliferation and is an important molecular target for SARS-CoV-2 and *S. aureus* immune escape in RA. Dendritic cells play an important role in this process. 1,25-Dihydroxy vitamin D3 may be an important therapeutic agent in treating RA with SARS-CoV-2 and *S. aureus* infections.

KEYWORDS

SARS-CoV-2, COVID-19, *Staphylococcus aureus*, Rheumatoid arthritis, IFI44, dendritic cells, 1,25-dihydroxy vitamin D_3

Introduction

Rheumatoid arthritis (RA) (1) is one of the most prevalent chronic inflammatory autoimmune diseases and has been the focus of intense study for decades (1–5). The prevalence of RA is about 1% (6). The clinical presentation of RA is characterized by chronic persistent synovitis, which, in turn, destroys bone and cartilage, leading to joint bone destruction and chronic disability (7–9). Therefore, patients with RA are more prone than the general population to requiring hip and knee replacements (10). There are three main categories of factors that influence the progression of RA: genetic, environmental, and immune (11, 12), with microbial infections (e.g., bacteria and viruses) constituting a significant subset of environmental factors that can trigger, induce, and exacerbate the disease process in RA (13–17). The balance between the impact of microorganisms on the host and the immune response of the host to microorganisms is crucial for maintaining the regular functioning of the body's immune system, and an imbalance between these reactions can exacerbate autoimmune inflammation in RA (18). In addition, disease-modifying antirheumatic drugs (DMARDs) and glucocorticoids, commonly used for RA, can affect the immune system to varying degrees (19–21). Although emerging biologic medicines (e.g., TNF inhibitors) have been employed in recent years to treat patients with RA with an inadequate response to DMARDs (22–25), studies have shown that their usage is linked with an increased risk of infection in patients with RA (26–28). Therefore, microbial infection is dangerous for individuals with RA, either in the illness itself or with the associated medicine, as well as after arthroplasty (29–31).

Staphylococcus aureus is a gram-positive human opportunistic pathogen (32) that frequently colonizes the human nasal cavity (33, 34) and can cause severe systemic or local infections if the immune system is compromised (35). First, *S. aureus* bacteremia (SAB) is a frequent systemic infection that is characterized by significant morbidity and mortality (36), and the majority of SAB are endogenous infections, predominantly from nasally colonized colonies (37). Second, local infections with *S. aureus* are prevalent in postoperative surgical-site infection (SSI) and prosthetic joint infection (PJI) (38, 39), which are not only the most prevalent postoperative complications (40) but also catastrophic consequences of joint replacement surgery (41, 42). According to studies, nasal

carriage of *S. aureus* is also a common source of postoperative infections (43, 44). Patients with RA are more likely than the general population to carry *S. aureus* in their nasal vestibules (45), and RA medications enhance nasal *S. aureus* carriage (46). In a Danish national observational cohort study, RA was identified as a significant risk factor for SAB, and intra-articular orthopedic implants enhanced the chance of infection (31). Another prospective cohort study found that patients with RA had a greater incidence of SAB and death and that RA-induced osteoarthritic damage made *S. aureus* more vulnerable to osteoarthritic infection (47). Patients with RA are susceptible to *S. aureus* primarily due to the following factors: First, the immune system disorder of patients with RA makes *S. aureus* easy to invade the host. Second, for the local situation of patients with RA, the bone and joint damage caused by the disease makes local infection with *S. aureus* easier. Third, patients with RA are susceptible to carrying *S. aureus*. Fourth, the medication of RA makes the nasal cavity more susceptible and carries more *S. aureus*. Fifth, it is easy for *S. aureus* to cause SSI and PJI in patients with RA who have had joint replacement surgery. Therefore, we aim to investigate the RA population's underlying susceptibility mechanism to *S. aureus*.

In 2019, COVID-19, caused by the severe acute respiratory syndrome coronavirus 2 (SARS-CoV-2), swiftly affected people and produced a significant public health concern, which was eventually classified as a worldwide pandemic (48–52). As of 12 June 2022, over 535 million confirmed cases and over six million deaths had been reported globally (53). COVID-19 is a systemic disease that can cause significant damage to several body systems, manifesting clinically as fever, cough, and respiratory distress, as well as skeletal and muscular symptoms, including arthralgia (54–57). SARS-CoV-2 has been reported to overstimulate the body's immune system and contribute to autoantibody production due to potential antigenic cross-reactivity with the body (58–60). Indeed, patients with COVID-19 frequently exhibit immunological dysregulation (61) and can trigger multiple autoimmune diseases (59, 62), and, conversely, patients with autoimmune disease are more vulnerable to SARS-CoV-2 infection (63), and the course of COVID-19 is more severe in hospitalized patients with autoimmune disease (64). As one of the most prevalent autoimmune diseases, RA merits in-depth investigation. According to studies, patients with RA infected with SARS-CoV-2 had a greater likelihood of hospitalization and mortality than non-RA patients (65, 66). Moreover, viral sequelae/combined bacterial infections are not only common consequences (67–69) but also significantly exacerbate disease severity and death (70–74). *Streptococcus pneumoniae*, β-hemolytic streptococci, *Haemophilus influenzae*, *Pseudomonas aeruginosa*, and *S. aureus* are often coinfected microorganisms (75–80). In COVID-19, *S. aureus* was the most common bacterium for SARS-CoV-2 sequel/combination (81, 82).

The RA population is one of the most numerous in the world for autoimmune diseases, with *S. aureus* being one of the most common human pathogens and COVID-19 caused by SARS-CoV-2, leading to a global pandemic. These three factors affect a wide range of populations and have a poor prognosis, and their combination leads to high rates of disability and mortality, posing a serious risk to global public health. This study aims to investigate the causes of RA susceptibility to SARS-CoV-2 and Aureus infection through bioinformatics analysis, to discover the common biomarkers and disease targets among the three, to search for the mechanisms of SARS-CoV-2 and *S. aureus* immune escape in the RA population, and to provide new directions for further analysis of their pathogenesis and targeted development of clinical treatments.

Materials and methods

Data collection

Three RA (GSE93272, GSE17755, GSE55235) and two *S. aureus* infection (GSE33341 and GSE13670) datasets were included in this study (83–87), using the National Center for Biotechnology Information Gene Expression Omnibus (GEO) (https://www.ncbi.nlm.nih.gov/geo/) for screening (Table 1). As test sets, the GSE93272 dataset with 232 patients with RA and 43 healthy individuals' whole blood samples and the GSE33341 dataset with 31 SAB patients and 43 healthy individuals' whole blood samples were utilized to identify the differentially expressed genes (DEGs). The GSE17755 dataset contains whole-blood samples from four patients with RA and 12 healthy individuals. The GSE55235 dataset contains synovial tissue samples from 10 patients with RA and 10 healthy individuals. GSE13670 dataset contains 15 *S. aureus*-infected

TABLE 1 Basic information of selected datasets.

Dataset ID	Platform	Tissue (*Homo sapiens*)	Experimental group	Normal control	Experiment type	Reference
GSE93272	GPL570	Whole blood	232	43	Array	Tasaki et al. (83)
GSE33341	GPL571	Whole blood	31	43	Array	Ahn et al. (84)
GSE17755	GPL1291	Whole blood	4	12	Array	Lee et al. (85)
GSE55235	GPL96	Synovium	10	10	Array	Woetzel et al. (86)
GSE13670	GPL570	PBMC	15	15	Array	Kozielet al. (87)

macrophage samples and 15 healthy human macrophage samples. These three datasets were utilized as validation sets for the hub genes.

Identification of DEGs

The empirical Bayesian approach of the limma R package (http://www.bioconductor.org/packages/release/bioc/html/limma.html) (88, 89) was used for differentially expressed genes between the RA and HC groups of GSE93272 and the SAB and HC groups of GSE33341 for analysis. The cutoff was |log2 FC| > 0.5 and P < 0.05. The volcano map was further drawn using the ggplot2 package to reflect the differential expression of DEGs. The common DEGs were obtained by taking the intersection of DEGs (GSE93272) and DEGs (GSE33341) using the Venn-diagram package in the R software.

GO, KEGG, and ClueGO enrichment analyses of DEGs

To explore the pathways and functions of the identified genes, GO and KEGG enrichment analyses of common-DEGs were performed with the R package "clusterProfiler" (90, 91). $P < 0.05$ indicates statistical significance. Finally, we visualized the common DEGs by using ClueGO (a plug-in for Cytoscape that uses the Kappa statistical analysis method) to display the interactive gene network map and analyze the function of the target gene set.

PPI network analysis, machine learning, and the identification of hub genes

The STRING database (https://string-db.org/) (92) was utilized to filter and construct PPI networks based on confidence values greater than 0.40. Machine learning is used to predict the interactions of PPI networks, specifically using the k-means algorithm (network is clustered to a specified number of clusters; number of clusters: 3) for clustering. K-means is an effective unsupervised machine learning approach for predicting protein pairings that interact without prior data labeling (93, 94). We construct and visualize PPI network data using The Cytoscape platform (95), then analyze PPI molecular networks using The MCODE (a Added to abbreviations Cytoscape plug-in). The cytoHubba tool was utilized to find hub genes, analyze each gene using the maximum centrality (MCC) algorithm, rank these genes, and filter the top 10 hub genes.

Metascape and GeneMANIA enrichment analyses of hub genes

Metascape (https://metascape.org/gp/index.html#/main/step1) is a statistical approach that can use all genes in the input genome as an enrichment background. Genes are grouped into clusters using terms with a *P*-value of 0.01, a minimum count of 3, and an enrichment factor > 1.5 to look for enrichment pathways and related functional annotations of target genes. In addition, terms with a similarity of greater than 0.30 were connected point to point by the Cytoscape visual network program to generate a network diagram that further illustrates the relationships between terms. GeneMANIA (http://www.genemania.org) is another website that integrates different databases and technologies to anticipate and identify the relevant activities of individual genes in hub genes and establish gene priority and linkages.

Identification of hub genes between RA, COVID-19, and SAB and functional enrichment analysis

The GeneCards database (https://www.genecards.org/) (96) was accessed and searched for "COVID-19" and "SARS-CoV-2" as keywords, and 4,778 and 4,055 related genes were found, respectively. There were 17, 28, and 25 SARS-CoV-2–associated genes from Ziegler et al. (97), Jain et al. (98), and Xiong et al. (99), respectively (Table 2). Finally, 5,103 related genes were obtained after summarizing these five parts of genes and removing duplicate data. Hub genes were obtained from the intersection of the top 10 hub genes and 5,103 SARS-CoV-2–related genes using the Venn Diagram package in R software. Finally, Metascape and GeneMANIA enrichment analyses of the hub gene were used.

Construction of TF-hub genes and miRNA-hub gene network

TF-hub gene and miRNAs-hub gene regulation networks were constructed utilizing NetworkAnalyst (https://www.networkanalyst.ca/) (100). We submitted the hub genes between RA, COVID-19, and SAB to NetworkAnalyst to acquire TFs from the ENCODE database and miRNA from miRTarBase v8.0 and TarBase v8.0 for hub genes. Cytoscape was used to display the networks of TF-hub genes and miRNA-hub genes.

TABLE 2 SARS-CoV-2–associated genes in the relevant reference.

Reference	Tissue (*Homo sapiens*)	Experiment type	Gene ID
Ziegler et al., 2020 (97)	Nasal polyps, lung lobe, ethmoid sinus surgical tissue, ileum	Array	STAT1,IFI6,IFNAR1, IFNGR2,GBP2,IFITM1,TRIM27, NT5DC1, ARL6IP1,TMPRSS2, ACE2, TRIM28, APOA1, FABP6, ENPEP, FI35, XAF1
Jain et al., 2020 (98)	Nasopharyngeal swabs	Array	IFI44,IFIT1,IFIT1B, IFIH1,IL6, IL10, IL11, IL19, IL3RA,IL21RA,IL18R1,CXCL5, CXCL12, CCL2, CCL4, CXCL10,CSF2, TNFSF11, TNFRSF11B, BMP2, BMP7, PDGFA,C4BPA, CCR6, CCR22, CCR25, SERPINE1, SERPINF2
Xiong et al., 2020 (99)	Peripheral blood mononuclear cells, bronchoalveolar lavage fluid	Array	CXCL1, CXCL2, CXCL6, CXCL8,CXCL10, CXCL10/IP-10,CCL2/MCP-1,CCL3/MIP-1A, CCL4/MIP1B, IL 33, IL18, IL10,TNFSF10, TIMP1, C5, AREG, NRG1, ADA2, HK1, GAT1,PGD, PLA2G15, CTSD, GAA, LAIR1

Validation of hub genes and identification of hub genes

The datasets GSE17755, GSE55235, and GSE13670 were included in our study as validation sets to strengthen the reliability and correctness of the results. The genes from the three validation sets were also individually processed using the limma R package to generate the volcano map of the corresponding DEGs. The hub genes were identified using the Venn Diagram tool, and the expression of the hub genes in each dataset was visualized using a box plot. The subject Receiver Operating Characteristic Curve (ROC) was then used to estimate the test's effect to determine the hub gene's sensitivity and specificity in various datasets (101). A value of 0.7 was regarded as diagnostically significant.

Analysis of immune cell infiltration and correlation analysis between immune cells

The CIBERSORT algorithm (http://CIBERSORT.stanford.edu/) is a method based on linear support vector regression (102). It was applied to evaluate the composition and quantity of immune cells in RA and HC. $P < 0.05$ prompted us to submit the data to CIBERSORT and receive the immune cell infiltration matrix. The ggplot2 package was used to display the distribution of LM22, whereas the corrplot package was utilized to display its correlation. Finally, we used Pearson's correlation coefficient analysis to reveal the relationship between the expression of target genes and the abundance of immune cells in RA to find immune cells associated with the target genes. The Github page for this study is HTTPS(https://github.com/zheng5862/IFI44).

Results

Identification of DEGs

The flowchart shows all our study's key and important procedures (Figure 1). A total of 338 DEGs were obtained from the GSE93272 dataset, of which 322 were upregulated genes and 16 were downregulated genes. In addition, 3,174 DEGs were obtained from the GSE33341 dataset, of which 1,429 were upregulated genes and 1,745 were downregulated genes. The distribution of DEGs for the two datasets was visualized using a volcano plot (Figure 2) and clustered heat map analysis (Figure 3). The analysis results of these two datasets were intersected using the Venn Diagram package to obtain a total of 199 DEGs (Figure 4A). The 199 DEGs had 192 upregulated genes in GSE93272, seven downregulated genes in GSE33341, 188 upregulated genes in GSE33341, and 11 downregulated genes in GSE33341. The distribution of the 199 DEGs in the microarray datasets GSE93272 and GSE33341, respectively, can be seen using the clustered heat map (Figures 4B,C).

Functional enrichment analyses of DEGs

The GO and KEGG methods were used to explore the functional correlation between the 199 DEGs sets of RA and SAB. From the GO analysis, it is clear that BP is mainly manifested in immune system process, immune response, defense response, immune effector process, innate immune response, response to biotic stimulus, response to other organisms, response to external biotic stimulus, defense response to other organism, and response to a virus (Figure 5A). CC is mainly enriched in the cytosol and cytosolic part (Figure 5B). MF mainly manifests in oxidoreductase activity, cytochrome-oxidase activity, pantetheine hydrolase activity, and immunoglobulin receptor activity (Figure 5C). The KEGG analysis shows the main enrichment in the NOD-like receptor signaling pathway, influenza A, oxidative phosphorylation, Epstein–Barr virus infection, and cytosolic DNA-sensing pathway (Figure 5D). From the ClueGO analysis, it can be visualized that the main enrichment is in the following pathways. First, regulation of innate immune responses includes IFN-I production, regulation of IFN-I production, regulation of IFN-I–mediated signaling pathway, IFN-I signaling pathway, IFN-α/β production,

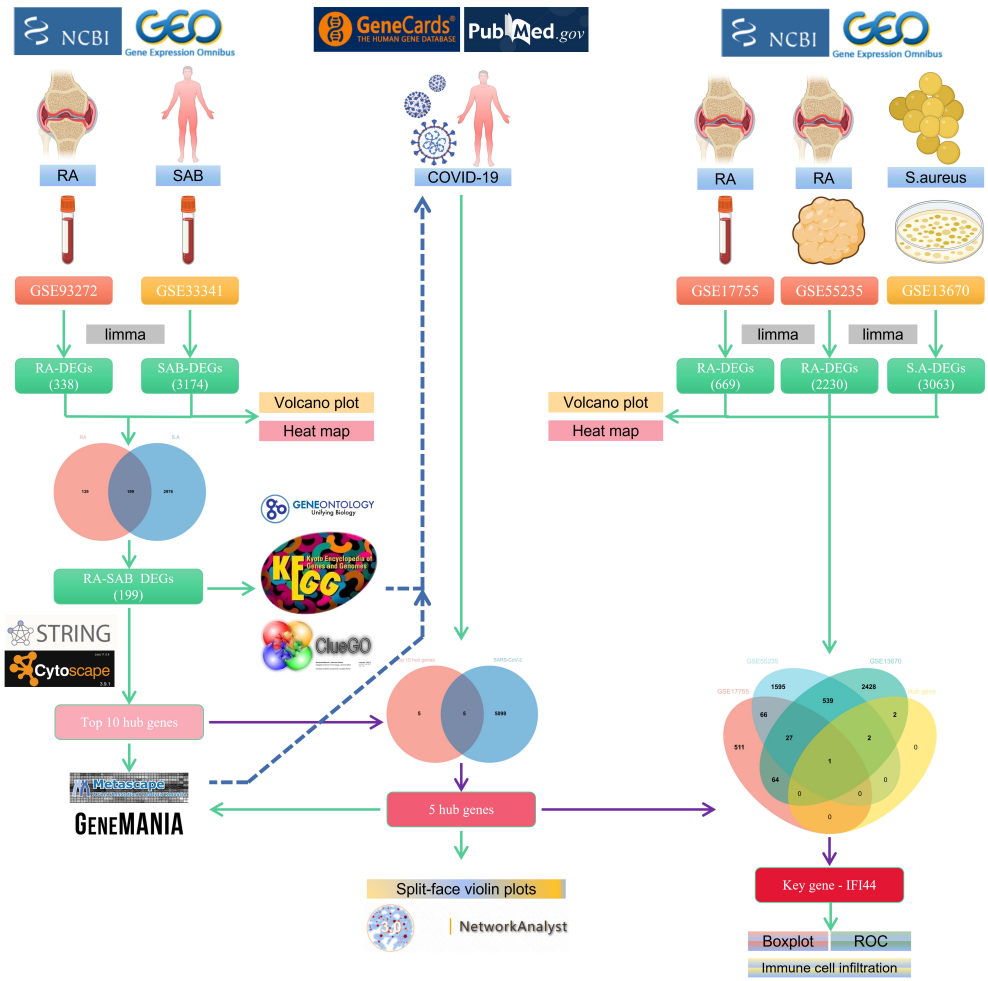

FIGURE 1
The schematic block diagram of the entire workflow of this study.

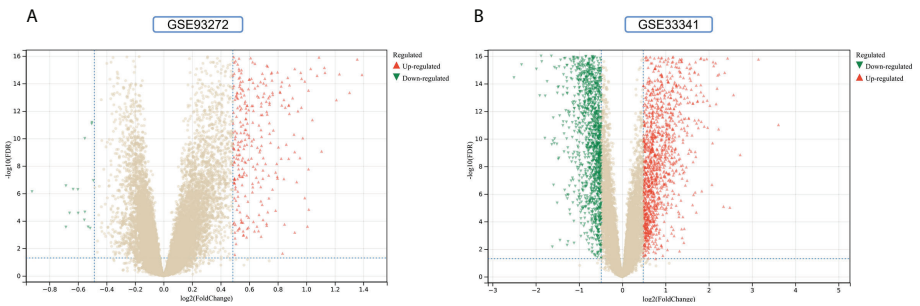

FIGURE 2
DEGs identification. **(A)** Gray dots represent genes not substantially differently expressed in RA and HC groups ($P > 0.05$), red triangles represent upregulated genes ($P < 0.05$), and green triangles represent downregulated genes ($P < 0.05$) in the GSE93272 dataset. **(B)** Gray dots represent genes not substantially differently expressed in *S. aureus* and HC groups ($P > 0.05$), red triangles represent upregulated genes ($P < 0.05$), and green triangles represent downregulated genes ($P < 0.05$) in the GSE33341 dataset.

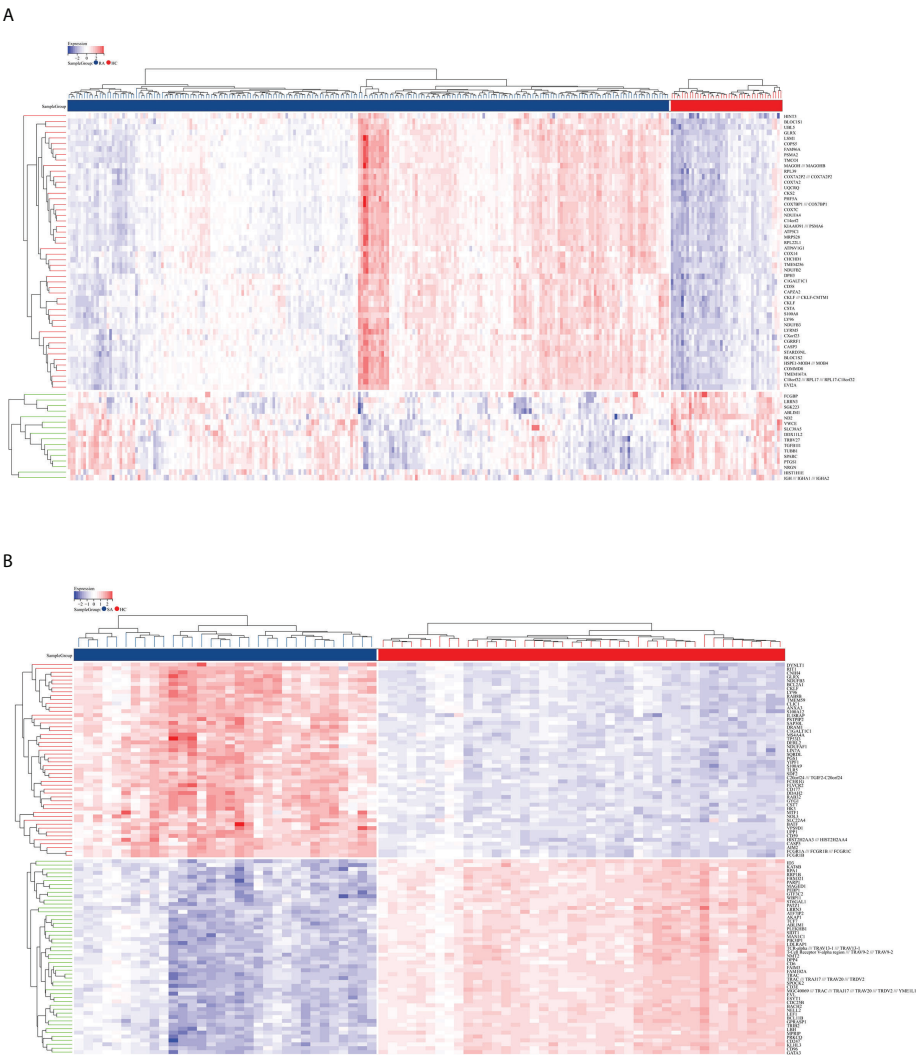

FIGURE 3
DEG distribution. **(A)** The clustering heat map shows the DEGs in the GSE93272 dataset. The RA group's samples are colored blue, whereas the HC group's samples are colored red. Red rectangles indicate elevated genes ($P < 0.05$), whereas blue rectangles indicate downregulated genes ($P < 0.05$). **(B)** The clustering heat map shows the intersection of DEGs in the GSE33341 dataset. The SA group's samples are colored blue, whereas the HC group's samples are colored red. Red rectangles indicate elevated genes ($P < 0.05$), whereas blue rectangles indicate downregulated genes ($P < 0.05$).

regulation IFN-α/β production, negative regulation of immune response, and negative regulation of innate immune response. Second, controlling viral infections involves regulating the viral replication process and immune, cellular, and defensive responses to a virus (Figure 5E).

PPI network, machine learning, and the identification of top 10 hub genes

PPI network data based on the STRING database were processed using Cytoscape software to further investigate the pathogenesis between RA and SAB. The results show that this PPI network has 184 nodes, 750 edges, an average node degree of 8.15, and an average local clustering coefficient of 0.461. The k-means cluster analysis graph based on the unsupervised machine learning algorithm of the PPI network can be seen: the green hexagon in the lower right corner is exactly the top 10 hub genes derived using the CytoHubba analysis method (Figure 6A). We then identified the top 10 genes in the enrichment ranking by the MCC algorithm of the CytoHubba package in Cytoscape software: RSAD2, IFIT3, GBP1, RTP4, IFI44, OAS1, IFI44L, ISG15, HERC5, and IFIT5 (Figure 6B), consistent with the PPI network using a k-means clustering algorithm to obtain the

10.3389/fimmu.2022.1013322

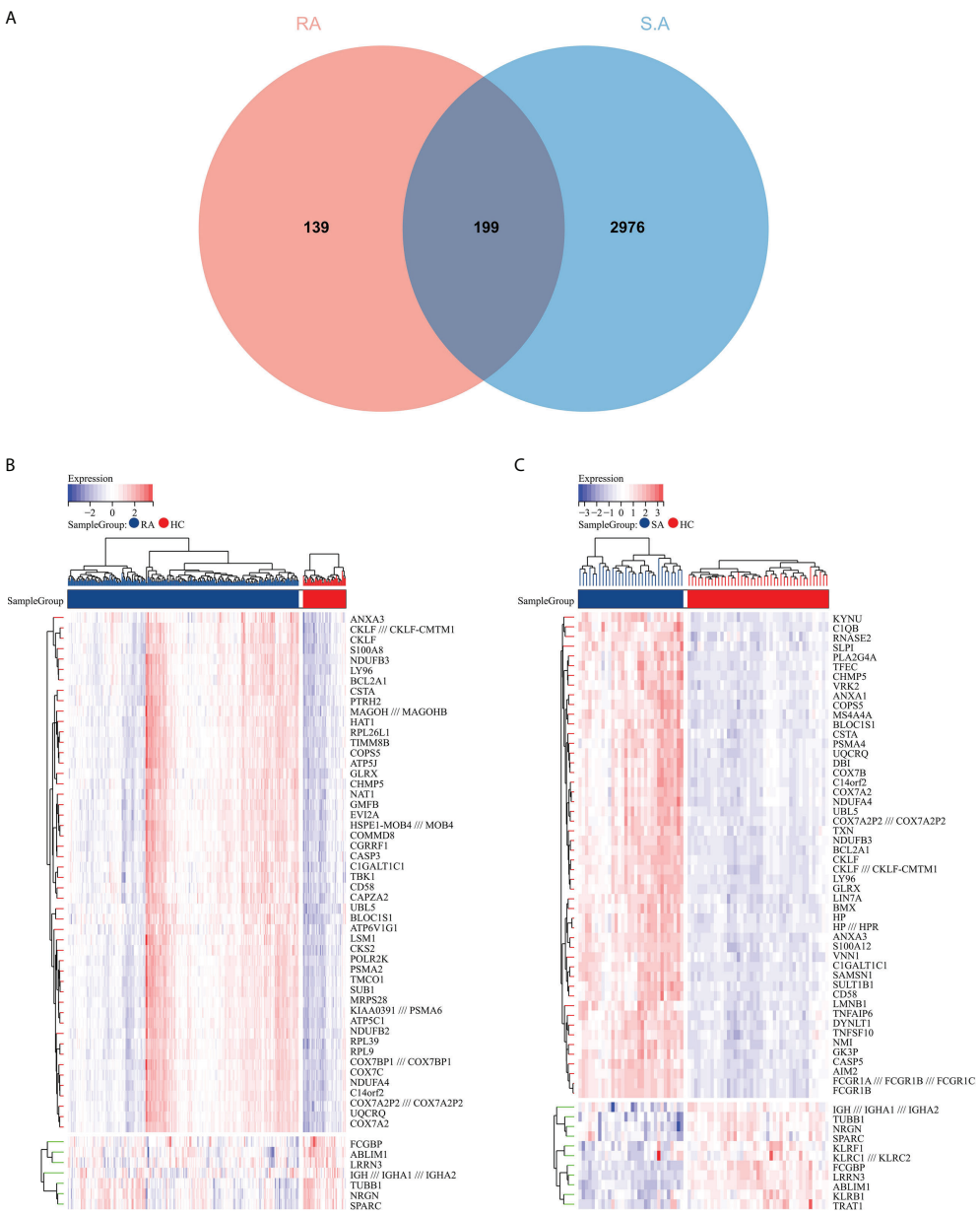

FIGURE 4
Common DEG screening. **(A)** Venn diagram on GSE93272 DEGs and GSE33341 DEGs. **(B)** Clustered heat map of common DEGs belonging to the RA group. **(C)** Clustered heat map of common DEGs in the SA group, with the RA/SA group colored blue and the HC group colored red. Red rectangles indicate elevated genes ($P < 0.05$), whereas blue rectangles indicate downregulated genes ($P < 0.05$).

same results. Tables 3, 4 give information about the top 10 hub genes in the GSE93272 and GSE33341 datasets, respectively.

Functional enrichment analyses of the top 10 hub genes

The top 10 hub genes were analyzed by the Metascape platform with the following findings. First, pathway and process enrichment analysis is mainly enriched in response to a virus, defense response to a virus, interferon (IFN) signaling, non-genomic actions of 1,25-dihydroxy vitamin D3, and cellular response to cytokine stimulus (Figure 7A). Second, DisGeNET[13] was mainly enriched in influenza A, bacterial infections, rhinovirus infections, and hepatitis C (chronic) (Figure 7B). Further network connection diagrams are used to visualize the connections between the pathways (Figure 7C). Finally,

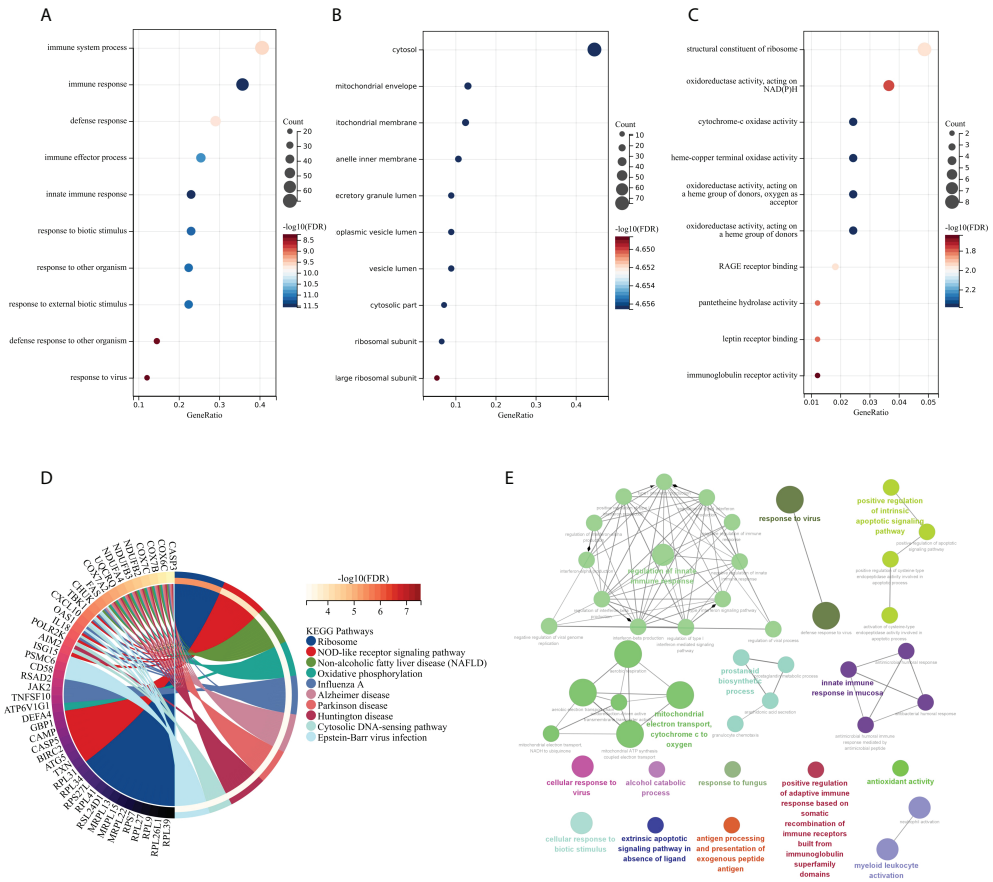

FIGURE 5
Functional enrichment analysis: GO, KEGG, and ClueGO analysis of DEGs. **(A)** BP gene enrichment of DEGs. **(B)** CC gene enrichment of DEGs. **(C)** MF gene enrichment of DEGs. **(D)** Analysis of DEGs using KEGG. **(E)** Analysis of DEGs using ClueGO.

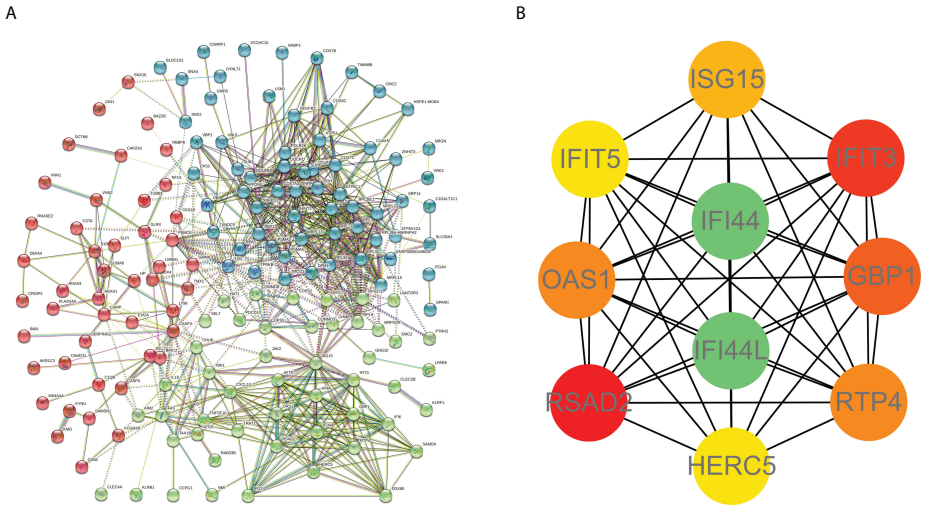

FIGURE 6
PPI interworking networks. **(A)** PPI network with 184 nodes and 750 edges. The green hexagon in the lower right corner is the top 10 hub genes derived using the CytoHubba analysis method. **(B)** Analysis of the top 10 hub genes with CytoHubba of Cytoscape.

TABLE 3 Information of the top 10 hub genes in GSE93272.

Gene ID	AveExpr	Log2FC(β)	P-Value
IFI44L	8.904949446	0.918840944	1.35×10^{-4}
ISG15	10.63569449	0.665205667	1.02×10^{-4}
OAS1	8.99533725	0.593634568	5.15×10^{-5}
RSAD2	9.132164541	1.008119022	4.29×10^{-5}
GBP1	8.752490808	0.489189707	2.69×10^{-5}
HERC5	9.587406065	0.69666656	1.19×10^{-5}
IFI44	7.849963939	1.017400799	1.66×10^{-6}
RTP4	7.814543847	0.590690331	3.71×10^{-7}
IFIT3	10.88045227	0.681499851	3.43×10^{-7}
IFIT5	8.712338631	0.698362888	1.02×10^{-10}

GeneMANIA was used to visualize the link between the 10 core genes and the most closely related genes (Figure 7D).

Identification of the hub genes between RA, COVID-19, and SAB and functional enrichment analysis

The genes associated with SARS-CoV-2 were selected from the Genecard database and related literature, and 5,103 genes were obtained after summarizing and removing duplicate data. The top 10 hub genes intersected with the SARS-CoV-2 gene set with five genes: IFI44, OAS1, IFI44L, ISG15, and HERC5 (Figure 8A). The expression of these five genes in the GSE93272 and GSE33341 datasets was analyzed using split-face violin plots, and it can be seen that the expression of all five genes in the RA and SAB datasets was significantly higher than that in the control group ($P < 0.01$) (Figures 8B, C). The functional enrichment analysis results using the Metascape platform are as follows. First, pathway and process enrichment analysis is mainly enriched in response to a virus, defense response to a virus, and response to a bacterium (Figure 9A). Second, DisGeNET[13] was mainly enriched in bacterial infections (Figure 9B). Further network connection diagrams are utilized to more precisely depict the links between the channels (Figure 9C). Finally, GeneMANIA was utilized to illustrate the relationship between the five hub genes and their closest relatives (Figure 9D).

Analyses of the network of TF-hub genes and miRNA-hub genes

The TF of five hub genes was predicted using the ENCODE database and the NetworkAnalyst web tool. The miRNAs of five hub genes were analyzed using the miRTarBase v8.0 package and the TarBase v8.0 package of the NetworkAnalyst web tool to build the networks of TF-hub genes and miRNA-hub genes, respectively. The TF-hub gene network includes three seeds, 81 edges, and 81 nodes (Figure 10A), and the simplified minimum network includes three seeds, four edges, and five nodes (Figure 10B). YY1 has the potential to regulate ISG15 and IFI44, and SIN3A and ZNF580 have the potential to regulate ISG15 and HERC5. The network structure of miRNA-hub genes analyzed using the miRTarBase v8.0 package includes four seeds, 26 edges, and 26 nodes (Figure 10C). The simplified minimum network includes four seeds, six edges, and six nodes (Figure 10D). The network structure of miRNA-hub genes analyzed by the TarBase v8.0 package includes five seeds, 188 edges, and 94 nodes (Figure 10E). The simplified minimum network includes five seeds, 16 edges, and 10 nodes (Figure 10F). The intersection of these two miRNA-hub gene networks could reveal that hsa-mir-1-3p and hsa-mir-146a-5p may play an important role in the expression of IFI44.

Validation of hub genes

To improve the reliability and reproducibility of the results, we used the datasets GSE17755, GSE55235, and GSE13670 for

TABLE 4 SARS-CoV-2-associated genes in the relevant reference.

Reference	Tissue(Homo sapiens)	Experiment type	Gene ID
Ziegler et al., 2020 (97)	Nasal polyps,Lung lobe,ethmoid sinus surgical tissue, Ileum	Array	STAT1,IFI6,IFNAR1, IFNGR2,GBP2,IFITM1,TRIM27, NT5DC1, ARL6IP1,TMPRSS2, ACE2, TRIM28, APOA1, FABP6, ENPEP, FI35, XAF1
Jain et al., 2020 (98)	Nasopharyngeal swabs	Array	IFI44,IFIT1,IFIT1B, IFIH1,IL6, IL10, IL11, IL19, IL3RA,IL21RA,IL18R1,CXCL5, CXCL12, CCL2, CCL4, CXCL10,CSF2, TNFSF11, TNFRSF11B, BMP2, BMP7, PDGFA,C4BPA, CCR6, CCR22, CCR25, SERPINE1, SERPINF2
Xiong et al., 2020 (99)	Peripheral blood mononuclear cells,Bronchoalveolar lavage fluid	Array	CXCL1, CXCL2, CXCL6, CXCL8,CXCL10, CXCL10/IP-10,CCL2/MCP-1,CCL3/MIP-1A, CCL4/MIP1B,IL 33, IL18, IL10,TNFSF10, TIMP1, C5, AREG, NRG1, ADA2, HK1, GAT1,PGD, PLA2G15, CTSD, GAA, LAIR1

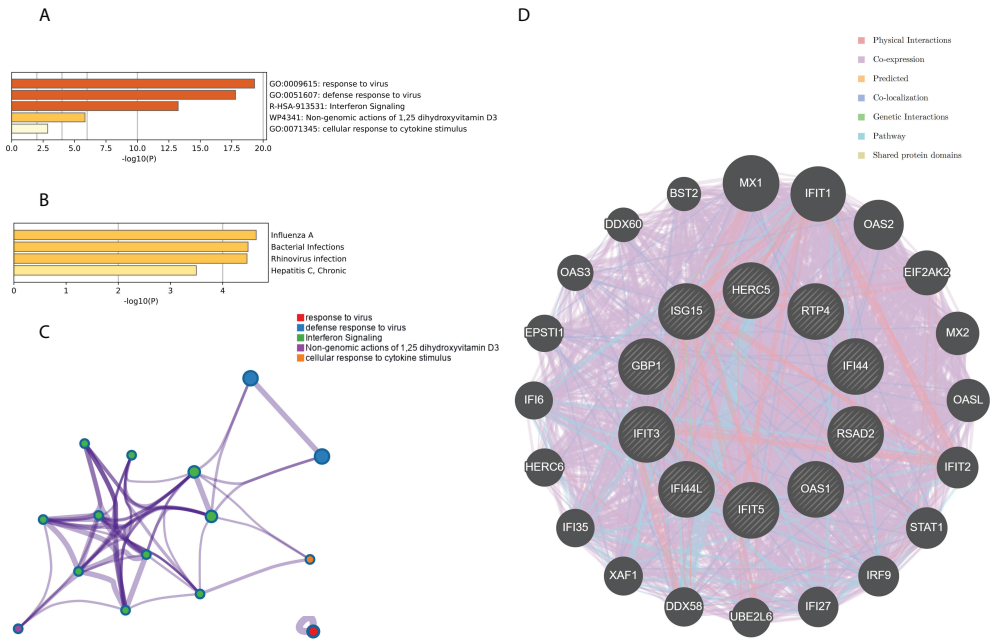

FIGURE 7
Functional enrichment analysis: Metascape and GeneMANIA of top 10 hub genes. **(A)** Pathway and process richness analysis of the Metascape platform. **(B)** Summary of enrichment analysis of DisGeNET [13] on Metascape platform. **(C)** The network is visualized using Cytoscape [5], colored by cluster IDs, and nodes sharing the same cluster ID are usually close to each other. **(D)** The gene–gene interaction network of the top 10 hub genes with the 20 most adjacent genes was analyzed using the GeneMANIA database. Each node represents a gene. The color of the linkage of the nodes represents the linkage between the corresponding genes.

validation. A total of 669 DEGs were obtained from the GSE17755 dataset, of which 471 were upregulated genes and 198 were downregulated genes. In addition, 2,230 DEGs were obtained from the GSE55235 dataset, of which 1,279 were upregulated genes and 951 were downregulated genes. A total of 3063 DEGs were obtained from the GSE13670 dataset, of which 1,100 upregulated genes and 1,963 downregulated genes were used. The distribution of DEGs in these three datasets was visualized using a volcano map, respectively (Figures 11A–C). The Venn diagram of five hub genes with the three validation sets of DEGs shows that IFI44 is the only intersection result (Figure 11D). IFI44 was highly expressed in all three validation sets ($P < 0.01$) (Figures 12A–C). Finally, the diagnostic validity of IFI44 as a biomarker was verified by ROC curves, which showed that the AUC values of IFI44 on the datasets GSE17755, GSE55235, and GSE13670 were 0.96 (95% CI, 0.95–0.96), 0.90 (95% CI, 0.77–1.00), and 0.79 (95% CI, 0.59–0.98). All had high sensitivity and high specificity (Figures 12D–F).

Immune infiltration analysis

We mapped 22 immune cell proportions in RA samples using CIBERSORT (Figure 13A) and then analyzed the differences in immune cell infiltration between RA and HC using box plots (Figure 13B). The results indicated that RA enriched four types of immune cells: B-cell memory, T-cell gamma delta, activated dendritic cells (DCs), and neutrophils ($P < 0.05$). Further correlation matrix analysis revealed that activated DCs were positively correlated with B-cell memory and T-cell gamma delta and negatively correlated with neutrophils ($P < 0.05$) (Figure 13C). Finally, we revealed the relationship between the expression of IFI44 and the abundance of immune cells in RA by Pearson's correlation coefficient analysis (Figure 13D), which showed that only activated DCs were closely and positively correlated with IFI44 ($R = 0.68$, $P = 3.7e\text{-}39$), and activated DCs were highly enriched in RA. Thus, IFI44 may be involved in RA progression by regulating immune cell infiltration, and activated DCs may play an important role in this regard.

Discussion

In this study, a total of 199 DEGs were obtained using a dataset of whole blood samples from RA and SAB (GSE93272 and GSE33341), and they were found to be closely associated with positive/negative regulation of the immune system and regulation of the IFN-I (IFN-α/β) pathway and related pathways of the immune system response to a virus by KEGG, GO, and

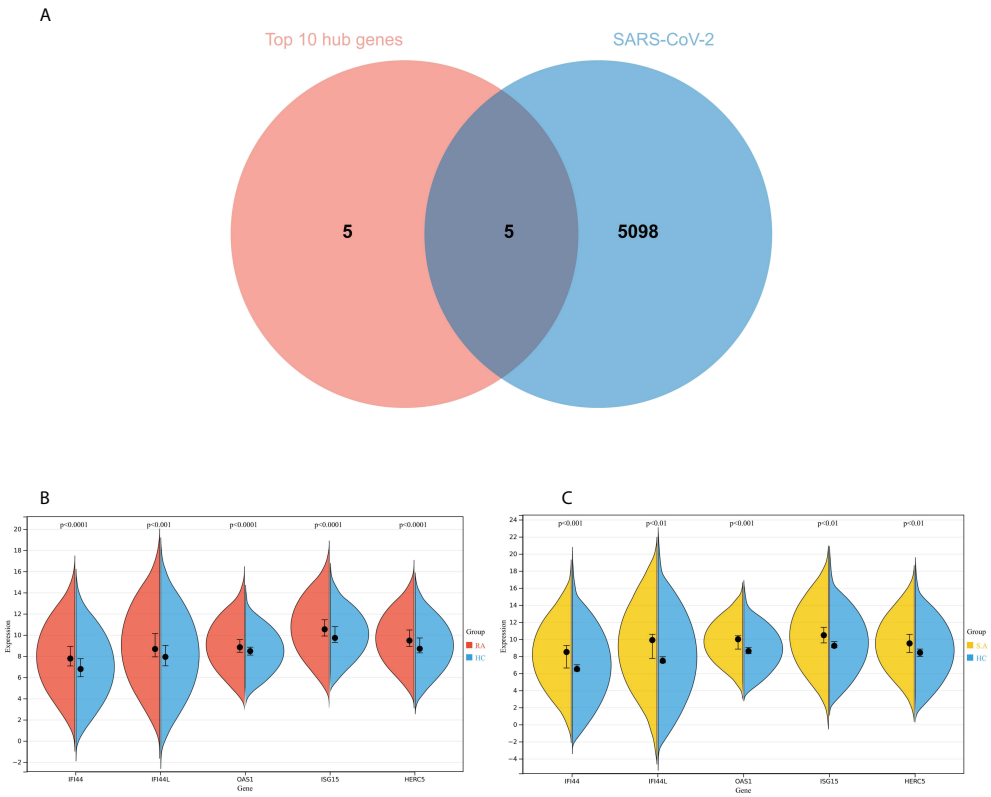

FIGURE 8
Identification of the hub gene between RA, COVID-19, and SAB. **(A)** Venn diagram of the top 10 hub genes and the SARS-CoV-2 gene set. **(B, C)** The expression of IFI44, OAS1, IFI44L, ISG15, and HERC5 in the GSE93272 and GSE33341 datasets was analyzed using split-face violin plots. Red indicates the RA group, yellow indicates the *S. aureus* group, and blue indicates the HC group.

ClueGO analyses. Ten hub genes were obtained using the PPI network and Cytoscape platform: RSAD2, IFIT3, GBP1, RTP4, IFI44, OAS1, IFI44L, ISG15, HERC5, and IFIT5, which were analyzed by Metascape platform and found to be associated with IFN signaling regulation and immune system response to viral infection and bacterial infection and were closely related. Five hub genes shared by RA, COVID-19, and SAB were IFI44, OAS1, IFI44L, ISG15, and HERC5, and they were found to be closely associated with the immune system response to viral infection and bacterial infection using Metascape analysis. TF-hub gene network and miRNA-hub gene network was constructed for these five hub genes, and one important TF (YY1) and two important miRNAs (hsa-mir-1-3p and hsa-mir-146a-5p) associated with IFI44 were obtained. To verify the reliability and comprehensiveness of the results, not only whole blood samples from RA (GSE17755) but also synovial tissue samples from RA (GSE55235) and blood samples from *S. aureus*-infected human mononuclear cells (GSE13670) were used to validate a core gene, which was obtained as IFI44. IFI44 was highly expressed in all five datasets, and its test efficacy was verified using ROC. Immune infiltration analysis reveals that the immune cells closely associated with IFI44 are activated DCs, which may play a significant connection between RA, SARS-CoV-2, and *S. aureus* infection. The pathway enrichment analysis revealed that 1,25-dihydroxy vitamin D3 might be an effective therapeutic agent for RA's SARS-CoV-2 and *S. aureus* infections.

Association of this study with The IFN-ISG pathways

IFNs are a family of cytokines having pleiotropic effects in humans (103, 104)—first recognized by Isaacs and Lindenmann in 1957 (105, 106) and characterized as antiviral inhibitors (107, 108). After more than 50 years of research by biologists, it was discovered that IFN is an essential regulator of the body's immune system (109), which plays a crucial role not only in viral infections (110–112) but also in bacterial infections (113, 114) and autoimmune illnesses (115, 116). There are three types of IFNs: IFN-I (IFN-α, β, ϵ, κ, and ω), IFN-II (IFN-γ), and IFN-

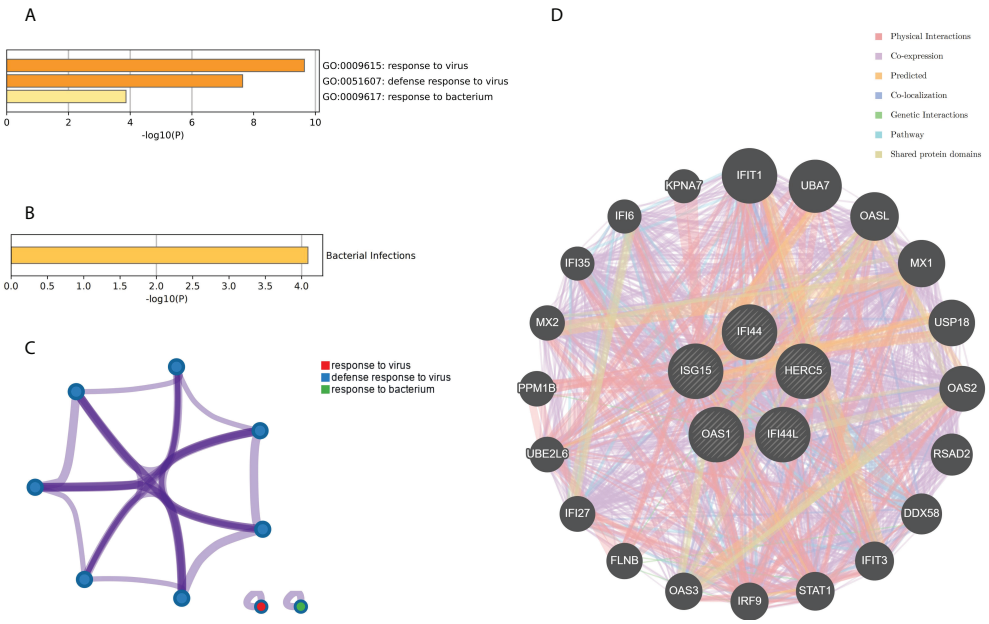

FIGURE 9
Functional enrichment analysis: Metascape and GeneMANIA of five hub genes. **(A)** Pathway and process richness analysis of the Metascape platform. **(B)** Summary of enrichment analysis of DisGeNET [13] on Metascape platform. **(C)** The network is visualized using Cytoscape [5], colored by cluster IDs, and nodes sharing the same cluster ID are usually close to each other. **(D)** The gene–gene interaction network of the five hub genes with the 20 most adjacent genes was analyzed using the GeneMANIA database. Each node represents a gene. The color of the linkage of the nodes represents the linkage between the corresponding genes.

III (IFN-λ), with IFN signaling through the Janus kinase (JAK)/STAT pathway (117).

Pattern recognition receptors (PRRs) recognize pathogen-associated molecular patterns (PAMPs) (118–120) and can activate transcription factors like IRF-3 and IRF-7, as well as the NF-κB pathway of B cells (121–124). NOD-like receptors are among the important PRRs that initiate the IFN pathway. TBK-1 and IKKε phosphorylate IRF-3 and IRF-7 to stimulate the transcription of IFN and proinflammatory genes (125, 126), with STING serving as the upstream signaling molecule that recruits TBK-1 and IKK (127). cGAS is an important cytosolic DNA sensing that can induce IFN formation by generating the cGAMP pathway that activates STING to form the cGAS-STING pathway (128–130). Activation of the cGAS-STING pathway is a double-edged sword that plays not only a crucial function in fighting viruses (131, 132) and bacteria (133, 134) but also an aberrant activation of cGAS by its DNA, which can provoke autoimmune disorders (135). The NOD-like receptor signaling pathway, oxidative phosphorylation, and cytosolic DNA sensing in the KEGG pathway of the intersecting genes of RA and SAB in this study are reflected in the IFN pathway. In cells that are not activated by the signal, NF-κB is prevented in the cytoplasm by IκBs, and only when IκBs are phosphorylated and hydrolyzed by proteases does NF-κB migrate to the nucleus to induce the production of IFN and proinflammatory genes (136, 137). IKK is responsible for the phosphorylation of IκBs, and it consists of two kinase subunits (IKKα and IKKβ) and one regulatory subunit (IKKγ) (138, 139). Notably, FKBP5 activates IKKε (140), interacts with the three subunits of IKK, and promotes IKK synthesis, leading to phosphorylation of IκBs, activation of NF-κB, and its migration into the nucleus, which eventually initiates the IFN signaling pathway (141, 142).

The receptor that binds IFN-I is composed of IFNAR1 and IFNAR2 subunits (143–145), whereas the receptor that binds IFN-III is composed of IFNLR1 and IL-10R subunits (146–148). By interacting with the receptor, IFN activates JAK1 and tyrosine kinase 2 (TYK2) (149–151). Activated JAK1 and TYK2 phosphorylate and activate STAT1 and STAT2 (152–154), whereas active STAT1 and STAT2 recruit and bind IRF-9 to form ISGF3 (155, 156). The ISGF3 complex can move from the cytoplasm to the nucleus and bind to the ISRE region in the ISG promoter, thereby beginning ISG transcription (143, 157, 158). ISGs influence cell activation and death in addition to viral aspects (159), and the antiviral, antiproliferative, and immunological stress actions of ISGs allow cells and organisms to survive (160). Although IFN-I and IFN-III produce ISGs through the same mechanism, the IFN-I pathway can induce ISG expression earlier, more swiftly, and more efficiently (157, 161), and IFN-I has been the subject of most studies, triggering the production of more than 300 ISGs (162). In this study,

10.3389/fimmu.2022.1013322

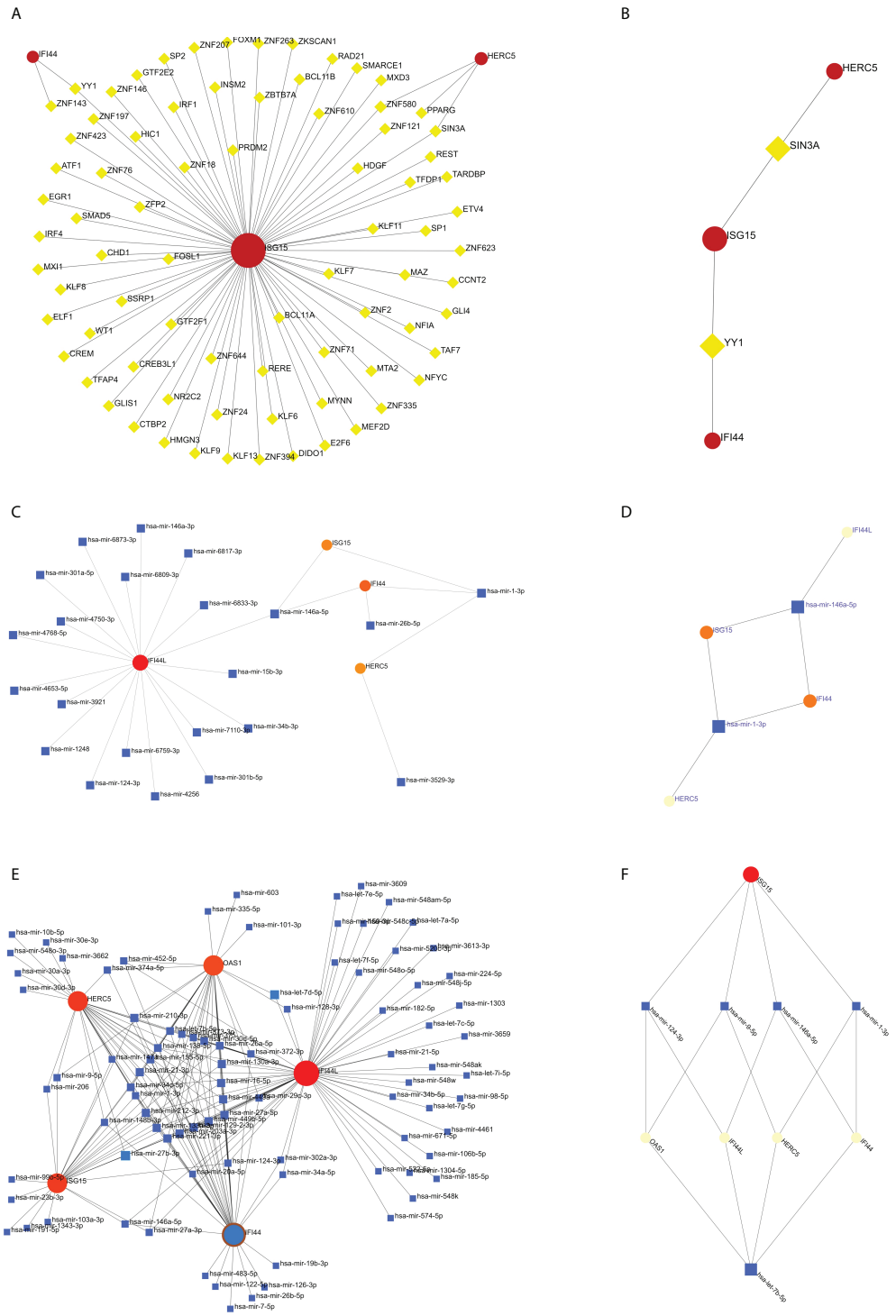

FIGURE 10
Construction of TF-hub gene and miRNA-hub gene network using NetworkAnalyst. **(A, B)** TF-hub gene network and simplified diagram. Red circles are genes, and yellow squares are TF. **(C, D)** miRNA-hub gene network (miRTarBase v8.0) and simplified diagram. **(E, F)** miRNA-hub gene network (TarBase v8.0) and simplified diagram. Circles are genes, and squares are miRNAs.

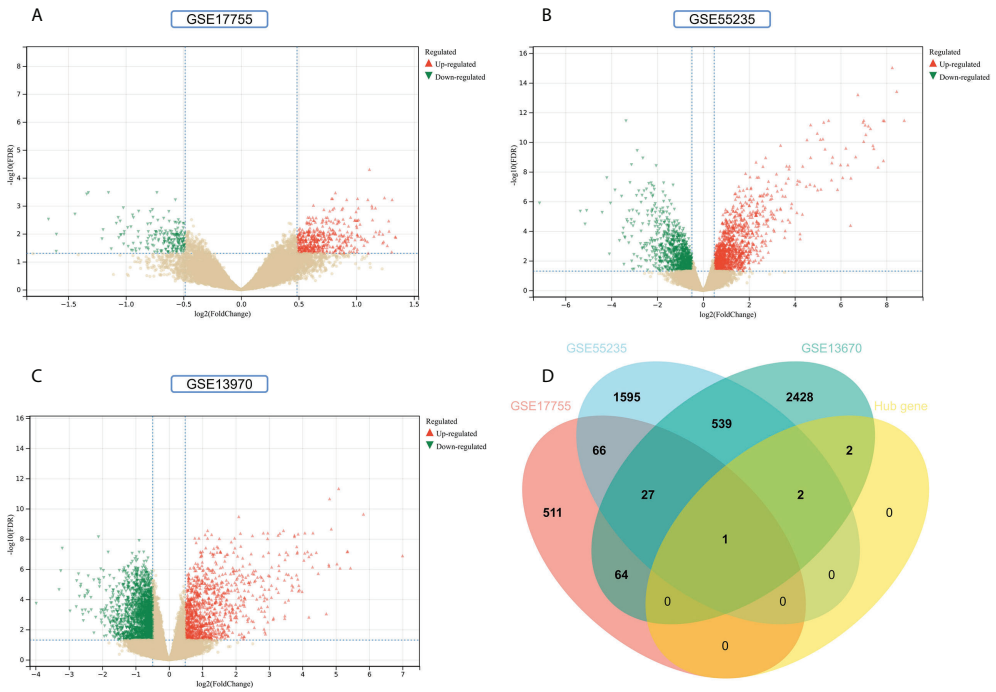

FIGURE 11
Screening for key genes. **(A, B)** Gray dots represent genes not substantially differently expressed in RA and HC groups ($P > 0.05$), red triangles represent upregulated genes ($P < 0.05$), and green triangles represent downregulated genes ($P < 0.05$) in GSE17755 and GSE55235 datasets. **(C)** Gray dots represent genes not substantially differently expressed in *S. aureus* and HC groups ($P > 0.05$), red triangles represent upregulated genes (P < 0.05), and green triangles represent downregulated genes ($P < 0.05$) in the GSE13670 dataset. **(D)** The Venn diagram of five hub genes with the three validation sets of DEGs.

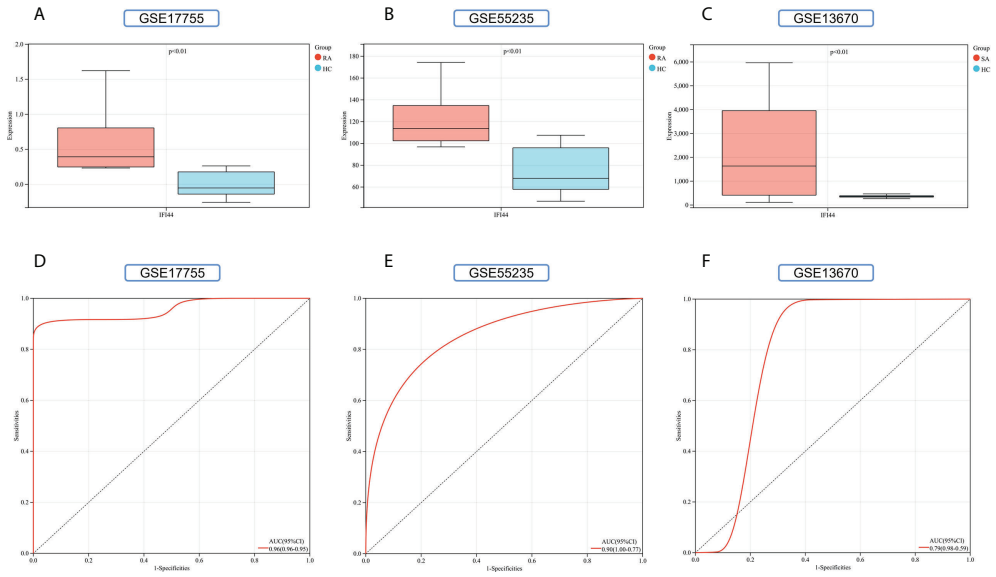

FIGURE 12
Validation of key genes. **(A–C)** The expression of IFI44 in GSE17755, GSE55235, and GSE13670. Red for RA/*S. aureus* group, and cyan for HC group. **(D–F)** The AUC of the ROC curve verifies the diagnostic validity of IFI44 in GSE17755, GSE55235, and GSE13670 ($P < 0.05$).

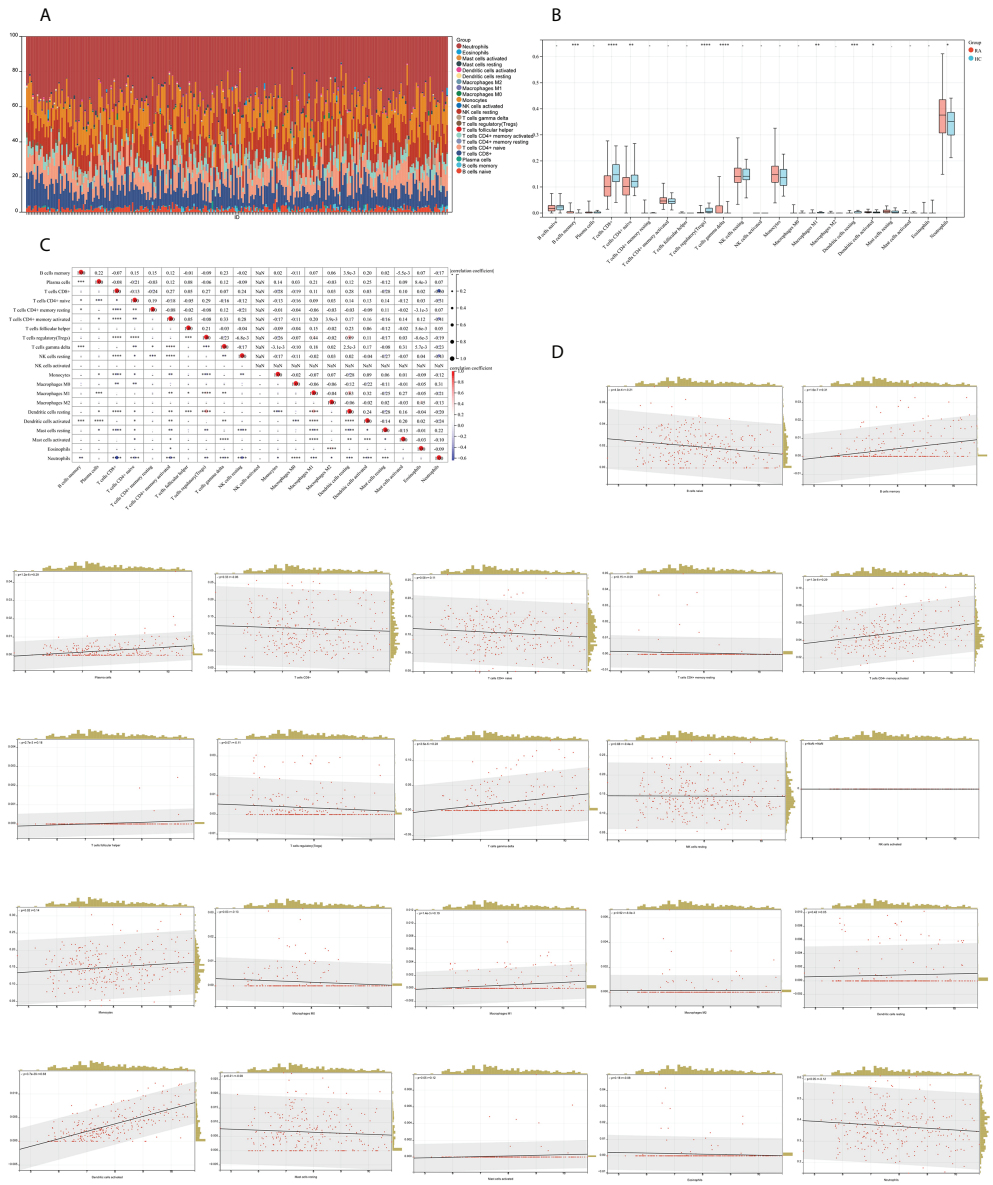

FIGURE 13
Analysis of immune cell infiltration. **(A)** A histogram of the proportion of LM22 in RA samples is depicted using the CIBERSORT algorithm, with the horizontal coordinate representing the sample and the vertical coordinate representing the percentage of individual immune cells. **(B)** Comparison of immune infiltrating cells between the RA and HC groups; red represents RA and cyan represents HC. **(C)** Correlation matrix between immune cells within the RA group. The horizontal and vertical coordinates are LM22, with red representing positive correlations and blue representing negative correlations (*$P < 0.05$, ** $P < 0.01$, and *** $P < 0.001$). **(D)** Correlation analysis between the expression of IFI44 and LM22.

ClueGO was used to analyze the intersectional gene enrichment pathways of RA and SAB in IFN-I production, regulation of IFN-I production, regulation of IFN-I–mediated signaling pathway, IFN-I signaling pathway, IFN-α/β production, regulation IFN-α/β production, negative regulation of immune response, negative regulation of innate immune response, regulation of viral replication process, response to a virus, defense response to viruses, and cellular response to a virus, which is reflected in the IFN-I pathway.

IFN, ISG, and IFI44 in RA

On the basis of the findings of this study, a portion of the route of the top 10 hub genes of RA and SAB was enriched in

IFN signaling and cellular response to cytokine stimulus; therefore, the association between RA and the IFN signaling pathway piqued our interest. Studies have shown that enhanced autoimmune responses can be detected in the presence of disease treated with IFN-α (163) and that 34% of patients have elevated rheumatoid factors (164), and that IFN-α treatment can contribute to the progression of RA (165, 166). In addition, the use of IFN-β1 in the treatment of MS promotes the development of RA (167). In contrast, TNF, a key driver of RA, enhances mtDNA release and initiates a cGAS/STING-dependent IFN response in inflammatory arthritis (168), and prolonged TNF therapy induces the creation of high quantities of IFN-I *via* a mechanism that stimulates IRF1 and IRF3 (169, 170). It has also been shown that significant amounts of IFN-I can be discovered in the peripheral blood of both patients with preclinical and clinical RA (115) and the synovial fluid of patients with RA (171). In reality, it dates back to 1979, when it was discovered that IFN levels were elevated in individuals with AID and positively linked with the disease's activity (172). The possible reason for this is that PAMPs are recognized by PRRs that produce IFN-I. These PRRs include TLR, RLR, and cGAS receptors that can sense nucleic acids (173, 174).

Interestingly, these PRRs can recognize viral nucleic acids and their nucleic acids to trigger AID (175). RA is one of the most common AIDs, and IFN-I plays an important role in contributing to the development of RA (115, 176). Furthermore, IFN-I can be used as an RA biomarker and a predictor of disease progression in patients with RA (177). Recent investigations have identified a significant expression of IFN-I–induced ISGs in the peripheral blood of patients with RA (176), and this elevated expression of ISGs induced by the IFN-I signaling pathway is referred to as the IFN signature of RA (178). In peripheral blood (179, 180) and synovial fluid of patients with RA (171, 176), elevated amounts of ISGs were found. Although patients with RA correlate unequally with IFN-I and ISGs (181), IFN-I and ISGs play a role in RA susceptibility (177), and thus, IFN and ISGs are considered biomarkers and disease targets for RA (179, 182, 183).

In combating pathogenic infections, many ISGs act directly on the signaling pathways of the pathogen's life cycle to inhibit its proliferation (158, 184). However, in RA, the excessive innate immune response and signaling dysregulation produce large amounts of IFNs that damage the organism (185). IFN desensitization is, therefore, of particular importance (158). The first aspect is cell intrinsic, which reduces signaling by blocking the JAK-STAT pathway *via* endocytosis and turnover of IFN receptors (186–189). The second aspect is that, during the immune response, some ISGs function as negative feedback regulators to maintain cellular homeostasis (158, 190, 191), and some ISGs can act as inhibitory proteins to reduce IFN pathway transduction (192). Common ISGs with negative regulatory functions include SOCS and USP18. Increased SOCS protein levels decrease the sensitivity of the JAK-STAT system, whose mechanism of action is to suppress JAK activity by binding to IFN receptors and tyrosine residues on JAK, thus preventing STAT-1 activation (193). By binding to the IFN-I receptor, USP18 can also prevent JAK activation and induce IFN-I desensitization (194). In addition, it was reported for the first time in 2019 that IFI44 also functions as a negative regulator of the IFN signaling pathway and that IFN-α treatment induces high expression of IFI44 (195) and also triggers the development of RA (196), which corresponds to our study's finding of high expression of IFI44 in patients with RA.

IFI44 is one of the IFN-I–induced ISGs (197, 198), which was initially found in hepatitis C virus–associated microtubule aggregation protein isolation (199). Therefore, we also observed hepatitis C (chronic) pathway enrichment in the top 10 hub genes of RA versus SAB. IFI44, with the assistance of FKBP5, is capable of exhibiting the two actions listed below. First, IFI44 significantly decreases the kinase activity of IKKβ, which inhibits the phosphorylation of IκBs, which, in turn, limits NF-κB activation and restricts its migration into the nucleus (200). Second, IFI44 can reduce the kinase activity of IKKε, resulting in the inhibition of IRF-3 phosphorylation (125), the restriction of STAT1 phosphorylation, and the reduction of ISG production (153). The reason for the high expression of IFI44 in patients with RA is that the high expression of IFNs and ISGs in patients with RA leads to an increase in the expression of IFI44 as an ISG, and it is the negative feedback regulation of IFI44 that makes its expression significantly higher than that of the healthy population. In the results of this study, a portion of the pathways of the top 10 hub genes of RA and SAB were enriched in immune responses to viral and bacterial infections. A portion of the pathways of the top five hub genes of RA, SAB, and COVID-19 was also enriched in immune responses to viral and bacterial infections. Therefore, we followed this thought regarding the IFN pathway and continued exploring the relationship between RA, SAB, and COVID-19.

Crosstalk between RA and SAB in terms of IFN, ISG, and IFI44

The average life expectancy of the RA population is reported to be shortened by 8 to 15 years, with infections, cardiovascular disease, and kidney disease being the three leading reasons (201–203). *S. aureus* seems inseparable from the topic of infection in patients with RA, as studies from the 1950s indicate that patients with RA are at a significantly increased risk of infection with *S. aureus* (201) and that invasion of patients with RA by *S. aureus* can result in severe deep bone and joint infections, as well as high rates of disability and mortality (47, 204). IFN-I has a

crucial role in bacterial invasion of the host (205, 206), which can be both useful and damaging to the organism (207, 208), depending on the type of invading bacteria and the organism's regulatory mechanisms (113, 209). IFN-I generated by *S. aureus* exacerbates the recruitment of leukocytes and the release of inflammatory cytokines, with detrimental effects on the organism (210–212). Because RA is an autoimmune disease capable of producing large levels of cytokines such as IFNs and ISGs, the relationship between RA and SAB *via* the IFN-I pathway can be described as follows.

On the one hand, the following points are of interest from the perspective of IFN-I–positive signaling. First, the TLR9 receptor identifies the DNA of *S. aureus*, causing DCs to produce IFN-I (213). Second, *S. aureus* detects TLR9-IRF1 *via* the Xr domain of SpA to activate the JAK-STAT pathway and NF-κB signaling pathway, resulting in the production of inflammatory cytokines such as TNF and IL-6, which promote inflammation and contribute to the progression of RA (211). Third, the autolysis process of *S. aureus* that produces peptidoglycan, among others, activates the NOD2/IRF5 pathway of DCs to mediate the IFN-I pathway, which enhances the virulence of *S. aureus* in the host to increase bacterial pathogenicity and also over-recruits neutrophils to promote inflammatory responses (210). Therefore, when patients with RA are infected with *S. aureus*, it leads to a severe proinflammatory response, probably because the superposition of the two proinflammatory mechanisms leads to an excessive inflammatory response and a severe imbalance in the immune system, followed by a collapse of the immune system, leading to a decrease in the body's defenses and further aggravating the *S. aureus* infection, thus creating a vicious circle. On the other hand, examining the issue from the standpoint of ISGs with a negative feedback regulatory effect on the IFN-I pathway yields the following conclusions. First, SOCS has a pro-bacterial effect because it makes it easier for *S. aureus* to invade an organism's defenses (214). SOCS not only inhibits the MYD88 molecule in macrophages to affect their antimicrobial effect (215, 216) but also inhibits the NF-κB pathway to reduce TNF release to act as an inhibitor of inflammation, thereby causing problems for host clearance of *S. aureus* (217), and an increase in phagocytosis and killing of *S. aureus* by the organism is observed when SOCS is inhibited (214). Second, USP18 can boost the susceptibility of *S. aureus* by negatively regulating the IFN-I pathway to reduce TNF-α signaling, and inhibition of USP18 can improve the body's bacterial infection status (218).

SOCS and USP18 proteins have been reported to promote bacterial infection, whereas few IFI44 proteins have been studied. In our study, IFI44 was found to be a key crosstalk gene between RA and SAB, and IFI44 is also an IFN-I–negative regulator, which can give a decrease in antimicrobial inflammatory factors by negatively regulating the NF-κB pathway and can also inhibit STAT1 activation from blocking the production of IFN-I and ISGs (195). Thus, IFI44 may also potentially promote RA susceptibility to *S. aureus*. Many studies have suggested that the IFN-I pathway acts as a paradoxical immune response during bacterial infection of the host (218), which may be due to the different focus of the IFN-I pathway on the different stages of bacterial infection. The high expression of IFI44 protein in patients with early RA facilitates further invasion of the organism by *S. aureus*, which is one of the reasons for *S. aureus* susceptibility, and the vicious cycle of immune imbalance in the organism resulting from the excessive IFN-I cascade response prompted by late RA and *S. aureus* stimulation is one of the reasons for the poor prognosis and high mortality. We, therefore, suggest that the negative regulation of the IFN-I pathway by IFI44 expression may be one of the mechanisms of immune escape from *S. aureus*. However, most of the functions of IFI44 are unknown, and further investigation of its mechanisms in bacterial infection is a direction of interest.

Crosstalk between RA, COVID-19, and SAB in terms of IFN, ISG, and IFI44

The coronavirus class is typically characterized by pandemic transmission and high pathogenicity; SARS-COV-2 is the ninth coronavirus identified as a severe threat to human health in 2019 (219–221). SARS-COV-2 is an enveloped virus of the genus *Betacoronavirus* with a positive-stranded single-stranded RNA genome of 26–32 kb in length (222–225). A virus is divided into four genera: α-, β-, δ-, and γ-CoV, characterized by high mutation rates and diverse recombination rates (226–229), and from 2019 to November 2021, the World Health Organization (WHO) has published Alpha (B.1.1.7), Beta (B.1.351), Gamma (P.1), Delta (B.1.617.2), and Omicron (B.1.1.529) for a total of five variants of concern (VOCs) (230). RA is associated with COVID-19 in the following points. On the one hand, SARS-CoV-2 can overstimulate the body's immune system and has the potential for antigenic cross-reactivity with the body to trigger the creation of autoantibodies (58, 60, 62). Thus, SARS-CoV-2 infection is considered a trigger for autoimmune disease and results in a worse prognosis (231–235). On the other hand, studies indicate that patients with rheumatic disorders are at a larger risk of SARS-COV-2 infection than the general population, with a worse prognosis and increased mortality (236, 237). In the COVID-19 Global Rheumatology Alliance (C19-GRA) Global Registry and other studies, the most common rheumatic disease among patients with COVID-19 was RA (238–241). Therefore, we prefer to propose that SARS-CoV-2 infection triggers the progression of RA, that patients with RA are more susceptible to SARS-CoV-2 infection, and that

the crosstalk between the two results in a vicious cycle of mutual disease progression that increases the risk of hospitalization and death (242–244), and that the crosstalk mechanism cannot be separated from the immune system and related inflammatory pathways (245).

In addition, COVID-19 combined/secondary *S. aureus* infection results in a considerable increase in mortality (246) primarily due to the following factors. First, patients with COVID-19 on admission had fewer coinfections with bacteria (3.5%) due to preventive administration of antibiotics, the most prevalent of which was *S. aureus* (81, 247–250). Second, in literature comprising 10 studies, a total of 132 bacterial species were reported as coinfections/secondary infections in patients with COVID-19 after admission, with *S. aureus* being the most common (n = 41.31%) (251). Third, according to a French study, 28% of critically ill COVID-19 patients admitted to the ICU had coinfections with bacteria, primarily *S. aureus* (252). We list a portion of the relevant literatures between RA, SAB, and COVID-19 (Table 5). In another bioinformatics investigation, *S. aureus* infection was shown to be the second highest in the KEGG analysis pathway enrichment order table for RA and COVID-19 (253), a result that was confirmed in our work, suggesting that there may be a connection between the IFN-I pathway in RA, COVID-19, and SAB.

IFN-I is among the most effective cytokines secreted by the organism against SARS-CoV-2 (254, 255). However, it is not always protective for the organism. In the late stage of COVID-19, the continual strong expression of IFN-I causes inflammatory damage to the immune system and many organs, increasing the organism's burden (256–258). It is undeniable that the IFN-I pathway had an important role in antagonizing the early stages of COVID-19 infection by secreting ISGs during the SARS-CoV-2 invasion (259, 260). However, the ISGs are not the only antiviral factors. Although most ISGs encode proteins capable of inhibiting different stages of the SARS-CoV-2 replication cycle (143, 261, 262), a few ISGs, including SOCS, USP18, and IFI44, can promote viral infection of the host (263–268). It was shown that silencing of IFI44 inhibits viral replication and overexpression of IFI44 promotes viral production due to negative regulation of the IFN-I pathway by IFI44 (195). Viruses mentioned in this study are not limited to SeV, LCMV, VSV, and IAV. Therefore, we suggest that the negative regulation of the IFN-I pathway by the expression of IFI44 may be one of the mechanisms of SARS-CoV-2 immune escape.

High expression of IFN-α in RA contributed to elevated levels of IFI44, promoted viral replication during the early stages of SARS-CoV-2 invasion, and increased susceptibility of *S. aureus*. Therefore, IFI44 may be an important target for the immune escape of SARS-CoV-2 and *S. aureus* infection in RA. Of course, we still need basic experiments and clinical trials to validate the results of our bioinformatics analysis.

$1,25(OH)_2VD_3$ may be an effective therapeutic agent in treating RA with SARS-CoV-2 and *S. aureus* infections

Finally, we also found that part of the pathway of the top 10 hub genes of RA and SAB was enriched in non-genomic actions of 1,25-dihydroxy vitamin D_3 and that IFI44 was positively correlated with DCs in an immune infiltration correlation analysis in RA. We put $1,25(OH)_2VD_3$ in series with RA, *S. aureus* infection, COVID-19, IFI44, and DCs (Figure 14). First, in RA, $1,25(OH)_2VD_3$ insufficiency is commonly reported among patients with RA (269–271). In a meta-analysis of 24 studies, $1,25(OH)_2VD_3$ was found to be inversely linked with RA disease activity (272), and the degree of deficiency was utilized as an indication of RA progression (273). Second, in SAB, $1,25(OH)_2VD_3$ was able to prevent the invasion of *S. aureus* by boosting the expression of mature macrophages, upregulating macrophage complement receptor immunoglobulin (CRIg), and encouraging macrophage phagocytosis (274, 275). Studies have

TABLE 5 Literature related to coinfection between RA, SAB, and COVID-19.

Reference	Disease	Coinfection	Conclusion
Dieperink et al., 2022 (31)	RA	*S. aureus*	RA is a high risk for SAB, and orthopedic implants increase the risk.
Joost et al., 2017 (47)	RA	*S. aureus*	Patients with RA exhibit a complex course of SAB and high mortality, and RA causes a significantly increased risk of leading to OAI.
Garcia-Vidal et al., 2021 (81)	COVID-19	*S. aureus*	Coinfection at COVID-19 diagnosis was mainly *S. aureus*.
Hughes et al., 2020 (82)	COVID-19	*S. aureus*	The most common co-infecting pathogen in early COVID-19 patients is *S. aureus*.
Conway et al., 2022 (236)	RA	SARS-CoV-2	Patients with RA have higher rates of SARS-CoV-2 infection and higher mortality.
Akiyama et al., 2021 (237)	RA	SARS-CoV-2	Patients with RA are at increased risk of contracting COVID-19.

10.3389/fimmu.2022.1013322

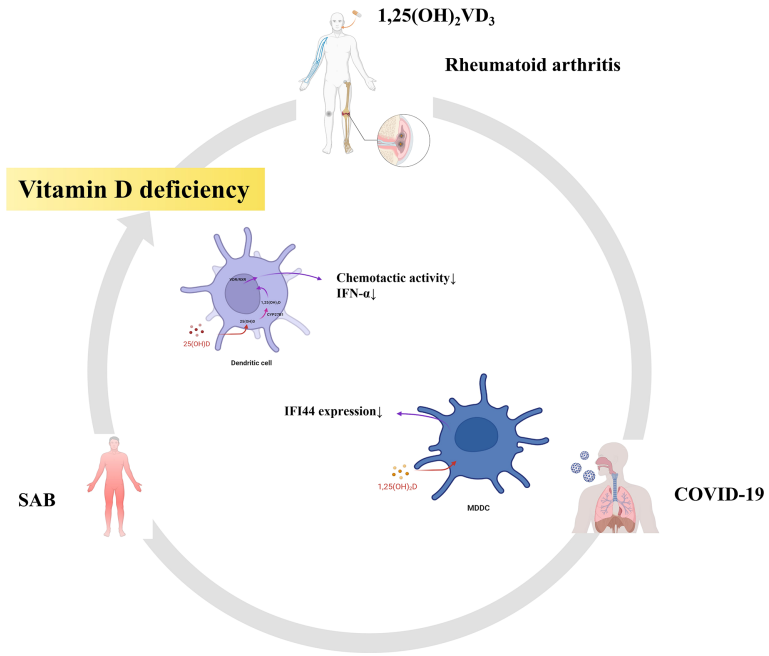

FIGURE 14
RA, SAB, and COVID-19 are often associated with vitamin D deficiency. This diagram shows that $1,25(OH)_2VD_3$ is the common target drug for RA, SAB, COVID-19, IFI44, and dendritic cells.

shown that $1,25(OH)_2VD_3$ levels are significantly lower in *S. aureus*-infected populations than in non–*S. aureus*–infected populations (276), and $1,25(OH)_2VD_3$ analogs reduce the incidence of PJI in *S. aureus* infections (277, 278). Third, in COVID-19, according to a study conducted in Israel, $1,25(OH)_2VD_3$ levels were adversely correlated with COVID-19 (279), and COVID-19 populations were frequently associated with vitamin D deficiency (280–282). $1,25(OH)_2VD_3$ insufficiency is positively associated with the severity and complications of COVID-19 and increases the chance of SARS-CoV-2 infection (283–286). The main reason for this is the ability to inhibit the cytokine storm and excessive inflammatory response in COVID-19 (287); thus, vitamin D can play a role in the prevention (288, 289), mitigation (285, 290), and treatment (291, 292) of COVID-19 (293). Fourth, in IFI44, the addition of $1,25(OH)_2VD_3$ to MDDCs in autoimmune diseases (SLE) resulted in a 34% reduction in IFI44 expression and the concentration of $1,25(OH)_2VD_3$ was negatively correlated with the activity of MDDCs in SLE (294). In our study, the expression of IFI44 was found to be positively correlated with DCs, so $1,25(OH)_2VD_3$ may also have some correlation with DCs. Fifth, in DCs, it was discovered that $1,25(OH)_2VD_3$ and its analogs inhibited DC chemotactic activity and IFN-α production, which decreased the expression of ISGs (295, 296). In addition, it has also been shown that DCs are potential target cells of $1,25(OH)_2VD_3$ for RA inhibition (297). Therefore, in this study, $1,25(OH)_2VD_3$ was found to be a drug target through the enrichment pathway of the shared genes of RA and SAB, and $1,25(OH)_2VD_3$ was found to be negatively associated with the expression of RA, COVID-19, SAB, IFI44, and the production and chemotactic activity of IFN-α in DCs from a new perspective.

Conclusions

In our present study, we screened the shared DEGs based on two datasets of RA (GSE93272) and SAB (GSE33341) and identified pathways associated with immunity and viral infection by multi-platform functional enrichment analysis. The following intersections were taken with the COVID-19 gene library to obtain hub genes, and functional enrichment analysis was performed to validate the pathway linkage of hub genes associated with RA, COVID-19, and SAB. The biomarker and disease target shared by RA, COVID-19, and SAB were validated and identified as IFI144 by GSE17755, GSE55235, and GSE13670 datasets. IFI44, a negative regulator of the IFN signaling pathway, promotes viral replication and bacterial proliferation and is an important molecular target for SARS-

CoV-2 and *S. aureus* immune escape in RA. DC activation was positively correlated with the expression of IFI44. 1,25(OH)$_2$VD$_3$ may be an important therapeutic agent in treating RA with SARS-CoV-2 and *S. aureus* infections. Our research can provide new directions for further analysis of its pathogenesis and targeted development of clinical treatments.

Data availability statement

The datasets presented in this study can be found in online repositories. The names of the repository/repositories and accession number(s) can be found in the article/supplementary material.

Author contributions

QZ analyzed and wrote the manuscript. DW designed the experiments and analyzed the data. WW devised the concept and supervised the study. All authors contributed to the article and approved the submitted version.

Acknowledgments

We acknowledge the GEO and Genecards databases for providing their platforms and contributors for uploading meaningful datasets.

Conflict of interest

The authors declare that the research was conducted in the absence of any commercial or financial relationships that could be construed as a potential conflict of interest.

Publisher's note

References

1. Lee DM, Weinblatt ME. Rheumatoid arthritis. *Lancet.* (2001) 358(9285):903–11. doi: 10.1016/S0140-6736(01)06075-5

2. Scott DL, Wolfe F, Huizinga TW. Rheumatoid arthritis. *Lancet.* (2010) 376 (9746):1094–108. doi: 10.1016/S0140-6736(10)60826-4

3. Smolen JS, Aletaha D, McInnes IB. Rheumatoid arthritis. *Lancet.* (2016) 388 (10055):2023–38. doi: 10.1016/S0140-6736(16)30173-8

4. McInnes IB, Schett G. The pathogenesis of rheumatoid arthritis. *N Engl J Med* (2011) 365(23):2205–19. doi: 10.1056/NEJMra1004965

5. Smolen JS, Aletaha D, Barton A, Burmester GR, Emery P, Firestein GS, et al. Rheumatoid arthritis. *Nat Rev Dis Primers.* (2018) 4:18001. doi: 10.1038/nrdp.2018.1

6. van der Woude D, van der Helm-van Mil AHM. Update on the epidemiology, risk factors, and disease outcomes of rheumatoid arthritis. *Best Pract Res Clin Rheumatol* (2018) 32:174–87. doi: 10.1016/j.berh.2018.10.005

7. McInnes IB, Schett G. Pathogenetic insights from the treatment of rheumatoid arthritis. *Lancet.* (2017) 389(10086):2328–37. doi: 10.1016/S0140-6736(17)31472-1

8. Choy E. Understanding the dynamics: pathways involved in the pathogenesis of rheumatoid arthritis. *Rheumatol (Oxford)* (2012) 51(Suppl 5):v3–11. doi: 10.1093/rheumatology/kes113

9. Liu L, Wong CW, Han M, Farhoodi HP, Liu G, Liu Y, et al. Meta-analysis of preclinical studies of mesenchymal stromal cells to treat rheumatoid arthritis. *EBioMedicine.* (2019) 47:47:563–577. doi: 10.1016/j.ebiom.2019.08.073

10. Cordtz RL, Hawley S, Prieto-Alhambra D, Højgaard P, Zobbe K, Overgaard S, et al. Incidence of hip and knee replacement in patients with rheumatoid arthritis following the introduction of biological DMARDs: an interrupted time-series analysis using nationwide Danish healthcare registers. *Ann Rheum Dis* (2018) 77 (5):684–9. doi: 10.1136/annrheumdis-2017-212424

11. Firestein GS, McInnes IB. Immunopathogenesis of rheumatoid arthritis. *Immunity* (2017) 46:183–96. doi: 10.1016/j.immuni.2017.02.006

12. Karami J, Aslani S, Jamshidi A, Garshasbi M, Mahmoudi M. Genetic implications in the pathogenesis of rheumatoid arthritis; an updated review. *Gene* (2019) 702:8–16. doi: 10.1016/j.gene.2019.03.033

13. Joo YB, Lim YH, Kim KJ, Park KS, Park YJ. Respiratory viral infections and the risk of rheumatoid arthritis. *Arthritis Res Ther* (2019) 21(1):199. doi: 10.1186/s13075-019-1977-9

14. Bartold PM, Marino V, Cantley M, Haynes DR. Effect of porphyromonas gingivalis-induced inflammation on the development of rheumatoid arthritis. *J Clin Periodontol* (2010) 37:405–11. doi: 10.1111/j.1600-051X.2010.01552.x

15. Puntis D, Malik S, Saravanan V, Rynne M, Heycock C, Hamilton J, et al. Urinary tract infections in patients with rheumatoid arthritis. *Clin Rheumatol* (2013) 32:355–60. doi: 10.1007/s10067-012-2129-7

16. Klatt T, Ouyang Q, Flad T, Koetter I, Bühring HJ, Kalbacher H, et al. Expansion of peripheral CD8+ CD28– T cells in response to Epstein-Barr virus in patients with rheumatoid arthritis. *J Rheumatol* (2005) 32:239–51.

17. Kawahito Y, Ichinose S, Sano H, Tsubouchi Y, Kohno M, Yoshikawa T, et al. Mycoplasma fermentans glycolipid-antigen as a pathogen of rheumatoid arthritis. *Biochem Biophys Res Commun* (2008) 369:561–6. doi: 10.1016/j.bbrc.2008.02.079

18. Hitchon CA, El-Gabalawy HS. Infection and rheumatoid arthritis: still an open question. *Curr Opin Rheumatol* (2011) 23(4):352–7. doi: 10.1097/BOR.0b013e3283477b7b

19. Rimoin DL, Wennberg JE, John E. Acute septic arthritis complicating chronic rheumatoid arthritis. *JAMA* (1966) 196:617–13. doi: 10.1001/jama.1966.03100200057018

20. Baum J. Infection in rheumatoid arthritis. *Arthritis Rheum* (1971) 14:135–7. doi: 10.1002/art.1780140119

21. McLean-Tooke A, Aldridge C, Waugh S, Spickett GP, Kay L. Methotrexate, rheumatoid arthritis and infection risk: what is the evidence? *Rheumatol (Oxford).* (2009) 48(8):867–71. doi: 10.1093/rheumatology/kep101

22. Singh JA, Furst DE, Bharat A, Curtis JR, Kavanaugh AF, Kremer JM, et al. Update of the 2008 American college of rheumatology recommendations for the use of disease-modifying antirheumatic drugs and biologic agents in the treatment of rheumatoid arthritis. *Arthritis Care Res (Hoboken)* (2012) 64(5):625–39. doi: 10.1002/acr.21641

23. Lahiri M, Dixon WG. Risk of infection with biologic antirheumatic therapies in patients with rheumatoid arthritis. *Best Pract Res Clin Rheumatol* (2015) 29:290–305. doi: 10.1016/j.berh.2015.05.009

24. Smolen JS, Landewe R, Breedveld FC, Buch M, Burmester G, Dougados M, et al. EULAR recommendations for the management of rheumatoid arthritis with synthetic and biological disease-modifying antirheumatic drugs: 2013 update. *Ann Rheum Dis* (2014) 73(3):492–509. doi: 10.1136/annrheumdis-2013-204573

25. Ramiro S, Sepriano A, Chatzidionysiou K, Nam JL, Smolen JS, van der Heijde D, et al. Safety of synthetic and biological DMARDs: a systematic literature review informing the 2016 update of the EULAR recommendations for management of rheumatoid arthritis. *Ann Rheum Dis* (2017) 76:1101–36. doi: 10.1136/annrheumdis-2016-210708

26. Singh JA, Cameron C, Noorbaloochi S, Cullis T, Tucker M, Christensen R, et al. Risk of serious infection in biological treatment of patients with rheumatoid arthritis: a systematic review and meta-analysis. *Lancet.* (2015) 386(9990):258–65. doi: 10.1016/S0140-6736(14)61704-9

27. Dixon WG. Rheumatoid arthritis: biological drugs and risk of infection. *Lancet.* (2015) 386(9990):224–5. doi: 10.1016/S0140-6736(14)61907-3

28. Bongartz T, Sutton AJ, Sweeting MJ, Buchan I, Matteson EL, Montori V. Anti-TNF antibody therapy in rheumatoid arthritis and the risk of serious infections and malignancies: systematic review and meta-analysis of rare harmful effects in randomized controlled trials. *JAMA: J Am Med Assoc* (2006) 295 (19):2275–85. doi: 10.1001/jama.295.19.2275

29. Arleevskaya MI, Larionova RV, Brooks WH, Bettacchioli E, Renaudineau Y. Toll-like receptors, infections, and rheumatoid arthritis. *Clin Rev Allergy Immunol* (2020) 58(2):172–81. doi: 10.1007/s12016-019-08742-z

30. Carty SM, Snowden N, Silman AJ. Should infection still be considered as the most likely triggering factor for rheumatoid arthritis? *J Rheumatol* (2003) 30 (3):425–9.

31. Dieperink SS, Glintborg B, Oestergaard LB, Nørgaard M, Benfield T, Mehnert F, et al. Risk of staphylococcus aureus bacteraemia in patients with rheumatoid arthritis and the effect of orthopaedic implants on the risk: a nationwide observational cohort study. *Scand J Rheumatol* (2022) 20:1–9. doi: 10.1080/03009742.2022.2049057

32. Lowy FD. Staphylococcus aureus infections. *N Engl J Med* (1998) 339 (8):520–32. doi: 10.1056/NEJM199808203390806

33. Foster TJ. Nasal colonization by staphylococcus aureus. *Nat Med* (2004) 10 (5):447. doi: 10.1038/nm0504-447a

34. Wertheim HF, Melles DC, Vos MC, van Leeuwen W, van Belkum A, Verbrugh HA, et al. The role of nasal carriage in staphylococcus aureus infections. *Lancet Infect Dis* (2005) 5:751–62. doi: 10.1016/S1473-3099(05)70295-4

35. Lowy FD. How staphylococcus aureus adapts to its host. *N Engl J Med* (2011) 364(21):1987–90. doi: 10.1056/NEJMp1100251

36. Naber CK. Staphylococcus aureus bacteremia: epidemiology, pathophysiology, and management strategies. *Clin Infect Dis* (2009) 48 Suppl 4: S231–7. doi: 10.1086/598189

37. von Eiff C, Becker K, Machka K, Stammer H, Peters G. Nasal carriage as a source of staphylococcus aureus bacteremia. study group. *N Engl J Med* (2001) 344 (1):11–6. doi: 10.1056/NEJM200101043440102

38. Hidron AI, Edwards JR, Patel J, Horan TC, Sievert DM, Pollock DA, et al. NHSN annual update: antimicrobial-resistant pathogens associated with healthcare-associated infections: annual summary of data reported to the national healthcare safety network at the centers for disease control and prevention, 2006–2007. *Infect Control Hosp Epidemiol* (2008) 29:996–1011. doi: 10.1086/591861

39. Lauderdale KJ, CL M, BR B, Morcuende J, Horswill AR. Biofilm dispersal of community-associated methicillin-resistant staphylococcus aureus on orthopedic implant material. *J Orthop Res* (2010) 28:55–61. doi: 10.1002/jor.20943

40. Magill SS, Hellinger W, Cohen J, Kay R, Bailey C, Boland B, et al. Prevalence of healthcare-associated infections in acute care hospitals in Jacksonville, Florida. *Infect Control Hosp Epidemiol* (2012) 33:283–91. doi: 10.1086/664048

41. Kapadia BH, Berg RA, Daley JA, Fritz J, Bhave A, Mont MA. Periprosthetic joint infection. *Lancet.* (2016) 387(10016):386–94. doi: 10.1016/S0140-6736(14) 61798-0

42. Melamed E, Cohen I, Robinson D. Prosthetic-joint infections. *N Engl J Med* (2005) 352(1):95–7.

43. Herwaldt LA. Staphylococcus aureus nasal carriage and surgical-site infections. *Surgery.* (2003) 134(5 Suppl):S2–9. doi: 10.1016/s0039-6060(03) 00390-8

44. Kluytmans J, van Belkum A, Verbrugh H. Nasal carriage of staphylococcus aureus: epidemiology, underlying mechanisms, and associated risks. *Clin Microbiol Rev* (1997) 10(3):505–20. doi: 10.1128/CMR.10.3.505

45. Tabarya D, Hoffman WL. Staphylococcus aureus nasal carriage in rheumatoid arthritis: antibody response to toxic shock syndrome toxin-1. *Ann Rheum Dis* (1996) 55(11):823–8. doi: 10.1136/ard.55.11.823

46. Goodman SM, Nocon AA, Selemon NA, Shopsin B, Fulmer Y, Decker ME, et al. Increased staphylococcus aureus nasal carriage rates in rheumatoid arthritis patients on biologic therapy. *J Arthroplasty.* (2019) 34(5):954–8. doi: 10.1016/j.arth.2019.01.025

47. Joost I, Kaasch A, Pausch C, Peyerl-Hoffmann G, Schneider C, Voll RE, et al. Staphylococcus aureus bacteremia in patients with rheumatoid arthritis - data from the prospective INSTINCT cohort. *J Infect* (2017) 74(6):575–84. doi: 10.1016/j.jinf.2017.03.003

48. Chen N, Zhou M, Dong X, Qu J, Gong F, Han Y, et al. Epidemiological and clinical characteristics of 99 cases of 2019 novel coronavirus pneumonia in wuhan, China: a descriptive study. *Lancet.* (2020) 395(10223):507–13. doi: 10.1016/S0140-6736(20)30211-7

49. Zhu N, Zhang D, Wang W, Li X, Yang B, Song J, et al. China Novel coronavirus investigating and research team. a novel coronavirus from patients with pneumonia in China, 2019. n. *Engl J Med* (2020) 382(8):727–33. doi: 10.1056/NEJMoa2001017

50. Huang C, Wang Y, Li X, Ren L, Zhao J, Hu Y, et al. Clinical features of patients infected with 2019 novel coronavirus in wuhan. *China. Lancet* (2020) 395 (10223):497–506. doi: 10.1016/S0140-6736(20)30183-5

51. Liang W, Guan W, Chen R, Wang W, Li J, Xu K, et al. Cancer patients in SARS-CoV-2 infection: a nationwide analysis in China. *Lancet Oncol* (2020) 21 (3):335–7. doi: 10.1016/S1470-2045(20)30096-6

52. Pollard CA, Morran MP, Nestor-Kalinoski AL. The COVID-19 pandemic: a global health crisis. *Physiol Genomics* (2020) 52(11):549–57. doi: 10.1152/physiolgenomics.00089.2020

53. Johns Hopkins Coronavirus Resource Center. *COVID-19 dashboard. JHU* (2021). Available at: https://coronavirus.jhu.edu/map.html.

54. Harrison AG, Lin T, Wang P. Mechanisms of SARS-CoV-2 transmission and pathogenesis. *Trends Immunol* (2020) 41(12):1100–15. doi: 10.1016/j.it.2020.10.004

55. Abd El-Aziz TM, Stockand JD. Recent progress and challenges in drug development against COVID-19 coronavirus (SARS-CoV-2) - an update on the status. *Infect Genet Evol* (2020) 83:104327. doi: 10.1016/j.meegid.2020.104327

56. Sohrabi C, Alsafi Z, O'Neill N, Khan M, Kerwan A, Al-Jabir A, et al. World health organization declares global emergency: A review of the 2019 novel coronavirus (COVID-19). *Int J Surg* (2020) 76:71–6. doi: 10.1016/j.ijsu.2020.02.034

57. Hu B, Guo H, Zhou P, Shi ZL. Characteristics of SARS-CoV-2 and COVID-19. *Nat Rev Microbiol* (2021) 19(3):141–54. doi: 10.1038/s41579-020-00459-7

58. Ruan Q, Yang K, Wang W, Jiang L, Song J. Clinical predictors of mortality due to COVID-19 based on an analysis of data of 150 patients from wuhan, China. *Intensive Care Med* (2020) 46(5):846–8. doi: 10.1007/s00134-020-05991-x

59. Dotan A, Muller S, Kanduc D, David P, Halpert G, Shoenfeld Y. The SARS-CoV-2 as an instrumental trigger of autoimmunity. *Autoimmun Rev* (2021) 20 (4):102792. doi: 10.1016/j.autrev.2021.102792

60. Vojdani A, Kharrazian D. Potential antigenic cross-reactivity between SARS-CoV-2 and human tissue with a possible link to an increase in autoimmune diseases. *Clin Immunol* (2020) 217:108480. doi: 10.1016/j.clim.2020.108480

61. Kim H, Byun JE, Yoon SR, Koohy H, Jung H, Choi I. SARS-CoV-2 peptides bind to NKG2D and increase NK cell activity. *Cell Immunol* (2022) 371:104454. doi: 10.1016/j.cellimm.2021.104454

62. Liu Y, Sawalha AH, Lu Q. COVID-19 and autoimmune diseases. *Curr Opin Rheumatol* (2021) 33(2):155–62. doi: 10.1097/BOR.0000000000000776

63. Zhong J, Shen G, Yang H, Huang A, Chen X, Dong L, et al. COVID-19 in patients with rheumatic disease in hubei province, China: a multicentre retrospective observational study. *Lancet Rheumatol* (2020) 2(9):e557–64. doi: 10.1016/S2665-9913(20)30227-7

64. Pablos JL, Galindo M, Carmona L, Lledó A, Retuerto M, Blanco R, et al. RIER investigators group; RIER investigators group. clinical outcomes of hospitalised patients with COVID-19 and chronic inflammatory and autoimmune rheumatic diseases: a multicentric matched cohort study. *Ann Rheum Dis* (2020) 79(12):1544–9. doi: 10.1136/annrheumdis-2020-218296

65. Raiker R, DeYoung C, Pakhchanian H, Ahmed S, Kavadichanda C, Gupta L, et al. Outcomes of COVID-19 in patients with rheumatoid arthritis: A multicenter research network study in the united states. *Semin Arthritis Rheumatol* (2021) 51 (5):1057–66. doi: 10.1016/j.semarthrit.2021.08.010

66. England BR, Roul P, Yang Y, Kalil AC, Michaud K, Thiele GM, et al. Risk of COVID-19 in rheumatoid arthritis: A national veterans affairs matched cohort study in At-risk individuals. *Arthritis Rheumatol* (2021) 73(12):2179–88. doi: 10.1002/art.41800

67. Paget C, Trottein F. Mechanisms of bacterial superinfection post-influenza: A role for unconventional T cells. *Front Immunol* (2019) 10:336. doi: 10.3389/fimmu.2019.00336

68. McArdle AJ, Turkova A, Cunnington AJ. When do co-infections matter? *Curr Opin Infect Dis* (2018) 31(3):209–15. doi: 10.1097/QCO.0000000000000447

69. Gupta RK, George R, Nguyen-Van-Tam JS. Bacterial pneumonia and pandemic influenza planning. *Emerg Infect Dis* (2008) 14(8):1187–92. doi: 10.3201/eid1408.070751

70. Metzger DW, Sun K. Immune dysfunction and bacterial coinfections following influenza. *J Immunol* (2013) 191(5):2047–52. doi: 10.4049/jimmunol.1301152

71. Jia L, Xie J, Zhao J, Cao D, Liang Y, Hou X, et al. Mechanisms of severe mortality-associated bacterial Co-infections following influenza virus infection. *Front Cell Infect Microbiol* (2017) 7:338. doi: 10.3389/fcimb.2017.00338

72. Quah J, Jiang B, Tan PC, Siau C, Tan TY. Impact of microbial aetiology on mortality in severe community-acquired pneumonia. *BMC Infect Dis* (2018) 18 (1):451. doi: 10.1186/s12879-018-3366-4

73. Katsurada N, Suzuki M, Aoshima M, Yaegashi M, Ishifuji T, Asoh N, et al. Adult pneumonia study group-japan. the impact of virus infections on pneumonia mortality is complex in adults: a prospective multicentre observational study. *BMC Infect Dis* (2017) 17(1):755. doi: 10.1186/s12879-017-2858-y

74. Beadling C, Slifka MK. How do viral infections predispose patients to bacterial infections? *Curr Opin Infect Dis* (2004) 17(3):185–91. doi: 10.1097/00001432-200406000-00003

75. Morens DM, Taubenberger JK, Fauci AS. Predominant role of bacterial pneumonia as a cause of death in pandemic influenza: implications for pandemic influenza preparedness. *J Infect Dis* (2008) 198(7):962–70. doi: 10.1086/591708

76. Rowe HM, Meliopoulos VA, Iverson A, Bomme P, Schultz-Cherry S, Rosch JW. Direct interactions with influenza promote bacterial adherence during respiratory infections. *Nat Microbiol* (2019) 4(8):1328–36. doi: 10.1038/s41564-019-0447-0

77. Mulcahy ME, McLoughlin RM. Staphylococcus aureus and influenza a virus: Partners in coinfection. *mBio*. (2016) 7(6):e02068–16. doi: 10.1128/mBio.02068-16

78. Sun K, Metzger DW. Influenza and staphylococcus aureus coinfection: TLR9 at play. *Trends Microbiol* (2019) 27(5):383–4. doi: 10.1016/j.tim.2019.02.006

79. Voiriot G, Visseaux B, Cohen J, Nguyen LB, Neuville M, Morbieu C, et al. Viral-bacterial coinfection affects the presentation and alters the prognosis of severe community-acquired pneumonia. *Crit Care* (2016) 20(1):375. doi: 10.1186/s13054-016-1517-9

80. Abelenda-Alonso G, Rombauts A, Gudiol C, Meije Y, Ortega L, Clemente M, et al. Influenza and bacterial coinfection in adults with community-acquired pneumonia admitted to conventional wards: Risk factors, clinical features, and outcomes. *Open Forum Infect Dis* (2020) 7(3):ofaa066. doi: 10.1093/ofid/ofaa066

81. Garcia-Vidal C, Sanjuan G, Moreno-García E, Puerta-Alcalde P, Garcia-Pouton N, Chumbita M, et al. COVID-19 researchers group. incidence of co-infections and superinfections in hospitalized patients with COVID-19: a retrospective cohort study. *Clin Microbiol Infect* (2021) 27(1):83–8. doi: 10.1016/j.cmi.2020.07.041

82. Hughes S, Troise O, Donaldson H, Mughal N, Moore LSP. Bacterial and fungal coinfection among hospitalized patients with COVID-19: a retrospective cohort study in a UK secondary-care setting. *Clin Microbiol Infect* (2020) 26 (10):1395–9. doi: 10.1016/j.cmi.2020.06.025

83. Tasaki S, Suzuki K, Kassai Y, Takeshita M, Murota A, Kondo Y, et al. Multi-omics monitoring of drug response in rheumatoid arthritis in pursuit of molecular remission. *Nat Commun* (2018) 9(1):2755. doi: 10.1038/s41467-018-05044-4

84. Ahn SH, Tsalik EL, Cyr DD, Zhang Y, van Velkinburgh JC, Langley RJ, et al. Gene expression-based classifiers identify staphylococcus aureus infection in mice and humans. *PloS One* (2013) 8(1):e48979. doi: 10.1371/journal.pone.0048979

85. Lee HM, Sugino H, Aoki C, Nishimoto N. Underexpression of mitochondrial-DNA encoded ATP synthesis-related genes and DNA repair genes in systemic lupus erythematosus. *Arthritis Res Ther* (2011) 13(2):R63. doi: 10.1186/ar3317

86. Woetzel D, Huber R, Kupfer P, Pohlers D, Pfaff M, Driesch D, et al. Identification of rheumatoid arthritis and osteoarthritis patients by transcriptome-based rule set generation. *Arthritis Res Ther* (2014) 16(2):R84. doi: 10.1186/ar4526

87. Koziel J, Maciag-Gudowska A, Mikolajczyk T, Bzowska M, Sturdevant DE, Whitney AR, et al. Phagocytosis of staphylococcus aureus by macrophages exerts cytoprotective effects manifested by the upregulation of antiapoptotic factors. *PloS One* (2009) 4(4):e5210. doi: 10.1371/journal.pone.0005210

88. Diboun I, Wernisch L, Orengo CA, Koltzenburg M. Microarray analysis after RNA amplification can detect pronounced differences in gene expression using limma. *BMC Genomics* (2006) 7:252. doi: 10.1186/1471-2164-7-252

89. Ritchie ME, Phipson B, Wu D, Hu Y, Law CW, Shi W, et al. Limma powers differential expression analyses for RNA-sequencing and microarray studies. *Nucleic Acids Res* (2015) 43(7):e47. doi: 10.1093/nar/gkv007

90. Huang da W, Sherman BT, Lempicki RA. Systematic and integrative analysis of large gene lists using DAVID bioinformatics resources. *Nat Protoc* (2009) 4:44–57. doi: 10.1038/nprot.2008.211

91. Yu G, Wang LG, Han Y, He QY. Clusterprofiler: An r package for comparing biological themes among gene clusters. *OMICS* (2012) 16(5):284–7. doi: 10.1089/omi.2011.0118

92. Szklarczyk D, Gable AL, Lyon D, Junge A, Wyder S, Huerta-Cepas J, et al. STRING v11: protein-protein association networks with increased coverage, supporting functional discovery in genome-wide experimental datasets. *Nucleic Acids Res* (2019) 47(D1):D607–13. doi: 10.1093/nar/gky1131

93. Sarkar D, Saha S. Machine-learning techniques for the prediction of protein-protein interactions. *J Biosci* (2019) 44(4):104. doi: 10.1007/s12038-019-9909-z

94. Choi J, Yun JS, Song H, Kim NH, Kim HS, Yook JI. Exploring the chemical space of protein-protein interaction inhibitors through machine learning. *Sci Rep* (2021) 11(1):13369. doi: 10.1038/s41598-021-92825-5

95. Shannon P, Markiel A, Ozier O, Baliga NS, Wang JT, Ramage D, et al. Cytoscape: a software environment for integrated models of biomolecular interaction networks. *Genome Res* (2003) 13:2498–504. doi: 10.1101/gr.1239303

96. Safran M, Dalah I, Alexander J, Rosen N, Iny Stein T, Shmoish M, et al. GeneCards version 3: the human gene integrator. *Database*. (2010) 2010:baq020. doi: 10.1093/database/baq020

97. Ziegler CG, Allon SJ, Nyquist SK, Mbano IM, Miao VN, Tzouanas CN, et al. SARS-CoV-2 receptor ACE2 is an interferon-stimulated gene in human airway epithelial cells and is detected in specific cell subsets across tissues. *Cell* (2020) 181:1016–35:e1019. doi: 10.1016/j.cell.2020.04.035

98. Jain R, Ramaswamy S, Harilal D, Uddin M, Loney T, Nowotny N, et al. Host transcriptomic profiling of COVID-19 patients with mild, moderate, and severe clinical outcomes. *Comput Struct Biotechnol J* (2021) 19:153–60. doi: 10.1016/j.csbj.2020.12.016

99. Xiong Y, Liu Y, Cao L, Wang D, Guo M, Jiang A, et al. Transcriptomic characteristics of bronchoalveolar lavage fluid and peripheral blood mononuclear cells in COVID-19 patients. *Emerg Microbes Infect* (2020) 9:761–70. doi: 10.1080/22221751.2020.1747363

100. Zhou G, Soufan O, Ewald J, Hancock REW, Basu N, Xia J. NetworkAnalyst 3.0: a visual analytics platform for comprehensive gene expression profiling and meta-analysis. *Nucleic Acids Res* (2019) 47(W1):W234–41. doi: 10.1093/nar/gkz240

101. Robin X, Turck N, Hainard A, Tiberti N, Lisacek F, Sanchez JC, et al. pROC: an open-source package for r and s+ to analyze and compare ROC curves. *BMC Bioinf* (2011) 12:77. doi: 10.1186/1471-2105-12-77

102. Chen B, Khodadoust MS, Liu CL, Newman AM, Alizadeh AA. Profiling tumor infiltrating immune cells with CIBERSORT. *Methods Mol Biol* (2018) 1711:243–59. doi: 10.1007/978-1-4939-7493-1_12

103. Maher SG, Romero-Weaver AL, Scarzello AJ, Gamero AM. Interferon: cellular executioner or white knight? *Curr Med Chem* (2007) 14(12):1279–89. doi: 10.2174/092986707780597907

104. Pestka S, Krause CD, Walter MR. Interferons, interferon-like cytokines, and their receptors. *Immunol Rev* (2004) 202:8–32. doi: 10.1111/j.0105-2896.2004.00204.x

105. Isaacs A, Lindenmann J. Virus interference. i. the interferon. *Proc R Soc Lond B Biol Sci* (1957) 147(927):258–67. doi: 10.1098/rspb.1957.0048

106. Isaacs A, Lindenmann J, Valentine RC. Virus interference. II. some properties of interferon. *Proc R Soc Lond B Biol Sci* (1957) 147:268–73. doi: 10.1098/rspb.1957.0049

107. Pestka S, Langer JA, Zoon KC, Samuel CE. Interferons and their actions. *Annu Rev Biochem* (1987) 56:727–77. doi: 10.1146/annurev.bi.56.070187.003455

108. Pestka S. Interferon from 1981 to 1986. *Methods Enzymol* (1986) 119:3–14. doi: 10.1016/0076-6879(86)19003-3

109. Duerr CU, Fritz JH. Editorial: Immunoregulatory mechanisms of interferon. *Front Immunol* (2020) 11:187. doi: 10.3389/fimmu.2020.00187

110. Interferon. *Lancet* (1970) 2(7681):1022–3.

111. Fensterl V, Chattopadhyay S, Sen GC. No love lost between viruses and interferons. *Annu Rev Virol* (2015) 2(1):549–72. doi: 10.1146/annurev-virology-100114-055249

112. Samuel CE. Antiviral actions of interferons. *Clin Microbiol Rev* (2001) 14 (4):778–809. doi: 10.1128/CMR.14.4.778-809.2001

113. Kovarik P, Castiglia V, Ivin M, Ebner F. Type I interferons in bacterial infections: A balancing act. *Front Immunol* (2016) 7:652. doi: 10.3389/fimmu.2016.00652

114. Perry AK, Chen G, Zheng D, Tang H, Cheng G. The host type I interferon response to viral and bacterial infections. *Cell Res* (2005) 15(6):407–22. doi: 10.1038/sj.cr.7290309

115. Barrat FJ, Crow MK, Ivashkiv LB. Interferon target-gene expression and epigenomic signatures in health and disease. *Nat Immunol* (2019) 20(12):1574–83. doi: 10.1038/s41590-019-0466-2

116. Wahren-Herlenius M, Dörner T. Immunopathogenic mechanisms of systemic autoimmune disease. *Lancet.* (2013) 382(9894):819–31. doi: 10.1016/S0140-6736(13)60954-X

117. Chow KT, Gale MJr. SnapShot: Interferon signaling. *Cell.* (2015) 163 (7):1808–1808.e1. doi: 10.1016/j.cell.2015.12.008

118. Takeuchi O, Akira S. Pattern recognition receptors and inflammation. *Cell.* (2010) 140(6):805–20. doi: 10.1016/j.cell.2010.01.022

119. Jensen S, Thomsen AR. Sensing of RNA viruses: a review of innate immune receptors involved in recognizing RNA virus invasion. *J Virol* (2012) 86(6):2900–10. doi: 10.1128/JVI.05738-11

120. Iwasaki A. A virological view of innate immune recognition. *Annu Rev Microbiol* (2012) 66:177–96. doi: 10.1146/annurev-micro-092611-150203

121. Yoneyama M, Suhara W, Fukuhara Y, Fukuda M, Nishida E, Fujita T. Direct triggering of the type I interferon system by virus infection: activation of a transcription factor complex containing IRF-3 and CBP/p300. *EMBO J* (1998) 17 (4):1087–95. doi: 10.1093/emboj/17.4.1087

122. Honda K, Yanai H, Negishi H, Asagiri M, Sato M, Mizutani T, et al. IRF-7 is the master regulator of type-I interferon-dependent immune responses. *Nature.* (2005) 434(7034):772–7. doi: 10.1038/nature03464

123. Honda K, Ohba Y, Yanai H, Negishi H, Mizutani T, Takaoka A, et al. Spatiotemporal regulation of MyD88-IRF-7 signalling for robust type-I interferon induction. *Nature.* (2005) 434(7036):1035–40. doi: 10.1038/nature03547

124. Visvanathan KV, Goodbourn S. Double-stranded RNA activates binding of NF-kappa b to an inducible element in the human beta-interferon promoter. *EMBO J* (1989) 8(4):1129–38. doi: 10.1002/j.1460-2075.1989.tb03483.x

125. Sharma S, tenOever BR, Grandvaux N, Zhou GP, Lin R, Hiscott J. Triggering the interferon antiviral response through an IKK-related pathway. *Science.* (2003) 300(5622):1148–51. doi: 10.1126/science.1081315

126. Fitzgerald KA, McWhirter SM, Faia KL, Rowe DC, Latz E, Golenbock DT, et al. IKKepsilon and TBK1 are essential components of the IRF3 signaling pathway. *Nat Immunol* (2003) 4(5):491–6. doi: 10.1038/ni921

127. Chen Q, Sun L, Chen ZJ. Regulation and function of the cGAS-STING pathway of cytosolic DNA sensing. *Nat Immunol* (2016) 17(10):1142–9. doi: 10.1038/ni.3558

128. Lio CW, McDonald B, Takahashi M, Dhanwani R, Sharma N, Huang J, et al. cGAS-STING signaling regulates initial innate control of cytomegalovirus infection. *J Virol* (2016) 90(17):7789–97. doi: 10.1128/JVI.01040-16

129. Zhang G, Chan B, Samarina N, Abere B, Weidner-Glunde M, Buch A, et al. Cytoplasmic isoforms of kaposi sarcoma herpesvirus LANA recruit and antagonize the innate immune DNA sensor cGAS. *Proc Natl Acad Sci U S A.* (2016) 113(8): E1034–43. doi: 10.1073/pnas.1516812113

130. Schoggins JW, MacDuff DA, Imanaka N, Gainey MD, Shrestha B, Eitson JL, et al. Pan-viral specificity of IFN-induced genes reveals new roles for cGAS in innate immunity. *Nature.* (2014) 505(7485):691–5. doi: 10.1038/nature12862

131. Li XD, Wu J, Gao D, Wang H, Sun L, Chen ZJ. Pivotal roles of cGAS-cGAMP signaling in antiviral defense and immune adjuvant effects. *Science.* (2013) 341(6152):1390–4. doi: 10.1126/science.1244040

132. Paijo J, Döring M, Spanier J, Grabski E, Nooruzzaman M, Schmidt T, et al. cGAS senses human cytomegalovirus and induces type I interferon responses in human monocyte-derived cells. *PloS Pathog* (2016) 12(4):e1005546. doi: 10.1371/journal.ppat.1005546

133. Watson RO, Bell SL, MacDuff DA, Kimmey JM, Diner EJ, Olivas J, et al. The cytosolic sensor cGAS detects mycobacterium tuberculosis DNA to induce type I interferons and activate autophagy. *Cell Host Microbe* (2015) 17(6):811–9. doi: 10.1016/j.chom.2015.05.004

134. Storek KM, Gertsvolf NA, Ohlson MB, Monack DM. cGAS and Ifi204 cooperate to produce type I IFNs in response to francisella infection. *J Immunol* (2015) 194(7):3236–45. doi: 10.4049/jimmunol.1402764

135. Crow YJ. Type I interferonopathies: mendelian type I interferon up-regulation. *Curr Opin Immunol* (2015) 32:7–12. doi: 10.1016/j.coi.2014.10.005

136. Karin M, Ben-Neriah Y. Phosphorylation meets ubiquitination: the control of NF-[kappa]B activity. *Annu Rev Immunol* (2000) 18:621–63. doi: 10.1146/annurev.immunol.18.1.621

137. Yaron A, Hatzubai A, Davis M, Lavon I, Amit S, Manning AM, et al. Identification of the receptor component of the IkappaBalpha-ubiquitin ligase. *Nature.* (1998) 396(6711):590–4. doi: 10.1038/25159

138. Karin M. How NF-kappaB is activated: the role of the IkappaB kinase (IKK) complex. *Oncogene.* (1999) 18(49):6867–74. doi: 10.1038/sj.onc.1203219

139. Zandi E, Chen Y, Karin M. Direct phosphorylation of IkappaB by IKKalpha and IKKbeta: discrimination between free and NF-kappaB-bound substrate. *Science.* (1998) 281(5381):1360–3. doi: 10.1126/science.281.5381.1360

140. Bouwmeester T, Bauch A, Ruffner H, Angrand PO, Bergamini G, Croughton K, et al. A physical and functional map of the human TNF-alpha/NF-kappa b signal transduction pathway. *Nat Cell Biol* (2004) 6(2):97–105. doi: 10.1038/ncb1086

141. Romano S, Xiao Y, Nakaya M, D'Angelillo A, Chang M, Jin J, et al. FKBP51 employs both scaffold and isomerase functions to promote NF-κB activation in melanoma. *Nucleic Acids Res* (2015) 43(14):6983–93. doi: 10.1093/nar/gkv615

142. Erlejman AG, De Leo SA, Mazaira GI, Molinari AM, Camisay MF, Fontana V, et al. NF-κB transcriptional activity is modulated by FK506-binding proteins FKBP51 and FKBP52: a role for peptidyl-prolyl isomerase activity. *J Biol Chem* (2014) 289(38):26263–76. doi: 10.1074/jbc.M114.582882

143. Schoggins JW, Rice CM. Interferon-stimulated genes and their antiviral effector functions. *Curr Opin Virol* (2011) 1(6):519–25. doi: 10.1016/j.coviro.2011.10.008

144. de Weerd NA, Vivian JP, Nguyen TK, Mangan NE, Gould JA, Braniff SJ, et al. Structural basis of a unique interferon-β signaling axis mediated via the receptor IFNAR1. *Nat Immunol* (2013) 14(9):901–7. doi: 10.1038/ni.2667

145. Shemesh M, Lochte S, Piehler J, Schreiber G. IFNAR1 and IFNAR2 play distinct roles in initiating type I interferon-induced JAK-STAT signaling and activating STATs. *Sci Signal* (2021) 14(710):eabe4627. doi: 10.1126/scisignal.abe4627

146. Kotenko SV, Rivera A, Parker D, Durbin JE. Type III IFNs: Beyond antiviral protection. semin. *Immunol.* (2019) 43:101303. doi: 10.1016/j.smim.2019.101303

147. Kotenko SV, Gallagher G, Baurin VV, Lewis-Antes A, Shen M, Shah NK, et al. IFN-lambdas mediate antiviral protection through a distinct class II cytokine receptor complex. *Nat Immunol* (2003) 4(1):69–77. doi: 10.1038/ni875

148. Sheppard P, Kindsvogel W, Xu W, Henderson K, Schlutsmeyer S, Whitmore TE, et al. IL-28, IL-29 and their class II cytokine receptor IL-28R. *Nat Immunol* (2003) 4(1):63–8. doi: 10.1038/ni873

149. Stark GR, Darnell JEJr. The JAK-STAT pathway at twenty. *Immunity.* (2012) 36(4):503–14. doi: 10.1016/j.immuni.2012.03.013

150. Schindler C, Plumlee C. Inteferons pen the JAK-STAT pathway. *Semin Cell Dev Biol* (2008) 19(4):311–8. doi: 10.1016/j.semcdb.2008.08.010

151. Schnepf D, Crotta S, Thamamongood T, Stanifer M, Polcik L, Ohnemus A, et al. Selective janus kinase inhibition preserves interferon-λ-mediated antiviral responses. *Sci Immunol* (2021) 6(59):eabd5318. doi: 10.1126/sciimmunol.abd5318

152. Li X, Leung S, Qureshi S, Darnell JEJr, Stark GR. Formation of STAT1-STAT2 heterodimers and their role in the activation of IRF-1 gene transcription by interferon-alpha. *J Biol Chem* (1996) 271(10):5790–4. doi: 10.1074/jbc.271.10.5790

153. Wang Y, Song Q, Huang W, Lin Y, Wang X, Wang C, et al. Stark GR. a virus-induced conformational switch of STAT1-STAT2 dimers boosts antiviral defenses. *Cell Res* (2021) 31(2):206–18. doi: 10.1038/s41422-020-0386-6

154. Ho J, Pelzel C, Begitt A, Mee M, Elsheikha HM, Scott DJ, et al. STAT2 is a pervasive cytokine regulator due to its inhibition of STAT1 in multiple signaling pathways. *PloS Biol* (2016) 14(10):e2000117. doi: 10.1371/journal.pbio.2000117

155. Platanitis E, Demiroz D, Schneller A, Fischer K, Capelle C, Hartl M, et al. A molecular switch from STAT2-IRF9 to ISGF3 underlies interferon-induced gene transcription. *Nat Commun* (2019) 10(1):2921. doi: 10.1038/s41467-019-10970-y

156. Rengachari S, Groiss S, JM D, Caron E, Grandvaux N, Panne D. Structural basis of STAT2 recognition by IRF9 reveals molecular insights into ISGF3 function. *Proc Natl Acad Sci U S A.* (2018) 115(4):E601–9. doi: 10.1073/pnas.1718426115

157. Zhou Z, Hamming OJ, Ank N, Paludan SR, Nielsen AL, Hartmann R. Type III interferon (IFN) induces a type I IFN-like response in a restricted subset of cells through signaling pathways involving both the jak-STAT pathway and the mitogen-activated protein kinases. *J Virol* (2007) 81(14):7749–58. doi: 10.1128/JVI.02438-06

158. Schneider WM, Chevillotte MD, Rice CM. Interferon-stimulated genes: a complex web of host defenses. *Annu Rev Immunol* (2014) 32:513–45. doi: 10.1146/annurev-immunol-032713-120231

159. Platanias LC. Mechanisms of type-i- and type-II-interferon-mediated signalling. *Nat Rev Immunol* (2005) 5(5):375–86. doi: 10.1038/nri1604

160. Schindler C, Levy DE, Decker T. JAK-STAT signaling: from interferons to cytokines. *J Biol Chem* (2007) 282(28):20059–63. doi: 10.1074/jbc.R700016200

161. Lazear HM, Schoggins JW, Diamond MS. Shared and distinct functions of type I and type III interferons. *Immunity.* (2019) 50(4):907–23. doi: 10.1016/j.immuni.2019.03.025

162. Der SD, Zhou A, Williams BR, Silverman RH. Identification of genes differentially regulated by interferon alpha, beta, or gamma using oligonucleotide arrays. *Proc Natl Acad Sci U S A.* (1998) 95(26):15623–8. doi: 10.1073/pnas.95.26.15623

163. Biggioggero M, Gabbriellini L, Meroni PL. Type I interferon therapy and its role in autoimmunity. *Autoimmunity.* (2010) 43(3):248–54. doi: 10.3109/08916930903510971

164. Borg FA, Isenberg DA. Syndromes and complications of interferon therapy. *Curr Opin Rheumatol* (2007) 19(1):61–6. doi: 10.1097/BOR.0b013e328010c547

165. Ionescu C, Micu L, Constantinescu I, Hortopan M, Ursaciuc C, Voiculescu M. Prolonged treatment with interferon alpha and peginterferon induces rheumatoid arthritis syndrome and erythema nodosum. *J Gastrointestin Liver Dis* (2008) 17(2):211–2. doi: 10.1007/s11749-008-0114-x

166. Chung A, Older SA. Interferon-alpha associated arthritis. *J Rheumatol* (1997) 24(9):1844–5.

167. Hojjati SM, Heidari B, Babaei M. Development of rheumatoid arthritis during treatment of multiple sclerosis with interferon beta 1-a. coincidence of two conditions or a complication of treatment: A case report. *J Adv Res* (2016) 7(5):611–3. doi: 10.1016/j.jare.2016.06.004

168. Willemsen J, Neuhoff MT, Hoyler T, Noir E, Tessier C, Sarret S, et al. TNF leads to mtDNA release and cGAS/STING-dependent interferon responses that support inflammatory arthritis. *Cell Rep* (2021) 37(6):109977. doi: 10.1016/j.celrep.2021.109977

169. Venkatesh D, Ernandez T, Rosetti F, Batal I, Cullere X, Luscinskas FW, et al. Endothelial TNF receptor 2 induces IRF1 transcription factor-dependent interferon-β autocrine signaling to promote monocyte recruitment. *Immunity.* (2013) 38(5):1025–37. doi: 10.1016/j.immuni.2013.01.012

170. Yarilina A, Park-Min KH, Antoniv T, Hu X, Ivashkiv LB. TNF activates an IRF1-dependent autocrine loop leading to sustained expression of chemokines and STAT1-dependent type I interferon-response genes. *Nat Immunol* (2008) 9(4):378–87. doi: 10.1038/ni1576

171. Hopkins SJ, Meager A. Cytokines in synovial fluid: II. the presence of tumour necrosis factor and interferon. *Clin Exp Immunol* (1988) 73(1):88–92.

172. Hooks JJ, Moutsopoulos HM, Geis SA, Stahl NI, Decker JL, Notkins AL. Immune interferon in the circulation of patients with autoimmune disease. *N Engl J Med* (1979) 301(1):5–8. doi: 10.1056/NEJM197907053010102

173. Tan X, Sun L, Chen J, Chen ZJ. Detection of microbial infections through innate immune sensing of nucleic acids. *Annu Rev Microbiol* (2018) 8:72:447–478. doi: 10.1146/annurev-micro-102215-095605

174. Levy DE, Marié IJ, Durbin JE. Induction and function of type I and III interferon in response to viral infection. *Curr Opin Virol* (2011) 1(6):476–86. doi: 10.1016/j.coviro.2011.11.001

175. Roers A, Hiller B, Hornung V. Recognition of endogenous nucleic acids by the innate immune system. *Immunity.* (2016) 44(4):739–54. doi: 10.1016/j.immuni.2016.04.002

176. Higgs BW, Liu Z, White B, Zhu W, White WI, Morehouse C, et al. Patients with systemic lupus erythematosus, myositis, rheumatoid arthritis and scleroderma share activation of a common type I interferon pathway. *Ann Rheum Dis* (2011) 70(11):2029–36. doi: 10.1136/ard.2011.150326

177. Rodríguez-Carrio J, López P, Suárez A. Type I IFNs as biomarkers in rheumatoid arthritis: towards disease profiling and personalized medicine. *Clin Sci (Lond).* (2015) 128(8):449–64. doi: 10.1042/CS20140554

178. Rönnblom L, Eloranta ML. The interferon signature in autoimmune diseases. *Curr Opin Rheumatol* (2013) 25(2):248–53. doi: 10.1097/BOR.0b013e32835c7e32

179. van der Pouw Kraan TC, van Baarsen LG, Wijbrandts CA, Voskuyl AE, Rustenburg F, Baggen JM, et al. Expression of a pathogen-response program in peripheral blood cells defines a subgroup of rheumatoid arthritis patients. *Genes Immun* (2008) 9(1):16–22. doi: 10.1038/sj.gene.6364438

180. Rodríguez-Carrio J, de Paz B, López P, Prado C, Alperi-López M, Ballina-García FJ, et al. IFNα serum levels are associated with endothelial progenitor cells imbalance and disease features in rheumatoid arthritis patients. *PloS One* (2014) 9(1):e86069. doi: 10.1371/journal.pone.0086069

181. Rodríguez-Carrio J, Alperi-López M, López P, Ballina-García FJ, Suárez A. Heterogeneity of the type I interferon signature in rheumatoid arthritis: A potential limitation for its use as a clinical biomarker. *Front Immunol* (2018) 8:2007. doi: 10.3389/fimmu.2017.02007

182. van der Pouw Kraan TC, Wijbrandts CA, van Baarsen LG, Voskuyl AE, Rustenburg F, Baggen JM, et al. Rheumatoid arthritis subtypes identified by genomic profiling of peripheral blood cells: assignment of a type I interferon signature in a subpopulation of patients. *Ann Rheum Dis* (2007) 66(8):1008–14. doi: 10.1136/ard.2006.063412

183. Muskardin TLW, Niewold TB. Type I interferon in rheumatic diseases. *Nat Rev Rheumatol* (2018) 14(4):214–28. doi: 10.1038/nrrheum.2018.31

184. Iwasaki A, Pillai PS. Innate immunity to influenza virus infection. *Nat Rev Immunol* (2014) 14(5):315–28. doi: 10.1038/nri3665

185. Rönnblom L. The type I interferon system in the etiopathogenesis of autoimmune diseases. *Ups J Med Sci* (2011) 116(4):227–37. doi: 10.3109/03009734.2011.624649

186. Coccia EM, Uzé G, Pellegrini S. Negative regulation of type I interferon signaling: facts and mechanisms. *Cell Mol Biol (Noisy-le-grand).* (2006) 52(1):77–87.

187. ten Hoeve J, de Jesus Ibarra-Sanchez M, Fu Y, Zhu W, Tremblay M, David M, et al. Identification of a nuclear Stat1 protein tyrosine phosphatase. *Mol Cell Biol* (2002) 22(16):5662–8. doi: 10.1128/MCB.22.16.5662-5668.2002

188. Irie-Sasaki J, Sasaki T, Matsumoto W, Opavsky A, Cheng M, Welstead G, et al. CD45 is a JAK phosphatase and negatively regulates cytokine receptor signalling. *Nature.* (2001) 409(6818):349–54. doi: 10.1038/35053086

189. Altman JB, Taft J, Wedeking T, Gruber CN, Holtmannspötter M, Piehler J, et al. Type I IFN is siloed in endosomes. *Proc Natl Acad Sci U S A.* (2020) 117(30):17510–2. doi: 10.1073/pnas.1921324117

190. Richards KH, Macdonald A. Putting the brakes on the anti-viral response: negative regulators of type I interferon (IFN) production. *Microbes Infect* (2011) 13(4):291–302. doi: 10.1016/j.micinf.2010.12.007

191. Komuro A, Bamming D, Horvath CM. Negative regulation of cytoplasmic RNA-mediated antiviral signaling. *Cytokine.* (2008) 43(3):350–8. doi: 10.1016/j.cyto.2008.07.011

192. Larner AC, Chaudhuri A, Darnell JEJr. Transcriptional induction by interferon. new protein(s) determine the extent and length of the induction. *J Biol Chem* (1986) 261(1):453–9. doi: 10.1016/S0021-9258(17)42492-6

193. Hong XX, Carmichael GG. Innate immunity in pluripotent human cells: attenuated response to interferon-β. *J Biol Chem* (2013) 288(22):16196–205. doi: 10.1074/jbc.M112.435461

194. Malakhova OA, Kim KI, Luo JK, Zou W, Kumar KG, Fuchs SY, et al. UBP43 is a novel regulator of interferon signaling independent of its ISG15 isopeptidase activity. *EMBO J* (2006) 25(11):2358–67. doi: 10.1038/sj.emboj.7601149

195. DeDiego ML, Nogales A, Martinez-Sobrido L, Topham DJ. Interferon-induced protein 44 interacts with cellular FK506-binding protein 5, negatively regulates host antiviral responses, and supports virus replication. *mBio.* (2019) 10(4):e01839-19. doi: 10.1128/mBio.01839-19

196. Nesher G, Ruchlemer R. Alpha-interferon-induced arthritis: clinical presentation treatment, and prevention. *Semin Arthritis Rheumatol* (1998) 27(6):360–5. doi: 10.1016/s0049-0172(98)80015-2

197. Bain VG, Yoshida EM, Kaita KD, Swain MG, Heathcote EJ, Garcia A, et al. Dynamics of interferon-specific gene expression in peripheral blood of interferon alfa-naïve patients with genotype 1 chronic hepatitis c infection treated with albumin-interferon alfa. *Hepatol Res* (2006) 35(4):256–62. doi: 10.1016/j.hepres.2006.04.005

198. Kitamura A, Takahashi K, Okajima A, Kitamura N. Induction of the human gene for p44, a hepatitis-c-associated microtubular aggregate protein, by interferon-alpha/beta. *Eur J Biochem* (1994) 224(3):877–83. doi: 10.1111/j.1432-1033.1994.00877.x

199. Honda Y, Kondo J, Maeda T, Yoshiyama Y, Yamada E, Shimizu YK, et al. Isolation and purification of a non-a, non-b hepatitis-associated microtubular aggregates protein. *J Gen Virol* (1990) 71(Pt 9):1999–2004. doi: 10.1099/0022-1317-71-9-1999

200. Zandi E, Rothwarf DM, Delhase M, Hayakawa M, Karin M. The IkappaB kinase complex (IKK) contains two kinase subunits, IKKalpha and IKKbeta, necessary for IkappaB phosphorylation and NF-kappaB activation. *Cell.* (1997) 91(2):243–52. doi: 10.1016/s0092-8674(00)80406-7

201. COBB S, ANDERSON F, BAUER W. Length of life and cause of death in rheumatoid arthritis. *N Engl J Med* (1953) 249(14):553–6. doi: 10.1056/NEJM195310012491402

202. England BR, Thiele GM, Anderson DR, Mikuls TR. Increased cardiovascular risk in rheumatoid arthritis: mechanisms and implications. *BMJ.* (2018) 361:k1036. doi: 10.1136/bmj.k1036

203. Suzuki A, Ohosone Y, Obana M, Mita S, Matsuoka Y, Irimajiri S, et al. Cause of death in 81 autopsied patients with rheumatoid arthritis. *J Rheumatol* (1994) 21(1):33–6.

204. Yeganeh MH, Kheir MM, Shahi A, Parvizi J. Rheumatoid arthritis, disease modifying agents, and periprosthetic joint infection: What does a joint surgeon need to know? *J Arthroplasty.* (2018) 33(4):1258–64. doi: 10.1016/j.arth.2017.11.031

205. Mancuso G, Midiri A, Biondo C, Beninati C, Zummo S, Galbo R, et al. Type I IFN signaling is crucial for host resistance against different species of pathogenic bacteria. *J Immunol* (2007) 178(5):3126–33. doi: 10.4049/jimmunol.178.5.3126

206. Manca C, Tsenova L, Freeman S, Barczak AK, Tovey M, Murray PJ, et al. Hypervirulent m. tuberculosis W/Beijing strains upregulate type I IFNs and

increase expression of negative regulators of the jak-stat pathway. *J Interferon Cytokine Res* (2005) 25(11):694–701. doi: 10.1089/jir.2005.25.694

207. Decker T, Müller M, Stockinger S. The yin and yang of type I interferon activity in bacterial infection. *Nat Rev Immunol* (2005) 5(9):675–87. doi: 10.1038/nri1684

208. McNab F, Mayer-Barber K, Sher A, Wack A, O'Garra A. Type I interferons in infectious disease. *Nat Rev Immunol* (2015) 15(2):87–103. doi: 10.1038/nri3787

209. Boxx GM, Cheng G. The roles of type I interferon in bacterial infection. *Cell Host Microbe* (2016) 19(6):760–9. doi: 10.1016/j.chom.2016.05.016

210. Parker D, Planet PJ, Soong G, Narechania A, Prince A. Induction of type I interferon signaling determines the relative pathogenicity of staphylococcus aureus strains. *PloS Pathog* (2014) 10(2):e1003951. doi: 10.1371/journal.ppat.1003951

211. Martin FJ, Gomez MI, Wetzel DM, Memmi G, O'Seaghdha M, Soong G, et al. Staphylococcus aureus activates type I IFN signaling in mice and humans through the xr repeated sequences of protein a. *J Clin Invest.* (2009) 119(7):1931–9. doi: 10.1172/jci35879

212. Stifter SA, Feng CG. Interfering with immunity: detrimental role of type I IFNs during infection. *J Immunol* (2015) 194(6):2455–65. doi: 10.4049/jimmunol.1402794

213. Parker D, Prince A. Staphylococcus aureus induces type I IFN signaling in dendritic cells. *via TLR9. J Immunol* (2012) 189(8):4040–6. doi: 10.4049/jimmunol.1201055

214. Klopfenstein N, Brandt SL, Castellanos S, Gunzer M, Blackman A, Serezani CH. SOCS-1 inhibition of type I interferon restrains staphylococcus aureus skin host defense. *PloS Pathog* (2021) 17(3):e1009387. doi: 10.1371/journal.ppat.1009387

215. Serezani CH, Lewis C, Jancar S, Peters-Golden M. Leukotriene B4 amplifies NF-κB activation in mouse macrophages by reducing SOCS1 inhibition of MyD88 expression. *J Clin Invest.* (2011) 121(2):671–82. doi: 10.1172/JCI43302

216. Piñeros Alvarez AR, Glosson-Byers N, Brandt S, Wang S, Wong H, Sturgeon S, et al. SOCS1 is a negative regulator of metabolic reprogramming during sepsis. *JCI Insight* (2017) 2(13):e92530. doi: 10.1172/jci.insight.92530

217. Duncan SA, Baganizi DR, Sahu R, Singh SR, Dennis VA. SOCS proteins as regulators of inflammatory responses induced by bacterial infections: A review. *Front Microbiol* (2017) 8:2431. doi: 10.3389/fmicb.2017.02431

218. Shaabani N, Honke N, Nguyen N, Huang Z, Arimoto KI, Lazar D, et al. The probacterial effect of type I interferon signaling requires its own negative regulator USP18. *Sci Immunol* (2018) 3(27):eaau2125. doi: 10.1126/sciimmunol.aau2125

219. Holmes EC, Goldstein SA, Rasmussen AL, Robertson DL, Crits-Christoph A, Wertheim JO, et al. The origins of SARS-CoV-2: A critical review. *Cell.* (2021) 184(19):4848–56. doi: 10.1016/j.cell.2021.08.017

220. Vlasova AN, Diaz A, Damtie D, Xiu L, Toh TH, Lee JS, et al. Novel canine coronavirus isolated from a hospitalized patient with pneumonia in East Malaysia. *Clin Infect Dis* (2022) 74(3):446–54. doi: 10.1093/cid/ciab456

221. Lednicky JA, Tagliamonte MS, White SK, Elbadry MA, Alam MM, Stephenson CJ, et al. Independent infections of porcine deltacoronavirus among Haitian children. *Nature.* (2021) 600(7887):133–7. doi: 10.1038/s41586-021-04111-z

222. Masters PS. The molecular biology of coronaviruses. *Adv Virus Res* (2006) 66:193–292. doi: 10.1016/S0065-3527(06)66005-3

223. Lu R, Zhao X, Li J, Niu P, Yang B, Wu H, et al. Genomic characterisation and epidemiology of 2019 novel coronavirus: implications for virus origins and receptor binding. *Lancet.* (2020) 395(10224):565–74. doi: 10.1016/S0140-6736(20)30251-8

224. Mittal A, Manjunath K, Ranjan RK, Kaushik S, Kumar S, Verma V. COVID-19 pandemic: Insights into structure, function, and hACE2 receptor recognition by SARS-CoV-2. *PloS Pathog* (2020) 16(8):e1008762. doi: 10.1371/journal.ppat.1008762

225. Chan JF, Yuan S, Kok KH, To KK, Chu H, Yang J, et al. A familial cluster of pneumonia associated with the 2019 novel coronavirus indicating person-to-person transmission: a study of a family cluster. *Lancet.* (2020) 395(10223):514–23. doi: 10.1016/S0140-6736(20)30154-9

226. Cui J, Li F, Shi ZL. Origin and evolution of pathogenic coronaviruses. *Nat Rev Microbiol* (2019) 17(3):181–92. doi: 10.1038/s41579-018-0118-9

227. Dai L, Gao GF. Viral targets for vaccines against COVID-19. *Nat Rev Immunol* (2021) 21(2):73–82. doi: 10.1038/s41577-020-00480-0

228. Jin Y, Yang H, Ji W, Wu W, Chen S, Zhang W, et al. Virology, epidemiology, pathogenesis, and control of COVID-19. *Viruses.* (2020) 12(4):372. doi: 10.3390/v12040372

229. Almazán F, Dediego ML, Galán C, Escors D, Alvarez E, Ortego J, et al. Construction of a severe acute respiratory syndrome coronavirus infectious cDNA clone and a replicon to study coronavirus RNA synthesis. *J Virol* (2006) 80(21):10900–6. doi: 10.1128/JVI.00385-06

230. WHO. *Tracking SARS-CoV-2 variants* (2021). Available at: https://www.who.int/en/activities/tracking-SARS-CoV-2-variants.

231. Sacchi MC, Tamiazzo S, Stobbione P, Agatea L, De Gaspari P, Stecca A, et al. SARS-CoV-2 infection as a trigger of autoimmune response. *Clin Transl Sci* (2021) 14(3):898–907. doi: 10.1111/cts.12953

232. Liew IY, Mak TM, Cui L, Vasoo S. Lim XR. a case of reactive arthritis secondary to coronavirus disease 2019 infection. *J Clin Rheumatol* (2020) 26(6):233. doi: 10.1097/RHU.0000000000001560

233. Ono K, Kishimoto M, Shimasaki T, Uchida H, Kurai D, Deshpande GA, et al. Reactive arthritis after COVID-19 infection. *RMD Open* (2020) 6(2):e001350. doi: 10.1136/rmdopen-2020-001350

234. Alivernini S, Cingolani A, Gessi M, Paglionico A, Pasciuto G, Tolusso B, et al. Comparative analysis of synovial inflammation after SARS-CoV-2 infection. *Ann Rheum Dis* (2021) 80(6):e91. doi: 10.1136/annrheumdis-2020-218315

235. Talarico R, Stagnaro C, Ferro F, Carli L, Mosca M. Symmetric peripheral polyarthritis developed during SARS-CoV-2 infection. *Lancet Rheumatol* (2020) 2(9):e518–9. doi: 10.1016/S2665-9913(20)30216-2

236. Conway R, Grimshaw AA, Konig MF, Putman M, Duarte-García A, Tseng LY, et al. COVID-19 global rheumatology alliance. SARS-CoV-2 infection and COVID-19 outcomes in rheumatic diseases: A systematic literature review and meta-analysis. *Arthritis Rheumatol* (2022) 74(5):766–75. doi: 10.1002/art.42030

237. Akiyama S, Hamdeh S, Micic D, Sakuraba A. Prevalence and clinical outcomes of COVID-19 in patients with autoimmune diseases: A systematic review and meta-analysis. *Ann Rheumatol Dis* (2020) 80:384–91. doi: 10.1136/annrheumdis-2020-218946

238. *The COVID-19 global rheumatology alliance global registry* (2020). Available at: https://rheum-covid.org/updates/combined-data.html.

239. Favalli EG, Ingegnoli F, Cimaz R, Caporali R. What is the true incidence of COVID-19 in patients with rheumatic diseases? *Ann Rheum Dis* (2021) 80(2):e18. doi: 10.1136/annrheumdis-2020-217615

240. Haberman R, Axelrad J, Chen A, Castillo R, Yan D, Izmirly P, et al. Covid-19 in immune-mediated inflammatory diseases - case series from new York. *N Engl J Med* (2020) 383(1):85–8. doi: 10.1056/NEJMc2009567

241. Sarzi-Puttini P, Marotto D, Caporali R, Montecucco CM, Favalli EG, Franceschini F, et al. Prevalence of COVID infections in a population of rheumatic patients from Lombardy and marche treated with biological drugs or small molecules: A multicentre retrospective study. *J Autoimmun* (2021) 116:102545. doi: 10.1016/j.jaut.2020.102545

242. Wang Y, D'Silva KM, Jorge AM, Li X, Lyv H, Wei J, et al. Increased risk of COVID-19 in patients with rheumatoid arthritis: A general population-based cohort study. *Arthritis Care Res (Hoboken).* (2022) 74(5):741–7. doi: 10.1002/acr.24831

243. Dewanjee S, Kandimalla R, Kalra RS, Valupadas C, Vallamkondu J, Kolli V, et al. COVID-19 and rheumatoid arthritis crosstalk: Emerging association, therapeutic options and challenges. *Cells.* (2021) 10(12):3291. doi: 10.3390/cells10123291

244. Favalli EG, Maioli G, Biggioggero M, Caporali R. Clinical management of patients with rheumatoid arthritis during the COVID-19 pandemic. *Expert Rev Clin Immunol* (2021) 17(6):561–71. doi: 10.1080/1744666X.2021.1908887

245. Schett G, Manger B, Simon D, Caporali R. COVID-19 revisiting inflammatory pathways of arthritis. *Nat Rev Rheumatol* (2020) 16(8):465–70. doi: 10.1038/s41584-020-0451-z

246. Mirzaei R, Goodarzi P, Asadi M, Soltani A, Aljanabi HAA, Jeda AS, et al. Bacterial co-infections with SARS-CoV-2. *IUBMB Life* (2020) 72(10):2097–111. doi: 10.1002/iub.2356

247. Vaughn VM, Gandhi TN, Petty LA, Patel PK, Prescott HC, Malani AN, et al. Empiric antibacterial therapy and community-onset bacterial coinfection in patients hospitalized with coronavirus disease 2019 (COVID-19): A multi-hospital cohort study. *Clin Infect Dis* (2021) 72(10):e533–41. doi: 10.1093/cid/ciaa1239

248. Karami Z, Knoop BT, Dofferhoff ASM, Blaauw MJT, Janssen NA, van Apeldoorn M, et al. Few bacterial co-infections but frequent empiric antibiotic use in the early phase of hospitalized patients with COVID-19: results from a multicentre retrospective cohort study in the Netherlands. *Infect Dis (Lond).* (2021) 53(2):102–10. doi: 10.1080/23744235.2020.1839672

249. Adler H, Ball R, Fisher M, Mortimer K, Vardhan MS. Low rate of bacterial co-infection in patients with COVID-19. *Lancet Microbe* (2020) 1(2):e62. doi: 10.1016/S2666-5247(20)30036-7

250. Fu Y, Yang Q, Xu M, Kong H, Chen H, Fu Y, et al. Secondary bacterial infections in critical ill patients with coronavirus disease 2019. *Open Forum Infect Dis* (2020) 7(6):ofaa220. doi: 10.1093/ofid/ofaa220

251. Westblade LF, Simon MS, Satlin MJ. Bacterial coinfections in coronavirus disease 2019. *Trends Microbiol* (2021) 29(10):930–41. doi: 10.1016/j.tim.2021.03.018

252. Contou D, Claudinon A, Pajot O, Micaëlo M, Longuet Flandre P, Dubert M, et al. Bacterial and viral co-infections in patients with severe SARS-CoV-2 pneumonia admitted to a French ICU. *Ann Intensive Care* (2020) 10(1):119. doi: 10.1186/s13613-020-00736-x

253. Hu H, Tang N, Zhang F, Li L, Li L. Bioinformatics and system biology approach to identify the influences of COVID-19 on rheumatoid arthritis. *Front Immunol* (2022) 13:860676. doi: 10.3389/fimmu.2022.860676

254. Lowery SA, Sariol A, Perlman S. Innate immune and inflammatory responses to SARS-CoV-2: Implications for COVID-19. *Cell Host Microbe* (2021) 29(7):1052–62. doi: 10.1016/j.chom.2021.05.004

255. Park A, Iwasaki A. Type I and type III interferons - induction, signaling, evasion, and application to combat COVID-19. *Cell Host Microbe* (2020) 27 (6):870–8. doi: 10.1016/j.chom.2020.05.008

256. Wilk AJ, Rustagi A, Zhao NQ, Roque J, Martínez-Colón GJ, McKechnie JL, et al. Blish CA. a single-cell atlas of the peripheral immune response in patients with severe COVID-19. *Nat Med* (2020) 26(7):1070–6. doi: 10.1038/s41591-020-0944-y

257. Lucas C, Wong P, Klein J, Castro TBR, Silva J, Sundaram M, et al. Longitudinal analyses reveal immunological misfiring in severe COVID-19. *Nature.* (2020) 584(7821):463–9. doi: 10.1038/s41586-020-2588-y

258. Lee JS, Park S, Jeong HW, Ahn JY, Choi SJ, Lee H, et al. Immunophenotyping of COVID-19 and influenza highlights the role of type I interferons in development of severe COVID-19. *Sci Immunol* (2020) 5(49): eabd1554. doi: 10.1126/sciimmunol.abd1554

259. Vanderheiden A, Ralfs P, Chirkova T, Upadhyay AA, Zimmerman MG, Bedoya S, et al. Type I and type III interferons restrict SARS-CoV-2 infection of human airway epithelial cultures. *J Virol* (2020) 94(19):e00985-20. doi: 10.1128/JVI.00985-20

260. Mantlo E, Bukreyeva N, Maruyama J, Paessler S, Huang C. Antiviral activities of type I interferons to SARS-CoV-2 infection. *Antiviral Res* (2020) 179:104811. doi: 10.1016/j.antiviral.2020.104811

261. Cheemarla NR, Watkins TA, Mihaylova VT, Wang B, Zhao D, Wang G, et al. Dynamic innate immune response determines susceptibility to SARS-CoV-2 infection and early replication kinetics. *J Exp Med* (2021) 218(8):e20210583. doi: 10.1084/jem.20210583

262. Martin-Sancho L, Lewinski MK, Pache L, Stoneham CA, Yin X, Becker ME, et al. Functional landscape of SARS-CoV-2 cellular restriction. *Mol Cell* (2021) 81(12):2656–68. doi: 10.1016/j.molcel.2021.04.008

263. Low ZY, Wen Yip AJ, Chow VTK, Lal SK. The suppressor of cytokine signalling family of proteins and their potential impact on COVID-19 disease progression. *Rev Med Virol* (2022) 32(3):e2300. doi: 10.1002/rmv.2300

264. Johnson HM, Lewin AS, Ahmed CM. SOCS, Factors IVTreatment of COVID-19, , Front ImmunAhmed CM, et al. SOCS1 mimetics and antagonists: A complementary approach to positive and negative regulation of immune function. *Front Immunol* (2015) 6:183. doi: 10.3389/fimmu.2015.00183

265. (2020) 11. doi: 10.3389/fimmu.2020.582102

266. Gold IM, Reis N, Glaser F, Glickman MH. Coronaviral PLpro proteases and the immunomodulatory roles of conjugated versus free interferon stimulated gene product-15 (ISG15). *Semin Cell Dev Biol* (2022) S1084-9521(22):00215–4. doi: 10.1016/j.semcdb.2022.06.005

267. Kirby D, Parmar B, Fathi S, Marwah S, Nayak CR, Cherepanov V, et al. Determinants of ligand specificity and functional plasticity in type I interferon signaling. *Front Immunol* (2021) 12:748423. doi: 10.3389/fimmu.2021.748423

268. Wilmes S, Beutel O, Li Z, Francois-Newton V, Richter CP, Janning D, et al. Receptor dimerization dynamics as a regulatory valve for plasticity of type I interferon signaling. *J Cell Biol* (2015) 209(4):579–93. doi: 10.1083/jcb.201412049

269. Kerr GS, Sabahi I, Richards JS, Caplan L, Cannon GW, Reimold A, et al. Prevalence of vitamin d insufficiency/deficiency in rheumatoid arthritis and associations with disease severity and activity. *J Rheumatol* (2011) 38(1):53–9. doi: 10.3899/jrheum.100516

270. Despotović M, Jevtović Stoimenov T, Stojanović S, Bašić J, Kundalić J, Đorđević B, et al. Association of vitamin d receptor genetic variants with bone mineral density and inflammatory markers in rheumatoid arthritis. *Clin Biochem* (2021) 87:26–31. doi: 10.1016/j.clinbiochem.2020.10.006

271. Murdaca G, Tonacci A, Negrini S, Greco M, Borro M, Puppo F, et al. Emerging role of vitamin d in autoimmune diseases: An update on evidence and therapeutic implications. *Autoimmun Rev* (2019) 18(9):102350. doi: 10.1016/j.autrev.2019.102350

272. Lin J, Liu J, Davies ML, Chen W. Serum vitamin d level and rheumatoid arthritis disease activity: Review and meta-analysis. *PloS One* (2016) 11(1): e0146351. doi: 10.1371/journal.pone.0146351

273. Mouterde G, Gamon E, Rincheval N, Lukas C, Seror R, Berenbaum F, et al. Association between vitamin d deficiency and disease activity, disability, and radiographic progression in early rheumatoid arthritis: The ESPOIR cohort. *J Rheumatol* (2020) 47(11):1624–8. doi: 10.3899/jrheum.190795

274. Small AG, Harvey S, Kaur J, Putty T, Quach A, Munawara U, et al. Vitamin d upregulates the macrophage complement receptor immunoglobulin in innate immunity to microbial pathogens. *Commun Biol* (2021) 4(1):401. doi: 10.1038/s42003-021-01943-3

275. Liu G, Fu Y, Yosri M, Chen Y, Sun P, Xu J, et al. CRIg plays an essential role in intravascular clearance of bloodborne parasites by interacting with complement. *Proc Natl Acad Sci USA* (2019) 116:24214–20. doi: 10.1073/pnas.1913443116

276. Thomason J, Rentsch C, Stenehjem EA, Hidron AI, Rimland D. Association between vitamin d deficiency and methicillin-resistant staphylococcus aureus infection. *Infection.* (2015) 43(6):715–22. doi: 10.1007/s15010-015-0815-5

277. Alamanda VK, Springer BD. The prevention of infection: 12 modifiable risk factors. *Bone Joint J* (2019) 101-B(1_Supple_A):3–9. doi: 10.1302/0301-620X.101B1.BJJ-2018-0233.R1

278. Hegde V, Dworsky EM, Stavrakis AI, Loftin AH, Zoller SD, Park HY, et al. Single-dose, preoperative vitamin-d supplementation decreases infection in a mouse model of periprosthetic joint infection. *J Bone Joint Surg Am* (2017) 99 (20):1737–44. doi: 10.2106/JBJS.16.01598

279. Merzon E, Tworowski D, Gorohovski A, Vinker S, Golan Cohen A, Green I, et al. Low plasma 25(OH) vitamin d level is associated with increased risk of COVID-19 infection: an Israeli population-based study. *FEBS J* (2020) 287 (17):3693–702. doi: 10.1111/febs.15495

280. Mercola J, Grant WB, Wagner CL. Evidence regarding vitamin d and risk of COVID-19 and its severity. *Nutrients.* (2020) 12(11):3361. doi: 10.3390/nu12113361

281. Grant WB, Lahore H, McDonnell SL, Baggerly CA, French CB, Aliano JL, et al. Evidence that vitamin d supplementation could reduce risk of influenza and covid-19 infections and deaths. *Nutrients* (2020) 12(4):988. doi: 10.3390/nu12040988

282. Rhodes JM, Subramanian S, Laird E, Griffin G, Kenny RA. Perspective: Vitamin d deficiency and COVID-19 severity - plausibly linked by latitude, ethnicity, impacts on cytokines, ACE2 and thrombosis. *J Intern Med* (2021) 289 (1):97–115. doi: 10.1111/joim.13149

283. Radujkovic A, Hippchen T, Tiwari-Heckler S, Dreher S, Boxberger M, Merle U. Vitamin d deficiency and outcome of COVID-19 patients. *Nutrients.* (2020) 12(9):2757. doi: 10.3390/nu12092757

284. Infante M, Buoso A, Pieri M, Lupisella S, Nuccetelli M, Bernardini S, et al. Low vitamin d status at admission as a risk factor for poor survival in hospitalized patients with COVID-19: An Italian retrospective study. *J Am Nutr Assoc* (2022) 41 (3):250–65. doi: 10.1080/07315724.2021.1877580

285. Pereira M, Dantas Damascena A, Galvão Azevedo LM, de Almeida Oliveira T, da Mota Santana J. Vitamin d deficiency aggravates COVID-19: systematic review and meta-analysis. *Crit Rev Food Sci Nutr* (2022) 62(5):1308–16. doi: 10.1080/10408398.2020.1841090

286. Panfili FM, Roversi M, D'Argenio P, Rossi P, Cappa M, Fintini D. Possible role of vitamin d in covid-19 infection in pediatric population. *J Endocrinol Invest.* (2021) 44(1):27–35. doi: 10.1007/s40618-020-01327-0

287. Gilani SJ, Bin-Jumah MN, Nadeem MS, Kazmi I. Vitamin d attenuates COVID-19 complications Via modulation of proinflammatory cytokines, antiviral proteins, and autophagy. . *Expert Rev Anti Infect Ther* (2022) 20(2):231–41. doi: 10.1080/14787210.2021.1941871

288. Kaufman HW, Niles JK, Kroll MH, Bi C, Holick MF. SARS-CoV-2 positivity rates associated with circulating 25-hydroxyvitamin d levels. *PloS One* (2020) 15(9):e0239252. doi: 10.1371/journal.pone.0239252

289. Ilie PC, Stefanescu S, Smith L. The role of vitamin d in the prevention of coronavirus disease 2019 infection and mortality. *Aging Clin Exp Res* (2020) 32 (7):1195–8. doi: 10.1007/s40520-020-01570-8

290. Xu Y, Baylink DJ, Chen CS, Reeves ME, Xiao J, Lacy C, et al. The importance of vitamin d metabolism as a potential prophylactic, immunoregulatory and neuroprotective treatment for COVID-19. *J Transl Med* (2020) 18(1):322. doi: 10.1186/s12967-020-02488-5

291. Murai IH, Fernandes AL, Sales LP, Pinto AJ, Goessler KF, Duran CSC, et al. Effect of a single high dose of vitamin D3 on hospital length of stay in patients with moderate to severe COVID-19: A randomized clinical trial. *JAMA*. (2021) 325(11):1053–60. doi: 10.1001/jama.2020.26848

292. Annweiler G, Corvaisier M, Gautier J, Dubée V, Legrand E, Sacco G, et al. Vitamin d supplementation associated to better survival in hospitalized frail elderly COVID-19 patients: The GERIA-COVID quasi-experimental study. *Nutrients.* (2020) 12(11):3377. doi: 10.3390/nu12113377

293. Tomaszewska A, Rustecka A, Lipińska-Opałka A, Piprek RP, Kloc M, Kalicki B, et al. The role of vitamin d in COVID-19 and the impact of pandemic

restrictions on vitamin d blood content. *Front Pharmacol* (2022) 13:836738. doi: 10.3389/fphar.2022.836738

294. Ben-Zvi I, Aranow C, Mackay M, Stanevsky A, Kamen DL, Marinescu LM, et al. The impact of vitamin d on dendritic cell function in patients with systemic lupus erythematosus. *PloS One* (2010) 5(2):e9193. doi: 10.1371/journal.pone.0009193

295. Suzuki T, Tatsuno K, Ito T, Sakabe JI, Funakoshi A, Tokura Y. Distinctive downmodulation of plasmacytoid dendritic cell functions by vitamin D3 analogue calcipotriol. *J Dermatol Sci* (2016) 84(1):71–9. doi: 10.1016/j.jdermsci.2016.06.003

296. Barragan M, Good M, Kolls JK. Regulation of dendritic cell function by vitamin d. *Nutrients*. (2015) 7(9):8127–51. doi: 10.3390/nu7095383

297. Bscheider M, Butcher EC. Vitamin d immunoregulation through dendritic cells. *Immunology*. (2016) 148(3):227–36. doi: 10.1111/imm.12610

10.3389/fimmu.2022.1013322

Glossary

Go	Gene Ontology
KEGG	Kyoto Encyclopedia of Genes and Genomes
PPI	Protein-Protein Interaction
TF	Transcription Factor
ROC	Receiver Operating Characteristic Curve
NLR	NOD-Like Receptor
RSAD2	Radical S-adenosyl Methionine Domain-containing Protein 2
IFIT3	Interferon Induced Protein with Tetratricopeptide Repeats 3
GBP1	Guanylate-Binding Protein 1
RTP4	Receptor Transporter Protein 4
IFI44	Interferon-Induced Protein 44
OAS1	2',5'-Oligoadenylate Synthetase 1
IFI44L	Interferon-induced Protein 44-Like
ISG15	Interferon-stimulated Gene 15
HERC5	HECT Domain and RCC1-Like Domain-Containing Protein 5
IFIT5	Interferon-Induced Protein with tetratricopeptide repeats 5
HC	Healthy Controls
NOD	Nucleotide-Binding Oligomerization Domain
AUC	Area Under the Curve
STAT	Signal Transducer and Activator of Transcription
IRF-3	Interferon Regulatory Factor 3
NF-κB	Nuclear Factor-kappa B
TBK-1	TANK-binding Kinase 1
cGAS	Cyclic GMP-AMP Synthase
IκBs	IκB proteins
ISGF3	Interferon-Stimulted Gene Factor 3
AID	Autoimmune Disease
TLR	Toll-Like Receptor
RLR	RIG-I-Like Receptor
SOCS	Suppressors of Cytokine Signaling
USP18	Ubiquitin-Specific Peptidase 18
SeV	Sendai Virus
LCMV	Lymphocytic Choriomeningitis Virus
VSV	Vesicular Stomatitis Virus
IAV	Influenza A Virus
SLE	Systemic Lupus Erythematosus

frontiers | Frontiers in Immunology

TYPE Original Research
PUBLISHED 23 September 2022
DOI 10.3389/fimmu.2022.983502

OPEN ACCESS

EDITED BY
Chenhe Su,
Wistar Institute, United States

REVIEWED BY
Xiaochuan Liu,
University of California, United States
Huibin Yu,
Yale University, United States
Dawei Zhou,
Wexner Medical Center, The Ohio State University, United States

*CORRESPONDENCE
Mudan Zhang
mudan@wh.iov.cn
Qinxue Hu
qhu@wh.iov.cn

SPECIALTY SECTION
This article was submitted to Viral Immunology, a section of the journal Frontiers in Immunology

RECEIVED 01 July 2022
ACCEPTED 06 September 2022
PUBLISHED 23 September 2022

CITATION
Hu H, Fu M, Li C, Zhang B, Li Y, Hu Q and Zhang M (2022) Herpes simplex virus type 2 inhibits TNF-α-induced NF-κB activation through viral protein ICP22-mediated interaction with p65. *Front. Immunol.* 13:983502. doi: 10.3389/fimmu.2022.983502

Herpes simplex virus type 2 inhibits TNF-α-induced NF-κB activation through viral protein ICP22-mediated interaction with p65

Huimin Hu[1,2], Ming Fu[1,3], Chuntian Li[1,2], Binman Zhang[1,2], Yuncheng Li[1,2], Qinxue Hu[1,4]* and Mudan Zhang[1]*

[1]State Key Laboratory of Virology, Wuhan Institute of Virology, Center for Biosafety Mega-Science, Chinese Academy of Sciences, Wuhan, China, [2]Savaid Medical School, University of Chinese Academy of Sciences, Beijing, China, [3]Department of Gastroenterology, Guangzhou Women and Children's Medical Center, Guangzhou Medical University, Guangzhou, China, [4]Institute for Infection and Immunity, St George's, University of London, London, United Kingdom

Herpes simplex virus type 2 (HSV-2) is a prevalent human pathogen and the main cause of genital herpes. After initial infection, HSV-2 can establish lifelong latency within dorsal root ganglia by evading the innate immunity of the host. NF-κB has a crucial role in regulating cell proliferation, inflammation, apoptosis, and immune responses. It is known that inhibition of NF-κB activation by a virus could facilitate it to establish infection in the host. In the current study, we found that HSV-2 inhibited TNF-α-induced activation of NF-κB-responsive promoter in a dose-dependent manner, while UV-inactivated HSV-2 did not have such capability. We further identified the immediate early protein ICP22 of HSV-2 as a vital viral element in inhibiting the activation of NF-κB-responsive promoter. The role of ICP22 was confirmed in human cervical cell line HeLa and primary cervical fibroblasts in the context of HSV-2 infection, showing that ICP22 deficient HSV-2 largely lost the capability in suppressing NF-κB activation. HSV-2 ICP22 was further shown to suppress the activity of TNF receptor-associated factor 2 (TRAF2)-, IκB kinase α (IKK α)-, IKK β-, IKK γ-, or p65-induced activation of NF-κB-responsive promoter. Mechanistically, HSV-2 ICP22 inhibited the phosphorylation and nuclear translocation of p65 by directly interacting with p65, resulting in the blockade of NF-κB activation. Furthermore, ICP22 from

Abbreviations: NF-κB, Nuclear factor κB; HIV, Human immunodeficiency virus; HSV, Herpes simplex virus; ICP22, Infected cell protein 22; IFNs, Interferons; IRF3, IFN-regulatory factor 3; TNF-α, Tumor necrosis factor alpha; TNFR, Tumor necrosis factor receptor; TRAF2, TNFR-associated factor 2; IKK, Inhibitor κB (IκB) kinase complex; IKK α, IκB kinase (IKK) α; ISGs, Interferon-stimulated genes; ISGF3, IFN-stimulated gene factor 3; RHD, Rel homology domain; NLS, Nuclear localization sequence.

10.3389/fimmu.2022.983502

several alpha-herpesviruses could also inhibit NF-κB activation, suggesting the significance of ICP22 in herpesvirus immune evasion. Findings in this study highlight the importance of ICP22 in inhibiting NF-κB activation, revealing a novel mechanism by which HSV-2 evades the host antiviral responses.

KEYWORDS

HSV-2, ICP22, NF-κB, p65, immune evasion

Introduction

HSV-2 is a large dsDNA virus, a member of the Herpesviridae family, belonging to genus Simplexvirus. The WHO reported that about 13% of the world's population aged 15 to 49 years were living with HSV-2 infection in 2016 (1). HSV-2 is mainly sexually transmitted and infects epithelial cells, causing genital herpes (2). It also infects leukocytes and neuronal cells (3–5), leading to encephalitis and disseminated diseases that affect other organ systems (6, 7). After initial infection, HSV-2 can establish life-long latency in the dorsal root ganglia (8).

It is known that HSV (HSV-1/2) has evolved countermeasures to evade the host innate immune responses. However, most of the studies to date have been focusing on HSV-1 (9). For instance, the UL2, UL24, UL42, RL2 and US3 of HSV-1 can interfere with the NF-κB signaling pathway by interacting with p65 or p50, the key component of NF-κB heterodimer (10–14), while HSV-1 UL36 suppresses NF-κB activation by cleaving the polyubiquitin chains of IκB α, an inhibitor of NF-κB activation (15). The RL2, RL1 and UL48 of HSV-1 suppress the production of type I interferons (IFN) by acting on IRF3 (16, 17), whereas the UL54, US11 and UL46 of HSV-1 act on TBK1 to block the production of type I IFN (18–20). In addition, the RL2 and UL41 of HSV-1 were reported to suppress the production of IFN-stimulated genes (ISGs) by degrading IFI16 (21). So far, little is known concerning how HSV-2 evades the host innate immune system. We previously demonstrated that the immediate early protein ICP22 of HSV-2 not only suppresses IFN-β production by blocking the association of IRF-3 with IFN-β promoter (22), but also inhibits the production of ISGs by directly degrading IFN-stimulated gene factor 3 (ISGF3) (23). Although ICP22 is a key mediator of HSV-2 immune evasion in type I IFN production and signaling, it remains to be determined whether HSV-2 ICP22 could inhibit the activation of NF-κB signaling pathway.

TNF receptor-associated factor 2 (TRAF2), IκB kinase (IKK) α (IKK α), IKK β, IKK γ and p65 are key components of the NF-κB signaling pathway. Under foreign stimuli, the IKK complex is first activated, resulting in the phosphorylation of IκB proteins and its subsequent degradation by the proteasome. Once IκB protein is detached, released NF-κB dimers are phosphorylated and then translocate to the nucleus to activate the transcription of target genes (24–26). Given that a number of viruses were previously shown to block the activation of NF-κB by acting on different components of NF-κB signaling pathway (27–33), we asked whether and how HSV-2 inhibits NF-κB activation.

In this study, we first revealed that HSV-2 blocks TNF-α-induced activation of NF-κB-responsive promoter. We further demonstrated that the immediate early protein ICP22 of HSV-2 inhibits NF-κB activation by directly interacting with p65, resulting in the blockade of p65 phosphorylation and nuclear translocation.

Materials and methods

Cell lines and viruses

HEK 293T, human cervical epithelial cell line HeLa, and African green monkey kidney cell line Vero were purchased from American Type Culture Collection and cultured in Dulbecco's modified Eagle medium (DMEM) (Gibico, C11995500BT) supplemented with 10% fetal bovine serum (FBS) (Gibico, 10099-141), and 100 U/mL of penicillin and streptomycin each (Genom, GMN15140) at 37°C in a 5% CO_2 incubator. Primary human cervical fibroblasts were purchased from Meisen Chinese Tissue Culture Collections (Meisen CTCC, CTCC-088-HUM) (Zhejiang, China) and cultured in primary fibroblast culture medium (Meisen CTCC, CTCC-003-PriMed). HSV-2 (G strain) was obtained from LGC standards and propagated in Vero cells. Virus stock supplemented with 10% FBS (Gibico, 10099-141) was stored at −80°C before being used for infection. UV-inactivated HSV-2 was obtained by exposure to UV irradiation for 30 min. HSV-2 titration was determined by plaque assay on Vero monolayers. ICP22 deficient HSV-2, named *us1* del HSV-2, was constructed and produced as previously described (22).

Antibodies, reagents and plasmids

Rabbit anti-p65 (10745-1-AP), mouse anti-β-actin (66009-1-Ig) and HA-tag (66006-2-Ig) polyclonal antibodies were purchased from Proteintech (Wuhan, China). Mouse anti-IκB α (L35A5) and phospho-p65 (ser536) (93H1) antibodies were purchased

from Cell Signaling Technology. Mouse antibodies against IKK α (sc-7606), IKK β (sc-271782), and IKK γ (sc-8032), respectively, were purchased from Santa Cruz Biotechnology. A mouse anti-Flag monoclonal antibody (mAb) (F1804) was obtained from Sigma-Aldrich. A sheep polyclonal antibody against HSV-2 (ab21112) was purchased from Abcam. Mouse normal IgG (A7028) was purchased from Beyotime. Rabbit normal IgG (A7016) was purchased from Beyotime. Recombinant human TNF-α (300-01A-50) was purchased from PeproTech. HA-tagged plasmids pHA-TRAF2, pHA-IKK α, pHA-IKK β, pHA-IKK γ, and Flag-tagged plasmid pFlag-p65 and the reporter plasmids phRL-TK and pNF-κB-Luc were kindly provided by Professor Hanzhong Wang at the Wuhan Institute of Virology, Chinese Academy of Sciences (34, 35). The coding sequences (CDS) of PRV ICP22 (Gene ID: 2952489) and VZV ICP22 (Gene ID: 1487700) were synthesized and cloned into pcDNA3.1(+) vector, respectively, by GeneCreate Biological Engineering Co, Ltd. (Wuhan, China). The Flag-tagged expression plasmids of HSV-1 ICP22 and HSV-2 UL46 and ICP22 were described in our previous studies (22, 36, 37). All the constructs were verified by DNA sequencing (Sunny Biotechnology, China).

Dual luciferase reporter assay

HEK 293T cells seeded in 24-well plates overnight were co-transfected with Firefly luciferase reporter plasmid pNF-κB-Luc, Renilla luciferase reporter plasmid phRL-TK and empty vector or plasmid encoding indicated viral protein. Transfections were performed using Lipofectamine 2000 (Invitrogen, 11668-027) according to the manufacturer's instructions. At 24 h post-transfection, cells were mock-treated or treated with TNF-α (20 ng/ml) for 6 h. In some cases, HEK 293T cells were co-transfected with pNF-κB-Luc, phRL-TK, plasmid expressing pFlag-p65, pHA-TRAF2, pHA-IKK α, pHA-IKK β or pHA-IKK γ and empty vector or plasmid expressing indicated viral protein for 30 h. For HeLa cells, after co-transfection with reporter plasmids pNF-κB-Luc and phRL-TK for 4 h, cells were infected or mock infected with HSV-2, UV-inactivated HSV-2 or *us1* del HSV-2 for 20 h, followed by stimulation with or without TNF-α (20 ng/ml) for 6 h. For primary human cervical fibroblasts, after co-transfection with reporter plasmids pNF-κB-Luc and phRL-TK for 4 h, cells were infected with HSV-2 or *us1* del HSV-2 for 20 h, followed by stimulation with or without TNF-α (20 ng/ml) for 6 h. Cells were subsequently harvested and lysed to measure Firefly and Renilla luciferase activities using a Dual Luciferase Reporter (DLR) Assay System (Promega, E1980) according to the manufacturer's instructions.

Western blot

The proteins from transfected or infected cells were prepared using Lysis Buffer supplemented with protease inhibitor cocktail (Roche, 11697498001). Prepared cell lysates or immunoprecipitates were subjected to 10% SDS-PAGE and transferred to 0.45 μm polyvinylidene difluoride (PVDF) membranes (Millipore, IPVH00010 PORE). The membrane was blocked using 5% non-fat milk in TBST (20 mM Tris-HCl buffer [pH 7.4] containing 37 mM NaCl and 0.1% Tween 20) at 4°C for 1 h, followed by incubation with a primary Ab overnight at 4°C. After three washes with TBST, the membrane was probed with a HRP-conjugated secondary Ab (Proteintech, SA00001-1 or SA00001-2) at room temperature for 1 h, and then washed five times with TBST. The bands were visualized by exposure to ChemiDoc MP Imaging System after the addition of chemiluminescent substrate.

RNA isolation and quantitative PCR

Cells were collected to extract total RNA using TRIzol (Invitrogen, 15596-026) according to the manufacturer's instructions. Subsequently, cDNA was synthesized with the HiScript II Q RT SuperMix for qPCR (+gDNA wiper) (Vazyme Biotech, R223-01). Relative real-time quantitative PCR was performed on a CFX Real-Time PCR system (Bio-Rad) using ChamQ SYBR qPCR Master Mix (High ROX Premixed) (Vazyme Biotech, Q341-02). The specific primer sequences were as follows: 5′-GCCATTCTGATTTGCTGC-3′ (forward) and 5′-CCTTTCCTTGCTAACTGC-3′ (reverse) for CXCL10, 5′-GGAAATCCCATCACCATC-3′ (forward) and 5′-CATCACGCCACAGTTTCC-3′ (reverse) for GAPDH. The expression difference was calculated on the basis of $2^{-\Delta\Delta Ct}$ values.

Co-immunoprecipitation assay

HeLa cells seeded in 6-well plates were transfected with Flag-tagged ICP22-expressing plasmid or empty vector. At 24 h post-transfection, cells were mock-treated or treated with TNF-α (20 ng/mL) for 6 h. Cells were subsequently harvested and lysed on ice for 30 min using 200 μL lysis buffer (50 mM Tris [pH 8.0], 150 mM NaCl, 1% NP40) containing protease inhibitor cocktail (Roche, 11697498001). 3 μg mouse anti-Flag Ab or mouse normal IgG (BOSTER, BA1051) was added to fresh Dynabeads protein G (Invitrogen, 10003D), and mixed with cell lysate, respectively. In some cases, 3 μg rabbit anti-p65 Ab or rabbit normal IgG (Beyotime, A7016) was mixed with fresh Dynabeads protein G, and the mixture was then added to cell lysates. After incubation with rotation overnight at 4°C, the Ag-Ab-dynabead complexes were washed three times with PBST, and then the target antigens (Ags) were subjected to western blot analysis after elution followed by boiling.

Binding kinetic analysis

Human recombinant p65 protein was purchased from SinoBiological Incorporation (12054-H09E, China). HA-tagged

ICP22 was purified as described previously (23). Briefly, for every 1 × 10^6 cells, 1.5 μg expression plasmid was transfected into HEK 293F cells using Polyethylenimine (PEI) transfection reagent (Polysciences, 23966-1, China). Cells were cultured in FreeStyle 293 Expression Medium (Gibico, 12338018, USA) at 37°C in a 5% CO_2 incubator shaker at 110 rpm. At day 3 post-transfection, cells were harvested and lysed by ultrasonic treatment. The HA-tagged protein was purified by anti-YPYDVPDYA Affinity Resin (DIA•AN, KAP0063, China) and eluted with 300 μg/mL YPYDVPDYA peptide (GenScript, RP11735, China). The purified protein was concentrated in PBS using 10 kDa Centrifugal Filter Units (Merck, UFC901096, Germany) for binding kinetic study.

The kinetics of binding was performed on a Forte-Bio Octet Red System. After Protein A Biosensors (Fortebio, 18-5010, USA) were soaked in 1× PBS, 5 μg/mL anti-p65 Ab was diluted and captured by the Biosensors. The Abs-captured Biosensors were used to bind p65, and then immersed in different concentration of ICP22 (62.5, 125, 250, 500 or 1000 nM) for association and disassociation. The response in nm shift was recorded as a function of time.

Immunofluorescence analysis

HeLa cells seeded in 35-mm glass-bottom dishes were transfected with Flag-tagged ICP22-expressing plasmid. At 24 h post-transfection, cells were treated with or without 20 ng/mL TNF-α for 6 h, and then fixed with 4% paraformaldehyde at room temperature for 10 min. After permeabilized with 0.2% Triton X-100 at room temperature for 10 min, cells were blocked in PBS containing 3% BSA at 4°C overnight. Thereafter, cells were incubated with the rabbit anti-human p65 polyclonal Ab (pAb) and the mouse anti-Flag mAb for 1 h at 37°C. After three washes with PBS, cells were then incubated with Alexa Fluor 488-labeled Goat anti-Mouse IgG (H+L) (Invitrogen, A-10667) and Alexa Fluor 647-labeled Goat anti-Rabbit IgG (H+L) (Invitrogen, A27018) for 1 h at 37°C. Cells were subsequently washed and incubated with DAPI for 10 min at 37°C. After washes, cells were observed under a fluorescence microscope (Nikon A1R/MP).

Statistical analysis

All experiments were repeated at least three times and the data were presented as mean ± SD unless otherwise specified. Data analyses were performed with GraphPad Prism 7.0 software (GraphPad). Comparison between two groups was analyzed by Student t-test, whereas comparisons among more than two groups were analyzed by one-way ANOVA with the Tukey's test. $P < 0.05$ was considered statistically significant.

Results

Productive HSV-2 infection suppresses TNF-α-induced NF-κB activation

It is known that HSV-2 can evade the host innate immunity to establish lifelong infection. Considering the critical role of NF-κB in the innate immunity, we examined the effect of HSV-2 infection on NF-κB activation. Given that human genital epithelial cells are the main targets of HSV-2 primary infection, we used human cervical epithelial cell line HeLa for the initial experiment. HeLa cells were co-transfected with the reporter plasmids pNF-κB-Luc and phRL-TK for 4 h, followed by infection with HSV-2 or UV-inactivated HSV-2 at an MOI of 1, 0.6, 0.3, or 0.1 for 20 h. After 6 h stimulation with TNF-α, the activities of luciferase were detected. As shown in Figure 1A, HSV-2 significantly inhibited the activation of NF-κB-responsive promoter, whereas UV-inactivated HSV-2 did not have such capability. We further confirmed that the viral proteins were barely detectable by WB after HSV-2 was inactivated by UV (Figure 1B), indicating that productive infection is necessary for HSV-2-mediated inhibition of NF-κB activation. Given that the chemokine CXCL10 could be induced *via* NF-κB activation (38, 39), we detected whether HSV-2 infection affects CXCL10 mRNA production. As showed in Figure 1C, HSV-2 infection indeed inhibited NF-κB activation-induced CXCL10 mRNA production, further suggesting the inhibitory effect of HSV-2 on NF-κB activation. These results indicate that HSV-2 infection suppresses TNF-α-induced NF-κB activation and that productive HSV-2 infection is necessary for such suppression.

HSV-2 ICP22 inhibits TNF-α-induced NF-κB activation

Our previous studies show that the HSV-2 ICP22 not only suppresses IFN-β production by blocking the association of IRF-3 with IFN-β promoter (22), but also inhibits the production of ISGs by directly degrading ISGF3 (23). Considering the key role of ICP22 in HSV-2-mediated immune evasion, we next assessed the involvement of HSV-2 ICP22 in interfering with NF-κB signaling pathway. HEK 293T cells were co-transfected with the reporter plasmids pNF-κB-Luc and phRL-TK together with ICP22-expressing plasmid. At 24 h post-transfection, cells were stimulated with TNF-α for 6 h. As shown in Figure 2A, HSV-2 ICP22 significantly inhibited the activation of NF-κB-responsive promoter. Moreover, HSV-2 ICP22 also suppressed CXCL10 mRNA production (Figure 2B). To confirm the role of ICP22 in the inhibition of NF-κB activation in the context of virus infection, HeLa cells or primary human cervical fibroblasts were transfected with the reporter plasmids pNF-κB-Luc and

10.3389/fimmu.2022.983502

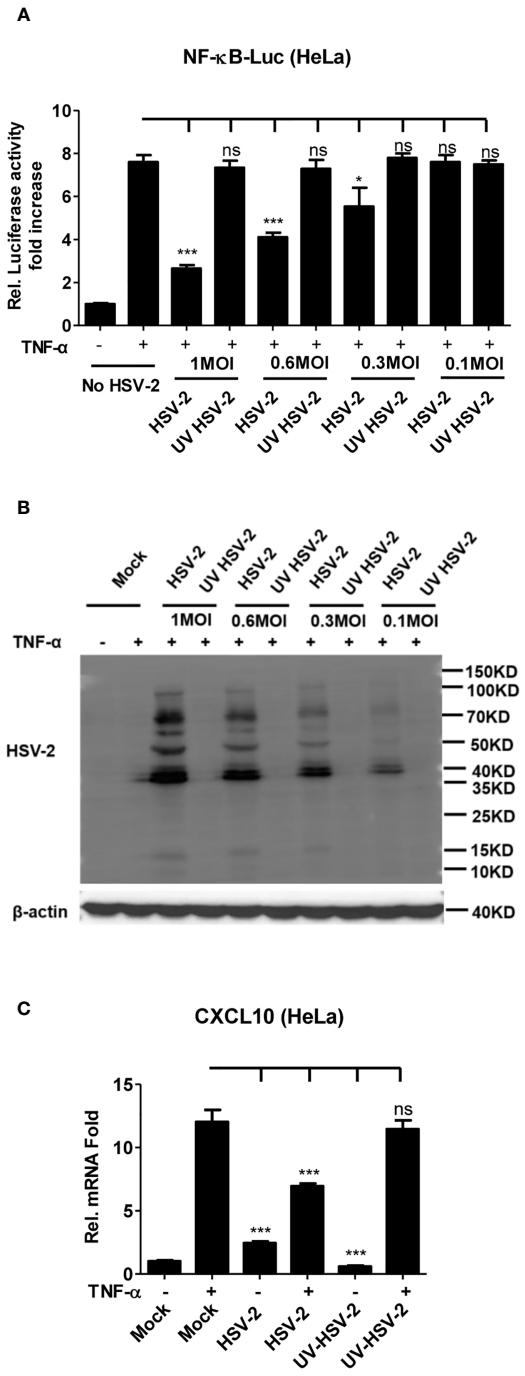

FIGURE 1
Productive HSV-2 infection suppresses TNF-α-induced NF-κB activation. **(A)** Productive HSV-2 infection suppresses TNF-α-induced NF-κB activation. HeLa cells were seeded in 24-well plates overnight and co-transfected with the reporter plasmids pNF-κB-Luc and phRL-TK. At 4 h post-transfection, cells were mock infected or infected with HSV-2 or UV-inactivated HSV-2 (UV HSV-2) at an MOI of 1, 0.6, 0.3, or 0.1. At 20 h post-infection, cells were stimulated with or without TNF-α (20 ng/ml) for 6 h. Reporter activities were determined by DLR assay. **(B)** Detection of viral protein expression in HSV-2-infected cells. HeLa cells were infected with HSV-2 or UV-inactivated HSV-2 at an MOI of 1, 0.6, 0.3, or 0.1 for 24 h. The expression of viral protein was detected by western blot using the anti-HSV-2 Ab. β-actin was used as a loading control. **(C)** HSV-2 infection inhibits CXCL10 mRNA production. HeLa cells seeded in 6-well plates were infected with HSV-2 or UV-inactivated HSV-2. At 24 h post-infection, cells were stimulated with TNF-α (20 ng/ml) for 6 h. Cells were harvested and total RNA was extracted. The expression of CXCL10 and GAPDH genes was evaluated by relative real-time quantitative PCR. For graphs, data shown are mean ± SD of three independent experiments with each condition performed in triplicate. For images, one representative experiment out of three is shown. *$p < 0.05$, ***$p < 0.001$. ns, not significantly. Rel, Relative.

10.3389/fimmu.2022.983502

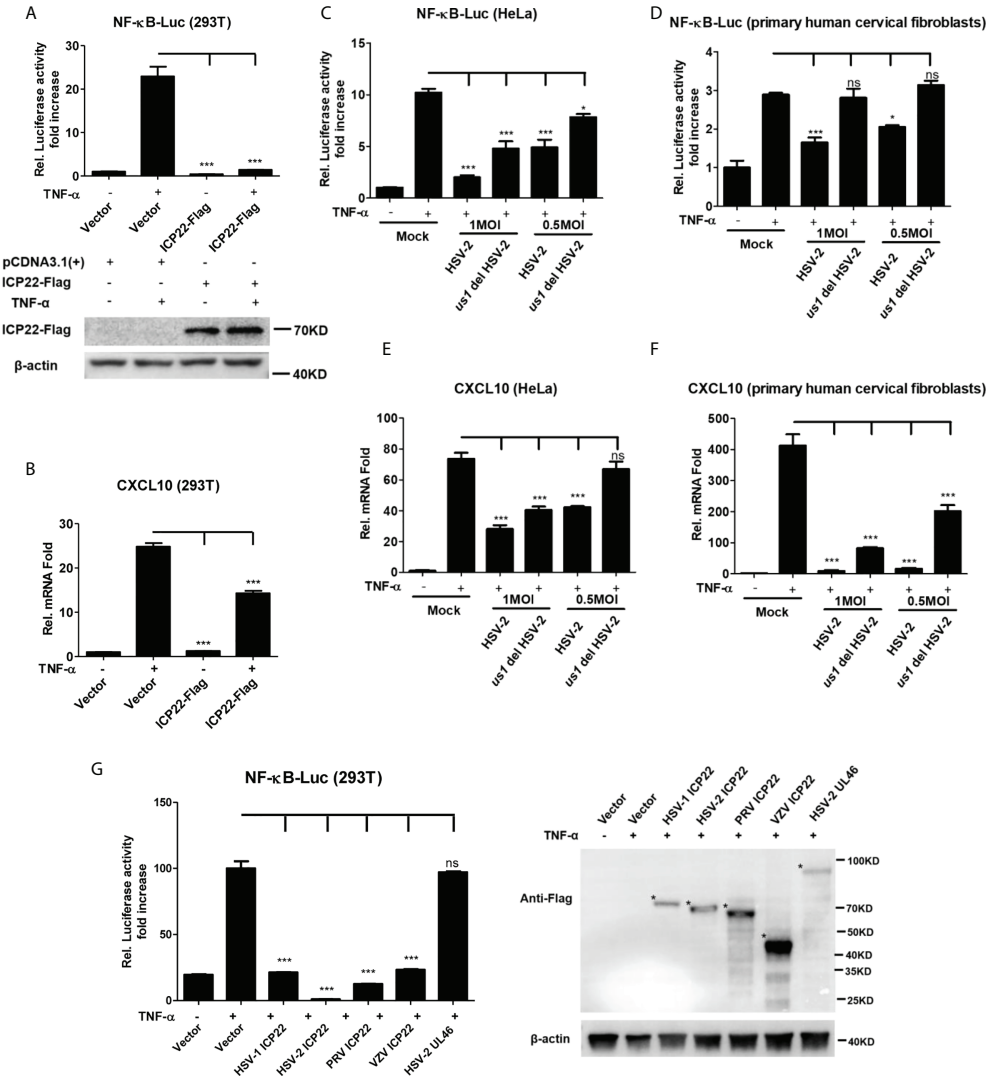

FIGURE 2
HSV-2 ICP22 inhibits TNF-α-induced NF-κB activation. **(A)** HSV-2 ICP22 suppresses TNF-α-induced NF-κB activation. HEK 293T cells were seeded in 24-well plates overnight and co-transfected with the reporter plasmids pNF-κB-Luc and phRL-TK together with ICP22-expressing plasmid. At 24 h post-transfection, cells were stimulated with TNF-α (20 ng/ml) for 6 h. Reporter activities were determined by DLR assay. The expression of ICP22 was detected by western blot using the anti-Flag Ab. **(B)** HSV-2 ICP22 suppresses the production of CXCL10 mRNA. HEK 293T cells seeded in 6-well plates were transfected with vector or ICP22-expressing plasmid. At 24 h post-transfection, cells were stimulated with TNF-α (20 ng/ml) for 6 h. Cells were harvested and total RNA was extracted. The expression of CXCL10 and GAPDH genes was evaluated by relative real-time quantitative PCR. **(C, D)**. ICP22 knockout impairs the inhibitory activity of HSV-2 on NF-κB activation. HeLa cells or primary human cervical fibroblasts were seeded in 24-well plates overnight and transfected with the reporter plasmids pNF-κB-Luc and phRL-TK, followed by infection with HSV-2 or *us1* del HSV-2. After stimulation with TNF-α for 6 h, reporter activities were determined by DLR assay. **(E, F)**. HSV-2 ICP22 knockout impairs the inhibitory activity of HSV-2 on CXCL10 mRNA production. HeLa cells or primary human cervical fibroblasts seeded in 6-well plates were infected with HSV-2 or *us1* del HSV-2 at an MOI of 1. After stimulation with TNF-α for 6 h, cells were harvested and total RNA was extracted. The expression of CXCL10 and GAPDH genes was evaluated by relative real-time quantitative PCR. **(G)** ICP22s from several alpha-herpesviruses significantly inhibit NF-κB activation. HEK 293T cells were co-transfected with the reporter plasmids pNF-κB-Luc and phRL-TK together with ICP22-expressing plasmid of HSV-1, PRV or VZV, or expression plasmid of HSV-2 UL46. At 24 h post-transfection, cells were stimulated with TNF-α (20 ng/ml) for 6 h. Reporter activities were determined by DLR assay. The expressions of HSV-1 ICP22-Flag, HSV-2 ICP22-Flag, PRV ICP22-Flag, VZV ICP22-Flag and HSV-2 UL46-Flag were detected by western blot. Asterisk indicated the locations of proteins. For graphs, data shown are mean ± SD of three independent experiments with each condition performed in triplicate. For images, one representative experiment out of three is shown. *p < 0.05, ***p<0.001, ns, not significantly. Rel, Relative.

phRL-TK for 4 h, followed by infection with HSV-2 or *us1* del HSV-2, which was constructed as described previously (22), for 20 h, and a stimulation with TNF-α for another 6 h. The results showed that ICP22 knockout significantly impaired the capability of HSV-2 in inhibiting NF-κB activation (Figures 2C, D) and CXCL10 mRNA production (Figures 2E, F) in both HeLa cells and primary human cervical fibroblasts. To address whether the inhibitory effect of HSV-2 ICP22 on NF-κB activation was virus specific, we assessed the effects of the ICP22s from several alpha-herpesviruses on NF-κB activation. The results showed that the ICP22s of alpha-herpesviruses HSV-1, PRV and VZV all significantly inhibited NF-κB activation, whereas HSV-2 UL46 had no such effect (Figure 2G), suggesting the significance of ICP22 in herpesvirus immune evasion. These results collectively indicate that HSV-2 ICP22 inhibits TNF-α-induced NF-κB activation.

HSV-2 ICP22 inhibits NF-κB activation by acting on the downstream of p65

IκB protein inhibits the activation of NF-κB by trapping NF-κB in the cytoplasm (40). Under foreigner stimuli, IKK complex phosphorylates IκB, resulting in the phosphorylation, and subsequent degradation of IκB. Once IκB is detached from NF-κB, NF-κB is phosphorylated and activated (41). To understand how HSV-2 ICP22 antagonizes NF-κB activation, HEK 293T cells were co-transfected with the reporter plasmids pNF-κB-Luc and phRL-TK, and the plasmid expressing TRAF2, IKK α, IKK β, IKK γ or p65, together with ICP22-expressing plasmid or empty vector for 30 h. As showed in Figures 3A–E, overexpression of TRAF2, IKK α, IKK β, IKK γ or p65 resulted in the activation of NF-κB-responsive promoter, whereas HSV-2 ICP22 significantly inhibited TRAF2, IKK α, IKK β, IKK γ or

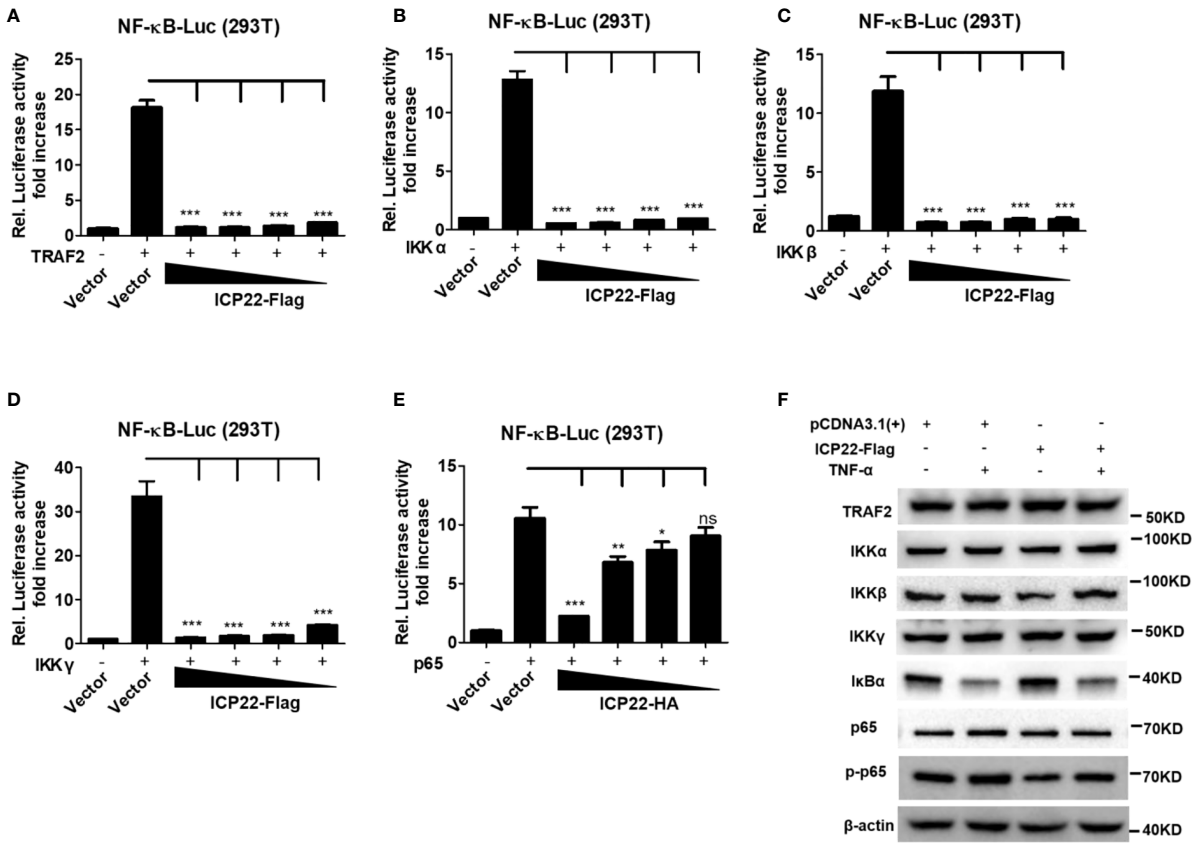

FIGURE 3
HSV-2 ICP22 inhibits NF-κB activation by acting on the downstream of p65. **(A–E)**. HSV-2 ICP22 inhibits TRAF2, IKK α, IKK β, IKK γ and p65-induced NF-κB activation. HEK 293T cells were seeded in 24 well plates overnight and co-transfected with the reporter plasmids pNF-κB-Luc and phRL-TK, and plasmid expressing TRAF2, IKK α, IKK β, IKK γ or p65, together with empty vector or ICP22-expressing plasmid. At 30 h post-transfection, the reporter activities were determined by DLR assay. **(F)**. HSV-2 ICP22 has no effect on the expression of TRAF2, IKK α, IKK β, IKK γ and p65 or degradation of IκB α. HEK 293T cells were seeded in 6 well plates overnight and transfected with plasmid expressing ICP22 or empty vector. At 24 h post-transfection, cells were stimulated with or without TNF-α (20 ng/ml) for 6 h. The expressions of TRAF2, IKK α, IKK β, IKK γ, IκB α, p65 and phospho-p65 were detected by western blot. For graphs, data shown are mean ± SD of three independent experiments with each condition performed in triplicate. For images, one representative experiment out of three is shown. *p<0.05, **p<0.01, ***p<0.001, ns, not significantly.

p65-induced NF-κB activation, without affecting the expression of TRAF2, IKK α, IKK β, IKK γ, and p65 (Figure 3F). As showed in Figure 3F, in the condition of TNF-α stimulation, the inhibitory factor IκB α was degraded in both vector- and ICP22-transfected cells indicating that HSV-2 ICP22 did not affect the degradation of IκB α, while the total level of phospho-p65 was decreased in ICP22-tranfected cells. These results collectively indicate that HSV-2 ICP22 inhibits the activation of NF-κB by acting on the downstream of p65.

HSV-2 ICP22 inhibits the phosphorylation and nuclear translocation of p65

Given that HSV-2 ICP22 inhibits the activation of NF-κB by acting on the downstream of p65, we next investigated the influence of ICP22 on p65 phosphorylation and nuclear translocation. HeLa cells were transfected with ICP22-expressing plasmid, followed by stimulation with TNF-α for 6 h. Cytoplasmic and nuclear proteins were subsequently isolated and detected by western blot to determine the distribution of p65. As showed in Figure 4A (Lane 1-4), the phosphorylation of p65 in the cytoplasm was inhibited by ICP22, although the expression of total p65 was not affected by ICP22 (Figure 3F). Meanwhile the phosphorylated p65 in the nucleus also decreased in ICP22-transfected cells (Figure 4B Lane 1-4). To further confirm the effect of ICP22 on p65 phosphorylation and nuclear translocation in the context of virus infection, HeLa cells were mock infected or infected with HSV-2 or *us1* del HSV-2. At 24 h post-infection, cells were stimulated with or without TNF-α for 6 h. As showed in Figures 4A, B, HSV-2 infection could inhibit the

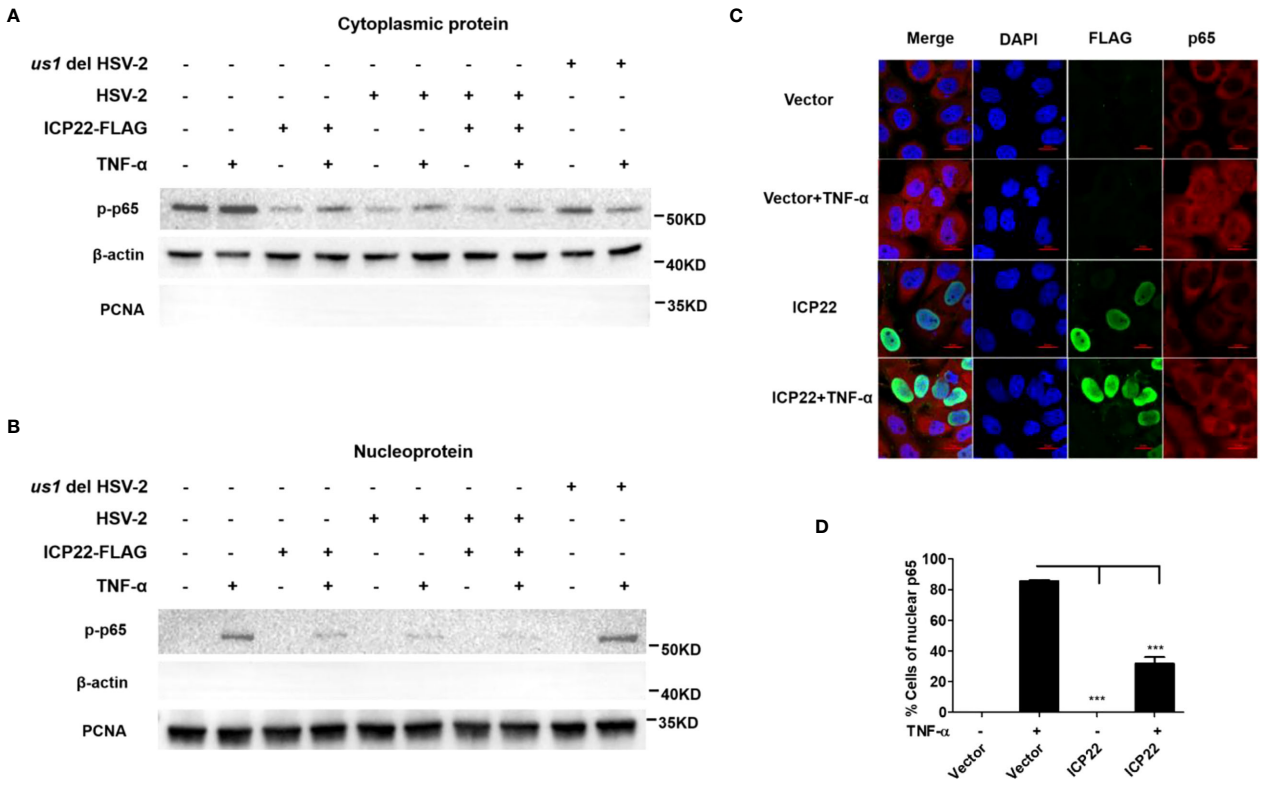

FIGURE 4
HSV-2 ICP22 inhibits the phosphorylation and nuclear translocation of p65. **(A, B)**. HSV-2 ICP22 inhibits the phosphorylation of p65. HeLa cells seeded in the 6 well plates were transfected with empty vector or ICP22-expressing plasmid. At 4 h post-transfection, cells were mock infected or infected with HSV-2 or *us1* del HSV-2 at an MOI of 1. At 20 h post-infection, cells were stimulated with or without TNF-α (20 ng/ml) for 6 h. The phosphorylated p65 in the cytoplasm and nucleus were detected by western blot. β-actin and PCNA were used as loading controls for cytoplasmic and nuclear proteins, respectively. **(C, D)**. HSV-2 ICP22 significantly inhibits the nuclear translocation of p65. HeLa cells were transfected with ICP22-expressing plasmid or empty vector. At 24 h post-transfection, cells were stimulated with or without TNF-α (20 ng/ml) for 6 h. Cells were stained using the mouse anti-Flag and the rabbit anti-p65 Ab. Alexa Fluor 488-conjugated goat anti-mouse (green) and Alexa Fluor 647-conjugated goat anti-rabbit (red) were used as secondary antibodies. Cell nuclei (blue) were stained with DAPI. The images were obtained by fluorescence microscopy using a 60× objective. The percentage of p65-positive nuclei was quantified in a number of fields **(D)**. The scale bar indicates 20 μm. For graphs, data shown are mean ± SD of three independent experiments with each condition performed in triplicate. For images, one representative experiment out of three is shown. ***p < 0.001.

phosphorylation and nuclear translocation of p65 (Lane 5-6), whereas ICP22 knockout obviously impaired the inhibitory effect of HSV-2 on p65 phosphorylation and nuclear translocation (Lane 9-10). Immunofluorescence assay further showed that p65 translocated from the cytoplasm into the nucleus in the majority of cells after stimulation with TNF-α, and such translocation was significantly blocked in ICP22-transfected cells (Figures 4C, D). These results together indicate that HSV-2 ICP22 inhibits the phosphorylation and nuclear translocation of p65.

HSV-2 ICP22 directly interacts with p65

To address how ICP22 suppresses the phosphorylation of p65, co-immunoprecipitation assay was performed to assess the interaction of HSV-2 ICP22 with p65. As showed in Figures 5A, B, HSV-2 ICP22 was found to interact with endogenous p65 in both pull-down experiments using the anti-Flag or anti-p65 antibody. To further confirm the results, recombinant HSV-2 ICP22 and human p65 were used to measure the binding kinetics of ICP22 with p65, showing that HSV-2 ICP22 indeed directly interacts with p65 (Figure 5C). p65 contains a conserved Rel homology domain (RHD) at the N terminus, which is responsible for nuclear localization, dimerization and DNA binding (24). To map the functional region of p65 interacting with ICP22, we constructed three truncation mutants Δ1, Δ2 and Δ3 (36). As showed in Figure 5D, Δ1 (19-306aa) retains complete RHD of p65, while Δ2 (19-300aa) is deficient in the nuclear localization signal (NLS) domain of RHD. Δ3 (19-187aa) only retains the DNA binding domain of RHD. Subsequently, His-tagged full-length p65 or its truncated mutants (named Δ1, Δ2, and Δ3) were used to identify the functional domain of p65 interacting with HSV-2 ICP22. Co-immunoprecipitation assay showed that full-length p65 and its three truncation mutants Δ1, Δ2 and Δ3 all interacted with ICP22 (Figure 5E). The interaction of ICP22 with p65 seemed to be weakened when the dimerization domain of p65 was deleted, indicating that the dimerization domain of p65 likely plays a more important role in the interaction. These results together inform that HSV-2 ICP22 directly interacts with p65, resulting in the blockade of p65 phosphorylation and nuclear translocation.

Discussion

HSV-2 is one of the most common sexually transmitted viruses worldwide, causing neonatal herpes and genital ulcer disease (42). HSV-2 and HSV-1 are closely related but exhibit substantial differences in latency and reactivation patterns (10–14, 43). NF-κB is a key regulator of a broad range of cellular responses, involved in the induction of inflammation (24, 44–46). Although a number of studies report that HSV-1 has evolved multiple countermeasures to subvert the activation of NF-κB signaling pathway (10–12, 15, 16, 20, 47), our current understanding of HSV-2 immune evasion against the activation of NF-κB is limited.

In this study, we found that HSV-2 infection inhibited TNF-α-induced activation of NF-κB-responsive promoter, whereas UV-inactivated HSV-2 did not have such inhibition, indicating that productive HSV-2 infection is necessary for the inhibition of NF-κB activation. Subsequent studies indicated that ICP22 has a significant inhibitory effect on the activation of NF-κB-responsive promoter, which was further confirmed in the context of viral infection using ICP22 deficient HSV-2. Moreover, we found that the ICP22s from several alpha-herpesviruses including HSV-1, PRV and VZV all inhibited NF-κB activation, which share 62%, 33% and 31% identity, respectively, with the amino acid sequence of HSV-2 ICP22, highlighting the significance of ICP22 in herpesvirus immune evasion. Given that HSV-2 ICP22 can also suppress the production of type I IFN and ISGs (22, 23), our findings collectively informed that ICP22 is a key viral element counteracting not only type I IFN production and signaling but also NF-κB activation.

It is known that NF-κB activation is an attractive target for common human viral pathogens to evade host antiviral responses (34, 48–50). The activation of NF-κB signaling cascade includes the phosphorylation and nuclear translocation of p65, a major component of NF-κB heterodimer. We found that HSV-2 ICP22 significantly blocked TRAF2, IKK α, IKK β, IKK γ and p65-induced NF-κB activation, but did not affect the expression of TRAF2, IKK α, IKK β, IKK γ and p65 or the degradation of IκB α, indicating that HSV-2 ICP22 likely affects p65 activation. We previously demonstrated that HSV-2 ICP22 functions as a novel E3 ubiquitin protein ligase to degrade ISGF3, resulting in the inhibition of type I IFN signaling (23). However, in the current study, HSV-2 ICP22 appears to inhibit NF-κB activation independent of its E3 ubiquitin protein ligase activity, and instead, it suppresses the phosphorylation and nuclear translocation of p65, leading to the inhibition of NF-κB activation.

Mechanistically, we found that HSV-2 ICP22 directly interacts with endogenous p65. In accordance with previous findings, several other viral proteins of HSV-1 have also been shown to interact with p65 (10–14).The NF-κB family shares the RHD at the N-terminus, which contains 300 amino acids and has three functions: sequence specific DNA-binding, dimerization and inhibitory protein binding (24, 41). By assessing three truncated p65, we found that full-length p65 and its three truncation mutants Δ1, Δ2 and Δ3 all interacted with ICP22. The p65 truncation mutant Δ3 (19-187aa) only

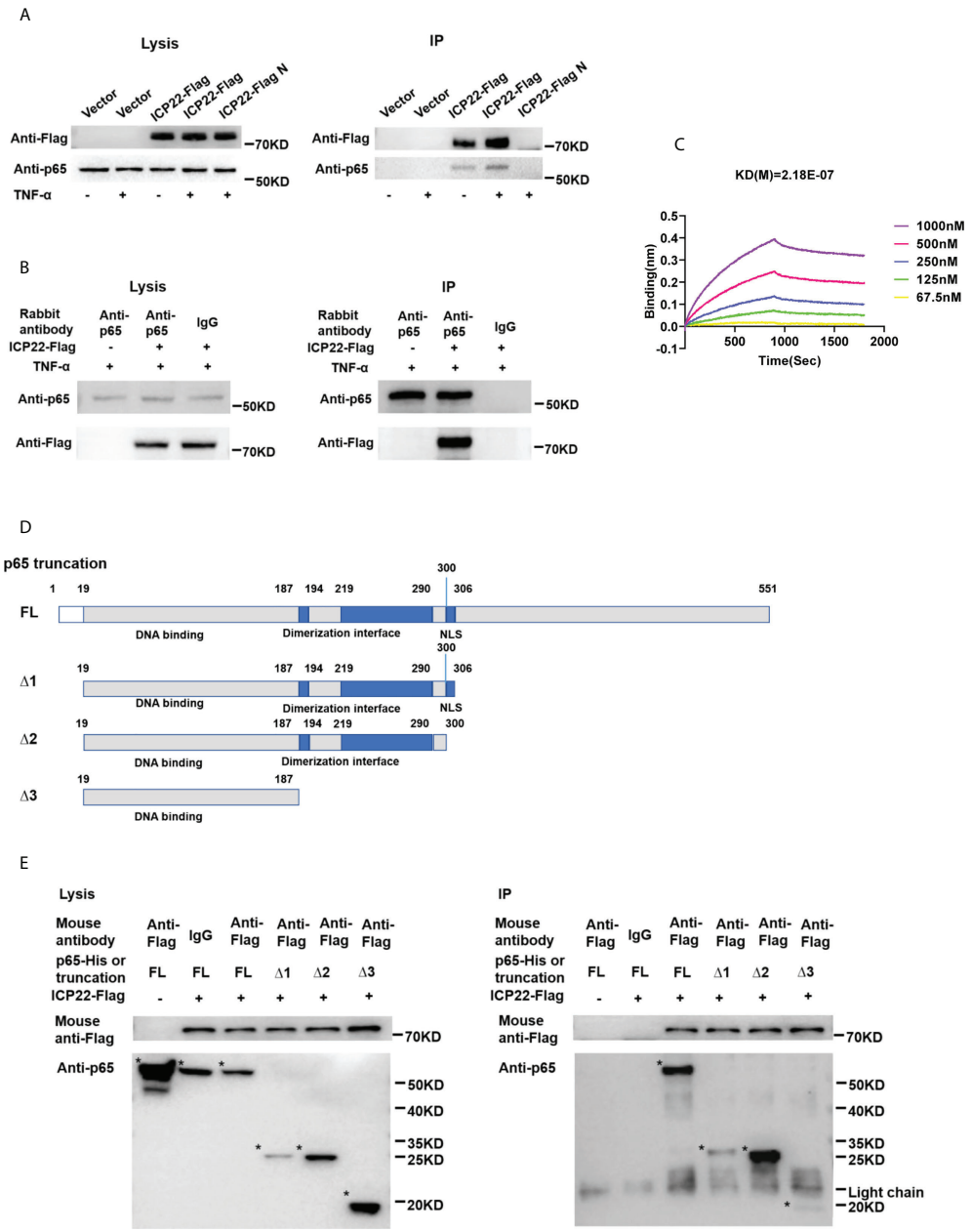

FIGURE 5
HSV-2 ICP22 directly interacts with p65. **(A)** HSV-2 ICP22 interacts with endogenous p65. **(B)** Endogenous p65 interacts with HSV-2 ICP22. HeLa cells seeded in the 6 well plates were transfected with empty vector or ICP22-expressing plasmid. At 24 h post-transfection, cells were mock-treated or treated with TNF-α (20 ng/ml) for 6 h. Cell lysates were then subjected to co-immunoprecipitation assays using the anti-Flag **(A)** or anti-p65 Ab **(B)**. The mouse **(A)** or rabbit **(B)** non-specific antibody was used as negative control. ICP22 and p65 were detected by western blot using the anti-Flag or anti-p65 Ab, respectively. **(C)** HSV-2 ICP22 directly interacts with p65. The kinetics of binding was performed on a Forte-Bio Octet Red System. 5 μg/mL rabbit anti-p65 Ab was coupled to Protein A biosensors. 25 μg/mL recombinant p65 was bound to Biosenors and immersed in different concentration of ICP22 (62.5, 125, 250, 500 or 1000 nM) for association and disassociation. The response in nm shift was recorded as a function of time. KD (M) = 2.18E-07. **(D)** Schematic representation of p65 truncations. **(E)** HSV-2 ICP22 interacts with the three truncation mutants Δ1, Δ2 and Δ3 of p65. Empty vector or ICP22-expressing plasmid and plasmid expressing full-length or truncated p65 were co-transfected into HEK 293T cells. At 24 h post-transfection, cells were mock-treated or treated with TNF-α (20 ng/ml) for 6 h. Cell lysates were then subjected to co-immunoprecipitation assays using the anti-Flag mAb. ICP22, truncated p65 were detected by western blot using the anti-Flag or anti-p65 Ab, respectively. Asterisk indicated the locations of proteins. One representative experiment out of three is shown.

retains the DNA binding domain of RHD. In agreement, our previous study showed that HSV-2 ICP22 also interacts with the DNA binding domain of IRF-3 (22) to suppress IFN-β production, which indirectly supports our co-immunoprecipitation results in this study. An interaction of ICP22 with the DNA binding domain of p65 likely blocks its association with phosphorylase, resulting in the suppression of p65 phosphorylation and nuclear translocation. Given that HSV-2 ICP22 interacts with the DNA binding domain of p65, it likely facilitates viral immune evasion by interfering with the binding of NF-κB with the promoters of regulatory genes in the nucleus.

It is known that HSV-1 ICP22 is an immediate-early protein and a multifunctional viral regulator. HSV-1 ICP22 not only interacts with RNA polymerase II (51–57) and P-TEFb (58) to regulate viral replication (59), but is also involved in posttranslational modification as viral protein kinases (60–63). To date, little is known about the functions of HSV-2 ICP22. We previously revealed that HSV-2 ICP22 functions as a novel E3 ubiquitin protein ligase to degrade ISGF3 (23) and a key viral element contributing to HSV-2 immune evasion (22). Although beyond the scope of this study, future work is warranted to explore the structural characteristics of HSV-2 ICP22 for its multiple functions.

In conclusion, we demonstrated that HSV-2 ICP22 blocks TNF-α-induced activation of NF-κB by directly interacting with p65. The findings highlight the significance of ICP22 in inhibiting NF-κB activation. We proposed a model as described in Figure 6. When the host recognizes foreign PAMPs, the innate immune system is activated by secreting cytokines such as TNF-α. The secreted TNF-α engages TNF receptor (TNFR), resulting in the activation of the IKK complex. Subsequently, the inhibitory protein of NF-κB, IκB α, is phosphorylated, degraded and detached from NF-κB. NF-κB dimers are then released and phosphorylated, and subsequently translocate to the nucleus to activate the expression of immunomodulatory genes. In the case of HSV-2 infection, the viral immediate early protein ICP22 directly interacts with p65 to suppress p65 phosphorylation and nuclear translocation, leading to the blockade of NF-κB activation, which would facilitate viral immune escape.

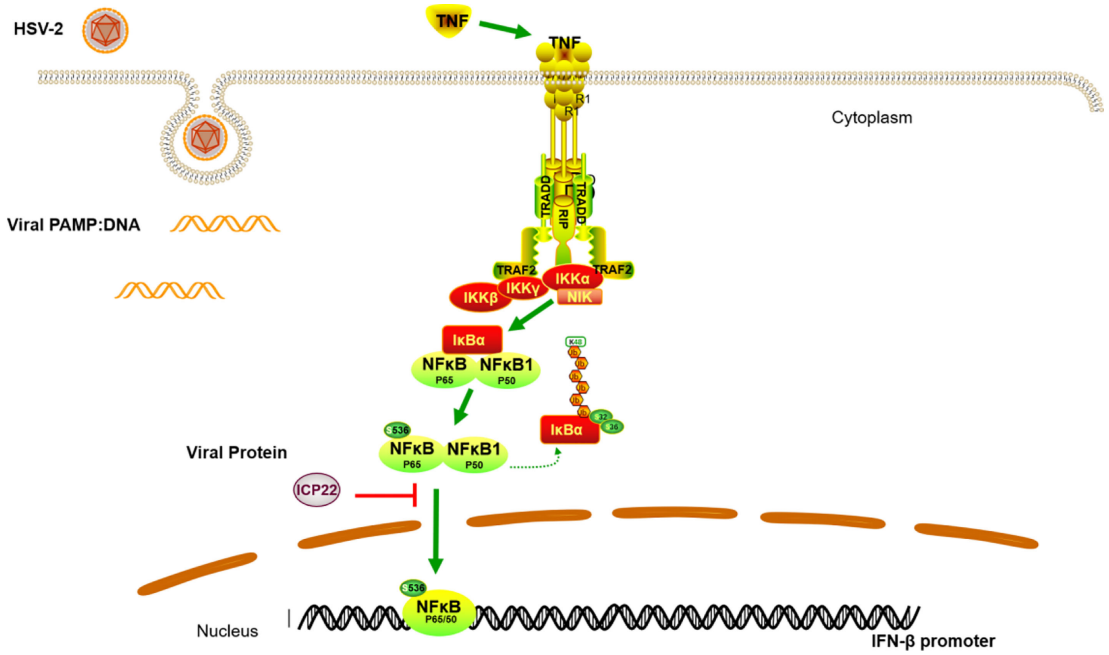

FIGURE 6
A schematic model of the mechanism by which HSV-2 ICP22 blocks TNF-α-induced NF-κB activation. The host recognizes foreign PAMPs and activates the innate immune system to secret cytokines such as TNF-α. TNF-α subsequently binds TNF receptor (TNFR), resulting in the activation of the IKK complex. The inhibitory protein of NF-κB, IκB α, is then phosphorylated, degraded and detached from NF-κB. NF-κB dimers are then released and phosphorylated, and subsequently translocate to the nucleus to activate the expression of immunomodulatory genes. In the case of HSV-2 infection, the viral immediate early protein ICP22 directly interacts with p65 to block p65 phosphorylation and nuclear translocation, leading to an inhibition of NF-κB activation.

Data availability statement

The raw data supporting the conclusions of this article will be made available by the authors, without undue reservation.

Author contributions

HH, MZ and QH conceived the study. HH and MZ conducted most experiments. CL constructed the truncation mutants of p65. MF, BZ and YL provided help in western blot experiments. HH, MZ and QH analyzed the data. HH, MZ and QH wrote the manuscript. All authors contributed to the article and approved the submitted version.

Funding

This work was supported by National Natural Science Foundation of China (82171736, 81772192 and 31970172), and the National Mega-Projects against Infectious Diseases (2018ZX10301406-002).

Acknowledgments

We thank Ding Gao at the Center for Instrumental Analysis and Metrology, Wuhan Institute of Virology, Chinese Academy of Sciences for technical assistance of Confocal Microscopy and BioLayer Interferometry.

Conflict of interest

The authors declare that the research was conducted in the absence of any commercial or financial relationships that could be construed as a potential conflict of interest.

Publisher's note

References

1. McQuillan G, Kruszon-Moran D, Flagg EW, Paulose-Ram R. Prevalence of herpes simplex virus type 1 and type 2 in persons aged 14-49: United states, 2015-2016. *NCHS Data Brief* (2018) 304):1–8.

2. Gupta R, Warren T, Wald A. Genital herpes. *Lancet* (2007) 370(9605):2127–37. doi: 10.1016/S0140-6736(07)61908-4

3. Martinelli E, Tharinger H, Frank I, Arthos J, Piatak MJr., Lifson JD, et al. Hsv-2 infection of dendritic cells amplifies a highly susceptible hiv-1 cell target. *PLoS Pathog* (2011) 7(6):e1002109. doi: 10.1371/journal.ppat.1002109

4. Wang K, Kappel JD, Canders C, Davila WF, Sayre D, Chavez M, et al. A herpes simplex virus 2 glycoprotein d mutant generated by bacterial artificial chromosome mutagenesis is severely impaired for infecting neuronal cells and infects only vero cells expressing exogenous hvem. *J Virol* (2012) 86(23):12891–902. doi: 10.1128/JVI.01055-12

5. Vahlne A, Svennerholm B, Sandberg M, Hamberger A, Lycke E. Differences in attachment between herpes simplex type 1 and type 2 viruses to neurons and glial cells. *Infect Immun* (1980) 28(3):675–80. doi: 10.1128/iai.28.3.675-680.1980

6. Gupta A, Rani PK, Bagga B, Dore P, Mittal A, Jalali S. Bilateral herpes simplex-2 acute retinal necrosis with encephalitis in premature twins. *J AAPOS* (2010) 14(6):541–3. doi: 10.1016/j.jaapos.2010.08.011

7. Miller S, Mateen FJ, Aksamit AJJr. Herpes simplex virus 2 meningitis: A retrospective cohort study. *J Neurovirol* (2013) 19(2):166–71. doi: 10.1007/s13365-013-0158-x

8. Whitley RJ. Herpes simplex virus infections of the central nervous system. *Continuum (Minneap Minn)* (2015) 21(6 Neuroinfectious Disease):1704–13. doi: 10.1212/CON.0000000000000243

9. Zhu H, Zheng C. The race between host antiviral innate immunity and the immune evasion strategies of herpes simplex virus 1. *Microbiol Mol Biol Rev* (2020) 84(4):e00099-20. doi: 10.1128/MMBR.00099-20

10. Xu H, Su C, Pearson A, Mody CH, Zheng C. Herpes simplex virus 1 Ul24 abrogates the DNA sensing signal pathway by inhibiting nf-kappab activation. *J Virol* (2017) 91(7):e00025-17. doi: 10.1128/JVI.00025-17

11. Zhang J, Wang S, Wang K, Zheng C. Herpes simplex virus 1 DNA polymerase processivity factor Ul42 inhibits tnf-Alpha-Induced nf-kappab activation by interacting with P65/Rela and P50/Nf-Kappab1. *Med Microbiol Immunol* (2013) 202(4):313–25. doi: 10.1007/s00430-013-0295-0

12. Zhang J, Wang K, Wang S, Zheng C. Herpes simplex virus 1 E3 ubiquitin ligase Icp0 protein inhibits tumor necrosis factor alpha-induced nf-kappab activation by interacting with P65/Rela and P50/Nf-Kappab1. *J Virol* (2013) 87 (23):12935–48. doi: 10.1128/JVI.01952-13

13. Cai M, Liao Z, Zou X, Xu Z, Wang Y, Li T, et al. Herpes simplex virus 1 Ul2 inhibits the tnf-Alpha-Mediated nf-kappab activity by interacting with P65/P50. *Front Immunol* (2020) 11:549. doi: 10.3389/fimmu.2020.00549

14. Wang K, Ni L, Wang S, Zheng C. Herpes simplex virus 1 protein kinase Us3 hyperphosphorylates P65/Rela and dampens nf-kappab activation. *J Virol* (2014) 88(14):7941–51. doi: 10.1128/JVI.03394-13

15. Ye R, Su C, Xu H, Zheng C. Herpes simplex virus 1 ubiquitin-specific protease Ul36 abrogates nf-kappab activation in DNA sensing signal pathway. *J Virol* (2017) 91(5):e02417-16. doi: 10.1128/JVI.02417-16

16. Xing J, Ni L, Wang S, Wang K, Lin R, Zheng C. Herpes simplex virus 1-encoded tegument protein Vp16 abrogates the production of beta interferon (Ifn) by inhibiting nf-kappab activation and blocking ifn regulatory factor 3 to recruit its coactivator cbp. *J Virol* (2013) 87(17):9788–801. doi: 10.1128/JVI.01440-13

17. Leib DA, Harrison TE, Laslo KM, Machalek MA, Moorman NJ, Virgin HW. Interferons regulate the phenotype of wild-type and mutant herpes simplex viruses *in vivo*. *J Exp Med* (1999) 189(4):663–72. doi: 10.1084/jem.189.4.663

18. Liu X, Matrenec R, Gack MU, He B. Disassembly of the Trim23-Tbk1 complex by the Us11 protein of herpes simplex virus 1 impairs autophagy. *J Virol* (2019) 93(17):e00497-19. doi: 10.1128/JVI.00497-19

19. You H, Zheng S, Huang Z, Lin Y, Shen Q, Zheng C. Herpes simplex virus 1 tegument protein Ul46 inhibits tank-binding kinase 1-mediated signaling. *mBio* (2019) 10(3):e00919-19. doi: 10.1128/mBio.00919-19

20. Kim JC, Lee SY, Kim SY, Kim JK, Kim HJ, Lee HM, et al. Hsv-1 Icp27 suppresses nf-kappab activity by stabilizing ikappabalpha. *FEBS Lett* (2008) 582 (16):2371–6. doi: 10.1016/j.febslet.2008.05.044

21. Lanfranca MP, Mostafa HH, Davido DJ. Hsv-1 Icp0: An E3 ubiquitin ligase that counteracts host intrinsic and innate immunity. *Cells* (2014) 3(2):438–54. doi: 10.3390/cells3020438

22. Zhang M, Liu Y, Wang P, Guan X, He S, Luo S, et al. Hsv-2 immediate-early protein Us1 inhibits ifn-beta production by suppressing association of irf-3 with ifn-beta promoter. *J Immunol* (2015) 194(7):3102–15. doi: 10.4049/jimmunol.1401538

23. Zhang M, Fu M, Li M, Hu H, Gong S, Hu Q. Herpes simplex virus type 2 inhibits type I ifn signaling mediated by the novel E3 ubiquitin protein ligase activity of viral protein Icp22. *J Immunol* (2020) 205(5):1281–92. doi: 10.4049/jimmunol.2000418

24. Hayden MS, Ghosh S. Shared principles in nf-kappab signaling. *Cell* (2008) 132(3):344–62. doi: 10.1016/j.cell.2008.01.020

25. Sun SC. The non-canonical nf-kappab pathway in immunity and inflammation. *Nat Rev Immunol* (2017) 17(9):545–58. doi: 10.1038/nri.2017.52

26. Ghosh S, Hayden MS. New regulators of nf-kappab in inflammation. *Nat Rev Immunol* (2008) 8(11):837–48. doi: 10.1038/nri2423

27. Wang TY, Yang YL, Feng C, Sun MX, Peng JM, Tian ZJ, et al. Pseudorabies virus Ul24 abrogates tumor necrosis factor alpha-induced nf-kappab activation by degrading P65. *Viruses* (2020) 12(1):51. doi: 10.3390/v12010051

28. Liao QJ, Ye LB, Timani KA, Zeng YC, She YL, Ye L, et al. Activation of nf-kappab by the full-length nucleocapsid protein of the sars coronavirus. *Acta Biochim Biophys Sin (Shanghai)* (2005) 37(9):607–12. doi: 10.1111/j.1745-7270.2005.00082.x

29. Hao W, Wang L, Li S. Fkbp5 regulates rig-I-Mediated nf-kappab activation and influenza a virus infection. *Viruses* (2020) 12(6):672. doi: 10.3390/v12060672

30. Mathers C, Schafer X, Martinez-Sobrido L, Munger J. The human cytomegalovirus Ul26 protein antagonizes nf-kappab activation. *J Virol* (2014) 88(24):14289–300. doi: 10.1128/JVI.02552-14

31. Li X, Liang D, Lin X, Robertson ES, Lan K. Kaposi's sarcoma-associated herpesvirus-encoded latency-associated nuclear antigen reduces interleukin-8 expression in endothelial cells and impairs neutrophil chemotaxis by degrading nuclear P65. *J Virol* (2011) 85(17):8606–15. doi: 10.1128/JVI.00733-11

32. Li Q, Zheng Z, Liu Y, Zhang Z, Liu Q, Meng J, et al. 2c proteins of enteroviruses suppress ikkbeta phosphorylation by recruiting protein phosphatase 1. *J Virol* (2016) 90(10):5141–51. doi: 10.1128/JVI.03021-15

33. Ye J, Chen Z, Li Y, Zhao Z, He W, Zohaib A, et al. Japanese Encephalitis virus Ns5 inhibits type I interferon (Ifn) production by blocking the nuclear translocation of ifn regulatory factor 3 and nf-kappab. *J Virol* (2017) 91(8):e00039-17. doi: 10.1128/JVI.00039-17

34. Liu Q, Zhang Z, Zheng Z, Zheng C, Liu Y, Hu Q, et al. Human bocavirus Ns1 and Ns1-70 proteins inhibit tnf-Alpha-Mediated activation of nf-kappab by targeting P65. *Sci Rep* (2016) 6:28481. doi: 10.1038/srep28481

35. Zheng Z, Li H, Zhang Z, Meng J, Mao D, Bai B, et al. Enterovirus 71 2c protein inhibits tnf-Alpha-Mediated activation of nf-kappab by suppressing ikappab kinase beta phosphorylation. *J Immunol* (2011) 187(5):2202–12. doi: 10.4049/jimmunol.1100285

36. Li C, Zhang M, Guan X, Hu H, Fu M, Liu Y, et al. Herpes simplex virus type 2 glycoprotein d inhibits nf-kappab activation by interacting with P65. *J Immunol* (2021) 206(12):2852–61. doi: 10.4049/jimmunol.2001336

37. Guan X, Zhang M, Fu M, Luo S, Hu Q. Herpes simplex virus type 2 immediate early protein Icp27 inhibits ifn-beta production in mucosal epithelial cells by antagonizing Irf3 activation. *Front Immunol* (2019) 10:290. doi: 10.3389/fimmu.2019.00290

38. Listwak SJ, Rathore P, Herkenham M. Minimal nf-kappab activity in neurons. *Neuroscience* (2013) 250:282–99. doi: 10.1016/j.neuroscience.2013.07.013

39. Mendez-Samperio P, Perez A, Rivera L. Mycobacterium bovis bacillus calmette-guerin (Bcg)-induced activation of Pi3k/Akt and nf-kb signaling pathways regulates expression of Cxcl10 in epithelial cells. *Cell Immunol* (2009) 256(1-2):12–8. doi: 10.1016/j.cellimm.2008.12.002

40. Oeckinghaus A, Hayden MS, Ghosh S. Crosstalk in nf-kappab signaling pathways. *Nat Immunol* (2011) 12(8):695–708. doi: 10.1038/ni.2065

41. Zhang Q, Lenardo MJ, Baltimore D. 30 years of nf-kappab: A blossoming of relevance to human pathobiology. *Cell* (2017) 168(1-2):37–57. doi: 10.1016/j.cell.2016.12.012

42. Khoury-Hanold W, Yordy B, Kong P, Kong Y, Ge W, Szigeti-Buck K, et al. Viral spread to enteric neurons links genital hsv-1 infection to toxic megacolon and lethality. *Cell Host Microbe* (2016) 19(6):788–99. doi: 10.1016/j.chom.2016.05.008

43. Zheng C. Evasion of cytosolic DNA-stimulated innate immune responses by herpes simplex virus 1. *J Virol* (2018) 92(6):e00099-17. doi: 10.1128/JVI.00099-17

44. Hayden MS, Ghosh S. Signaling to nf-kappab. *Genes Dev* (2004) 18 (18):2195–224. doi: 10.1101/gad.1228704

45. Li Q, Verma IM. Nf-kappab regulation in the immune system. *Nat Rev Immunol* (2002) 2(10):725–34. doi: 10.1038/nri910

46. Vallabhapurapu S, Karin M. Regulation and function of nf-kappab transcription factors in the immune system. *Annu Rev Immunol* (2009) 27:693–733. doi: 10.1146/annurev.immunol.021908.132641

47. Hargett D, Rice S, Bachenheimer SL. Herpes simplex virus type 1 Icp27-dependent activation of nf-kappab. *J Virol* (2006) 80(21):10565–78. doi: 10.1128/JVI.01119-06

48. Du H, Yin P, Yang X, Zhang L, Jin Q, Zhu G. Enterovirus 71 2c protein inhibits nf-kappab activation by binding to Rela(P65). *Sci Rep* (2015) 5:14302. doi: 10.1038/srep14302

49. Fu YZ, Su S, Zou HM, Guo Y, Wang SY, Li S, et al. Human cytomegalovirus DNA polymerase subunit Ul44 antagonizes antiviral immune responses by suppressing Irf3- and nf-Kappab-Mediated transcription. *J Virol* (2019) 93(11): e00181-19. doi: 10.1128/JVI.00181-19

50. Yu H, Bruneau RC, Brennan G, Rothenburg S. Battle royale: Innate recognition of poxviruses and viral immune evasion. *Biomedicines* (2021) 9 (7):765. doi: 10.3390/biomedicines9070765

51. Asai R, Ohno T, Kato A, Kawaguchi Y. Identification of proteins directly phosphorylated by Ul13 protein kinase from herpes simplex virus 1. *Microbes Infect* (2007) 9(12-13):1434–8. doi: 10.1016/j.micinf.2007.07.008

52. Bastian TW, Livingston CM, Weller SK, Rice SA. Herpes simplex virus type 1 immediate-early protein Icp22 is required for vice domain formation during productive viral infection. *J Virol* (2010) 84(5):2384–94. doi: 10.1128/JVI.01686-09

53. Bastian TW, Rice SA. Identification of sequences in herpes simplex virus type 1 Icp22 that influence rna polymerase ii modification and viral late gene expression. *J Virol* (2009) 83(1):128–39. doi: 10.1128/JVI.01954-08

54. Cun W, Chen J, Zhang Y, Liu LD, Li QH. Analysis of the cellular localization of herpes simplex virus 1 immediate-early protein Icp22. *Virol Sin* (2010) 25 (3):158–67. doi: 10.1007/s12250-010-3118-0

55. Fraser KA, Rice SA. Herpes simplex virus immediate-early protein Icp22 triggers loss of serine 2-phosphorylated rna polymerase ii. *J Virol* (2007) 81 (10):5091–101. doi: 10.1128/JVI.00184-07

56. Long MC, Leong V, Schaffer PA, Spencer CA, Rice SA. Icp22 and the Ul13 protein kinase are both required for herpes simplex virus-induced modification of the Large subunit of rna polymerase ii. *J Virol* (1999) 73(7):5593–604. doi: 10.1128/JVI.73.7.5593-5604.1999

57. Rice SA, Long MC, Lam V, Schaffer PA, Spencer CA. Herpes simplex virus immediate-early protein Icp22 is required for viral modification of host rna-Polymerase-Ii and establishment of the normal viral transcription program. *J Virol* (1995) 69(9):5550–9. doi: 10.1128/JVI.69.9.5550-5559.1995

58. Guo L, Wu WJ, Liu LD, Wang LC, Zhang Y, Wu LQ, et al. Herpes simplex virus 1 Icp22 inhibits the transcription of viral gene promoters by binding to and blocking the recruitment of p-tefb. *PLoS One* (2012) 7(9):e45749. doi: 10.1371/journal.pone.0045749

59. Mostafa HH, Davido DJ. Herpes simplex virus 1 Icp22 but not us 1.5 is required for efficient acute replication in mice and vice domain formation. *J Virol* (2013) 87(24):13510–9. doi: 10.1128/JVI.02424-13

60. Purves FC, Ogle WO, Roizman B. Processing of the herpse simplex virus regulatory protein A22 mediated by the Ul13 protein kinase determines the accumulation of a subset of a and y mrnas and proteins in infected cells. *Proc Natl Acad Sci U S A* (1993) 90:6701–5. doi: 10.1073/pnas.90.14.6701

61. Mitchell C, Blaho JA, Roizman B. Casein kinase ii speciallynucleotidylylates in vitro the amino acid sequence of the protein encoded by the A22 gene of herpse simplex virus 1. *Proc Natl Acad Sci U S A* (1994) 91:11864–8. doi: 10.1073/pnas.91.25.11864

62. Blaho JA, Mitchell C, Roizman B. Guanylylation and adenylylation of the alpha-regulatory proteins of herpes simplex virus require a viral-beta or viral-gamma function. *J Virol* (1993) 67(7):3891–900. doi: 10.1128/JVI.67.7.3891-3900.1993

63. Purves FC, Roizman B. The Ul13 gene of herpes-simplex virus 1 encodes the functions for posttranslational processing associated with phosphorylation of the regulatory protein A22. *Proc Natl Acad Sci U S A* (1992) 89(16):7310–4. doi: 10.1073/pnas.89.16.7310

frontiers | Frontiers in Immunology

TYPE Opinion
PUBLISHED 26 September 2022
DOI 10.3389/fimmu.2022.1027539

OPEN ACCESS

EDITED BY
Chenhe Su,
Wistar Institute, United States

REVIEWED BY
Yuexiu Zhang,
The Ohio State University, United States
Biao Qiu,
NewYork-Presbyterian, United States

*CORRESPONDENCE
Zi-Guo Yuan
ziguoyuan@scau.edu.cn

SPECIALTY SECTION
This article was submitted to Viral Immunology, a section of the journal Frontiers in Immunology

RECEIVED 25 August 2022
ACCEPTED 31 August 2022
PUBLISHED 26 September 2022

CITATION
Yuan H, Song Y, Zhang X-X, Zhai J, Zhang J and Yuan Z-G (2022) Public awareness should be raised on a crucial but neglected factor for COVID-19 vaccination.
Front. Immunol. 13:1027539.
doi: 10.3389/fimmu.2022.1027539

Public awareness should be raised on a crucial but neglected factor for COVID-19 vaccination

Hao Yuan[1], Yining Song[1], Xiu-Xiang Zhang[1], Jingbo Zhai[2,3], Jin Zhang[4] and Zi-Guo Yuan[1]*

[1]Guangdong Provincial Key Laboratory of Zoonosis Prevention and Control, College of Veterinary Medicine, South China Agricultural University, Guangzhou, China, [2]Medical College, Inner Mongolia Minzu University, Tongliao, China, [3]Key Laboratory of Zoonose Prevention and Control at Universities of Inner Mongolia Autonomous Region, Tongliao, China, [4]Department of Pharmacy and Toxicology, University of Missippi Medical Center, Jackson, MS, United States

KEYWORDS

COVID19, vaccination, neglected factor, public awareness, Toxoplasma gondii, immunosuppressive pathogens

According to the current epidemic trend, herd immunity can be achieved *via* a vaccination program on a wide scale, representing one of the important ways to block the spread of COVID-19 (Corona Virus Disease 2019). Herd immunity is largely affected by the frequency of vaccination and the type of vaccine. Currently, the low vaccine protection rate is mostly attributed to a) there is no vaccine for children under 6 months, and exemption of partial population with neurologic disorder and anaphylactic disease and immunocompromised patients from receiving the vaccine, and b) the emergence of variant strains across the world has greatly reduced the protection of the vaccine. In addition, a significant factor may be neglected: the influence of immunosuppressive parasite infection.

As of August 2022. 343.0624 million COVID-19 vaccines have been vaccinated across China (1). Due to the differences in the coverage of COVID-19 vaccines worldwide and the prevalence of delta mutants and Omicron. Due to decreased vaccine protective efficacy in humans over time, new cases still emerge in an endless stream. In the interim analysis data of Phase III clinical trial released by Johnson & Johnson Ad26 adenovirus vector COVID-19 vaccine on January 29, 2021, 468 of the 43,783 subjects were infected with COVID-19. This unique pattern raises an important question, why does infection still occur during the period of antibody protection after vaccination? a) It may be related to antibody production time and titer. b) immunosuppressive parasite infection could be an important factor that has been ignored and never been investigated as a potential cause of vaccine failure.

Nowadays, with the development of the economy, people are petting cats for emotional support (2). Feline is the definitive host of *Toxoplasma gondii* (*T. gondii*), where oocysts, the

infective stage, can be discharged, causing environmental contamination and widespread infection. According to statistics, the seroprevalence of *T. gondii* varies from less than 10-60% in the world's nations (3). *T. gondii*, as a zoonotic parasitic disease, acute or chronic infections, can cause systemic or local immunosuppression of the host. Studies have shown that 65% of patients with HIV die from the re-activation of *T. gondii* infection in the first year after diagnosis (4). It is well documented that *T. gondii* has developed mechanisms to evade the attack by the host immune system (5, 6). Serological testing for *T. gondii* is not compulsory, and there is no *T. gondii* vaccine. In the case of such a high seropositivity rate, the antibody titers of the people injected with COVID-19 vaccines may be affected by suppressive *T. gondii* infection. We hypothesize that this could be one of the important neglected reasons for the low vaccine protection rate and should raise the attention of the Centers for Disease Control and Prevention worldwide.

Even though we are unsure whether *T. gondii* infection is connected to COVID-19 vaccination failure, we should test for immunosuppressive pathogens like *T. gondii* in vaccination failure patients to confirm the connection between vaccination failure and immunosuppression and to increase the efficacy and protection rate of COVID-19 vaccines.

Author contributions

HY, YS, X-XZ, and JZ are responsible for writing the draft. JZ is responsible for revising the manuscript. Z-GY is responsible for the conception and polishing the MS. All authors contributed to the article and approved the submitted version.

Funding

This work was supported by the National Natural Science Foundation of China (31972707) and Guangdong Provincial Forestry Department's Provincial Financial Special Fund for Ecological Forestry Construction-Wildlife Conservation.

Acknowledgments

We sincerely thank the support of Yasser Mahmmod for his overview and precious suggestion on the article.

Conflict of interest

The authors declare that the research was conducted in the absence of any commercial or financial relationships that could be construed as a potential conflict of interest.

Publisher's note

References

1. National Health Commission of the People's Republic of China. Up to 24:00 on 24th August, the latest situation of new coronavirus vaccination. Availble at: https://www.nhc.gov.cn/jkj/s7915/202208/6c767517c5c446dc9fe733956bfb7fdb.shtml

2. Kochanowsky JA, Koshy AA. Toxoplasma gondii. *Curr Biol* (2018) 28:R770–1. doi: 10.1016/j.cub.2018.05.035

3. Pappas G, Roussos N, Falagas ME. Toxoplasmosis snapshots: global status of *Toxoplasma gondii* seroprevalence and implications for pregnancy and congenital toxoplasmosis. *Int J Parasitol* (2009) 39:1385–94. doi: 10.1016/j.ijpara.2009.04.003

4. Mayor AM, Santos DF, Dworkin MS, Rios-Olivares E, Hunter RF. Toxoplasmic encephalitis in an AIDS cohort at Puerto Rico before and after highly active antiretroviral therapy (HAART). *Am J Trop Med* (2011) 84:838–41. doi: 10.4269/ajtmh.2011.10-0718

5. Melchor SJ, Ewald SE. Disease tolerance in *Toxoplasma* infection. *Front Cell Infect Microbiol* (2019) 9:185. doi: 10.3389/fcimb.2019.00185

6. Zhao XY, Ewald SE. The molecular biology and immune control of chronic *Toxoplasma gondii* infection. *J Clin Invest* (2020) 130:3370–80. doi: 10.1172/JCI136226

frontiers | Frontiers in Immunology

TYPE Original Research
PUBLISHED 28 September 2022
DOI 10.3389/fimmu.2022.1026509

OPEN ACCESS

EDITED BY
Chenhe Su,
Wistar Institute, United States

REVIEWED BY
Song Jiaxing,
Guangxi Medical University, China
Huan Qin,
South China Normal University, China

*CORRESPONDENCE
Ping Chen
stemph2021@163.com
Xianwang Wang
275379987@qq.com

†These authors have contributed equally to this work and share first authorship

SPECIALTY SECTION
This article was submitted to Viral Immunology, a section of the journal Frontiers in Immunology

RECEIVED 24 August 2022
ACCEPTED 06 September 2022
PUBLISHED 28 September 2022

CITATION
Hu S, Hu Y, Long P, Li P, Chen P and Wang X (2022) The effect of tai chi intervention on NLRP3 and its related antiviral inflammatory factors in the serum of patients with pre-diabetes. *Front. Immunol.* 13:1026509. doi: 10.3389/fimmu.2022.1026509

The effect of tai chi intervention on NLRP3 and its related antiviral inflammatory factors in the serum of patients with pre-diabetes

Shujuan Hu[1,2†], Yingxing Hu[3†], Peilin Long[2], Peixiong Li[2], Ping Chen[2*] and Xianwang Wang[3*]

[1]School of Education and Physical Education, Yangtze University, Jingzhou, China, [2]School of Physical Education and Science, Jishou University, Jishou, China, [3]Department of Biochemistry and Molecular Biology, Center for Molecular Medicine, Health Science Center, Yangtze University, Jingzhou, China

Background: NLRP3 inflammasome and its related antiviral inflammatory factors have been implicated in the pathogenesis of type 2 diabetes mellitus (T2DM) and insulin resistance, but its contribution to pre-diabetes remains poorly understood.

Objective: To investigate the effects and the potential mechanism of Tai Chi intervention on NLRP3 inflammasome and its related inflammatory factors in the serum of middle-aged and older people with pre-diabetes mellitus (PDM).

Methods: 40 pre-diabetic subjects were divided into a pre-diabetic control group (PDM-C group, N=20) and a Tai Chi group (PDM-TC group, N=20) by random number table. 10 normoglycemic subjects (NG) were selected as controls. We measured clinical metabolic parameters and collected blood samples before and after the 12 weeks of Tai Chi intervention. Antiviral inflammatory factors in serum were detected by enzyme-linked immunosorbent assay.

Results: The blood glucose, insulin resistance, and inflammation in PDM groups were higher than those in the NG group ($P<0.05$ and $P<0.01$, respectively). The results also suggested that 12 weeks of Tai Chi intervention could reduce body weight, blood pressure, blood glucose, insulin resistance, blood lipid, and the expressions of serum inflammatory factors in the pre-diabetic population.

Conclusion: Tai Chi intervention may improve blood glucose, lipid levels, and insulin resistance in middle-aged and elderly pre-diabetic patients by reducing the level of NLRP3 inflammasome and its related inflammatory factors.

KEYWORDS

tai chi intervention, NLRP3 inflammasome, pre-diabetes mellitus, inflammatory factors, insulin resistance

Introduction

Diabetes mellitus is a common and complex chronic disease that has become a serious threat to human health after cancer, cardiovascular, and cerebrovascular diseases, of which 90% are type 2 diabetes mellitus (T2DM) (1). Diabetes mellitus (in particular T2DM) develops slowly and may have a pre-diabetes mellitus (PDM) state, which is a high-risk state for diabetes (2). PDM is the only stage that can be reversed the occurrence of diabetes as it is a necessary stage for the normal progression to T2DM (2). Therefore, it is a wise option to ameliorate diabetes by developing an effective strategy for the PDM population. The Guidelines for Prevention and Treatment of T2DM in China (2020 edition) explicitly recommended that the prevention and relief of T2DM require adjustment of unhealthy lifestyle and persistence of exercise (1). Naturally, exercise is an important scheme of lifestyle adjustment, which has been recommended for managing pre-diabetes and diabetes. Previous studies have found that exercise intervention significantly improved fasting blood glucose (FBG), plasma glucose after 2 hours (2 hPG), and Glycosylated hemoglobin (HbA_1C) in patients with PDM (3). In addition, exercise intervention has been shown to ameliorate glucose tolerance, and effectively prevent impaired glucose tolerance from progressing to diabetes (4).

Inflammation is an adaptive biological response of the immune system (5). Chronic inflammation is an important pathophysiological factor leading to diabetes (6), which is manifested by higher levels of Nod-like receptor protein 3 (NLRP3), Caspase-1, Interleukin-1β (IL-1β), and various antiviral inflammatory cytokines (7), inducing a strong inflammatory response in the body. NLRP3 inflammasome is a multi-protein complex composed of the nod-like receptor (NLR) family core member (NLRP3), apoptosis-associated spot-like protein (ASC), and Caspase-1 (8). Nuclear factor κB (NF-κB), and reactive oxygen species (ROS) have been regarded as the important upstream signal to activate the NLRP3 inflammasome (9). Activation of NLRP3 inflammasome could activate Caspase-1, which cleaves the pro-IL-1β precursor to form mature IL-1β secreted out of the cell, thereby inducing the body's inflammatory response (10). In addition, the NLRP3 inflammasome has become a regulator of inflammatory response and protective immunity (11), which plays an important role in the antiviral innate immune signaling pathway (12).

Much evidence has shown that aerobic exercise could reduce the expressions of NLRP3, Caspase-1, IL-1β and other inflammatory factors (13, 14). Zaidi et al. found that one year of exercise training in patients with T2DM significantly reduced the levels of pro-inflammatory markers, especially IL-18 (15). After 8 weeks of aerobic exercise, the activity of NF-κB and NLRP3 in the prefrontal cortex of diabetic rats decreased. The activity of Phosphatidylinositol 3-hydroxy kinase (PI3K)/protein kinase B (Akt) was enhanced, and the insulin signaling pathway was improved by inhibiting the inflammatory signaling (14). These findings suggested that moderate-intensity aerobic exercise may ameliorate insulin sensitivity by inhibiting over-activation of the NLRP3 inflammasome, thereby alleviating insulin resistance. In brief, aerobic exercise could relieve diabetes by suppressing inflammation.

Tai Chi is an aerobic exercise with a long history, and Tai Chi has been widely used in the clinical prevention and treatment of diabetes. At the same time, the exercise intensity is moderate, which is favored by the middle-aged and elderly. Tai Chi has been shown to improve the level of blood glucose and lipid in diabetic patients, and the potential mechanism may be driven by insulin resistance, and reduction in inflammatory factors (16, 17). Studies have found that Tai Chi can stimulate innate and adaptive immune cell responses and regulate inflammatory biomarkers, enhancing participants' immune system function (5, 18). However, whether Tai Chi plays a vital role in regulating pre-diabetic symptoms remains unknown. The evidence of beneficial therapeutic effects of exercise interventions on reducing inflammatory markers is also unclear in pre-diabetic rat models (19) and the pre-diabetic population. Therefore, we aimed to explore the effect and potential mechanism of Tai Chi intervention on the NLRP3 inflammasome and its related inflammatory factors in pre-diabetic population, and we seek an economical and effective strategy to alleviate and improve diabetes.

Materials and methods

Studied subject and study design

In this study, a randomized controlled study design was adopted, cases were screened strictly following the inclusion and exclusion criteria established in the study protocol, eligible cases were randomly grouped, intervened, observed and followed up, and relevant data were collected. The sample size was determined based on literature reports of similar studies (20). A total of 40 pre-diabetic patients and 10 healthy subjects recruited from Jishou University from April to July 2021 were selected, among which 2 patients withdrew due to the reason of health. At last, 38 participants were randomly divided into the PDM control group (PDM-C, N=19) with an age of (61.58 ± 6.62) years and a height of (1.60 ± 0.09) meters; the PDM Tai Chi group (PDM-TC, N=19), age was (62.68 ± 7.33) years, height was (1.57 ± 0.06) meters; normoglycemic subjects (NG, N=10), age of (55.20 ± 7.45) years, the height of (1.59 ± 0.07) meters. All groups had no significant differences in age, height, and body weight (P>0.05).

Eating habits of all recruited participants are relatively stable. They were asked to continue their daily routines without changing physical activity and eating habits.

Monthly one-on-one interviews with a valid questionnaire, including nutritional intake and physical activity, were conducted to assess their compliance. All participants underwent clinical assessment at recruitment to the project, followed by an oral glucose tolerance test (OGTT) and blood test. All tests were performed before the intervention and repeated 3 months following each participant's final exercise session. The Ethics Committee approved this study of Jishou University (approval number: JSDX-2021-0055). All study participants provided written informed consent.

Inclusion criteria: 1. PDM patients (N=38), (i) Subjects with impaired fasting glucose (IFG) or impaired glucose tolerance (IGT), defined as FBG 100-125 mg/dL or 2 hPG 140-199 mg/dL. (ii)Age: 50-70 years old. (iii) Ability to perform exercise training. 2. NG group (N=10), (i) Subjects with normal fasting glucose and normal glucose tolerance, defined as FBG <100 mg/dL and 2 hPG <140 mg/dL. (ii)Age: 45-70 years old. Exclusion criteria: (i) Highly active lifestyle. (ii) Patients with type 1 or 2 diabetes, other special types of diabetes and abnormal liver and kidney function were excluded. (iii) Patients with a history of cancer and other serious diseases were excluded.

Tai Chi exercise intervention

PDM-TC group

All patients underwent a 12-week Tai Chi intervention. 24 simplified Tai Chi intervention was conducted for 12 weeks under the guidance of a professional Tai Chi instructor (group instruction). Practice venue: Jishou University New Campus sports ground. Practice period: April to July 2021. The training frequency was four sessions per week for 12 weeks, for a total of 48 pieces of training. Only subjects who performed at least 80% of all planned training were included in this study. Each training lasted approximately 80 min, beginning with a warm-up (20 min), Tai Chi exercises (50 min), followed by relaxation exercises (10 min). The first 1-3 weeks of Tai Chi learning period, 4-12 weeks of Tai Chi consolidation and strengthening.

Before enrollment, the researcher conducted relevant training and education for all PDM-TC group subjects, and informed them of the specific details of the exercise program and matters needing attention. The blood pressure and heart rate of subjects were measured before each exercise. Exercise intensity was maintained to keep the heart rate within 50%~60% of the maximum heart rate (male maximum heart rate=220-age, female maximum heart rate=210-age), and wear a polar watch randomly for real-time monitoring. The most significant feature of the exercise intervention is that it was 100% supervised to ensure uniformity among patients in the exercise intervention. If the patients show any discomfort, the exercise will be terminated immediately.

PDM-C group and NG group

Do not exercise regularly in any other way than to maintain their previous lifestyle. Both groups were visited weekly to know their states of life, to ensure they did not engage in other forms of disciplined exercise and did not change their diet.

Biochemical measurements of subjects

Anthropometrics and body composition

Anthropometric measurements and body composition analyses were performed in the fasted state using a calibrated body composition analyzer Model N40 (Korea). BMI was calculated as body mass (kg) divided by height (m) squared. Blood pressure is measured continuously 3 times in a calm state, and its average value is taken. A tape measure was used to measure the subjects' waist and hip measurements, and the waist-hip ratio was calculated.

OGTT and laboratory measurements

The OGTT procedure was conducted following ADA recommendations (21). Blood glucose was measured in plasma using a blood glucose detector with Kyoto U-Test (Kyoto, Japan). Blood samples were collected from all subjects before and after Tai Chi intervention. Fasting for more than 8 h was required, and 5 ml of venous blood was taken on an empty stomach from 7:00 to 9:00 the next morning. Fasting insulin (FINs), total cholesterol (TC), triglyceride (TG), low-density cholesterol (LDL-C), high-density cholesterol (HDL-C), FBG, and other biochemical indexes were determined by Hitachi 7600 automatic biochemical analyzer. HbA_1C was determined by Hitachi 7170A automatic glycated hemoglobin analyzer. The homeostatic model assessment for insulin resistance was calculated to evaluate insulin resistance: homeostatic model assessment for insulin resistance (HOMA-IR) = (FBG×FINs)/22.5. The concentrations of NF-κB, ROS, NLRP3, ASC, Caspase-1, GSDMD, IL-1β, and IL-18 in serum of all subjects were detected by enzyme-linked immunosorbent assay (ELISA). The ELISA kits were purchased from Sin-Troch (China). The instrument was Rayto and RT-6100 microplate reader, and the operation was completed according to the kit instructions. The operation is completed according to the operating instructions.

Statistical analyses

SPSS23.0 statistical software was used to process the measured data, and the experimental data were expressed as the mean ± standard deviation ($\bar{x} \pm s$). Paired *t*- test was used for intra-group comparison before and after the intervention. Comparison among the three groups was performed by one-

10.3389/fimmu.2022.1026509

way ANOVA. $P<0.05$ or $P<0.01$ means the difference is statistically significant.

Results

Tai Chi intervention reduced the related indexes of body weight and blood pressure in patients with pre-diabetes

To determine the effect of Tai Chi intervention on weight and blood pressure indexes in the pre-diabetic population. As shown in Table 1, of 48 enrolled subjects, 10 (21%) were normoglycemic; 38 (79%) were pre-diabetic with impaired fasting glucose or glucose tolerance. PDM participants were randomly divided into the PDM-C group (N=19) and the PDM-TC group (N=19). 10 NG group (N=10) were selected as controls. The results showed no statistically significant difference in Wt, BMI, SBP, DBP and WHR among PDM-C, PDM-TC, and NG groups ($P>0.05$). After 12 weeks of Tai Chi intervention in the PDM-TC group, there were significant differences in Wt, BMI, SBP, and DBP ($P<0.01$). Compared with the PDM-C group, we found that there were significantly decreased DBP and WHR in the PDM-TC group ($P<0.01$). These results demonstrated that Tai Chi intervention for 12 weeks could reduce body weight and blood pressure in the pre-diabetic population.

Tai Chi intervention decreased blood glucose and insulin resistance in pre-diabetes

To examine whether Tai Chi intervention for 12 weeks influences blood glucose and insulin resistance in pre-diabetes, patients' blood analysis was performed. As shown in Table 1, before 12 weeks of Tai Chi intervention, we observed that there are significant differences in FBG, 2 hPG, HbA_1C, HbA_1, FINs, and HOMA-IR among PDM-C, PDM-TC, and NG groups ($P<0.05$ or $P<0.01$), suggesting that the blood glucose and insulin resistance in PDM groups were significantly higher than those in NG group. Nevertheless, there were no significant differences between the PDM-C and PDM-TC groups in FBG, 2 hPG, HbA_1C, HbA_1, FINs, and HOMA-IR ($P>0.05$). After 12 weeks of Tai Chi intervention in the PDM-TC group, FBG, 2 hPG, HbA_1C, HbA_1, FINs, and HOMA-IR were decreased. Compared with the PDM-C group, we found that FBG, 2 hPG, HbA_1C, and HbA_1 were reduced significantly in the PDM-TC group ($P<0.05$ or $P<0.01$). Specifically, there was statistical significance in insulin resistance-related indexes, including FINs and HOMA-IR ($P<0.05$ or $P<0.01$) between the PDM-C and PDM-TC groups. Taken together, 12 weeks of Tai Chi intervention could decrease blood glucose and insulin resistance in pre-diabetes (Table 1).

TABLE 1 Clinical characteristics of subjects.

Parameter (Unit)	PDM-TC (N = 19)		PDM-C (N = 19)		NG (N = 10)	
	Before	After	Before	After	Before	After
Wt (kg)	61.58 ± 9.42	59.21 ± 9.05^{b}	65.49 ± 11.08	65.37 ± 11.05	60.45 ± 7.17	60.38 ± 8.27
BMI (kg/m^2)	24.99 ± 3.64	24.15 ± 3.42^{b}	25.41 ± 2.57	25.34 ± 2.38	23.89 ± 1.80	23.83 ± 1.97
SBP (mmHg)	143.05 ± 19.80	124.79 ± 14.56^{b}	138.16 ± 18.37	136.53 ± 19.66	128.20 ± 14.73	126.90 ± 16.70
DBP (mmHg)	80.84 ± 8.20	74.00 ± 10.01^{bd}	84.32 ± 7.82	82.27 ± 7.04	84.80 ± 13.61	83.10 ± 10.50
WHR	0.91 ± 0.05	0.89 ± 0.04^{d}	0.91 ± 0.05	0.96 ± 0.04	0.89 ± 0.06	0.91 ± 0.06
FBG (mmol/L)	6.39 ± 0.31^{d}	6.04 ± 0.31^{bd}	6.40 ± 0.31	6.60 ± 0.34	5.42 ± 0.42	5.44 ± 0.30
2 hPG (mmol/L)	9.17 ± 2.17^{d}	7.56 ± 2.47^{bc}	8.62 ± 0.77	8.66 ± 0.72	6.70 ± 0.73	6.94 ± 0.72
CRP (mg/dl)	1.94 ± 0.11^{c}	1.86 ± 0.11^{bd}	2.06 ± 0.15	2.09 ± 0.13	1.95 ± 0.12	1.92 ± 0.11
HbA_1C (%)	6.23 ± 0.33^{d}	6.00 ± 0.34^{bd}	6.24 ± 0.29	6.32 ± 0.50	5.60 ± 0.28	5.65 ± 0.18
HbA_1 (%)	7.65 ± 0.53^{d}	7.39 ± 0.44^{bd}	7.65 ± 0.39	7.56 ± 0.65	6.64 ± 0.44	6.62 ± 0.36
FINs (μU/mL)	12.22 ± 5.97^{c}	9.73 ± 4.72^{bc}	13.98 ± 5.23	13.08 ± 4.62	8.76 ± 2.84	9.54 ± 3.28
HOMA-IR	3.13 ± 1.71^{d}	2.27 ± 1.15^{bd}	3.74 ± 1.41	3.66 ± 1.35	1.92 ± 0.73	2.04 ± 0.81
TG (mmol/L)	1.65 ± 0.83	1.56 ± 0.86	2.00 ± 0.87	2.19 ± 0.95	1.44 ± 1.07	1.68 ± 0.73
TC (mmol/L)	5.58 ± 1.05	5.33 ± 1.05^{b}	5.03 ± 1.01	5.06 ± 0.92	5.17 ± 1.05	5.16 ± 0.78
HDL-C (mmol/L)	1.41 ± 0.34	1.41 ± 0.33	1.58 ± 0.52	1.65 ± 0.63	1.37 ± 0.32	1.34 ± 0.28
LDL-C (mmol/L)	3.32 ± 0.84	3.11 ± 0.88^{b}	3.42 ± 0.72	3.44 ± 0.73	3.15 ± 0.67	3.17 ± 0.49

Comparison in the group,$^{a}P < 0.05$, $^{b}P < 0.01$; Comparison between groups, $^{c}P < 0.05$, $^{d}P < 0.01$. Wt, weight; BMI, body mass index; WHR, waist-to-hip ratio; FBG, fasting blood glucose; 2 h PG, 2 hours plasma glucose; HDL-C, high-density lipoprotein cholesterol; LDL-C, low-density lipoprotein cholesterol; TG, triglycerides; TC, total cholesterol; CRP, C-reactive protein; HbA_1c, haemoglobinA1c; HbA_1, total glycosylated hemoglobin; FINs, fasting insulin; HOMA-IR, homeostatic model assessment for insulin resistance.

Tai Chi intervention has a positive effect on blood lipid in pre-diabetes

To detect the influence of Tai Chi intervention on blood lipid in the pre-diabetic population. Before Tai Chi intervention, there were no significant differences among the PDM-C group, PDM-TC group, and NG group in blood lipid-related indexes, including TG, TC, HDL-C, and LDL-C ($P>0.05$), respectively, indicating that the difference is not obvious in blood lipids among the three groups. After 12 weeks of Tai Chi intervention in the PDM-TC group, there were significant differences in TC and LDL-C ($P<0.01$), however, the improvements in TG and HDL-C were not significant (Table 1). These results indicated that a 12-week Tai Chi intervention positively affects blood lipid-related indexes in the pre-diabetic population. Compared with the PDM-C group, we found no significant difference in TG, TC, HDL-C, and LDL-C ($P>0.05$), possible resulting from the small sample size and the short intervention time.

Tai Chi intervention reduced serum inflammatory factors in prediabetes

An ELISA assay was employed to confirm the effect of Tai Chi intervention on serum inflammatory factors in the pre-diabetic population. Before Tai Chi intervention, we did not find any significant differences in inflammation markers in the serum between PDM-TC and PDM-C groups. As shown in Figures 1A–J, most inflammatory indexes in the NG group were lower than those in the PDM groups. However, the mean value of irisin was slightly higher in the NG group than in the PDM groups. Intra group comparison results showed that there were significantly reduced the expressions of NEK7, ROS, NF-κB, NLRP3, ASC, Caspase-1, GSDMD, IL-1β, and IL-18, while the expression of irisin was increased in PDM-TC group after 12 weeks Tai Chi intervention ($P<0.05$ or $P<0.01$). Compared with the PDM-C group, the expressions of NEK7, ROS, NF-κB, NLRP3, ASC, Caspase-1, IL-1β, and IL-18 were significantly decreased in the PDM-TC group ($P<0.05$ or $P<0.01$). However, there was no significant difference in the expression level of irisin in the PDM-TC group. These results suggest that Tai Chi intervention for 12 weeks can significantly reduce the expression of serum inflammatory factors in pre-diabetes.

Discussion

Diabetes is a metabolic disease mainly characterized by hyperglycemia, presenting a "chronic low-grade inflammatory" state (22). Chronic inflammation is also considered a key inducer in the development of diabetes and permeates the whole process of diabetes (23). NLRP3 inflammasome, IL-1β, and IL-18 can affect blood glucose control and insulin resistance, which are related to the pathogenesis of diabetes (23, 24), and play an important role in diabetes-induced systemic chronic inflammation and insulin signal transduction (15, 25). Our study showed that the expressions of NLRP3 inflammasome and other antiviral inflammatory cytokines in the NG group were lower than those in the PDM groups, suggesting that the pre-diabetes is indeed in a chronic inflammatory state. Consistent with our findings, studies have found that NLRP3 inflammasome, Caspase-1, IL-1β, IL-18, and other inflammatory factors were significantly increased in multiple tissues of diabetic patients (26, 27). Many studies showed that hyperglycemia could produce excessive ROS (28) and activate NF-κB (29), thereby triggering the activation of intracellular signal transduction and NLRP3 inflammasome in the occurrence and development of diabetes (30). It is reported that NEK7 directly regulates the activation of NLRP3 inflammasome (31). A previous study also showed that the expressions of NEK7 and NLRP3 inflammasome in vascular cells of patients with diabetes were significantly increased (32). In this work, we found that ROS, NF-κB, and NEK7 were significantly higher in PDM groups than in the NG group (as shown in Figures 1A, C, D). Additionally, irisin plays a crucial role in diabetes and energy metabolism (33). A previous study showed that the level of circulating irisin in patients with diabetes was lower when compared with that of the non-diabetic control group (34). Our study found that the average irisin of the NG group was slightly higher than that of the PDM groups (as shown in Figure 1B), but there was no statistical significance. The possible reasons are that the sample size is small and the study object is pre-diabetes. In addition, irisin can reduce the excessive production of ROS and oxidative stress (35), and inhibit the formation and activation of NLRP3 inflammasome (36). To sum up, ROS, NF-κB, and NEK7 could activate NLRP3 inflammasome, while irisin inhibits the activation of these inflammatory cytokines.

Aerobic exercise is believed to be a promising intervention to reduce the expressions of ROS, NF-κB (37), NEK7, NLRP3, ASC, Caspase-1, IL-1β, and other inflammatory factors (38–40), and improves diabetes-induced inflammation and reduces insulin resistance. Tai Chi is a typical aerobic exercise, as well as a physical and mental exercise method of both internal and external cultivation and coordinating the balance of mind-body (41). The data detected by ELISA suggested that Tai Chi intervention for 12 weeks could significantly reduce the concentration of the serum inflammatory factors including ROS, NF-κB, NEK7, NLRP3, ASC, Caspase-1, GSDMD, IL-1β, and IL-18 in patients with pre-diabetes, indicating that Tai Chi intervention could relieve vascular and systemic inflammation. Another important finding of our study is that the level of irisin in the blood of patients with pre-diabetes increased slightly after 12 weeks of Tai Chi intervention ($P<0.01$) (as shown in Figure 1B), which is consistent with the study of Jia (42). Therefore, 12 weeks of Tai Chi intervention can significantly decrease the

10.3389/fimmu.2022.1026509

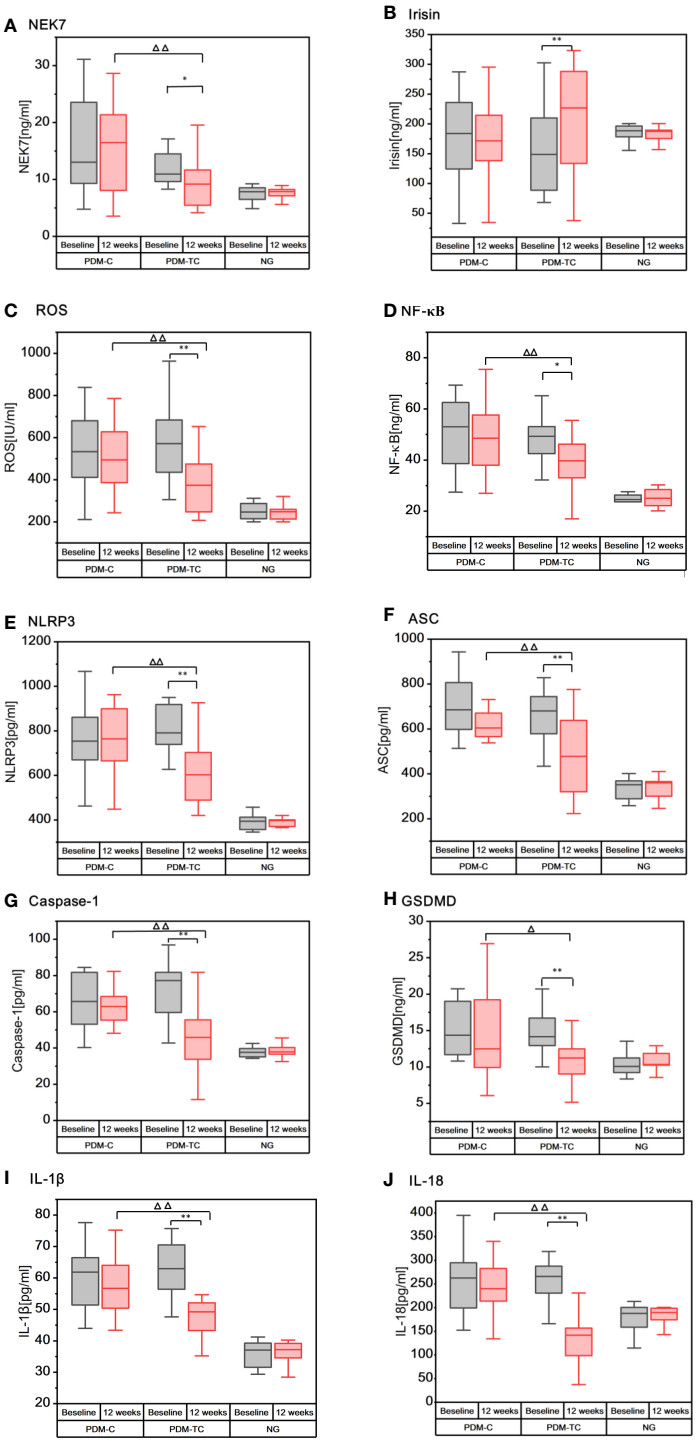

FIGURE 1
The expressions of inflammatory cytokines in the serum of patients with PDM-C, PDM-TC and NG groups, before and after 12 weeks of Tai Chi intervention. "*" indicates that there are differences within the group ($P < 0.05$), and "**" indicates that there is significant difference in the group ($P < 0.01$). "Δ" indicates differences between the PDM-TC group and the PDM-C group ($P < 0.05$), and "ΔΔ" indicates significant differences between the PDM-TC group and the PDM-C group ($P < 0.01$).

expressions of NEK7, NLRP3, ASC, Caspase-1, GSDMD, IL-1β, and IL-18, while increasing the expression of irisin in pre-diabetes.

We showed that the 12 weeks of Tai Chi intervention effectively alleviated glucose homeostasis and anthropometric parameters in both PDM-TC and PDM-C relative to normoglycemia. Thus, Tai Chi is an important form of exercise in pre-diabetes, which may be useful in preventing the development of T2DM. Previous studies have also confirmed that Tai Chi intervention can significantly reduce TC,TG, FBG, and HbA_1C in T2DM patients (43). This study also found that Tai Chi intervention can reduce the expressions of blood glucose, blood lipid, and inflammatory factors in pre-diabetes. However, does Tai Chi intervention improve blood glucose, blood lipid, and insulin resistance by reducing the expression of inflammatory factors?

Previous studies have shown that ROS, NF-κB, and NEK7 can activate the NLRP3 inflammasome, which secretes IL-1β. IL-1β activates C-Jun N-terminal kinase (JNK) and induces serine phosphorylation of insulin receptor substrate 1 (IRS-1), inhibits the expression of Akt protein kinase (44) and weakens the insulin/PI3K/Akt signaling pathway in insulin-sensitive tissues, leading to insulin resistance (45). Irisin can inhibit the formation and activation of NLRP3 inflammasome (36), thereby improving insulin resistance. Studies have shown that exercise can increase the expression of irisin in skeletal muscle, increasing of circulating irisin (35). Therefore, we speculated that Tai Chi intervention might increase irisin level in skeletal muscle, lead to

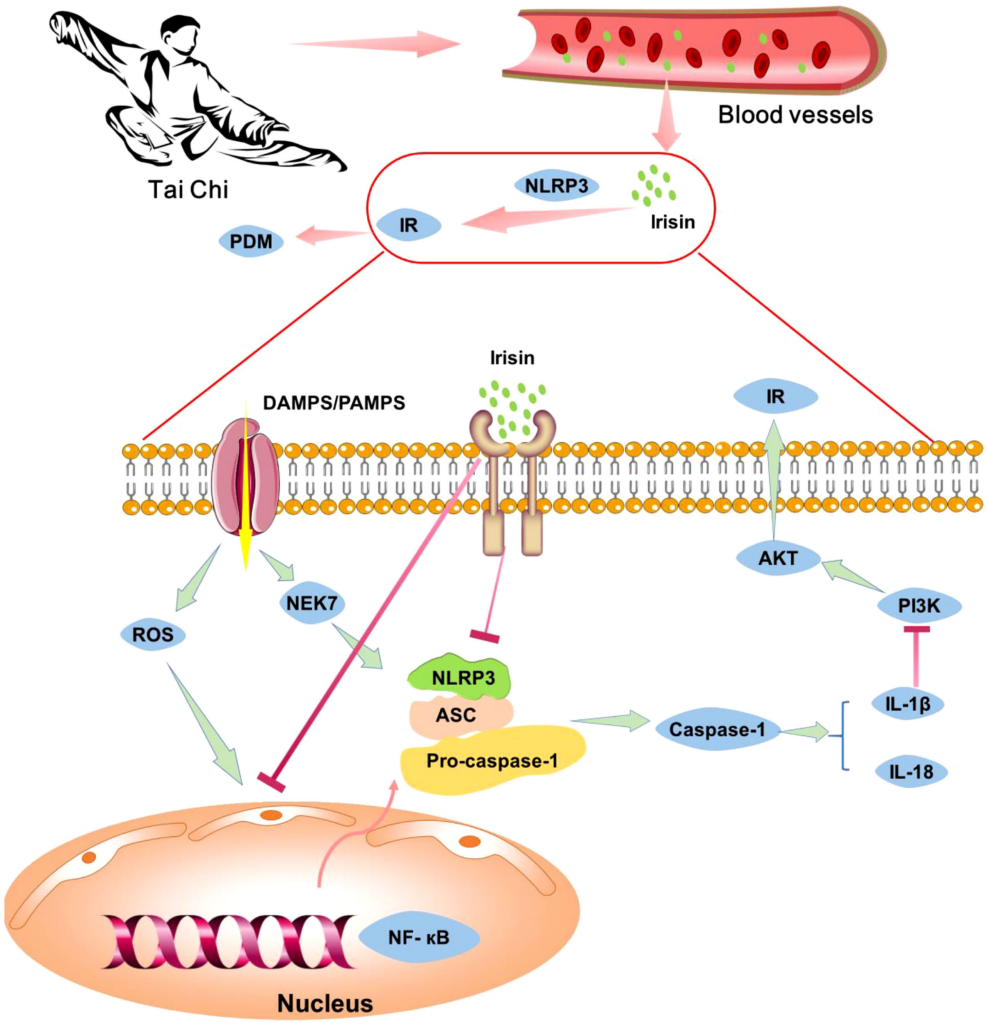

FIGURE 2
The potential mechanism of Tai Chi intervention relieves pre-diabetes by inhibiting inflammation cytokines. Tai Chi intervention can increase the level of irisin in the blood, thus inhibiting the expression of NLRP3 inflammasome and other inflammatory factors, enhancing insulin receptor sensitivity, relieving insulin resistance and pre-diabetes.

a high concentration of irisin in blood, and thus inhibit the expressions of NLRP3 and other inflammatory factors. The decrease of inflammatory factors could further enhance insulin receptor sensitivity and improve insulin resistance (Figure 2). In general, Tai Chi intervention may improve insulin resistance by reducing the expression of inflammatory factors.

However, as the objects of study are the pre-diabetes population, the expressions of inflammatory-related factors in the tissues cannot be detected. It is suggested that the mouse model should also be used in future studies. Secondly, the sample size can be increased in the follow-up study. Finally, its follow-up research can try applying inflammation-related factors to the study of exercise in mice with pre-diabetes to explore the molecular mechanism of how different exercise patterns reduce inflammation.

Conclusion

Tai Chi intervention can reduce blood glucose, blood lipid, and insulin resistance levels and decrease the serum levels of inflammatory factors, including NF-κB, ROS, NLRP3, IL-1β, and IL-18 in pre-diabetes. The potential mechanism is that Tai Chi intervention could increase the level of irisin in the blood, and inhibit the expression of the NLRP3 inflammatory signal pathway, thereby reducing inflammation and relieving insulin resistance. Therefore, based on effective control of blood glucose, NLRP3 inflammasome and its related inflammatory factors may become important targets for Tai Chi intervention to ameliorate pre-diabetes.

Data availability statement

The original contributions presented in the study are included in the article/supplementary material. Further inquiries can be directed to the corresponding authors.

Ethics statement

The studies involving human participants were reviewed and approved by Ethics Committee of Jishou University (approval number: JSDX-2021-0055). Written informed consent to participate in this study was provided by the participants' legal guardian/next of kin.

Author contributions

SH, PC, and XW designed the study. SH and XW drafted the manuscript. SH and YH drew the figures and filled the table. XW, PC, PLi and PLong revised the manuscript. All authors contributed to the article and approved the submitted version.

Funding

This work was supported by grants from the Philosophy and Social Science Research Project of the Hubei Education Department (21Q050), the Key scientific research project of the Hunan Provincial Department of Education (20A414). The Central Government guides local funds for scientific and Technological Development (XZ202201YD0024C), Key R & D Program of Hubei Province (2021BGD010), Hubei Province Scientific and Technological Research Project (D20201306), Hubei Province Key Project of Research and Development Plan (to XW), Hubei Province Health Research Project (WJ2019-01), Hubei Medical Youth Tip-Top Talent (to XW), and Leading Talent Program of Yangtze Talent Project (to XW).

Conflict of interest

The authors declare that the research was conducted in the absence of any commercial or financial relationships that could be construed as a potential conflict of interest.

Publisher's note

All claims expressed in this article are solely those of the authors and do not necessarily represent those of their affiliated organizations, or those of the publisher, the editors and the reviewers. Any product that may be evaluated in this article, or claim that may be made by its manufacturer, is not guaranteed or endorsed by the publisher.

References

1. Association DBoCM. Chinese Clinical guidelines for the prevention and treatment of type 2 diabetes mellitus in the elderly (2020). *Chin J Diabetes* (2021) 13:315–409. doi: 10.3760/cma.j.cn115791-20210221-00095

2. Endocrinology. CSo, Society. CD and Association CE. Expert consensus on adult prediabetes intervention in China. *Chin J Endocrinol Metab* (2020)36:371–80. doi: 10.3760/cma.j.cn311282-20200115-00022

3. Jadhav RA, Hazari A, Monterio A, Kumar S, Maiya AG. Effect of physical activity intervention in prediabetes: A systematic review with meta-analysis. *J Phys activity Health* (2017) 14:745–55. doi: 10.1123/jpah.2016-0632

4. Hemmingsen B, Gimenez-Perez G, Mauricio D, Roque IFM, Metzendorf MI, Richter B. Diet, physical activity or both for prevention or delay of type 2 diabetes mellitus and its associated complications in people at increased risk of developing type 2 diabetes mellitus. *Cochrane Database Syst Rev* (2017) 12:CD003054. doi: 10.1002/14651858.CD003054.pub4

5. Oh B, Bae K, Lamoury G, Eade T, Boyle F, Corless B, et al. The effects of tai chi and qigong on immune responses: A systematic review and meta-analysis. *Medicines (Basel)* (2020)7:39. doi: 10.3390/medicines7070039

6. Wang Y, Zhong J, Zhang X, Liu Z, Yang Y, Gong Q, et al. The role of HMGB1 in the pathogenesis of type 2 diabetes. *J Diabetes Res* (2016) 2016:2543268. doi: 10.1155/2016/2543268

7. Luo B, Li B, Wang W, Liu X, Xia Y, Zhang C, et al. NLRP3 gene silencing ameliorates diabetic cardiomyopathy in a type 2 diabetes rat model. *PloS One* (2014) 9:e104771. doi: 10.1371/journal.pone.0104771

8. Liang F, Huang T, Li B, Zhao Y, Zhang X, Xu B. High-intensity interval training and moderate-intensity continuous training alleviate beta-amyloid deposition by inhibiting NLRP3 inflammasome activation in APPswe/PS1dE9 mice. *Neuroreport* (2020) 31:425–32. doi: 10.1097/WNR.0000000000001429

9. Elliott EI, Sutterwala FS. Initiation and perpetuation of NLRP3 inflammasome activation and assembly. *Immunol Rev* (2015) 265:35–52. doi: 10.1111/imr.12286

10. Heid ME, Keyel PA, Kamga C, Shiva S, Watkins SC, Salter RD. Mitochondrial reactive oxygen species induces NLRP3-dependent lysosomal damage and inflammasome activation. *J Immunol* (2013) 191:5230–8. doi: 10.4049/jimmunol.1301490

11. Liu W, Guo WJ, Xu Q, Sun Y. Advances in mechanisms for NLRP3 inflammasomes regulation. *Yao xue xue bao = Acta Pharm Sin* (2016) 51:1505–12. doi: 10.16438/j.0513-4870.2016-0380

12. Zheng C. The emerging roles of NOD-like receptors in antiviral innate immune signaling pathways. *Int J Biol Macromol* (2021) 169:407–13. doi: 10.1016/j.ijbiomac.2020.12.127

13. Khakroo Abkenar I, Rahmani-Nia F, Lombardi G. The effects of acute and chronic aerobic activity on the signaling pathway of the inflammasome NLRP3 complex in young men. *Medicina (Kaunas)* (2019) 55:105. doi: 10.3390/medicina55040105

14. Wang Q, Hu J, Liu Y, Li J, Liu B, Li M, et al. Aerobic exercise improves synaptic-related proteins of diabetic rats by inhibiting FOXO1/NF-kappaB/NLRP3 inflammatory signaling pathway and ameliorating PI3K/Akt insulin signaling pathway. *J Mol Neurosci* (2019) 69:28–38. doi: 10.1007/s12031-019-01302-2

15. Zaidi H, Byrkjeland R, Njerve IU, Akra S, Solheim S, Arnesen H, et al. Effects of exercise training on inflammasome-related mediators and their associations to glucometabolic variables in patients with combined coronary artery disease and type 2 diabetes mellitus: Sub-study of a randomized control trial. *Diabetes Vasc Dis Res* (2019) 16:360–8. doi: 10.1177/1479164119836922

16. Irwin MR, Olmstead R, Breen EC, Witarama T, Carrillo C, Sadeghi N, et al. Tai chi, cellular inflammation, and transcriptome dynamics in breast cancer survivors with insomnia: a randomized controlled trial. *J Natl Cancer Inst Monogr* (2014) 2014:295–301. doi: 10.1093/jncimonographs/lgu028

17. Lu WA, Chen YS, Wang CH, Kuo CD. Effect of a single session of tai chi chuan practice on glucose and lipid metabolism and related hormones. *Life (Basel)* (2020) 10:145. doi: 10.3390/life10080145

18. Bower JE, Irwin MR. Mind-body therapies and control of inflammatory biology: A descriptive review. *Brain Behav Immun* (2016) 51:1–11. doi: 10.1016/j.bbi.2015.06.012

19. Sumneang N, Oo TT, Singhanat K, Maneechote C, Arunsak B, Nawara W, et al. Inhibition of myeloid differentiation factor 2 attenuates cardiometabolic impairments *via* reducing cardiac mitochondrial dysfunction, inflammation, apoptosis and ferroptosis in prediabetic rats. *Biochim Biophys Acta Mol Basis Dis* (2022) 1868:166301. doi: 10.1016/j.bbadis.2021.166301

20. Szczerbinski L, Taylor MA, Puchta U, Konopka P, Paszko A, Citko A, et al. The response of mitochondrial respiration and quantity in skeletal muscle and adipose tissue to exercise in humans with prediabetes. *Cells* (2021) 10:3013. doi: 10.3390/cells10113013

21. American Diabetes A. Classification and diagnosis of diabetes: Standards of medical care in diabetes-2020. *Diabetes Care* (2020) 43:S14–31. doi: 10.2337/dc20-S002

22. Hotamisligil GS. Inflammation and metabolic disorders. *Nature* (2006) 444:860–7. doi: 10.1038/nature05485

23. Gora IM, Ciechanowska A, Ladyzynski P. NLRP3 inflammasome at the interface of inflammation, endothelial dysfunction, and type 2 diabetes. *Cells* (2021) 10:314. doi: 10.3390/cells10020314

24. Rheinheimer J, de Souza BM, Cardoso NS, Bauer AC, Crispim D. Current role of the NLRP3 inflammasome on obesity and insulin resistance: A systematic review. *Metabolism* (2017) 74:1–9. doi: 10.1016/j.metabol.2017.06.002

25. Sepehri Z, Kiani Z, Afshari M, Kohan F, Dalvand A, Ghavami S. Inflammasomes and type 2 diabetes: An updated systematic review. *Immunol Lett* (2017) 192:97–103. doi: 10.1016/j.imlet.2017.10.010

26. Unamuno X, Gomez-Ambrosi J, Ramirez B, Rodriguez A, Becerril S, Valenti V, et al. NLRP3 inflammasome blockade reduces adipose tissue inflammation and extracellular matrix remodeling. *Cell Mol Immunol* (2021) 18:1045–57. doi: 10.1038/s41423-019-0296-z

27. Kursawe R, Dixit VD, Scherer PE, Santoro N, Narayan D, Gordillo R, et al. A role of the inflammasome in the low storage capacity of the abdominal subcutaneous adipose tissue in obese adolescents. *Diabetes* (2016) 65:610–8. doi: 10.2337/db15-1478

28. Li J. Effects of aerobic exercise on vascular inflammation and SIRT1 /NF-κB signaling pathway in type 2 diabetic ats. *J Beijing Sport Univ* (2018) 41:57–63. doi: 10.19582/j.cnki.11-3785/g8.2018.05.009

29. Li Y, Xu P, Wang Y, Zhang J, Yang M, Chang Y, et al. Different intensity exercise preconditions affect cardiac function of exhausted rats through regulating TXNIP/TRX/NF-kBp65/NLRP3 inflammatory pathways. *Evid Based Complement Alternat Med* (2020) 2020:5809298. doi: 10.1155/2020/5809298

30. Chen C, Ma X, Yang C, Nie W, Zhang J, Li H, et al. Hypoxia potentiates LPS-induced inflammatory response and increases cell death by promoting NLRP3 inflammasome activation in pancreatic beta cells. *Biochem Biophys Res Commun* (2018) 495:2512–8. doi: 10.1016/j.bbrc.2017.12.134

31. Liu G, Chen X, Wang Q, Yuan L. NEK7: a potential therapy target for NLRP3-related diseases. *Biosci Trends* (2020) 14:74–82. doi: 10.5582/bst.2020.01029

32. Cai H, Wang P, Zhang B, Dong X. Expression of the NEK7/NLRP3 inflammasome pathway in patients with diabetic lower extremity arterial disease. *BMJ Open Diabetes Res Care* (2020) 8:e001808. doi: 10.1136/bmjdrc-2020-001808

33. Ma C, Ding H, Deng Y, Liu H, Xiong X, Yang Y. Irisin: A new code uncover the relationship of skeletal muscle and cardiovascular health during exercise. *Front Physiol* (2021) 12:620608. doi: 10.3389/fphys.2021.620608

34. Shelbaya S, Abu Shady MM, Nasr MS, Bekhet MM, Mageed YA, Abbas M. Study of irisin hormone level in type 2 diabetic patients and patients with diabetic nephropathy. *Curr Diabetes Rev* (2018) 14:481–6. doi: 10.2174/1573399813666170829163442

35. Benedini S, Dozio E, Invernizzi PL, Vianello E, Banfi G, Terruzzi I, et al. Irisin: A potential link between physical exercise and metabolism-an observational study in differently trained subjects, from elite athletes to sedentary people. *J Diabetes Res* (2017) 2017:1039161. doi: 10.1155/2017/1039161

36. Yue R, Zheng Z, Luo Y, Wang X, Lv M, Qin D, et al. NLRP3-mediated pyroptosis aggravates pressure overload-induced cardiac hypertrophy, fibrosis, and dysfunction in mice: cardioprotective role of irisin. *Cell Death Discovery* (2021) 7:50. doi: 10.1038/s41420-021-00434-y

37. Li J, Liu Y, Liu B, Li F, Hu J, Wang Q, et al. Mechanisms of aerobic exercise upregulating the expression of hippocampal synaptic plasticity-associated proteins in diabetic rats. *Neural Plast* (2019) 2019:7920540. doi: 10.1155/2019/7920540

38. Kaufmann FN, Costa AP, Ghisleni G, Diaz AP, Rodrigues ALS, Peluffo H, et al. NLRP3 inflammasome-driven pathways in depression: Clinical and preclinical findings. *Brain Behav Immun* (2017) 64:367–83. doi: 10.1016/j.bbi.2017.03.002

39. Kar S, Shahshahan HR, Hackfort BT, Yadav SK, Yadav R, Kambis TN, et al. Exercise training promotes cardiac hydrogen sulfide biosynthesis and mitigates pyroptosis to prevent high-fat diet-induced diabetic cardiomyopathy. *Antioxidants (Basel)* (2019) 8:638. doi: 10.3390/antiox8120638

40. Bian XP, Ji RF, Liu BB, Hu JY, Li MM, Xue XL, et al. Aerobic exercise reduces the expression of pyroptosis-related proteins and inflammatory factors in hippocampus of mice with insulin resistance. *Sheng li xue bao [Acta physiologica Sinica]* (2020) 72:455–62. doi: 10.13294/j.aps.2020.0002

41. Tao J, Chen X, Liu J, Egorova N, Xue X, Liu W, et al. Tai chi chuan and baduanjin mind-body training changes resting-state low-frequency fluctuations in the frontal lobe of older adults: A resting-state fMRI study. *Front Hum Neurosci* (2017) 11:514. doi: 10.3389/fnhum.2017.00514

42. Jia S, Yang Y, Bai Y, Wei Y, Zhang H, Tian Y, et al. Mechanical stimulation protects against chondrocyte pyroptosis through irisin-induced suppression of PI3K/Akt/NF-kappaB signal pathway in osteoarthritis. *Front Cell Dev Biol* (2022) 10:797855. doi: 10.3389/fcell.2022.797855

43. Chao M, Wang C, Dong X, Ding M. The effects of tai chi on type 2 diabetes mellitus: A meta-analysis. *J Diabetes Res* (2018) 2018:7350567. doi: 10.1155/2018/7350567

44. Czech MP. Insulin action and resistance in obesity and type 2 diabetes. *Nat Med* (2017) 23:804–14. doi: 10.1038/nm.4350

45. Rovira-Llopis S, Apostolova N, Banuls C, Muntane J, Rocha M, Victor VM. Mitochondria, the NLRP3 inflammasome, and sirtuins in type 2 diabetes: New therapeutic targets. *Antioxid Redox Signal* (2018) 29:749–91. doi: 10.1089/ars.2017.7313

frontiers | Frontiers in Immunology

TYPE Original Research
PUBLISHED 06 October 2022
DOI 10.3389/fimmu.2022.1028458

OPEN ACCESS

EDITED BY
Hongjuan You,
Xuzhou Medical University, China

REVIEWED BY
Biao Qiu,
NewYork-Presbyterian, United States
Jiangning Liu,
Chinese Academy of Medical Sciences and Peking Union Medical College, China
Tao Jiang,
Beijing Institute of Microbiology and Epidemiology, China

*CORRESPONDENCE
Rongbao Gao
gaorongbao@cnic.org.cn

†These authors have contributed equally to this work and share first authorship

SPECIALTY SECTION
This article was submitted to Viral Immunology, a section of the journal Frontiers in Immunology

RECEIVED 26 August 2022
ACCEPTED 20 September 2022
PUBLISHED 06 October 2022

CITATION
Zhang Z, Gao Y, Li L, Luo J and Gao R (2022) Deficiency of C-reactive protein or human C-reactive protein transgenic treatment aggravates influenza A infection in mice. *Front. Immunol.* 13:1028458. doi: 10.3389/fimmu.2022.1028458

Deficiency of C-reactive protein or human C-reactive protein transgenic treatment aggravates influenza A infection in mice

Zhuohan Zhang[1,2†], Yongjun Gao[1,2†], Li Li[1,2], Junhao Luo[1,2] and Rongbao Gao[1,2*]

[1]National Health Commission of People's Republic of China (NHC) Key Laboratory of Biosafety, National Institute for Viral Disease Control and Prevention, Chinese Center for Disease Control and Prevention, Beijing, China, [2]National Health Commission of People's Republic of China (NHC) Key Laboratory of Medical Virology and Viral Diseases, National Institute for Viral Disease Control and Prevention, Chinese Center for Disease Control and Prevention, Beijing, China

C-reactive protein (CRP) has been shown to be a potential candidate target in the immunotherapy of severe influenza A infection. However, it is unclear on the pathogenesis associated with CRP in influenza infections. Here, we used influenza A H1N1 CA04 to infect human CRP transgenic mice (KI), CRP knockout mice (KO), and wild-type mice (WT), respectively, and compared the viral pathogenicity and associated immune response in those mice. The results showed that CA04 infection resulted in 100%, 80%, and 60% death in KO, KI, and WT mice, respectively. Compared to WT mice, CA04 infection resulted in higher TCID50 in lungs on day 3 after infection but lowered HI antibody titers in sera of survivors on day 21 after infection in KI mice. ELISA assay showed that IFN-γ concentration was significantly increased in sera of WT, KI, or KO mice on day 7 after infection, and IL-17 was remarkably increased in sera of WT mice but decreased in sera of KI mice while no significant change in sera of KO mice on day 3 or 7 after infection. Quantitative RT-PCR showed that the relative expression levels of immune checkpoint CTLA-4, LAIR-1, GITR, BTLA, TIM-3, or PD-1 mRNA in the lung presented decreased levels on day 3 or 7 after infection in KI or KO mice. The correlation analysis showed that mRNA expression levels of the 6 molecules positively correlated with viral TICD50 in WT mice but negatively correlated with viral TCID50 in KI or KO mice. However, only LAIR-1 presented a significant correlation in each lung tissue of WT, KI, or KO mice with CA07 infection statistically. IHC results showed that LAIR-1 positive cells could be found in WT, KO, or KI mice lung tissues with CA04 infection, and the positive cells were mainly distributed in an inflammatory dense area. Our results suggested that deficiency of CRP or human CRP transgenic treatment aggravates influenza A virus infection in mice. CRP is a double sword in immune regulation of influenza infection in which IL-17 and immune checkpoint may be involved.

KEYWORDS

influenza, C-reactive protein, pneumonia, immune response, immune checkpoint

Introduction

The influenza virus that causes annually recurrent acute respiratory disease in humans is responsible for a large proportion of morbidity and mortality (1). The WHO estimates that annual influenza epidemics result in ~1 billion infections, 3-5 million cases of severe illness, and 290,000-650,000 deaths (2). Severe disease and/or mortality in patients with influenza virus infection are generally due to virus-induced pneumonia or secondary bacterial superinfection (1). Primary viral pneumonia is characterized by high levels of viral replication in the lower respiratory tract accompanied by strong pro-inflammatory responses. Influenza-mediated alveolar epithelial cell injury is due to inherent viral pathogenicity and imbalanced host immune response triggered by the virus (3, 4).

C-reactive protein (CRP), a pentameric protein found in almost all organisms where the presence of CRP has been sought, is an inflammatory biomarker and an immune mediator (5, 6). It was first named because of its ability to precipitate C-polysaccharide from Streptococcus pneumoniae *in vivo* and became a protein expressed as a component of the acute phase response in humans and some other species (7). Growing studies have shown that CRP plays important roles in inflammatory processes and host responses to infection, including the complement pathway, apoptosis, phagocytosis, nitric oxide release, and the production of cytokines. Several studies suggested that CRP is a potential candidate target in the immunotherapy of severe influenza A infection (5, 8–10). However, to our knowledge, it is unclear on the pathogenesis associated with CRP on severe influenza infection.

In this study, to understand the pathogenesis associated with CRP on severe influenza infection, we used influenza A H1N1 virus to infect mice with human CRP transgenic treatment, mice with deficiency of CRP, and wild-type mice, respectively, and compared the viral pathogenicity and associated immune response in the three typed mice.

Materials and methods

Mice and infection

All animal studies were performed according to the guidelines approved by the Investigational Animal Care and Use Committee of the National Institute for Viral Diseases Control and Prevention of the China CDC and were conducted following the guidelines of the Council for Animal Care. The CRP knockout (KO), human CRP knock-in (KI), or wild-type (WT) C57BL/6J mice were purchased from Cyagen Biosciences (Suzhou, China). The KO or KI mice were detected by PCR, sequencing, and southern blotting to determine the knockout of mouse CRP or knock-in of human CRP on the sampled tail of each mouse. We performed a viral challenge by i.n. Inoculation of 1.5×10^4 TCID50 of A/California/04/2009 (H1N1) to anesthetized 8- to 10-week aged KO, KI, or WT female mice in 50 µL PBS. After the mice were infected with the virus, their body weight was measured daily to observe the changes. If the mice lost over 25% of their initial body weight, they were humanely euthanized and necropsied.

Viral titration

The influenza viruses used in this study were titrated by a TCID50 (50% tissue culture infectious dose) in MDCK cells. Briefly, 100 µl/well of MDCK cells (3×10^5 cells/ml) were seeded one day before infection in 96-well microtiter plates. Serial semi-logarithmic dilutions of each virus or supernatants of mouse lung homogenates were made with Dulbecco modified Eagle medium containing 1% bovine serum albumin and 2 µg/ml TPCK-treated trypsin from 10^{-2} to 10^{-7}. Each virus or sample's dilution was added to MDCK cells (4 wells for each dilution, 100 µl/well). The cells were incubated for 72 h at 35°C. The contents of each well were tested for hemagglutination by incubating 50 µl of the tissue culture supernatant with 0.5% turkey erythrocytes. The TCID50 was calculated according to the Reed and Muench method. For mouse lung tissue processing, in brief, left lung tissues from each mouse were homogenized in 1 mL of phosphate-buffered saline (PBS) by the tissue lyser (Qiagen). The supernatant was sampled after centrifugation at 3000 rpm for 15 min at 4°C.

Hemagglutination-inhibition (HI) assay

Prior to testing by the HI assay with turkey RBC, the serum samples were treated with 4-fold receptor destroying enzyme (RDE) dilutions at 37°C for 18 h, followed by incubation at 56°C for 30 min. The serum samples were titrated in 2-fold dilutions of PBS and tested at an initial dilution of 1:10. Virus was added at a concentration of 4 HAU/25 µL. After 1 hour, 50 µL of 1% turkey RBC was added.

Histopathological and immunohistochemical staining

Routine hematoxylin and eosin staining was used for histopathology evaluation. For immunohistochemistry, 4µm deparaffinized formalin-fixed paraffin-embedded sections were stained with polyclonal antibody against LAIR-1 (51030-R119, Sinobilogical, China) by using a polymer-based colorimetric indirect peroxidase method (ZSBio, China).

Cytokine IL-17 and IFN-γ assay

The concentration of IL-17 and IFN-γ in mice sera was determined using an enzyme-linked immunosorbent assay (ELISA) according to the manufacturer's instructions (R&D system, USA). The serum samples were detected in 10-fold dilutions of PBS. The concentrations of IL-17 and IFN-γ were calculated through standard curves using the standard product (Supplemental Figure 1).

RNA extraction and quantitative RT-PCR

RNA was extracted from mouse lung tissues using an animal tissue total RNA extraction kit (TIANGEN BIOTECH, China) per the kit's protocol. To quantify the relative expression levels of immune checkpoint glucocorticoid-induced TNF receptor family-related protein (GITR), B- and T-lymphocyte attenuator (BTLA), T-cell immunoglobulin and mucin-3 (TIM-3), cytotoxic T lymphocyte-associated antigen-4 (CTLA-4), human leukocyte associated Ig-like receptor-1 (LAIR-1) or programmed death 1 (PD-1) mRNA in mice lung tissues, a quantitative real-time RT-PCR was performed by QuantiFast SYBR Green RT-PCR Kit (Life Science Technologies, USA) on a real-time PCR detection system (Agilent Technologies Inc., Santa Clara, CA). The housekeeping gene GAPDH was used as the internal control. The specific primer sets were used as follows: GITR forward: GCCAGACGCTACAAGACT, GITR reverse: ATCGTAACTCACCGCTCT; BTLA forward: GTGACTTGGTGTAAGCACAATGGAA, BTLA reverse: TACGACCCGTTATCACTGAGATGTA; TIM-3 forward: AACCCTGCGAAAGGCAAACTT, TIM-3 reverse: GGTGACGACTGTCCTCCCAAA; CTLA-4 forward: AACCTTCAGTGGTGTTGGCTAG, CTLA-4 reverse: CCTCAGTCATTTGGTCATTTGT; LAIR-1 forward: TTGTCTTTCCGCCCTTCTGTTCTG, LAIR-1 reverse: CTGCTGCTGTCTTTTGTTGTTTGG; PD-1 forward: TATAACCTTGACGCAAACCA, PD-1 reverse: CTTGCTCATTTCAGAGTCCT; GAPDH reverse: ATGGGAGTTGTTTTCTTG, GAPDH forward: CTCGTCTTCTGTCATCTCTGCTG. The relative expression level was displayed by ΔCt in previous studies (11, 12).

Statistical analysis

The mouse survival curve analysis was performed using Fischer's exact test. Mouse body weight changes, viral TCID50 in mouse lung tissue, sera HI antibody titers, sera concertation of cytokines, and mRNA expression levels of immune checkpoints in mouse lung tissues were observed using unpaired t-tests for significant differences. The correlations between mRNA levels of checkpoint and sera levels of cytokines were analyzed by Pearson's correlation method. Differences were considered significant at P <.05 with a two-tailed test. All analyses were performed using Instat software (Vision 5.0; GraphPad Prism).

Results

The impact of CRP on pathogenicity of influenza virus in mice

CA04 infection resulted in 60% (n=10), 80% (n=10), or 100% (n=10) fatality in WT, KI, or KO mice respectively. The body weight changes suggested that the body weight loss of KO mice was higher than one of WT or KI mice after day 4 of infection, and the body weight loss of KI mice presented higher than one of the WT mice on day 7 after infection till to day 14 after infection (Figure 1). Furthermore, histopathological

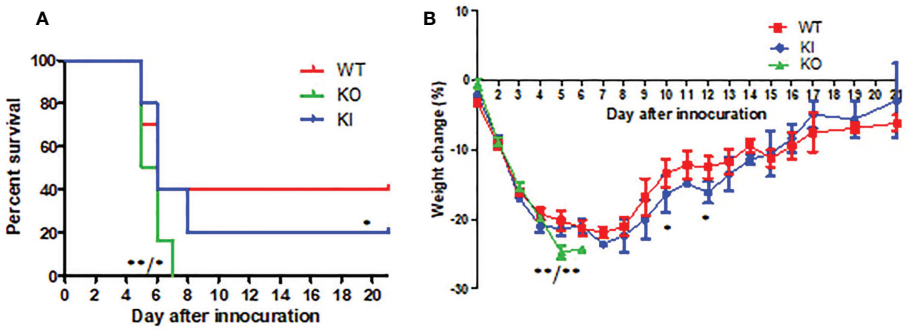

FIGURE 1
The survival rate and body weight changes in WT, KO, or KI mice with CA07 infection. **(A)** Kaplan-Meier survival curves were recorded. n=10 mice for each group. *P <0.05, **P <0.01 (log-rank test) when comparing the WT or KI mice. **(B)** Body weight loss was recorded for all survived mice until 21 days post-infection. *P <0.05, **P <0.01 (two-tailed t-test) when comparing the WT or KI mice.

changes were observed on WT, KI, or KO mice with CA07 infection lung tissues. The results showed that, compared to MOCK, the CA04 resulted in typical histopathological damages, including infiltration of inflammatory cells and congestion and edema of alveoli and bronchus in the lungs of WT mice as well as in the lungs of KO or KI mice (Figure 2). On day 3 after infection, CA04 raised focal damages with scatted bronchopneumonia in WT, KO, or KI mice.

In comparison, the infiltration of inflammatory cells presented more in WT or KI mice than in KO mice (Figures 2A–C). On day 7 after infection, defuse alveolar damages were observed in the lungs of WT, KO, or KI mice. In comparison, the damages were more serious and extensive in the lungs of KO or KI mice than those of WT mice (Figures 2D–F). Taken together, the results suggested that deficiency of CRP or human CRP transgenic treatment enhanced the pathogenicity of influenza virus in mice.

The impact of CRP on viral replication and antibody response in mice with influenza virus infection

Viral titration showed that the viral TCID50 presented a significantly higher level in the lungs of KI mice than WT or KO mice on day 3 after infection. In contrast, no significant difference was observed between them, although viral TCID50 presented a higher level in the lungs of KO mice than KI or WT mice on day 7 after infection (Figure 3A). The HI assay showed that the sera HI antibody titer against CA07 presented a much higher level in WT survivors than in KI survivors (Figure 3B). The results suggested that CRP was related to the viral clearance and antibody response in influenza infection.

The impact of CRP on levels of cytokine IFN-γ and IL-17

As shown in Figure 4, the ELISA assay showed that IFN-γ concentration was significantly increased in sera of WT, KI, or KO mice on day 7 after infection, and no significant difference was observed between them. However, compared to PBS inoculated mice, IL-17 was remarkably increased in sera of WT mice with CA04 infection but decreased in sera of KI mice with CA04 infection on day 3 or 7 after infection, while there was no significant change in sera of KO mice infected with CA04 on day 3 or 7 after infection. The results suggested that deficiency of CRP or human CRP transgenic treatment decreased IL-17 immune response in influenza infection.

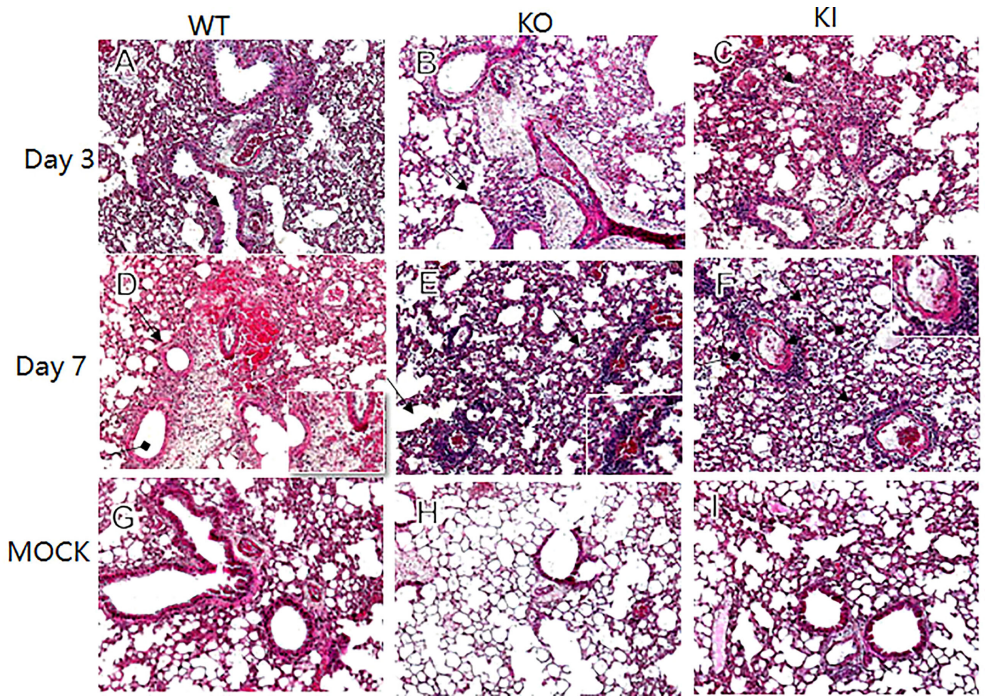

FIGURE 2
Histopathological damage in lung tissues of WT, KO or KI mice infected with CA04. Representative lung histopathology of CA04 or PBS challenged WT **(A, D, G)**, KO **(B, E, H)** or KI **(C, F, I)** mice on day 3 or 7 after infection. The lungs of PBS inoculated WT **(G)**, KO **(H)** or KI **(I)** mice were set as MOCK. The infiltration of inflammatory cells (black arrow) and hyaline membrane formation (black square arrow) were presented in lung sections. Original magnification: ×10.

10.3389/fimmu.2022.1028458

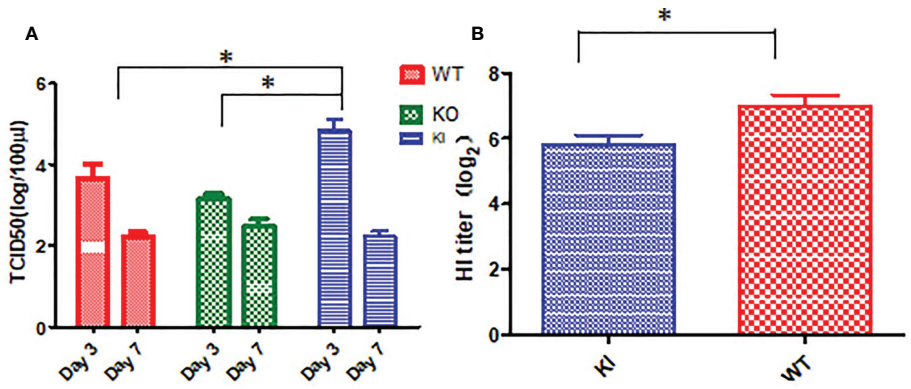

FIGURE 3
Viral load and HI antibody titer in mice with CA04 infection. **(A)** The viral TCID50 in lung tissues of CA04 infected WT, KI, or KO mice on day3 or 7 after infection, n=5 mice per group (mean ± SEM). **(B)** HI antibody titers in sera of CA04 infected WT or KI mice on day21 or 7 after infection. Unpaired t-tests were performed to assess statistical significance, *P <0.05, (two-tailed).

The impact of CRP on immune checkpoint mRNA expression of infected mice

To observe the correlation of CRP with the local immune response of lung in mice to influenza infection, we quantified the relative expression levels of 6 immune checkpoint mRNAs in lung tissues of mice, including GITR, BTLA, TIM-3, PD-1, CTLA-4, and LAIR-1. The results showed that compared to PBS inoculated mice, relative expression levels of GITR, BTLA, TIM-3, and PD-1 mRNA were significantly decreased on day 3 or 7 after infection in KI or KO mice with CA07 infection but not in WT mice with CA07 infection, and their levels were significantly higher in WT mice than in KI or KO mice (Figures 5A–D). Whereas the relative expression levels of CTLA-4 and LAIR-1 were increased on day 3 or 7 after infection in WT, KI, and KO mice, and their levels were significantly higher in WT mice than in KI or KO mice on day 7 after infection (Figures 5E, F). In addition, the correlation analysis showed that mRNA expression levels of the 6 molecules presented a respectively positive correlation with viral TICD50 in WT mice but a negative correlation with viral TCID50 in KI or KO mice (Figure 6). However, only LAIR-1 presented a significant correlation in each lung tissues of WT, KI, or KO mice with CA07 infection statistically (Figure 6A). In addition, IHC results showed that LAIR-1 positive cells could be seen in lung tissues of WT, KO, or KI mice with CA04 infection, and the positive cells were mainly distributed in an inflammatory dense area. Given the comparison, more stained cells were seen on day 7 after infection than on day 3 after infection and in WT and KI mice than in KO mice on day 7 after infection (Figure 7).

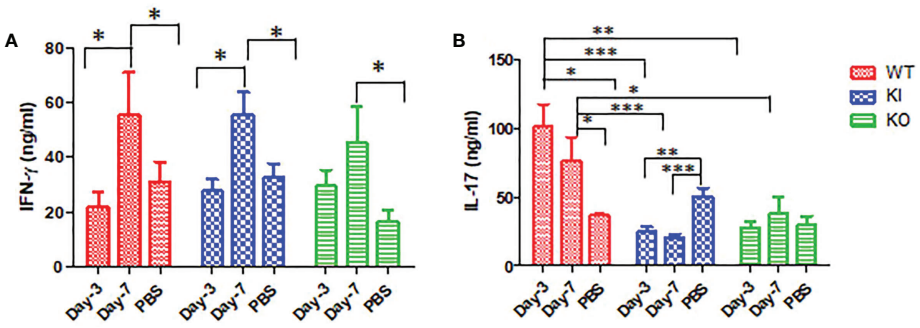

FIGURE 4
IFN-γ and IL-17 levels in WT, KO, or KI mice sera. **(A)** The concentration of IFN-γ tested by ELISA in sera of WT, KO, or KI mice infected with CA04 on day 3 or 7 after infection, PBS inoculated mice were set as mock control. **(B)** The concentration of IL-17 tested by ELISA in sera of WT, KO, or KI mice infected with CA04 on day 3 or 7 after infection, PBS inoculated mice were set as mock control. Unpaired t-tests were performed to assess statistical significance, *P <0.05, **P <0.01, ***P <0.001 (two-tailed)..

10.3389/fimmu.2022.1028458

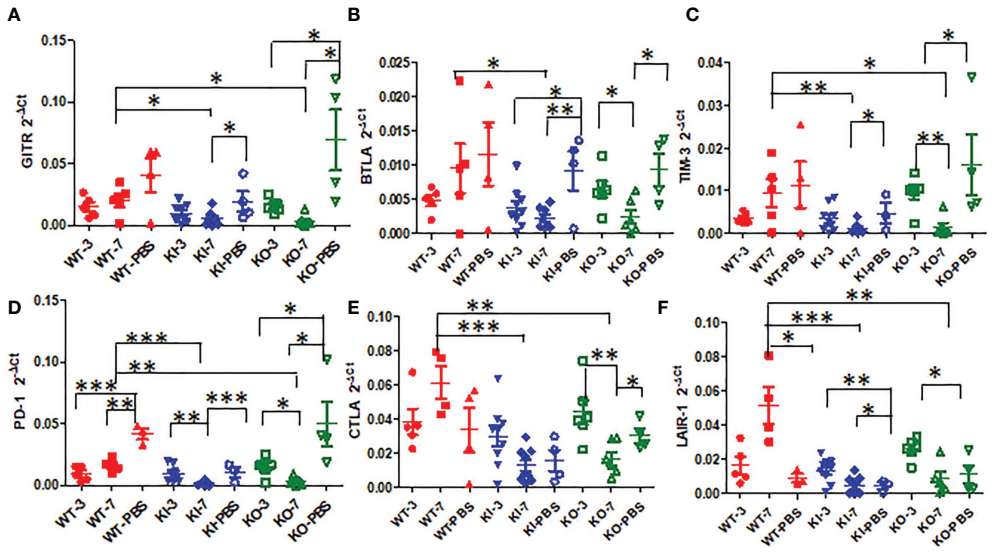

FIGURE 5
The relative quantification level of checkpoint mRNA GITR **(A)**, BTLA **(B)**, TIM-3 **(C)**, CTLA-4 **(D)**, PD-1 **(E)**, or LAIR-1 **(F)** in lung tissues of WT, KO, or KI mice with CA04 infection on day 3 or 7 after infection. PBS inoculated mice were set as mock control. Unpaired *t*-tests were performed to assess statistical significance, $*P < 0.05$, $**P < 0.01$, $***P < 0.001$ (two-tailed).

Discussion

The modulation of host factors involved in regulating viral replication and/or injury or tissue recovery has been demonstrated to be a potential strategy against viral diseases, including influenza (13, 14). Whereas, CRP has been considered a potential therapeutic target for inflammatory diseases, including infections, since CRP bound to a multivalent ligand can efficiently initiate the assembly of a C3 convertase through the classical pathway and thus decorate the surface of the ligand with opsonic complement fragments (6, 15, 16). However, the detailed response pathway of CRP to the disease is still unknown, although CRP is related to the outcome of severe influenza disease and joined in the mediation of immunopathological lesions (8, 17, 18).

Our data demonstrated that deficiency of CRP or human CRP transgenic treatment aggravated influenza A virus infection in mice, and deficiency of CRP resulted in a much more severer outcome than human CRP transgenic treatment. Human CRP transgenic mice have been demonstrated to be a good model for studying the *in vivo* function of the protein (19) and have been used to study infectious diseases (6, 20–25). Transgenic or passively administered human CRP was protective against lethal bacterial infection in transgenic mice (6). In contrast, increasing studies have shown that excessively high CRP level was a risk factor for virus infection's severity or fatal outcome, including influenza (8, 17, 26–28). Studies have demonstrated that the antiviral immune response represents a balancing act between the elimination of the virus and immune-mediated pulmonary injury (29). Our previous study showed that CRP joined in mediating immunopathological lesions in severe influenza (8). Hence, our results here indicated that CRP might play an important role in the immune balance of influenza infection, and the role may be a double-edged sword in influenza infection, overexpression or deficiency of CRP would be a disadvantage to the infection. Besides survival rate and body weight loss, our results showed that human CRP transgenic treatment or deficiency of CRP resulted in more serious and extensive damage to the lung in mice with influenza A infection on day 7 after infection, and human CRP transgenic treatment increased the viral load in the lung of mice with influenza A infection on day 3 after infection but decreased the HI antibody titer in survivor on day 21 after infection. The results indicated that deficiency of CRP or human CRP transgenic treatment impacted the immune response associated with tissue damage, viral clearance, and/or antibody production.

Our results also suggested that deficiency of CRP or human CRP transgenic treatment decreased or blocked the immune response of IL-17 in influenza A infection. Studies showed that IL-17 plays a critical role in mediating the recruitment of B cells to the site of pulmonary influenza virus infection in mice (29) and suggested that anti-IL-17A or anti-IFN-γ treatment attenuated the severity of immunopathology by influenza virus (30, 31). However, studies also suggested that IL-17 plays a crucial role in enhancing effective antiviral immune responses, including the maintenance of tissue integrity and the generation of protective immune responses to infectious microorganisms,

10.3389/fimmu.2022.1028458

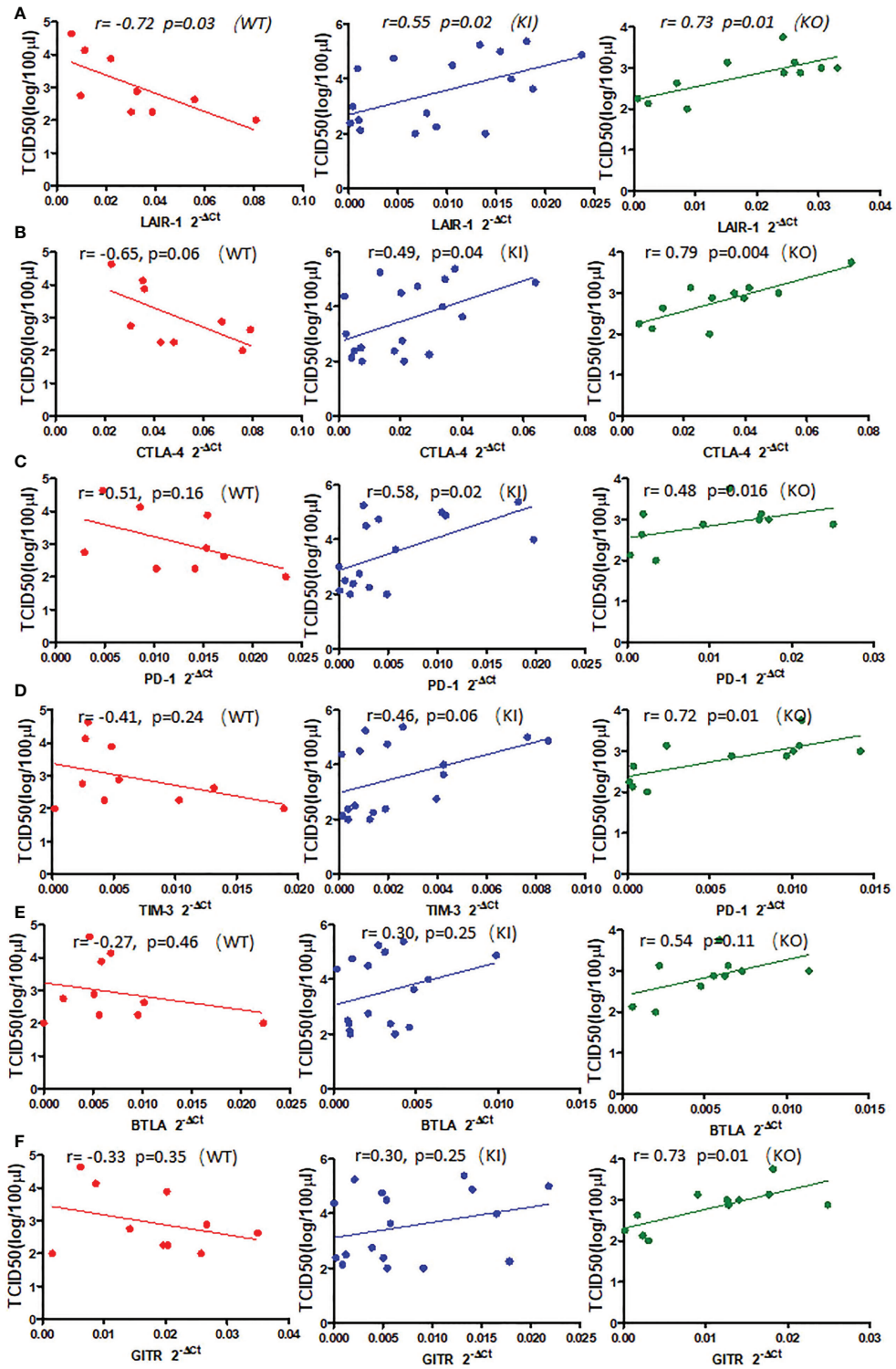

FIGURE 6
The correlation between relative quantification level of checkpoint mRNA LAIR-1 **(A)**, CTLA-4 **(B)**, PD-1 **(C)**, TIM-3 **(D)**, BTLA **(E)**, GITR **(F)**, and viral TCID50 in lung tissue of WT, KO, or KI mice infected with CA04 on day 3 or 7 after infection. Pearson correlation analysis was performed.

10.3389/fimmu.2022.1028458

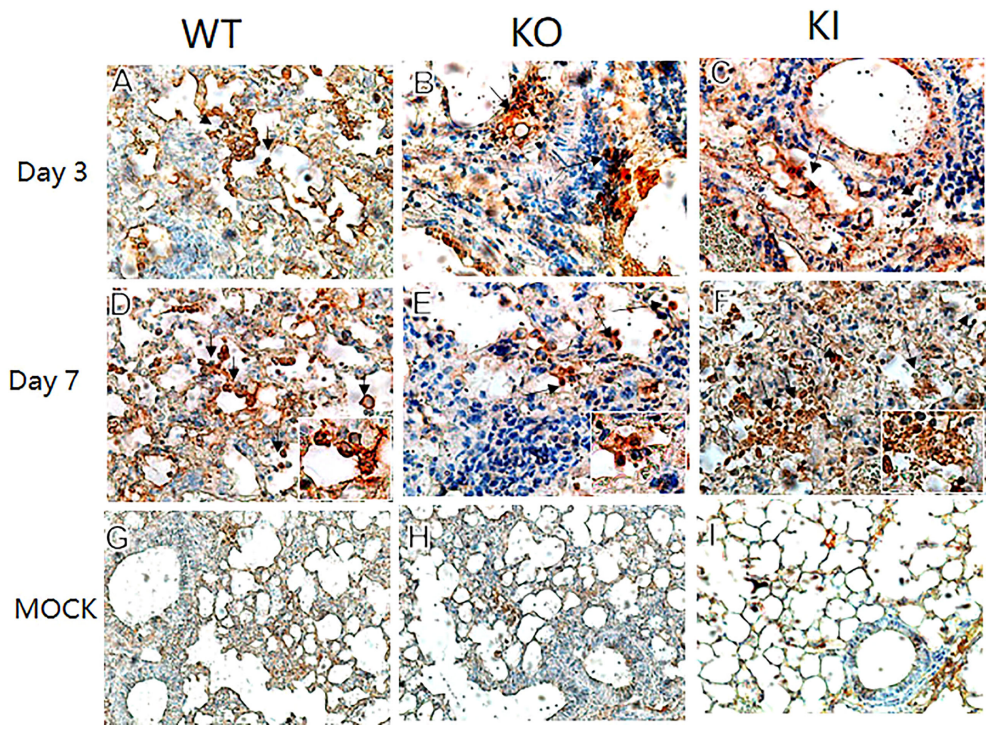

FIGURE 7
LAIR-1 immunopathology of lung sections from WT, KO, or KI mice. Immunohistochemistry for LAIR-1 + pulmonary cells (black arrows) in representative lung sections of WT, KO, or KI mice infected with CA04 on day 3 **(A–C)** or 7 after infection **(D–F)**. PBS inoculated mice were set as mock control **(G–I)**. Original magnification: ×40 **(A–F)** or ×20 **(G–I)**.

especially at epithelial barrier sites (32–34). Our results showed that both deficiencies of CRP and human CRP transgenic treatment decreased IL-17 response but had no influence on IFN-γ response in mice with influenza A infection, indicating that IL-17 antiviral response was deficient or decreased in influenza A infection in mice with deficiency of CRP or human CRP transgenic treatment or.

We further analyzed the impact of CRP on the expression of immune checkpoint molecules in lung tissues of mice with influenza A infection because several immune checkpoint molecules have been demonstrated to be crucial for maintaining self-tolerance and for modulating the length and magnitude of effector immune responses in peripheral tissues to minimize tissue damage (35–37). In addition, studies of the interplay between immune activation and suppression have shown an important role for immune checkpoint molecules in the pathogenesis of infectious diseases (37). In this study, our results showed that, compared to WT mice, influenza A infection resulted in decreased expression of checkpoint molecules GITR, BTLA, TIM-3, PD-1, CTLA-4, and LAIR-1 in lung tissues of KI or KO mice on day 7 after infection, and expression levels of these molecules presented a positive correlation with viral TICD50 in lungs of WT mice but negative correlation with TCID50 in lungs of KI or KO mice although the significant correlation was not observed in all them (Figure 5 and Supplemental Figure 1). And the results showed the only LAIR-1 presented significant correlation with viral TCID50 in each infection of the three typed mice. The IHC stains also showed that LAIR-1 positive cells were mainly distributed in the inflammatory dense area of lung tissues in WT, KO, or KI mice with CA04 infection. Studies showed that LAIR-1 plays a role in regulating immune cells (38) and limits neutrophilic airway inflammation as a functional inhibitory receptor on airway-infiltrated neutrophils (39, 40). The results indicated that deficiency of CRP or human CRP transgenic treatment impacted the balance of immune regulation by immune checkpoint molecules. In contrast, the delicate immune balance is a key factor in maintaining normal immune responses such as viral clearance (41), tissue tolerance, antibody responses, and tissue repairment (29, 42, 43).

In summary, we observed the impact of human CRP transgenic treatment and deficiency of CRP on the pathogenicity of influenza A virus in mice and analyzed immune factors associated with innate immune regulation in those mice. Our results showed that both deficiencies of CRP and human CRP transgenic treatment aggravated influenza A infection in mice, and the aggravation may be owed to imbalance immune regulation, including decreased antibody

response, IL-17 levels, and/or expression of several immune checkpoint molecules.

Data availability statement

The original contributions presented in the study are included in the article/Supplementary Material. Further inquiries can be directed to the corresponding author.

Ethics statement

The animal study was reviewed and approved by Investigational Animal Care and Use Committee of the National Institute for Viral Diseases Control and Prevention of the China CDC.

Author contributions

RG designed the study and wrote the report. ZZ, YG, and LL performed the experiments. RG, ZZ, and YG joined in the data analysis. All authors contributed to the review and revision of the manuscript and have read and approved the final version.

Funding

This work was supported by the National Natural Scientific Foundation of China (grant number 81971946) and the National Key R&D Program of China (grant number 2019YFC1605001). The contents of this article are solely the responsibility of the authors and do not necessarily represent the views of China CDC and other organizations.

Conflict of interest

The authors declare that the research was conducted in the absence of any commercial or financial relationships that could be construed as a potential conflict of interest.

Publisher's note

Supplementary material

The Supplementary Material for this article can be found online at: https://www.frontiersin.org/articles/10.3389/fimmu.2022.1028458/full#supplementary-material

SUPPLEMENTARY FIGURE 1
The ELISA standard curves of IL-17 **(A)** and IFN-γ **(B)**.

References

1. Peteranderl C, Herold S, Schmoldt C. Human influenza virus infections. *Semin Respir Crit Care Med* (2016) 37:487–500. doi: 10.1055/s-0036-1584801

2. Iuliano AD, Roguski KM, Chang HH, Muscatello DJ, Palekar R, Tempia S, et al. Estimates of global seasonal influenza-associated respiratory mortality: a modelling study. *Lancet* (2018) 391:1285–300. doi: 10.1016/S0140-6736(17)33293-2

3. Flerlage T, Boyd DF, Meliopoulos V, Thomas PG, Schultz-Cherry S. Influenza virus and SARS-CoV-2: pathogenesis and host responses in the respiratory tract. *Nat Rev Microbiol* (2021) 19:425–41. doi: 10.1038/s41579-021-00542-7

4. Narasaraju T, Yang E, Samy RP, Ng HH, Poh WP, Liew AA, et al. Excessive neutrophils and neutrophil extracellular traps contribute to acute lung injury of influenza pneumonitis. *Am J Pathol* (2011) 179:199–210. doi: 10.1016/j.ajpath.2011.03.013

5. Pathak A, Agrawal A. Evolution of c-reactive protein. *Front Immunol* (2019) 10:943. doi: 10.3389/fimmu.2019.00943

6. Volanakis JE. Human c-reactive protein: expression, structure, and function. *Mol Immunol* (2001) 38:189–97. doi: 10.1016/S0161-5890(01)00042-6

7. Kushner I. The phenomenon of the acute phase response. *Ann NY Acad Sci* (1982) 389:39–48. doi: 10.1111/j.1749-6632.1982.tb22124.x

8. Gao R, Wang L, Bai T, Zhang Y, Bo H, Shu Y. C-reactive protein mediating immunopathological lesions: A potential treatment option for severe influenza a diseases. *EBioMedicine* (2017) 22:133–42. doi: 10.1016/j.ebiom.2017.07.010

9. Li HY, Tang ZM, Wang Z, Lv JM, Liu XL, Liang YL, et al. C-reactive protein protects against acetaminophen-induced liver injury by preventing complement overactivation. *Cell Mol Gastroenterol Hepatol* (2022) 13:289–307. doi: 10.1016/j.jcmgh.2021.09.003

10. Pepys MB, Hirschfield GM. C-reactive protein: a critical update. *J Clin Invest* (2003) 111:1805–12. doi: 10.1172/JCI200318921

11. Livak KJ, Schmittgen TD. Analysis of relative gene expression data using real-time quantitative PCR and the 2(-delta delta C(T)) method. *Methods* (2001) 25:402–8. doi: 10.1006/meth.2001.1262

12. Rao X, Huang X, Zhou Z, Lin X. An improvement of the 2^(-delta delta CT) method for quantitative real-time polymerase chain reaction data analysis. *Biostat Bioinforma Biomath* (2013) 3:71–85.

13. Chen N, Zhang B, Deng L, Liang B, Ping J. Virus-host interaction networks as new antiviral drug targets for IAV and SARS-CoV-2. *Emerg Microbes Infect* (2022) 11:1371–89. doi: 10.1080/22221751.2022.2071175

14. Lin KL, Sweeney S, Kang BD, Ramsburg E, Gunn MD. CCR2-antagonist prophylaxis reduces pulmonary immune pathology and markedly improves survival during influenza infection. *J Immunol* (2011) 186:508–15. doi: 10.4049/jimmunol.1001002

15. Ridker PM. From c-reactive protein to interleukin-6 to interleukin-1: Moving upstream to identify novel targets for atheroprotection. *Circ Res* (2016) 118:145–56. doi: 10.1161/CIRCRESAHA.115.306656

16. Yao X, Huang J, Zhong H, Shen N, Faggioni R, Fung M, et al. Targeting interleukin-6 in inflammatory autoimmune diseases and cancers. *Pharmacol Ther* (2014) 141:125–39. doi: 10.1016/j.pharmthera.2013.09.004

17. Vasileva D, Badawi A. C-reactive protein as a biomarker of severe H1N1 influenza. *Inflammation Res* (2019) 68:39–46. doi: 10.1007/s00011-018-1188-x

18. Zimmerman O, Rogowski O, Aviram G, Mizrahi M, Zeltser D, Justo D, et al. C-reactive protein serum levels as an early predictor of outcome in patients with pandemic H1N1 influenza a virus infection. *BMC Infect Dis* (2010) 10:288. doi: 10.1186/1471-2334-10-288

19. Ciliberto G, Arcone R, Wagner EF, Ruther U. Inducible and tissue-specific expression of human c-reactive protein in transgenic mice. *EMBO J* (1987) 6:4017–22. doi: 10.1002/j.1460-2075.1987.tb02745.x

20. Gang TB, Hanley GA, Agrawal A. C-reactive protein protects mice against pneumococcal infection *via* both phosphocholine-dependent and phosphocholine-independent mechanisms. *Infect Immun* (2015) 83:1845–52. doi: 10.1128/IAI.03058-14

21. Simons JP, Loeffler JM, Al-Shawi R, Ellmerich S, Hutchinson WL, Tennent GA, et al. C-reactive protein is essential for innate resistance to pneumococcal infection. *Immunology* (2014) 142:414–20. doi: 10.1111/imm.12266

22. Suresh MV, Singh SK, Ferguson DAJr., Agrawal A. Role of the property of c-reactive protein to activate the classical pathway of complement in protecting mice from pneumococcal infection. *J Immunol* (2006) 176:4369–74. doi: 10.4049/jimmunol.176.7.4369

23. Suresh MV, Singh SK, Ferguson DAJr., Agrawal A. Human c-reactive protein protects mice from streptococcus pneumoniae infection without binding to pneumococcal c-polysaccharide. *J Immunol* (2007) 178:1158–63. doi: 10.4049/jimmunol.178.2.1158

24. Szalai AJ, Briles DE, Volanakis JE. Human c-reactive protein is protective against fatal streptococcus pneumoniae infection in transgenic mice. *J Immunol* (1995) 155:2557–63.

25. Yother J, Volanakis JE, Briles DE. Human c-reactive protein is protective against fatal streptococcus pneumoniae infection in mice. *J Immunol* (1982) 128:2374–6.

26. Wang C, Yu H, Horby PW, Cao B, Wu P, Yang S, et al. Comparison of patients hospitalized with influenza a subtypes H7N9, H5N1, and 2009 pandemic H1N1. *Clin Infect Dis* (2014) 58:1095–103. doi: 10.1093/cid/ciu053

27. Zeng F, Huang Y, Guo Y, Yin M, Chen X, Xiao L, et al. Association of inflammatory markers with the severity of COVID-19: A meta-analysis. *Int J Infect Dis* (2020) 96:467–74. doi: 10.1016/j.ijid.2020.05.055

28. Zou S, Liu J, Yang Z, Xiao D, Cao D. SAA and CRP are potential indicators in distinction and severity assessment for children with influenza. *Int J Infect Dis* (2021) 108:357–62. doi: 10.1016/j.ijid.2021.05.057

29. Newton AH, Cardani A, Braciale TJ. The host immune response in respiratory virus infection: balancing virus clearance and immunopathology. *Semin Immunopathol* (2016) 38:471–82. doi: 10.1007/s00281-016-0558-0

30. Liu X, Nguyen TH, Sokulsky L, Li X, Garcia Netto K, Hsu AC, et al. IL-17A is a common and critical driver of impaired lung function and immunopathology induced by influenza virus, rhinovirus and respiratory syncytial virus. *Respirology* (2021) 26:1049–59. doi: 10.1111/resp.14141

31. Liu B, Bao L, Wang L, Li F, Wen M, Li H, et al. Anti-IFN-gamma therapy alleviates acute lung injury induced by severe influenza a (H1N1) pdm09 infection in mice. *J Microbiol Immunol Infect* (2021) 54:396–403. doi: 10.1016/j.jmii.2019.07.009

32. Bagri P, Anipindi VC, Nguyen PV, Vitali D, Stampfli MR, Kaushic C. Novel role for interleukin-17 in enhancing type 1 helper T cell immunity in the female genital tract following mucosal herpes simplex virus 2 vaccination. *J Virol* (2017) 91. doi: 10.1128/JVI.01234-17

33. Ma WT, Yao XT, Peng Q, Chen DK. The protective and pathogenic roles of IL-17 in viral infections: friend or foe? *Open Biol* (2019) 9:190109. doi: 10.1098/rsob.190109

34. Wang X, Ma K, Chen M, Ko KH, Zheng BJ, Lu L. IL-17A promotes pulmonary b-1a cell differentiation *via* induction of blimp-1 expression during influenza virus infection. *PLoS Pathog* (2016) 12:e1005367. doi: 10.1371/journal.ppat.1005367

35. Baumeister SH, Freeman GJ, Dranoff G, Sharpe AH. Coinhibitory pathways in immunotherapy for cancer. *Annu Rev Immunol* (2016) 34:539–73. doi: 10.1146/annurev-immunol-032414-112049

36. Pardoll DM. The blockade of immune checkpoints in cancer immunotherapy. *Nat Rev Cancer* (2012) 12:252–64. doi: 10.1038/nrc3239

37. Wykes MN, Lewin SR. Immune checkpoint blockade in infectious diseases. *Nat Rev Immunol* (2018) 18:91–104. doi: 10.1038/nri.2017.112

38. Tang X, Tian L, Esteso G, Choi SC, Barrow AD, Colonna M, et al. Leukocyte-associated ig-like receptor-1-deficient mice have an altered immune cell phenotype. *J Immunol* (2012) 188:548–58. doi: 10.4049/jimmunol.1102044

39. Burgstaller G, Oehrle B, Gerckens M, White ES, Schiller HB, Eickelberg O. The instructive extracellular matrix of the lung: basic composition and alterations in chronic lung disease. *Eur Respir J* (2017) 50. doi: 10.1183/13993003.01805-2016

40. Kumawat K, Geerdink RJ, Hennus MP, Roda MA, van Ark I, Leusink-Muis T, et al. LAIR-1 limits neutrophilic airway inflammation. *Front Immunol* (2019) 10:842. doi: 10.3389/fimmu.2019.00842

41. Zinkernagel RM. Immunology taught by viruses. *Science* (1996) 271:173–8. doi: 10.1126/science.271.5246.173

42. Allard B, Panariti A, Martin JG. Alveolar macrophages in the resolution of inflammation, tissue repair, and tolerance to infection. *Front Immunol* (2018) 9:1777. doi: 10.3389/fimmu.2018.01777

43. Incorvaia E, Sicouri L, Petersen-Mahrt SK, Schmitz KM, Hormones and AID. Balancing immunity and autoimmunity. *Autoimmunity* (2013) 46:128–37. doi: 10.3109/08916934.2012.748752

frontiers | Frontiers in Immunology

TYPE Original Research
PUBLISHED 02 November 2022
DOI 10.3389/fimmu.2022.1031868

OPEN ACCESS

EDITED BY
Chenhe Su,
Wistar Institute, United States

REVIEWED BY
Yuexiu Zhang,
The Ohio State University, United States
Gongguan Liu,
Nanjing Agricultural University, China
Biao Qiu,
NewYork-Presbyterian, United States

*CORRESPONDENCE
Lin Yi
yilin@scau.edu.cn
Jinding Chen
jdchen@scau.edu.cn

SPECIALTY SECTION
This article was submitted to Viral Immunology, a section of the journal Frontiers in Immunology

RECEIVED 30 August 2022
ACCEPTED 10 October 2022
PUBLISHED 02 November 2022

CITATION
Liu C, Zhao W, Su J, Chen X, Zhao F, Fan J, Li X, Liu X, Zou L, Zhang M, Zhang Z, Zhang L, Fan S, Li Y, Zhao M, Chen J and Yi L (2022) HSP90AA1 interacts with CSFV NS5A protein and regulates CSFV replication *via* the JAK/STAT and NF-κB signaling pathway. *Front. Immunol.* 13:1031868. doi: 10.3389/fimmu.2022.1031868

HSP90AA1 interacts with CSFV NS5A protein and regulates CSFV replication *via* the JAK/STAT and NF-κB signaling pathway

Chenchen Liu[1,2], Wei Zhao[3], Jia Su[3], Xiaochun Chen[3], Feifan Zhao[1,2], Jindai Fan[1,2], Xiaowen Li[1,2], Xiaodi Liu[1,2], Linke Zou[1,2], Mengru Zhang[1,2], Zilin Zhang[1,2], Liangliang Zhang[1,2], Shuangqi Fan[1,2], Yuwan Li[1,2], Mingqiu Zhao[1,2], Jinding Chen[1,2]* and Lin Yi[1,2]*

[1]College of Veterinary Medicine, South China Agricultural University, Guangzhou, China, [2]Key Laboratory of Zoonosis Prevention and Control of Guangdong Province, Guangzhou, China, [3]China Institute of Veterinary Drug Control, Beijing, China

Classical swine fever (CSF), caused by the classical swine fever virus (CSFV), is a highly contagious and fatal viral disease, posing a significant threat to the swine industry. Heat shock protein 90 kDa alpha class A member 1 (HSP90AA1) is a very conservative chaperone protein that plays an important role in signal transduction and viral proliferation. However, the role of HSP90AA1 in CSFV infection is unknown. In this study, we found that expression of HSP90AA1 could be promoted in PK-15 and 3D4/2 cells infected by CSFV. Overexpression of HSP90AA1 could inhibit CSFV replication and functional silencing of HSP90AA1 gene promotes CSFV replication. Further exploration revealed that HSP90AA1 interacted with CSFV NS5A protein and reduced the protein levels of NS5A. Since NS5A has an important role in CSFV replication and is closely related to type I IFN and NF-κB response, we further analyzed whether HSP90AA1 affects CSFV replication by regulating type I IFN and NF-κB pathway responses. Our research found HSP90AA1 positively regulated type I IFN response by promoting STAT1 phosphorylation and nuclear translocation processes and promoted the nuclear translocation processes of p-P65. However, CSFV infection antagonizes the activation of HSP90AA1 on JAK/STAT and NF-κB pathway. In conclusion, our study found that HSP90AA1 overexpression significantly inhibited CSFV replication and may inhibit CSFV replication by interacting with NS5A and activating JAK/STAT and NF-κB signaling pathways. These results provide new insights into the mechanism of action of HSP90AA1 in CSFV infection, which abundant the candidate library of anti-CSFV.

KEYWORDS

CSFV, HSP90AA1, NS5A, JAK/STAT, NF-κB

Introduction

Classical swine fever (CSF), caused by the classical swine fever virus (CSFV), is a highly contagious disease in pigs (1), and listed as a notifiable disease by the World Organization for Animal Health (OIE) (2, 3). CSFV, which belongs to the genus *Pestivirus* within the *Flaviviridae* family, is an enveloped virus containing a single-stranded, positive-sense RNA genome of approximately 12.3 kb (4, 5). The genome encodes a poly protein that is processed into 4 structural proteins (C、E^{rns}、E1 and E2) and 8 non-structural proteins (N^{pro}、p7、NS2、NS3、NS4A、NS4B、NS5A and NS5B) by protease of the virus and host cells (6, 7). These structural and non-structural proteins have been proposed to play diverse roles in proliferation and virulence. Among these proteins, the essential roles of NS5A protein in regulation of viral replication are getting increasing attention with the deepening of research.

CSFV NS5A protein consists of 496 amino acid (aa) residues, with a molecule of mass 55 kDa (8, 9). In spite of the exact function of NS5A is still unknown, many researches on it seem to imply that the NS5A protein is an important tool of CSFV to generate a favorable environment for viral replication. CSFV NS5A protein could interact with a variety of host proteins. For instance, a few studies indicate that NS5A protein interacts with eukaryotic translation initiation factor 3 subunit E (eIF3E), ras-related protein 18 (Rab-18), glucose-regulated protein 78 (GRP78), heat shock protein 70 (Hsp70) and so on to facilitate viral replication (10–13). Recent studies revealed that NS5A induces autophagy to enhance replication of CSFV (14, 15). It has also been shown that CSFV NS5A protein could inhibit the secretion of inflammatory cytokines by suppressing the NF-κB pathway (16). Although the effect of CSFV NS5A on type I IFNs pathway is not well understood, sufficient studies have shown that many flaviviruses NS5 have an antagonism of type I IFN (17). For example, Japanese encephalitis virus (JEV) NS5 could competitively bind to the nuclear transport proteins KPNA3 and KPNA4, which inhibited the nuclear translocation of IRF3 and NF-κB, resulting in the suppression of type I IFN (18). The NS5A protein of hepatitis C virus (HCV) which also belongs to the *Flaviviridae* family, suppresses type I interferon signaling and the phosphorylation of STAT1 (19). Moreover, a study also reveals that binding of the NS5 to Hsp90 could disrupt the interaction of Hsp90 with Janus kinase (JAK), which can help flaviviruses to broadly inhibit JAK/STAT pathway (20).

As is well known, type I IFN (IFN-α/β) is one of the critical lines of defense against viral infections widely (21, 22). IFN-dependent anti-viral response, is initiated by intracellular signaling cascade through the Janus protein kinase (JAK) family members, JAK and Tyk2 (23, 24). The binding of type I IFNs with the receptor (IFNAR) trigger JAK and STATs phosphorylation (25, 26). Subsequently, the phosphorylated STATs dimerize and translocate to the nucleus where they bind to IFN-response elements (ISRE) in ISG promoters to activate transcription of ISGs (24, 26, 27). The antiviral response induced by IFN/JAK/STAT could prevent viral replication directly and quickly (28). ISGs those are amplified effect factors of the IFN signaling cascades have been proved to block various steps of the viral life (26, 29). These ISG-encoded proteins could act directly on the virus to limit viral infection (22, 29). For instance, IFN-α inducible Mx2 could inhibit HBV replication and RNA transcription (30). Studies have shown that ISG15, Mx1 and OAS could inhibit CSFV replication (31, 32).

NF-κB pathway also plays an important role in the control of immunity, inflammation and other processes (33). The binding of viral pathogen-associated molecular patterns (PAMPs) to their receptor host pathogen recognition receptors (PRRs) triggers natural immunity and activates IFN regulatory factor (IRF) family members as well as NF-κB and thus promotes the expression of downstream ISGs (34). The transcription factor NF-κB proteins consist of the Rel family of proteins which include RelA (P65), RelB, c-Rel, p105/p50 (NF-κB1) and p100/p52 (NF-κB2) (35). In most resting cells, the NF-κB protein binds to its inhibitory protein IκB and maintains inactive in the cytoplasm (36). When is activated, the IκB phosphorylates and degrads rapidly, which in turn exposes NF-κB to the nuclear localization sequence (NLS) before translocating to the nucleus to drive the corresponding gene transcription (33). Activation of the NF-κB signaling pathway also play a key role to restrict virus replication (37). Studies have shown that activation of NF-κB is necessary for the generation of ROS to limit HSV-1 replication (38), and may affect HBV viral replication levels by regulating antiviral immunity (39). However, CSFV NS5A inhibits NF-κB nuclear translocation and NF-κB activity (16).

Heat shock protein 90 (HSP90), which family includes HSP90α, HSP90β, glucose-regulated protein 94 (GRP94) and tumor necrosis factor receptor-associated protein 1 (TRAP1) isoforms, is an essential molecular chaperon that is highly conserved in evolution (40, 41). It is involved in diverse biological processes such as virus infection, immune regulation, signal transduction. (42, 43). Many viruses depend on cellular HSP90 to complete their life cycles, especially depend on HSP90α and HSP90β isoforms (44). Studies have revealed that HSP90 is vital for the reverse transcriptase viability of Hepatitis B Virus (HBV), which is essentially required to initiate and maintain HBV reverse transcription (45, 46). In addition to direct binding to viral proteins, HSP90 can also affect the viral infection by regulating the expression of cytokines and antigen presentation (47). It is worth pointing out that HSP90 is required by JAK and IKK to enhance kinase activity, which promotes activation and nuclear translocation of STAT and NF-κB (43, 48).

In previous studies, we found that HSP90AB1 interacts with CSFV NS5A protein (15). However, it is currently unknown whether one of the HSP90 family members, HSP90AA1, also interacts with NS5A and the association of HSP90AA1 with JAK/STAT and NF-κB affects CSFV replication. Therefore, we sought to explore the regulatory effect of HSP90AA1 on JAK/STAT and NF-κB in CSFV infection.

Here, we found that there is a regulatory relationship between CSFV infection and the expression of HSP90AA1. The over-expression of HSP90AA1 inhibits CSFV replication. Further, HSP90AA1 interacts with viral protein NS5A and decreased the protein levels of NS5A. Mechanistically, our results show that over-expression of HSP90AA1 could activate JAK/STAT and NF-κB signaling pathways, which antagonize CSFV infection. Thus, HSP90AA1 is a key host factor limiting CSFV proliferation, it could interact with CSFV NS5A protein and its upregulation could activate host cell antiviral responses.

Material and methods

Cells, virus, and plasmids

Porcine alveolar macrophages 3D4/2 were cultured in RPMI 1640 medium (Thermo Fisher, 11875500) with 10% fetal bovine serum (FBS) (Thermo Fisher, 10100147). The swine kidney cell line PK-15 (ATCC, CCL-33) and human embryonic kidney cell line HEK293T (ATCC, CRL-1573) were cultured in Dulbecco's minimal essential medium (Thermo Fisher, 11965092) with 8% FBS. All cells were cultured at 37°C in a 5% CO_2 incubator. The CSFV strain (Shimen) used in this study was stored in our laboratory and was propagated in PK-15 cells. pMD18-T-NS5B, p3×Flag-CMV10, pEGFP-C3, pEGFP-NS4A and pEGFP-NS5A were deposited in our laboratory. Lipo3000 (Thermo Fisher, L3000075) reagent was used for transient transfection of plasmids.

Virus titration by indirect immunofluorescence assay (IFA)

The PK-15 cells were transferred to a 96-well plate, and CSFV virus solution was inoculated when the mono-layer cells reached 70%~80% confluence. The CSFV virus solution was inoculated in 1.5 mL centrifuge tubes with DMEM for 10-fold serial dilution (10-1 to 10-7), and 4 wells were repeated for each dilution.

IFA was used to determine CSFV titers in the culture supernatant. With 48-hour post infection (hpi), cells were washed three times with PBS and fixed with pre-chilled absolute ethanol (200 μL/well) at -20°C for 20 minutes. Following three washes with PBS, the cells were dried at room temperature for about 10 min to completely evaporate the absolute ethanol. The cells were incubated CSFV E2 antibody (JBT, 9011) at 4°C overnight (in dilute E2 protein antibody with PBS at a ratio of 1:200 (40 μL/well). After five washes, the cells were incubated with FITC-labeled or Alexa488-labeled goat anti-mouse IgG antibody (Beyotime, A0428) at 37°C for 1 h. After five washes, Immunofluorescence was observed using a fluorescence microscope (Nikon, Japan). Mock-infected cells were used as controls to establish background staining levels.

Quantitative real-time RT-PCR (qPCR)

The relative mRNA expression of HSP90AA1, ISGs and IFN-α was tested by RT-PCR using specific primers (Table 1). Total RNA from cells was extracted using Total RNA Kit I (OMEGA, R6834) and Viral RNA extraction using Viral RNA Kit (OMEGA, R6874). Subsequently, the cDNA was synthesized by reverse transcription using the HiScript II Q RT SuperMix for qPCR (Vazyme, R223-01). RT-PCR was performed with ChamQ Universal SYBR qPCR Master Mix (Vazyme, Q711-02) according to the manufacturer's protocol. Relative quantification of mRNA levels was conducted using ΔΔCT method and β-actin as an internal reference gene. Calculation of the gene copy numbers of CSFV was carried out using the absolute quantification method. A standard curve generated from the amplification results of the standard (10-fold serial dilution of the pMD18-T-NS5B plasmid of known concentration) was used to calculate the CSFV gene copy numbers.

Western blot analysis

Cell lysates were prepared in radioimmunoprecipitation (RIPA) (Beyotime, P0013) buffer with protease and phosphatase inhibitor cocktail (Beyotime, P1050). The protein concentration was determined with Pierce™ BCA Protein Assay Kit (Thermo Fisher, 23225). The samples were separated by 10% or 12.5% SDS-PAGE that prepared with PAGE Gel Rapid Prep Kit (Jacob enzyme Biotech, PG112) followed by transfer onto polyvinylidene difluoride (PVDF) membranes. After blocking

TABLE 1 Primers used in this study.

Primers	Sequence (5'~3')
NS5B-F	CCTGAGGACCAAACACATGTTG
NS5B-R	GGCACCACACCTTCTACAACGAG
β-actin-F	TCATCTTCTCACGGTTGGCTTTGG
β-actin-R	CCTGACCCTCAAGTACCCCA
HSP90AA1-F	CAGAGGCGGACAAGAACGACAAG
HSP90AA1-R	GATCCTGTTGGCGTGCGTCTG
IFN-α-F	CATCCTGGCTGTGAGGAAATA
IFN-α-R	CAGGTTTCTGGAGGAAGAGAAG
Mx1-F	GAACGAAGAAGACGAATGGAAGG
Mx1-R	GATGCCAGGAAGGTCTATGAGG
OAS2-F	CCAACGGACCCAACCAATAA
OAS2-R	GTCCAGGTGACTCATTCAGAAA
ISG15-F	CTGACCAGTTCTGGCTGACTTTCG
ISG15-R	GCACATAGGCTTGAGGTCATACTCC
Flag-HSP90AA1-F	ACGAATTCAATGCCCGAGGAAACCCA
Flag-HSP90AA1-R	GCTCTAGACTAATCGACTTCCTCCATGCG
siHSP90AA1-F	GGAUCUACAGGAUGAUCAATT
siHSP90AA1-R	UUGAUCAUCCUGUAGAUCCTT

with 5% skim milk at room temperature for 1 h, the membranes were incubated with primary antibodies overnight at 4°C. Primary antibodies used include mouse anti-HSP90AA1 monoclonal antibody (mAb) (Santa Cruz, sc-515081), mouse anti-phospho-STAT1 polyclonal antibody (pAb) (Santa Cruz, sc-136229), mouse anti-tubulin mAb (Beyotime, AT819), mouse anti-Flag mAb (Beyotime, AF5051), rabbit anti-GFP mAb (Beyotime, AF1483), rabbit anti-STAT1 pAb (Beyotime, AF0288), rabbit anti-phospho-JAK1 pAb (Beyotime, AF5857), rabbit anti-P65 mAb (Abmart, AF1234), rabbit anti-JAK1 mAb (Abmart, AT8190), rabbit anti-IκBα mAb (Abmart, T55026S), rabbit anti-phospho-IκBα mAb (Abmart, T57246S), rabbit anti-OAS2 pAb (Sangon Biotech, D121064) and rabbit anti-ISG15 pAb (Sangon Biotech, D225264). After three washes with PBST, the membranes were incubated with horseradish peroxidase (HRP)-conjugated goat anti-mouse IgG (Beyotime, A0216) secondary antibody at 37°C in a thermal shaker for 1 h. Finally, the results were visualized by ECL chemiluminescence kit (Jacob enzyme Biotech, SQ201) and X-ray film exposure (Tanon, China).

Plasmid construction and synthesis of small interfering RNA

HSP90AA1 PCR amplification primers were designed according to the HSP90AA1 sequence (NM_213973.2) published by NCBI using Primer Premier 5. HSP90AA1 was amplified by PCR from PK-15 cells cDNA and cloned into p3×Flag CMV10. The siRNA targeting HSP90AA1 and a negative control siNC were designed and synthesized by Sangon Biotech. All primers and sequence of siRNA were listed in Table 1.

Immunoprecipitation

The p3×Flag-HSP90AA1 was co-transfected into 293T cells with pEGFP-NS5A or pEGFP-NS4A using Lipofectamine™ 3000, respectively. Controls were represented by cells cotransfected with p3×Flag-HSP90AA1 and pEGFP, p3×Flag-CMV and pEGFP-NS5A. Cells were harvested at 24h after plasmid transfection using Western blot and IP lysis buffer (Beyotime, p0013) containing a protease inhibitor. After centrifugation for 10 min at 4°C, a part of the supernatant was boiled for 10 min with loading buffer (Beyotime, P0015L) as whole cell extracts (Input). The remaining lysate, used for IP experiment, was first incubated with Protein A+G at 4°C with slow rotation for 4h, and then incubated with the corresponding Flag or GFP antibody at 4°C overnight. After incubation, samples were centrifuged at 4°C for 2 min (2000 g/min). The supernatant was discarded and the precipitate was washed five times with pre-cooled PBS. Finally, loading buffer was added to the precipitate and boiled for 10 minutes to perform Western blot experiments with the input samples.

Confocal microscopy

The HEK-293T cells were cultured in laser confocal dishes to 60% confluence. The p3×Flag-HSP90AA1 was co-transfected into 293T cells with pEGFP-NS5A using Lipofectamine™ 3000, respectively. While setting two controls: 293T cells respectively cotransfected with p3×Flag-HSP90AA1 and pEGFP, p3×Flag-CMV and pEGFP. After culturing for 24 h, the cells were washed twice with PBS and fixed with pre-cooled absolute ethanol at room temperature for 10 minutes. Absolute ethanol was discarded and the cells were washed 3 times with PBS, then permeabilized with 0.1% Triton X-100 for 10 min at room temperature and discarded. Cells were washed 3 times with PBS and incubated with goat anti-mouse Flag antibody (Beyotime, AF5051) overnight at 4°C (antibody was diluted 1:200 in PBS), then washed 3 times with PBS and incubated with Cy3-labeled fluorescent secondary antibody (Beyotime, A0521) at 37°C for 1 Hour. The nucleus was counterstained with DAPI for 10 min. Finally, anti-fluorescence quencher was added dropwise to the cells. Observation of cell fluorescence signals under a laser confocal microscope.

In the experiment of the effect of HSP90AA1 on the phosphorylation and nuclear translocation of STAT1 and P65, p3×Flag-HSP90AA1 was transfected into PK-15 cells and 3D4/2 cells. Primary antibodies include rabbit anti-p-STAT1 pAb (Bioss, bs-3427R), rabbit-anti-p-P65 pAb (Affinity Biosciences, AF2006) and mouse anti-Flag mAb. Fluorescent secondary antibodies include FITC-labeled goat anti-mouse IgG (Beyotime, A0568) and Cy3-labeled goat anti-rabbit IgG (Beyotime, A0516).

Results

CSFV infection Up-regulates HSP90AA1 expression

To explore whether CSFV infection affects the expression of HSP90AA1, CSFV-infected (MOI=1) and CSFV-uninfected PK-15 and 3D4/2 cells were harvested at 24 hpi and 48 hpi to detect the mRNA and levels of HSP90AA1. The results showed that there was a significant increase in mRNA and protein levels of HSP90AA1 in PK-15 and 3D4/2 cells compared with control cells (Figure 1). The results show that CSFV infection prompted HSP90AA1 expression.

HSP90AA1 overexpression decreases CSFV replication

In order to determine the effect of HSP90AA1 on CSFV replication, PK-15 and 3D4/2 cells was transfected with p3×Flag-HSP90AA1 and then infected with CSFV (MOI=1). The replication of CSFV was detected by qRT-PCR, Western blot and IFA, respectively. The results showed that over-expression of HSP90AA1 inhibited CSFV replication in PK-15 and 3D4/2 cells. (Figure 2).

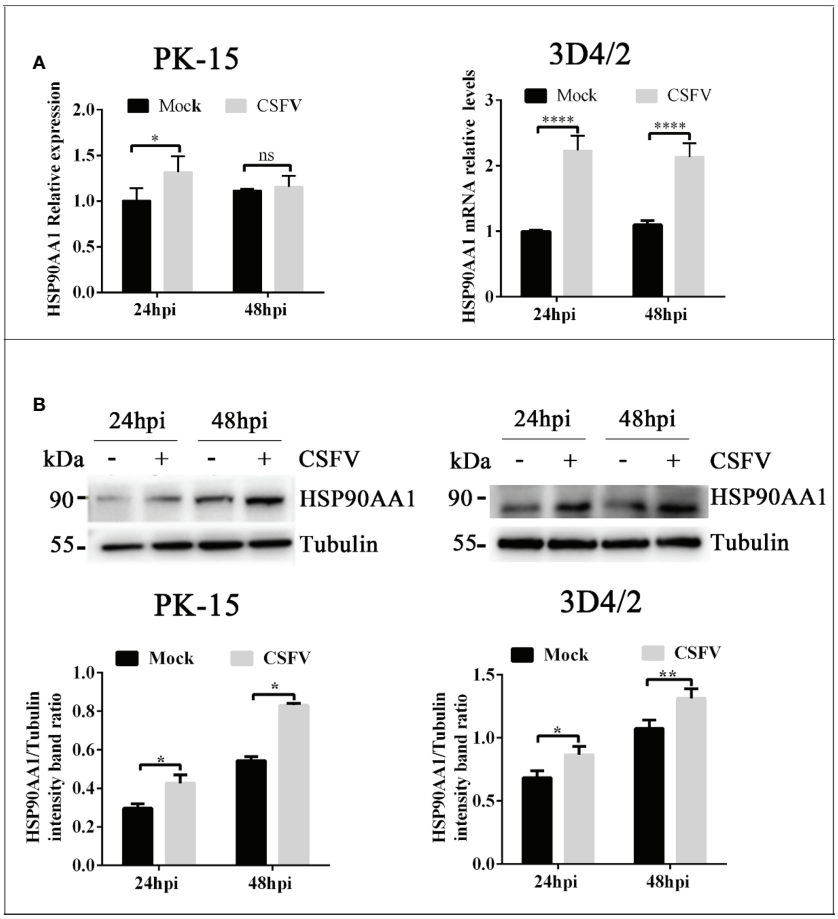

FIGURE 1
CSFV infection Up-regulates HSP90AA1 expression. **(A)** HSP90AA1 mRNA relative levels in PK-15 and 3D4/2 cells was analyzed by qRT-PCR; **(B)** Western blot showing HSP90AA1 protein expression and the relative protein levels of HSP90AA1 in PK-15 and 3D4/2 cells were estimated by histograms representing density readings of the gel bands with Image J, and the ratios were calculated relative to Tubulin control. (*p < 0.05, **p < 0.01 and ****p < 0.0001 calculated using two-way ANOVA, ns, not significant).

HSP90AA1 inhibition promotes CSFV replication

To investigate whether silencing HSP90AA1 expression affects CSFV replication, small interfering RNA targeting HSP90AA1 (siRNA-HSP90AA1) was transfected into PK-15 and 3D4/2 cells and then the cells were infected with CSFV (MOI=1). Similarly, the replication of CSFV was detected by qRT-PCR, Western blot and IFA, respectively. The results showed that silencing of HSP90AA1 gene function increased CSFV replication in PK-15 and 3D4/2 cells (Figure 3).

HSP90AA1 interacts with CSFV NS5A protein

Our previous works have found that CSFV NS5A protein interacted with HSP90 by liquid chromatography-mass spectrometry (15). Due to that HSP90AA1 was one of the members of the HSP90 family, this study further confirms the interaction of HSP90AA1 with CSFV NS5A protein. The results of confocal laser microscopiclaser showed that CSFV NS5A co-localized with HSP90AA1 in the cytoplasm in 293T, PK-15 and 3D4/2 cells (Figures 4A, C, D). And the results of co-immunoprecipitation experiments showed that HSP90AA1 interacted with CSFV NS5A protein in 293T cells (Figure 4B).

HSP90AA1 reduces the protein levels of CSFV NS5A

To investigate effects of HSP90AA1 on CSFV NS5A protein levels, we co-transfected pEGFP-NS5A with different amounts of p3×Flag-HSP90AA1 into PK-15 and 3D4/2 cells, and the cells were harvested to assess protein levels of fusion protein EGFP-

10.3389/fimmu.2022.1031868

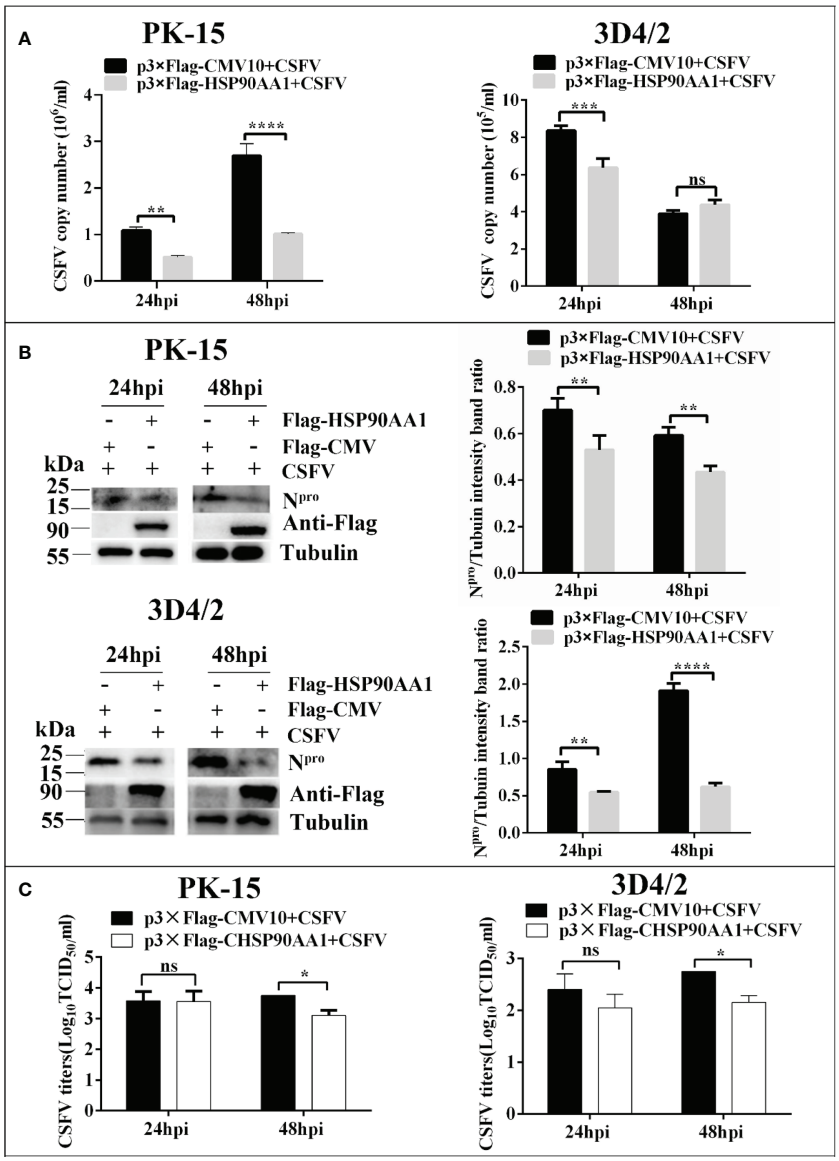

FIGURE 2
Over-expression of HSP90AA1 inhibits CSFV replication. **(A)** CSFV NS5B copy numbers were determined by RT-PCR at 24 and 48 hpi in HSP90AA1-overexpression PK-15 and 3D4/2 cells. **(B)** Western blot for HSP90AA1 and CSFV N^{pro} expression in HSP90AA1-overexpression PK-15 and 3D4/2 cells, and the relative protein levels of N^{pro} in HSP90AA1-overexpression PK-15 and 3D4/2 cells were estimated by histograms representing density readings of the gel bands with Image J, and the ratios were calculated relative to Tubulin control. **(C)** Infectious progeny viral titers in supernatants from HSP90AA1-overexpressing PK-15 and 3D4/2 cells. Viral titers from the supernatants collected at 24 and 48 hpi were determined and expressed as $TCID_{50}$/ml. (*$p < 0.05$, **$p < 0.01$, ***$p < 0.001$ and ****$p < 0.0001$ calculated using two-way ANOVA. ns, not significant).

NS5A by Western blot. Meanwhile, co-transfected NS4A was used as a control. We found that the protein levels of NS5A decreased gradually with the increasing expression of HSP90AA1 in PK-15 and 3D4/2 cells without dose-dependent inhibition of NS4A (Figure 5). It suggested that HSP90AA1 was not required to maintain the stability of CSFV NS5A. On the contrary, it can specifically reduce the protein levels of CSFV NS5A.

HSP90AA1 over-expression activates STAT1 and P65

To study the effect of HSP90AA1 on JAK/STAT and NF-κB signaling pathways, we detected the phosphorylation and nuclear translocation of STAT1 and P65 in HSP90AA1-overexpressing PK-15 and 3D4/2 cells by laser confocal microscopy. As a result, it was observed that higher levels of p-STAT1 in HSP90AA1-

10.3389/fimmu.2022.1031868

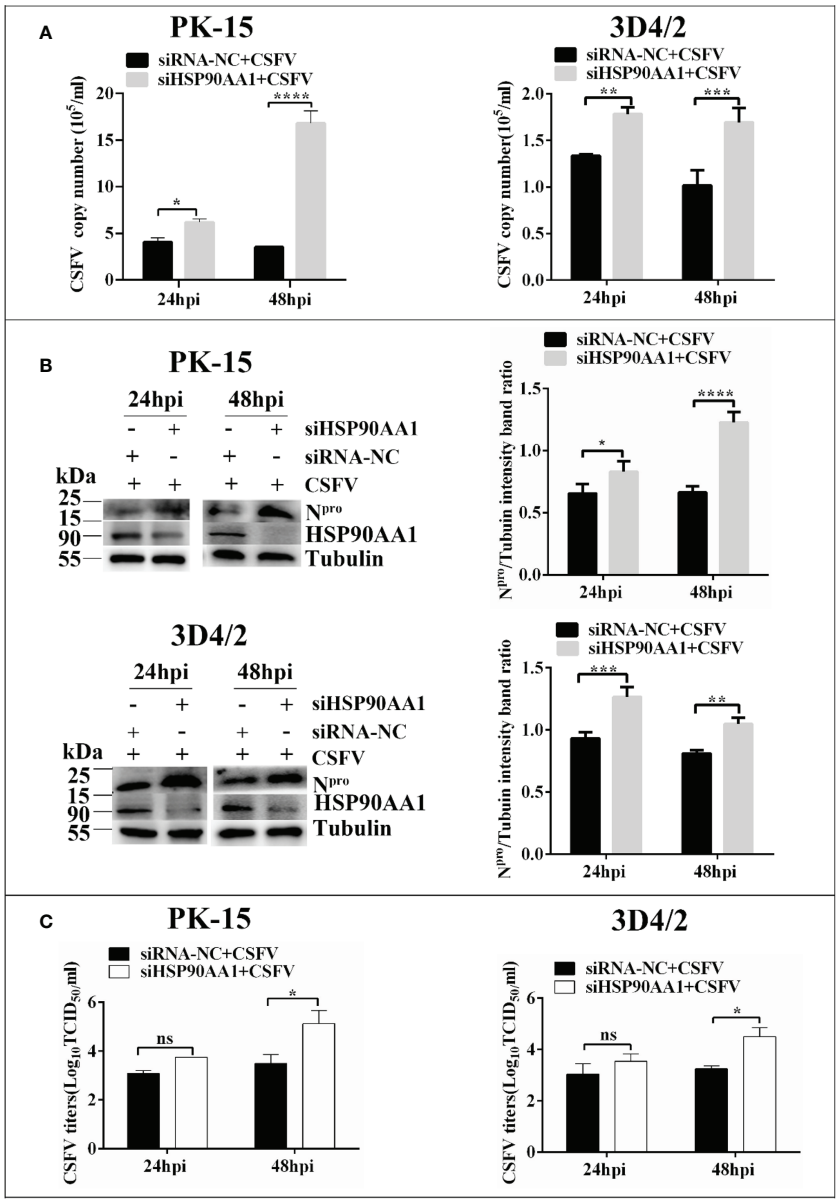

FIGURE 3
Knockdown of HSP90AA1 promoted CSFV replication. **(A)** RT-PCR determined CSFV NS5B copy numbers at 24 and 48 hpi in HSP90AA1 knockdown PK-15 and 3D4/2 cells. **(B)** Western blot for HSP90AA1 and CSFV N^{pro} expression in HSP90AA1 knock-downed PK-15 and 3D4/2 cells, and the relative levels of N^{pro} in HSP90AA1 knock-downed PK-15 and 3D4/2 cells were estimated by histograms representing density readings of the gel bands with Image J, and the ratios were calculated relative to tubulin control. **(C)** Infectious progeny viral titers in supernatants from HSP90AA1-knockdown PK-15 and 3D4/2 cells. Viral titers from the supernatant collected at 24 and 48 hpi were determined and expressed as $TCID_{50}$/ml. (*$p < 0.05$, **$p < 0.01$, ***$p < 0.001$ and ****$p < 0.0001$ calculated using two-way ANOVA, ns, not significant).

overexpressing PK-15 and 3D4/2 cells than that observed in control cells. And p-STAT1 was mostly distributed in the nucleus of HSP90AA1-overexpressing PK-15 while p-STAT1 in control cells was mainly distributed in the cytoplasm (Figure 6A). In addition, the nuclear distribution of p-P65 in HSP90AA1-overexpressing PK-15 and 3D4/2 cells was more than that in control cells (Figure 6B). These results indicated that HSP90AA1 over-expression promoted nuclear translocation of p-STAT1 and p-P65.

HSP90AA1 over-expression does not promote the expressions of ISGs and IFN-α under CSFV infection

To investigate the effect of HSP90AA1 on the regulation of JAK/STAT and NF-κB pathways under CSFV infection, we first analyzed the expression levels of ISGs and IFN-α in HSP90AA1-overexpressing PK-15 and 3D4/2 cells which were infected with

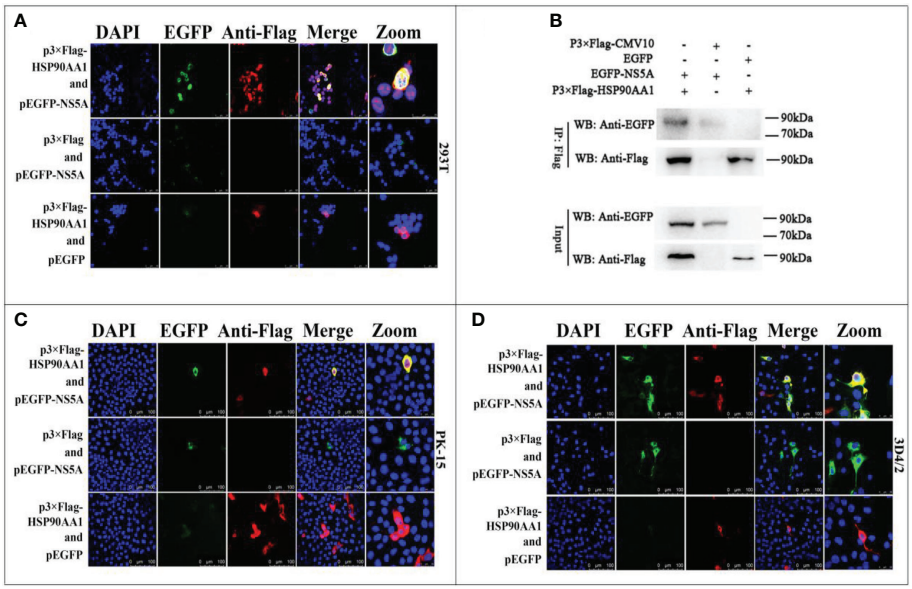

FIGURE 4
Validation for the interaction of HSP90AA1 with CSFV NS5A protein. **(A)** Identification of the colocalization of HSP90AA1 with NS5A protein in 293T cells. 293T cells co-expressing pEGFP-NS5A and p3×Flag-HSP90AA1 were analyzed by laser-scanning confocal microscopy. 293T Cells were co-transfected with pEGFP and p3×Flag-HSP90AA1 and pEGFP-NS5A with p3×Flag-CMV as negative controls. **(B)** Exogenous Co-IP analysis of NS5A with HSP90AA1 in 293T cells. 293T cells were co-transfected with p3×Flag-HSP90AA1 and EGFP-NS5A. 293T Cells were co-transfected with pEGFP and p3×Flag-HSP90AA1 and pEGFP-NS5A with p3×Flag-CMV as negative controls. **(C, D)** Identification of the colocalization of HSP90AA1 with NS5A protein in PK and 3D4/2 cells. PK-15 and 3D4/2 cells co-expressing pEGFP-NS5A and p3×Flag-HSP90AA1 were analyzed by laser-scanning confocal microscopy. PK-15 and 3D4/2 Cells were co-transfected with pEGFP and p3×Flag-HSP90AA1 and pEGFP-NS5A with p3×Flag-CMV as negative controls.

CSFV (MOI=1). The cells were harvested at 24 hpi and 48 hpi to detect the mRNA relative levels of ISGs and IFN-α by RT-PCR. The results showed that over-expression of HSP90AA1 could significantly promote the expressions of ISGs (ISG-15, OAS2 and Mx1) in PK-15 and 3D4/2 cells and significantly promote the expressions of IFN-α in 3D4/2 cells (Figure 7). However, HSP90AA1 Over-expression does not promote the expressions of ISGs under CSFV infection (Figure 7). This suggests that the facilitation effect of HSP90AA1 on ISGs is diminished or even disappeared after CSFV infection.

CSFV infection antagonizes the activation of HSP90AA1 on JAK/STAT and NF-κB pathway

To further verify the effects of HSP90AA1 on JAK/STAT and NF-κB pathway under CSFV infection, we detected changes in the levels of proteins related to above two pathways from CSFV infection in HSP90AA1 over-expression or knock-down PK-15 and 3D4/2 cells. The results showed that HSP90AA1 activated JAK/STAT pathway, while CSFV infection attenuates activation of HSP90AA1 on JAK/STAT pathway (Figure 8). HSP90AA1 significantly promoted the phosphorylation of IκBα, but had no significant effect on the protein expressions of P65 and IκBα, while CSFV infection inhibited the phosphorylation of HSP90AA1 on IκBα (Figure 9). These results showed that CSFV infection antagonizes the activation of HSP90AA1 on JAK/STAT and NF-κB pathway. It is suggested that HSP90AA1 may inhibit CSFV replication *via* activating JAK/STAT and NF-κB pathway.

Discussion

The production of type I IFNs are triggered by virus infection, which in turn activates the synthesis of interferon-stimulated genes to limit viral proliferation (49). The activation of JAK/STAT and NF-κB signaling pathway plays a key role in establishing the antiviral state (17, 29). However, CSFV suppresses the production of type I IFN, which facilitates its massive replication and persistent infection in tropic cells (15, 50). Moreover, like other members of the *Flaviviridae* family, CSFV NS5A also plays a critical role in regulation of type I IFN response (15, 16). In the current study, we found that HSP90AA1 could inhibit CSFV replication as a host antiviral

10.3389/fimmu.2022.1031868

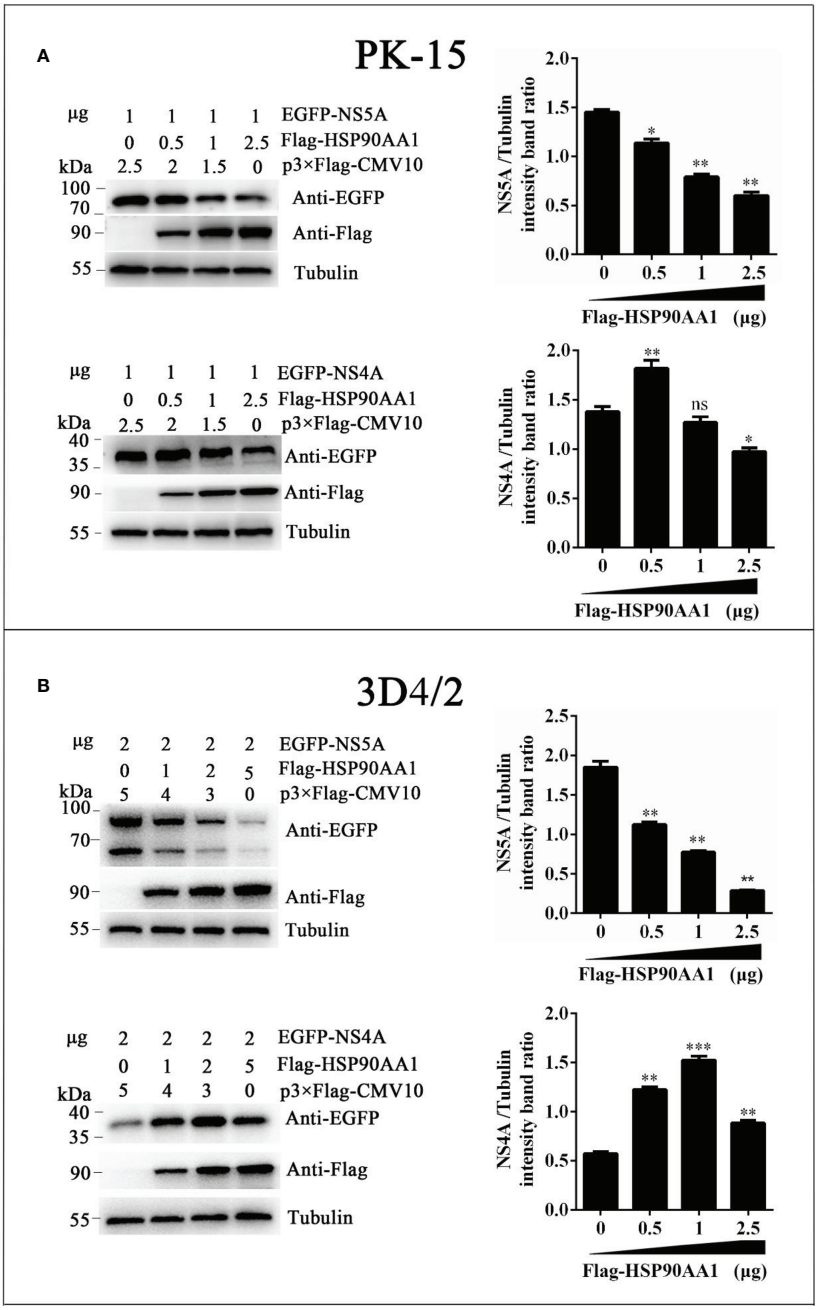

FIGURE 5
HSP90AA1 reduces the protein levels of CSFV NS5A. **(A, B)** EGFP-NS5A or EGFP-NS4A protein expression in HSP90AA1-expressing PK-15 and 3D4/2 cells. PK-15 and 3D4/2 cells were co-transfected with pEGFP-NS5A or EGFP-NS4A with a different amount of p3×Flag-HSP90AA1. Western blot analyzed EGFP-NS5A or EGFP-NS4A protein expression at 24 hours post co-transfected. Tubulin served as an internal control. The relative levels of EGFP-NS5A or EGFP-NS4A were estimated by histograms representing density reading of the gel bands with Image J, and the ratios were calculated relative to tubulin control. (*$p < 0.05$, **$p < 0.01$ and ***$p < 0.001$ calculated using one-way ANOVA, ns, not significant).

factor. Further research found that HSP90AA1 may inhibit CSFV replication by inhibiting CSFV NS5A protein expression in a dose-dependent manner and activating JAK/STAT and NF-κB signaling pathway.

The critical role of HSP90 in type I IFN response has been well described (51, 52). HSP90 inhibition can lead to dysregulation of JAK/STAT pathway activation and suppress the activation of NF-κB (53, 54). Our results highlight that

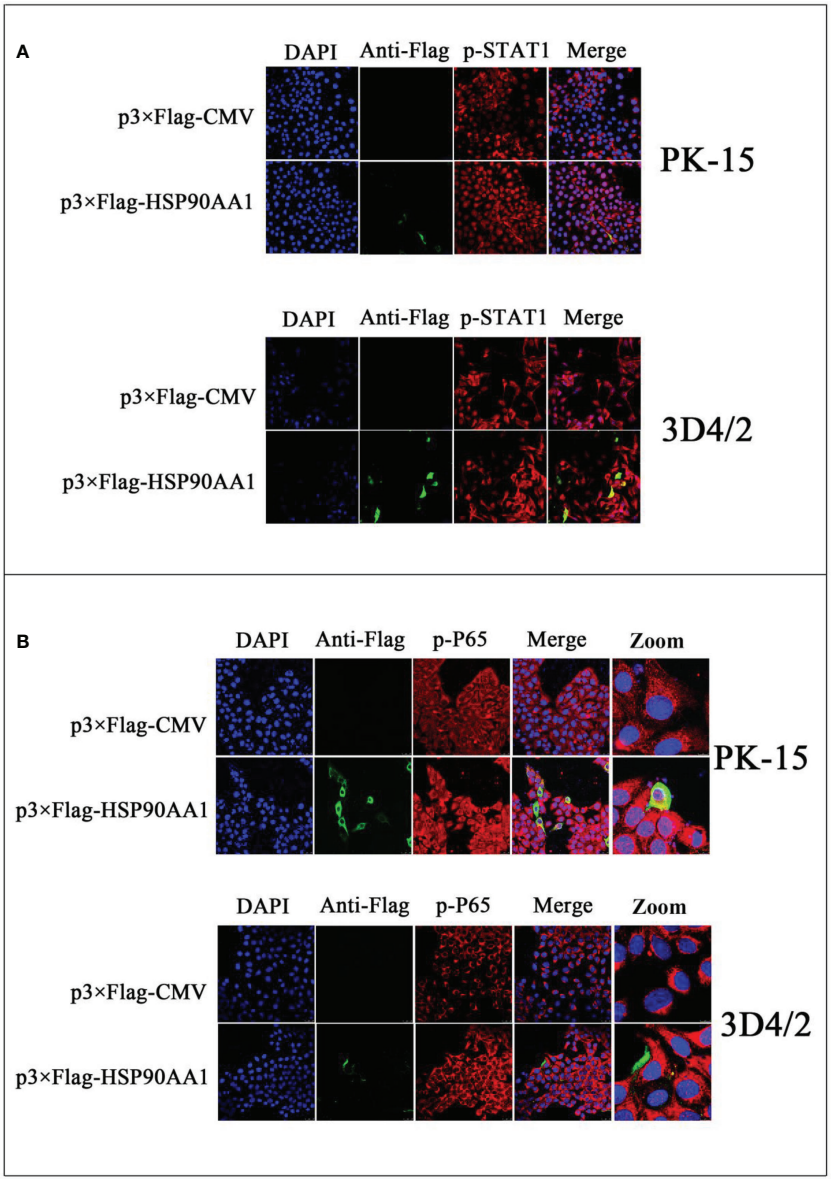

FIGURE 6
HSP90AA1 over-expression activates STAT1 and P65 in PK-15 and 3D4/2 cells. **(A)** HSP90AA1 over-expression affected the phosphorylation of STAT1 and nuclear translocation of p-STAT1 in PK-15 and 3D4/2 cells were observed by laser confocal microscopy. **(B)** HSP90AA1 over-expression affected the nuclear translocation of p-P65 in PK-15 and 3D4/2 cells were observed by laser confocal microscopy.

HSP90AA1 positively regulates type I IFN response by promoting the stability of JAK, and STAT1 phosphorylation and nuclear translocation processes. It also promotes the activation of NF-kB signaling pathway. However, the promotion of type I IFN and ISGs by HSP90AA1 was inhibited in the CSFV-infected state. We hypothesize that HSP90AA1 is not the main molecule for CSFV to escape innate immunity, there are still other key proteins that help CSFV to escape innate immunity, but HSP90AA1 is important for establishing an intracellular antiviral immune state, which helps to limit viral infection.

Like other members of the *Flaviviridae* family, CSFV infection significantly inhibits the activation of the JAK/STAT signaling pathway (50, 55). Although the mechanism of the inhibition is not fully elucidated, many studies suggest that flavivirus nonstructural protein NS5 plays an important role in this process (56–58). Justin A. et al. proposed that the binding of the flavivirus nonstructural protein NS5 to HSP90 resulting in

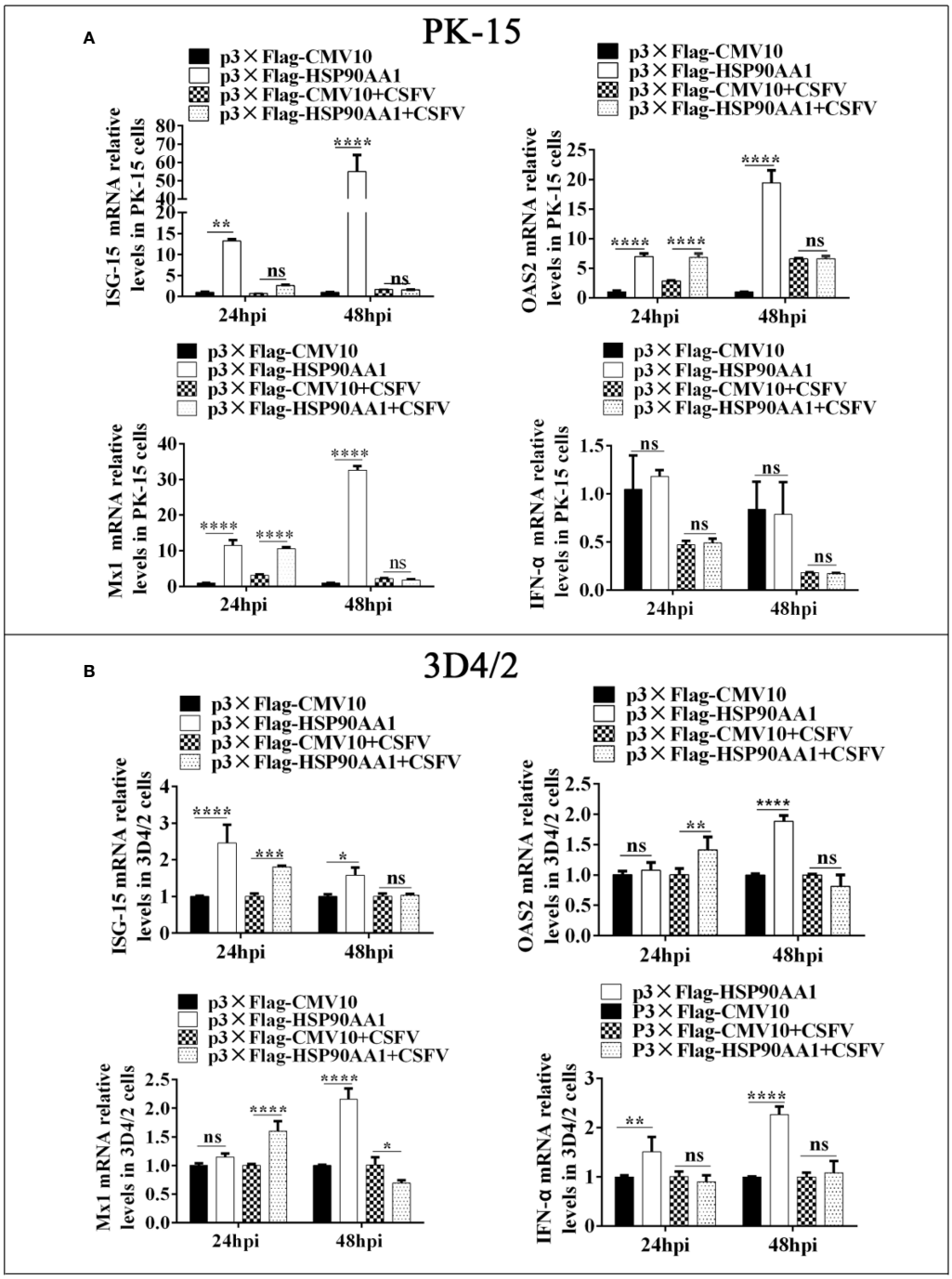

FIGURE 7
HSP90AA1 over-expression does not promote the expressions of ISGs and IFN-α under CSFV Infection. **(A, B)** Relative mRNA levels of ISGs and IFN-α in PK-15 and 3D4/2 cells were determined by RT-PCR. Cells were transfected with p3×Flag-HSP90AA1 first and then infected with CSFV (MOI=1). Cells were harvested at 24hpi and 48hpi. Total cellular RNA was extracted to determine relative mRNA expression levels of ISGs and IFN-α. (*$p < 0.05$, **$p < 0.01$, ***$p < 0.001$ and ****$p < 0.0001$ calculated using two-way ANOVA, ns, not significant)

an imbalance in JAK/STAT pathway signal transduction (20). Our results show that HSP90AA1 is not necessary to maintain NS5A stability, but rather dose-dependently inhibits the protein levels of NS5A. It suggests that HSP90AA1 can act as a key host restriction factor to limit CSFV replication by inhibiting the CSFV NS5A protein.

It seems to be evident that HSP90 is able to enhance the homeostasis of signal transduction proteins in stressful stress states

10.3389/fimmu.2022.1031868

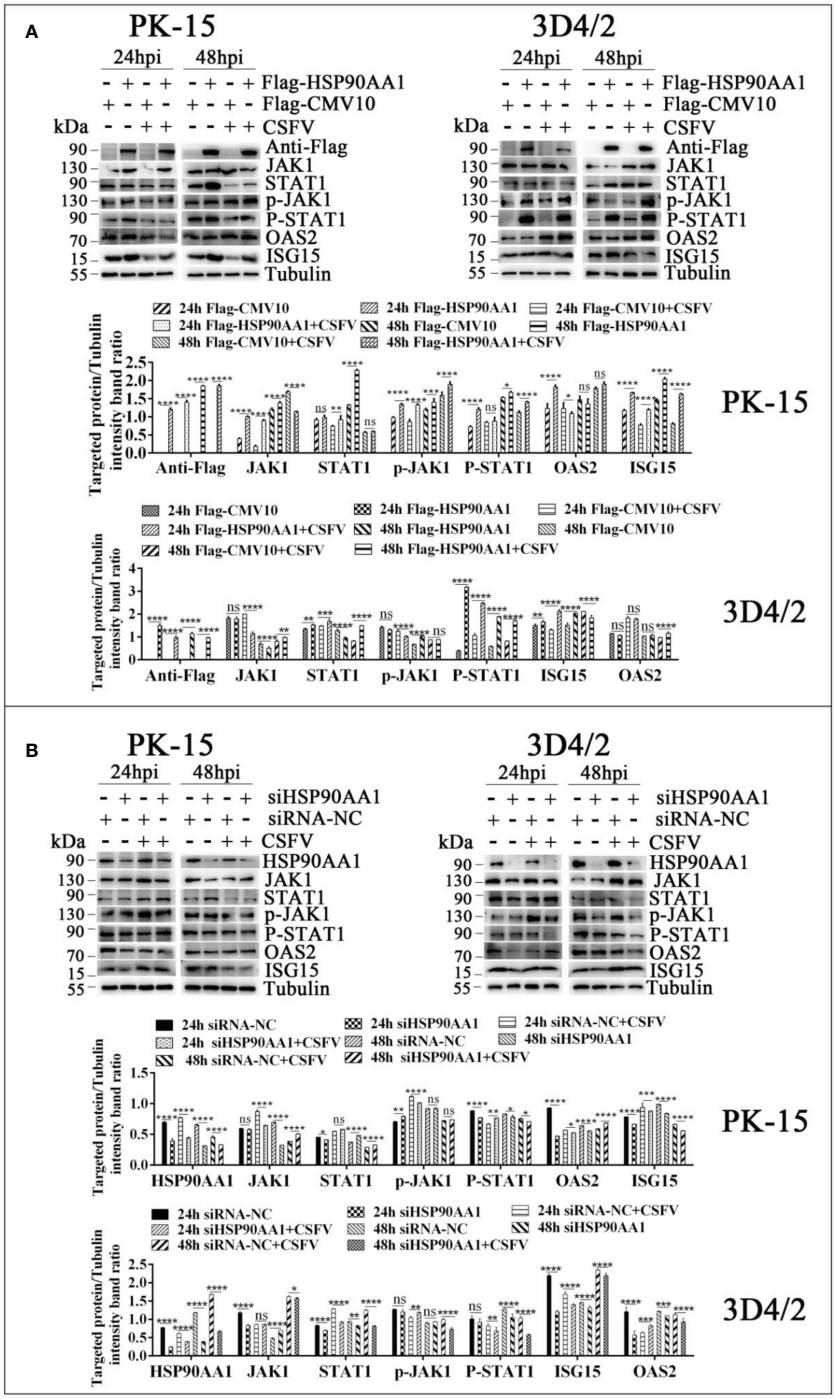

FIGURE 8
CSFV infection antagonizes the activation of HSP90AA1 on JAK/STAT pathway. **(A, B)** Western blot for JAK1, STAT1, p-JAK1, p-STAT1, OAS2, ISG-15 and HSP90AA1 expression in HSP90AA1-overexpression or knock-downed PK-15 and 3D4/2 cells. Cells were infected with CSFV (MOI=1) after transfection p3×Flag-HSP90AA1 or siHSP90AA1. The cells were not infected with CSFV as a control. Cells were harvested at 24hpi and 48hpi served to Western blot. The relative levels of proteins were estimated by histograms representing density reading of the gel bands with Image J, and the ratios were calculated relative to tubulin control. (*p < 0.05, **p < 0.01, ***p < 0.001 and ****p < 0.0001 calculated using two-way ANOVA, ns, not significant).

10.3389/fimmu.2022.1031868

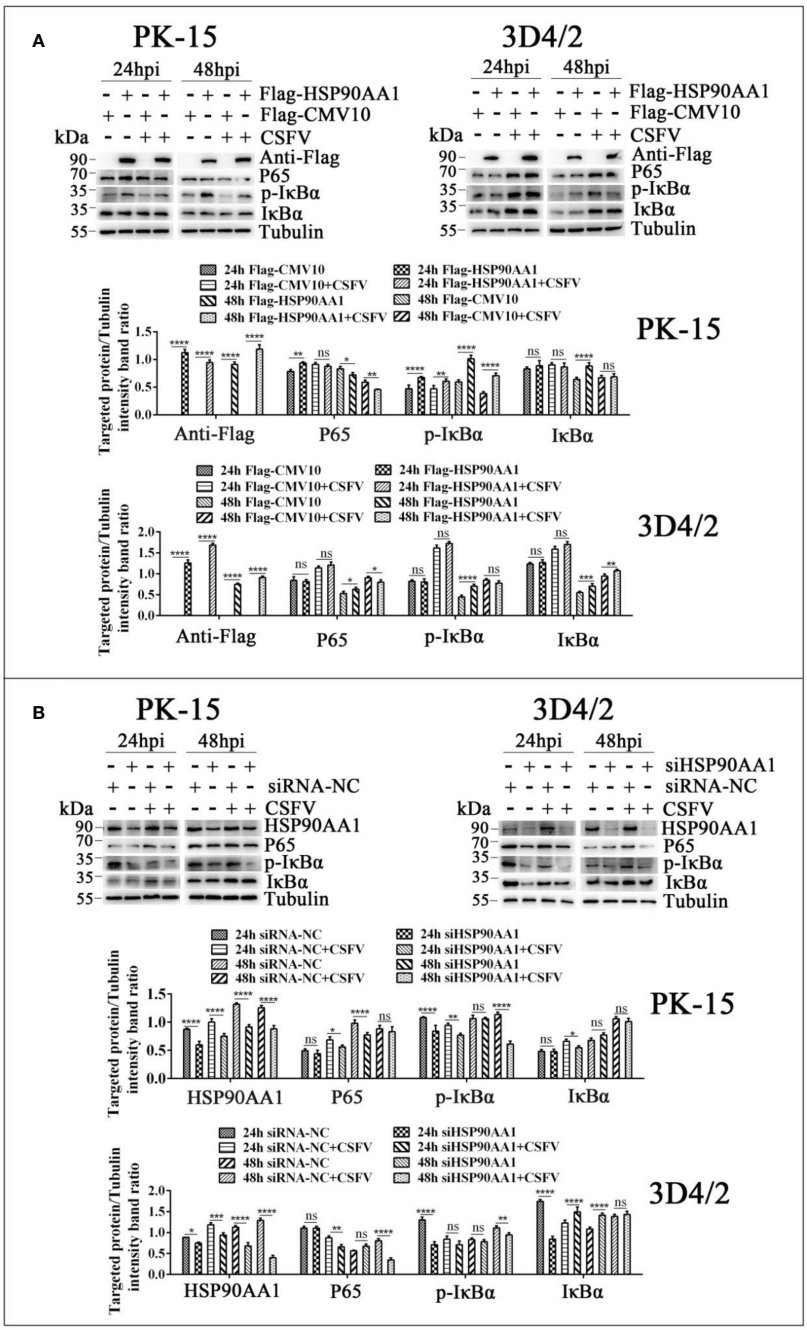

FIGURE 9
CSFV infection antagonizes the activation of HSP90AA1 on NF-κB pathway. **(A, B)** Western blot for P65, p-IκBα and IκBα in HSP90AA1-overexpression or knock-downed PK-15 and 3D4/2 cells. Cells were infected with CSFV (MOI=1) after transfection p3×Flag-HSP90AA1 or siHSP90AA1, and the cells were not infected with CSFV as a control. Cells were harvested at 24hpi and 48hpi served to Western blot. The relative levels of proteins were estimated by histograms representing density reading of the gel bands with Image J, and the ratios were calculated relative to tubulin control. (*p < 0.05, **p < 0.01, ***p < 0.001 and ****p < 0.0001 calculated using two-way ANOVA, ns, not significant).

(42, 59). However, there are also distinct effects of HSP90 in different viral infections. It has been shown that HSP90AA1 can promote rabies virus (RABV) proliferation by binding to P protein (60). Enterovirus 71 (EV71) in human rhabdomyosarcoma enters cells by binding to HSP90β on the surface of cells and the cytoplasmic HSP90β can prevent viral proteins from being degraded by proteasome (61). However, our results revealed that CSFV infection induces upregulation of HSP90AA1 expression and

that HSP90AA1 overexpression activates innate immunity to in turn inhibit CSFV replication. We hypothesize that inhibition of type I interferon response by CSFV infection may lead to the accumulation of HSP90AA1, which has a regulatory effect on innate immunity. Although upregulation of HSP90AA1 did not alter the inhibition of the type I interferon response by CSFV, it may act as a negative feedback signal to promote cell survival and protect cellular proteins from the risk of damage. Moreover, our study found that HSP90 is not essential for protein stabilization of CSFV NS5A of the *Flaviviridae* family, but restricts CSFV infection by activating the type I IFN signaling pathway. It shares similarities with the involvement of HSP90 in the regulation of cellular and inflammatory factors during flavivirus infection (20). It suggests that the role of HSP90 in flavivirus infection may be specific. It remains relevant to explore the important mechanisms of HSP90 action during flavivirus infection.

The important role of molecular chaperone proteins like HSP70 and HSP90 in viral infections has been studied extensively and heat shock proteins are very conserved in evolution (62, 63). Therefore, some researchers have also suggested that inhibitors of the above two chaperone proteins can be used as broad-spectrum antiviral drugs (64, 65). However, the mechanisms of regulation of viral homeostasis and regulation of intracellular protein homeostasis by molecular chaperones are complex and even opposite for different viral infection processes. So, it is very necessary to investigate the mechanism of interaction between heat shock proteins and flavivirus proteins and the effects of the interaction on immune and inflammatory. It can provide new ideas to elucidate the molecular mechanism of viral infection and help to screening of broad-spectrum anti-flavivirus drugs.

Data availability statement

The datasets presented in this study can be found in online repositories. The names of the repository/repositories and accession number(s) can be found in the article/supplementary material.

Author contributions

CL, SF, JF, and JC conceived and designed the study. CL, MeZ, XLiu, FZ, LZo, ZZ, WZ, JS, and LZh performed the experiments. CL, SF, XLi, XC, YL, and JF analyzed the data. CL, SF, MiZ, LY, and JC wrote the manuscript. All authors read and agreed upon the final manuscript.

Funding

This work was supported by the Program of National Natural Science Foundation of China (No.321728243、No.32102643), the Science and Technology Program of Guangzhou, China, (No. 202206010161), the Key Research Projects of Universities in Guangdong Province (No.2019KZDXM026), Quality and Efficiency Improvement Project of South China Agricultural University(No.C18).

Conflict of interest

The authors declare that the research was conducted in the absence of any commercial or financial relationships that could be construed as a potential conflict of interest.

Publisher's note

References

1. Wei Q, Liu Y, Zhang G. Research progress and challenges in vaccine development against classical swine fever virus. *Viruses* (2021) 13(3):445. doi: 10.3390/v13030445

2. Edwards S, Fukusho A, Lefevre PC, Lipowski A, Pejsak Z, Roehe P, et al. Classical swine fever: The global situation. *Veterinary Microbiol* (2000) 73(2-3):103–19. doi: 10.1016/S0378-1135(00)00138-3

3. Liu C, Liu Y, Cheng Y, Zhang Y, Zhang J, Liang X, et al. The ESCRT-I subunit tsg101 plays novel dual roles in entry and replication of classical swine fever virus. *J Virol* (2021) 95(6):e01928–20. doi: 10.1128/JVI.01928-20

4. Ruggli N, Tratschin JD, Schweizer M, McCullough KC, Hofmann MA, Summerfield A. Classical swine fever virus interferes with cellular antiviral defense: Evidence for a novel function of n(pro). *J Virol* (2003) 77(13):7645–54. doi: 10.1128/JVI.77.13.7645-7654.2003

5. Tautz N, Tews BA, Meyers G. The molecular biology of pestiviruses. *Adv Virus Res* (2015) 93:47–160. doi: 10.1016/bs.aivir.2015.03.002

6. Elbers K, Tautz N, Becher P, Stoll D, Rümenapf T, Thiel HJ. Processing in the pestivirus E2-NS2 region: Identification of proteins p7 and E2p7. *J Virol* (1996) 70 (6):4131–5. doi: 10.1128/jvi.70.6.4131-4135.1996

7. Ruggli N, Summerfield A, Fiebach AR, Guzylack-Piriou L, Bauhofer O, Lamm CG, et al. Classical swine fever virus can remain virulent after specific elimination of the interferon regulatory factor 3-degrading function of npro. *J Virol* (2009) 83(2):817–29. doi: 10.1128/JVI.01509-08

8. Reed KE, Gorbalenya AE, Rice CM. The NS5A/NS5 proteins of viruses from three genera of the family flaviviridae are phosphorylated by associated Serine/ Threonine kinases. *J Virol* (1998) 72(7):6199–206. doi: 10.1128/JVI.72.7.6199-6206.1998

9. Sheng C, Zhu Z, Yu J, Wan L, Wang Y, Chen J, et al. Characterization of NS3, NS5A and NS5B of classical swine fever virus through mutation and complementation analysis. *Veterinary Microbiol* (2010) 140(1-2):72–80. doi: 10.1016/j.vetmic.2009.07.026

10. Liu X, Wang X, Wang Q, Luo M, Guo H, Gong W, et al. The eukaryotic translation initiation factor 3 subunit e binds to classical swine fever virus NS5A and facilitates viral replication. *Virol (New York N.Y.)* (2018) 515:11–20. doi: 10.1016/j.virol.2017.11.019

11. Okamoto T, Nishimura Y, Ichimura T, Suzuki K, Miyamura T, Suzuki T, et al. Hepatitis c virus RNA replication is regulated by FKBP8 and Hsp90. *EMBO J* (2006) 25(20):5015–25. doi: 10.1038/sj.emboj.7601367

12. Zhang L, Zhao D, Jin M, Song M, Liu S, Guo K, et al. Rab18 binds to classical swine fever virus NS5A and mediates viral replication and assembly in swine umbilical vein endothelial cells[J]. *Virulence* (2020) 11(1):489–501. doi: 10.1080/21505594.2020.1767356

13. Chengcheng Z, Fuxi Z, Mengjiao G, Baoyang R, Xuefeng W, Yantao W, et al. CSFV protein NS5A activates the unfolded protein response to promote viral replication. *Virology* (2020) 541:75–84. doi: 10.1016/j.virol.2019.12.006

14. Zhang C, Wang X, Sun J, Guo M, Zhang X, Wu Y. Autophagy induced by the n-terminus of the classic swine fever virus nonstructural protein 5A protein promotes viral replication. *Front Microbiol* (2021) 12:733385. doi: 10.3389/fmicb.2021.733385

15. Xie B, Zhao M, Song D, Wu K, Yi L, Li W, et al. Induction of autophagy and suppression of type I IFN secretion by CSFV. *Autophagy* (2021) 17(4):925–47. doi: 10.1080/15548627.2020.1739445

16. Dong XY, Tang SQ. Classical swine fever virus NS5A protein changed inflammatory cytokine secretion in porcine alveolar macrophages by inhibiting the NF-kappaB signaling pathway. *Virol J* (2016) 13:101. doi: 10.1186/s12985-016-0545-z

17. Latanova A, Starodubova E, Karpov V. Flaviviridae nonstructural proteins: The role in molecular mechanisms of triggering inflammation. *Viruses* (2022) 14 (8):1808. doi: 10.3390/v14081808

18. Ye J, Chen Z, Li Y, Zhao Z, He W, Zohaib A, et al. Japanese Encephalitis virus NS5 inhibits type i interferon (IFN) production by blocking the nuclear translocation of IFN regulatory factor 3 and NF-κB. *J Virol* (2017) 91(8):e00039–17. doi: 10.1128/JVI.00039-17

19. Kumthip K, Chusri P, Jilg N, Zhao L, Fusco DN, Zhao H, et al. Hepatitis c virus NS5A disrupts STAT1 phosphorylation and suppresses type I interferon signaling. *J Virol* (2012) 86(16):8581–91. doi: 10.1128/JVI.00533-12

20. Roby JA, Esser-Nobis K, Dewey-Verstelle EC, Fairgrieve MR, Schwerk J, Lu AY, et al. Flavivirus nonstructural protein NS5 dysregulates HSP90 to broadly inhibit JAK/STAT signaling. *Cells* (2020) 9(4):899. doi: 10.3390/cells9040899

21. Wan Y, Cao W, Han T, Ren S, Feng J, Chen T, et al. Inducible Rubicon facilitates viral replication by antagonizing interferon production. *Cell Mol Immunol* (2017) 14(7):607–20. doi: 10.1038/cmi.2017.1

22. Yuan H, You J, You H, Zheng C. Herpes simplex virus 1 UL36USP antagonizes type i interferon-mediated antiviral innate immunity. *J Virol* (2018) 92(19):e01161–18. doi: 10.1128/JVI.01161-18

23. Ezeonwumelu IJ, Garcia-Vidal E, Ballana E. JAK-STAT pathway: A novel target to tackle viral infections. *Viruses* (2021) 13(12):2379. doi: 10.3390/v13122379

24. Schindler C, Levy DE, Decker T. JAK-STAT signaling: From interferons to cytokines. *J Biol Chem* (2007) 282(28):20059–63. doi: 10.1074/jbc.R700016200

25. Kessler DS, Veals SA, Fu X, Levy DE. Interferon-α regulates nuclear translocation and DNA-binding affinity of ISGF3, a multimeric transcriptional activator. *Genes Dev* (1990) 4(10):1753–65. doi: 10.1101/gad.4.10.1753

26. Rojas JM, Alejo A, Martin V, Sevilla N. Viral pathogen-induced mechanisms to antagonize mammalian interferon (IFN) signaling pathway. *Cell Mol Life Sci* (2021) 78(4):1423–44. doi: 10.1007/s00018-020-03671-z

27. Darnell JE. STATs and gene regulation. *Science* (1997) 277(5332):1630–5. doi: 10.1126/science.277.5332.1630

28. Nan Y, Wu C, Zhang Y. Interplay between janus Kinase/Signal transducer and activator of transcription signaling activated by type i interferons and viral antagonism. *Front Immunol* (2017) 8:1758. doi: 10.3389/fimmu.2017.01758

29. Zhu H, Zheng C. The race between host antiviral innate immunity and the immune evasion strategies of herpes simplex virus 1. *Microbiol Mol Biol Rev* (2020) 84(4):e00099–20. doi: 10.1128/MMBR.00099-20

30. Wang YX, Niklasch M, Liu T, Wang Y, Shi B, Yuan W, et al. Interferon-inducible MX2 is a host restriction factor of hepatitis b virus replication. *J Hepatol* (2020) 72(5):865–76. doi: 10.1016/j.jhep.2019.12.009

31. Zhou J, Chen J, Zhang XM, Gao Z, Liu C, Zhang Y, et al. Porcine mx1 protein inhibits classical swine fever virus replication by targeting nonstructural protein NS5B. *J Virol* (2018) 92(7):e02147–17. doi: 10.1128/JVI.02147-17

32. Li C, Wang Y, Zheng H, Dong W, Lv H, Lin J, et al. Antiviral activity of ISG15 against classical swine fever virus replication in porcine alveolar macrophages *via* inhibition of autophagy by ISGylating BECN1. *Veterinary Res* (2020) 51(1):22. doi: 10.1186/s13567-020-00753-5

33. Hayden MS, Ghosh S. Shared principles in NF-kappaB signaling. *Cell* (2008) 132(3):344–62. doi: 10.1016/j.cell.2008.01.020

34. Cai C, Tang Y, Zhai J, Zheng C. The RING finger protein family in health and disease. *Signal transduction targeted Ther* (2022) 7(1):1–23. doi: 10.1038/s41392-022-01152-2

35. Barnabei L, Laplantine E, Mbongo W, Rieux-Laucat F, Weil R. NF-kappaB: At the borders of autoimmunity and inflammation. *Front Immunol* (2021) 12:716469. doi: 10.3389/fimmu.2021.716469

36. Baeuerle PA, Baltimore D. IκB: A specific inhibitor of the NF-κB transcription factor. *Science* (1988) 242(4878):540–6. doi: 10.1126/science.3140380

37. Jensen S, Thomsen AR. Sensing of RNA viruses: A review of innate immune receptors involved in recognizing RNA virus invasion. *J Virol* (2012) 86(6):2900–10. doi: 10.1128/JVI.05738-11

38. Marino-Merlo F, Papaianni E, Frezza C, Pedatella S, De Nisco M, Macchi B, et al. NF-kappaB-Dependent production of ROS and restriction of HSV-1 infection in u937 monocytic cells. *Viruses* (2019) 11(5):428. doi: 10.3390/v11050428

39. Lu X, Chen Q, Liu H, Zhang X. Interplay between non-canonical NF-kappaB signaling and hepatitis b virus infection. *Front Immunol* (2021) 12:730684. doi: 10.3389/fimmu.2021.730684

40. Maloney A, Workman P. HSP90 as a new therapeutic target for cancer therapy: The story unfolds. *Expert Opin On Biol Ther* (2005) 2(1):3–24. doi: 10.1517/14712598.2.1.3

41. Serwetnyk MA, Blagg B. The disruption of protein-protein interactions with co-chaperones and client substrates as a strategy towards Hsp90 inhibition. *Acta Pharm Sin B* (2021) 11(6):1446–68. doi: 10.1016/j.apsb.2020.11.015

42. Saibil H. Chaperone machines for protein folding, unfolding and disaggregation. *Nat Rev Mol Cell Biol* (2013) 14(10):630–42. doi: 10.1038/nrm3658

43. Schopf FH, Biebl MM, Buchner J. The HSP90 chaperone machinery. *Nat Rev Mol Cell Biol* (2017) 18(6):345–60. doi: 10.1038/nrm.2017.20

44. Geller R, Taguwa S, Frydman J. Broad action of Hsp90 as a host chaperone required for viral replication. *Biochim Biophys Acta (BBA) - Mol Cell Res* (2012) 1823(3):698–706. doi: 10.1016/j.bbamcr.2011.11.007

45. Hu J. Hepadnavirus assembly and reverse transcription require a multi-component chaperone complex which is incorporated into nucleocapsids. *EMBO J* (1997) 16(1):59–68. doi: 10.1093/emboj/16.1.59

46. Hu J, Seeger C. Hsp90 is required for the activity of a hepatitis b virus reverse transcriptase. *Proc Natl Acad Sci* (1996) 93(3):1060–4. doi: 10.1073/pnas.93.3.1060

47. Joshi P, Maidji E, Stoddart CA. Inhibition of heat shock protein 90 prevents HIV rebound. *J Biol Chem* (2016) 291(19):10332–46. doi: 10.1074/jbc.M116.717538

48. Echeverría PC, Bernthaler A, Dupuis P, Mayer B, Picard D. An interaction network predicted from public data as a discovery tool: Application to the hsp90 molecular chaperone machine. *PloS One* (2011) 6(10):e26044. doi: 10.1371/journal.pone.0026044

49. Nie Y, Ran Y, Zhang HY, Huang ZF, Pan ZY, Wang SY, et al. GPATCH3 negatively regulates RLR-mediated innate antiviral responses by disrupting the assembly of VISA signalosome. *PloS Pathog* (2017) 13(4):e1006328. doi: 10.1371/journal.ppat.1006328

50. Goraya MU, Ziaghum F, Chen S, Raza A, Chen Y, Chi X. Role of innate immunity in pathophysiology of classical swine fever virus infection. *Microb Pathog* (2018) 119:248–54. doi: 10.1016/j.micpath.2018.04.020

51. Shang L, Tomasi TB. The heat shock protein 90-CDC37 chaperone complex is required for signaling by types I and II interferons. *J Biol Chem* (2006) 281 (4):1876–84. doi: 10.1074/jbc.M509901200

52. Bocchini CE, Kasembeli MM, Roh SH, Tweardy DJ. Contribution of chaperones to STAT pathway signaling. *JAKSTAT* (2014) 3(3):e970459. doi: 10.4161/21623988.2014.970459

53. Schoof N, von Bonin F, Trumper L, Kube D. HSP90 is essential for jak-STAT signaling in classical Hodgkin lymphoma cells. *Cell Communication Signaling* (2009) 7:17. doi: 10.1186/1478-811X-7-17

54. Nollen EA, Morimoto RI. Chaperoning signaling pathways: Molecular chaperones as stress-sensing 'heat shock' proteins. *J Cell Sci* (2002) 115(Pt 14):2809–16. doi: 10.1242/jcs.115.14.2809

55. Liniger M, Gerber M, Renzullo S, García-Nicolás O, Ruggli N. TNF-mediated inhibition of classical swine fever virus replication is IRF1-, NF-κB- and JAK/STAT signaling-dependent. *Viruses* (2021) 13(10):2017. doi: 10.3390/v13102017

56. Grant A, Ponia SS, Tripathi S, Balasubramaniam V, Miorin L, Sourisseau M, et al. Zika virus targets human STAT2 to inhibit type i interferon signaling. *Cell Host Microbe* (2016) 19(6):882–90. doi: 10.1016/j.chom.2016.05.009

57. Best SM, Pierson TC. The many faces of the flavivirus NS5 protein in antagonism of type i interferon signaling. *J Virol* (2017) 91(3):e01970–16. doi: 10.1128/JVI.01970-16

58. Laurent-Rolle M, Boer EF, Lubick KJ, Wolfinbarger JB, Carmody AB, Rockx B, et al. The NS5 protein of the virulent West Nile virus NY99 strain is a potent

antagonist of type I interferon-mediated JAK-STAT signaling. *J Virol* (2010) 84 (7):3503–15. doi: 10.1128/JVI.01161-09

59. Balchin D, Hayer-Hartl M, Hartl FU. *In vivo* aspects of protein folding and quality control. *Sci (American Assoc Advancement Science)* (2016) 353(6294):42. doi: 10.1126/science.aac4354

60. Xu Y, Liu F, Liu J, Wang D, Yan Y, Ji S, et al. The co-chaperone Cdc37 regulates the rabies virus phosphoprotein stability by targeting to Hsp90AA1 machinery. *Sci Rep* (2016) 6(1):27123. doi: 10.1038/srep27123

61. Tsou Y, Lin Y, Chang H, Lin HY, Shao HY, Yu SL, et al. Heat shock protein 90: Role in enterovirus 71 entry and assembly and potential target for therapy. *PloS One* (2013) 8(10):e77133. doi: 10.1371/journal.pone.0077133

62. Lubkowska A, Pluta W, Strońska A, Lalko A. Role of heat shock proteins (HSP70 and HSP90) in viral infection. *Int J Mol Sci* (2021) 22(17):9366. doi: 10.3390/ijms22179366

63. Robert J. Evolution of heat shock protein and immunity. *Dev Comp Immunol* (2003) 27(6-7):449–64. doi: 10.1016/S0145-305X(02)00160-X

64. Taguwa S, Yeh M, Rainbolt TK, Nayak A, Shao H, Gestwicki JE, et al. Zika virus dependence on host Hsp70 provides a protective strategy against infection and disease. *Cell Rep (Cambridge)* (2019) 26(4):906–20. doi: 10.1016/j.celrep.2018.12.095

65. Taguwa S, Maringer K, Li X, Bernal-Rubio D, Rauch JN, Gestwicki JE, et al. Defining hsp70 subnetworks in dengue virus replication reveals key vulnerability in flavivirus infection. *Cell* (2015) 163(5):1108–23. doi: 10.1016/j.cell.2015.10.046

frontiers | Frontiers in Immunology

TYPE Original Research
PUBLISHED 15 November 2022
DOI 10.3389/fimmu.2022.1016440

OPEN ACCESS

EDITED BY
Hongjuan You,
Xuzhou Medical University, China

REVIEWED BY
Dragica Bozic,
Faculty of Pharmacy, University of Belgrade, Serbia
Jiandong Guo,
Hangzhou Ninth People's Hospital, China
Dan Zhang,
State Key Laboratory of Molecular Developmental Biology (CAS), China

*CORRESPONDENCE
Wei Muyun
wmy2940@163.com
Ma Xiaowei
m138902y@hotmail.com
Li Lixin
lilixinsjz@163.com
Chen Xiaoying
chenxiaoying@renji.com

†These authors have contributed equally to this work and share first authorship

SPECIALTY SECTION
This article was submitted to Viral Immunology, a section of the journal Frontiers in Immunology

RECEIVED 10 August 2022
ACCEPTED 10 October 2022
PUBLISHED 15 November 2022

CITATION
Zhaoyang S, Guowei S, Jing P, Yundong Z, Xinhua L, Muyun W, Xiaowei M, Lixin L and Xiaoying C (2022) Clinical characteristics of the host DNA-removed metagenomic next-generation sequencing technology for detecting SARS-CoV-2, revealing host local immune signaling and assisting genomic epidemiology. *Front. Immunol.* 13:1016440. doi: 10.3389/fimmu.2022.1016440

Clinical characteristics of the host DNA-removed metagenomic next-generation sequencing technology for detecting SARS-CoV-2, revealing host local immune signaling and assisting genomic epidemiology

Sun Zhaoyang[1†], Song Guowei[2†], Pan Jing[2†], Zhou Yundong[3], Lu Xinhua[1], Wei Muyun[1*], Ma Xiaowei[1*], Li Lixin[2*] and Chen Xiaoying[1*]

[1]Department of Laboratory Medicine, Ren Ji Hospital, Shanghai Jiao Tong University School of Medicine, Shanghai, China, [2]Department of Laboratory Medicine, Shijiazhuang People's Hospital, Shijiazhuang, China, [3]Shanghai Medical Innovation Fusion Biomedical Research Center, Shanghai, China

Background: Metagenomic next-generation sequencing (mNGS) technology has been central in detecting infectious diseases and helping to simultaneously reveal the complex interplay between invaders and their hosts immune response characteristics. However, it needs to be rigorously assessed for clinical utility. The present study is the first to evaluate the clinical characteristics of the host DNA-removed mNGS technology for detecting SARS-CoV-2, revealing host local immune signaling and assisting genomic epidemiology.

Methods: 46 swab specimens collected from COVID-19 patients were assayed by two approved commercial RT-qPCR kits and mNGS. The evolutionary tree of SARS-CoV-2 was plotted using FigTree directly from one sample. The workflow of removing the host and retaining the host was compared to investigate the influence of host DNA removal on the performances of mNGS. Functional enrichment analysis of DEGs and xCell score were used to explore the characteristics of host local immune signaling.

Results: The detection rate of mNGS achieved 92.9% (26/28) for 28 samples with a Ct value ≤ 35 and 81.1% (30/37) for all 46 samples. The genome coverage of SARS-CoV-2 could reach up to 98.9% when the Ct value is about 20 in swab samples. Removing the host could enhance the sensitivity of mNGS for detecting SARS-CoV-2 from the swab sample but does not affect the species abundance of microbes RNA. Improving the sequencing depth did not show a positive effect on improving the detection sensitivity of SARS-CoV-2. Cell type

enrichment scores found multiple immune cell types were differentially expressed between patients with high and low viral load.

Conclusions: The host DNA-removed mNGS has great potential utility and superior performance on comprehensive identification of SARS-CoV-2 and rapid traceability, revealing the microbiome's transcriptional profiles and host immune responses.

KEYWORDS

mNGS, RT-PCR, SARS-CoV-2, the removal of host, traceability

Introduction

Infectious diseases have been, and still are, a leading cause of human morbidity and mortality worldwide and are also a tremendous challenge for the biomedical sciences. Accurate and rapid diagnosis of infectious diseases will be of great significance for reducing the medical therapies burden on patients, straining the increasingly drug-resistant organisms and standardizing antibiotic stewardship (1, 2). However, clinical diagnosis of infectious diseases is often characterized as complex and difficult for the following critical reasons: (a) Many abnormal indicators caused by suspected infection may be part of symptoms of complicated underlying disease; (b) The human pathogens are so rich and diverse that it is difficult to explicitly definite the species of the suspected pathogen.

Traditional diagnostic techniques in the microbiology laboratory include culture techniques, detection of pathogen-specific antibodies (serology) or antigens, and molecular identification of microbial nucleic acids (DNA or RNA), most commonly *via* PCR (3–5). However, these techniques detect only one or a small number of pathogens in a given reaction (6). Comprehensive screening of all species of pathogens is extremely important for the precision diagnosis and therapy of infectious disease and is also part of precision medicine, which requires precision at all levels. Considering its paramount clinical importance, improving microbiological diagnosis needs more reliable detection technologies. In recent years, untargeted metagenomic next-generation sequencing (mNGS) has emerged as a promising technique because of its special strengths and abilities for comprehensively detecting all pathogens in samples (7–9). Compared with most traditional diagnostic techniques that only target a limited number of pathogens using specific primers or probes or specific antigens, metagenomic approaches characterize all DNA or RNA present in a sample, enabling analysis of the entire microbiome as well as the human host genome or transcriptome in patient samples (3).

However, the clinical application of mNGS is still in its early stages and is not yet routinely established in the clinical environment. There are also no uniform criteria for pathogen identification by mNGS because of its extremely high level of complexity in the entire detection process (10). The draft guidance issued by Food and Drug Administration (FDA) points out exactly that the clinical performance characteristics of NGS technology for microbial identification lie in its limit of detection (LOD), inclusivity, interfering substances, repeatability, cross-contamination and stability (11). These indicators used to evaluate the detection performance of mNGS require more comprehensive and in-depth studies.

Emerging pieces of evidence demonstrated that mNGS could yield a higher sensitivity for pathogen identification than conventional culture-based techniques and has sensitivity similar to specific PCR assays (12–14). Interestingly, unlike current traditional diagnostic techniques, the sensitivity of mNGS for pathogens detection is affected by a series of variables: efficiency of nucleic acid extraction (bias toward some species), pathogen genome size (at the same organism load, more reads are generated from longer genomes), the robustness of library preparation, the total number of sequences reads generated from a given specimen (more reads ≈higher sensitivity), specimen composition and background reads, bioinformatics pipeline used for analysis (availability of appropriate reference sequences in databases), sequence similarity with related organisms (confident differentiation of close relatives requires greater sequencing depth than the identification of unique sequences), the accuracy of classification algorithms, and required confidence for pathogen identification (15).

For the reasons above, our present study aims to evaluate the sensitivity of DNA-removed mNGS by detecting 46 swab sample from patients with COVID-19 infection and comparing the mNGS and two approved quantitative real-time PCR (qRT-PCR). In addition, our results will also provide further insight into understanding the superior performance of DNA-removed mNGS in the comprehensive identification of the pathogen and simultaneously reveal the transcriptional profiles of the microbiome and host responses.

Methods

Swab specimen collection from the hospital in patients with COVID-19 infection

46 swab specimens were collected from inpatients diagnosed with COVID-19 infection from Shijiazhuang People's Hospital. All patients were treated in isolation between January 2021 and March 2021. This study has been approved by Shijiazhuang People's Hospital Ethics Committee. The Ethics Approval Number: [2020]-046.

Nucleic acid extraction of swab specimen

The nucleic acid was extracted from a 200μl swab sample using an automatic nucleic acid extraction instrument (Smart Lab Assist) and its supporting reagents (Taiwan Advanced Nanotech, Taiwan, China) according to the manufacturer's protocol. Isolated nucleic acid was eluted in a 50μl elution buffer. Then, 33μl nucleic acid from each swab sample was used to performed the mNGS assay, and 5μl was performed for qRT-PCR detection by using two commercial RT–PCR kits-DAAN and BioGerm, which have been both approved by the China National Medical Products Administration (NMPA).

SARS-CoV-2 detection by two different clinical RT-PCR kits

The primers of two RT–PCR kits were both targeted to the regions of the SARS-Cov-2 N gene and ORF1ab gene. According to the judgment criteria of two RT–PCR kits, cycle threshold (Ct) values below 40 were regarded as positive and above 40 as negative.

The schematic flow of mNGS detection

The detection process of untargeted host-removed mNGS is as follows. (a) After extracting the nucleic acid from the swab specimen, 33μl nucleic acid of each sample was mixed with 3uL DNA enzyme and DNA enzyme buffer to digest DNA and enrich RNA. (b) Reverse transcription and cDNA synthesis. (c) cDNA library preparation using the PMseq RNA infectious pathogens high throughput detection kit (probe anchored polymer sequencing method) (Green Pine Capital Partners Co. LTD, Wuhan, China). The qualification of the cDNA libraries concentration was quantified using the Qubit4.0. (d) The DNB (DNA nano ball) was prepared after the qualification of cDNA libraries and then loaded into the sequencing chip. (e) Sequencing was performed on the MGSEQ-2000 platform (MGI Tech Co., Ltd. Shenzhen, China, https://en.mgi-tech.com/about/). The sequence was generated with a single-end, 50 bp size reading (SE50). We defined samples with positive SARS-CoV-2 results when the specific reads of SARS-CoV-2 detected from samples was greater than or equal to 1. Specific reads of SARS-CoV-2 were those mapped exclusively to SARS-CoV-2 species, to discriminate those aligned to other species.

Bioinformatic analysis

After the sequencing was completed, we first removed adaptor sequences from raw reads and discarded low-quality reads. Then, two different bioinformatics analysis workflows were performed to analyze the transcriptome sequence profile of human and the sequence information of microbial species in swab samples, respectively. For microbiota analysis workflow, the sequences aligned to the human reference genome were removed, followed by comparing the microbiota sequences with the reference genome sequences in the database to determine the microbial species information. The sequence of SARS-CoV-2 was extracted and used to assemble the viral genome, followed by aligning the full genome sequences with reference genomes derived from NCBI. Then the phylogenetic trees were constructed using the Maximum Parsimony method included in evolutionary tree analysis software MEGA based on the 50 optimum alignment genomes. For analysis workflow of human transcriptome sequence, we screened raw data to make clean data by removing contaminants, adaptors, low-quality reads using the Trimmomatic program (version.0.39) (https://github.com/timflutre/trimmomatic), which removed the leading and trailing low-quality bases below quality 3 or N bases, cut the sliding window which average quality per base drops below 15, and dropped reads below the 36 bases long. A quality control using FastQC was performed on the reads (https://www.bioinformatics.babraham.ac.uk/projects/fastqc/, v0.11.9). Then, sequences were aligned to the reference human genome version GRCh38 (Gencode, version 39) (15). Transcript abundance was computed using Salmon version 1.8.0 (16).

Data analysis and statistics

Data analyses were performed using R statistical language (version 4.1.0) and Origin 2018 64Bit. Comparison of the test results between the host removed and the host retained workflow was tested using two-tailed paired t-test. GO enrichment is visualized using the GOplot R package. Differential gene expression and signature enrichment analysis were performed using a two-sided Wilcoxon rank sum test, and statistical significance was defined as P <0.05.

Results

Compared with two approved RT-qPCR kits, mNGS presented credible sensitivity for detecting SARS-CoV-2 from swab samples

To strengthen the reliability of the results, we compared the detection rate of mNGS for detecting SARS-CoV-2 with two approved commercial RT-qPCR kits, both approved by NMPA and widely used for risk screening of COVID-19 in the majority of health care institutions across China. The detailed results of 46 swab samples derived from mNGS and two RT-qPCR detections are given in Supplementary Table 1. Among 46 swab samples from 46 hospitalized patients, the result of the 9 sample (Samples 38-46) was simultaneously confirmed to be negative by two different RT-PCR kits based on the judging criteria; the remaining 37 samples were confirmed to be positive. As shown in Figure 1, among 37 samples that showed positive RT-PCR results, 30 (30/37, 81.1%) samples were found the SARS-CoV-2 sequences (reads≥1) and were considered to be consistent with the results of RT-PCR assays; residual 7 (7/37, 18.9%) samples with positive RT-PCR results fail to detect the SARS-CoV-2 sequence. Notably, for RT-PCR positive samples with Ct value ≤ 35, the positive rates of mNGS was 92.9% (26/28).

The relationship between the total reads and the genome coverage of SARS-CoV-2

Recent advances in next-generation sequencing (NGS) technologies have markedly increased the amount of data (=Total reads, 1M=10^7reads) produced by a single sample in each test and significantly reduced the sequencing cost. However, almost no previous research has elucidated the clinical and research significance of increased total data amount. In this study, we first revealed the relationship between the amount of data (total reads) and the genome coverage of SARS-CoV-2. The 30 samples with positive mNGS results were ranked according to the detection reads of SARS-CoV-2. The result is consistent with the theory, which suggests that the genome coverage of SARS-CoV-2 increases with the increasing reads of SARS-CoV-2. However, it was unexpected that the genome coverage of SARS-CoV-2 could reach up to 98.9% when the reads number of SARS-CoV-2 was 5653 in the sample, corresponding to the Ct value of approximately 20 (Figure 2A).

Next, the sample with the highest coverage (98.9%) of SARS-CoV-2 was conducted genome assembly using MUSCLE (http://www.ebi.ac.uk/Tools/msa/muscle/). The assembled contigs sequence was aligned with the online NCBI alignment tools to obtain the 50 optimal genome alignment. Then,

FIGURE 1
Results comparison between mNGS and two approved RT-qPCR methods. From left to right, the 37 samples were sorted according to the Ct value of N gene from DAAN (red curve). From top to bottom are the host reads, the percentage of host read in each sample, microbes read in each sample, detection read number of 2019-nCoV, Ct values of two RT-PCR kits and total reads (including the reads from host and microbes in swab sample) generated from each sample.

phylogenetic trees were constructed using the MEGA software to explore their evolutionary relationship in terms of geographical locations. The genomic epidemiology analysis showed that our sample-GenomenCoV5653 presents a close orthologous relationship with the genomes of the viruses from Germany (Figure 2B).

Comparison results from the workflow of removing host and workflow of retaining host

As an unbiased detection method, mNGS could efficiently detect all RNA in the sample without bias, including all RNA from microbes and hosts. Removing the host DNA could theoretically improve the sensitivity of this technique for the analysis of all RNA in the sample. However, little evidence exists to demonstrate whether such removal of host DNA will cause the loss of part of RNA form viruses, microbes, and hosts in the sample. Given this, our study represents the first investigation of the efficacy and influence of host DNA removal for analyzing all RNA in the sample. Eight samples were selected and simultaneously performed the remove host and retain host process. As shown in Figure 3, the procedure of removal host can significantly improve the detection read number of 2019-nCoV (Figure 3A) and decrease the host rate (Figure 3B) in all 8 samples when comparing the procedure of retaining the host ($p<0.05$). In contrast, the microbes' reads (Figure 3C) and the host reads (Figure 3D) do not present the same changing trend after removing the host for an identical sample (ns: no significance). These results demonstrate that the removal of the host could enhance the sensitivity of mNGS for detecting SARS-CoV-2 from swab sample

Removing the host does not affect the species' abundance of microbes RNA

To enhance the sensitivity of untargeted mNGS for detecting and analyzing the RNA from viruses and transcriptomic information from hosts and microbes, our study removed host DNA by introducing DNA enzymes before library preparation. We have demonstrated that the removal of host DNA positively affects the detection of virus RNA in the sample based on the result above. However, it is unclear that whether this method will cause the untargeted degradation of microbes' RNA and influence the microbe species' abundance based on the analysis of microbes' RNA. Given this, our study first compared species abundance in removing host DNA and retaining host DNA at the RNA level in eight pairs of samples. Our results found that the species, proportion, and abundance of microbe in removing and retaining host DNA were almost identical (Figures 4A–F) (Figures S2A, B), demonstrating that the removal of the host does not affect the species abundance of microbes RNA.

Improving the sequencing depth did not show a positive effect on improving the detection sensitivity of SARS-CoV-2

Our study first explored the relationship between the sequencing depth and the detection sensitivity of SARS-CoV-2 based on untargeted host-removed mNGS technology. 25 samples were selected and assayed using two or more different sequencing depths (M), the relevance between sequencing depths and SARS-CoV-2 detection reads was exhibited in Figure 5. The SARS-CoV-2 detection reads of 7 samples

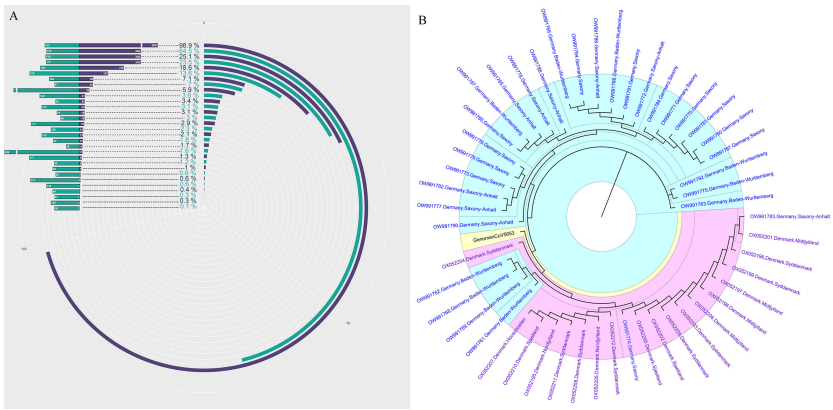

FIGURE 2
The genome of SARS-CoV-2 analysis based on mNGS. **(A)** The genome coverage of SARS-CoV-2 increases with the increasing reads of SARS-CoV-2. **(B)** The evolutionary tree analysis between our sample-GenomenCoV5653 and the 50 optimal genome alignment from NCBI.

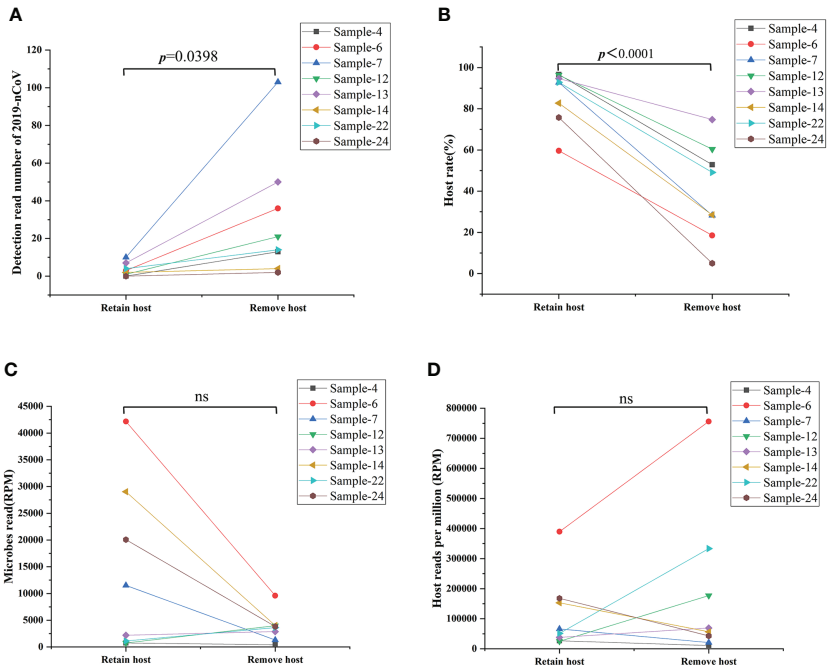

FIGURE 3
Comparison results from removing host and retaining host workflow. **(A)** Removing the host significantly improved the detection read number of 2019-nCoV ($p<0.05$). **(B)** Removing the host decreased significantly the host rate in the swab sample ($p<0.05$). **(C, D)** Removing the host on the detection reads of microbes reads and the host reads varies in different samples. RPM: Numbers of mapped reads per million; ns: no significance.

(Figures 5A–G) showed low a Ct value at around 40 based on RT-PCR were consistently negative (y=0) for mNGS, even when the sequencing depths were improved up to sixfold for Sample-34 (Figure 5F). Only one sample witch from negative (y=0) to positive (y=1) (Figure 5H). Further investigations on 17 samples with positive results for mNGS detection showed that there was only slight improvement in SARS-CoV-2 detection read even when the sequencing depths were enhanced for several folds (Figures 5I–Y). To some extent, these results demonstrate that the enhancement of sequencing depths will not yield much improvement for SARS-CoV-2 detection reads.

Determining the compositions of both the fungal and bacterial communities by untargeted host-removed mNGS

Another important aspect of data analysis of such metagenomic data from untargeted host-removed mNGS is determining the microbial composition and quantifying the microbial abundances based on the metagenomic sequencing data. Until now, most studies have determined respiratory microbial composition using 16S ribosomal DNA (16S rDNA) gene sequencing, whether the host-removed mNGS possess the same utility has not yet been fully explored. The entire sequence alignment from all 37 samples is presented in Figures 6A, B, we found that the bacterial community structures determined by mNGS were highly abundant with various bacterial, fungal and bacterial species. More importantly, mNGS can comprehensively reveal the normal upper respiratory tract flora, such as Veillonella, Actinomyces, Streptococcus and Prevotella, all recognized as oral commensals (Figure 6A) (17, 18). Malassezia, a dominant fungal genus on the human skin and upper airways of most healthy people and related to human autoimmunity and skin diseases (19–21), was detected in all samples. Aspergillus species, one of the most common pathogenic fungi causing upper and lower airway disorders, was also detected in all samples (Figure 6B) (22). These results demonstrated that the bacterial and fungal community structures revealed by mNGS are similar to the microbial communities commonly reported in previous studies based on other technologies like 16S rDNA gene sequencing.

Functional enrichment analysis of DEGs and xCell score between patients with high and low virus load

Taking the CT value of 35 as the critical point, a total of 462 differentially expressed genes (DEGs) were identified between patients with high and low CT values of SARS-CoV-2, including

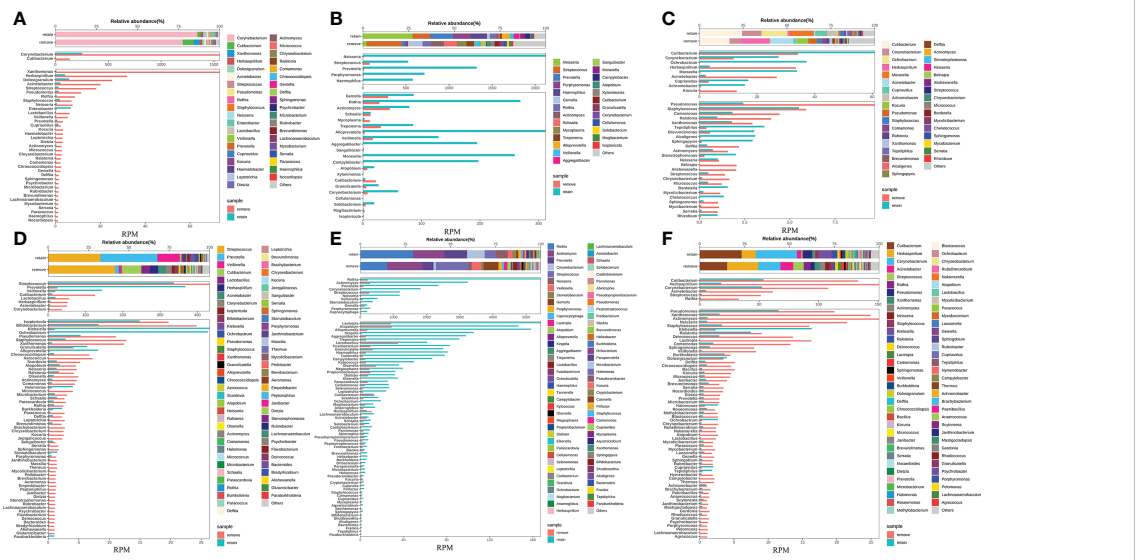

FIGURE 4
Removing host DNA detection workflow show identical species abundance of bacteria with the workflow of retaining host DNA and will not cause the loss of RNA from bacterial species. **(A–F)** Eight samples simultaneously performed the workflow of removing and retaining host DNA and compared the bacterial species composition between the two workflows.

127 up-regulated and 335 down-regulated genes (Figure 7A). To determine the functional annotation of the DEGs between patients with high and low CT values of SARS-CoV-2, we performed the Gene Ontology (GO) analysis and presented the expression levels of genes in each term in a GO circle plot using the R package GO plot. Based on GO enrichment analysis, DEGs were divided into the three principal GO organization categories: biological process (31 genes) (Figure 7B), cellular component (25 genes) (Figure 7C), and molecular function (31 genes) (Figure 7D). Next, we analyzed the xCell score using the R package 'xCell' (https://github.com/dviraran/xCell). xCell is a newly published method based on ssGSEA that estimates the abundance scores of 64 immune cell types, including adaptive and innate immune cells, epithelial cells, hematopoietic progenitors, and extracellular matrix cells. Based on the comparison between 18 patients with high viral load and 19 patients with low viral load, we found that the cellular proportions of $CD4^+$ memory T cells, $CD8^+$ naive T cells, $CD8^+$ T cells, Fibroblasts, HSC, Microenvironment Score and Stroma Score in patients with low viral load were significantly higher than that in patients with high viral load; while the Sebocytes have a higher proportion in patients with high viral load ($p<0.05$) (Figure 7E) (Supplementary Figure S1).

Discussion

mNGS is a revolutionary diagnostic tool capable of simultaneously detecting all microbial and host gene expressions. However, it is not very clear what the sensitivity level of this technology is compared with traditional detection methods, especially PCR. In the present study, we systematically evaluated the sensitivity of untargeted host-removed mNGS between the mNGS and two approved qRT-PCR methods. Further series analyses revealed that mNGS have superior performance in the comprehensive identification of the pathogen and simultaneously reveal the transcriptional profiles of the microbiome and host responses.

In recent years, mNGS has emerged with more rapid and accurate diagnostic advantages than traditional methods, especially in culture-negative samples. The sensitivity of mNGS varies in different kinds of pathogens, and while many studies have demonstrated that mNGS is more sensitive than conventional culture (9, 23, 24), there has not been fully proven that whether mNGS could yield high sensitivity than qPCR, which is widely considered as the high-sensitivity. To stringently evaluate the sensitivity of mNGS, 37 samples confirmed to be positive by two different RT-PCR kits simultaneously were used to assayed by mNGS. Results showed that the detection rate of mNGS achieved 92.9% (26/28) for 28 samples with Ct value ≤ 35 and 81.1% (30/37) for all 37 samples (Figure 1), this compliance was similar to other studies (25). A recent study demonstrated that the infectious virus will no longer be isolated from the patients with Ct value of qPCR>35 and there was no viral shedding from infectious patients when the Ct value was>28 (26). In view of this, the detection rate of mNGS would meet clinical need and diagnosis of COVID-19.

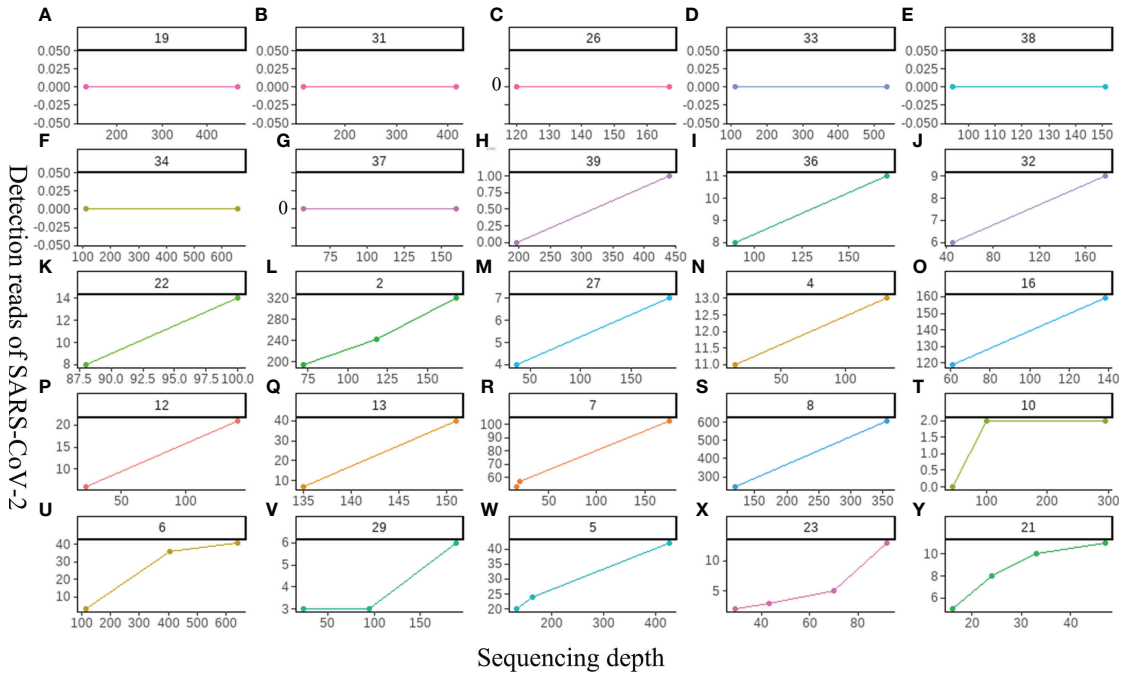

FIGURE 5
The relationship between the sequencing depth and the detection sensitivity of SARS-CoV-2 based on untargeted host-removed mNGS technology. **(A-Y)** 25 samples were assayed by mNGS using sequencing depth, respectively.

Recent advances and the growing popularity of mNGS have enabled the rapid identification and traceability of emerging infectious diseases in basic medical institutions or medical laboratories worldwide. The three major pathogenic human coronaviruses (CoVs) are the SARS-CoV, the Middle East respiratory syndrome (MERS)-CoV and SARS-CoV-2 (27). The nucleotide sequence of SARS-CoV-2 is ~79% similar to SARS-CoV-1 and about 50% with MERS-CoV (Middle East respiratory syndrome coronavirus) (28). In addition, SARS-CoV-2 is genetically very similar to other Coronaviruses (29), so fully understanding its RNA sequence is the key to identifying SARS-CoV-2, especially in the early stage of the epidemic. Our research demonstrated that the mNGS can could not only accurately diagnose COVID-19, but also simultaneously achieve traceability at the first time point.

The sensitivity of mNGS for detecting pathogen-derived genomes could be improved by increasing sequencing depth or decreasing the high human host DNA background (8). However, the effect of the removal of host cell-derived nucleic acids is still controversial, especially for samples with low microbial content, the removal of human host DNA background can significantly reduce the detection rate of target microorganisms (30). Different strategies of host removal may cause different outcomes for various pathogens; further research with larger sample sizes is needed to define its clinical utility. Our data provided the first evidence that removing human host DNA can improve the detection sensitivity for SARS-CoV-2 in swab samples (Figure 3A). More interestingly, our study also first demonstrates that the removal of the host does not affect the species abundance of microbes reflected by mNGS (Figure 4), indicating that this method can be reliably used to study the microbiome community structure and function.

Hospitalized COVID-19 patients often present with a large spectrum of clinical pictures—from only mild upper respiratory symptoms to severe disease characterized by pneumonia, acute respiratory distress syndrome, and even diverse systemic effects impacting various tissues (31). How infection influences spread from the upper respiratory tract to the lower respiratory tract and cause respiratory failure remains incompletely understood. Recently, an increasing number of researchers are starting to focus on studying the host local immune characteristics related to the SARS-CoV-2 infection based on detecting and analyzing the nasopharyngeal samples from COVID-19 patients (32, 33). It has been demonstrated that SARS-CoV-2 infection can induce unique host immune responses different from infection caused by other respiratory viruses (34, 35). Similar result was also confirmed with the data in our study, which found that there are 462 DEGs between patients with high and low CT values of SARS-CoV-2 (Figure 7A).

Further GO enrichment analyses showed that the BP clusters were primarily enriched in functions related to the induction of

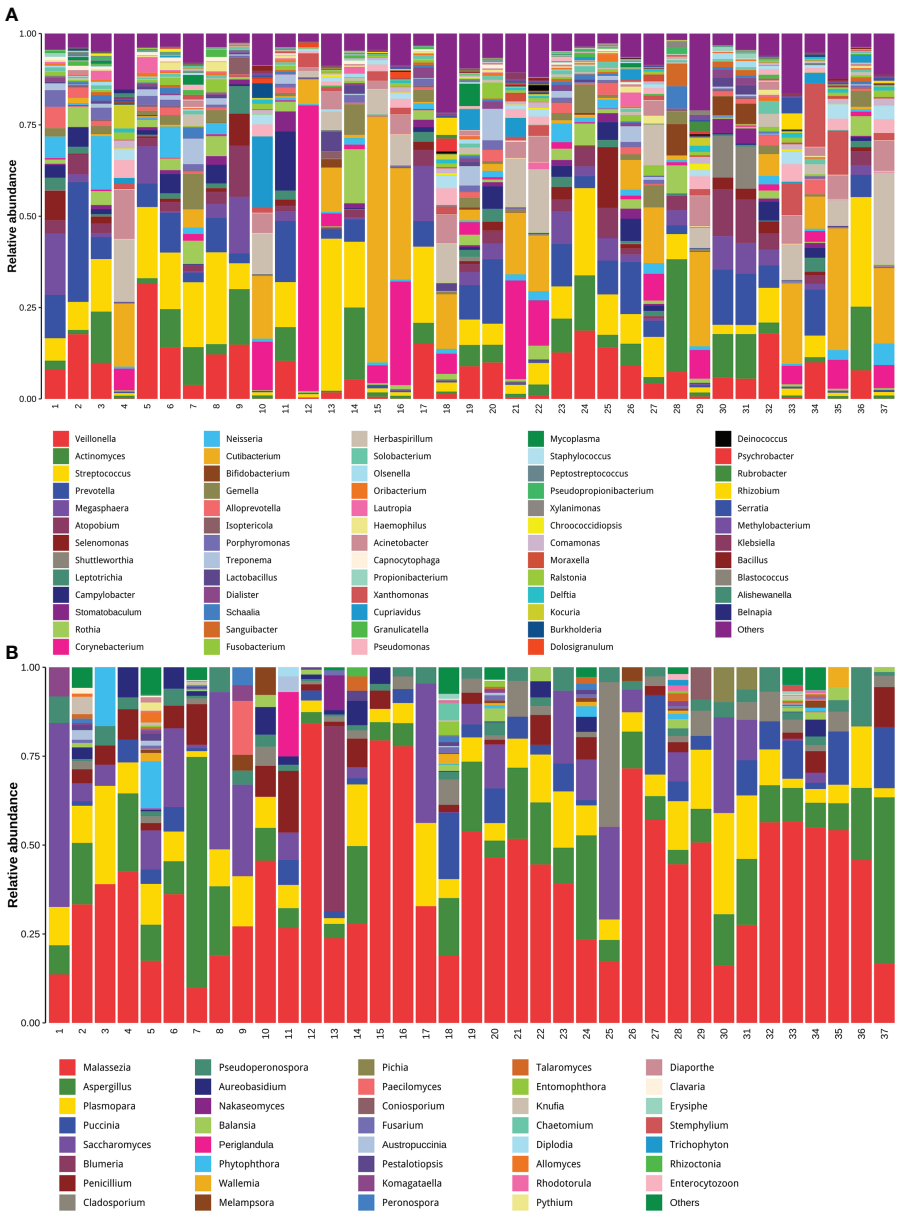

FIGURE 6
Untargeted host-removed mNGS accurately revealed the compositions of both the bacterial and fungal and bacterial communities. The bacterial **(A)** and fungal **(B)** with abundance greater than 1% were presented, and less than 1% of the total abundance were combined into the "Other <1%" category.

the inflammasome pathway including granulocyte migration, neutrophil migration, granulocyte chemotaxis and myeloid leukocyte migration (Figure 7B). In view of the above series of analysis results, we speculated that differentiating protective host mechanisms might support rapid viral clearance or spread from limited local nasopharynx infection to severe and fatal outcomes. In addition, local nasopharyngeal immune microenvironment analysis also indicated that patients with low viral load presented more intense immune responses than patients with high viral load (Figure 7E). This result may also suggest that the host transcriptomic profiling of the host, utilized alone or in combination with the detection results of SARS-CoV-2 from qRT-PCR, is characterized by the ability to establish close connections between viral load and host immune response in the nasopharynx. However, the limitation of this study was the small number of subjects. Future research with larger sample

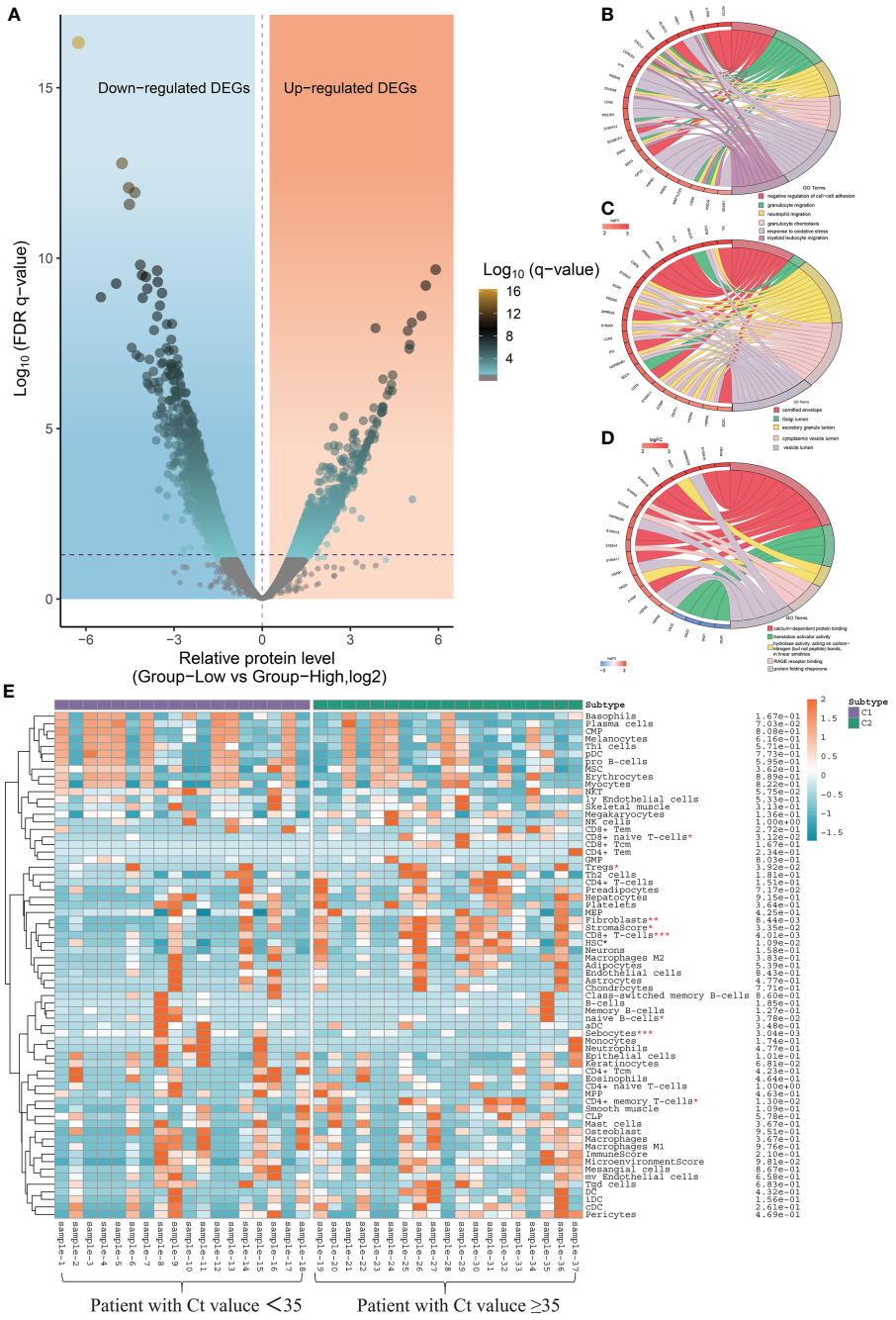

FIGURE 7
Local nasopharyngeal immune microenvironment analysis between high and low virus load patients. **(A)** Differentially expressed genes (DEG) by volcano diagram. **(B)** Functional enrichment analysis of the biological process (BP) **(C)** Functional enrichment analysis of cellular component (CC). **(D)** Functional enrichment analysis of molecular function (MF). **(E)** xCell immune score identifies the difference in abundance scores of 64 immune cell types between patients with high and low viral load.

sizes is needed to investigate the relationship between viral load and host immune characteristics and identify biomarkers from the point of view of the human host for distinguishing the degree of infection progress.

In summary, our study offered the first comprehensive description of the practical application and value of untargeted host-removed mNGS for SARS-CoV-2 identification, as well as a comprehensive analysis of the genomic epidemiology of SARS-

CoV-2 and the transcriptional profiles of the host responses and microbiome, simultaneously.

Data availability statement

Metagenome sequencing data data for this study is deposited in the NCBI SRA BioProject repository with the accession PRJNA894695. All other relevant data generated in this manuscript that support the findings of this study are available upon request from the authors. Source data are provided with this paper.

Ethics statement

The studies involving human participants were reviewed and approved by Shijiazhuang People's Hospital Ethics Committee. The Ethics Approval Number: [2020]-046.

Author contributions

SZ, SG and PJ contributed equally to this work. SZ, SG, PJ and LL collected the samples. SZ, MX, CX performed the qPCR and mNGS experiments, SZ and ZY analyzed the data. SZ and WM wrote manuscript. All authors contributed to the article and approved the submitted version.

Funding

This work was supported by Science and Technology Research and Developmental Guidance Program of Shijiazhuang City (No. 201460503A).

Conflict of interest

The authors declare that the research was conducted in the absence of any commercial or financial relationships that could be construed as a potential conflict of interest.

Publisher's note

All claims expressed in this article are solely those of the authors and do not necessarily represent those of their affiliated organizations, or those of the publisher, the editors and the reviewers. Any product that may be evaluated in this article, or claim that may be made by its manufacturer, is not guaranteed or endorsed by the publisher.

Supplementary material

The Supplementary Material for this article can be found online at: https://www.frontiersin.org/articles/10.3389/fimmu.2022.1016440/full#supplementary-material

References

1. Jian Y, Li T, Zhao L, Zhao N, Liu Y, Lv H, et al. Regulation ofbla system in ST59-related oxacillin-susceptiblemecA -positiveStaphylococcus aureus. *J Antimicrob Chemoth* (2021) 77:604–14. doi: 10.1093/jac/dkab460

2. Liu Y, Liu Y, Du Z, Zhang L, Chen J, Shen Z, et al. Skin microbiota analysis-inspired development of novel anti-infectives. *Microbiome* (2020) 8:85. doi: 10.1186/s40168-020-00866-1

3. Chiu CY, Miller SA. Clinical metagenomics. *Nat Rev Genet* (2019) 20:341–55. doi: 10.1038/s41576-019-0113-7

4. Sun Z, Liu W, Zhang J, Wang S, Yang F, Fang Y, et al. The direct semi-quantitative detection of 18 pathogens and simultaneous screening for nine resistance genes in clinical urine samples by a high-throughput multiplex genetic detection system. *Front Cell Infect Mi* (2021) 11:660461. doi: 10.3389/fcimb.2021.660461

5. Sun Z, Meng J, Wang S, Yang F, Liu T, Zeng X, et al. A new multiplex genetic detection assay method for the rapid semi-quantitative detection of six common curable sexually transmitted pathogens from the genital tract. *Front Cell Infect Mi* (2021) 11:704037. doi: 10.3389/fcimb.2021.704037

6. Ackerman CM, Myhrvold C, Thakku SG, Freije CA, Metsky HC, Yang DK. Massively multiplexed nucleic acid detection with Cas13. *Nature* (2020) 582:277–82. doi: 10.1038/s41586-020-2279-8

7. Qu J, Zhang J, Chen YH, Huang Y, Xie Y. Aetiology of severe community acquired pneumonia in adults identified by combined detection methods: A multi-centre prospective study in China. *Emerg Microbes Infect* (2022) 11:556–66. doi: 10.1080/22221751.2022.2035194

8. Liu D, Zhou H, Xu T, Yang Q, Mo X, Shi D, et al. Multicenter assessment of shotgun metagenomics for pathogen detection. *Ebiomedicine* (2021) 74:103649. doi: 10.1016/j.ebiom.2021.103649

9. Gu W, Deng X, Lee M, Sucu YD, Arevalo S, Stryke D, et al. Rapid pathogen detection by metagenomic next-generation sequencing of infected body fluids. *Nat Med* (2021) 27:115–24. doi: 10.1038/s41591-020-1105-z

10. Bharucha T, Oeser C, Balloux F, Brown JR, Carbo EC. STROBE-metagenomics: A STROBE extension statement to guide the reporting of metagenomics studies. *Lancet Infect Dis* (2020) 20:e251–60. doi: 10.1016/s1473-3099(20)30199-7

11. *Infectious disease next generation sequencing based diagnostic devices: Microbial identification and detection of antimicrobial resistance and virulence markers* (2016). Available at: https://www.fda.gov/regulatory-information/search-fda-guidance-documents/infectious-disease-next-generation-sequencing-based-diagnostic-devices-microbial-identification-and (Accessed 2022-3-22).

12. Miller S, Chiu C. The role of metagenomics and next-generation sequencing in infectious disease diagnosis. *Clin Chem* (2022) 68:115–24. doi: 10.1093/clinchem/hvab173

13. Yang L, Song J, Wang Y, Feng J. Metagenomic next-generation sequencing for pulmonary fungal infection diagnosis: Lung biopsy versus bronchoalveolar lavage fluid. *Infect Drug Resist* (2021) 14:4333–59. doi: 10.2147/IDR.S333818

14. Wang L, Guo W, Shen H, Guo J, Wen D, Yu Y, et al. Plasma microbial cell-free DNA sequencing technology for the diagnosis of sepsis in the ICU. *Front Mol Biosci* (2021) 8:659390. doi: 10.3389/fmolb.2021.659390

15. Schlaberg R, Chiu CY, Miller S, Procop GW, Weinstock G. Validation of metagenomic next-generation sequencing tests for universal pathogen detection. *Arch Pathol Lab Med* (2017) 141:776–86. doi: 10.5858/arpa.2016-0539-RA

16. Patro R, Duggal G, Love MI, Irizarry RA, Kingsford C. Salmon provides fast and bias-aware quantification of transcript expression. *Nat Methods* (2017) 14:417–9. doi: 10.1038/nmeth.4197

17. Tsay JJ, Wu BG, Sulaiman I, Gershner K, Schluger R, Li Y, et al. Lower airway dysbiosis affects lung cancer progression. *Cancer Discovery* (2021) 11:293–307. doi: 10.1158/2159-8290.CD-20-0263

18. Hong B, Sobue T, Choquette L, Dupuy AK, Thompson A, Burleson JA, et al. Chemotherapy-induced oral mucositis is associated with detrimental bacterial dysbiosis. *Microbiome* (2019) 7:66 doi: 10.1186/s40168-019-0679-5

19. Zhu T, Duan Y, Kong F, Galzote C, Quan Z. Dynamics of skin mycobiome in infants. *Front Microbiol* (2020) 11:1790. doi: 10.3389/fmicb.2020.01790

20. Flowers L, Grice EA. The skin microbiota: Balancing risk and reward. *Cell Host Microbe* (2020) 28:190–200. doi: 10.1016/j.chom.2020.06.017

21. Lee K, Zhang I, Kyman S, Kask O, Cope EK. Co-Infection of malassezia sympodialis with bacterial pathobionts pseudomonas aeruginosa or staphylococcus aureus leads to distinct sinonasal inflammatory responses in a murine acute sinusitis model. *Front Cell Infect Mi* (2020) 10:472. doi: 10.10.3389/fcimb.2020.00472

22. Barac A, Ong DSY, Jovancevic L, Peric A, Surda P, Tomic Spiric V, et al. Fungi-induced upper and lower respiratory tract allergic diseases: One entity. *Front Microbiol* (2018) 9:583. doi: 10.3389/fmicb.2018.00583

23. Xing X, Zhang J, Ma Y, He M, Yao G, Wang W, et al. Metagenomic next-generation sequencing for diagnosis of infectious encephalitis and meningitis: A large, prospective case series of 213 patients. *Front Cell Infect Mi* (2020) 10:88. doi: 10.3389/fcimb.2020.00088

24. Zhang X, Guo L, Liu L, Shen A, Feng W, Huang W, et al. The diagnostic value of metagenomic next-generation sequencing for identifying streptococcus pneumoniae in paediatric bacterial meningitis. *BMC Infect Dis* (2019) 19:495. doi: 10.1186/s12879-019-4132-y

25. Thi Kha Tu N, Thi Thu Hong N, Thi Han Ny N, My Phuc T, Thi Thanh Tam P, Doorn HRV, et al. The virome of acute respiratory diseases in individuals at risk of zoonotic infections. *Viruses* (2020) 12:960. doi: 10.3390/v12090960

26. Ke R, Martinez PP, Smith RL, Gibson LL, Mirza A, Conte M, et al. Daily longitudinal sampling of SARS-CoV-2 infection reveals substantial heterogeneity in infectiousness. *Nat Microbiol* (2022) 7:640–52. doi: 10.1038/s41564-022-01105-z

27. Malik YS, Ansari MI, Kattoor JJ, Kaushik R, Sircar S, Subbaiyan A, et al. Evolutionary and codon usage preference insights into spike glycoprotein of SARS-CoV-2. *Brief Bioinform* (2021) 22:1006–22. doi: 10.1093/bib/bbaa383

28. Raghav S, Ghosh A, Turuk J, Kumar S, Jha A, Madhulika S, et al. Analysis of indian SARS-CoV-2 genomes reveals prevalence of D614G mutation in spike protein predicting an increase in interaction with TMPRSS2 and virus infectivity. *Front Microbiol* (2020) 11:594928. doi: 10.3389/fmicb.2020.594928

29. Kostarelos K. Nanoscale nights of COVID-19. *Nat Nanotechnol* (2020) 15:343–4. doi: 10.1038/s41565-020-0687-4

30. Han D, Gao P, Li R, Tan P, Xie J, Zhang R, et al. Multicenter assessment of microbial community profiling using 16S rRNA gene sequencing and shotgun metagenomic sequencing. *J Adv Res* (2020) 26:111–21. doi: 10.1016/j.jare.2020.07.010

31. Tang J, Ravichandran S, Lee Y, Grubbs G, Coyle EM, Klenow L, et al. Antibody affinity maturation and plasma IgA associate with clinical outcome in hospitalized COVID-19 patients. *Nat Commun* (2021) 12:1221. doi: 10.1038/s41467-021-21463-2

32. Chua RL, Lukassen S, Trump S, Hennig BP, Wendisch D, Pott F, et al. COVID-19 severity correlates with airway epithelium–immune cell interactions identified by single-cell analysis. *Nat Biotechnol* (2020) 38:970–9. doi: 10.1038/s41587-020-0602-4

33. Ziegler CGK, Miao VN, Owings AH, Navia AW, Tang Y, Bromley JD, et al. Impaired local intrinsic immunity to SARS-CoV-2 infection in severe COVID-19. *Cell* (2021) 184:4713–33. doi: 10.1016/j.cell.2021.07.023

34. Mick E, Kamm J, Pisco AO, Ratnasiri K, Babik JM, Castaneda G, et al. Upper airway gene expression reveals suppressed immune responses to SARS-CoV-2 compared with other respiratory viruses. *Nat Commun* (2020) 11:5854. doi: 10.1038/s41467-020-19587-y

35. Butler D, Mozsary C, Meydan C, Foox J, Rosiene J, Shaiber A, et al. Shotgun transcriptome, spatial omics, and isothermal profiling of SARS-CoV-2 infection reveals unique host responses, viral diversification, and drug interactions. *Nat Commun* (2021) 12:1660 doi: 10.1038/s41467-021-21361-7

frontiers | Frontiers in Immunology

TYPE Original Research
PUBLISHED 28 November 2022
DOI 10.3389/fimmu.2022.1054407

OPEN ACCESS

EDITED BY
Chenhe Su,
Wistar Institute, United States

REVIEWED BY
Rawan Muhammad Shady,
Cairo University, Egypt
Yusha Araf,
Shahjalal University of Science and Technology, Bangladesh

*CORRESPONDENCE
Hou'an Xiao
xiaohouan@163.com

†These authors have contributed equally to this work and share first authorship

SPECIALTY SECTION
This article was submitted to Viral Immunology, a section of the journal Frontiers in Immunology

RECEIVED 26 September 2022
ACCEPTED 08 November 2022
PUBLISHED 28 November 2022

CITATION
Wang P, Zhang Z, Lin R, Lin J, Liu J, Zhou X, Jiang L, Wang Y, Deng X, Lai H and Xiao H (2022) Machine learning links different gene patterns of viral infection to immunosuppression and immune-related biomarkers in severe burns. *Front. Immunol.* 13:1054407. doi: 10.3389/fimmu.2022.1054407

Machine learning links different gene patterns of viral infection to immunosuppression and immune-related biomarkers in severe burns

Peng Wang[1†], Zexin Zhang[2†], Rongjie Lin[3†], Jiali Lin[4], Jiaming Liu[1], Xiaoqian Zhou[1], Liyuan Jiang[1], Yu Wang[1], Xudong Deng[1], Haijing Lai[1] and Hou'an Xiao[1*]

[1]Department of Burns and Plastic and Cosmetic Surgery, Xi'an Ninth Hospital, Xi'an, China, [2]Department of Burns and Plastic and Wound Repair Surgery, Xiang'an Hospital of Xiamen University, School of Medicine, Xiamen University, Xiamen, China, [3]Department of Orthopedics, 900th Hospital of Joint Logistics Support Force, Fuzhou, China, [4]Obstetrics and Gynecology Hospital, Institute of Reproduction and Development, Fudan University, Shanghai, China

Introduction: Viral infection, typically disregarded, has a significant role in burns. However, there is still a lack of biomarkers and immunotherapy targets related to viral infections in burns.

Methods: Virus-related genes (VRGs) that were extracted from Gene Oncology (GO) database were included as hallmarks. Through unsupervised consensus clustering, we divided patients into two VRGs molecular patterns (VRGMPs). Weighted gene co-expression network analysis (WGCNA) was performed to study the relationship between burns and VRGs. Random forest (RF), least absolute shrinkage and selection operator (LASSO) regression, and logistic regression were used to select key genes, which were utilized to construct prognostic signatures by multivariate logistic regression. The risk score of the nomogram defined high- and low-risk groups. We compared immune cells, immune checkpoint-related genes, and prognosis between the two groups. Finally, we used network analysis and molecular docking to predict drugs targeting *CD69* and *SATB1*. Expression of *CD69* and *SATB1* was validated by qPCR and microarray with the blood sample from the burn patient.

Results: We established two VRGMPs, which differed in monocytes, neutrophils, dendritic cells, and T cells. In WGCNA, genes were divided into 14 modules, and the black module was correlated with VRGMPs. A total of 65 genes were selected by WGCNA, STRING, and differential expression analysis. The results of GO enrichment analysis were enriched in Th1 and Th2 cell differentiation, B cell receptor signaling pathway, alpha-beta T cell activation, and alpha-beta T cell differentiation. Then the 2-gene signature was constructed by RF, LASSO, and LOGISTIC regression. The signature was an independent prognostic factor and performed well in ROC, calibration, and

10.3389/fimmu.2022.1054407

decision curves. Further, the expression of immune cells and checkpoint genes differed between high- and low-risk groups. *CD69* and *SATB1* were differentially expressed in burns.

Discussion: This is the first VRG-based signature (including 2 key genes validated by qPCR) for predicting survival, and it could provide vital guidance to achieve optimized immunotherapy for immunosuppression in burns.

KEYWORDS

burn, immunosuppression, machine learning, prognostic model, virus infection

Introduction

According to the Global Burden of Diseases, Injuries, and Risk Factors Study, there were approximately 8.4 million burn incidents worldwide in 2019, resulting in 110,000 deaths (1). Burn emergency techniques have advanced significantly over the past 20 years, bringing about a significant reduction in burn mortality, but the burden of infection remains high (2). Infections are triggered by the accompanying immunosuppression in burn patients. Most studies focused on infections including the bacterial ones primarily caused by *Pseudomonas aeruginosa* or *Klebsiella pneumonia*. However, burn wounds are also highly susceptible to viral infections mainly due to the impaired immune responses and functions of the immune cells within the wound micro-environment (3).

Herpes simplex virus (HSV), varicella-zoster virus (VZV), cytomegalovirus (CMV), human papillomavirus (HPV), and Epstein-Barr virus (EBV) are common pathogens in burn patients with a viral infection which are mainly latent infections (3). Post-burn immunosuppression is a common pathological process, and immunosuppression increases the risk of viral reactivation. In addition, viral infections can weaken the body's immunity, leading to increased bacterial susceptibility (4). Viral infection is hard to detect because blisters and skin damage make the skin symptoms of viral infection unobvious. In addition, severe viral infection can lead to liver failure and severe encephalitis, easily misdiagnosed as multiple organ failure in severe burns (5–7). Although viral infection is vital to prognosis, there is still a lack of prognostic and therapeutic biomarkers related to viral infection. It is of great value to study viral markers.

Current prognostic indicators have some limitations. Total body surface area (TBSA) is the most common indicator, but it ignores age and gender and cannot accurately assess complex complications such as inhalation injury (8). The ABSI and Baux scales are used at the beginning of the burn, which cannot dynamically track the progression, and cannot evaluate the state of inflammation and the patient's immune function (9). Some inflammatory mediators and cytokines such as IL-1, IL-6, IL-8, MCP-1, and GCS-F reflect inflammation and immune function, but are still limited (10). Immunosuppression and infections are responsible for the deaths of more than 60% of patients (11, 12). Therefore, developing new markers related to immune function and prognosis is necessary. With the advancement of artificial intelligence and medical big data technology, machine learning has become part of precision medicine to validate therapeutic and prognostic biomarkers (13–15). Based on transcriptome data, unsupervised consensus clustering has been used to reveal different patterns in diabetes and cardiovascular disease (16–18), which can be used to search for similarity and heterogeneity between transcriptome data and to divide samples into groups with different prognostic clusters (14, 19–21). Random forest and LASSO are machine learning algorithms that can screen out biomarkers related to the prognosis of many genes, and have been used to screen key genes for cardiovascular diseases and other diseases (22–24). Conjoint analysis of multiple machine learning methods can improve the accuracy of prognostic biomarkers. Therefore, combining transcriptomic data and machine learning techniques is promising for developing new prognostic markers for severe burns.

This study used VRGs as hallmarks to identify patients grouped by two different VRGMPs by consensus clustering. Function and immune infiltration analysis between groups were

Abbreviations: VRGs, Virus-related genes; VRGMPs, VRGs molecular patterns; TBSA, total body surface area; VRGMPG, VRGMP groups; PAC, Proportion of ambiguous clustering; CDF, Cumulative distribution function; PCA, Principal component analysis; GSEA, Gene Set Enrichment Analysis; KEGG, Kyoto Encyclopedia of Genes and Genomes; ssGSEA, Single sample Gene Set Enrichment Analysis; PPI, Protein-protein interaction; GO, Gene Oncology; WGCNA, Weighted gene co-expression network analysis; RF, Random forest; LASSO, least absolute shrinkage and selection operator; HSV, Herpes simplex virus; VZV, varicella-zoster virus; CMV, Cytomegalovirus; HVP, human papilloma virus; EBV, Epstein-Barr virus.

assessed from four aspects: immune infiltration analysis, immune score, enrichment analysis, and clinical features. Next, in WGCNA, we identified gene sets associated with VRGMPs. The functions of these genes were fully assessed by network analysis and enrichment analysis. Further, we used RF and LASSO regression to screen for key genes associated with prognosis and constructed a nomogram by multivariate logistic regression to divide patients into high- and low-risk groups. Finally, we assessed differences in immune cells and checkpoints between patients in different risk groups and predicted potential drugs targeting key genes by molecular docking. The experimental process is shown in the flow chart (Figure 1).

Methods

Data acquisition and processing

The blood samples of burn patients were downloaded from the GEO database (GSE19743, GSE77791, and GSE37069). The patients aged 18-55, total body surface area (TBSA) >25% and sampling time after burning 7-30 days were included. Data preprocessing included transforming gene probes into gene symbols, data consolidation, and batch normalization. Probes without gene symbols or genes with more than one probe were deleted or averaged, respectively. The merged data was prepossessed by the SVA package in R software (version 4.0.5) to remove batch effects (25).

VRGs were selected from GeneOntology (GO) database (http://geneontology.org/) by keyword "Herpes simplex virus, varicella-zoster virus, cytomegalovirus, human papillomavirus, and Epstein-Barr virus".

The *in vitro* validation cohort was obtained from GSE37069, GSE26440, and blood samples from the Department of Burns and Plastic and Cosmetic Surgery, Xi'an Ninth Hospital. Data acquisition was approved by the Ethics Committee of Xi'an Ninth Hospital (200268).

Identification of VRGMP groups by consensus clustering

The GSE19743 dataset was included in consensus clustering analysis to explore differences in clinical traits and immunology between the different VRGMPGs. Through the k-means machine learning algorithm, the "ConsensusClusterPlus" R package was used to perform unsupervised consensus clustering, which allows for dividing or condensing cases to multiple clusters according to the provided hallmarks or signatures. Hallmarks were VRGs. In detail, we used the consensus clustering algorithm with 1,000 iterations by sampling 80% of the data in each iteration. The item-Consensus plot, the proportion of ambiguous clustering (PAC) algorithm, and the relative change in the area under the cumulative distribution function (CDF) curves confirmed the optimal cluster number. Principal component analysis (PCA) was performed to assess gene expression patterns between the VRGMPGs.

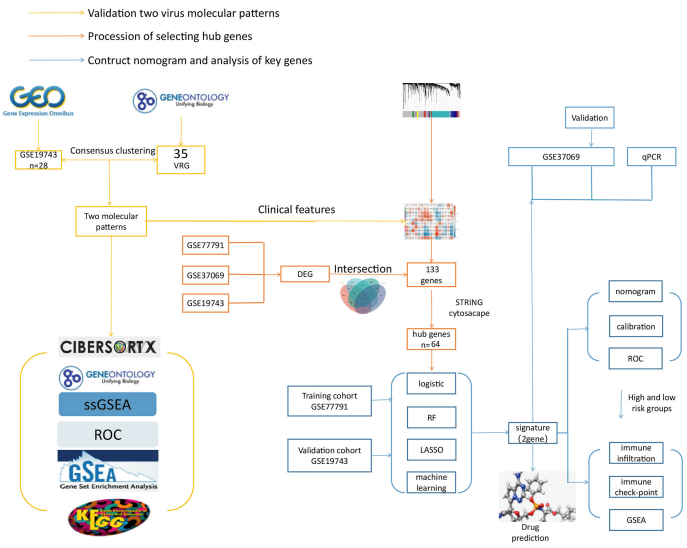

FIGURE 1
The flow chart. The yellow line is the validation of two viral molecular patterns. The orange line is the process of selecting hub genes. The blue line is the contructed nomogram and analysis of key genes.

Analysis of immune and clinical features between two VRGMPGs

The proportions of the immune cells and functions between VRGMPGs were determined by CIBERSORT, Gene Set Enrichment Analysis (GSEA), and single sample Gene Set Enrichment Analysis (ssGSEA). The ssGSEA was performed by R package "GSVA" to explore the different infiltration degrees of immune cell types, immune-related functions, and immune-related pathways between Virus 1 and 2 groups (26). GSEA software (version 3.0) was obtained from the GSEA website (http://software.Broadinstitute.org/gsea/index.Jsp), and "c2.cp.kegg.v7.4.symbols. gmt" subset was downloaded from the Molecular Signatures Database (http://www.gsea-msigdb.Org/gsea/downloads.jsp). CIBERSORT was performed online (https://cibersortx.stanford.edu/) (27). Based on gene expression profiles and VRGMPGs, the minimum gene set was set to 5 and the maximum gene set to 5000, with one thousand re-samplings, and $P < 0.05$ was considered statistically significant. The top 7 terms with the smallest p-values are shown. The prognostic value of immune cells was assessed by the receiver operating curve (ROC). We downloaded clinical information from the GSE19743 dataset to analyze clinical features (survival, ABSI, Baux, TBSA, age, sex, inhalation injury, and hospital time) between VRGMPGs.

WGCNA and identification of VRDEGs

WGCNA is a systems biology approach that can identify modules of highly correlated genes based on linkages between gene sets and phenotypes. Gene modules associated with VRGMPGs in GSE19743 were identified using the "WGCNA" package. The "limma" package was applied to calculate the differential expression genes between healthy controls and burns in GSE19743, GSE77791, and GSE37069, respectively. We took the intersection of WGCNA module genes and burn differential genes to obtain virus-related differentially expressed genes (VRDEGs) for further analysis.

Network analysis of VRDEGs

The functions of VRDEGs were assessed by GO and Kyoto Encyclopedia of Genes and Genomes (KEGG) enrichment analysis in The Database for Annotation, Visualization and Integrated Discovery (DAVID) (https://david.ncifcrf.gov/). We constructed a PPI network based on the STRING database (https://cn.string-db.org/), visualized it using Cytoscape, and used the MCODE plugin to identify hub genes in the network.

Screening for prognosis-related genes

In GSE77791, univariate logistic regression analysis was performed based on the hub genes, and variables with $P < 0.05$ were used for the subsequent analysis; LASSO regression analysis was performed with the hub genes, and variables with non-zero coefficients were screened out for the next analysis; Random forest analysis was utilized to screen out the most important genes for prognosis (top 20). The results of LASSO, logistic and random forest were intersected to obtain prognostic genes for multivariate logistic regression.

Constructing risk scoring models and independence verification

In GSE77791, multivariate logistic regression analysis was performed on prognostic genes to find key genes ($P < 0.05$). Visualize the relationship between variables and predictive models using the "rms" package. The nomogram was constructed to predict the risk of death using *CD69* and *SATB1*. Its performance was assessed by the area under the receiver operating characteristic curve (AUC), calibration curve, and decision curve. According to the nomogram risk score, patients were divided into high- and low-risk groups with a median cutoff value. To verify the independence of risk scores, univariate and multivariate logistic regression analyses were performed for risk scores, TBSA, AGE, SEX, BUAX, and ABSI, respectively.

Immune analysis between high- and low-risk groups

Immune infiltration and immune checkpoint analysis in the high- and low-risk groups.We performed the CIBERSORT, GSEA, and ssGSEA analysis to assess immune cell expression and immune score between high- and low-risk groups. In addition, we also analyzed differences in the expression of immune checkpoint genes between high- and low-risk groups. $P < 0.05$ was considered significant. Furthermore, we performed a Pearson correlation analysis between key genes, T cell subtypes, and T cell activation/suppression.

Drug prediction and molecular docking

Using the online network analysis tool "Networkanalysis" (https://www.Networkanalyst.ca/), the interaction network of key genes and chemicals was constructed based on the Comparative Toxicogenomics Database (CTD), and the compounds that acted on both genes at the same time were selected for the next step of molecular docking. The ".sdf" format structures of compounds

were downloaded from The PubChem Project (https://pubchem.ncbi.nlm.nih.gov/). We downloaded the structures of proteins from the RSCB PDB database (https://www.rcsb.org/). PyMOL 2.2.0 software (https://pymol.org) was used to process small molecule ligands, including removal of water molecules, ligand removal, and addition of hydrogen. AutoDockTools 1.5.6 (https://autodock.scripps.edu/) was used to process receptor proteins, such as adding polar hydrogen and a charge. Molecular docking was performed by using AutoDock Vina 1.1.2 software (28). By analyzing the binding energy of the molecule, choosing the conformation with the lowest binding energy and observing the formation of hydrogen bonds, we used Pymol software to map and display the three-dimensional structures, protein residues and binding bonds of proteins.

Validation expression of key genes

The immune system of burn patients was in dynamic changes, so we detected the expression of key genes in five different periods (0-24h, 24-72h, 72h-7d, 7d-30d, >30d) in the whole blood PCR group and the microarray group. The PCR samples (blood) were obtained from the Department of Burns and Plastic and Cosmetic Surgery, Xi'an Ninth Hospital, and data acquisition was approved by the Ethics Committee of Xi'an Ninth Hospital (202268). The Microarray group samples were collected from the public dataset (GSE37069) and do not require ethical approval. Peripheral blood mononuclear cells (PBMC) were isolated from blood using Ficoll sodium diatrizoate gradient centrifugation (Sigma-Aldrich, St. Louis, MO, USA) and were dissolved in TRIzol reagent (Invitrogen, Carlsbad, CA, USA). The total RNA was extracted using an RNeasy kit (Qiagen, Hilden, Germany) and stored at −80°C. The RR047A cDNA synthesis kit (TaKaRa, China) was used to perform the reverse-transcription of the extracted RNA, and the 2X SG Fast qPCR Master Mix (High Rox, B639273, BBI) was used for quantitative PCR of hub genes on an ABI PRISM 3700 instrument (Foster, CA, USA). GAPDH was used as an internal control, and primers are as follows:

CD69-F: 5'-ATTGTCCAGGCCAATACACATT-3'
CD69-R: 5' –CCTCTCTACCTGCGTATCGTTTT-3'
SATB1-F: 5'-GATCATTTGAACGAGGCAACTCA-3'
SATB1-R: 5'-TGGACCCTTCGGATCACTC-3'
GAPDH-F: 5' -TGGGTGTGAACCATGAGAAGT-3'
GAPDH-R: 5' -TGAGTCCTTCCACGATACCAA-3'

Statistical methods

The independent Student's t-test was used to compare the continuous data with normal distribution, and the $\chi 2$ test for categorical data was utilized for pairwise comparisons between subgroups. The Mann–Whitney U test was used to compare differences between two independent groups when the dependent variable was either ordinal or continuous but not normally distributed. All statistical analyses were performed using the R programming language (Version 4.0.5) and SPSS software. A difference of $P < 0.05$ indicates statistical significance unless specified otherwise.

Result

Data acquisition and processing

We included 28 burns and 25 controls in GSE19743, 76 burns and 14 controls in GSE77791, and 83 burns and 36 controls in GSE37069. The three datasets for burns were processed with the batch effect shown below (Figure 2). A total of 20,441 genes were integrated from the three datasets (Figure 2), and the datasets were directly comparable (Figure 2).

Through the GO database, we extracted 35VRGs that were used to be Hallmarks in Consensus clustering.

We obtained 6 blood samples of severe burn patients (total body surface area, TBSA > 25%) aged 18-55, with sampling times including (0-24h, 24-72h, 72h-7d, 7d-30d, >30d) and 6 healthy adults with peripheral blood samples from Department of Burns and Plastic and Cosmetic Surgery, Xi'an Ninth Hospital.

Since immune cells were significantly different at different time points after burning, we selected the samples in GSE37069 to evaluate the expression of key genes at different time points, including 0-24h, 24-72h, 72h-7d, 7d-30d, >30d.

Analysis of immune and clinical features between two VRGMPGs

To explore the association between severe burn patients and viral infection, we performed unsupervised clustering using genes associated with VRGs as hallmarks. Based on the machine learning algorithm "ConsensusClusterPlus", we divided patients into two distinct virus-associated molecular patterns (C1:Virus-1 and C2:Virus-2 groups) (Figure 3A). According to the results of principal component analysis, different VRGMPs have different gene expression patterns (Figure 3). In GSEA analysis, genes in the C1 group were more enriched in INTESTINAL_IMMUNE_NETWORK_FOR_IGA_PRODUCTION, GRAFT_VERSUS_HOST_DISEASE, ASTHMA, T_CELL_RECEPTOR_ SIGNALING_PATHWAY, VIRAL_MYOCARDITIS, SYSTEMIC_LUPUS_ERYTHEMATOSUS, and ETHER_LIPID_METABOLISM (Figure 3). In the CIBERSORT immune infiltration analysis, the proportions of plasma cells, Tregs, monocytes, and neutrophils significantly differed between different virus-

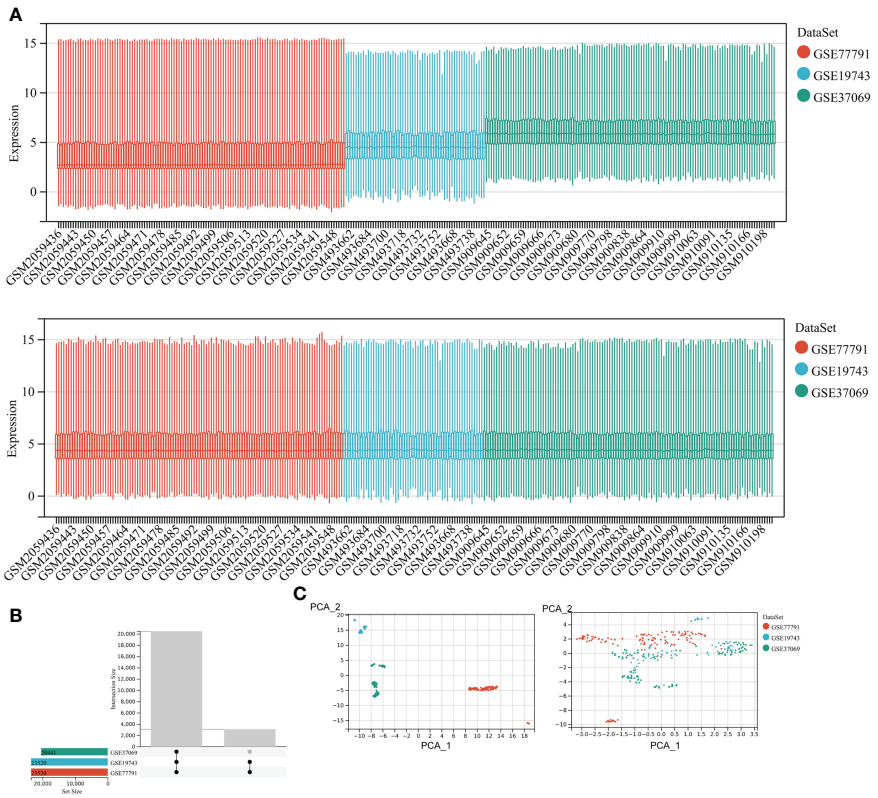

FIGURE 2
Correcting for batch effects. **(A)** Bar graphs with different colors represent different data sets. The ordinate is the expression value of the microarray data, and the abscissa is the sample number. **(B)** Overlapping genes after converting gene names between different datasets. **(C)** Sample expression profiles before batch correction and after batch correction.

associated molecular patterns (Figure 3). In ssGSEA analysis, CD8 T cells and effector CD4 T cells differed significantly between different virus-associated molecular patterns. Gamma delta T cell, CD56 bright natural killer cell, and Activated dendritic cell have better prognostic values (Figure 3G). TBSA and survival also differed significantly between different VRGMPGs (Figure 3).

WGCNA and identification of VRDEGs

In the WGCNA analysis, two outlier samples were excluded with a soft threshold of 16 (Figure 4A). The genes of GSE19743 can be divided into 14 modules (Figure 4). The black modules containing 244 genes were significantly correlated with VRGMPGs ($P < 0.01$, coefficient=-0.48) (Figure 4). In GSE19743, there were 5481 differentially expressed genes (DEGs) ($|LogFC > 1|$, FDR < 0.05) between burn patients and healthy adults. In GSE77791, there are 2246 DEGs. In GSE37069, there are 2765DEGs (Figure 4G). Finally, there were 133 intersections between the black modules of WGCNA and differently expressed genes (Figure 4). These genes were used in the next step of network analysis to screen the hub genes further.

Network analysis of VRDEGs

Using the MCODE plugin for Cytoscape, we identified 65 hub genes with dense interaction networks (Figure 5). In GO and KEGG enrichment analysis, these genes are highly correlated with T cell-related pathways, such as T cell activation and differentiation, T cell receptor signaling, T cell receptor complex, and Th1, Th2, and Th17 cell differentiation (Figure 5B). Furthermore, there are highly shared genes among these pathways, illustrating the high possibility of interaction between these genes (Figure 5G).

Screening for prognosis-related genes

When the number of decision trees is 500, there is a lower error in RF, and the top 20 important genes are screened out

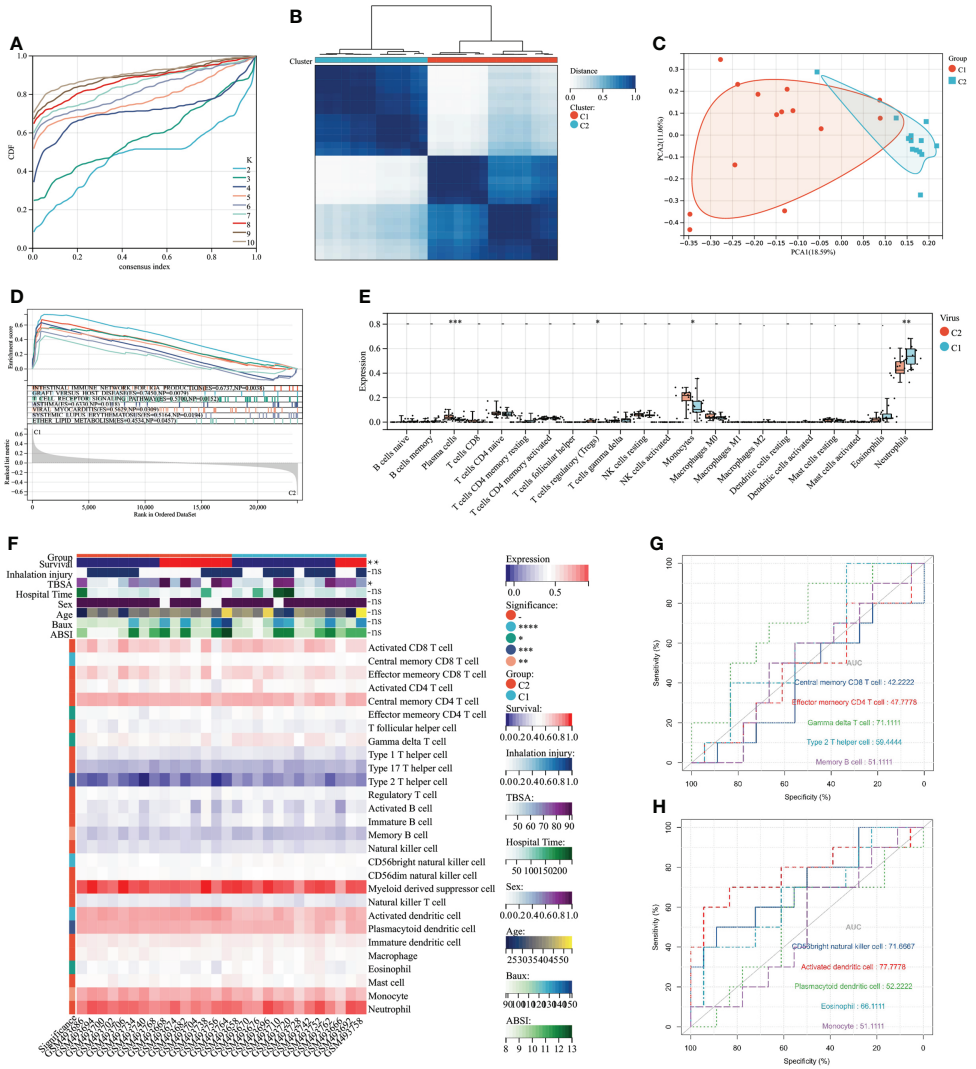

FIGURE 3
Consensus clustering and its grouping for clinical properties and immunological analysis. **(A)** Different colored lines represent different K (number of sample groups). According to the evaluation of the area under the CDF curve, the area under the CDF curve gradually increases when the K value increases. Here, the clusters with the highest average consistency in the group are the number of clusters is K=2, and the number of the next highest cluster is K=4. **(B)** When K=2, the samples can be divided into 2 groups with different expression patterns (C1 and C2). **(C)** The dots of different colors represent different groups. PCA is performed according to the gene expression data. The gene expression profiles of the two groups of patients in the figure are significantly different. **(D)** The results of GSEA showed that different colors represent enriched pathways; ES > 0 indicates that the genes of C1 are enriched in this pathway, and ES < 0 means that the genes of C2 are enriched in this pathway. **(E)** Comparison of 22 immune cells between C1 and C2 subgroups. The vertical axis represents the proportion of immune cells. Cells with $P < 0.05$ were considered to be different between groups. **(F)** ssGSEA results. In the C1 and C2 subgroups, showing differences in clinical shape, immune cells, and immune function, $P < 0.05$ was considered to be different between the different subgroups. **(G)** Immune cells and immune function ROC curves with significant differences. The larger the AUC value, the better the predictor of the patient's prognosis. $P < 0.05$:*, $P < 0.01$:**, $P < 0.001$:***P < 0.0001:****, P > 0.05:ns.

(Figure 6A). 16 variables had non-zero coefficients in the least absolute shrinkage and selection operator (LASSO) regression model (Figure 6C). In GSE77791, 25 genes were significantly associated with survival ($P < 0.05$) according to the univariate analysis (Figure 6). Finally, we obtained 4 prognostic genes for further study (Figure 6).

Constructing risk scoring models and independence verification

Multivariate logistic regression analysis revealed that *CD69* and *SATB1* were independent risk factors for severe burns (Table 1). These two independent factors were used to

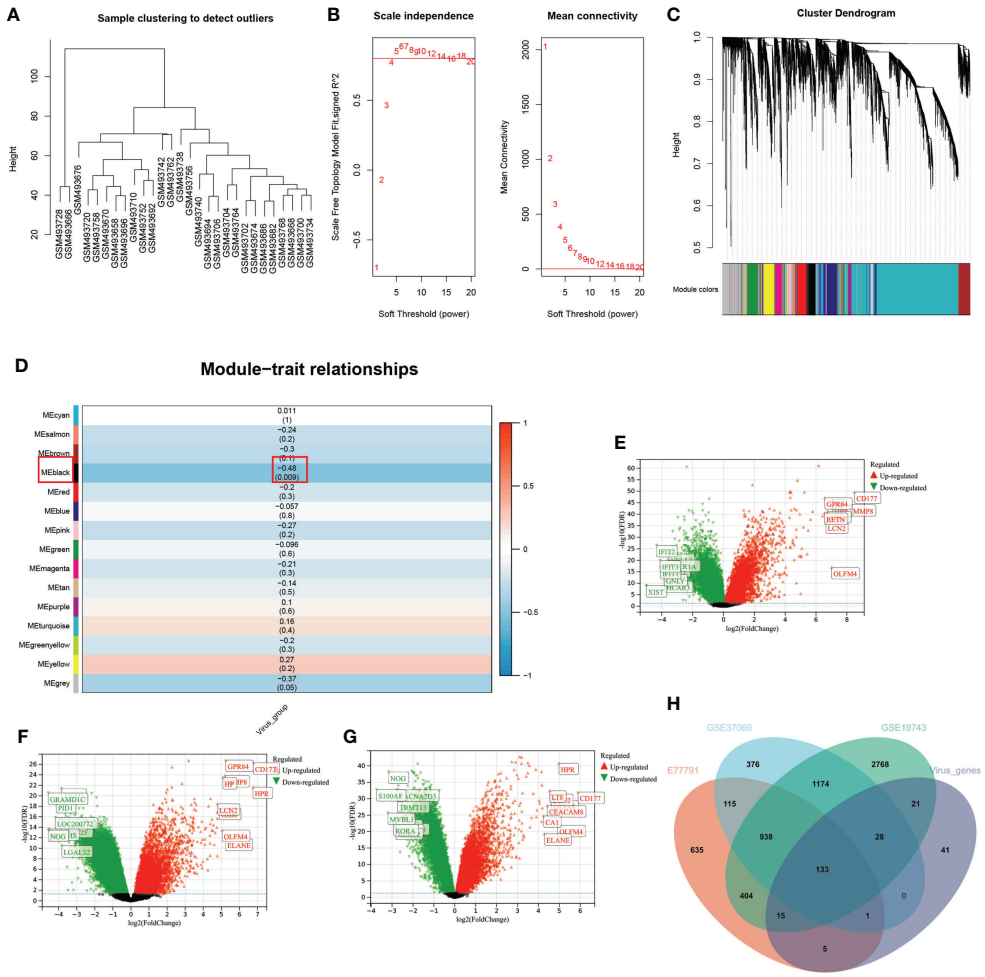

FIGURE 4
WGCNA and differential expression analysis **(A)** In the cluster analysis results of the GSE19743 dataset, abnormal samples can be eliminated according to the height value. **(B)** Analysis of scale-free fit indices (left) and average connectivity (right) to select various soft power (β). Soft threshold: select the soft threshold when R2>0.85. **(C)** Cluster dendrogram of burn trait genes; each color below represents a co-expressed gene module. **(D)** Correlation of consensus clustering groupings with gene modules. The values are the correlation coefficients (p), respectively. Red represents positive correlation, and blue represents negative correlation. Black modules have a significant correlation with virus grouping. **(E–G)**. Differential expression analysis of genes in three burn datasets. Green represents down-regulated genes, and red represents up-regulated genes. The genes in black are not significantly different. **(H)** The intersection of the three burn datasets and the black module in WGCNA.

construct the nomogram (Figure 7). The AUC value of the nomogram was 0.825 (95% CI): (Figure 7), which indicated that the model had good predictability. Furthermore, the calibration curve showed a high consistency between prediction and actual observation (Figure 7). The AUCs of TBSA, hospital time, halation injury, Baux, AGE, and ABSI were 0.73, 0.73, 0.63, 0.7, 0.56, and 0.7, respectively (Figure 7I). The AUC of the nomogram was 0.75 in the validation set (Figure 7). The calibration curve also showed a relatively low consistency between prediction and actual observation (Figure 7). The decision curve analysis (DCA) showed that the Risk_score had the best ability to identify survival than any other clinical factor in the validation sets (Figure 7M). Multivariate logistic regression analysis revealed that risk scores were independent risk factors for severe burns (Table 2).

Immune analysis between high- and low-risk groups

In CIBERSORT analysis, T cells *CD4* naive, T cells *CD4* memory resting, and *T* cells *CD4* memory activated were higher in the low-risk group (Figure 8). Similarly, in ssGSEA, the score of *CD4* T cells was higher in the low-risk group (Figure 8). In addition, the scores of immature B cell, *CD56* bright natural killer cell, *MDSC*, and T cell co-stimulation were also higher in

10.3389/fimmu.2022.1054407

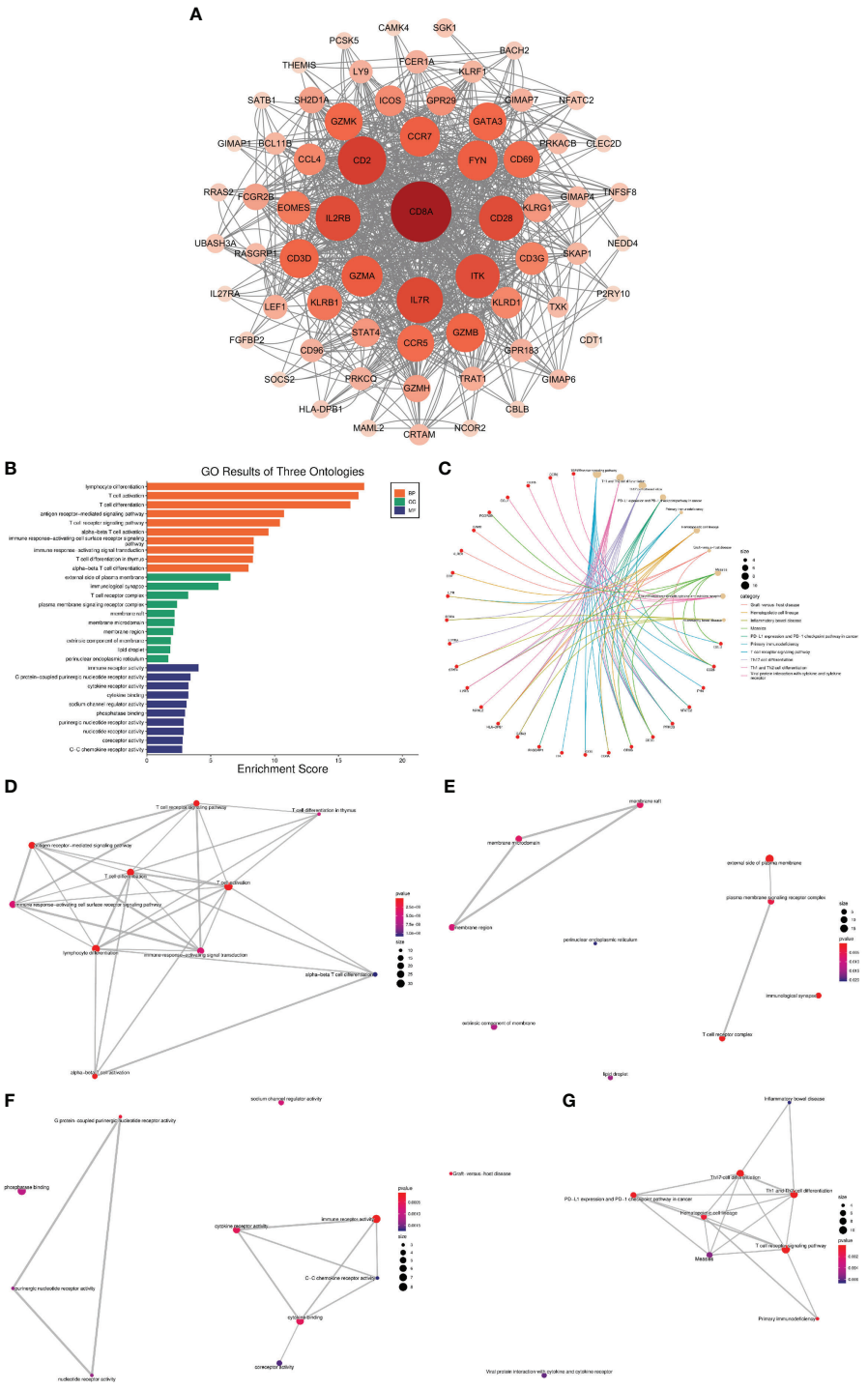

FIGURE 5
Network analysis of VRDEGs **(A)** The core gene network after the intersection of genes was screened by the MCODE plugin. The darker the color and the larger the circle, the more nodes the gene plays. **(B)** GO enrichment analysis results, orange is BP, green is CC, blue is MF, the abscissa is the enrichment score, and the ordinate is the pathway name. **(C)** KEGG enrichment analysis results. The red is the gene, and the yellow is the pathway. The larger the circle is, the more genes are enriched in the pathway. Different colors represent different enrichment results. **(D–G)**. Network plot of KEGG and GO enrichment analysis. Each link represents a commonly enriched gene between pathways, and the thicker the connecting line, the greater the number of common genes. The more enriched genes, the bigger the dots, and the smaller the P value, the redder the dots.

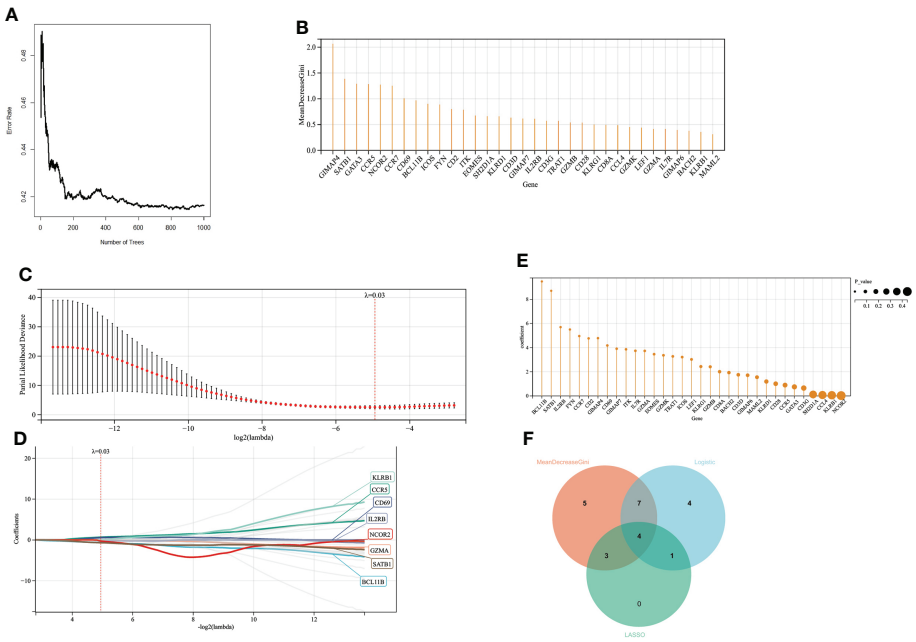

FIGURE 6
Screening variables by machine learning **(A)** When the random forest selects different numbers of decision trees, the error rate of the classification results. When the decision tree is 500, it has a lower error rate. **(B)** The ordinate is the Gini value, representing the variable's importance in the random forest analysis. **(C, D)**. LASSO regression results have a better screening effect when the coefficient is set at 0.03. **(E)** The results of univariate logistic analysis. The ordinate is the regression coefficient, and the size of the circle is proportional to the P value. **(F)** Intersection of random forest, lasso regression, and univariate logistic regression results.

the low-risk group (Figure 8). Interestingly, the low-risk group's expression of immune checkpoint-related genes, such as *CD28*, *CD86*, *CD276*, *ICOS*, *TIGIT*, and *TNFSF4*, was upregulated (Figure 8). *CD69* significantly correlates with Activated *CD4* T cell, Activated *CD8* T cell, Gamma-delta T cell, Treg, Th2, and T cell co-inhibition. *SATB1* significantly correlates with Activated CD8 T cell, Gamma-delta T cell, T follicular helper cell, Th2, T cell co-inhibition, and T cell co-stimulation (Figure 8). In GSEA, Low-risk group genes were mainly enriched in AXON_GUIDANCE, TGF_BETA_ SIGNALING_PATHWAY, GRAFT_VERSUS_ HOST_DISEASE, ALDOSTERONE_ REGULATED_SODIUM_ REABSORPTION,TYPE_I_DIABETES_MELLITUS,T_CELL_ RECEPTOR_SIGNALING_PATHWAY,CELL_ADHESION_ MOLECULES_CAMS, and CIRCADIAN_RHYTHM_MAMMAL while high-risk group in GLYCOSAMINOGLYCAN_ DEGRADATION,FOLATE_BIOSYNTHESIS (Figures 8E, F).

Drug prediction and molecular docking

A total of seven chemicals were found to be effective against both *CD69* and *SATB1* (Figure 9). We excluded two toxic chemicals and molecularly docked five chemicals, including Acetaminophen, decitabine, Cyclosporine, NickelSulfate, and JQ1, to confirm their potential as immunosuppressive drugs for the treatment of burns. Generally, binding energy less than 0 indicates that the ligand can bind the receptor spontaneously (29); binding energy less than -5.00 kcal/mol indicates strong

TABLE 1 Univariate and multivariate logistic regression for 4 genes.

Genes	Univariate analysis			Multivariate analysis		
	P	OR	95% CI	P	OR	95% CI
SATB1	0.021	0.047	(0.003-0.634)	0.008	0.025	(0.003-0.191)
CD69	0.003	10.716	(2.258-50.85)	0.001	5.001	(1.508-16.577)
BCL11B	0.008	1.456	(0.102-0.709)	0.774	–	–
IL2RB	0.026	0.111	(0.016-0.768)	0.69	–	–

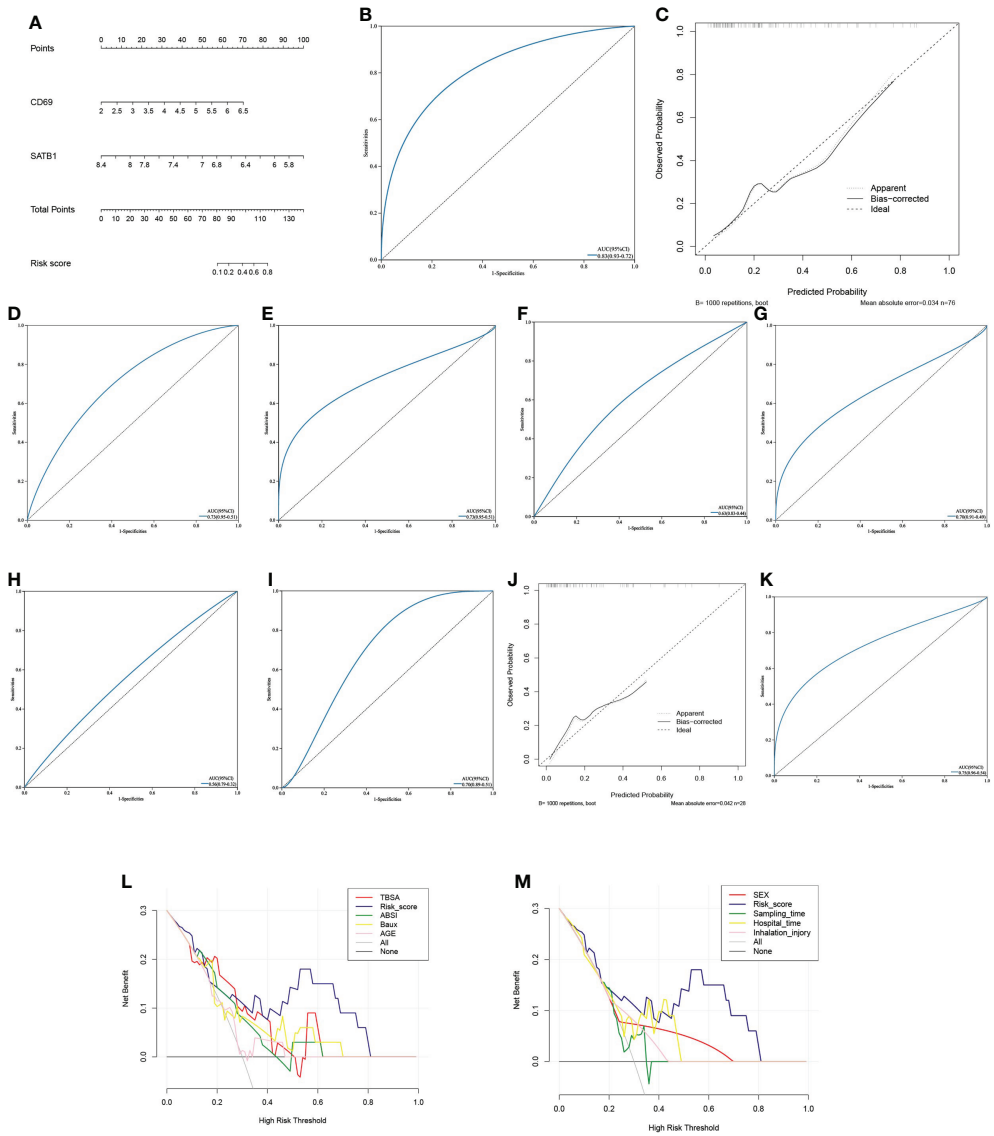

FIGURE 7
Predictive model **(A)** The Nomogram chart is constructed by multivariate logistic regression, which scores patients according to the gene value, and then predicts the risk of death. **(B)** The ROC curve of the nomogram in the training set: the larger the AUC value, the better the prediction performance. **(C)** The calibration curve of the nomogram in the training set: the higher the degree of coincidence with the diagonal line, the better the prediction performance. **(D–I)**. ROC curves of TBSA, hospital time, inhalation injury, Baux, age, and ABSI in the validation set **(J)** The calibration curve of the nomogram in the validation set. **(K)** ROC curve of the nomogram in the validation set. **(L, M)**. In the decision curve of the validation set's nomogram, the risk cutoff value is the horizontal axis, and the larger the vertical axis, the better the prediction performance. Nomoram's risk score has the best predictive power.

binding activity (30). As illustrated in Figure 9B, *CD69* and *SATB1* could form ligands primarily through hydrogen bonding or hydrophobic interaction. Cyclosporin, JQ1, and Decitabine performed better than the other two compounds for *CD69*. However, the binding energy of all 5 compounds was less than -5.00 kcal/mol for *SATB1*, which indicates weak binding activity (Table 3). The docking results could help validate the regulatory relationship between the target and the ligand.

Validation expression of key genes

In the microarray group, *CD69* was significantly down-regulated at five time periods (0-24h, 24-72h, 72h-7d, 7d-30d, >30d), as was *SATB1*. In the PCR group, *SATB1* was significantly down-regulated at five time periods (0-24h, 24-72h, 72h-7d, 7d-30d, >30d), while there was no significant difference between burns and healthy controls at 24-72h and 30d (Figures 10A–J).

TABLE 2 Univariate and multivariate logistic regression for risk score and clinical features.

Variables	Univariate analysis			Multivariate analysis		
	P	OR	95% CI	P	OR	95% CI
Risk_score	0.049	2.324	(1.003-5.383)	0.024	6.286	(0.88-44.9)
INJURY_INHALATION	0.887	1.154	(0.161-8.274)	–	–	–
TBSA	0.024	1.054	(0.986-1.127)	–	–	–
HOSPITAL TIME	0.696	1.003	(0.989-1.017)	–	–	–
SEX	0.999	–	–	–	–	–
AGE	0.622	0.947	(0.761-1.177)	–	–	–
HOURS POST INJURY	0.212	0.987	(0.967-1.008)	–	–	–
Baux	0.503	1.069	(0.88-1.299)	–	–	–
ABSI	0.823	1.258	(0.169-9.357)	–	–	–

Discussion

Infection and sepsis are the leading causes of death in burn patients who are often accompanied by viral infections, especially those with immunosuppression (31). However, the diagnostic, therapeutic, and prognostic value associated with the virus remains underestimated because burn patients are accompanied by fever, damaged skin structure, and immune system disturbances, which makes the virus infection less noticeable (3).

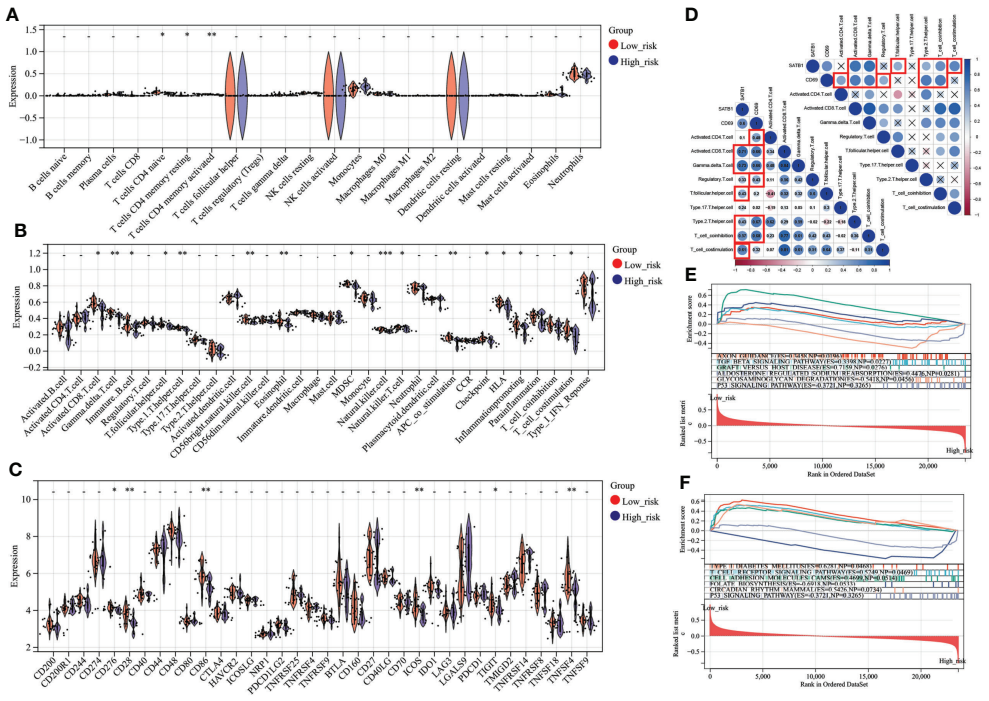

FIGURE 8
Immune analysis grouped by different risk scores **(A)** Comparison of 22 immune cells between different risk score groups. The vertical axis represents the proportion of immune cells. Cells with $P < 0.05$ were considered to be different between groups. **(B)** Comparison of immune cell and immune function scores between different risk score groups. The vertical axis is the rating. Cells with $P < 0.05$ were considered to be different between groups. **(C)** Comparison of immune checkpoint-related gene expression between different risk score groups. The vertical axis represents the gene expression level. Genes with $P < 0.05$ were considered to be different between groups. **(D)** Key genes, correlation analysis with T cell number and function. In the bottom left plot, blue represents a positive correlation, and red is a negative correlation. $P > 0.05$ is drawn as "×" in the upper right corner. Correlation coefficients > 0.4 and $P < 0.05$ are highlighted with red lines. $P < 0.05$:*, $P < 0.01$:**, $P < 0.001$:***. **(E, F)**. In the results of GSEA, different colors represent enriched pathways, and ES > 0 indicates that the genes of the low-risk group are enriched in this pathway, and ES < 0 means that the genes of the high-risk group are enriched in this pathway.

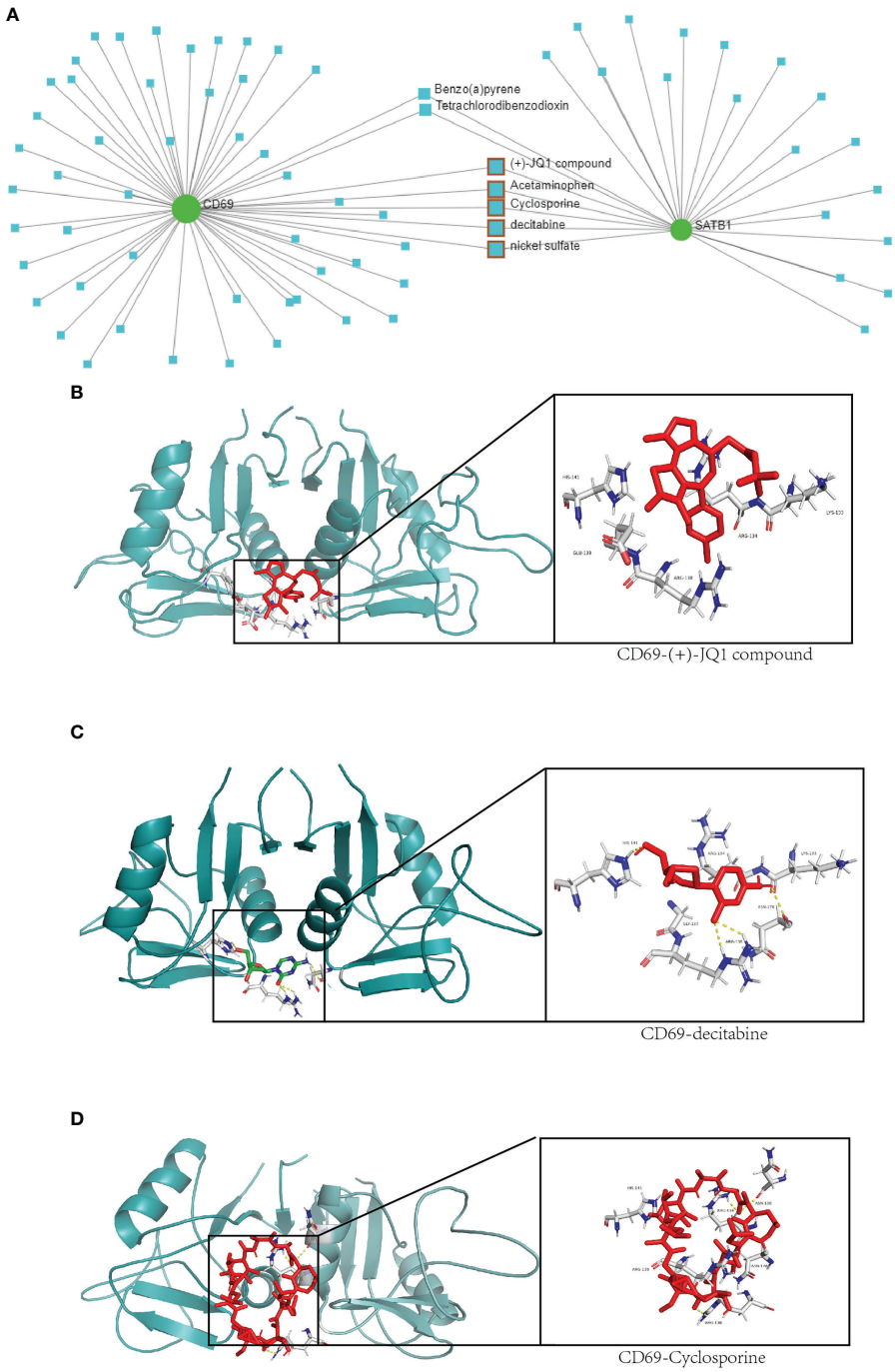

FIGURE 9
Drug network and molecular docking. **(A)** Compounds that may act on *CD69* and *SATB1* genes are predicted in the network analysis database. The compounds with therapeutic effects are selected by the red squares. **(B–D)** Molecular docking of *CD69* and JQ1, decitabine and cyclosporine compounds. The protein structure of *CD69* is in green, and the structure of the compound and its hydrogen-bonding site with *CD69* is on the right.

In this study, we performed a machine learning algorithm, consensus clustering, with hallmarks (related to HSV, CMV, HPV, VZV, and EBV) to divide burn patients into two virus molecular patterns (C1 vs. C2). In follow-up studies, significant differences in enrichment analysis, the ratio of immune cells, and clinical features were found between C1 and C2. It means there are different viral infection response profiles between C1 and C2 patients. In the C1 group, genes were significantly enriched in

TABLE 3 Main parameters of molecular docking of key genes and compounds, including binding energies and hydrogen bonding and hydrophobic interaction sites.

	CD69			SATB1		
	Score (kcal/mol)	hydrogen bonding	hydrophobic interaction	Score (kcal/mol)	hydrogen bonding	hydrophobic interaction
Acetaminophen	142.1	ALA136 GLU139 ARG138	TYR191 HIS141 ARG134 ASN178	262	SER117	LEU118 VAL99 LEU100
Cyclosporin	-5.2	ARG138 ARG134 ASN130	HIS141 ARG138 ASN178	-3.8	GLU97 PHE98 VAL76 VAL99 LEU10 MET113	VAL101 ALA114
Decitabine	-5.6	HIS141 ARG138 ASN178	ARG134 GLY137 LYS133	-3.6	LEU100	LEU118 SER117 GLU97 MET73
JQ1	-6.4	–	HIS141 GLU139 ARG138 ARG134 LYS133	23.6	NONE	SER117 LEU118 GLU97 MET73 LEU100 MET73
NickelSulfate	-1	–	ARG138 GLY137 ARG134 TYR135	-1	NONE	ALA114 VAL99 CYS78 VAL79 GLU97 ALA96

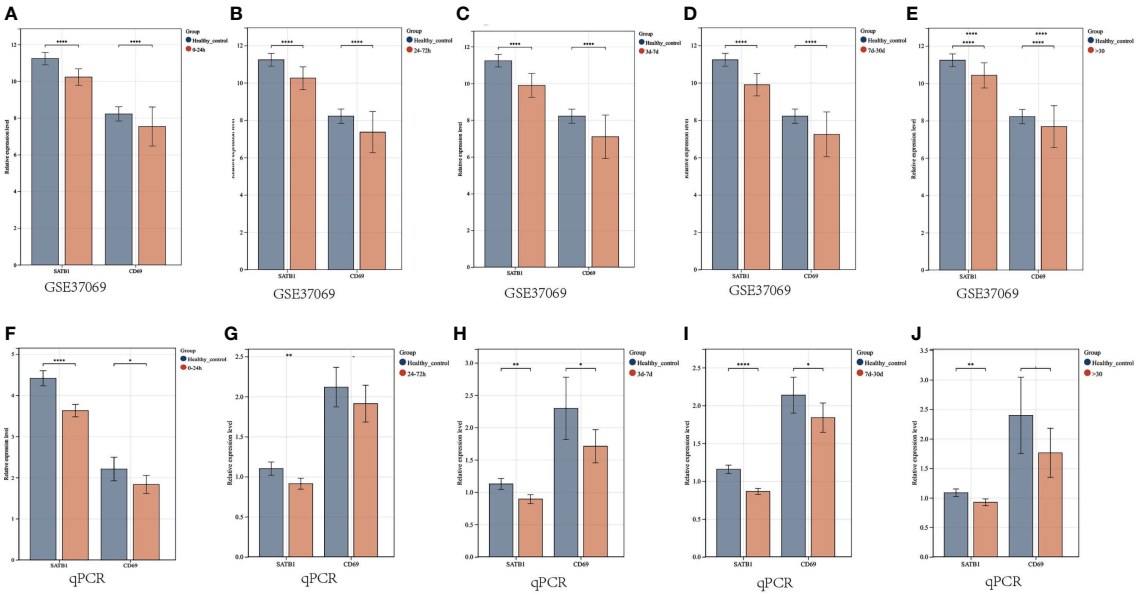

FIGURE 10
Validation of key gene expression. **(A–E)** Relative expression levels of key genes grouped by microarray at different periods (0-24h, 24-72h, 72h-7d, 7d-30d, >30d). The ordinate is the relative expression level, and the abscissa is the gene. Red bars are burn patients, and blue are normal controls. **(F–J)** Relative expression levels of key genes in PCR groups at different periods. $P < 0.05$:*, $P < 0.01$:**, $P < 0.001$:***, P>0.05: ns.

INTESTINAL_IMMUNE_NETWORK_FOR_IGA_PRODUCTION. The immune capacity of the intestinal mucosa is significantly reduced after burns. First, burns can lead to severe dysbiosis of the intestinal microbiota, reducing beneficial bacteria and increasing opportunistic pathogens (32). Secondly, the function of the intestinal mucosal barrier was damaged after burns, and bacteria invaded the blood from the intestine to induce sepsis (33). CMV latency occurs within the bone marrow, mainly within the monocyte/granulocyte progenitor cells (34), and the rate of CMV reactivation in burn patients varies from 55% to 71% (35). CMV infection reduces the immune response and exacerbates susceptibility to this bacteria (36). Our experimental results reveal the possibility of interaction between viral infection and intestinal mucosal immunity, and it will be interesting to explore further whether viral infection can exacerbate intestinal mucosal immune abnormalities.

"T_CELL_RECEPTOR_SIGNALING_PATHWAY" has been enriched in C1 groups. In addition, plasma cells, Tregs, monocytes, neutrophils, CD8 T cells, CD4 T cells, NK cells, and dendritic cells were different between VRGMPGs. After severe burns, the immune system fluctuates violently, which can generally be summarized as excessive activation of innate immune cells causing extensive inflammatory responses and immunosuppression caused by impaired adaptive immune cell function and apoptosis (37). Innate immune cells such as monocytes, neutrophils, and dendritic cells are increasing. Still, in patients with TBSA > 40%, and the ability of monocytes to migrate was damaged (38), the ability of neutrophils to phagocytosis and chemotaxis was reduced (39). The ability of dendritic cells to phagocytosis and antigen presentation was decreased (40).

Furthermore, the activation of adaptive immune response was inhibited. T cells' landscape after burn decreased proliferation, increased apoptosis, and decreased secretion of cytokines, thereby inhibiting adaptive immunity (41, 42). In WGCNA and differential expression analysis, we obtained 133 VRDEGs significantly associated with T cell proliferation and differentiation. In GO terms, VRDEGs were mainly enriched in lymphocyte differentiation, T cell activation, and T cell activation. In KEGG analysis, VRDEGs were mainly enriched in the TCR signaling pathway, Th1, Th2, and Th17 differentiation, and viral protein interaction with cytokine and cytokine receptors. Inhibition of proliferation of T cells (especially Th cells) was a major feature of adaptive immune dysfunction after burns (43). T cells were one of the key cells against VZV infection (44), and viral infection reshapes T cell phenotype (45). Immunosuppression after burns increases the risk of VZV infection, and severe viral infection further weakens immune function and leads to death (31, 46). Inhibition of T cell also increased the risk of HSV infection. HSV induced the down-regulation of Toll-like receptor (TLR)-mediated nuclear factor-κB (NF-κB) cytokine production, which enhances further viral replication, and such patients are more susceptible to bacterial infections (4, 47). Different T cell-related pathways in two VRGMPs may be both the cause and the result of viral infection, and these mechanisms are worthy of further study. Survival and TBSA were significantly correlated with VRGMPs. The above findings illustrated that VRGMPs were associated with abnormal immune function in patients, and related therapeutic targets and prognostic markers had important prospects.

We identified the 64 hub genes related to viral infection based on the PPI network. Further, through RF, LASSO, and logistic analysis, we developed a nomogram composed of two key genes, *CD69* and *SATB1*. We confirmed that the nomogram was an independent prognostic value in multivariate logistic analysis. TBSA, ABSI, and Baux were often used to assess the severity and prognosis of burn patients (48, 49). Some researchers have also constructed prognostic models related to age, gender, length of hospital stay, and inhalation injury. Although these indicators have good prognostic value, they are often evaluated at the time of admission and cannot dynamically track the progression of burns. Changes in immune function cannot be reflected. In both training and validation sets, the AUC values of the nomogram are significantly higher (0.82 and 0.75) than those of TBSA, ABSI, and Baux, and the calibration curve shows the good performance of the nomogram. The DCA curve showed that the prognostic value of the nomogram was significantly better than any other clinical feature.

Patients could be divided into high- and low-risk groups based on the median risk score calculated from the nomogram as a cutoff. We found that CD4+T cell and CD8+T cell expression were lower in the high-risk group, which is consistent with previous findings. In addition, we also found significant differences in immune checkpoint gene expression between different risk groups. Immune checkpoint therapy was of great value in improving patient immune function and has been extensively studied in sepsis but is still unclear in severe burns. PD-L1 expression was upregulated in neutrophils and monocytes after severe burn, as was PD-1 co-inhibitory receptor expression on T cells (50, 51), which may be an important mechanism of T cell suppression. Increased IFN-γ in burn patients may be associated with increased PD-1/PDL1 expression in similar sepsis (52, 53). Anti-PD-L1 antibody therapy improves T cell suppression and survival in burnt mice (54). *PD-1* and *CTLA-4* were also a co-suppressor involved in T cell suppression in sepsis. Preclinical studies have shown that bacterial sepsis leads to increased expression of *CTLA-4* on CD4+ and CD8+ T cells, and anti-CTLA-4 treatment exhibits dose-dependent reductions in CD4+ and CD8+ T lymphocyte apoptosis and improved survival (51, 55). BTLA, another immune checkpoint inhibitor, has been associated with increased morbidity and mortality in preclinical studies (56). Increased BTLA expression on circulating CD4+ T cells in sepsis patients was associated with nosocomial infection. In a CLP mouse model of sepsis, *BTLA*

knockout mice had reduced bacterial numbers, reduced organ damage markers, and improved survival (57). Immune checkpoint inhibitors have enormous value in treating burn patients with immunosuppression and sepsis. However, the current clinical efficacy is still not good, which is related to the lack of effective targets (58). Our study identified potential immune checkpoint genes in burn patients with different VRGMPs, such as *CD28*, *CD86*, *CD276*, *ICOS*, *TIGIT*, and *TNFSF4*, which were of great value for the development of new immunotherapy targets.

Immunosuppression is mainly manifested by enhanced innate immunity, such as excessive activation of neutrophils, and weakened adaptive immune responses, such as T cell apoptosis in burn patients. *CD69* and *SATB1* were significantly differentially expressed between burn patients and healthy adults. Our correlation analysis showed that its expression pattern had an important relationship with γδ T-cells, CD4/8 T cells, Th2 cells, and T cell co-inhibition.

CD69 is a member of the C-type lectin superfamily. Once activated, *CD69* acts as a co-stimulatory molecule for T cell activation and proliferation. In burn patients, *CD69* expression was suppressed on αβ T cells, but increased on γδ T-cells in the burn wound (59). The role of *CD69* on T cell differentiation is multifaceted. Activated γδ T-cells can induce T cell subtypes to differentiate into Th2 and Th17 (60), and Th17 can inhibit the differentiation of Th1 cells, which may be an important factor in the imbalance of Th1 and Th2 differentiation after burns, and the imbalance of Th1 and Th2 differentiation is an important cause of immunosuppression. *CD69* significantly correlates with immune disorders, making it important for prognostic significance. In addition, *CD69* is an important target in regulating inflammation and immunity. Knockout of *CD69* can effectively reduce the susceptibility to inflammation caused by Th17 and play an important role for regulating immune response (61). High expression of *CD69* can promote the inhibition of T cell function while blocking *CD69* enhances the immunity of T cells. In addition to mature T cells, *CD69* is indelibly expressed by immature thymocytes, natural killer (NK) cells, monocytes, and neutrophils and is constitutively expressed by mature thymocytes. Activated NK cells also highly express *CD69*. Inhibiting NK cell function can reduce *CD69* expression and improve wound healing (62).

Similarly, high *CD69* expression was found in hyper-activated neutrophils, which mediate suppression of lymphocyte function (63). *CD69* is also associated with viral susceptibility. Activated monocytes highly express *CD69*, and activated monocytes have a higher viral load during virus infection than non-activated monocytes (64). EBV-activated specific cytotoxic T lymphocytes (CTL) highly express *CD69* and can inhibit the proliferation of lymphocytes (65). High expression of *CD69* in burn patients is associated with over-enhanced innate immunity and attenuated adaptive immune response, and this correlation gives it the ability to predict prognosis. At the same time, high *CD69* expression is associated with viral infections and is a promising therapeutic target that can improve immunosuppression in burn patients.

Special AT-rich binding protein-1 (*SATB1*) is a global chromatin organizer capable of activating or repressing gene transcription in mice and humans (66). The role of *SATB1* is pivotal for T-cell development and differentiation, with *SATB1*-knockout mice being neonatally lethal and having dysregulation of Th17 (67, 68). *SATB1*-dependent T cell activation is crucial for the correct differentiation of T cell subtypes, and inhibition of *SATB1* can inhibit Treg cell activation and differentiation (69). Apoptosis of T cells is an important factor leading to post-burn immunosuppression, and immunosuppression-induced infection leads to the death of patients (59). Our study found that *SATB1* was lowly expressed in burn patients, and the expression level of *SATB1* was significantly correlated with prognosis, demonstrating the great prognostic value of *SATB1*. *SATB1* exhibits excellent prognostic value in many diseases due to its close association with T cell development (66). However, there is still no research in the field of burns. Our study identifies the ability of *SATB1* as a prognostic marker in burn patients, and given its association with burn immunosuppression, we consider the results to be of high confidence.

Further study will be promising. Furthermore, *SATB1* is proposed to suppress transcription of *PDCD1*, encoding the immune checkpoint protein 1 (PD-1) (67). In patients with burn sepsis, *PD1* is highly expressed on immune cells, and reversing this high expression is of great help in improving immune function. In our findings, *SATB1* is down-expressed in burn patients, and reversing this underexpression is a promising immunotherapy.

Both *CD69* and *SATB1* may be involved in immunosuppression in burn patients and are promising therapeutic targets. In our study, *CD69* and *SATB1* interacted with decitabine, Cyclosporine, and JQ1. Decitabine is a chemotherapy drug used for hematological tumors. Studies have shown that decitabine can inhibit pro-inflammatory factors, which may help improve the excessive inflammatory response in burns (70). In addition, decitabine can also regulate the differentiation of T cell subtypes. Decitabine could upregulate major histocompatibility complex class I-related chains B and UL16-binding protein 1 expression, and combination treatment involving γδ T cell immunotherapy and decitabine could be used to enhance the cytotoxic killing of osteosarcoma cells by γδ T cells (71). In general, its application in burns is rare, and relevant research will be of great significance. Cyclosporine is a potent immunomodulatory agent with an increasing number of clinical applications. Its major mode of action is inhibiting the production of cytokines involved in the regulation of T-cell activation (72). Cyclosporine can inhibit *CD69*-mediated T cell activation and maturation (69), which may help regulate T cell differentiation disorders (73). However, it should be noted that systemic administration of cyclosporine can significantly suppress the immune response, which in turn induces more serious infections (31). Therefore, it

is necessary to develop more precise treatment methods to explore further the therapeutic value of Cyclosporine in burn patients with immunosuppression. The Bromo- and Extra-terminal domain (BET) signaling pathway plays an important role in cell proliferation, immune responses, and pro-inflammatory events. The bromodomain inhibitor JQ1, a first-in-class potent and selective inhibitor of the Bromodomain-containing protein 4 (BRD4) signaling pathway, is widely used for various diseases (74). In sepsis, JQ1 protects the intestinal mucosal barrier and reduces levels of pro-inflammatory cytokines IL6, IL1β and IL18 (75). Over-activation of Th17 can inhibit Th1 cells (impaired in burn immunosuppression), while JQ1 impairs p300-mediated RORγt acetylation in human Th17 cells (76), which is expected to enhance the differentiation and proliferation of Th1 cells. However, JQ1 can also inhibit the function of Th1 cells from secreting IFN-γ (77). Therefore, the recovery of immune function by JQ1 is complicated, and further studies on its role in immunosuppression in burns are needed.

Viral infection in burn patients is often insidious and often misdiagnosed clinically. However, viral infection can profoundly affect the immune system of burn patients, but the crosstalk between viral infection and the immune system is currently unclear. Our study is the first to identify VRGMP in burn patients by machine learning and fully explore the differences in immune cells, immune scores, and enrichment pathways between VRGMPGs. Our study found significant differences in the activation and differentiation of T cells, especially Th cells, between VRGMPGs, which may be vital clues for diagnosis, treatment, and prognostic biomarkers. In addition, the dysfunction of Th cells is of great significance in burn patients. We believe that viral infection may affect the body's immunity by disturbing the function of Th cells, which promotes the development of immunosuppression. Therefore, genes associated with viral molecular patterns have important prognostic and therapeutic value. We developed a reliable nomogram based on VRGs with significantly better predictive power than traditional burn indicators such as TBSA, ABSI, and Baux.

Furthermore, we predicted by network analysis and molecular docking that drugs targeting *CD69* and *SATB1* have important links to immunosuppression in burn patients. Our study also has certain limitations. First, although we identified genes associated with prognosis, the samples lacked clinical information on whether the patients were infected with the virus. If such information is available, we can construct a transcriptome-based virus diagnostic nomogram, which is important for discovering occult viral infections. Second, our study found a correlation between T cells, especially Th cells, and viral infection, but more cell and animal experiments are needed to explore the exact mechanism, which is useful for studying the mechanism between viral infection and burn immunosuppression significantly. Finally, we fully evaluated the possibility of immune checkpoint target genes and key genes as targets, which will greatly help the treatment of burn immunosuppression if they can be verified in further experiments. Overall, this study provides an overlooked perspective on post-burn viral infection and fully discusses its potential to interact with the immune system. We identified nomograms with strong prognostic, and predictive power and developed related drug targets, which have important guiding significance for future research on burn virus infection.

Conclusion

We identified two VRGMPs in burn patients with significantly different T-cell proliferation-differentiation-related gene expression patterns and T-cell ratios. We constructed a nomogram including *CD69* and *SATB1* with stronger prognostic efficacy than common clinical indicators such as ABSI, TBSA, and Baux. In addition, we identified possible immune checkpoint inhibitor targets and immunotherapy drugs, Cyclosporin, JQ1, and Decitabine.

Data availability statement

The datasets presented in this study can be found in online repositories. The names of the repository/repositories and accession number(s) can be found below: https://www.ncbi.nlm.nih.gov/geo/, GSE19743, GSE77791, GSE37069, GSE26440.

Ethics statement

Ethical approval was obtained from the Ethics Committee of Xi'an Ninth Hospital (202268).

Author contributions

PW, ZZ and RL: Consulted the literature and prepared materials. PW, ZZ, RL, JML, XZ, LJ, YW and XD: Experimented and analysed the data. PW and ZZ: Drawn up the manuscript. HX: Conceived and designed the study. HX: Financial support and final approval of the manuscript. All authors contributed to the article and approved the submitted version.

Funding

Key Research and Development Plan of Shaanxi Province, Grant/Award Number: S2021-YF-YBSF-0936. Open Project of

Provincial Key Laboratory of Union Hospital Affiliated to Fujian Medical University in 2020, Grant/Award Number: XHZDSYS202004. Xi'an Health Commission Fund Project, Grant/Award Number: 2020yb21; 2022yb03; 2022yb04; 2022yb05. China Red Cross Foundation Xu Rongxiang Regenerative Life Public Welfare Fund Research Project, Grant/Award Number: RXRL2021-05.

Acknowledgments

We would like to thank the staff of the Department of Burns and Plastic and Cosmetic Surgery, the Ninth Affiliated Hospital of Xi'an Jiaotong University for their help in this study.

Conflict of interest

The authors declare that the research was conducted in the absence of any commercial or financial relationships that could be construed as a potential conflict of interest.

Publisher's note

References

1. Leigh J, John O, Fischer F, Rabiee N, Mirzaei M, Abbafati C, et al. Global burden of 369 diseases and injuries in 204 countries and territories, 1990-2019: A systematic analysis for the global burden of disease study 2019. *Lancet* (2020) 396:1204–22. doi: 10.1016/S0140-6736(20)30925-9

2. Lionelli GT, Pickus EJ, Beckum OK, Decoursey RL, Korentager RA. A three decade analysis of factors affecting burn mortality in the elderly. *Burns* (2005) 31:958–63. doi: 10.1016/j.burns.2005.06.006

3. Baj J, Korona-Głowniak I, Buszewicz G, Forma A, Sitarz M, Teresiński G. Viral infections in burn patients: A state-Of-The-Art review. *Viruses 12* (2020) 12 (11):1315. doi: 10.3390/v12111315

4. Daubeuf S, Singh D, Tan Y, Liu H, Federoff HJ, Bowers WJ, et al. HSV ICP0 recruits USP7 to modulate TLR-mediated innate response. *Blood* (2009) 113:3264–75. doi: 10.1182/blood-2008-07-168203

5. Sen S, Szoka N, Phan H, Palmieri T, Greenhalgh D. Herpes simplex activation prolongs recovery from severe burn injury and increases bacterial infection risk. *J burn Care Res* (2012) 33:393–7. doi: 10.1097/BCR.0b013e3182331e28

6. Norvell JP, Blei AT, Jovanovic BD, Levitsky J. Herpes simplex virus hepatitis: an analysis of the published literature and institutional cases. *Liver Transplant* (2007) 13:1428–34. doi: 10.1002/lt.21250

7. Ellul M, Solomon T. Acute encephalitis - diagnosis and management. *Clin Med* (2018) 18:155–9. doi: 10.7861/clinmedicine.18-2-155

8. Kishawi D, Wozniak AW, Mosier MJ. TBSA and length of stay impact quality of life following burn injury. *Burns* (2020) 46:616–20. doi: 10.1016/j.burns.2019.09.007

9. Yoshimura Y, Saitoh D, Yamada K, Nakamura T, Terayama T, Ikeuchi H, et al. Comparison of prognostic models for burn patients: A retrospective nationwide registry study. *Burns* (2020) 46:1746–55. doi: 10.1016/j.burns.2020.10.008

10. Hur J, Yang HT, Chun W, Kim JH, Shin SH, Kang HJ, et al. Inflammatory cytokines and their prognostic ability in cases of major burn injury. *Ann Lab Med* (2015) 35:105–10. doi: 10.3343/alm.2015.35.1.105

11. Barrow RE, Spies M, Barrow LN, Herndon DN. Influence of demographics and inhalation injury on burn mortality in children. *Burns* (2004) 30:72–7. doi: 10.1016/j.burns.2003.07.003

12. Schwacha MG, Holland LT, Chaudry IH, Messina JL. Genetic variability in the immune-inflammatory response after major burn injury. *Shock (Augusta Ga.)* (2005) 23:123–8.10.1097/01.shk.0000148073.19717.a9

13. Thongprayoon C, Kaewput W, Kovvuru K, Hansrivijit P, Kanduri SR, Bathini T, et al. Promises of big data and artificial intelligence in nephrology and transplantation. *J Clin Med 9* (2020) 9(4):1107. doi: 10.3390/jcm9041107

14. MacEachern SJ, Forkert ND. Machine learning for precision medicine. *Genome* (2021) 64:416–25. doi: 10.1139/gen-2020-0131

15. Jiang Z, Bo L, Xu Z, Song Y, Wang J, Wen P, et al. An explainable machine learning algorithm for risk factor analysis of in-hospital mortality in sepsis survivors with ICU readmission. *Comput Methods programs biomedicine* (2021) 204:106040. doi: 10.1016/j.cmpb.2021.106040

16. Nedyalkova M, Madurga S, Simeonov V. Combinatorial K-means clustering as a machine learning tool applied to diabetes mellitus type 2. *Int J Environ Res Public Health* (2021) 18(4):1919. doi: 10.3390/ijerph18041919

17. Lachmann M, Rippen E, Schuster T, Xhepa E, von Scheidt M, Pellegrini C, et al. Subphenotyping of patients with aortic stenosis by unsupervised agglomerative clustering of echocardiographic and hemodynamic data. *JACC. Cardiovasc Interventions* (2021) 14:2127–40. doi: 10.1016/j.jcin.2021.08.034

18. Wilkerson MD, Hayes DN. ConsensusClusterPlus: a class discovery tool with confidence assessments and item tracking. *Bioinf (Oxford England)* (2010) 26:1572–3. doi: 10.1093/bioinformatics/btq170

19. Thongprayoon C, Mao MA, Keddis MT, Kattah AG, Chong GY, Pattharanitima P, et al. Hypernatremia subgroups among hospitalized patients by machine learning consensus clustering with different patient survival. *J Nephrol* (2022) 35:921–9. doi: 10.1007/s40620-021-01163-2

20. Thongprayoon C, Dumancas CY, Nissaisorakarn V, Keddis MT, Kattah AG, Pattharanitima P, et al. Machine learning consensus clustering approach for hospitalized patients with phosphate derangements. *J Clin Med* (2021) 10 (19):4441. doi: 10.3390/jcm10194441

21. Xue Y, Shen J, Hong W, Zhou W, Xiang Z, Zhu Y, et al. Risk stratification of ST-segment elevation myocardial infarction (STEMI) patients using machine learning based on lipid profiles. *Lipids Health Dis* (2021) 20:48. doi: 10.1186/s12944-021-01475-z

22. Chen Z, Wang M, De Wilde RL, Feng R, Su M, Torres-de la Roche LA, et al. A machine learning model to predict the triple negative breast cancer immune subtype. *Front Immunol* (2021) 12:749459. doi: 10.3389/fimmu.2021.749459

23. Tian Y, Yang J, Lan M, Zou T. Construction and analysis of a joint diagnosis model of random forest and artificial neural network for heart failure. *Aging* (2020) 12:26221–35. doi: 10.18632/aging.202405

24. Dai P, Chang W, Xin Z, Cheng H, Ouyang W , Luo A. Retrospective study on the influencing factors and prediction of hospitalization expenses for chronic renal failure in China based on random forest and LASSO regression. *Front Public Health* (2021) 9:678276. doi: 10.3389/fpubh.2021.678276

25. Leek JT, Johnson WE, Parker HS, Jaffe AE, Storey JD. The sva package for removing batch effects and other unwanted variation in high-throughput experiments. *Bioinf (Oxford England)* (2012) 28:882–3. doi: 10.1093/bioinformatics/bts034

26. Xia MD, Yu RR, Chen DM. Identification of hub biomarkers and immune-related pathways participating in the progression of antineutrophil cytoplasmic antibody-associated glomerulonephritis. *Front Immunol* (2021) 12:809325. doi: 10.3389/fimmu.2021.809325

27. Newman AM, Liu CL, Green MR, Gentles AJ, Feng W, Xu Y, et al. Robust enumeration of cell subsets from tissue expression profiles. *Nat Methods* (2015) 12:453–7. doi: 10.1038/nmeth.3337

28. Trott O, Olson AJ. AutoDock vina: improving the speed and accuracy of docking with a new scoring function, efficient optimization, and multithreading. *J Comput Chem* (2010) 31:455–6110.1002/jcc.21334

29. Chu M, Gao T, Zhang X, Kang W, Feng Y, Cai Z, et al. Elucidation of potential targets of San-Miao-San in the treatment of osteoarthritis based on network pharmacology and molecular docking analysis. *Evidence-Based complementary Altern Med eCAM* (2022) 2022:7663212. doi: 10.1155/2022/7663212

30. Dan W, Liu J, Guo X, Zhang B, Qu Y, He Q. Study on medication rules of traditional Chinese medicine against antineoplastic drug-induced cardiotoxicity based on network pharmacology and data mining. *Evidence-Based complementary Altern Med eCAM* (2020) 2020:7498525. doi: 10.1155/2020/7498525

31. Murata K, Hoshina T, Onoyama S, Tanaka T, Kanno S, Ishimura M, et al. Reduction in the number of varicella-zoster virus-specific T-cells in immunocompromised children with varicella. *Tohoku J Exp Med* (2020) 250:181–90. doi: 10.1620/tjem.250.181

32. Wang X, Yang J, Tian F, Zhang L, Lei Q, Jiang T, et al. Gut microbiota trajectory in patients with severe burn: A time series study. *J Crit Care* (2017) 42:310–6. doi: 10.1016/j.jcrc.2017.08.020

33. Luck ME, Herrnreiter CJ, Choudhry MA. Gut microbial changes and their contribution to post-burn pathology. *Shock (Augusta Ga.)* (2021) 56:329–4410.1097/SHK.0000000000001736

34. Prösch S, Döcke WD, Reinke P, Volk HD, Krüger DH. Human cytomegalovirus reactivation in bone-marrow-derived granulocyte/monocyte progenitor cells and mature monocytes. *Intervirology* (1999) 42:308–13. doi: 10.1159/000053965

35. Bordes J, Goutorbe P, Montcriol A, Boret H, Dantzer E, Meaudre E. Cytomegalovirus reactivation in critically ill burn patients: it's time to worry about it! *Crit Care (London England)* (2014) 18:410. doi: 10.1186/cc13742

36. Mansfield S, Grießl M, Gutknecht M, Cook CH. Sepsis and cytomegalovirus: foes or conspirators? *Med Microbiol Immunol* (2015) 204:431–7. doi: 10.1007/s00430-015-0407-0

37. Fang H, Xu L, Zhu F. [Advances in the research of persistent inflammation-immunosuppression-catabolism syndrome in severe burn]. *Zhonghua shao shang za zhi* (2019) 35:548–51. doi: 10.3760/cma.j

38. Wang GQ, Zhang Y, Wu HQ, Zhang WW, Zhang J, Wang GY, et al. Reduction of CD47 on monocytes correlates with MODS in burn patients. *Burns* (2011) 37:94–8. doi: 10.1016/j.burns.2010.04.007

39. Sakuma M, Khan MAS, Yasuhara S, Martyn JA, Palaniyar N. Mechanism of pulmonary immunosuppression: extrapulmonary burn injury suppresses bacterial endotoxin-induced pulmonary neutrophil recruitment and neutrophil extracellular trap (NET) formation. *FASEB J* (2019) 33:13602–16. doi: 10.1096/fj.201901098R

40. Meng Y, Zhao Z, Zhu W, Yang T, Deng X, Bao R. CD155 blockade improves survival in experimental sepsis by reversing dendritic cell dysfunction. *Biochem Biophys Res Commun* (2017) 490:283–9. doi: 10.1016/j.bbrc.2017.06.037

41. Ni Choileain N, MacConmara M, Zang Y, Murphy TJ, Mannick JA, Lederer JA. Enhanced regulatory T cell activity is an element of the host response to injury. *J Immunol (Baltimore Md. 1950)* (2006) 176:225–36. doi: 10.4049/jimmunol.176.1.225

42. Wang SX, Liu QY, Li Y. Lentinan ameliorates burn sepsis by attenuating CD4(+) CD25(+) tregs. *Burns* (2016) 42:1513–21. doi: 10.1016/j.burns.2016.04.003

43. Hargreaves RG, Borthwick NJ, Gilardini Montani MS, Piccolella E, Carmichael P, Lechler RI, et al. Induction of apoptosis following antigen presentation by T cells: anergy and apoptosis are two separate phenomena. *Transplant Proc* (1997) 29:1102–4. doi: 10.1016/S0041-1345(96)00433-2

44. Weinberg A, Levin MJ. VZV T cell-mediated immunity. *Curr topics Microbiol Immunol* (2010) 342:341–57. doi: 10.1007/82_2010_31

45. Sen N, Mukherjee G, Arvin AM. Single cell mass cytometry reveals remodeling of human T cell phenotypes by varicella zoster virus. *Methods (San Diego Calif.)* (2015) 90:85–94. doi: 10.1016/j. ymeth.2015.07.008

46. Wurzer P, Guillory A, Parvizi D, Clayton RP, Branski LK, Kamolz LP, et al. Human herpes viruses in burn patients: A systematic review. *Burns* (2017) 43:25–33. doi: 10.1016/j.burns.2016.02.003

47. Xu H, Su C, Pearson A, Mody CH, Zheng C. Herpes simplex virus 1 UL24 abrogates the DNA sensing signal pathway by inhibiting NF-κB activation. *J Virol* (2017) 91(7):e00025-17. doi: 10.1128/JVI.00025-17

48. Billner M, Reif S, Registry GB, Reichert B. The effect of self-inflicted burns on ABSI score prediction power: A four-year prospective multicenter study of the German burn registry. *Burns* (2021) 48(7):1710–8. doi: 10.1016/j.burns.2021.11.016

49. Saadat GH, Toor R, Mazhar F, Bajani F, Tatebe L, Schlanser V, et al. Severe burn injury: Body mass index and the baux score. *Burns* (2021) 47:72–7. doi: 10.1016/j.burns.2020.10.017

50. Brahmamdam P, Inoue S, Unsinger J, Chang KC, McDunn JE, Hotchkiss RS. Delayed administration of anti-PD-1 antibody reverses immune dysfunction and improves survival during sepsis. *J leukocyte Biol* (2010) 88:233–40. doi: 10.1189/jlb.0110037

51. Chang KC, Burnham CA, Compton SM, Rasche DP, Mazuski RJ, McDonough JS, et al. Blockade of the negative co-stimulatory molecules PD-1 and CTLA-4 improves survival in primary and secondary fungal sepsis. *Crit Care (London England)* (2013) 17:R85. doi: 10.1186/cc12711

52. Rožman P, Švajger U. The tolerogenic role of IFN-γ. *Cytokine Growth factor Rev* (2018) 41:40–53. doi: 10.1016/j.cytogfr.2018.04.001

53. Wilson JK, Zhao Y, Singer M, Spencer J, Shankar-Hari M. Lymphocyte subset expression and serum concentrations of PD-1/PD-L1 in sepsis - pilot study. *Crit Care (London England)* (2018) 22:95. doi: 10.1186/s13054-018-2020-2

54. Patil NK, Luan L, Bohannon JK, Hernandez A, Guo Y, Sherwood ER. Frontline science: Anti-PD-L1 protects against infection with common bacterial pathogens after burn injury. *J leukocyte Biol* (2018) 103:23–33. doi: 10.1002/JLB.5HI0917-360R

55. Inoue S, Bo L, Bian J, Unsinger J, Chang K, Hotchkiss RS. Dose-dependent effect of anti-CTLA-4 on survival in sepsis. *Shock (Augusta Ga.)* (2011) 36:38–44. doi: 10.1097/SHK.0b013e3182168cce

56. Shubin NJ, Chung CS, Heffernan DS, Irwin LR, Monaghan SF, Ayala A. BTLA expression contributes to septic morbidity and mortality by inducing innate inflammatory cell dysfunction. *J leukocyte Biol* (2012) 92:593–603. doi: 10.1189/jlb.1211641

57. Shubin NJ, Monaghan SF, Heffernan DS, Chung CS, Ayala A. B and T lymphocyte attenuator expression on CD4+ T-cells associates with sepsis and subsequent infections in ICU patients. *Crit Care (London England)* (2013) 17:R276. doi: 10.1186/cc13131

58. Blears E, Sommerhalder C, Toliver-Kinsky T, Finnerty CC, Herndon DN. Current problems in burn immunology. *Curr problems Surg* (2020) 57:100779. doi: 10.1016/j.cpsurg.2020.100779

59. Rani M, Schwacha MG. The composition of T-cell subsets are altered in the burn wound early after injury. *PloS One* (2017) 12:e0179015. doi: 10.1371/journal.pone.0179015

60. Rani M, Zhang Q, Schwacha MG. Burn wound γδ T-cells support a Th2 and Th17 immune response. *J burn Care Res* (2014) 35:46–53. doi: 10.1097/01.bcr.0000440705.91099.cc

61. González-Amaro R, Cortés JR, Sánchez-Madrid F, Martín P. Is CD69 an effective brake to control inflammatory diseases? *Trends Mol Med* (2013) 19:625–32. doi: 10.1016/j.molmed.2013.07.006

62. Schneider DF, Palmer JL, Tulley JM, Kovacs EJ, Gamelli RL, Faunce DE. Prevention of NKT cell activation accelerates cutaneous wound closure and alters local inflammatory signals. *J Surg Res* (2011) 171:361–73. doi: 10.1016/j.jss.2010.03.030

63. Sun R, Huang J, Liu L, Yang Y, Song M, Shao Y, et al. [Neutrophils mediate T lymphocyte function in septic mice *via* the CD80/cytotoxic T lymphocyte antigen-4 signaling pathway]. *Zhonghua wei zhong bing ji jiu yi xue* (2021) 33:849–54. doi: 10.3760/cma.j.cn121430-20210113-00047

64. Munsaka SM, Agsalda M, Troelstrup D, Hu N, Yu Q, Shiramizu B. Characteristics of activated monocyte phenotype support R5-tropic human immunodeficiency virus. *Immunol immunogenetics Insights* (2009) 1:15–20. doi: 10.4137/III.S2011

65. Wilkie GM, Taylor C, Jones MM, Burns DM, Turner M, Kilpatrick D, et al. Establishment and characterization of a bank of cytotoxic T lymphocytes for immunotherapy of epstein-barr virus-associated diseases. *J immunotherapy (Hagerstown Md. 1997)* (2004) 27:309–16. doi: 10.1097/00002371-200407000-00007

66. Zelenka T, Spilianakis C. SATB1-mediated chromatin landscape in T cells. *Nucleus (Austin Tex.)* (2020) 11:117–31. doi: 10.1080/19491034.2020.1775037

67. Nüssing S, Koay HF, Sant S, Loudovaris T, Mannering SI, M. Lappas DUY, et al. Divergent SATB1 expression across human life span and tissue compartments. *Immunol Cell Biol* (2019) 97:498–511. doi: 10.1111/imcb.12233

68. Yasuda K, Kitagawa Y, Kawakami R, Isaka Y, Watanabe H, Kondoh G, et al. Satb1 regulates the effector program of encephalitogenic tissue Th17 cells in chronic inflammation. *Nat Commun* (2019) 10:549. doi: 10.1038/s41467-019-08404-w

69. Kitagawa Y, Ohkura N, Kidani Y, Vandenbon A, Hirota K, Kawakami R, et al. Guidance of regulatory T cell development by Satb1-dependent super-enhancer establishment. *Nat Immunol* (2017) 18:173–83. doi: 10.1038/ni.3646

70. Han P, Hou Y, Zhao Y, Liu Y, Yu T, Sun Y, et al. Low-dose decitabine modulates T-cell homeostasis and restores immune tolerance in immune thrombocytopenia. *Blood* (2021) 138:674–88. doi: 10.1182/blood.2020008477

71. Wang Z, Wang Z, Li S, Li B, Sun L, Li H, et al. Decitabine enhances Vγ9Vδ2 T cell-mediated cytotoxic effects on osteosarcoma cells *via* the NKG2DL-NKG2D axis. *Front Immunol* (2018) 9:1239. doi: 10.3389/fimmu.2018.01239

72. Russell G, Graveley R, Seid J, al-Humidan AK, Skjodt H. Mechanisms of action of cyclosporine and effects on connective tissues. *Semin Arthritis rheumatism* (1992) 21:16–22. doi: 10.1016/0049-0172(92)90009-3

73. Conde M, Montaño R, Moreno-Aurioles VR, Ramirez R, Sanchez-Mateos P, Sanchez-Madrid F, et al. Anti-CD69 antibodies enhance phorbol-dependent glucose metabolism and Ca2+ levels in human thymocytes. antagonist effect of cyclosporin a. *J leukocyte Biol* (1996) 60:278–84. doi: 10.1002/jlb.60.2.278

74. Shi X, Liu C, Liu B, Chen J, Wu X, Gong W. JQ1: A novel potential therapeutic target. *Die Pharmazie* (2018) 73:491–3. doi: 10.1691/ph.2018.8480

75. Chen L, Zhong X, Cao W, Mao M, Li W, Yang H, et al. JQ1 as a BRD4 inhibitor blocks inflammatory pyroptosis-related acute colon injury induced by LPS. *Front Immunol* (2021) 12:609319. doi: 10.3389/fimmu.2021.609319

76. Wang X, Yang Y, Ren D, Xia Y, He W, Wu Q, et al. JQ1, a bromodomain inhibitor, suppresses Th17 effectors by blocking p300-mediated acetylation of RORγt. *Br J Pharmacol* (2020) 177:2959–73. doi: 10.1111/bph.15023

77. Gibbons HR, Mi DJ, Farley VM, Esmond T, Kaood MB, Aune TM. Bromodomain inhibitor JQ1 reversibly blocks IFN-γ production. *Sci Rep* (2019) 9:10280. doi: 10.1038/s41598-019-46516-x

frontiers | Frontiers in Immunology

TYPE Original Research
PUBLISHED 01 December 2022
DOI 10.3389/fimmu.2022.1053059

OPEN ACCESS

EDITED BY
Junji Xing,
Houston Methodist Research Institute, United States

REVIEWED BY
Xing Liu,
Nanjing Agricultural University, China
Fusheng Si,
Shanghai Academy of Agricultural Sciences, China

*CORRESPONDENCE
Zhuoran Li
lizhuoran85@126.com
Huachun Li
li_huachun@hotmail.com

†These authors have contributed equally to this work and share first authorship

SPECIALTY SECTION
This article was submitted to Viral Immunology, a section of the journal Frontiers in Immunology

RECEIVED 25 September 2022
ACCEPTED 15 November 2022
PUBLISHED 01 December 2022

CITATION
Lu D, Li Z, Zhu P, Yang Z, Yang H, Li Z, Li H and Li Z (2022) Whole-transcriptome analyses of sheep embryonic testicular cells infected with the bluetongue virus. *Front. Immunol.* 13:1053059. doi: 10.3389/fimmu.2022.1053059

Whole-transcriptome analyses of sheep embryonic testicular cells infected with the bluetongue virus

Danfeng Lu[1†], Zhuoyue Li[2†], Pei Zhu[3], Zhenxing Yang[3], Heng Yang[3,4], Zhanhong Li[3], Huachun Li[3*] and Zhuoran Li[3*]

[1]School of Medicine, Kunming University, Kunming, Yunnan, China, [2]School of Medicine and Pharmacy, Ocean University of China, Qingdao, Shandong, China, [3]Yunnan Tropical and Subtropical Animal Virus Diseases Laboratory, Yunnan Animal Science and Veterinary Institute, Kunming, Yunnan, China, [4]College of Agriculture and Life Sciences, Kunming University, Kunming, Yunnan, China

Introduction: bluetongue virus (BTV) infection triggers dramatic and complex changes in the host's transcriptional profile to favor its own survival and reproduction. However, there is no whole-transcriptome study of susceptible animal cells with BTV infection, which impedes the in-depth and systematical understanding of the comprehensive characterization of BTV-host interactome, as well as BTV infection and pathogenic mechanisms.

Methods: to systematically understand these changes, we performed whole-transcriptome sequencing in BTV serotype 1 (BTV-1)-infected and mock-infected sheep embryonic testicular cells, and subsequently conducted bioinformatics differential analyses.

Results: there were 1504 differentially expressed mRNAs, 78 differentially expressed microRNAs, 872 differentially expressed long non-coding RNAs, and 59 differentially expressed circular RNAs identified in total. Annotation from the Gene Ontology, enrichment from the Kyoto Encyclopedia of Genes and Genomes, and construction of competing endogenous RNA networks revealed differentially expressed RNAs primarily related to virus-sensing and signaling transduction pathways, antiviral and immune responses, inflammation, and development and metabolism related pathways. Furthermore, a protein-protein interaction network analysis found that BTV may contribute to abnormal spermatogenesis by reducing steroid biosynthesis. Finally, real-time quantitative PCR and western blotting results showed that the expression trends of differentially expressed RNAs were consistent with the whole-transcriptome sequencing data.

Discussion: this study provides more insights of comprehensive characterization of BTV-host interactome, and BTV infection and pathogenic mechanisms.

KEYWORDS

Bluetongue virus, sheep embryonic testicular cells, RNA sequencing, ceRNA network, protein-protein interaction network

Introduction

Bluetongue (BT) is one of the major arboviral diseases of ruminants, especially sheep, and manifests as various clinical symptoms in sick animals, ranging from subclinical symptoms to lethal hemorrhagic fever. It is estimated that BT is responsible for up to US$ 3 billion in annual economic losses in morbidity, mortality, production, reproduction, and animal-related trade restrictions (1, 2). Thus, the World Organization for Animal Health (OIE) listed BT as a notifiable disease. Bluetongue virus (BTV), the prototype virus of the *Orbivirus* genus within the *Reoviridae* family, is the pathogen of BT, which is mainly transmitted by *Culicoides* spp. midges. The genome of BTV is constituted by 10 segments of double-stranded RNAs (dsRNAs; Seg-1 to Seg-10) ranging in length from about 0.9 Kb to 4 Kb, encoding 7 structural proteins (VP1 to VP7) and 5 non-structural proteins (NS1 to NS4 and NS3A), in which VP2 and VP5 are the determinants of the viral serotypes (3). In total, 28 serotypes of BTV have been recognized globally, and additional novel serotypes have been identified continuously (4–6). There are 13 serotypes of BTV prevalent in China, including BTV-1, -2, -3, -4, -5, -7, -9, -12, -15, -16, -21, -24 and putative BTV-29 (5). The BTV-1 strain (Y863), in particular, caused the first recorded outbreak of BT in Shizong County, Yunnan <cp>Province</cp>, in 1979 (7). Furthermore, the Chinese national BTV surveillance program from 2013 to 2017 revealed that BTV was widely prevalent in Southern China, and Eastern-Western topotype reassorted strains were also derived through the genomic segments reassortment, potentially endangering animal husbandry safety production (5, 7). Therefore, an in-depth understanding of the pathogenesis of BTV and then exploring new strategies for BT prevention and control still rely on studying the interactions between BTV and the hosts.

Previous studies have pointed out that BTV replicates principally in endothelial cells and mononuclear phagocytic cells of sheep. However, it can also multiply efficiently in a variety of mammalian cell lines, such as primary sheep testicular (ST) cells, a cloned derivative baby hamster kidney (BSR) cells, and human cervical epithelial carcinoma (HeLa) cells, and subsequently release a large number of viral particles to trigger cytopathic effects (CPEs) in these infected cells, which is characterized by rounding, swelling, granular degeneration and detachment of cells (8–11). The infection and multiplication processes of viruses involve complex virus-host interactions. BTV's success stems from its ability to actively manipulate antiviral defense, effectively subvert or take advantage of the host intracellular mechanisms, reform the environment of host cells by employing a set of virulence factors, and eventually produce virus-specific components. For example, BTV utilizes its nonstructural protein NS4 to antagonize the host interferon (IFN) response, downregulate the transcription levels of type I IFN (IFN-I) and IFN-stimulated genes (*ISGs*), and contribute to the virulence of BTV decisively (12). In addition, BTV regulated a series of host signaling pathways, such as mitogen-activated protein kinase (MAPK), phosphatidylinositide 3-kinase (PI3K)-serine/threonine kinase (Akt), and nuclear factor-kappa B (NF-κB) signaling pathways, by altering the expression profile of host microRNAs (miRNAs) (10).

Recently, lots of studies have reported that long noncoding RNAs (lncRNAs) and circular RNAs (circRNAs) function in the infection and replication processes of viruses through modifying the transcriptomic responses of hosts and participating in various cellular processes, including but not limited to antiviral immunity, metabolic pathways, and cellular apoptosis (13, 14). For instance, circRNAs serves as sponges of miRNAs and constitute an interactive competing endogenous RNA (ceRNA) network with miRNAs and mRNAs to modulate RNA transcription and protein production. Viruses destroy or utilize the networks, which can significantly influence the viral life cycle and pathogenicity (14). However, studies on the transcriptional profiles of BTV-infected cells have either been conducted in human cell lines or have only sequenced the miRNAs/mRNAs sector (10, 12, 15). There is no whole-transcriptome study of susceptible animal cells with BTV infection, which impedes the in-depth and systematical understanding of the comprehensive characterization of BTV-host interactome, as well as BTV infection and pathogenic mechanisms.

In this study, we performed whole-transcriptome sequencing in BTV-1-infected sheep embryonic testicular cells, conducted a series of bioinformatics analyses, clearly portrayed the RNAs expression profile underlying responses to BTV infection at a critical time point, and finally gained some insights into the basic molecular mechanisms of host-virus interactions.

Materials and methods

Cell culture and infection

Sheep embryonic testicular (OA3.Ts) cells were purchased from the Kunming Branch of the National Experimental Cell Resource Sharing Platform, Chinese Academy of Science. The cells were cultured in F12: DMEM =1: 1 medium supplemented with 10% FBS at 37 °C/5% CO_2. OA3.Ts cells were seeded in 10 cm dishes (NEST, China), grown to approximately 80%~90% confluency, and inoculated with the BTV-1 (Y863 strain) with a multiplicity of infection (MOI) of 1. The supernatants were discarded after 1 hour of incubation. OA3.Ts cells were then maintained with F12: DMEM =1: 1 medium supplemented with 1% FBS. The uninfected OA3.Ts cells served as the mock-infected control. The CPEs were observed under a light microscope (Olympus, Japan) at 0, 24 and 48 h post-infection (hpi).

RNA extraction and qualification

Total RNA from each sample was extracted with TRIzol reagent (Invitrogen, USA) according to the manufacturer's instructions. The RNA amount and purity of each sample were quantified using NanoDrop ND-100 (NanoDrop, USA). The RNA integrity was assessed by Bioanalyzer 2100 and RNA 6000 Nano LabChip Kit (Agilent, USA) with RIN number >7.0 and confirmed by electrophoresis with denaturing agarose gel. The extracted RNA was stored at -80 °C until use.

Library construction and sequencing

Poly(A) RNA was purified for two rounds from 2 μg total RNA using Dynabeads Oligo(dT)25-61005 (Thermo Fisher, USA) to construct mRNA library. Approximately 2 μg of total RNA was used to remove ribosomal RNA according to the manuscript of the Ribo-Zero Gold Kit (Epicentre Biotechnologies, USA) to construct lncRNA or circRNA library. The poly(A) RNA and the remaining RNA after ribosomal RNA removal were fragmented into small pieces using Magnesium RNA Fragmentation Module (NEB, USA). The cleaved RNA fragments were reverse-transcribed into cDNA by SuperScript II Reverse Transcriptase (Invitrogen), which was subsequently used to synthesize U-labeled second-stranded DNAs with *E. coli* DNA polymerase I (NEB), RNase H (NEB) and dUTP Solution (Thermo Fisher). An A-base was then added to the blunt ends of each strand, followed by the ligation of indexed adapters. Each adapter contained a T-base overhang for ligating the adapter to the A-tailed fragmented DNA. Next, single- or dual-index adapters were ligated to the fragments, and size selection was performed with AMPure XP beads (Beckman Coulter, USA). After the heat-labile UDG enzyme (NEB) treatment of the U-labeled second-stranded DNAs, the ligated products were amplified with PCR. The average insert size for the final cDNA library was 300 ± 50 bp.

Approximately 1 μg of total RNA was used to prepare the miRNA library following the protocol of TruSeq small RNA Sample Prep Kits (Illumina, USA). Briefly, the miRNA molecules were ligated to a 5' adaptor and a 3' adaptor by T4 RNA ligase (Promega, USA). Subsequently, the adaptor-ligated miRNAs were reverse transcribed into cDNA and PCR amplified. Finally, PCR products were purified and DNA fragments of 150 ± 10 bp (the length of small RNA inserts plus the 5' and 3' adaptors) were quantified following the Solexa sequencing protocol (Illumina). At last, the 2×150 bp paired-end sequencing for mRNA, lncRNA, and circRNA, and the 1×50 bp single-end sequencing for miRNA were performed on Illumina Novaseq 6000 and Illumina Hiseq2500 (LC-Bio Technology Co. Ltd., Hangzhou, China) following the vendor's recommended protocol, respectively. The obtained sequence reads were deposited into the NCBI Gene Expression Omnibus (GEO) database and can be accessed *via* accession numbers GSE213637 and GSE213638.

Bioinformatics analyses

Fastp (v0.14.1) was used to remove the mRNA, lncRNA and circRNA reads that contained adaptor contamination, low-quality bases and undetermined bases and verify the sequence quality (16). Hisat2 (v2.0.4) for mRNA, as well as Bowtie2 (v2.2.5) and Tophat2 (v2.0.13) for lncRNA were used to map reads to the genome of *Ovis aries* (GCA_000298735.1) (17–19). StringTie (v1.3.0) was used to assemble the mapped mRNA and lncRNA reads from each sample, and then the mRNA or lncRNA transcripts from all samples were merged to reconstruct a comprehensive transcript profile using GffCompare (20, 21). Subsequently, transcripts annotated as known mRNAs, known lncRNAs, and less than 200 nt in length were discarded. Coding Potential Calculator (CPC) software (v0.9-r2) and Coding-Non-Coding Index (CNCI) software (v2.0) were unutilized to predict transcripts with coding potential. All transcripts with CPC score <-1 and CNCI score <0 was removed. The remaining transcripts with class code (l, j, o, u, and x) were considered novel lncRNAs (22, 23). The expression levels of mRNAs and lncRNAs were calculated using fragments per kb per million reads (FPKM = [total exon fragments/mapped reads (millions) × exon length (Kb)]) (20).

Bowtie2 (v2.2.5) and Tophat2 (v2.0.13) for circRNA were used to map reads to the *Ovis aries* genome (GCA_000298735.1) (18, 19). The remaining unmapped circRNA reads were further mapped to the genome using Tophat-Fusion (v2.0.12) (24). As for mapped circRNA reads, they firstly were *de novo* assembled to circular using CIRCexploer (v1.1.10) and CircRNA Identifier (CIRI) (v2) (25–27). Then, back-splicing reads were identified in unmapped reads by Tophat-Fusion (v2.0.12) and CIRCexploer (v1.1.10) (24–26). All samples generated unique circular RNAs. Spliced reads per billion mapping (SRPBM) calculated circRNAs expression levels (SRPBM = number of back-spliced junction reads/number of mapped reads × 1,000,000,000).

The miRNA raw data were processed through an in-house program, ACGTA101-miR (v4.2) (LC Science, USA) to remove adapter dimers, junk, low complexities, common RNA families (rRNA, tRNA, snRNA, and snoRNA), repeats, and sequences <18 nt or >26 nt in length were filtered out using Rfam (v13.0) and Repbase Update (28, 29). The 18~26 nt unique reads were mapped to miRNA sequences in miRBase (v22.0) (30). Mapping was also performed on pre-miRNA against *Ovis aries* genomic data (GCA_000298735.1). The unique sequences that aligned to the known miRNA sequences in miRBase (v22.0) were identified as known miRNAs (30). The secondary structure of pre-miRNAs was presented as a hairpin, including 5p- and 3p-derived miRNA. The unique sequences mapping to the other

arm of the pre-miRNA sequences that were not annotated in the miRBase (v22.0) were considered to be 5p- or 3p-derived miRNA candidates (30). In order to find candidate novel miRNAs, the remaining unmapped sequences were compared to the *Ovis aries* genomic sequences (GCA_000298735.1). In order to identify the results of putative miRNAs of *Ovis aries*, all the obtained miRNAs were used to predict the secondary structures using RNAfold software (31).

R package edgeR (v3.14.0) was used to analyze the differentially expressed RNAs (dif-RNAs) (32). The thresholds of $|\log_2$ fold change (FC)| ≥1.0 and *p*-value <0.05 were used to filter out differentially expressed mRNAs (dif-mRNAs), differentially expressed lncRNAs (dif-lncRNAs), and differentially expressed circRNAs (dif-circRNAs), while only the comparisons with *p*-value <0.05 were considered differentially expressed miRNAs (dif-miRNAs) based on normalized deep-sequencing counts. Hierarchical clustering and volcano plot were drawn on the dif-RNAs using the pheatmap R package (v1.0.12) and ggplot2 R package (v3.3.6), respectively (33, 34).

Target gene prediction and functional analyses

To further explore the function of dif-RNAs, potential *cis*-target mRNAs of dif-lncRNAs were predicted (35). The *cis*-targets of dif-lncRNAs were predicted using Blast2GO (v4.0.7) (36). The mRNAs in the dif-lncRNAs' upstream or downstream 100 Kb regions were considered potential *cis*-targets.

The target mRNAs for each dif-miRNAs were predicted using the TargetScan (v5.0) and miRanda (v3.3a) algorithms (37). TargetScan score ≥50 and miRanda energy <-10 were set as thresholds for screening. Finally, the data predicted by both algorithms were combined and the overlaps were analyzed.

Gene Ontology (GO) annotations were performed on dif-mRNAs, and target or host mRNAs of dif-lncRNAs, dif-miRNAs, and dif-circRNAs using gene ontology resource (38). In addition, the Kyoto Encyclopedia of Genes and Genomes (KEGG) enrichment analyses were conducted to understand high-level functions and utilities of biological systems (39). GO bubble diagrams and KEGG scatter diagrams were visualized using the GOplot R package (v1.0.2) and ggplot2 R package (v3.3.6), and all terms with *p*-value <0.05 were considered significantly (34, 40).

ceRNA networks construction

In constructing the lncRNA- and circRNA-miRNA-mRNA axes, the most meaningfully interacting pairs were selected and presented according to the following criteria: 1) Among miRNA-mRNA interaction pairs, dif-miRNAs and dif-mRNAs were selected when their $|\log_2$ FC| values were ≥1.5 and ≥2.0, respectively. At the same time, the pairs should comply with a standard of TargeScan score ≥50 and miRanda energy <-10; 2) For miRNA-lncRNA interaction pairs, the values of $|\log_2$ FC| were the same as those of miRNA-mRNA pairs; while the TargeScan score ≥80 and miRanda energy <-20 were set as a further filter criterion; 3) As for miRNA-circRNA interaction pairs, the thresholds of $|\log_2$ FC|, TargetScan score, and miRanda energy were consistent with those of miRNA-mRNA pairs. Subsequently, the lncRNA- and circRNA-miRNA-mRNA axes were constructed with miRNAs as the central nodes, and ceRNA networks were built and visually displayed using the ggalluvial R package (v0.12.3) based on these axes (41). The differential transcripts of mRNAs involved in the ceRNA networks were performed GO and KEGG analyses. These results were graphically displayed with the GOplot R package (v1.0.2) and ggplot2 R package (v3.3.6), and all terms with *p*-value <0.05 were considered significantly (34, 40).

Protein-protein interaction (PPI) network and module analysis of dif-mRNAs

The interactions between dif-mRNAs encoded proteins were analyzed using the Search Tool for the Retrieval of Interacting Genes/Proteins (STRING) online database (v11.5) (42). The species was set as *Ovis aries* with the interaction score >0.4 selected as the cut-off value. Subsequently, the PPI network was visualized utilizing Cytoscape software (v3.8.2) (43). The Cytoscape's Molecular Complex Detection (MCODE) plugin was applied to extract densely connected modules from the PPI network, with degree cut-off = 2, node score cut-off = 0.2, K-score = 2, and max depth = 100. The downregulated and upregulated mRNAs involved in the PPI network were performed GO and KEGG enrichment and visualized using the ggplot2 R package (v3.3.6), respectively (34). All terms with *p*-value <0.05 were considered significantly.

Real-time quantitative PCR (qRT-PCR)

Real-time qRT-PCR was conducted on an ABI 7500 fast system (Applied Biosystems, USA) using One Step PrimeScript Real Time RT-PCR Kit (Takara Biomedical Technology, China) with extracted total RNA from OA3.Ts cells served as templates to verify the successful infection of BTV-1 (Y863 strain) (44).

In order to validate the expression profile of dif-RNAs, real-time qRT-PCR was performed using PrimeScript RT reagent Kit with gDNA Eraser (Takara Biomedical Technology) and TB Green Premix Ex Taq II (Takara Biomedical Technology) for dif-mRNAs, dif-lncRNAs, and dif-circRNAs, as well as Mir-X miRNA First-Stranded Synthesis Kit (Takara Biomedical Technology) and Mir-X miRNA qRT-PCR TB Green Kit (Takara Biomedical Technology) for dif-miRNAs on an ABI

7500 fast system (Applied Biosystems) according to the manufacturer's instructions. The specific primers were designed using Oligo 7 software or referred to as the reported primers. The primer sequences are shown in Supplementary Table 1. Transcriptional levels of the gene for *β-actin* and *U6* were determined to normalize total RNA input. Relative dif-RNAs expression was evaluated using the $2^{-\Delta\Delta Ct}$ method.

Western blotting (WB)

The infected cells were washed with cold phosphate-buffered saline (PBS) and lysed for 30 min at 4°C in lysis buffer (Beyotime Biotechnology, China) containing protease inhibitor cocktails (BioTool, China). Total protein quantities of the sample supernatants were determined using TaKaRa BCA Protein Assay Kit (Takara Biomedical Technology). Equal amounts (20 μg) of each quantified cell proteins were separated on 10% SDS-PAGE and then transferred onto the PVDF membrane (Millipore, USA). After blocking with 5% bovine serum albumin (BSA) (Sangon Biotech, China) in PBS containing 0.1% Tween (Sangon Biotech), the blots were incubated with Rig-I (D33H10) Rabbit mAb (CST, USA), IκBα (L35A5) Mouse mAb (CST), IKKγ antibody (CST), Caspase-8 (D35G2) Rabbit mAb (CST), Anti-CTGF antibody (Abcam, UK), PIK3IP1 Ab (Affinity Biosciences, China), NS3 (33H7) mouse monoclonal antibody (Ingenasa, Spain), anti-β-tubulin mouse monoclonal antibody (Transgen Biotech, China), and Anti-beta Actin antibody (Abcam) at 4°C overnight, respectively. This was followed by incubation with horseradish peroxidase (HRP)-conjugated goat anti-mouse IgG antibody (Beyotime Biotechnology) or HRP-conjugated goat anti-rabbit IgG antibody (Beyotime Biotechnology). In addition, the immunoreactivity of blots with antibodies was visualized under ChemiScope 3300mini (Clinx, China) using the BeyoECL Plus Detection Kit (Beyotime Biotechnology). The relative optical densities of bands were assessed using ImageJ software (Bethesda, USA) and normalized according to optical densities of corresponding β-tubulin bands.

Statistical analysis

Data were presented as mean ± SD with an error bar representing at least three independent experiments. In addition, the student's t test was performed for statistical analysis with GraphPad Prism 7.0 software (GraphPad Software, USA). Symbols * and ** indicate that the difference between the indicated groups was significant (p-value <0.05) or very significant (p-value <0.01), respectively.

Results

Cells infection and harvest

OA3.Ts cells were infected with BTV-1 at a MOI of 1, and the infection was confirmed by observing CPEs and monitoring virus replication by qRT-PCR and WB at 0, 24 and 48 hpi. As it showed in Figure 1A, no CPE was observed in mock-infected OA3.Ts cells, while the pathological cellular state in the BTV-1-infected group, with cells shrinkage and rounding, could begin to be recognized at 24 hpi, and the CPEs were more obvious at 48 hpi. The results of virus replication were displayed in the form of cycle threshold (Ct) values and viral NS3 protein bands of WB (Figure 1B). The gradual increase in viral replication from 24 hpi to 48 hpi was reflected in decreasing Ct values and increased NS3 protein bands, indicating the development of persistent infection. The OA3.Ts cells at 24 hpi were harvested for whole-transcriptome sequencing.

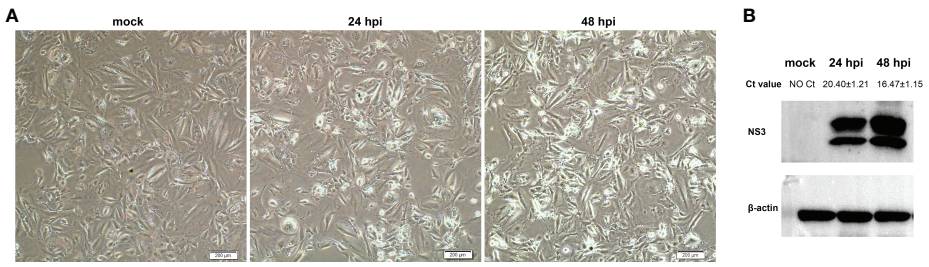

FIGURE 1
Validation of BTV-1 infection in OA3.Ts cells at 0, 24 and 48 dpi. **(A)** CPEs were observed in OA3.Ts cells infected with BTV-1 (Y863 strain) under microscope at 0, 24 and 48 hpi (×4 magnification). Scale bar, 200 μM. **(B)** qRT-PCR and WB were also used to verify the successful infection of BTV-1 (Y863 strain) in OA3.Ts cells. The infection status of BTV-1-infected- and mock-infected groups at different time points was represented by mean Ct values ± SD from three independent experiments. NS3 was detected as control for successful infection, whereas β-actin served as an internal control.

Differential expression profiles analyses

Whole-transcriptome sequencing was applied to profile the expression of mRNAs, miRNAs, lncRNAs, and circRNAs in BTV-1-infected OA3.Ts cells. Overall, 1504 dif-mRNAs, containing 687 upregulated and 817 downregulated mRNAs, were identified in the infected group compared with the mock-infected group (Figure 2A and Supplementary Table 2). According to the screening criteria, 78 dif-miRNAs were determined, of which 45 were transcriptionally increased and 33 were decreased (Figure 2B and Supplementary Table 3). A total of 872 dif-lncRNAs, consisting of 863 novel lncRNAs and 9 known lncRNAs, were obtained, including 748 upregulated and 124 downregulated lncRNAs (Figure 2C and Supplementary Table 4). In addition, the expression levels of 24 circRNAs were increased, and 35 circRNAs were decreased among 59 dif-circRNAs, (Figure 2D and Supplementary Table 5). Hierarchical clustering was performed to generate heatmaps of dif-RNAs, from which it was found that the infected samples could be significantly separated from the mock-infected samples (Figures 3A–D). Moreover, consistent with the previous study conducted in BTV-16-infected peripheral blood mononuclear cells (PBMCs), our study similarly obtained more than 1000 dif-mRNAs; some of the 1504 dif-mRNAs involved in antiviral activities and immune responses also presented high expression levels, including *ISG20*, IFN-induced protein with tetratricopeptide repeats-1 (*IFIT1*) and *IFIT2* (Figure 3A and Supplementary Table 2) (15). Although the number of identified dif-miRNAs was limited, the expression patterns of certain dif-miRNAs were similar to the results of microRNA sequencing in BTV-1 (GS/11 strain)-infected ST cells, such as chi-miR-33b-3p, chi-miR-34c-5p and oar-miR-194_R+1 (Figure 3B and Supplementary Table 3) (10). All these data indicated that the results of the differential expression analyses were reliable.

Functional enrichment analyses of dif-RNAs

To better understand the potential roles of host factors in BTV infection, all dif-RNAs were subjected to GO term classification statistics from the biological processes (BP), cellular components (CC), and molecular function (MF) ontologies.

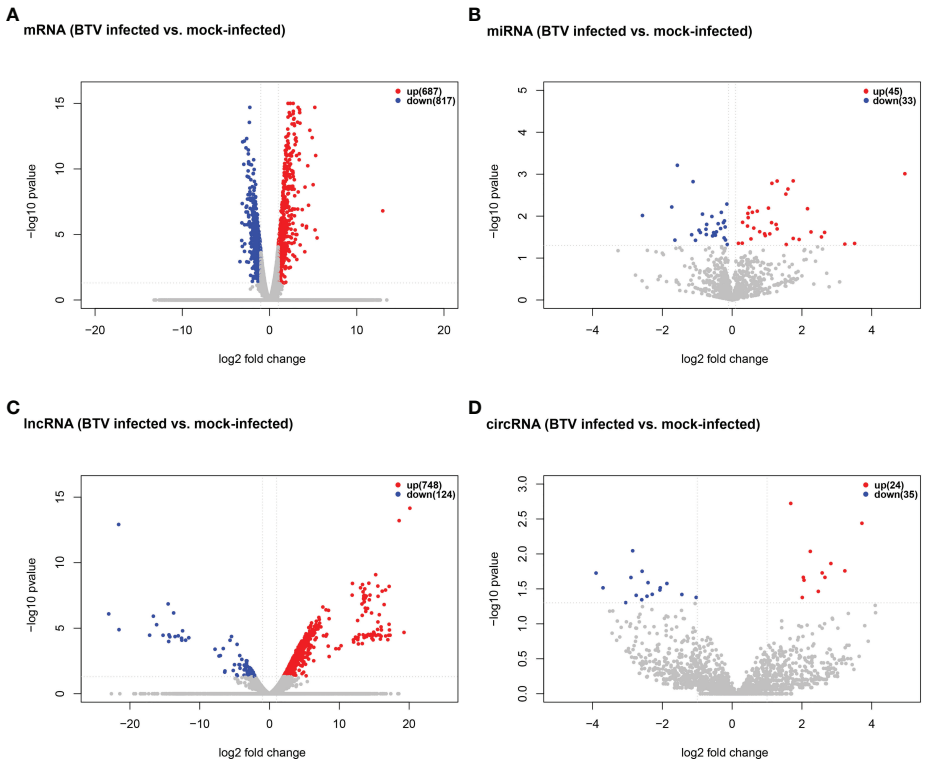

FIGURE 2
Volcano plots of **(A)** dif-mRNAs, **(B)** dif-miRNAs, **(C)** dif-lncRNAs, and **(D)** dif-circRNAs between BTV-1-infected and mock-infected OA3.Ts cells. Red and blue dots represented upregulated and downregulated dif-RNA, respectively. The total numbers of upregulated and downregulated dif-RNAs were marked in the upper right corner of each figure.

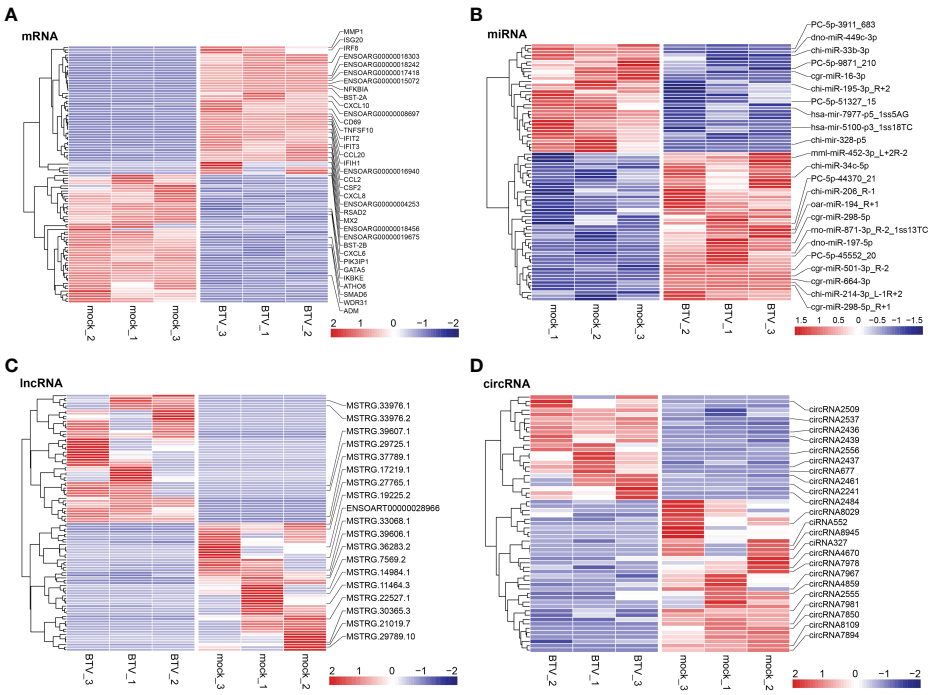

FIGURE 3
Hierarchical cluster analyses of **(A)** dif-mRNAs, **(B)** dif-miRNAs, **(C)** dif-lncRNAs, and **(D)** dif-circRNAs between BTV-1-infected and mock-infected OA3.Ts cells. The top 50 upregulated and downregulated dif-mRNAs and dif-lncRNAs, as well as all dif-miRNAs and dif-circRNAs were selected and displayed in the heatmaps. The color of the color blocks from blue to red represented the dif-RNAs expression levels from downregulated to upregulated. Several important dif-RNAs were labeled to the right of the corresponding heatmaps.

Similar to the research performed in BTV-16-infected sheep PBMCs, BTV-1 infection induced significant enrichment of defense response to virus (GO: 0051607) and immune response (GO: 0006955) under BP ontology, and protein binding (GO: 0005515) and metal ion binding (GO: 0046872) under MF ontology in OA3.Ts cells (Figure 4A and Supplementary Table 2) (15). Compared with the mock-infected group, in addition to well-known antiviral genes, such as *IFITs* and radical S-adenosyl methionine domain containing 2 (*RSAD2*), several antiluteolysin genes belonging to the IFN-I family and relevant to preventing pregnant ewes from luteolytic, for example *ENSOARG00000008675*, *ENSOARG00000008697*, and *ENSOARG00000008791*, also transcriptionally increased under cytokine activity (GO: 0005125) and defense response to virus (GO: 0051607) terms, indicating that these antiluteolysin genes potentially contribute to host antiviral responses (Figure 3A and Supplementary Table 2) (15, 45). The other dif-mRNAs in comparison with mock-infected and infected samples were mostly associated with negative regulation of viral genome replication (GO: 0045071), response to virus (GO: 0009615), I kappa B kinase (IKK)/nuclear factor-kappa B (NF-κB) signaling (GO: 0007249), cytokine activity (GO: 0005125) and DNA-binding transcription factor activity (GO: 0003700) under BP and MF ontologies, respectively (Figure 4A and Supplementary Table 2). Interestingly, the key activators of the NF-κB signaling pathway, which had been reported to be activated by BTV infection, were downregulated, for instance, an inhibitor of NF-κB kinase subunit ϵ (*IKBKE*) and *IKBKG* (also known as NF-κB essential modulator, *NEMO*). While inhibitors of NF-κB signaling pathway, such as NF-κB inhibitor α (*NFKBIA* encoding IκBα) and *NFKBIB*, were upregulated significantly. These transcriptional alternations were accompanied by increases in the expression of tumor necrosis factor (TNF) receptor-associated factor family member associated NF-κB activator (*TANK*), NF-κB functional subunit *REL*, NF-κB p105 subunit (*NFKB1*), and *RELB* (Figure 3A and Supplementary Table 2) (11, 46–48). A similar phenomenon was also found in the BTV-16-infected sheep PBMCs, for example, a significant decrease in *IKBKE* transcription (15). These results indicated that canonical and non-canonical NF-κB pathways might play a more complicated and changeable role in BTV infection and pathogenic processes.

MiRNAs regulate gene expression at the post-transcriptional level through interactions between their seed sequences and the target mRNAs (49). The dif-miRNAs target genes in this study were primarily enriched in the BP ontology of proteolysis (GO: 0006508) and oxidation-reduction process (GO: 0055114), the CC ontology of cytoplasm (GO: 0005737), and the MF ontology

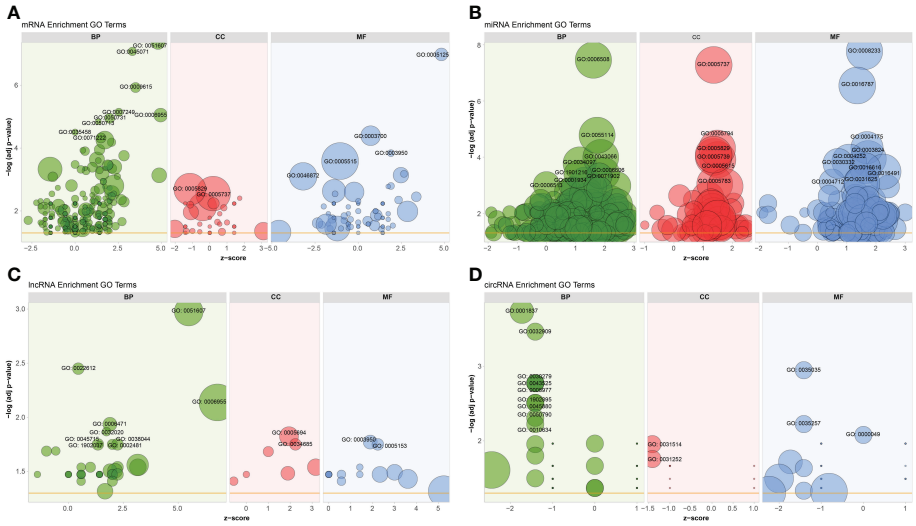

FIGURE 4
GO annotations of **(A)** dif-mRNAs, target mRNAs of **(B)** dif-miRNAs, **(C)** dif-lncRNAs, and **(D)** host mRNAs of dif-circRNAs under BP, CC, and MF ontologies, respectively. Z-score was equal to the total number of transcriptional increased dif-mRNAs minus the total number of decreased dif-mRNAs and then divided by the square root of the total number of dif-mRNAs in a certain GO term and was used to measure whether the term was upregulated or downregulated overall. The size of the solid circulars represented the number of enriched dif-mRNAs under specific GO terms. GO: 0051607: defense response to virus, GO: 0045071: negative regulation of viral genome replication, GO: 0009615: response to virus, GO: 0007249: I-kappaB kinase/NF-kappaB signaling, GO: 0006955: immune response, GO: 0050731: positive regulation of peptidyl-tyrosine phosphorylation; GO: 0050713: negative regulation of interleukin-1 beta secretion, GO: 0035458: cellular response to interferon-beta, GO: 0071222: cellular response to lipopolysaccharide, GO: 0005829: cytosol, GO: 0005737: cytoplasm, GO: 0005125: cytokine activity, GO: 0003700: DNA-binding transcription factor activity, GO: 0003950: NAD+ADP-ribosyltransferase activity, GO: 0005515: protein binding, GO: 0046872: metal ion binding; GO: 0006508: proteolysis, GO: 0055114: oxidation-reduction process, GO: 0043066: negative regulation of apoptotic process, GO: 0034097: response to cytokine, GO: 0006606: protein import into nucleus, GO:1901216: positive regulation of neuron death, GO: 0071902: positive regulation of protein serine/threonine kinase activity, GO: 0001934: positive regulation of protein phosphorylation, GO: 0006513: protein monoubiquitination, GO: 0005794: Golgi apparatus, GO: 0005739: mitochondrion, GO: 0005615: extracellular space, GO: 0005783: endoplasmic reticulum, GO: 0008233: peptidase activity, GO: 0016787: hydrolase activity, GO: 0004175: endopeptidase activity, GO: 0003824: catalytic activity, GO: 0004252: serine-type endopeptidase activity, GO: 0030332: cyclin binding, GO: 0016616: oxidoreductase activity, acting on the CH-OH group of donors, NAD or NADP as acceptor, GO: 0016491: oxidoreductase activity, GO: 0004712: protein serine/threonine/tyrosine kinase activity, GO: 0031625: ubiquitin protein ligase binding; GO: 0022612: gland morphogenesis, GO: 0006471: protein ADP-ribosylation, GO: 0032020: ISG15-protein conjugation, GO: 0038044: transforming growth factor-beta secretion, GO: 0002481: antigen processing and presentation of exogenous protein antigen *via* MHC class Ib, TAP-dependent, GO:1902037: negative regulation of hematopoietic stem cell differentiation, GO: 0045715: negative regulation of low-density lipoprotein particle receptor biosynthetic process, GO: 0005694: chromosome, GO: 0034685: integrin alphav-beta6 complex, GO: 0005153: interleukin-8 receptor binding; GO: 0001837: epithelial to mesenchymal transition, GO: 0032909: regulation of transforming growth factor beta2 production, GO: 0030279: negative regulation of ossification, GO: 0043525: positive regulation of neuron apoptotic process, GO: 0005977: glycogen metabolic process, GO:1902895: positive regulation of pri-miRNA transcription by RNA polymerase II, GO: 0045880: positive regulation of smoothened signaling pathway, GO: 0050790: regulation of catalytic activity, GO: 0010634: positive regulation of epithelial cell migration, GO: 0031514: motile cilium, GO: 0031252: cell leading edge, GO: 0035035: histone acetyltransferase binding, GO: 0035257: nuclear hormone receptor binding, GO: 0000049: tRNA binding.

of peptidase activity (GO: 0008233), hydrolase activity (GO: 0016787) and endopeptidase activity (GO: 0004175) (Figure 4B and Supplementary Table 6). By analyzing the GO classification of dif-miRNA target genes in BTV-1-infected ST cells, it was found that under BP and MF ontologies, the enriched GO terms involved in both our current and previous studies are related to metabolic process and catalytic activity, respectively. In contrast, under CC ontology, our study is mainly associated with cytoplasm rather than cell and cell part (10). According to the definition of lncRNA function mode and the prediction of target genes, 622 dif-lncRNAs might influence the expression or chromatin state of 1077 of their nearby genes in *cis* (Supplementary Table 7) (35). The target genes mainly involved in the BP ontology of defense response to virus (GO: 0051607), gland morphogenesis (GO: 0022612), immune response (GO: 0006955), protein adenosine-diphosphate (ADP)-ribosylation (GO: 0006471) and IFN-stimulated gene 15 (ISG15)-protein conjugation (GO: 0032020), and the CC ontology of chromosome (GO: 0005694) (Figure 4C and Supplementary Table 7). For instance, two significantly elevated dif-lncRNAs, MSTRG.33976.1 and MSTRG.33976.2, were probably responsible for the several folds upregulation of their target gene C-X-C motif chemokine 8 (*CXCL8*, also known as *IL-8*) in immune response (GO: 0006955) term (Figure 3A, C;

Figure 4C and Supplementary Table 7). Among 59 dif-circRNAs, 38, 3, and 18 were back-spliced from exons, introns, and intergenic RNAs, respectively (Supplementary Table 5). The linear transcripts of the 41 dif-circRNAs were identified. Following that, the corresponding transcripts were subjected to GO enrichment analysis. These linear cognates were significantly assigned to BP and MF ontologies, including epithelial to mesenchymal transition (GO: 0001837), regulation of transforming growth factor β (TGF-β)-2 production (GO: 0032909), negative regulation of ossification (GO: 0030279), positive regulation of neuron apoptotic process (GO: 0043525), glycogen metabolic process (GO: 0005977), and histone acetyltransferase binding (GO: 0035035) (Figure 4D and Supplementary Table 8). These results suggested that dif-RNAs induced by BTV-1 infection are not only related to antiviral and immune responses of the host, but also participate in the development and metabolism processes.

Enrichment analyses of dif-RNAs

It is well known that signaling pathway analyses conduce to better understanding of the biological functions of genes. KEGG pathway enrichment analyses of dif-RNAs can be used to determine the biochemical metabolic and signal transduction pathways, further facilitating the exploration of host-virus interactions.

KEGG analysis showed that unlike the results of previous research, dif-mRNAs lacked primary enrichment in Ras, MAPK, Janus tyrosine kinase (JAK)-signal transducer and activator of transcription protein (STAT) and vascular endothelial growth factor (VEGF) signaling pathways. At the same time, they were significantly enriched in cytoplasmic retinoic acid-inducible gene I (RIG-I)-like receptor (RLR) signaling pathway, Influenza A, TNF signaling pathway, cytosolic DNA-sensing pathway, nucleotide-binding and oligomerization domain (NOD)-like receptor (NLR) signaling pathway, and HSV-1 infection (Figure 5A and Supplementary Table 2) (15). The RIG-I and melanoma differentiation-associated gene 5 (MDA5) proteins, encoded by DEXH (Asp-Glu-X-His) box polypeptide 58 (*DDX58*) and IFN-induced helicase C domain-containing protein 1 (*IFIH1*) respectively, are both important dsRNA recognition receptor in the RLR signaling pathway, and BTV infection induced transcriptional level of *IFIH1* was higher than that of *DDX58* in our study (Figure 3A and Supplementary Table 2) (50). In addition to being assigned in typical dsRNA sensing signal pathway, dif-mRNAs were also enriched in DNA virus infection-related signaling pathways, such as Herpes simplex virus 1 (HSV-1) infection, Epstein-Barr virus (EBV) infection and Kaposi sarcoma-associated herpesvirus (KSHV)

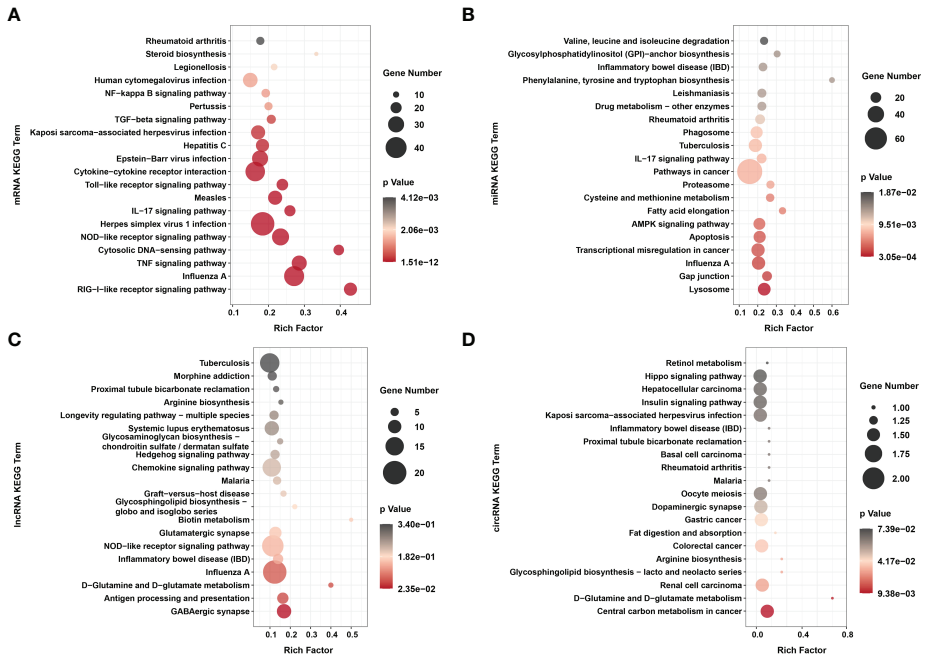

FIGURE 5
KEGG enrichments of **(A)** dif-mRNAs, target mRNAs of **(B)** dif-miRNAs, **(C)** dif-lncRNAs, and **(D)** host mRNAs of dif-circRNAs. Top 20 KEGG pathways were shown. Rich factor indicated the ratio of dif-mRNAs enriched to the specific pathway. The size and the color of the solid circulars represented the number of enriched dif-mRNAs and significance of the enrichment, respectively.

infection (Figure 5A) (50). Using the HSV-1 pathway as an example, 45 dif-mRNAs were involved, with 25 dif-mRNAs being transcriptionally increased and 20 dif-mRNAs being transcriptionally decreased. The 25 upregulated dif-mRNAs contained not only typical dsRNA activated genes, such as Toll/IL-1 receptor domain-containing adapter molecule 1 (*TICAM1*, also known as *TRIF*), an adapter of TLR3, but also traditional DNA recognition receptor, for instance, Toll-like receptor 9 (*TLR9*) (Supplementary Table 2) (51, 52). The 20 decreased dif-mRNAs mainly were zinc finger proteins relevant to DNA binding and transcription (Supplementary Table 2) (53).

The target genes of dif-miRNAs mainly were associated with the lysosome, gap junction, Influenza A, transcriptional misregulation in cancer, apoptosis, and adenosine 5'-monophosphate-activated protein kinase (AMPK) signaling pathway (Figure 5B and Supplementary Table 6). Previous studies have shown that apoptosis triggered by BTV infection in mammalian cells is the leading cause of CPE/cell lysis *in vitro* and virus-induced pathogenesis *in vivo* (9, 54, 55). The target genes of dif-miRNAs, calcium-activated neutral proteinase 1 (*CAPN1*), a requirement of apoptosis in some cell lines, and caspase-7 (*CASP7*), served as one of the readouts for the activation of apoptosis, were both transcriptionally upregulated by BTV-1 infection. On the other hand, downregulated dif-miRNAs, hsa-mir-5100-p3_1ss18TC, and chi-miR-195-3p_R+2, possibly contributed to the expression increases of the two genes mentioned above (Figure 3B and Supplementary Table 6) (56). The dif-lncRNAs targeting genes were primarily involved in the γ-aminobutyric acid (GABA)ergic synapse, antigen processing and presentation, D-Glutamine and D-glutamate metabolism, Influenza A, inflammatory bowel disease (IBD) and NLR signaling pathway (Figure 5C and Supplementary Table 7). In addition, most linear transcripts of dif-circRNAs were related to the central carbon metabolism in cancer, D-Glutamine and D-glutamate metabolism, renal cell carcinoma, glycosphingolipid biosynthesis-lacto and neolacto series, arginine biosynthesis and colorectal cancer (Figure 5D and Supplementary Table 8). These results showed that except for virus-sensing and signaling transduction pathways, the dif-RNAs induced by BTV-1 infection also involve in a variety of pathways, such as cancer-, transcription-, and metabolism-related pathways, indicating that BTV can regulate the expression profiles of OA3.Ts cells and hijacks the metabolic pathways of the host in order to complete its life cycle.

ceRNA networks construction and enrichment analyses

Noncoding RNAs (ncRNAs) involve a wide range of regulatory functions that interact with DNA and RNA to control transcription and translation. In addition, lncRNAs and circRNAs possess miRNA binding sites, which allow them to compete for binding miRNAs, serve as miRNA sponges, and counteract the repressive transcriptional activity of miRNA on target genes, thereby achieving indirect regulation of gene expression. These lncRNAs and circRNAs are called ceRNAs (13, 14). Based on the ceRNA theory, lncRNA-miRNA-mRNA and circRNA-miRNA-mRNA ceRNA networks were constructed, using lncRNAs or circRNA as the decoy, miRNA as the core, and mRNA as the target. According to the screening criteria, 53 dif-lncRNAs and 22 dif-circRNAs regulating 33 dif-mRNAs mainly through 10 dif-miRNAs were selected for display (Figures 6A, B and Supplementary Table 9). The heatmaps depicted the expression patterns of partial dif-RNAs in the infected and mock-infected groups (Figures 3A–D).

According to GO analysis, the regulated genes in the ceRNA networks are primarily enriched in BP and CC ontologies, such as the negative regulation of IFN-I production (GO: 0032480), positive regulation of cholesterol efflux (GO: 0010875), positive regulation of glucose import (GO: 0046326), regulation of intracellular pH (GO: 0051453), positive regulation of IL-12 production (GO: 0032735), and protein-containing complex (GO: 0032991) (Figure 7A and Supplementary Table 9). Ubiquitin-specific protease (USP4), a key modulator of RLR signaling pathway, increases the stability of RIG-I protein through deubiquitination and further promotes the production of IFN-I (57). BTV-1 infection downregulated a series of lncRNAs and circRNAs, such as MSTRG.19225.2 and circRNA7978, and probably deprived their competitive binding with the corresponding miRNAs, cgr-miR-298-5p_R+1, and ultimately led to a certain extent of decrease in the transcription of *USP4* (Figures 6A, B). KEGG pathway analysis indicated that the modulated target genes are mostly assigned to the NF-κB signaling pathway, TNF signaling pathway, transcriptional misregulation in cancer, prostate cancer, C-type lectin receptor signaling pathway, and IL-17 signaling pathway (Figure 7B and Supplementary Table 9). Except for transcriptional misregulation in cancer, IκBα was mentioned to function in the above 5 pathways (Supplementary Table 9) (47, 52, 58). Several significantly elevated lncRNAs and circRNAs, MSTRG.37789.1, MSTRG.29725.1, circRNA2437, and circRNA2439, served as sponges of hsa-mir-7977-p5_1ss5AG, and contributed to the increased transcription level of *NFKBIA*. The GO and KEGG enrichment analyses suggested that most dif-mRNAs in the ceRNA networks are associated with the host's inflammatory responses, such as IL-12-, IL-17-, and TNF-related biological processes or signaling pathways (52, 59, 60).

Protein-protein interaction network, modules extraction, and functional enrichment analyses

The PPI network based on dif-mRNAs consisted of 1306 nodes and 7052 interaction pairs (Supplementary Figure 1). In the PPI network, six modules were determined, which were

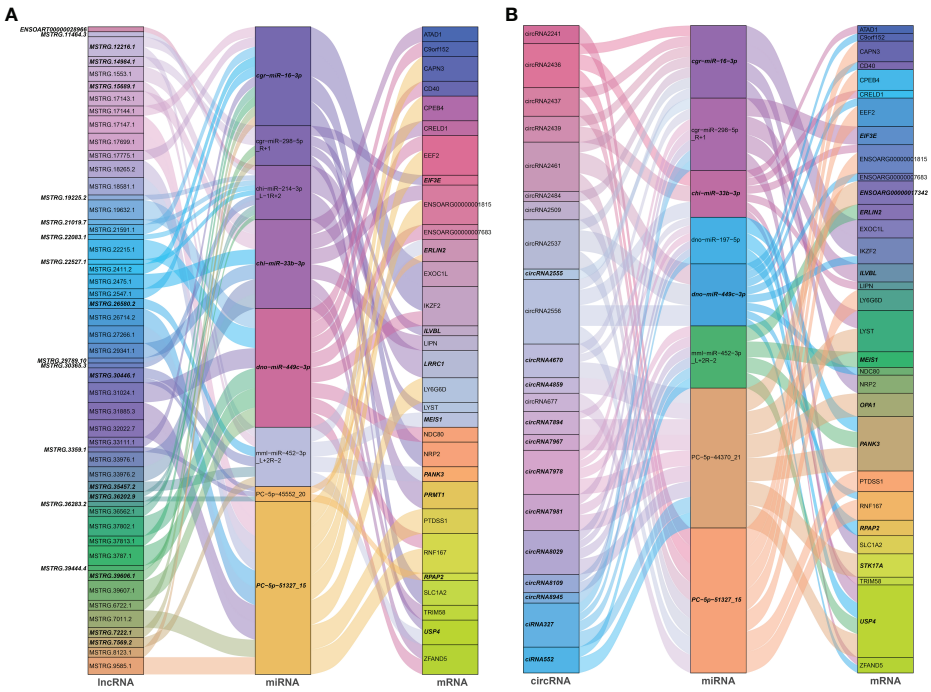

FIGURE 6
Sankey diagrams of ceRNA network based on **(A)** lncRNA-miRNA-mRNA, and **(B)** circRNA-miRNA-mRNA interaction pairs. Different colored blocks represented different dif-RNA nodes, and the downregulated dif-RNAs were indicated with bold italic font. The flow charts from dif-lncRNAs or dif-circRNAs to dif-miRNAs, and finally to dif-mRNAs represented lncRNAs or circRNAs regulated the expression of mRNAs through different miRNAs.

mainly related to viral nucleic acids sensing, antiviral effects, inflammatory responses, development, cell cycle (Module A, C, D and E), ribosome structural constituent proteins (Module B), and cholesterol and steroid metabolism process (Module F), respectively (Figure 8).

Furthermore, dif-mRNAs in these modules were extracted and performed for GO enrichment and KEGG analyses (Supplementary Tables 10–13). Functional enrichment analysis showed that according to the numbers of enriched dif-mRNAs, the elevated dif-mRNAs are primarily relevant to defense response to virus, immune response, cytoplasm, integral component of membrane, extracellular space, and protein binding under BP, CC and MF ontologies, respectively (Figure 9A and Supplementary Table 10). In contrast, the declined dif-mRNAs were mainly associated with regulation of transcription (DNA-templated), cholesterol biosynthetic process, nucleus, integral component of membrane, membrane, and protein binding under BP, CC and MF ontologies, respectively (Figure 9B and Supplementary Table 11). Taking Module A as an example, it contained 35 nodes and 284 interaction pairs, including expression-increased *DDX58*, *IFIH1*, *ISG20*, IFN-α inducible protein 6 (*IFI6*), IFN-induced protein 44-like (*IFI44L*), bone marrow stromal cell antigen 2A (*BST-2A*), *BST-2B*, IFN regulatory factor 1 (*IRF1*), and ribonuclease L (*RNASEL*) in defense response to virus term under BP ontology, and transcriptional-elevated *ENSOARG00000019675* and *ENSOARG00000010819* in ribosome term under CC ontology (Figure 8) (15, 50, 61–65).

The top 20 KEGG pathways for upregulated and downregulated dif-mRNAs in the modules were chosen for display in the order of significance. The upregulated dif-mRNAs primarily enriched in Influenza A, TNF signaling pathway, cytosolic DNA-sensing pathway, cytokine-cytokine receptor interaction, Measles, and Hepatitis C (Figure 9C and Supplementary Table 12). The downregulated dif-mRNAs mainly enriched in steroid biosynthesis, TGF-β signaling pathway, cell cycle, viral carcinogenesis, small cell lung cancer, and cellular senescence (Figure 9D and Supplementary Table 13). Steroids and steroid hormones function in metabolism, stress responses, immune activities, sexual differentiation and reproduction, and several genes related to steroid biosynthesis were decreased significantly in BTV-1-infected OA3.Ts cells, such as lanosterol synthase (*LSS*), cytochrome P450 lanosterol 14-α demethylase (*CYP51A1*), 7-dehydrocholesterol reductase (*DHCR7*), and *DHCR24* (Figure 8) (66). Moreover, the transcription level of another member of the cytochrome P450 family, *CYP11A1*, also declined (Supplementary Table 2). CYP11A1 is the first and rate-limiting

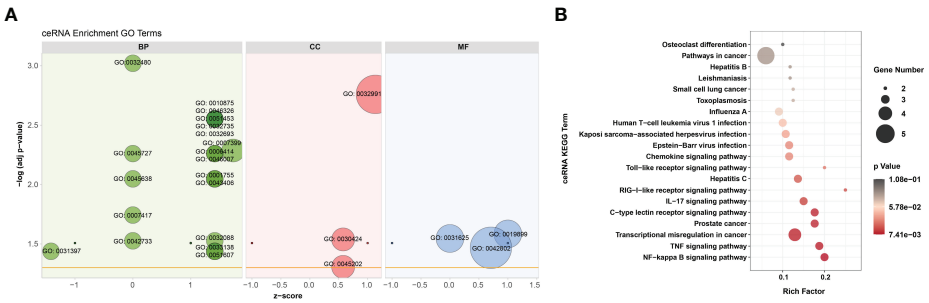

FIGURE 7
GO annotation and KEGG enrichment of dif-mRNAs involved in ceRNA networks. **(A)** Z-score in the GO bubble diagram was equal to the total number of transcriptional increased dif-mRNAs minus the total number of decreased dif-mRNAs and then divided by the square root of the total number of dif-mRNAs in a certain GO term and was used to measure whether the term was upregulated or downregulated overall. The size of the solid circulars represented the number of enriched dif-mRNAs under specific GO terms. GO: 0032480: negative regulation of type I interferon production, GO: 0045727: positive regulation of translation, GO: 0045638: negative regulation of myeloid cell differentiation, GO: 0007417: central nervous system development, GO: 0042733: embryonic digit morphogenesis, GO: 0031397: negative regulation of protein ubiquitination, GO: 0010875: positive regulation of cholesterol efflux, GO: 0046326: positive regulation of glucose import, GO: 0051453: regulation of intracellular pH, GO: 0032735: positive regulation of interleukin-12 production, GO: 0032693: negative regulation of interleukin-10 production, GO: 0007399: nervous system development, GO: 0006414: translational elongation, GO: 0046007: negative regulation of activated T cell proliferation, GO: 0001755: neural crest cell migration, GO: 0043406: positive regulation of MAP kinase activity, GO: 0032088: negative regulation of NF-kappaB transcription factor activity, GO: 0033138: positive regulation of peptidyl-serine phosphorylation, GO: 0051607: defense response to virus, GO: 0032991: protein-containing complex, GO: 0030424: axon, GO: 0045202: synapse, GO: 0019899: enzyme binding, GO: 0031625: ubiquitin protein ligase binding, GO: 0042802: identical protein binding. **(B)** Top 20 KEGG pathways were selected to display. Rich factor indicated the ratio of dif-mRNAs enriched to the specific pathway. The size of and the color of the solid circulars represented the number of enriched dif-mRNAs and significance of the enrichment, respectively.

enzyme in steroidogenesis and converts cholesterol to pregnenolone, the precursor of steroid hormones (67). Pregnenolone further produces 17α-hydroxypregnenolone, dehydroepiandrosterone, androstenedione, and testosterone under the catalysis of enzymes, which plays an important role in spermatogenesis (68). Downregulated genes, mothers against decapentaplegic homolog 5 (*SMAD5*), *SMAD6*, and *SMAD9*, showed in Module E, are all associated with TGF-β signaling pathway, which involves cell fate, proliferation, terminal differentiation, and cell death (Figure 8) (69). BTV caused repression of this pathway by reducing the expression of cell cycle-related genes, such as cyclin E2 (*CCNE2*), cyclin-

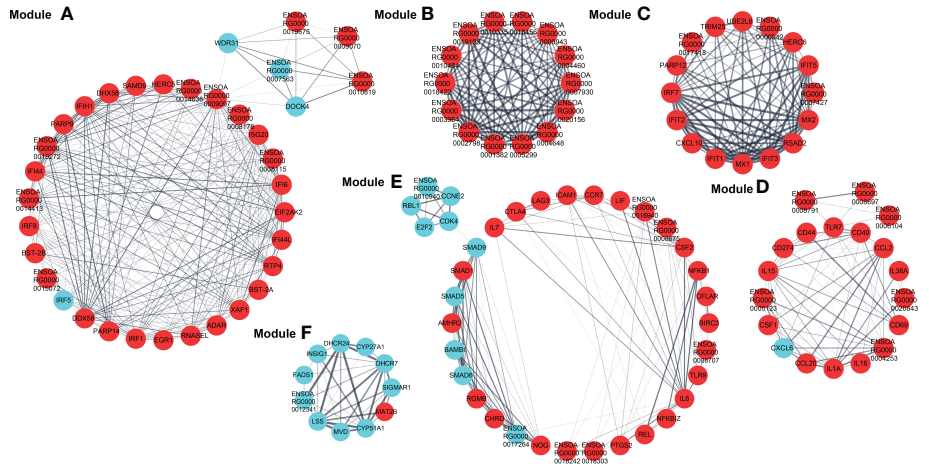

FIGURE 8
Modules **(A–F)** extracted from PPI network. The MCODE plugin in Cytoscape was applied to extract densely connected modules from PPI network, with degree cut-off = 2, node score cut-off = 0.2, K-score = 2, and max depth = 100. Red and blue circles represented upregulated and downregulated dif-mRNAs, respectively, whereas the thickness of the solid black line indicated the strength of the corresponding protein interactions.

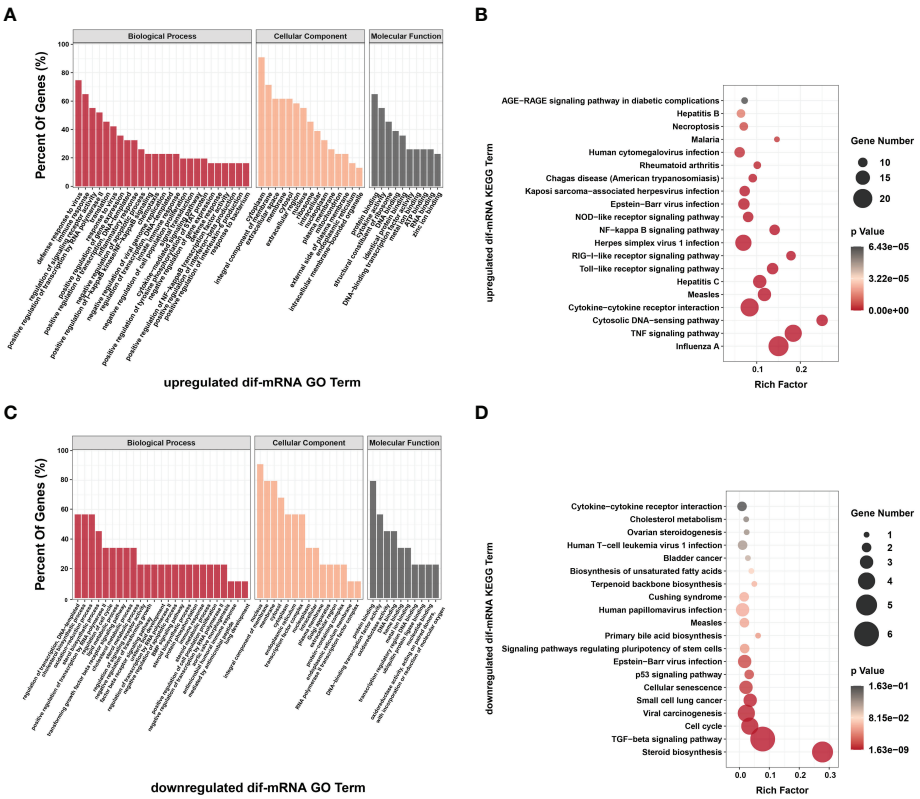

FIGURE 9
Go annotation and KEGG enrichment of upregulated and downregulated dif-mRNAs displayed in the extracted six modules. Top 50 GO terms and top 20 KEGG pathways were shown. **(A, C)** The height of bar chart represented the ratio of enriched dif-mRNAs under specific GO terms. **(B, D)** Rich factor of the KEGG scatter diagrams indicated the ratio of dif-mRNAs enriched to the specific pathway. The size of and the color of the solid circulars represented the number of enriched dif-mRNAs and significance of the enrichment, respectively.

dependent kinase 4 (*CDK4*), S-phase kinase associated protein 2 (*ENSOARG00000019040*), and retinoblastoma transcriptional corepressor like 1 (*RBL1*), and might further lead to cell cycle arrest in infected OA3.Ts cells (Figure 8) (70).

Validation of dif-RNAs using qRT-PCR and WB

Eight each of dif-mRNAs, dif-miRNAs, dif-lncRNAs, and dif-circRNAs were selected for qRT-PCR verification. As shown in Figure 10, the expression trends of the vast majority of selected dif-RNAs were highly consistent with the sequencing results, with significant differences between the infected and mock-infected groups, except for rno-miR-871-3p_R-2_1ss13TC, chi-mir-328-p5, MSTRG.14318.1, circRNA2484, and circRNA7981. In addition, some validated dif-RNAs in the infected and mock-infected groups were labeled in the heatmaps, respectively (Figures 3A–D).

Six proteins CASP8, connective tissue growth factor (CTGF, also known as CCN2), NEMO, IκBα, PI3K interacting protein 1 (PIK3IP1), and RIG-I were selected for further WB validation. Except for RIG-I, the expression patterns of other proteins coincided with the sequencing results (Figure 11).

Discussion

BTV pathogenicity and its interactome with the host are highly complex. Moreover, alternations in the host transcription profiles caused by BTV infection are enormous and systemic. However, the RNA expression profiles and involved biological processes in host cells responding to BTV infection have not been comprehensively elucidated. As an increasingly popular method to detect genome-wide gene expression, the combination of expression profile data and bioinformatics analyses has become an effective modality for identifying potential biomarkers and key pathways in various pathogens' infections. In this study, in order to gain some clues for an in-depth understanding of BTV infection and pathogenic relevant mechanisms, we determined the differential expression profiles of mRNAs, miRNAs, lncRNAs, and circRNAs in OA3.Ts cells

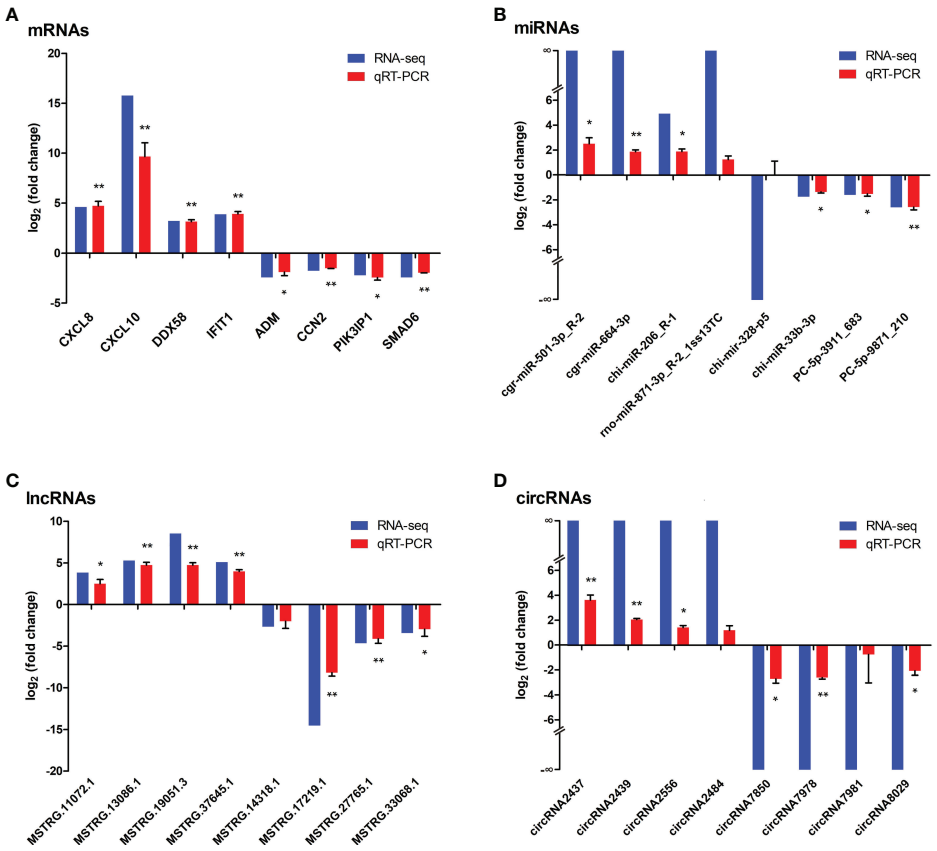

FIGURE 10
Verification the expressions of **(A)** dif-mRNAs, **(B)** dif-miRNAs, **(C)** dif-lncRNAs, and **(D)** dif-circRNAs using qRT-PCR, respectively. Blue and red bars represented the whole transcription sequencing results and qRT-PCR validation results respectively, whereas qRT-PCR validation results were displayed as mean $\log_2$ (fold change) ± SD with error bars from three independent experiments. Symbols * and ** indicated the difference between the indicated groups was significant (p-value < 0.05) or very significant (p-value < 0.01 respectively.

infected with BTV-1 through high-throughput whole-transcriptome sequencing, analyzed the GO terms and signaling pathways enriched by dif-RNAs, predicted the potential interactions between dif-RNAs, and verified the sequencing results of some dif-RNAs using qRT-PCR and WB.

BTV regulates the transcription system, hijacks biological pathways, and utilizes factors of the mammalian host to complete its life processes, such as infection, replication, packaging, and release, which can lead to a series of reactions in the host cells, including but not limited to autophagy, apoptosis, and cell lysis (9, 54, 71, 72). These reactions are a wrestle between BTV and the host cells, progressively advanced and completed. Therefore, some critical time nodes are significant to completing the virus life cycle. As observed in Figure 1A, previous studies also pointed out that the autophagy and apoptosis phenomenon gradually appeared from 24 hpi (10, 11, 71). In addition, the IFN levels decreased and became undetectable at 24 hpi (55); As for reversible protein phosphorylation, the most pervasive control and regulatory mechanism within cells, also began to transit from 24 hpi, for example, the phosphorylation status of Akt exhibited a significant conversion from increasing to decreasing at 24 hpi (73). Hence, we selected OA3.Ts cells infected with BTV-1 for 24 h as samples for whole-transcriptome sequencing to clarify the transcription profiles changes induced by BTV infection.

Although human lung adenocarcinoma (A549) cells were thoughted to be a good model for studying BTV infection, our sequencing data identified relatively few dif-mRNAs compared to the 2863 dif-mRNAs previously found between BTV-8-infected and mock-infected A549 cells. While a comparable number of dif-mRNAs was obtained in our study in comparation with 1152 dif-mRNAs determined in research conducted in BTV-16-infected sheep PBMCs (Supplementary Table 2) (12, 15). There was no doubt that A549 cells and OA3.Ts cells derived from different species is one reason for the differences, whereas another more important reason was that the BTV-8 strain with stronger virulence and higher MOI of 4 was used to infect A549 cells and induced more dramatic host responses, which ultimately manifested as extensive changes in the expression of genes. Although the same serotype strains were

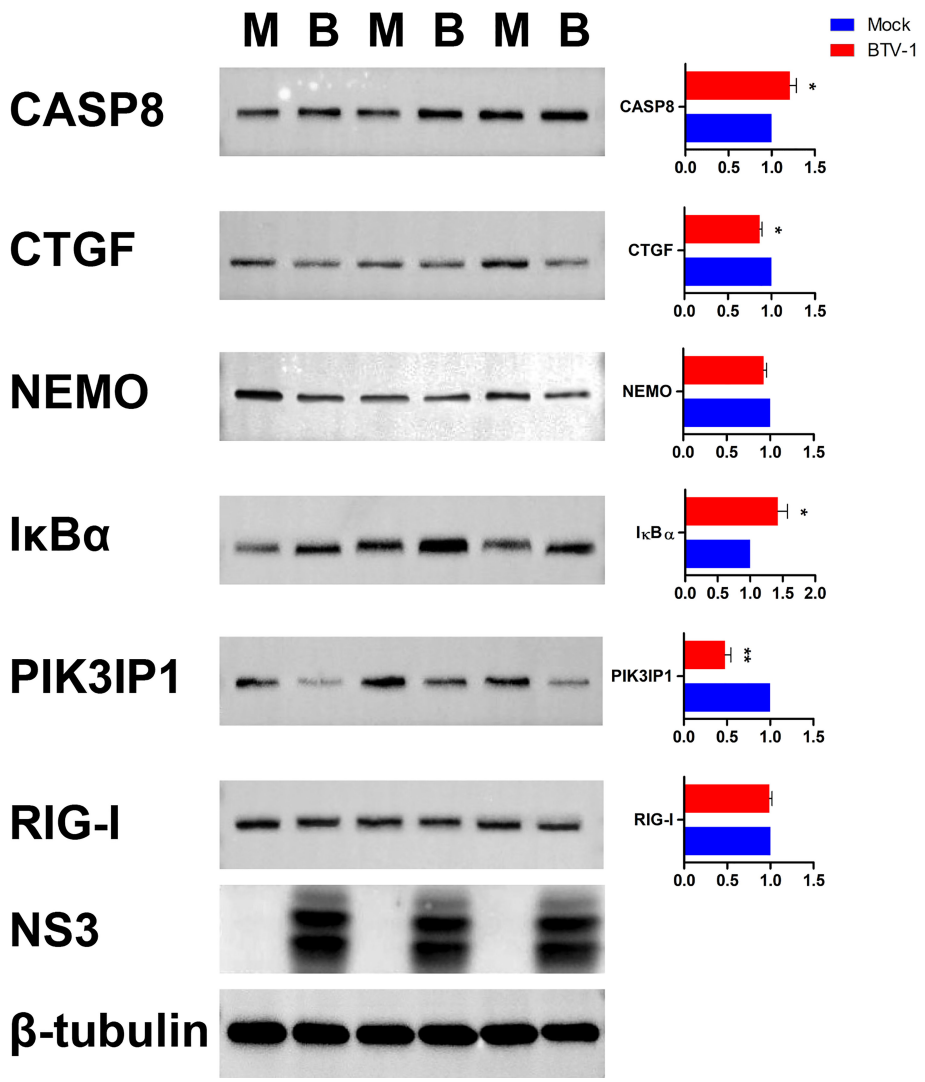

FIGURE 11
Validation the expressions of six dif-mRNAs using WB. The expression patterns of CASP8, CTGF, NEMO, IκBα, PIK3IP1, and RIG-I were validated using WB with specific antibodies. M and B indicated mock-infected and BTV-1-infected groups, respectively. NS3 was detected as control for successful infection, whereas β-tubulin served as an internal control. Symbols * and ** indicated the difference between the indicated groups was significant (p-value <0.05) or very significant (p-value <0.01), respectively.

used to infect sheep-derived cell lines, the highly tissue-specific expression of some miRNAs and the difference in infection time may lead to divergences in miRNA expression profiles, similar to the changes caused by other RNA viruses (74, 75). Therefore, only 9 dif-miRNAs were shared between the 78 dif-miRNAs identified in our study and the 265 dif-miRNAs obtained in the previous study, and merely 6 dif-miRNAs possessed similar expression patterns (Supplementary Table 3) (10).

Through functional analyses, it was found that a total of 35 dif-mRNAs are enriched in the defense responses to virus term (GO: 0051607), which involved RLR signaling pathway, TLR signaling pathway, and NLR signaling pathway (Figures 4A, 5A and Supplementary Table 2). RLR and TLR signaling pathways are primarily responsible for sensing viral RNAs (50). RIG-I and MDA5 act as dsRNA sensors within the RLRs family and recognize relatively short and long dsRNAs, respectively, which explains why the expression level of *IFIH1* encoding MDA5 induced by BTV infection was higher than that of *DDX58* encoding RIG-I (Supplementary Table 2) (52, 76). Despite the role of LGP2, another member of the RLRs family encoded by DEXH (Asp-Glu-X-His) box polypeptide 58 (*DHX58*), in resisting RNA virus infection is not yet fully understood, the transcriptional level of *DHX58* was upregulated, although the fold change was lower than those of the other two members (Supplementary Table 2). The same expression pattern of *DDX58*, *DHX58*, and *IFIH1* was also

detected in BTV-8-infected A549 cells (12). TLR3, TLR7, and TLR9 of the TLRs family sense dsRNA, single-stranded RNA, and DNA, respectively. Despite the previous study pointing out that BTV-activated IFN-I responses *via* TLR3 recognition, the expression level of TLR3 was not induced by BTV infection in our study (77). Instead, the expression levels of TLR7 and TLR9 were significantly increased, which were partially consistent with the previous studies (Supplementary Table 2) (12, 15). Nevertheless, whether the TLR signaling pathway is activated by virus infection cannot be generalized. For instance, Chauveau et al. (2012) indicated that impairment of TLR3 exhibits no or weak effect on IFN-I transcription induced by BTV-8; Singh et al. (2017) regarded TLR7 as an important immune gene for resisting BTV-16 infection in sheep PBMCs; Ruscanu et al. (2012) noted that BTV-8 induces IFN-I production in sheep plasmacytoid dendritic cells (DCs) *via* a TLR7-independent signaling pathway; As for the TLR9-related signaling pathway, a typical DNA sensing pathway, could be activated by the dengue virus in human DCs (15, 76, 78, 79). Hence, whether TLRs are activated depends on the virus species and the type of cells it infects, and the transcription levels of TLRs induced by BTV infection might also be relevant to cell types.

In response to BTV infection, RNA virus and DNA virus sensing receptor and adaptor proteins showed a degree of versatility, and their downstream signal transmitters present extensive crosstalk to save resources and improve the efficiency of the host (80). Just like Z-DNA binding protein 1 (*ENSOARG00000017418* also known as *ZBP1*) and cyclic GMP-AMP synthase (*ENSOARG00000006104* also known as *cGAS*), which play important roles in restricting RNA and DNA virus infections, were all transcriptionally elevated obviously in our study (Supplementary Table 2) (80, 81). Furthermore, RNA virus infection plausibly prompts DNA damage in the host cell, and the leaked self-DNA further activates DNA recognition pathways and increases the production of IFNs and inflammatory cytokines (82). Thus, it was not unexpected that dif-mRNAs induced by BTV infection were enriched in HSV-1, EBV and KSHV infection related signaling pathways (Figure 5A and Supplementary Table 2).

The final result of recognizing viral DNA or RNA is the production of IFNs, the core effector of the host's innate immune system. Thus, the confrontation between BTV and the innate immune system was reflected in both sides' modulation of IFN-I production. Aside from *USP4*, some other ubiquitin transferases, such as RING-type E3 ubiquitin transferase (*RNF125*) and SMAD ubiquitylation regulatory factor 1 (*SMURF1*), which are negative regulators of RIG-I, MDA5, as well as mitochondrial antiviral-signaling (MAVS), were significantly induced expression by BTV (Supplementary Table 2) (83). As a counterattack from the host, tripartite motif 25 (*TRIM25*), an indispensable positive regulator of RIG-I, was also obviously upregulated, which functions to activate the activity of RIG-I. However, the extent of the increase was slightly inferior to that of *RNF125* (Supplementary Table 2) (83). Our sequencing data also revealed that in contrast to the increased expression of RLRs family members, transcription of *MAVS* and tumor necrosis factor receptor-associated factor 3 (*TRAF3*) within the RLR signaling pathway did not change significantly, potentially further weakening signal transduction downstream. Furthermore, the downregulation of *IKBKE* and *IKBKG* could cause the profound interruption of signal transduction and direct impairment of IFN-I production through IRF3 (Supplementary Table 2) (52, 84). Nevertheless, the transcription of other important regulators that negatively modulate IFN-I production by targeting RIG-I downstream proteins and NEMO, such as *TRIM18* and *TRIM29*, showed no significant concomitant changes (85–87). In order to defeat BTV, the host cells also arranged other trumps. Poly(ADP-ribose) polymerases (PARPs) modulate the innate immune responses through recognition of viral RNAs, inhibiting viral transcription and replication, degradation of viral proteins, and facilitating transcription of *ISGs* to defend against virus invasion (88). In our study, the expression of *PARP9*, a non-canonical sensor for RNA virus, along with its binding partner, Deltex E3 ubiquitin ligase 3L (*DTX3L*), were all elevated; moreover, *PARP10*, *PARP12*, and *PARP14* were concomitantly upregulated significantly (Supplementary Table 2) (88, 89). The target genes of dif-lncRNAs were also responsible for the enrichment in protein ADP-ribosylation (GO: 0006471) and nicotinamide adenine dinucleotide (NAD) + ADP-ribosyltransferase activity (GO: 0003950) terms under BP and MF ontologies (Figure 4C and Supplementary Table 7). In conclusion, despite BTV intensively regulated IFN-I production, it was still a strong IFN-I inducer. ISG15 is an IFN-induced expression protein that mediates ISG15ylation by conjugating itself with other proteins and causing the degradation of corresponding proteins (90). The transcription levels of homologous to E6AP carboxyl terminus (HECT) domain and regulator of chromosome condensation 1 (RCC1)-like domain-containing protein 5 (*HERC5*) and *HERC6*, which are associated with ISG15ylation, were all elevated significantly (Supplementary Table 2) (90). Similarly, *HERC5* was upregulated in BTV-16-infected sheep PBMCs and functioned as a critical immune gene (15).

The NLR signaling pathway, the third pathway involved in defense responses to virus, mainly recognizes invading bacteria and regulates the host's inflammatory responses (52, 91). Our study did not observe alternations of important sensors in NLR signaling pathway, such as NOD1 and NOD2, contrary to the study conducted in BTV-16-infected sheep PBMCs (Supplementary Table 2) (15). At the same time, the expression of other members of the NLRs family was significantly changed, just like increases of NLRs family pyrin domain-containing 3 (*NLRP3*) relevant to inflammasome formation. Elevation of caspase-1-like protein (*ENSOARG00000003068*), which belongs to the mammalian inflammatory caspase family and catalyzes the

maturation of proinflammatory cytokine IL-1β, was also accompanied (Supplementary Table 2) (91). In addition to the abovementioned members of the NLRs family, the enrichment in the TNF, IL-12, and IL-17 production or signaling pathways, the high expression of *CXCL8* and *CXCL10*, and the upregulation of *IL-6* and prostaglandin-endoperoxide synthase 2 (*PTGS2*) positively contributed to the inflammatory responses of the host (Figures 5, 7, and Supplementary Table 2) (8, 92). However, pro-inflammatory cytokines are a double-edged sword. On one side, they control the scope of viral infection. On the other side, they also contributed to cytokines storm, capillary vessels damage and increased vascular permeability, coupled with the transcriptionally enhanced vascular endothelial growth factor (*VEGF*) and vascular endothelial growth factor receptor 2 (*KDR*), which would eventually lead to an aberrant systemic inflammatory response and severe hemorrhages in infected animals (Supplementary Table 2) (8, 92, 93).

In this still stalemate war, the virus has already narrowly won some important battles, such as transcription and translation regulations, cell proliferation and differentiation, metabolism, autophagy, and apoptosis. Seventy dif-mRNAs were enriched in DNA-binding transcription factor activity (GO: 0003700) term under MF ontology, and the expression of several essential transcription factors was downregulated. The transcription of a considerable amount of zinc finger proteins was also reduced (Figure 4 and Supplementary Table 2). The general elevation of dif-mRNAs encoding ribosome constitutive proteins exhibited in Figure 8 Module B suggested that BTV hijacks the host's translation system to synthesize viral proteins (94). Given that the dysregulation of transcription and translation is bound to influence the proliferation and differentiation of host cells, the expression declined *SMAD6* and *SMAD9* were the direct executors of inhibiting these processes (Figure 8 and Supplementary Table 2) (69). Additionally, there was a widespread transcriptional reduction of cholesterol and steroid metabolism-relevant genes (Supplementary Table 2), which might be the underlying mechanism behind the phenomenon of testicular degeneration and azoospermia in BTV-infected rams described in a previous study (2). Similarly, BTV infection elicited wide-ranging transcriptional misregulation of dif-miRNAs and dif-circRNAs enriched in cancer-related pathways (Figures 5B, D; Supplementary Tables 6, 8). Glutamine, a crucial extracellular carbon source, is relied upon to replicate of various viruses (95, 96). BTV also modulated the D-glutamine and D-glutamate metabolism in infected OA3.Ts cells through dif-lncRNAs and dif-circRNAs (Figures 5C, D; Supplementary Tables 7, 8). In a word, the abnormal regulation of transcription, translation, and metabolism by BTV inevitably caused various dysfunction in the host cells.

Talking about the slightly superior victory of BTV, we have to mention autophagy and apoptosis. Because, on one hand, although the host activates autophagy and apoptosis to clear damaged organelles and infected cells, limiting the spread of virus. It also carefully controls the extent of autophagy and apoptosis to mitigate the self-damage. On the other hand, the viruses enhancing autophagy and apoptosis to complete their life cycle are their customary means (11, 71). As observed in Figure 1, BTV infection had prompted apoptosis steadily, and the visible CPEs gradually expanded from 24 hpi to 48 hpi. Moreover, apoptosis implicates the ordered function of multiple proteases, including peptidase, hydrolase, and endopeptidase (97). The proteases CASP8 and CASP7, activator and executor of apoptosis, were inductively highly transcribed (Supplementary Table 2) (55). Matrix metalloproteinases (MMPs) are proteolytic enzymes that cleave almost all extracellular matrix components. MMP1, MMP3, MMP12, and MMP13 served as collagenase, stromelysins, and elastase, respectively, and the genes encoding these four proteases were upregulated in our study, which would change the extracellular environment and exacerbate apoptosis (Supplementary Table 2) (98). At the same time, dif-miRNAs also appreciably contributed to the positive regulation of apoptosis flux (Figure 4B and Supplementary Table 6). Additionally, the elevated autophagy related 2B (*ATG2B*), an indicator of late steps of autophagy, and other relevant dif-mRNAs all played positive roles in the eventual execution of autophagy (Supplementary Table 2) (99). Simultaneously, GO analysis indicated that there are about a dozen of dif-circRNAs that also probably make contributions to the regulation of autophagy (Supplementary Table 8).

Finally, we needed to investigate the NF-κB signaling pathway separately because it is involved in transcription regulation, inflammation, and apoptosis (11, 41, 100). In our study, the elevated transcription levels of *REL*, *NFKB1*, *RELB*, *TANK*, *IL-1α*, *IL-6*, and *CXCL8* suggested that canonical and non-canonical NF-κB signaling pathway were activated, at least before 24 hpi. This was consistent with the findings of Stewart et al. (2010) that the NF-κB signaling pathway was activated in the early stage of BTV infection, thereby inhibiting BTV replication (Supplementary Table 2) (11). From 24 hpi, the activity of canonical and non-canonical NF-κB signaling pathway was suppressed by BTV, as evidenced by increased transcription levels of their repressors, *NFKBIA* and *NFKBIB*, as well as decreased expression levels of *IKBKG* and *IKBKE* with the intermediary centrality in the NF-κB interactive network (Supplementary Table 2) (47). Although the expression levels of some downstream genes and facilitators remained high, just like *REL*, *NFKB1*, *RELB*, and *TANK*, these high levels of transcription were likely in vain relative to the downregulation of the betweenness center, and the upregulation of repressor genes since the anti-apoptotic function of the NF-κB signaling pathway was progressively lost starting from 24 hpi. Apoptosis and its resulting CPEs significantly expanded their influences at 48 hpi, the most common and best-characterized form of inflammation-induced cell death (Supplementary Table 2) (11, 47).

Our study presented a whole transcriptome map of BTV-infected sheep embryonic testicular cells for the first time, outlined the context of virus-and-host cell interactions, and provided new clues to elucidate the underly mechanisms of the host by which

BTV exploited or hijacked. Unfortunately, the NF-κB complex interactive network involves more than 300 members, and it is difficult to identify its role in the BTV infection process from the current results. Our sequencing data could only suggest similar conclusions to previous studies: BTV activated NF-κB signaling pathway in the early stage of infection, but inhibited it in the late stage, and BTV-induced apoptosis did not depend on the activation of this signaling pathway (11). We speculate that other signaling pathways, similar to NF-κB pathway, are regulated differently in different stages of infection with the progression of BTV infection. At the same time, further transcriptome sequencing and experimental verification at more intensive infection time points will help us to understand the different regulations of these signaling pathway more clearly in the process of BTV infection.

The variation of the transcriptional profile implicated a series of transcription factors, and the changes in transcription factors and validation of transcriptomic sequencing data could be further analyzed in conjunction with an assay for transposase-accessible chromatin with high-throughput sequencing (ATAC-seq). The OA3.Ts cell is a sheep embryo-derived cell line with differentiation potential, resulting in a relatively complex cell type composition. The transcriptional profile changes involved in the BTV infection process vary widely among different type of cells, which may cause the expression of some transcripts to be annihilated, and then exert an impact on our analysis results. Single-cell transcriptional profiling is also a promising technology for elucidating the infection and pathogenic mechanisms of BTV at the transcriptional level.

Data availability statement

The datasets presented in this study can be found in online repositories. The names of the repository/repositories and accession number(s) can be found below: https://www.ncbi.nlm.nih.gov/geo/, GSE213637, GSE213638.

Author contributions

ZrL and HL conceived and designed the experiments. ZrL, PZ, ZY, HY, and ZhL performed the experiments. DL and ZyL analyzed the data. ZrL and DL wrote the paper. All authors contributed to the article and approved the submitted version.

Funding

This study was supported by the Ten Thousand Talent for Youth Top-notch Talents of Yunnan Province (Project No. YNWR-QNBJ-2020-211), the Applied Basic Research Program of Yunnan Province (Project No. 2019FB041), the National Natural Science Foundation of China (Project No. 31802177), and the Special Fund for Agro-scientific Research in the Public Interest (Project No. 201303035).

Conflict of interest

The authors declare that the research was conducted in the absence of any commercial or financial relationships that could be construed as a potential conflict of interest.

Publisher's note

Supplementary material

The Supplementary Material for this article can be found online at: https://www.frontiersin.org/articles/10.3389/fimmu.2022.1053059/full#supplementary-material

SUPPLEMENTARY FIGURE 1
The PPI network based on dif-mRNAs constructed using STRING online database which was consisted of 1306 nodes and 7052 interaction pairs. Red and blue circles represented upregulated and downregulated dif-mRNA, respectively, whereas the thickness of the solid black line indicated the strength of the corresponding protein interactions.

References

1. Rushton J, Lyons N. Economic impact of bluetongue: A review of the effect on production. *Vet Ital* (2015) 51:401–6. doi: 10.12834/VetIt.646.3183.1

2. Puggioni G, Pintus D, Melzi E, Meloni G, Rocchigiani AM, Maestrale C, et al. Testicular degeneration and infertility following arbovirus infection. *J Virol* (2018) 92:e01131–18. doi: 10.1128/JVI.01131-18

3. Zhu J, Yang H, Li H, Xiao L, Wang J, Li N, et al. Full-genome sequence of bluetongue virus serotype 1 (BTV-1) strain Y863, the first BTV-1 isolate of eastern origin found in China. *Genome Announc* (2013) 1:e00403–13. doi: 10.1128/genomeA.00403-13

4. Bumbarov V, Golender N, Jenckel M, Wernike K, Beer M, Khinich E, et al. Characterization of bluetongue virus serotype 28. *Transbound Emerg Dis* (2020) 67:171–82. doi: 10.1111/tbed.13338

5. Yang H, Gu W, Li Z, Zhang L, Liao D, Song J, et al. Novel putative bluetongue virus serotype 29 isolated from inapparently infected goat in xinjiang of China. *Transbound Emerg Dis* (2021) 68:2543–55. doi: 10.1111/tbed.13927

6. Ries C, Vögtlin A, Hüssy D, Jandt T, Gobet H, Hilbe M, et al. Putative novel atypical BTV serotype '36' identified in small ruminants in Switzerland. *Viruses* (2021) 13:721. doi: 10.3390/v13050721

7. Yang H, Xiao L, Meng J, Lv M, Liao D, Song J, et al. Phylogenetic characterization genome segment 2 of bluetongue virus strains belonging to serotype 5, 7 and 24 isolated for the first time in China during 2012 to 2014. *Transbound Emerg Dis* (2017) 64:1317–21. doi: 10.1111/tbed.12479

8. DeMaula CD, Leutenegger CM, Bonneau KR, MacLachlan NJ. The role of endothelial cell-derived inflammatory and vasoactive mediators in the pathogenesis of bluetongue. *Virology* (2002) 296:330–7. doi: 10.1006/viro.2002.1476

9. Gu L, Musiienko V, Bai Z, Qin A, Schneller SW, Li Q. Novel virostatic agents against bluetongue virus. *PloS One* (2012) 7:e43341. doi: 10.1371/journal.pone.0043341

10. Du J, Gao S, Tian Z, Xing S, Huang D, Zhang G, et al. MicroRNA expression profiling of primary sheep testicular cells in response to bluetongue virus infection. *Infect Genet Evol* (2017) 49:256–67. doi: 10.1016/j.meegid.2017.01.029

11. Stewart ME, Roy P. Role of cellular caspases, nuclear factor-kappa b and interferon regulatory factors in bluetongue virus infection and cell fate. *Virol J* (2010) 7:362. doi: 10.1186/1743-422X-7-362

12. Ratinier M, Shaw AE, Barry G, Gu Q, Gialleonardo LD, Janowicz A, et al. Bluetongue virus NS4 protein is an interferon antagonist and a determinant of virus virulence. *J Virol* (2016) 90:5427–39. doi: 10.1128/JVI.00422-16

13. Liu S, Liu X, Li J, Zhou H, Carr MJ, Zhang Z, et al. Long noncoding RNAs: novel regulators of virus-host interactions. *Rev Med Virol* (2019) 29:e2046. doi: 10.1002/rmv.2046

14. Choudhary A, Madbhagat P, Sreepadmanabh M, Bhardwaj V, Chande A. Circular RNA as an additional player in the conflicts between the host and the virus. *Front Immunol* (2021) 12:602006. doi: 10.3389/fimmu.2021.602006

15. Singh M, Prasad M, Mishra B, Manjunath S, Sahu AR, Priya GB, et al. Transcriptome analysis reveals common differential and global gene expression profiles in bluetongue virus serotype 16 (BTV-16) infected peripheral blood mononuclear cells (PPBMCs) in sheep and goats. *Genom Data* (2016) 11:62–72. doi: 10.1016/j.gdata.2016.12.001

16. Chen S, Zhou Y, Chen Y, Gu J. Fastp: An ultra-fast all-in-one FASTQ preprocessor. *Bioinformatics* (2018) 34:i884–90. doi: 10.1093/bioinformatics/bty560

17. Kim D, Langmead B, Salzberg SL. HISAT: A fast spliced aligner with low memory requirements. *Nat Methods* (2015) 12:357–60. doi: 10.1038/nmeth.3317

18. Langmead B, Salzberg SL. Fast gapped-read alignment with bowtie 2. *Nat Methods* (2012) 9:357–9. doi: 10.1038/nmeth.1923

19. Kim D, Pertea G, Trapnell C, Pimentel H, Kelley R, Salzberg SL. TopHat2: Accurate alignment of transcriptomes in the presence of insertions, deletions and gene fusions. *Genome Biol* (2013) 14:R36. doi: 10.1186/gb-2013-14-4-r36

20. Pertea M, Pertea GM, Antonescu CM, Chang TC, Mendell JT, Salzberg SL. StringTie enables improved reconstruction of a transcriptome from RNA-seq reads. *Nat Biotechnol* (2015) 33:290–5. doi: 10.1038/nbt.3122

21. Pertea G, Pertea M. GFF utilities: GffRead and GffCompare. *F1000Res* (2020) 9:J–304. doi: 10.12688/f1000research.23297.2

22. Kong L, Zhang Y, Ye ZQ, Liu XQ, Zhao SQ, Wei L, et al. CPC: Assess the protein-coding potential of transcripts using sequence features and support vector machine. *Nucleic Acids Res* (2007) 35:W345–9. doi: 10.1093/nar/gkm391

23. Sun L, Luo H, Bu D, Zhao G, Yu K, Zhang C, et al. Utilizing sequence intrinsic composition to classify protein-coding and long non-coding transcripts. *Nucleic Acids Res* (2013) 41:e166. doi: 10.1093/nar/gkt646

24. Kim D, Salzberg SL. Tophat-fusion: An algorithm for discovery of novel fusion transcripts. *Genome Biol* (2011) 12:R72. doi: 10.1186/gb-2011-12-8-r72

25. Zhang XO, Wang HB, Zhang Y, Lu X, Chen LL, Yang L, et al. Complementary sequence-mediated exon circularization. *Cell* (2014) 159:134–47. doi: 10.1016/j.cell.2014.09.001

26. Zhang XO, Dong R, Zhang Y, Zhang JL, Luo Z, Zhang J, et al. Diverse alternative back-splicing and alternative splicing landscape of circular RNAs. *Genome Res* (2016) 26:1277–87. doi: 10.1101/gr.202895.115

27. Gao Y, Wang J, Zhao F. CIRI: An efficient and unbiased algorithm for *de novo* circular RNA identification. *Genome Biol* (2015) 16:4. doi: 10.1186/s13059-014-0571-3

28. Griffiths-Jones S, Bateman A, Marshall M, Khanna A, Eddy SR. Rfam: An RNA family database. *Nucleic Acids Res* (2003) 31:439–41. doi: 10.1093/nar/gkg006

29. Jurka J, Kapitonov VV, Pavlicek A, Klonowski P, Kohany O, Walichiewicz J. Repbase update, a database of eukaryotic repetitive elements. *Cytogenet Genome Res* (2005) 110:462–7. doi: 10.1159/000084979

30. Shen J, Hao Z, Luo Y, Zhen H, Liu Y, Wang J, et al. Deep small RNA sequencing reveals important miRNAs related to muscle development and intramuscular fat deposition in longissimus dorsi muscle from different goat breeds. *Front Vet Sci* (2022) 9:911166. doi: 10.3389/fvets.2022.911166

31. Hofacker IL. Vienna RNA Secondary structure server. *Nucleic Acids Res* (2003) 31:3429–31. doi: 10.1093/nar/gkg599

32. Robinson MD, McCarthy DJ, Smyth GK. edgeR: A bioconductor package for differential expression analysis of digital gene expression data. *Bioinformatics* (2010) 26:139–40. doi: 10.1093/bioinformatics/btp616

33. Kolde R. Pheatmap: Pretty heatmaps. R package Version 1.0.12 (2019). Available at: https://cran.r-project.org/web/packages/pheatmap/index.html.

34. Villanueva RAM, Chen ZJ. ggplot2: Elegant graphics for data analysis (2nd ed.). *Meas-Interdiscip Res* (2019) 17:160–7. doi: 10.1080/15366367.2019.1565254

35. Kopp F, Mendell JT. Functional classification and experimental dissection of long noncoding RNA. *Cell* (2018) 172:393–407. doi: 10.1016/j.cell.2018.01.011

36. Conesa A, Götz S, García-Gómez JM, Terol J, Talón M, Robles M. Blast2GO: a universal tool for annotation, visualization and analysis in functional genomics research. *Bioinformatics* (2005) 21:3674–6. doi: 10.1093/bioinformatics/bti610

37. Lewis BP, Burge CB, Bartel DP. Conserved seed paring, often flanked by adenosines, indicates that thousands of human genes are microRNA targets. *Cell* (2005) 120:15–20. doi: 10.1016/j.cell.2004.12.035

38. Gene Ontology Consortium. Creating the gene ontology resource: design and implementation. *Genome Res* (2001) 11:1425–33. doi: 10.1101/gr.180801

39. Kanehisa M, Goto S. KEGG: Kyoto encyclopedia of genes and genomes. *Nucleic Acids Res* (2000) 28:27–30. doi: 10.1093/nar/28.1.27

40. Walter W, Sánchez-Cabo F, Ricote M. GOplot: An r package for visually combining expression data with functional analysis. *Bioinformatics* (2015) 31:2912–4. doi: 10.1093/bioinformatics/btv300

41. Brunson JC. Ggalluvial: Layered grammar for alluvial plots. *J Open Source Software* (2020) 5:2017. doi: 10.21105/joss.02017

42. Szklarczyk D, Gable AL, Lyon D, Junge A, Wyder S, Huerta-Cepas J, et al. STRING v11: protein-protein association networks with increased coverage, supporting functional discovery in genome-wide experimental datasets. *Nucleic Acids Res* (2019) 47:D607–13. doi: 10.1093/nar/gky1131

43. Kohl M, Wiese S, Warscheid B. Cytoscape: Software for visualization and analysis of biological networks. *Methods Mol Biol* (2011) 696:291–303. doi: 10.1007/978-1-60761-987-1_18

44. Orrù G, Ferrando ML, Meloni M, Liciardi M, Savini G, De Santis P. Rapid detection and quantitation of bluetongue virus (BTV) using a molecular beacon fluorescent probe assay. *J Virol Methods* (2006) 137:34–42. doi: 10.1016/j.jviromet.2006.05.028

45. Flint AP, Burton RD, Gadsby JE, Heap RB, Sheldrick EL. Embryonic steroid synthesis and luteal oxytocin production: Controlling mechanisms for the maternal recognition of pregnancy. *J Steroid Biochem* (1983) 19:973–8. doi: 10.1016/0022-4731(83)90042-0

46. Mortola E, Noad R, Roy P. Bluetongue virus outer capsid proteins are sufficient to trigger apoptosis in mammalian cells. *J Virol* (2004) 78:2875–83. doi: 10.1128/jvi.78.6.2875-2883.2004

47. Tieri P, Termanini A, Bellavista E, Salvioli S, Capri M, Franceschi C. Charting the NF-κB pathway interactome map. *PloS One* (2012) 7:e32678. doi: 10.1371/journal.pone.0032678

48. Nomura F, Kawai T, Nakanishi K, Akira S. NF-κB activation through IKK-i-dependent I-TRAF/TANK phosphorylation. *Genes Cells* (2000) 5:191–202. doi: 10.1046/j.1365-2443.2000.00315.x

49. Gulyaeva LF, Kushlinskiy NE. Regulatory mechanisms of microRNA expression. *J Transl Med* (2016) 14:143. doi: 10.1186/s12967-016-0893-x

50. Goubau D, Deddouche S, Reis e Sousa C. Cytosolic sensing of viruses. *Immunity* (2013) 38:855–69. doi: 10.1016/j.immuni.2013.05.007

51. Vitour D, Doceul V, Ruscanu S, Chauveau E, Schwartz-Cornil I, Zientara S. Induction and control of the type I interferon pathway by bluetongue virus. *Virus Res* (2014) 182:59–70. doi: 10.1016/j.virusres.2013.10.027

52. Takeuchi O, Akira S. Pattern recognition receptors and inflammation. *Cell* (2010) 140:805–20. doi: 10.1016/j.cell.2010.01.022

53. Cassandri M, Smirnov A, Novelli F, Pitolli C, Agostini M, Malewicz M, et al. Zinc-finger proteins in health and disease. *Cell Death Discovery* (2017) 3:17071. doi: 10.1038/cddiscovery.2017.71

54. Mortola E, Larsen A. Bluetongue virus infection: Activation of the MAP kinase-dependent pathway in required for apoptosis. *Res Vet Sci* (2010) 89:460–4. doi: 10.1016/j.rvsc.2010.04.001

55. Saminathan M, Singh KP, Khorajiya JH, Dinesh M, Vineetha S, Maity M, et al. An updated revies on bluetongue virus: Epidemiology, pathobiology, and advances in diagnosis and control with special reference to India. *Vet Q* (2020) 40:258–321. doi: 10.1080/01652176.2020.1831708

56. Fan TJ, Han LH, Cong RS, Liang J. Caspase family proteases and apoptosis. *Acta Biochim Biophys Sin* (2005) 37:719–27. doi: 10.1111/j.1745-7270.2005.00108.x

57. Wang L, Zhao W, Zhang M, Wang P, Zhao K, Zhao X, et al. USP4 positively regulates RIG-I mediated antiviral response through deubiquitination and stabilization of RIG-I. *J Virol* (2013) 87:4507–15. doi: 10.1128/JVI.00031-13

58. Han X, Zhang JJ, Yao N, Wang G, Mei J, Li B, et al. Polymorphisms in NFKB1 and NFKBIA genes modulate the risk of developing prostate cancer among han Chinese. *Med Sci Monit* (2015) 21:1707–15. doi: 10.12659/MSM.893471

59. Hamza T, Barnett JB, Li B. Interleukin 12 a key immunoregulator cytokine in infection applications. *Int J Mol Sci* (2010) 11:789–806. doi: 10.3390/ijms11030789

60. Veldhoen M. Interleukin 17 is a chief orchestrator of immunity. *Nat Immunol* (2017) 18:612–21. doi: 10.1038/ni.3742

61. Richardson RB, Ohlson MB, Eitson JL, Kumar A, McDougal MB, Boys IN, et al. A CRISPR screen identities IFI6 as an ER-resident interferon effector that blocks flavivirus replication. *Nat Microbiol* (2018) 3:1214–23. doi: 10.1038/s41564-018-0244-1

62. DeDiego ML, Martinez-Sobrido L, Topham DJ. Novel functions of IFI44L as a feedback regulator of host antiviral responses. *J Virol* (2019) 93:e01159–19. doi: 10.1128/JVI.01159-19

63. Takeda E, Nakagawa S, Nakaya Y, Tanaka A, Miyazawa T, Yasuda J, et al. Identification and functional analysis of three isoform of bovine BST-2. *PloS One* (2012) 7:e41483. doi: 10.1371/journal.pone.0041483

64. Barnes B, Lubyova B, Pitha PM. On the role of IRF in host defense. *J Interferon Cytokine Res* (2002) 22:59–71. doi: 10.1089/107999002753452665

65. Drappier M, Michiels T. Inhibition of the OAS/RNase l pathway by viruses. *Curr Opin Virol* (2015) 15:19–26. doi: 10.1016/j.coviro.2015.07.002

66. Schiffer L, Barnard L, Baranowski ES, Gilligan LC, Taylor AE, Arlt W, et al. Human steroid biosynthesis, metabolism and excretion are differentially reflected by serum and urine steroid metabolomes: A comprehensive review. *J Steroid Biochem Mol Biol* (2019) 194:105439. doi: 10.1016/j.jsbmb.2019.105439

67. Slominski AT, Li W, Kim TK, Semak I, Wang J, Zjawiony JK, et al. Novel activities of CYP11A1 and their potential physiological significance. *J Steroid Biochem Mol Biol* (2015) 151:25–37. doi: 10.1016/j.jsbmb.2014.11.010

68. Sato Y, Asahina K, Yoshiike M, Nozawa S, Otoi T, Iwamoto T. A change in the steroid metabolic pathway in human testes showing deteriorated spermatogenesis. *Reprod Biol* (2020) 20:210–9. doi: 10.1016/j.repbio.2020.02.008

69. Massagué J. TGF-β signaling in development and disease. *FEBS Lett* (2012) 586:1833. doi: 10.1016/j.febslet.2012.05.030

70. Otto T, Sicinski P. Cell cycle proteins as promising targets in cancer therapy. *Nat Rev Cancer* (2017) 17:93–115. doi: 10.1038/nrc.2016.138

71. Lv S, Xu QY, Sun EC, Zhang JK, Wu DL. Dissection and integration of the autophagy signaling network initiated by bluetongue virus infection: crucial candidates ERK1/2, akt and AMPK. *Sci Rep* (2016) 6:23130. doi: 10.1038/srep23130

72. Celma CCP, Roy P. A viral nonstructural proteins regulates bluetongue virus trafficking and release. *J Virol* (2009) 83:6806–16. doi: 10.1128/JVI.00263-09

73. Mohl BP, Emmott E, Roy P. Phosphoproteomic analysis reveals the importance of kinase regulation during orbivirus infection. *Mol Cell Proteomics* (2017) 16:1990–2005. doi: 10.1074/mcp.M117.067355

74. Liu X, Wang T, Wakita T, Yang W. Systematic identification of microRNA and messenger RNA profiles in hepatitis c virus-infected human hepatoma cells. *Virology* (2010) 398:57–67. doi: 10.1016/j.virol.2009.11.036

75. Loveday EK, Svinti V, Diederich S, Pasick J, Jean F. Temporal- and strain-specific host microRNA molecular signatures associated with swine-origin H1N1 and avian-origin H7N7 influenza a virus infection. *J Virol* (2012) 86:6109–22. doi: 10.1128/JVI.06892-11

76. Chauveau E, Doceul V, Lara E, Adam M, Breard E, Sailleau C, et al. Sensing and control of bluetongue virus infection in epithelial cells *via* RIG-I and MDA5 helicases. *J Virol* (2012) 86:11789–99. doi: 10.1128/JVI.00430-12

77. Dai M, Wang X, Li JL, Zhou Y, Sang M, Liu JB, et al. Activation of TLR3/interferons signaling pathway by bluetongue virus results in HIV inhibition in macrophages. *FASEB J* (2015) 29:4978–88. doi: 10.1096/fj.15-273128

78. Ruscanu S, Pascale F, Bourge M, Hemati B, Elhmouzi-Younes J, Urien C, et al. The double-stranded RNA bluetongue virus induces type I interferon in plasmacytoid dendritic cells *via* a MYD88-dependent TLR7/8-independent signaling pathway. *J Virol* (2012) 86:5817–28. doi: 10.1128/JVI.06716-11

79. Lai JH, Wang MY, Huang CY, Wu CH, Hung LF, Yang CY, et al. Infection with the dengue RNA virus activates TLR9 signaling in human dendritic cells. *EMBO Rep* (2018) 19:e46182. doi: 10.15252/embr.201846182

80. Cai C, Tang YD, Xu G, Zheng C. The crosstalk between viral RNA- and DNA-sensing mechanisms. *Cell Mol Life Sci* (2021) 78:7427–34. doi: 10.1007/s00018-021-04001-7

81. Maelfait J, Liverpool L, Bridgeman A, Ragan KB, Upton JW, Rehwinkel J. Sensing of viral and endogenous RNA by ZBP1/DAI induces necroptosis. *EMBO J* (2017) 36:2529–43. doi: 10.15252/embj.201796476

82. Kirsch-Volders M, Fenech M. Inflammatory cytokine storms severity may be fueled by interactions of micronuclei and RNA viruses such as COVID-19 virus SARS-CoV-2. a hypothesis. *Mutat Res Rev Mutat Res* (2021) 788:108395. doi: 10.1016/j.mrrev.2021.108395

83. Zhou Y, He C, Wang L, Ge B. Post-translational regulation of antiviral innate signaling. *Eur J Immunol* (2017) 47:1414–26. doi: 10.1002/eji.201746959

84. Chauveau E, Doceul V, Lara E, Breard E, Sailleau C, Vidalain PO, et al. NS3 of bluetongue virus interferes with the induction of type I interferon. *J Virol* (2013) 87:8241–6. doi: 10.1128/JVI.00678-13

85. Fang M, Zhang A, Du Y, Lu W, Wang J, Minze LJ, et al. TRIM18 is a critical regulator of viral myocarditis and organ inflammation. *J BioMed Sci* (2022) 29:55. doi: 10.1186/s12929-022-00840-z

86. Xing J, Weng L, Yuan B, Wang Z, Jia L, Jin R, et al. Identification of a role for TRIM29 in the control of innate immunity in the respiratory tract. *Nat Immunol* (2016) 17:1373–80. doi: 10.1038/ni.3580

87. Xing J, Zhang A, Minze LJ, Li XC, Zhang Z. TRIM29 negatively regulates the type I IFN production in response to RNA virus. *J Immunol* (2018) 201:183–92. doi: 10.4049/jimmunol.1701569

88. Malgras M, Garcia M, Jousselin C, Bodet C, Lévêque N. The antiviral activities of poly-ADP-ribose polymerase. *Viruses* (2021) 13:582. doi: 10.3390/v13040582

89. Xing J, Zhang A, Du Y, Fang M, Minze LJ, Liu YJ, et al. Identification of poly (ADP-ribose) polymerase 9 (PARP9) as a noncanonical sensor for RNA virus in dendritic cells. *Nat Commun* (2021) 12:2681. doi: 10.1038/s41467-021-23003-4

90. Paparisto E, Woods MW, Coleman MD, Moghadasi SA, Kochar DS, Tom SK, et al. Evolution-guided structural and functional analyses of the HERC family reveal an ancient marine origin and determinants of antiviral activity. *J Virol* (2018) 92:e00528–18. doi: 10.1128/JVI.00528-18

91. Platnich JM, Muruve DA. NOD-like receptors and inflammasomes: review of their canonical and non-canonical signaling pathways. *Arch Biochem Biophys* (2019) 670:4–14. doi: 10.1016/j.abb.2019.02.008

92. Coperchini F, Chiovato L, Croce L, Magri F, Rotondi M. The cytokine storm in COVID-19: An overview of the involvement of the chemokine/chemokine-receptor system. *Cytokine Growth Factor Rev* (2020) 53:25–32. doi: 10.1016/j.cytogfr.2020.05.003

93. Weis SM, Cheresh DA. Pathophysiological consequences of VEGF-induced vascular permeability. *Nature* (2005) 437:497–504. doi: 10.1038/nature03987

94. Huang L, Shi Y, Gong B, Jiang L, Zhang Z, Liu X, et al. Dynamic blood single-cell immune responses in patients with COVID-19. *Signal Transduct Targe Ther* (2021) 6:110. doi: 10.1038/s41392-021-00526-2

95. Datta PK, Deshmane S, Khalili K, Merali S, Gordon JC, Fecchio C, et al. Glutamate metabolism in HIV-1 infected macrophages: Role of HIV-1 vpr. *Cell Cycle* (2016) 15:2288–98. doi: 10.1080/15384101.2016.1190054

96. Krishnan S, Nordqvist H, Ambikan AT, Gupta S, Sperk M, Svensson-Akusjärvi S, et al. Metabolic perturbation associated with COVID-19 disease severity and SARS-CoV-2 replication. *Mol Cell Proteomics* (2021) 20:100159. doi: 10.1016/j.mcpro.2021.100159

97. Moffitt KL, Martin SL, Walker B. Proteases implicated in apoptosis: Old and new. *J Pharm Pharmacol* (2010) 62:563–76. doi: 10.1211/jpp.62.05.0002

98. Kimura-Ohba S, Yang Y. Oxidative DNA damage mediated by intranuclear MMP activity is associated with neuronal apoptosis in ischemic stroke. *Oxid Med Cell Longev* (2016) 2016:6927328. doi: 10.1155/2016/6927328

99. Lin XT, Zheng XB, Fan DJ, Yao QQ, Hu JC, Lian L, et al. MicroRNA-143 targets ATG2B to inhibit autophagy and increase inflammatory responses in crohn's disease. *Inflammation Bowel Dis* (2018) 24:781–91. doi: 10.1093/ibd/izx075

100. Tak PP, Firestein GS. NF-κB: A key role in inflammatory diseases. *J Clin Invest* (2001) 107:7–11. doi: 10.1172/JCI11830

Frontiers in Immunology

Explores novel approaches and diagnoses to treat immune disorders.

The official journal of the International Union of Immunological Societies (IUIS) and the most cited in its field, leading the way for research across basic, translational and clinical immunology.

Discover the latest Research Topics

See more →

Frontiers

Avenue du Tribunal-Fédéral 34
1005 Lausanne, Switzerland
frontiersin.org

Contact us

+41 (0)21 510 17 00
frontiersin.org/about/contact